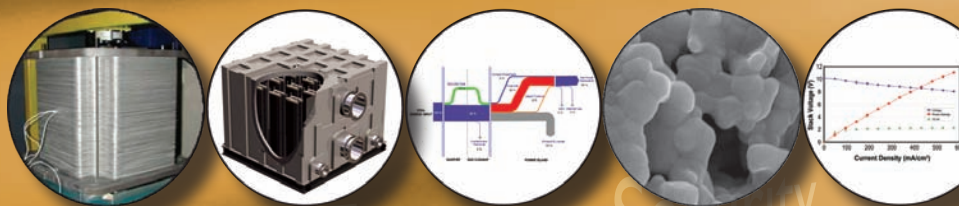


2008  
Office of Fossil Energy  
Fuel Cell Program Annual Report



Increase Energy Security  
Reduce Carbon Footprint  
Enhance Water Conservation



Solid State Energy Conversion Alliance





**2008**  
**OFFICE OF FOSSIL ENERGY**  
**FUEL CELL PROGRAM ANNUAL REPORT**

November 2008

---

**Disclaimer**

This report was prepared as an account of work sponsored by an agency of the United States Government. Neither the United States Government nor any agency thereof, nor any of their employees, makes any warranty, express or implied, or assumes any legal liability or responsibility for the accuracy, completeness, or usefulness of any information, apparatus, product, or process disclosed, or represents that its use would not infringe privately owned rights. Reference therein to any specific commercial product, process, or service by trade name, trademark, manufacturer, or otherwise does not necessarily constitute or imply its endorsement, recommendation, or favoring by the United States Government or any agency thereof. The views and opinions of authors expressed therein do not necessarily state or reflect those of the United States Government or any agency thereof.

---

# Table of Contents

<b>I. INTRODUCTION</b>	<b>1</b>
<b>II. SECA INDUSTRY TEAMS</b>	<b>15</b>
A. COAL-BASED SYSTEMS	15
1 FuelCell Energy, Inc.: FuelCell Energy’s (FCE) Solid State Energy Conversion Alliance (SECA) Coal-Based Solid Oxide Fuel Cell Power Plant Development Project	17
2 Siemens Power Generation, Inc.: Coal Gas Fueled SOFC Hybrid Power Systems with CO <sub>2</sub> Separation	22
B. COST REDUCTION	25
1 Delphi Automotive Systems LLC: Solid State Energy Conversion Alliance Delphi SOFC	27
<b>III. INNOVATIVE CONCEPTS</b>	<b>31</b>
1 GE Global Research: Solid Oxide Fuel Cell Coal-Based Power Systems	33
<b>IV. SECA CORE RESEARCH &amp; DEVELOPMENT</b>	<b>37</b>
A. CATHODES	37
1 Argonne National Laboratory: Synchrotron X-Ray Studies of SOFC Cathodes	39
2 Carnegie Mellon University: SOFC Cathode Surface Chemistry and Optimization Studies	42
3 Carnegie Mellon University: TEM Investigations of Cr-Contamination in SOFC Cathodes	47
4 Georgia Institute of Technology: Characterization of Atomic and Electronic Structure of Electrochemically Active SOFC Cathode Surfaces	52
5 Georgia Institute of Technology: Functionally Graded Cathodes for Solid Oxide Fuel Cells	56
6 Lawrence Berkeley National Laboratory: Development of Metal Supported SOFC	59
7 Massachusetts Institute of Technology: Local Electronic Structure and Surface Chemistry of SOFC Cathodes	63
8 NexTech Materials Ltd.: Intermediate Temperature Solid Oxide Fuel Cell Cathode Enhancement through Infiltration Fabrication Techniques	67
9 University of Florida: SECA Coal-Based Systems Core Research – University of Florida	70
10 Walter A. Harrison/Stanford University: Electronic Structure of Cathode Materials	75
B. ANODES AND COAL CONTAMINANTS	79
1 Georgia Institute of Technology: Novel Sulfur-Tolerant Anodes for Solid Oxide Fuel Cells	81
2 National Energy Technology Laboratory: Coal-Based Fuel Cells	86
3 Ohio University: Combined Theoretical and Experimental Investigation and Design of H <sub>2</sub> S Tolerant Anode for Solid Oxide Fuel Cells	89
4 Pacific Northwest National Laboratory: SECA Coal-Based Systems Core Research: Anode Reactions in Coal-Derived Fuels	92
5 SRI International: Effect of Coal Contaminants on Solid Oxide Fuel System Performance and Service Life	96
6 West Virginia University: Direct Utilization of Coal Syngas in High Temperature Fuel Cells	99
C. INTERCONNECTS	105
1 ATI Allegheny Ludlum: Evaluation of a Functional Interconnect System for SOFCs	107
2 Arcomac Surface Engineering, LLC: Oxidation Resistant, Cr Retaining, Electrically Conductive Coatings on Metallic Alloys for SOFC Interconnects	111
3 National Energy Technology Laboratory: Materials Development for the Solid Oxide Fuel Cell Environment	115
4 Pacific Northwest National Laboratory: Cathode-Interconnect Contact and Cathode Chemical Compatibility Studies	120

<b>IV. SECA CORE RESEARCH &amp; DEVELOPMENT (CONTINUED)</b>	
<b>C. INTERCONNECTS (CONTINUED)</b>	
5 Pacific Northwest National Laboratory: SOFC Interconnect Materials Development at PNNL.....	124
6 Tennessee Technological University: Development of Low-Cr Fe-Ni-Based Alloys for Intermediate Temperature SOFC Interconnect Application.....	128
<b>D. SEALS.....</b>	133
1 Pacific Northwest National Laboratory: Development of Seals and Seal/Interconnect Interfaces.....	135
2 Sandia National Laboratories: Reliable Seals for Solid Oxide Fuel Cells.....	139
3 University of Cincinnati: Innovative Seals for Solid Oxide Fuel Cells (SOFCs).....	144
4 Missouri University of Science & Technology: Thermochemically Stable Sealing Materials for Solid Oxide Fuel Cells.....	147
<b>E. CONTACT MATERIALS.....</b>	151
1 Pacific Northwest National Laboratory: SECA Coal-Based Systems Core Research: Contact Paste Development.....	153
2 Tennessee Technological University: Novel Composite Materials for SOFC Cathode-Interconnect Contact.....	157
<b>F. CROSS-CUTTING MATERIALS AND MANUFACTURING.....</b>	161
1 Argonne National Laboratory: SOFC Research and Development in Support of SECA.....	163
2 Oak Ridge National Laboratory: Reliability and Durability of Materials and Components for Solid Oxide Fuel Cells.....	166
3 Pacific Northwest National Laboratory: SECA Core Technology Program Activities - PNNL.....	170
4 Pacific Northwest National Laboratory: Development and Implementation of Stack Fixture Tests.....	174
5 University of Texas at San Antonio: Novel Low Temperature Solid State Fuel Cells.....	177
<b>G. FUEL PROCESSING.....</b>	181
1 Aspen Products Group, Inc.: Waterless 5 kWe Diesel Reformer.....	183
2 Ceramatec, Inc.: SOFC Integrated Multi-Mode Diesel Reformer.....	186
3 Delevan d.b.a. Goodrich Turbine Fuel Technologies: An Innovative Injection and Mixing System for Diesel Fuel Reforming.....	191
4 Eltron Research and Development Inc.: Reformer for Conversion of Diesel Fuel into CO and Hydrogen.....	195
5 Lynntech, Inc.: Low Cost, Compact Plasma Fuel Reformer for APUs.....	200
6 National Energy Technology Laboratory: Liquid Hydrocarbon Fuel Reforming Studies.....	203
7 National Energy Technology Laboratory: Oxide-Based Reforming Catalysts: Evaluation and Development.....	206
8 Precision Combustion Inc.: Novel Water-Neutral Diesel Fuel Processor and Sulfur Trap.....	210
9 University of Michigan: Carbon Tolerant Steam Reforming and SOFC Anode Catalysts.....	213
<b>H. POWER ELECTRONICS.....</b>	217
1 National Institute of Standards and Technology: Advanced Power Conditioning System (PCS) Technologies for High-Megawatt Fuel Cell Power Plants.....	219
2 Virginia Polytechnic Institute and State University: A Low-Cost Soft-Switched DC-DC Converter for Solid Oxide Fuel Cells.....	225

---

<b>IV. SECA CORE RESEARCH &amp; DEVELOPMENT (CONTINUED)</b>	
<b>I. MODELING AND SIMULATION</b> . . . . .	229
1 American Society of Mechanical Engineers: SOFC Design Basis Development Project . . . . .	231
2 Pacific Northwest National Laboratory: Modeling and Experiments of SOFC Stacks and Materials at PNNL . . . . .	233
3 University of California, Irvine: High Efficiency Coal Gasification-Based SOFC Power Plants . . . . .	237
<b>J. BALANCE OF PLANT</b> . . . . .	243
1 Acumentrics Corporation: Hybrid Ceramic/Metallic Recuperator for SOFC Generator. . . . .	245
2 Phoenix Analysis & Design Technologies: Anode and Cathode Blower Systems for SOFC . . . . .	248
3 R&D Dynamics Corporation: Foil Gas Bearing Supported High Speed Centrifugal Anode Gas Recycle Blower . . . . .	251
<b>V. ADVANCED RESEARCH</b> . . . . .	255
1 Ceramtec, Inc.: Proton Conducting Solid Oxide Fuel Cell. . . . .	257
2 Ceramtec, Inc.: Intermediate Temperature Solid Oxide Fuel Cell Development. . . . .	261
3 Montana State University: SECA Coal-Based Systems Core Research – Montana State University. . . . .	264
4 National Energy Technology Laboratory: Oxide Contaminant Removal in Liquid Tin Anode Fuel Cells by Direct Reduction with Coal. . . . .	272
5 Naval Undersea Warfare Center: Testing and Evaluation of Solid Oxide Fuel Cells in Extreme Conditions. . . . .	274
6 University of Utah: A High Temperature Electrochemical Energy Storage System Based on Sodium Beta Alumina Solid Electrolyte (BASE) . . . . .	277
<b>VI. ACRONYMS &amp; ABBREVIATIONS</b> . . . . .	281
<b>VII. PRIMARY CONTACT INDEX</b> . . . . .	289
<b>VIII. ORGANIZATION INDEX</b> . . . . .	291
<b>IX. CONTRACT NUMBER INDEX</b> . . . . .	293
<b>X. INDEX OF PREVIOUS PROJECTS</b> . . . . .	295



---

# I. INTRODUCTION



---

## I. Introduction

### Competitive Innovation: Accelerating Technology Development

The U.S. Department of Energy (DOE) Office of Fossil Energy, through the National Energy Technology Laboratory (NETL) and in collaboration with the Pacific Northwest National Laboratory, is forging government/industry partnerships under the Solid State Energy Conversion Alliance (SECA) to reduce the cost of fuel cells and to develop integrated gasification fuel cell (IGFC) systems utilizing coal for clean and efficient central power generation. These goals equate to removing environmental and climate change concerns associated with fossil fuel use while simultaneously establishing a foundation for a secure energy future in the United States. With the successful completion of the first phase of the SECA Cost Reduction program element in 2006, SECA is one step closer to realizing its vision of cost-effective, near-zero-emission fuel cell technology for commercial applications.

The Administration's Office of Management and Budget previously cited the SECA program as leading the way in Government-industry partnerships.

*"The SECA program leverages private-sector ingenuity by providing Government funding to Industry Teams developing fuel cells, as long as the Teams continue to exceed a series of stringent technical performance hurdles. This novel incentive structure has generated a high level of competition between the Teams and an impressive array of technical approaches. The SECA program also develops certain core technologies that can be used by all the Industry Teams to avoid duplication of effort. The program exceeded its 2005 performance targets, and it is on track to meet its goal for an economically competitive technology by 2010."*

The SECA fuel cell program is a critical element of the DOE's Office of Fossil Energy technology portfolio. From an energy security perspective, coal is a primary resource for reducing dependence on imported oil and natural gas. More than half of the nation's electricity supply is generated from coal - developing technology to ensure its environmentally clean and climate friendly use is of crucial national importance. SECA technology offers greater than 90 percent carbon capture, less than 0.5 ppm NO<sub>x</sub> emission, reduced water requirements, and a coal-to-electricity efficiency exceeding 50 percent on a higher heating value (HHV) basis. The SECA cost goal of \$400/kW pursued under the SECA Cost Reduction program element will ensure that the cost of electricity to the user will not exceed what is typical today.

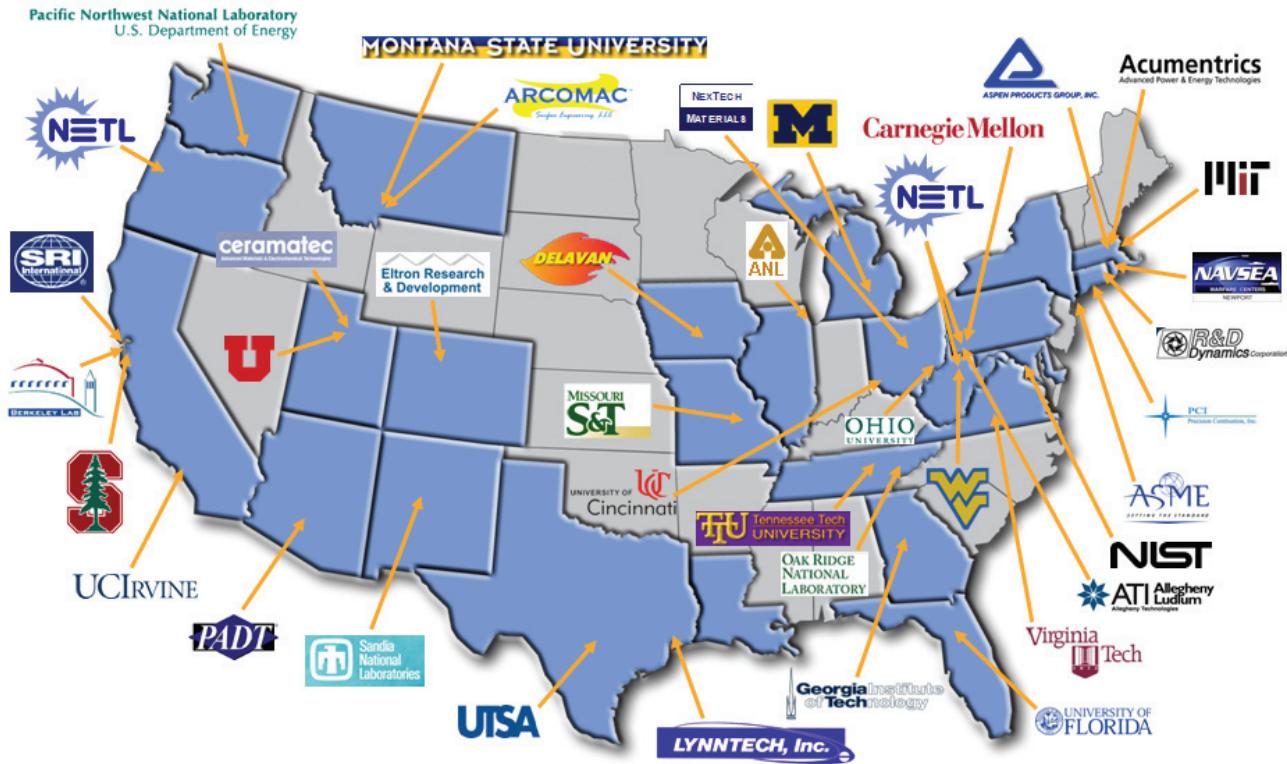


Concurrently, the SECA Coal-Based Systems program element will scale and integrate SECA solid oxide fuel cell (SOFC) technology for use in large IGFC systems. Cross-cutting research and development (R&D) and testing support is provided by SECA's Core Technology program element.

SECA is comprised of three groups: Industry Teams, Core Technology participants, and federal government management. The Industry Teams within the SECA Cost Reduction and Coal-Based Systems program elements design the fuel cells and handle most hardware and market penetration issues. The Core Technology program element, made up of universities, national laboratories, small businesses, and other R&D organizations, addresses applied technological issues common to all Industry Teams. Findings and inventions under the Core Technology program are made available to all Industry Teams under unique intellectual property provisions that serve to accelerate development. The federal government management facilitates interaction between Industry Teams and the Core Technology program as well as establishes technical priorities and approaches.

Across the United States, SECA Core Technology participants are working on dozens of fuel cell projects, led by the brightest minds from leading universities, national laboratories and businesses. These competitively-selected projects provide vital R&D and testing in support of the Industry Teams.

In the same spirit of healthy competition, the Industry Teams leverage the collective ingenuity of the Core Technology participants to independently pursue innovations in fuel cell design that can be mass-produced at lower cost. Focusing on Cost Reduction and Coal-Based Systems, the Industry Teams are working to solve the challenges of fuel cell technology, each using different design and manufacturing



SECA Core Technology and Advanced Research Participants

approaches. As a result, the SECA program is rich in innovation, allowing it to reach its goals much faster.

**Fuel Cell Research and Development**

The Office of Fossil Energy and NETL are pleased to present this FY 2008 Office of Fossil Energy Fuel Cell Program Annual Report, a compilation of abstracts from the fuel cell projects managed through these offices. These abstracts are divided into subsections as detailed below.

**SECA Industry Teams - Coal-Based Systems:**

Through its Coal-Based Systems program element, SECA seeks to leverage successes in the Cost Reduction program element; scale SOFC cells and stacks to sizes appropriate for central power generation applications; and integrate the SOFC, associated balance of plant, and coal gasification technology to create an IGFC system. Industry Teams will focus on developing large MW-scale systems while continuing SECA Cost Reduction activities through 2010. It is anticipated that the best technology from any Industry Team will be available for incorporation into one or more of the SECA Coal-Based Systems projects. Key R&D topics include coal contaminants, pressurization, failure analysis, system

integration, balance of plant, materials, manufacturing, and controls and instrumentation.

**SECA Industry Teams - Cost Reduction:**

To achieve cost targets, Industry Teams are refining and validating advanced technology in 3-10 kW SOFC modules that can be mass produced, aggregated, and scaled to meet a broad range of applications. This development activity is blending established manufacturing processes with state-of-the-art fuel cell technology advancements in order to leverage the advantages of economies of production (high-volume mass production) and scale to reduce fuel cell costs. Achieving the cost targets requires reaching a full spectrum of large markets, such as auxiliary power units (APUs) for trucks and recreational vehicles, and other markets such as residential-commercial-industrial power, a wide range of distributed generation, and specialized applications for the military. Producing a common module for these vast markets will create the opportunity for the high-volume production required to reduce cost to the necessary level.

### Innovative Concepts:

One of the Industry Teams, General Electric, is working to identify degradation mechanisms in high-performance cathodes and develop strategies for retaining high performance over the lifetime of an operating SOFC. In addition, a thermal spray process will be developed and demonstrated for depositing the electrolyte layer – this technology would permit expanded stack design and manufacturing options and lower cost. Optimal solutions to the degradation mechanisms, including the thermal spray process, will be tested and evaluated. The goal is to reduce power degradation rates while maintaining high initial power levels.

### SECA Core R&D:

The Core Technology program provides comprehensive applied research support in ten focus areas. This structure and special intellectual property provisions reduce cost by leveraging resources so that all Industry Teams do not engage in separate applied research programs, paying multiple times for the same research. This approach also ensures that only major issues are addressed. SECA's goal is to raise the technology bar in large strides rather than small steps. Core Technology program areas are also funded by special topics under DOE Science Initiatives, Small Business Innovative Research (SBIR), Basic Energy Sciences, and Historically Black Colleges and Universities. The Core Technology focus areas include the following:

- **Cathodes** – Improve the stability and performance of fuel cell cathodes, using state-of-the-art concepts and methodologies;
- **Anodes and Coal Contaminants** – Determine potential coal syngas contaminants and their potential impact on anode performance;
- **Interconnects** – Develop stable, low-cost metallic interconnects operating in the temperature range of 650 to 850°C with acceptably low area-specific resistance (ASR) over the service lifetime;
- **Seals** – Develop materials and designs exhibiting adequate sealing performance with the requisite chemical and phase stability in long-term service;
- **Contact Materials** – Develop interconnect contact materials that result in low, stable ASRs;
- **Cross-Cutting Materials and Manufacturing** – Develop materials and manufacturing technologies that improve fuel cell reliability, performance, and ability to tolerate any fuel or air contaminants, and that achieve cost reductions;
- **Fuel Processing** – Develop fuel processing technologies that will meet application requirements

such as zero water, space and volume, and transient capability;

- **Power Electronics** – Optimize fuel cell power system efficiency and cost in conversion of fuel cell output to usable DC (direct current) and AC (alternating current) power;
- **Modeling and Simulation** – Create models to determine a reliable operating space and to guide manufacturing; and
- **Balance of Plant** – Develop high temperature heat exchangers and blowers to enable high system efficiency and low cost.

### Advanced Research:

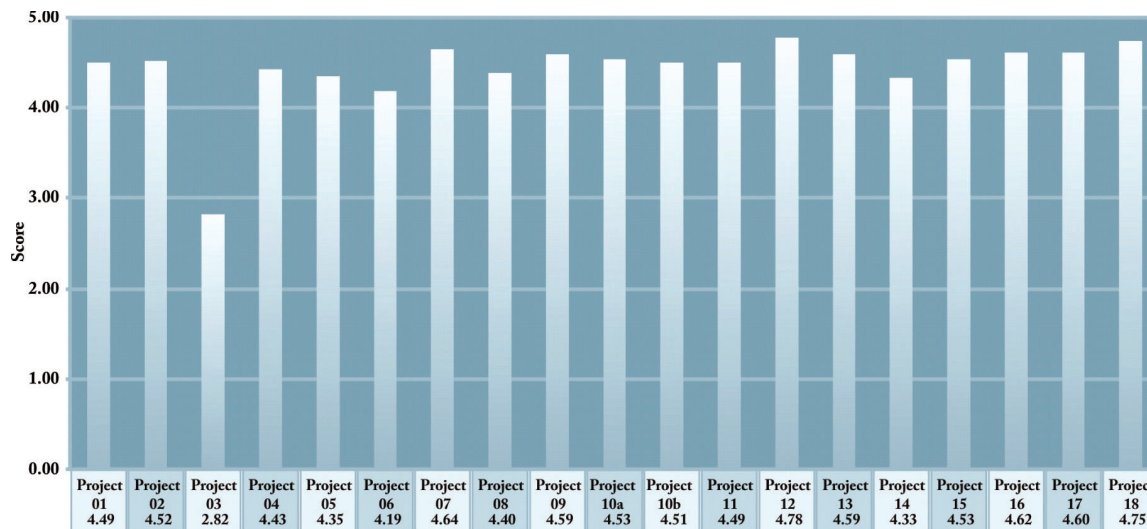
The SECA Advanced Research program provides cross-cutting, multidisciplinary research that leads to advanced electrochemical technologies minimizing the environmental consequences of using fossil fuels in energy generation. This program supports future advances in the SECA and Office of Fossil Energy Coal and Power programs by developing novel electrochemical energy-conversion and integrated technologies that advance the efficiency, reliability, and cost goals of fuel cell systems.

## Key Program Accomplishments

### SECA Peer Review Demonstrates Strength and Success:

Eighteen projects were evaluated during the 2008 Fuel Cells Peer Review at Sheraton Station Square, Pittsburgh, PA, on April 21-25, 2008. A group of nine reviewers from industry and academia assessed the projects across nine criteria: A) Existence of clear, measurable milestones, B) Rate of progress, C) Technical approach, D) Economic analysis, E) Utilization of government resources, F) Scientific and technical merit, G) Anticipated benefits if successful, H) Commercialization potential, and I) Possible adverse effects considered. Scores were based on a whole number scale of 1 to 5, with 1 being “results not demonstrated” and 5 being “effective”.

Results were extremely supportive of the Fuel Cells/SECA program and Core R&D as shown in the following figure. Seventeen of the 18 of the projects evaluated had average project scores ranging from 4.19 to 4.78 for the nine criteria. The overall average score for these 17 projects was an outstanding 4.52. The outlier project, an earmark, was rated 2.82, between ineffective and adequate, and including this project in the overall average score lowers it to 4.43. These results



SECA Peer Review Project Average Score Results

clearly demonstrate the effectiveness, strength, and success of the Fuel Cells/SECA Program.

SECA Industry Teams – Coal-Based Systems:

- SOFCs Successfully Scaled for Centralized Power Generation.** FuelCell Energy (FCE) and its technology partner Versa Power Systems (VPS) made significant progress in scaling SOFCs to sizes amenable to central generation (greater than 100 MWe) applications. In October 2007, VPS successfully completed a 1.3 kWe, 6-cell stack test incorporating scaled cells, each with an active area 550 cm<sup>2</sup> – an increase of over 350 percent compared to the baseline VPS cell (121 cm<sup>2</sup>). Furthermore, the scaling to larger area cells was achieved with less than 5 percent performance loss compared to the performance of the baseline cell. These cells were manufactured using VPS’ existing proprietary manufacturing processes that are both economical and suitable for high-volume manufacturing. Fuel cell active area is an important aspect of fuel cell design which effects stack cost and, ultimately, fuel cell system cost. The larger the fuel cell active area, the fewer non-repeat parts – end plates, manifolds, electrical connections between stacks, and other hardware – will be required. This FCE/VPS accomplishment substantially contributes to achievement of the SECA cost goal of \$400/kW fuel cell power blocks by 2010.
- Siemens Delta-8 SOFC Cell Surpasses Previous Performance by Five-Fold.** The performance of Siemens Power Generation’s (SPG) “Delta8” SOFC cell has surpassed the performance of all

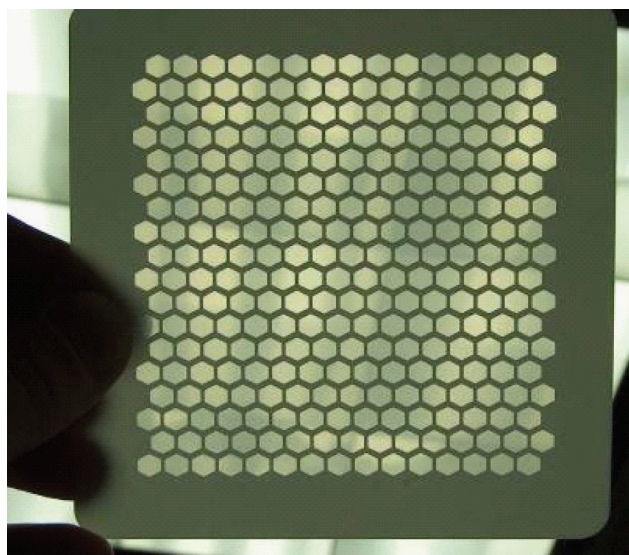
previous SPG cell designs with no noticeable voltage degradation. On a power per cell basis, the Delta8 cell is an almost five-fold improvement over the earlier tubular designs. At a cell voltage of 0.70 Volts, the Delta8 cell generates 525 watts per cell versus 110 watts per cell for the tubular cells. Furthermore, the Delta8 cell represents a 60 percent increase in active area over the largest previous cell, and a 125 percent increase over the-baseline SPG tubular cell. The Delta8 design, the latest within SPG’s High Power Density (HPD) cell design series, utilizes a 15-cm-wide flattened tube (which shortens current conduction paths, thereby reducing cell resistance and increasing performance) with 8 triangular corrugations on one side for increased active area. The cell active length is 75 cm, resulting in a cell active area of 1900 cm<sup>2</sup>. An increase in active length to 100 cm is planned, which will increase the cell active area to 2600 cm<sup>2</sup>. The 75 cm Delta8 cell has achieved a peak power density of 0.28 W/cm<sup>2</sup> to date – which was limited by the test stand equipment. This result was achieved at 1,000°C, atmospheric pressure, and 80 percent fuel utilization using humidified hydrogen as fuel. Projected peak power density is over 0.33 Watts/cm<sup>2</sup>. The cell test has operated for over 2,000 hours under load and an additional 609 hours at open circuit through April 2008. This performance improvement is indicative of the advancements achieved by SPG and other Industry Teams under the SECA program towards the R&D performance goals necessary for commercialization of SOFCs.

## SECA Industry Teams – Cost Reduction:

- **Delphi SOFC Auxiliary Power Unit Demonstrated.** Leveraging development supported by the DOE Office of Energy Efficiency and Renewable Energy (EERE) and Office of Fossil Energy's SECA program, Delphi Automotive Systems and Peterbilt Motors Company successfully demonstrated a Delphi SOFC APU powering a Peterbilt Model 386 truck's "hotel" loads. The Delphi/Peterbilt test, conducted at Peterbilt's Texas headquarters, replicated a typical trucker's day to evaluate the real-world usefulness and capacity of the SOFC. As part of the test, the Delphi SOFC provided ten hours of power for the Model 386's electrical system and air conditioning and maintained the truck's batteries – all while the Model 386's diesel engine was turned off, simulating an overnight hotel load requirement. Throughout the test, the Delphi SOFC APU provided an average of 800 watts of electricity to the Peterbilt Model 386. Delphi's SOFC technology directly addresses increasingly stringent anti-idling legislation and other proposals addressing commercial truck emissions, noise and fuel consumption. By limiting idling time and running a SOFC instead of the main engine, emissions are reduced, noise is nearly eliminated, and operators realize significant fuel savings. The Peterbilt Model 386 was chosen as the test bed for the SOFC due to its aerodynamic and fuel-efficient performance. It merges conventional Peterbilt styling with leading aerodynamic design and has been recognized as fuel efficient and environmentally friendly by the Environmental Protection Agency's SmartWay program.

## SECA Core R&amp;D – Cathodes:

- **SOFC Cathode Surface Chemistry Characterized with Synchrotron X-rays.** Researchers at the Advanced Photon Source at Argonne National Laboratory (ANL), Carnegie Mellon University, Massachusetts Institute of Technology, and Stanford University are collaborating to understand the chemistry and structure of SOFC cathodes. Recently, ANL illuminated the surface of model cathodes with synchrotron X-rays to determine their surface chemistry and surface structure. The cathodes were systematically exposed to variations in oxygen pressure, temperature, and electrochemical loading. Preliminary results show that in strontium-containing cathodes, electrochemical loading can cause strontium to surface segregate. Analysis of cathodes with analytical techniques that require room-temperature
- ultra-high vacuum (UHV) conditions has been hampered by a poor understanding of differences between laboratory conditions and SOFC operating conditions. This revolutionary work provides a solid underpinning to the use of UHV techniques by discovering that the surface chemistry and structure of some cathodes are very similar under room-temperature laboratory conditions and high-temperature SOFC operating conditions. When coupled with validating studies such as this, UHV techniques, known for their spatial and energetic sensitivities, will permit direct access to the electronic structure of the cathodes and establish accurate descriptions of the local chemical and structural landscape. The new data being generated by this study are guiding theoreticians and engineers in their understanding of the role of surfaces in fuel cell cathode performance.
- **New Electrode Architecture Leads to Lower Polarization Resistance and Better Stability.** Georgia Institute of Technology has successfully demonstrated that the performance and long-term stability of the state-of-the-art LSCF cathodes can be enhanced by infiltration of a catalytically active coating (e.g., LSM or SSC). The unique features of this new electrode architecture derive from its effective use of the high ionic and electronic conductivity of the backbone (e.g., LSCF) and the high stability and catalytic activity of the surface coating (e.g., LSM or SSC). The novelty of the cathodes is in the selection and the detailed microstructure of the catalysts and backbone materials that create a better performing cathode. Further, a methodology for reliably evaluating the intrinsic surface catalytic properties of mixed-conducting cathode materials has been developed, which is vital to systematically characterizing the effect of surface morphology, composition, and thickness of the coating materials on the electrochemical behavior of the cathodes. Reduction in cathode polarization resistance and improvement in stability will ultimately reduce the cost of SOFC technology and help to meet DOE cost goals.
  - **FlexCell Design and Analysis Initiated.** NexTech Materials, Ltd. recently initiated work on a DOE-SECA project to validate the performance, robustness, cost and scalability of a novel planar cell design for use in coal-based SOFC power systems. NexTech's planar cell design, termed the FlexCell, is a patent-pending, electrolyte-supported planar SOFC. The structure is comprised of a thin (<40 microns) electrolyte membrane layer that is mechanically supported by a thicker "honeycomb"



NexTech's FlexCell Design

mesh layer of electrolyte material. More than 80 percent of the electrolyte membrane within the active area is thin. The FlexCell may offer improved strength and therefore higher reliability, and higher efficiency due to the thin electrolyte. The objectives of this project are to demonstrate high performance from FlexCells made with yttrium-stabilized zirconia, to achieve stable performance in FlexCells operating with syngas fuels typical of gasified coal after clean up, and to scale up the size of the FlexCell design. A manufacturing cost analysis also will be performed to determine FlexCell manufacturing costs at full-scale production levels (250 MW/year).

- Novel Catalysis Techniques Provide Fundamental Approach to Improve Performance of SOFC Cathodes.** Researchers at the University of Florida used novel *in situ* oxygen-isotope experiments to determine the kinetics of the oxygen reduction mechanism on  $\text{LaSrMnO}_3$  and  $\text{LaSrCoFeO}_3$  cathode materials. The results show that the observed greater performance of  $\text{LaSrCoFeO}_3$  cathodes is due to their greater overall kinetics for the oxygen reduction reaction. Mechanistically, both cathode materials were demonstrated to have comparable rates of oxygen dissociation, but  $\text{LaSrCoFeO}_3$  exhibited a  $\sim 3$ -order-of-magnitude faster oxygen incorporation step than  $\text{LaSrMnO}_3$ . Moreover, the results indicate that  $\text{LaSrCoFeO}_3$  cathode performance could be further improved if the surface could be modified to increase oxygen surface coverage. Since currently SOFC performance is limited by the cathodes, this could have a dramatic impact on SOFC performance.

- Understanding of Electronic Structure of Manganates and Ferrites Improved.** In a theoretical program in support of the R&D of oxide cathode structures for fuel cells, Professor Walter Harrison of Stanford University has sought a simplified description of the electronic structure of the manganates and ferrites, analogous to the bond-orbital theory of semiconductors. In this formulation, cluster orbitals, based upon a transition-metal ion and its six oxygen neighbors, play the role of the bond orbitals in semiconductor theory. He began with the simpler systems, manganese oxides  $\text{MnO}$ ,  $\text{Mn}_2\text{O}_3$ , and  $\text{MnO}_2$ , and found that such orbitals, based upon free-atom atomic term values and his universal couplings, reasonably described the cohesion in these systems. He extended the description to the cohesion of the cathode materials  $\text{La}_{1-x}\text{Sr}_x\text{MnO}_3$  (LSM) and  $\text{La}_{1-x}\text{Sr}_x\text{Co}_y\text{Fe}_{1-y}\text{O}_3$  (LSCF) with similar success. Since this is a theory of the electronic structure, not just the cohesion, it is applicable to the entire array of structural, conducting, and magnetic properties of these systems, providing a general elementary understanding of these systems such as that which has supported the development of traditional semiconductor systems.

#### SECA Core R&D – Anodes and Coal Contaminants:

- Methodology for Improving Sulfur Tolerance of Anodes Developed.** Georgia Institute of Technology has successfully evaluated the effect of  $\text{H}_2\text{S}$  contaminants on the performance of SOFCs. For exposure to low concentration of  $\text{H}_2\text{S}$  (e.g., 1 ppm in hydrogen humidified at room temperature), the degradation (or the drop in power output or voltage at a constant current) due to the initial  $\text{H}_2\text{S}$  exposure appears to be independent of operating conditions (e.g., cell potential). In contrast, for exposure to high concentration of  $\text{H}_2\text{S}$  (e.g., 10 ppm), the degradation appears to be more severe at a higher operating current density (or lower cell potential). The degradation due to initial  $\text{H}_2\text{S}$  exposure occurs quickly, typically within hours, and performance then remains relatively constant for continuous operation up to thousands of hours at 200 and 400  $\text{mA}/\text{cm}^2$ . For cells operated at 600  $\text{mA}/\text{cm}^2$ , however, there appears a second stage degradation in performance after the degradation due to the initial  $\text{H}_2\text{S}$  exposure, but at a much smaller rate. Further, a methodology for reducing the sensitivity to  $\text{H}_2\text{S}$  has been developed. Development of sulfur-tolerant anodes will improve the stability and performance of SOFCs and help to meet DOE cost goals.



NETL researcher Rich Pineault installs the SOFC multi-cell array at the PSDF gasification facility in Alabama, with the gasifier visible in the background

- Novel Design Accelerates Integrated SOFC-Coal Gasifier Performance Testing.** A collaborative effort between researchers at NETL and the Power Systems Development Facility (PSDF) operated by Southern Company has successfully proven a novel SOFC test hardware design which permits accelerated performance testing of SOFCs fueled with direct syngas derived from gasification of coal. The unique design, known as the multi-cell array or MCA, permits simultaneous parallel testing of up to 12 SOFC test specimen for extended periods. The MCA test skid was deployed to the PSDF gasification unit from January to August of 2008 and, after being successfully validated, was operated to collect 1,200 sample-hours of SOFC performance data. The data collected during this effort will be used to predict gas cleanup targets for high-performance, high-efficiency IGFC systems. The test system is scheduled for re-deployment to PSDF next year to support continued research efforts on coal syngas fuelled SOFC.
- Highlight on Coal Gas Contaminant Testing.** Researchers at Pacific Northwest National Laboratory (PNNL) have evaluated the consequences of SOFC exposure to low concentrations of phosphorus and arsenic in gasified coal. This work is part of a collaborative effort involving NETL, SRI International, and

PNNL to establish acceptable concentrations of contaminants that may be present in coal gas used to fuel SOFCs. Both phosphorus and arsenic, even at sub-parts-per-million levels, were found to react strongly with nickel in the SOFC anode to form alteration phases, consistent with expectations based on thermodynamic assessments. Both of these contaminants were preferentially captured within a short distance of the fuel inlet in reactions with nickel. An important degradation mode involved loss of electronic percolation, the result of alteration phase formation, grain growth, and inducement of micro-fractures within the affected portions of the anode support. Even with extensive anode support conversion, rates of SOFC performance loss remained very low, with the active anode remaining unaffected until nickel conversion to alteration phases was nearly complete. These results suggest that nearly complete removal of phosphorus and arsenic from coal gas is necessary for SOFC applications, and that a nickel-based guard bed would be very effective in lowering phosphorus and arsenic concentrations to negligible concentrations.

#### SECA Core R&D – Interconnects:

- New Processes Improve SOFC Performance and Cost Efficiency.** In an inter-agency/industrial partner collaboration, researchers at ATI Allegheny Ludlum (an Allegheny Technologies company), NETL, and PNNL have successfully modified the metallic alloy AISI 441 to help achieve SOFC electrical interconnect requirements for lifetimes of 40,000 hours or more. AISI 441 is an inexpensive ferritic stainless steel that, with the addition of a manganese cobalt spinel coating, hinders chromium depletion and reduces oxidation in the SOFC environment. Experimental work at PNNL and ATI Allegheny Ludlum indicated that coated AISI 441 exhibited a very low and nearly constant area-specific resistance over 5,000 hours of testing. A rare earth treatment integral to the coating that reduces oxidation and a manufacturing process that reduces silica formation, both without vacuum melt, have been developed by NETL and ATI, respectively. In addition to these breakthroughs, the cost of commercially available AISI 441 is predicted to be considerably lower than the cost of producing state-of-the-art, high-temperature metal alloys suitable for SOFC electrical interconnect service.

#### SECA Core R&D – Seals:

- Refractory Glass Seals Show Promise.** Planar SOFC stacks require adequate seals between the interconnects and adjacent cell components in order

to prevent mixing of the oxidant and fuel gases within the stack, and leakage of the gas streams from the stack. Devitrifying glass seals represent a relatively easy means of sealing an SOFC stack (at least initially), but they face challenges in meeting the stringent SOFC requirements, including long-term operation at elevated temperatures and thermal cycling between operating and room temperatures. Most SOFC sealing glasses are designed to seal at temperatures fairly close to stack operating conditions. As an alternative, “refractory” glass seals, which seal at relatively high temperatures, are under development at PNNL. Refractory sealing glasses potentially offer improved stability in terms of thermal expansion, chemical compatibility, interfacial strength, and minimal interfacial reactivity during long-term operations. In addition, the higher stack fabrication temperature may result in increased strength and electrical conductivity of contact materials at the cathode/interconnect contact zones. Optimized refractory sealing glass compositions in the Sr-Ca-Y-B-Si-O system exhibit low volatility, high electrical resistance, stable coefficients of thermal expansion (CTEs) in the desired range of 11.5-12.5 ppm/°C, and sealing temperatures in the 950-1000°C range. However, similar to other SOFC sealing glasses, microstructure analysis did reveal a tendency to form alkaline earth chromate at the glass/interconnect interfaces. The formation of the chromate must be mitigated due to its high CTE, which leads to reduced interfacial strength due to large residual stresses. To prevent this problem, PNNL investigated alloy surface modifications intended to stabilize the seal/interconnect interface by preventing the formation of the chromate phase. One of the most promising mitigation approaches involves the formation of an aluminum oxide layer on the alloy surface, which can prevent the chromium oxide-containing scale on steel from contacting, and subsequently reacting with, alkaline earth constituents in the glass seal. While the tensile strength of refractory glass seals to as-received interconnect steel decreased significantly (by ~90 percent) during aging in air at SOFC operating temperatures, the strength of seals to aluminized steel actually increased (by ~40 percent) when aged under identical conditions.

### SECA Core R&D – Contact Materials:

- **Low-Temperature Sintering of Cathode-Side Contact Pastes Demonstrated.** Researchers at PNNL have found a way to lower the sintering temperature of lanthanum strontium manganite (LSM) contact pastes by hundreds of degrees

through atmospheric cycling. Contact pastes are employed in planar SOFCs to facilitate low-resistance electrical contacts between the cathode and metallic interconnects. It is preferred that the contact paste either be compliant or provide a good thermal expansion match to other fuel cell components, be of low cost, stable, and processible at temperatures compatible with the glass seal. LSM meets most requirements, with the exception of an air sintering temperature that is higher than preferred (>1,200°C). PNNL researchers exploited the unique defect chemistry of LSM in enhancing sinterability, where alternating exposure to air and nitrogen created transient cation vacancy gradients that resulted in high mobility. Tensile bond strengths to coated ferritic steel coupons of ~6 MPa were typically achieved at less than 1,000°C within two hours, while stable cathode/interconnect contact resistances of less than 10 milliohm-cm<sup>2</sup> were routinely obtained. The technology has been demonstrated successfully using the Core Technology program’s planar SOFC test fixture. Research is continuing in collaboration with Oak Ridge National Laboratory (ORNL) to evaluate mechanical properties of sintered contact pastes at high temperature, and to model stresses that develop in planar stacks during operation.

### SECA Core R&D – Cross-Cutting Materials and Manufacturing:

- **The Impact of Chromium on the Polarization Resistance of SOFCs Elucidated.** Planar SOFC stacks operating below 800°C can use metallic interconnects to provide electrical contact between the individual cells. Of the available alloys, ferritic stainless steels have been the primary focus due to a favorable combination of properties and cost. Various stack developers have used different types of ferritic stainless steels and even developed some specifically for this application. However, it became apparent that when stainless steel interconnects were used, the stacks developed higher polarization resistances than expected from single cell tests (without stainless steel interconnects). Initially, this phenomenon was attributed to the electrical resistance of the scales formed on the stainless steels, but through systematic investigations at ANL, it is now clear that chromium migration from the stainless steel is responsible for a majority of the increase in polarization resistance. Building on the data in the literature, which showed that chromium forms a variety of volatile species at SOFC operating conditions (primarily an oxy-hydroxide), ANL showed that this chromium oxy-hydroxide is electrochemically reduced to chromium

oxide ( $\text{Cr}_2\text{O}_3$ ) at the active triple phase boundary sites. The chromium oxide deposits interfere with the normal oxygen reduction reaction, resulting in an increase in the polarization resistance. The chromium oxide has also been observed to react with a lanthanum strontium manganite cathode, forming chromium manganite, lanthanum oxide and strontium chromite (all of which increase the polarization resistance as well). ANL has demonstrated that this deposition phenomenon is dependant upon the operating potential of the cell, and by maintaining an operating potential of approximately 0.85 volts or higher, this degradation mechanism appears to be avoidable.

- **Test Fixture Commissioned.** Simulated stack testing, currently being developed and optimized within the SECA Core Technology program, provides a unique capability to accelerate the evaluation and validation of advanced materials, fabrication processes, and design concepts developed by PNNL and other SECA Core R&D participants. The testing is performed using a stack test fixture (based on an initial design by Lawrence Berkeley National Laboratory/NETL) with modifications and implementation by PNNL which incorporates the full set of planar SOFC stack components (cell, cell frame, interconnects, seals, and contact materials). As a result, the performance and stability of newly developed materials, processes, etc. can be assessed in a realistic stack operating environment. To date, several new materials developed at PNNL have been evaluated via the stack tests, including refractory glass seals and low-cost steel interconnect alloys with protective cathode-side and seal region coatings. It is anticipated that this capability, which will be transferred to other Core R&D participants including NETL, will help bridge the gap between typical bench-scale characterization and the full-scale cells and stacks produced by SECA Industry Teams, and thus enhance technology transfer from the SECA Core Technology program to Industry Teams.

#### SECA Core R&D – Fuel Processing:

- **Innovative Injection and Mixing System for Diesel Fuel Reforming Achieved.** Fuel reformers are a critical component of SOFC systems, enabling them to compete with conventional auxiliary power units in remote stationary and mobile power generation markets. Currently, liquid fuel processing technology is not yet viable for commercial applications in SOFC systems. To achieve SECA goals of improved feed stream preparation, Goodrich (Delevan) has developed and evaluated two promising fuel injection concepts:

fuel preheat and piezoelectric atomizers. The key performance parameters evaluated included fuel atomization, droplet evaporation, mixing, uniformity of mixture temperature, velocity and concentration, wall impingement, flow recirculation, carbon deposition, feed stream supply pressure, power consumption, complexity, and reliability. One obstacle with preheating the fuel before injection into the feed stream is carbon formation in the internal fuel passages of the fuel injector. Carbon can restrict the fuel flow in the injector and reduce atomizer performance. Several anti-carbon coating applications were evaluated to determine their ability to reduce carbon formation within the fuel circuit of the preheating atomizer. The piezoelectric atomizer demonstrated an exceptionally large turndown ratio but was limited to a specific atomizer orientation. Both injectors developed showed promise for various applications.

- **Advancements in Diesel Fuel Reformer Lower Parasitic Power.** Eltron Research and Development, Inc. is developing a reformer for converting diesel fuel into a mixture of hydrogen and CO suitable for use in solid oxide fuel cells. A laboratory reformer has been constructed incorporating a porous cylinder of yttria-stabilized zirconia (YSZ). Air is effused into the reformer through the porous walls in order to maintain high partial pressure of oxygen near the inner walls needed to suppress deposition of carbon, which otherwise plugs reactors. Zirconia is chosen because of its stability under both oxidizing and reducing conditions above  $1,000^\circ\text{C}$ , its ability to be thermally cycled and its low likelihood of poisoning fuel cell catalysts downstream, which are in contact with YSZ. Sulfur-tolerant platinum-rhodium wire gauze has been replaced with perovskite catalysts of general formula,  $\text{La}_{1-x}\text{Sr}_x\text{FeO}_{3-\delta}$ . Iron acts as a “Reverse Fischer-Tropsch Catalyst” converting hydrocarbons and oxygen into synthesis gas. Strontium introduces oxygen-ion vacancies, enhancing diffusion of oxygen and allowing attack of adsorbed carbon from beneath. Work continues to lower parasitic power and to develop a practical device.
- **Non-Conventional Materials Used to Enhance Hydrocarbon Reforming to Improve SOFC Integration and Operation.** Researchers at NETL have been utilizing unique properties of oxide-based materials to develop effective catalysts for the reforming of heavy hydrocarbon fuels/compounds (i.e., coal-based, diesel, etc.). Conventional supported metal-based catalysts can suffer from poor performance and lifetimes without the use of excess water (a common

commercially employed strategy). For applications where water management/storage is an issue, alternative approaches are needed. NETL utilized the properties of pyrochlore oxide materials and modified their compositions to add catalytic activity, which shows an improved performance and stability when undergoing dry or low-water content reforming relative to the more commercial version of traditional catalyst systems. Long-term testing is currently underway to characterize and further demonstrate the readiness of these catalyst systems.

- **From Molecular Insights to Novel Electro-Catalysts for SOFCs.** A team led by Professor Suljo Linic at the University of Michigan (Ann Arbor), funded by NETL, has developed Ni alloy (electro) catalysts that exhibit superior tolerance to carbon-induced deactivation compared to standard monometallic Ni catalysts. The alloy materials have been tested in hydrocarbon steam reforming under close to stoichiometric steam-to-carbon ratios and as electrocatalysts for direct utilization of hydrocarbons in solid oxide fuel cells. The novel alloy materials were designed based on a detailed molecular understanding of chemical transformations that lead to the carbon-induced deactivation of Ni. The discovery represents a rare example where novel (electro) catalytic materials were designed based on detailed molecular insights.

### SECA Core R&D – Power Electronics:

- **DC-DC Converter Successfully Tested with Solid Oxide Fuel Cell.** Virginia Polytechnic Institute and State University (Virginia Tech) has successfully developed a low-cost, high-efficiency DC-DC converter for low-voltage SOFC applications. The converter consists of multiple phases to allow ripple cancellation and thus significantly reduces the passive component size and cost. The switching devices operate at zero-voltage soft switching condition to eliminate the switching loss and thus improve the efficiency. Switching loss elimination also allows high switching frequency to further reduce the passive component size and cost. As compared to existing commercial designs in which the inductor size and weight dominate the entire unit, the Virginia Tech DC-DC converter cuts the size of the inductor to less than 10 percent. For stationary applications where the DC-DC output stage is a single-phase DC-AC inverter, a low-frequency ripple tends to propagate back to the fuel cell source, which causes a higher peak power and typically requires 15 percent additional fuel cell capacity. Virginia Tech has developed a novel active current control method to regulate the output

current to pure DC so that the fuel cell current is also pure DC, thus reducing the need for additional fuel cell capacity. The added current regulation loop in the active control can also be used for DC output battery charging control. With collaboration between Virginia Tech as a Core Technology program partner and Delphi as an Industrial Team partner, the entire DC-DC converter has been successfully tested with a Delphi SOFC, showing well-regulated charging current from 0 to 200 A and efficiency higher than 97 percent for the power level of 500 W and higher.

### SECA Core R&D – Modeling and Simulation:

- **Design Guide Documents Best Practices.** A SOFC Design Guide has been prepared in a collaborative effort between NETL, PNNL, ORNL, and the American Society of Mechanical Engineers (ASME). The objective of the guide is to provide recommended design practices and associated modeling and analysis procedures, for use by U.S. designers and fabricators of SOFCs, to optimize design of durable and reliable SOFCs. The guide is based on past successful usage and advances in the state of knowledge. It describes suggested analytical procedures developed by the SECA Core Technology program to model electrochemical and thermo-mechanical performance of SOFCs; as well as how these tools and other simulation tools can be used in designing a structurally-reliable and durable SOFC stack. The recommended modeling procedures contained in the guide attempt to quantify the variability in material properties and design parameters of all elements in the SOFC structure. These modeling procedures address the coupled electro-chemical and thermo-mechanical nature of SOFCs by quantifying the electro-chemistry activities and the associated thermal-mechanical behaviors of various SOFC components for different design configurations. The guide is intended to facilitate development of cost-effective, reliable, SOFC designs. Further, the guide is a living document, to be updated and expanded on a regular basis.
- **Numerical Modeling Guides Cell Design.** Numerical modeling tools developed at PNNL have been used to provide insight to the distribution of thermal-mechanical loads within SOFC stacks and the corresponding demands on the sealing system. Perimeter seals for planar cells must accommodate thermal expansion mismatch forces between the ceramic cell and metallic support structure, but simulations have shown that the load path can be favorably altered by introducing strong, stiff contact

paste layers between the cell and interconnects. Good mechanical bonds here can better distribute the developed mismatch forces directly to the stack support structure and beneficially reduce the shear loads on the seal by up to 20 percent. These observations indicate that a cell design and processing procedure to simultaneously form the refractory sealant and contact paste layers is viable, and the numerical models are currently being used to identify the relative stiffness properties required for each layer to minimize the seal loads and improve their reliability.

- SOFC Model Predictions Agree with Experimental Results.** A stand-alone finite element SOFC model that is transferable and executable without special software purchase requirements is under development by the University of California, Irvine. This model includes flexibility to accept user inputs and produce steady state operating results based upon sound and rigorous analysis of expected future SOFC performance. The fuel cell model is highly configurable, which enables investigation of various parameters that may affect the performance of an SOFC. Besides producing results such as fuel cell power output, heat loss, and exhaust stream properties, which are essential for systems analysis, the fuel cell model also provides the temperature, composition and current density profiles within the fuel cell that are helpful in determining if the fuel cell is being operated under realistic conditions. The planar SOFC model predictions have thus far been compared against those of the International Energy Agency (IEA) and the PNNL SOFC-MP model. The model predictions are in reasonably good agreement with the IEA and PNNL results. Discrepancies amongst the predictions are attributed to different solution methodologies, different heat transfer models and different parameters for calculating the activation and diffusion polarizations.

#### SECA Core R&D – Balance of Plant:

- Lower-Cost Recuperator Prototype Manufactured.** Acumentrics Corporation, in conjunction with Blasch Precision Ceramics, has successfully integrated a ceramic monolith into a combination cross flow ceramic and counter flow metallic cathode air recuperator. This arrangement takes advantage of a high temperature, near net shape cast cross flow ceramic core, while enabling the use of lower grade metallic alloys in the medium-to-low temperature counter flow metallic section. Thermal modeling predicts that an effectiveness of >80 percent with a reduction in heat transfer metal

temperatures of 100°C is attainable. This will permit the use of less expensive alloys for the metallic components of the recuperator. This recuperator configuration also permits the use of low cost, automotive catalytic converter type, sealing between the ceramic and metallic sections without the need for complex plenums. An initial prototype of the recuperator has been manufactured and testing of the unit is underway.

#### Advanced Research:

- SOFC Stacks and Blower Pass Proof-of-Concept Tests.** Two technologies developed under the SECA fuel cell program recently passed successful proof-of-concept tests by the U.S. Navy's Naval Undersea Warfare Center Division located in Newport, Rhode Island. The tests mark a breakthrough for SOFC-based power systems and reflect the potential of SOFC technology for other spinoff market applications. The proof-of-concept tests incorporated two technologies developed under the SECA program: SOFC stacks manufactured by Delphi Corporation of Flint, Michigan, and a specialized blower developed for SECA SOFC systems by R&D Dynamics, Bloomfield, Connecticut, under DOE's SBIR program. The blower was used successfully in the test to recycle high-temperature fuel exhaust flows back to the fuel reformer. The proof-of-concept system met the U.S. Navy's targets for power output and efficiency. SECA fuel cells are well-suited to unmanned undersea vehicles because they can operate on logistic fuels (such as jet fuels), tolerate fuel impurities, generate high-quality heat for fuel reforming, and are highly efficient in converting fuel energy into electricity.

#### SECA Adds Coal-Based Systems Industry Teams:

In early 2005, the SECA program was accelerated to deliver megawatt-class fuel cell systems in response to the emerging national need for low-cost carbon capture technologies, the need for more efficient and cost-effective use of fuels abundantly available in the United States, and the need to address reduced water usage in power plants. Initially, three Industry Teams – Siemens Power Generation, FuelCell Energy / Versa Power Systems, and General Electric – transitioned their cost-reduction projects into Coal-Based Systems projects to develop fuel cell systems for central generation IGFC plants with capacities of 100 megawatts or greater. In May 2008, DOE selected two new Industry Teams: one led by UTC Power, a United Technologies Corporation,

in partnership with Delphi Corporation, and the other led by Rolls-Royce Fuel Cell Systems (U.S.) Inc. The Rolls-Royce project will include work at Ohio's Stark State College Fuel Cell Prototyping Center, which is also supported through a National Science Foundation grant.

### SECA Adds Core Technology Projects:

Research consistently shows that the majority of the losses in SOFC performance are concentrated at the air electrode cathode that provides electrons for the reaction of oxygen gas with the fuel cell. The following six new projects will employ state-of-the-art concepts and methodologies to improve the stability and performance of fuel cell cathodes: Boston University, Carnegie Mellon University, General Electric Global Research, Georgia Tech Research Corporation, Massachusetts Institute of Technology, and Montana State University. Four more projects will provide other research. CellTech Power will perform lab-scale cell experimental work and develop a conceptual design for a direct-coal power plant based on the liquid tin anode (LTA) fuel cell. NexTech Materials will validate the anticipated advantages of NexTech's FlexCell technology, which include high performance and stability in sulfur-containing fuels, scalability to large cells, and potential for low-cost manufacture. The University of Cincinnati will engineer and demonstrate innovative sealing concepts for SOFCs using a promising viscous glass. Similarly, Alfred University will explore the compositional space for viscous glasses, providing a thorough characterization of promising candidates.

### 2008 Annual SECA Workshop in Pittsburgh, Pennsylvania:

The SECA program held its 9<sup>th</sup> annual workshop August 5-7, 2008, in Pittsburgh, Pennsylvania. Principal Investigators of projects provided presentations. The findings and recommendations will be used by the DOE Project Managers to guide their future work and by the Technology Manager to make programmatic and funding decisions for the upcoming fiscal years. The workshop proceedings will be found on the program's website at <http://www.netl.doe.gov/seca/>.

## Summary

Peer review results clearly demonstrate the effectiveness, strength, and success of the Fuel Cells/SECA program. In light of the substantial technical progress realized in Fiscal Year 2008, ongoing cell performance and scaling improvements will undoubtedly result in additional cost reduction and the testing of larger SOFC stacks. The maximum obtainable performance of cathode materials is limited by stability and activity, and results show that both are directly related to surface chemistry and structure where characterization is more appropriate. Technological spinoffs of SOFCs into a variety of other applications, especially within the Department of Defense, will add to market penetration, increase manufacturing production volume, and lower SOFC cost.

By developing fuel cells to operate cost effectively on coal gas as well as natural gas, bio-fuels, diesel, and hydrogen, SECA is solving today's environmental, climate change, fuel availability, and energy security issues. SECA fuel cells are ideal for use in central generation applications, enabling high efficiency, diverse opportunities for carbon capture (e.g., post-power block), lower criteria pollutant emissions (e.g., less than 0.5 ppm NO<sub>x</sub>, regardless of fuel), and water conservation. IGFC system configurations utilizing near-term gasification and syngas cleaning technologies will generate power from coal with overall efficiencies of greater than 45 to 50 percent (HHV, coal to AC power) or more, including the coal gasification and CO<sub>2</sub> capture processes. Advanced systems are capable of efficiencies of greater than 50 percent, approaching 60 percent for some configurations. In conjunction with SECA-driven fuel cell cost reduction, these IGFC systems will enable the clean, efficient and cost-effective use of the nation's most abundant fossil fuel. The once distant vision of using clean, low-cost fuel cell technology for everyday applications is now within reach.

---

## II. SECA INDUSTRY TEAMS

### A. Coal-Based Systems



## II.A.1 FuelCell Energy's (FCE) Solid State Energy Conversion Alliance (SECA) Coal-Based Solid Oxide Fuel Cell Power Plant Development Project

Hossein Ghezel-Ayagh

FuelCell Energy, Inc.  
3 Great Pasture Road  
Danbury, CT 06813  
Phone: (203) 825-6048  
E-mail: hghezel@fce.com  
Website: www.fce.com

DOE Project Manager: Travis Shultz

Phone: (304) 285-1370  
E-mail: Travis.Shultz@netl.doe.gov

Subcontractors:

- Versa Power Systems, Inc., Littleton, CO
- Gas Technology Institute, Des Plaines, IL
- WorleyParsons, Inc., Reading, PA
- Nexant, Inc., San Francisco, CA
- SatCon Power Systems Inc., Burlington, ON, Canada
- Pacific Northwest National Laboratory, Richland, WA

Contract Number: 41837

Start Date: February 27, 2004

Project End Date: September 30, 2008

### Objectives

The objective of this project is to develop low-cost, high-performance solid oxide fuel cell (SOFC) technology to support multi-MW coal-fueled central power systems. This three-phase project has the following supporting objectives:

- Resolve barrier issues concerning larger-size SOFCs and demonstrate a SOFC building block for multi-MW applications.
- Develop and optimize a design for a large-scale (>100 MWe) baseline integrated gasifier fuel cell power plant (IGFC) incorporating a SOFC that will produce electrical power from coal. The system will be:
  - Highly efficient (>50% coal higher heating value [HHV]).
  - Environmentally friendly (CO<sub>2</sub> separation for 90% of syngas carbon capture).
  - Cost-effective (<\$400/kWe, exclusive of coal gasification, syngas clean-up, and CO<sub>2</sub> separation subsystems).
- Design, manufacture, and test a proof-of-concept system derived from the IGFC design.

### Accomplishments

Since initiation of the coal-based SOFC project, several significant technical accomplishments in cell and stack development have been achieved:

- SOFC manufacturing scale-up from the baseline size of 156 cm<sup>2</sup> to greater than 1,000 cm<sup>2</sup> has been successfully demonstrated at Versa Power Systems Inc (VPS). Production capacity for scaled-up 625 cm<sup>2</sup> components has been successfully validated. This validation is based on the manufacture of over 600 cell components meeting design specifications and targeted production yields.
- Efforts are well underway to enhance stack manufacturing capacity to 500 kW/year and cell manufacturing capacity to 1,000 kW/year by the end of Phase I (September 2008). Plans are being made to increase SOFC pilot plant manufacturing capacity to 2 MW/year in Phase II and 10 MW/year in Phase III of the project to meet production requirements for the MW module and multi-MW power plant demonstrations.
- Performance and reliability (thermal cycle) of scaled-up 625 cm<sup>2</sup> cell components has been validated in numerous single cell and over 20 short stack tests. No significant performance or reliability differences were observed with the scaled-up components as compared to the baseline, smaller area cell sizes.
- Single cell testing of advanced cell components has demonstrated ~8-10% performance improvement over baseline cell components. At low SOFC operating temperatures (700°C), these advanced cell components exhibited an even greater performance improvement of 15% as compared to the baseline.
- Advanced cell components have shown significant improvement in endurance (decreased decay rate) over the baseline cells in single cell tests. The degradation rate demonstrated with advanced cell components at the single cell level meets the final program goal for commercial applications. Validation in large area cells and stacks is planned.
- Preliminary cost analysis of the SOFC multi-MW baseline power plant stack and system shows a clear path to achieving the SECA cost goals.
- Preliminary computational modeling and engineering analysis conducted jointly with the WorleyParsons group has led to a SOFC power plant system design with greater than 50% overall efficiency operating on coal syngas fuel.

This progress and these technical advancements present a clear indicator that SOFC development is well on the path to becoming a credible, viable option for clean, reliable, highly efficient and cost effective power generation from a coal-based fuel source with negligible emissions.

## Introduction

FCE was engaged in a Department of Energy (DOE) managed SECA program to develop a 3-10 kW SOFC power plant system since April 2003. As shown in Table 1, the FCE team successfully completed Phase I of this SOFC development program, surpassing all specified metrics for performance, reliability, endurance and cost. In September 2006, this project was merged with a multi-phase project for development of very efficient coal-to-electricity, large scale (multi-MW) SOFC power plants with near zero-emissions. The SOFC technology developed and verified in the SECA 3-10 kW development program will serve as the basis for further development and scale-up in this multi-MW, SECA Coal-Based System Phase I project. FCE is ideally suited for this project based on experience in various DOE managed programs to develop commercial large scale, MW-size fuel cell power plants, high efficiency hybrid fuel cell-turbine systems, fuel cell operation on coal syngas and SOFC development with their technology partner, VPS. The primary objectives of these SECA programs are to develop affordable, SOFC-based

power plant systems with high efficiency that are cost competitive with other power generating technologies of similar capacity without incentive funding support. Some of the key program objectives are the development of SOFC technologies, cell and stack size scale-up, SOFC performance optimization, increased stack manufacturing capacity development and MW class module engineering design. FCE uses the VPS planar cell and stack technology for all its SOFC development projects. VPS has been actively engaged in cost-effective SOFC manufacturing process research and development since 1998 and has well establish processes, quality procedures and equipment for the manufacture of small to intermediate size cells and stacks. This serves as a solid basis for cell area and stack size scale-up. The achievement of the cost targets is a key facet of the SECA programs. In order to be cost competitive with other power generating technologies of similar capacity without the need for incentive funding programs, significant SOFC stack and system cost reduction must occur from the current low volume development level to high volume, mass production prices. The DOE specified metric for the final program (Phase III) system cost that is determined to be competitive with other power generating technologies of similar capacity without incentive funding is \$400/kW for a multi-MW power plant, exclusive of coal gasification, syngas clean-up, and CO<sub>2</sub> separation subsystem costs. Another key objective is implementation of an innovative system concept design for a multi-MW power plant with anticipated efficiencies exceeding 50% coal HHV. The final project deliverable will be a ~5 MW proof-of-concept power plant demonstration to be conducted at a suitable SECA selected site. The development of this SOFC technology will significantly advance the nation's energy security and independence interests, address pollution and greenhouse gases concerns and help enhance the nation's economic growth.

**TABLE 1.** SECA Cost Reduction Program Phase I Metric Test Results

	Steady State Operation (BOT)	Steady State Operation (EOT)	Peak Power Operation	SECA Metric	
Net DC Electrical Power	3.39 kW	3.13 kW	5.26 kW	3 to 10 kW	✓
Net DC Electrical Efficiency	38.7%	36.4%	33.3%	>35% (Steady State)	✓
Stack Power Density	280 mW/cm <sup>2</sup>	260 mW/cm <sup>2</sup>	430 mW/cm <sup>2</sup>	N/A	
Steady State Degradation		1.2%/500 hrs	N/A	<2%/500 hrs	✓
Transient Degradation (7 load interruptions, 3 thermal cycles)		0.7%	N/A	<1.0%	✓
Availability		98.6%	N/A	>80%	✓

✓ All SECA 3 kW Phase I Cost Reduction Program performance metrics have been successfully demonstrated!

## Approach

The project is organized in three phases according to schedule and technical objectives:

- Phase I of the project will focus on cell and stack development. This will include the scale-up of existing SOFC cell area and stack size (number of cells) and performance improvements. Preliminary engineering design and analysis for multi-MW power plant systems will also be conducted. The Phase I deliverable will be a test demonstration of a SOFC stack building block unit, that is representative of a MW class module, on simulated coal syngas.
- Upon successful completion of Phase I and notice by DOE to continue, Phase II of the project will focus on modularization of the Phase I stack building block units into a MW-size module.

Detailed design engineering and analysis for multi-MW power plant systems will also be conducted. The Phase II deliverable will be a test demonstration of a representative SOFC stack module in the size range of several hundreds of kilowatts to megawatt power output, on simulated coal syngas.

- Upon successful completion of Phase II and notice by DOE to continue, Phase III of the project will focus on design and fabrication of a proof-of-concept multi-MW power plant including turbine for high efficiency and CO<sub>2</sub> separation for low emissions. The Phase III deliverable will be long-term testing of a 5 MW SOFC power plant at a suitable SECA selected site on a coal gasifier with carbon separation for sequestration.

**Results**

FCE utilizes the planar cell and stack technology of its SOFC provider, VPS, for all its SOFC development programs. In September 2006, FCE completed a SECA Phase I SOFC Cost Reduction Program to develop a 3-10 kW SOFC power plant system. Two major objectives of the Phase I development effort were to demonstrate the technical performance of a 3 kW prototype SOFC system and to develop factory cost estimates showing that SOFC systems can be manufactured on a cost-effective basis. Based on tests conducted over a 2,100-hour operational period, the FCE 3 kW prototype system successfully met all DOE-specified technical targets as shown in Table 1. These targets included power output, system efficiency, system availability and overall system endurance. SOFC cost estimates also surpassed the DOE metric target. Both the performance tests and the factory cost estimate were audited and confirmed by independent third party consultants approved by the DOE. This VPS cell and stack technology serves as the basis for further development and scale-up in this multi-MW, coal-based system SECA Phase I project.

Since beginning the Coal-Based SOFC project in October 2006, several significant technical milestones in cell and stack development have been achieved:

- SOFC cell manufacturing scale-up from the baseline size of 156 cm<sup>2</sup> to greater than 1,000 cm<sup>2</sup> has been successfully demonstrated as shown in Figure 1. Production capacity for scaled-up 625 cm<sup>2</sup> components has been successfully validated. This validation is based on the manufacture of over 600 cell components meeting component design specifications and targeted production yields. Performance repeatability of scaled-up, 625 cm<sup>2</sup> size components has been validated with several repeat single cell and short stack tests. These results indicate no significant electrochemical performance loss due to cell scale-up from an active area of 81 cm<sup>2</sup> to 550 cm<sup>2</sup>.

- Assembly scale-up of SOFC stack building block units from the baseline size of 28 cells to 64 cells has been successfully demonstrated as shown in Figure 2. New test facilities are being fabricated for testing of these larger stack building block sizes.
- For the coal-based multi-MW power plant, a cell size of 625 cm<sup>2</sup> and a stack building block size of 64 cells has been chosen to pursue based on manufacturing and performance experience, technical risk and program requirements. Five of these stacks will be constructed into a 50 kW stack tower and 20 stack towers will be assembled into a single MW size module to be used for the multi-MW power plant systems as illustrated in Figure 3. This design configuration has undergone significant computational modeling analysis at FCE, VPS and Pacific Northwest National Laboratories.
- Efforts are well underway at VPS to enhance stack manufacturing capacity to 500 kW/year and cell manufacturing capacity to 1,000 kW/year by the end

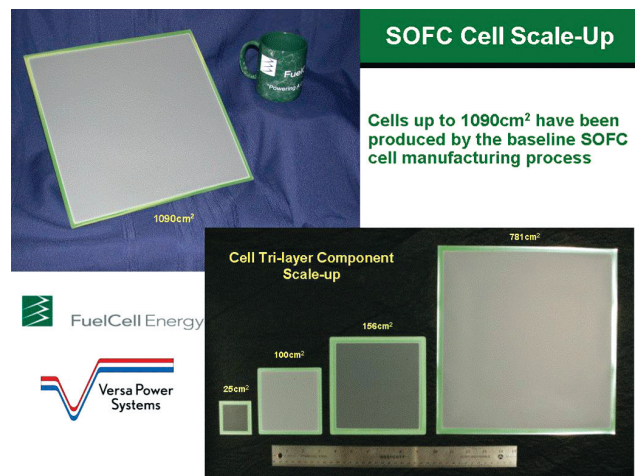


FIGURE 1. Scale-Up of SOFC Cell Components

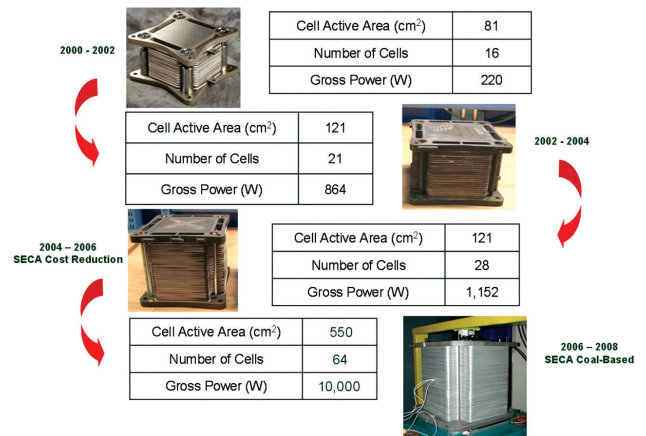


FIGURE 2. Scale-Up of SOFC Stack Building Blocks

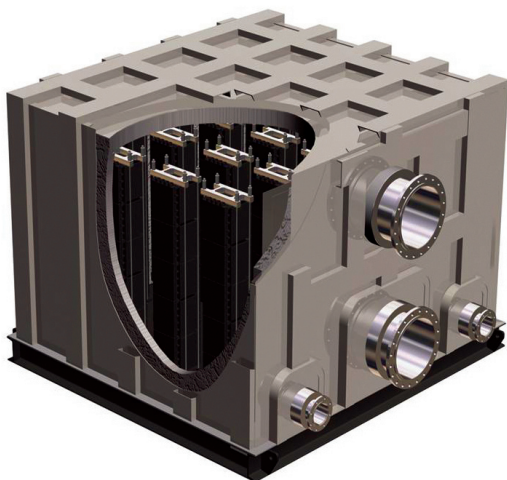


FIGURE 3. MW SOFC Module Illustration

of Phase I (October 2008). Plans are being made to increase SOFC pilot plant manufacturing capacity to 2 MW/year in Phase II and 10 MW/year in Phase III of the project to meet production requirements for the MW module and multi-MW power plant demonstrations.

- Single cell testing of advanced cell components has demonstrated ~8-10% performance improvement over baseline cell components. At low SOFC operating temperatures (700°C), these advanced cell components exhibited an even greater performance improvement of 15% as compared to the baseline. Stack tests are planned to validate these findings.
- Advanced cell components have also shown significant improvement in endurance (decreased

decay rate) over the baseline cells. The degradation rate demonstrated with advanced cell components at the single cell level meets the final project goal for commercial applications. Validation in large area cells and stacks is planned.

- Much progress has been made in detailed engineering and design analysis for the baseline power plant system, with special attention to the coal-gas clean-up system and turbine combined cycle technology for maximum efficiency with minimum cost. Preliminary cost analysis of the SOFC multi-MW baseline power plant stack and system shows a clear path to achieving the SECA cost goals. Preliminary computational modeling and engineering analysis conducted jointly with the WorleyParsons group has led to a baseline SOFC power plant system design with greater than 50% overall efficiency operating on coal syngas fuel. Typical breakdown of power generation and losses for an IGFC power plant is shown in the energy flow diagram of Figure 4.

### Conclusions and Future Directions

- The development of SOFC technology will significantly advance the nation’s energy security and independence interests, address pollution and greenhouse gases concerns, and help enhance the nation’s economic growth. Specifically, SOFC technology for large-scale coal-based power generation:
  - Reduces nation’s dependency on foreign fuel sources.

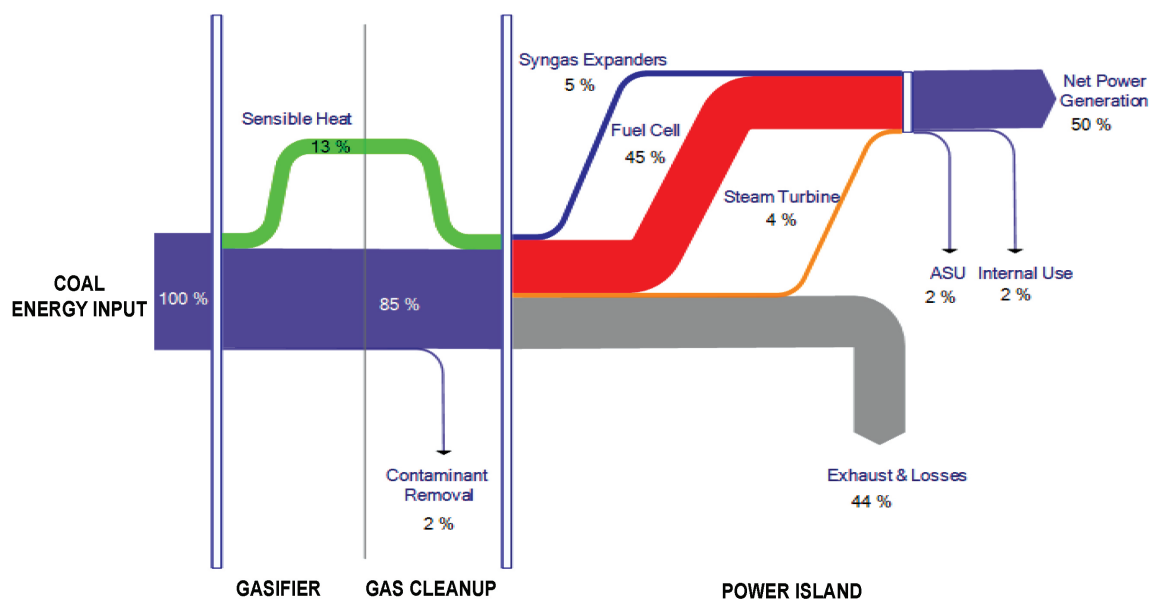


FIGURE 4. SOFC System Energy Flow

- Makes use of the largest natural fuel source in the U.S., coal, with an estimated 250 years of reserves.
- Provides highest power plant efficiency with lowest cost of electricity.
- Has lowest pollution emissions (NO<sub>x</sub>, SO<sub>x</sub>) as compared to conventional power generation technologies.
- Addresses greenhouse gas concerns; enables simple power plant system design for carbon separation and sequestration.
- Enables power plant fuel flexibility/tolerance to varying coal gasifier syngas compositions (H<sub>2</sub>, CH<sub>4</sub>, CO, CO<sub>2</sub>).
- Has lowest water consumption requirements as compared to other power generation technologies.
- Enhances the nation's economic growth through high value, domestic job creation and factory/equipment investment.
- Offers simplified system for H<sub>2</sub> co-production from a coal gasifier and/or fuel cell power block as an enabler for use in smaller, low temperature fuel cell types to help our nation address the transportation energy sector needs for a clean, efficient, domestic alternative to foreign fossil fuels.
- Enhances the nation's economic growth and prosperity with domestic job creation and factory/equipment investment. The technologies developed under this DOE Cooperative Agreement requires substantial manufacturing within the U.S., thereby contributing to economic competitiveness.

The progress and technical advancements made in the project thus far present a clear indicator that SOFC development is well on the path to becoming a credible, viable option for clean, reliable, highly efficient and cost effective power generation from a coal-based fuel source with negligible emissions.

### **FY 2008 Publications/Presentations:**

1. J. Doyon, "Coal-Based Solid Oxide Fuel Cell Power Plant Development", DOE Office of Fossil Energy Fuel Cell Program, 2007 Annual Report, II.1, p. 11-14.
2. J. Doyon, "SECA Solid Oxide Fuel Cell Power Plant System Cost Reduction", DOE Office of Fossil Energy Fuel Cell Program, 2006 Annual Report, III.4, p. 31-34.
3. J. Doyon, "SECA SOFC Programs At FuelCell Energy Inc.", 8<sup>th</sup> Annual SECA Workshop, San Antonio, Texas, August 7-9, 2007.
4. J. Doyon, H. Ghezal-Ayagh, J. Walzak, S. T. Junker, D. Patel, A. Adriani, P. Huang, D. Stauffer, V. Vaysman, J. S. White, B. Borglum, E. Tang, R. Petri, C. Sishla, "SECA Coal-Based Multi-MW SOFC Power Plant Development", Abstracts, 2007 FuelCell Seminar. Also in ECS Transactions - 2007 Fuel Cell Seminar & Exposition, Volume 12 (1B) - "High Temperature Fuel Cell R&D II (SECA)", 2008.
5. B. Borglum, "Development of solid oxide fuel cells at Versa Power Systems", Abstracts, 2007 Fuel Cell Seminar, p. 85-88.
6. J. Doyon, "High Temperature Fuel Cell Activities at FuelCell Energy Inc & Versa Power Systems Inc.", 2007 Materials Sciences & Technology Conference, 2007 Presentation.
7. J. Doyon, "FuelCell Energy Inc. Coal-Based, Multi-MW SOFC SECA Program", NETL Peer Review Meeting, 2008.
8. H. Ghezal-Ayagh, "Coal Based Integrated Gasification SOFC System Development", International Colloquium on Environmentally Preferred Advanced Power Generation, 2008.
9. J. Doyon, "High Temperature Fuel Cells for Stationary Power Applications", Electric Power Conference, 2008.

---

## II.A.2 Coal Gas Fueled SOFC Hybrid Power Systems with CO<sub>2</sub> Separation

Joseph F. Pierre

Siemens Power Generation, Inc.  
Stationary Fuel Cells (SFC)  
1310 Beulah Road  
Pittsburgh, PA 15235  
Phone: (412) 256-5313; Fax: (412) 256-2012  
E-mail: joseph.pierre@siemens.com

DOE Project Manager: Travis Shultz  
Phone: (304) 285-1370  
E-mail: Travis.Shultz@netl.doe.gov

Contract Number: 42613

Start Date: October 1, 2005  
Project End Date: September 30, 2008

### Objectives

- Optimization of the Siemens DeltaN solid oxide fuel cell (SOFC) and scale-up of its dimensions to its largest practical size.
- Verification by test of cell, thermally self-sustaining stack, and module on simulated coal-gas.
- Corroboration of the technical and economic feasibility of a >50% efficient SOFC-based large capacity (>100 MWe) coal-fueled baseline power plant.
- Design, manufacture, and test on coal syngas of a fully functional 50% efficient proof-of-concept of lesser multi-MWe capacity.

### Approach

- Analytical modeling to optimize the DeltaN cell geometry.
- Develop a viable cell manufacturing process and fabricate cells.
- Verify by parametric testing cell performance and durability.
- Analyze, design, and develop a fuel cell stack.
- Prepare the preliminary design of a module aggregating fuel cell stacks.
- Test a thermally self-sustaining fuel cell stack on simulated coal syngas at the power system operating pressure.
- Identify and analyze cycle concepts.
- Select a baseline system cycle.
- Prepare the conceptual design for the baseline system.

- Corroborate via independent audit the technical and economic feasibility of the baseline system.
- Develop the conceptual design, performance analysis, and cost analysis for the proof-of-concept (POC) system.

### Accomplishments

- Identified the Delta8 as the preferred cell configuration.
- Achieved a Delta8 cell power density of >250 mW/cm<sup>2</sup>.
- Manufactured the Delta8 cells and bundles for the end-of-phase stack test.
- Initiated assembly of the end-of-phase stack test article.
- Validated a stack cost that achieves and exceeds the \$225/kWe milestone.
- Continued the development of the Advanced Module concept.
- Defined the preferred cycle configuration for the proof-of-concept system in sufficient detail to specify the major system components.
- Confirmed the coal-fueled SOFC baseline power system configuration.
- Developed conceptual design-level specifications for major baseline power system components that will be used as the basis for the baseline system performance and cost estimate.

### Future Directions

- Optimize atmospheric plasma spray operating parameters.
- Initiate the end-of-phase stack test.
- Continue the conceptual design for the advanced module.
- Update the high-efficiency and maximum power performance levels for the baseline power system.
- Complete the cost estimate for the baseline power system.
- Update and complete the conceptual design of POC system.

---

### Introduction

Siemens Power Generation SFC will develop a MWe-class SOFC power system to operate on coal-derived synthesis gas and demonstrate operation at

greater than 50% electrical efficiency (based on higher heating value, HHV, of coal) with greater than 90% CO<sub>2</sub> capture. The system will be scalable to sizes greater than 100 MWe output and, when offered in commercial quantities, will have a target cost of \$400/kWe including any extraordinary costs of integration to the balance of plant. Corroboration of the technical and economic feasibility of the SOFC power system will be achieved through the conceptual design of a large (>100 MWe) baseline power plant and the subsequent design, development, fabrication, and test of a POC system. The POC system will be representative of the baseline system, have multi-MWe capacity, and demonstrate an electrical efficiency >50% (coal HHV).

The coal-fueled SOFC baseline power system will generate ~128 MWe net alternating current (AC) power at >50% efficiency (net AC/coal HHV) while separating for sequestration 90% of the CO<sub>2</sub>. A maximum power output of ~170 MWe can be achieved by firing the gas turbine combustor, albeit at an efficiency of <50%. The baseline power system includes an oxygen-blown gasification system selected for its relatively high cold gas efficiency and ability to meet the 90% CO<sub>2</sub> separation requirement when coupled in series with a Selexol CO<sub>2</sub> removal process. Oxygen for the coal gasification process will be provided by an ion transport membrane. The SOFC system incorporates the high power density Delta8 cell configuration. The Delta8 cells are packaged into a pressurized module, rated at approximately 1.2 MWe per module. To achieve the baseline system power rating, the modules are arranged in two banks of 40 modules per bank. Centrally located between the two banks of modules is the gas turbine-generator and heat recovery system. The gas turbine delivers the air oxidant/coolant to the SOFC system and in return receives the high temperature, high pressure SOFC exhaust. During normal operation the gas turbine is not fired. Following expansion, the lower grade heat remaining in the gas turbine exhaust is delivered to a dual pressure heat recovery steam generator. The steam produced herein is supplied to a steam turbine cycle, generating additional electric power.

## Approach

The pressurized SOFC baseline power system is fueled by coal-derived syngas. The overall objectives are high electrical efficiency and CO<sub>2</sub> separation capability. The baseline system power capacity is to exceed 100 MWe whereas the POC system is to be in the MWe-class range. Several candidate system configurations were identified, modeled, and evaluated to estimate electrical efficiency of the system and values of key operating parameters (e.g. mass flow rate, temperature, and pressure) for major components. Also to be considered in addition to system efficiency are cost as reflected by system complexity and the potential for

POC testing at the MWe-class capacity. The efficiency target for the POC is 50% (net AC/coal HHV). The candidate system configurations were then subjected to a figure-of-merit comparison and the preferred baseline power system selected.

SFC is continuing the development of the DeltaN cell and stack design that combines the seal-less stack feature and a cell with triangular channels. This new design has a closed end similar to the Siemens circular tubular design. Analytical modeling was utilized to optimize the number and dimensions of ribs for maximum power, the distribution of fuel flow and air flow, and structural stability against thermal stresses during operation from atmospheric to elevated pressure. Additionally, active length and width were optimized based on practical limitations for cell fabrication and generator utility. The optimized DeltaN cells will be bundled into an array or bundle (stack) of electrically connected fuel cells forming a monolithic structure. A typical stack will consist of bundles connected in series arranged in parallel rows. The proposed SOFC stack and module concepts are based on technology that has been developed and proven as part of previous generator design and testing programs, a series of atmospheric and pressurized bundle tests, and the 220 kWe pressurized SOFC generator designed, built and operated in the pressurized SOFC/gas turbine hybrid power system. Further innovation will be required, particularly in development of low cost ceramic materials, net shape component fabrication, and a high power density stack configuration to reduce the overall cost of the system. Cell and stack performance at atmospheric and elevated pressure will be characterized via a series of single, multi-cell, and stack tests.

## Results

A figure-of-merit system was employed in a rigorous down selection process of candidate system configurations, resulting in the preferred baseline configuration depicted in Figure 1. The baseline power system meets the efficiency objective, separates the required 90% of the CO<sub>2</sub>, and based on a preliminary cost estimate will meet the targeted cost goal.

Cell development efforts, incorporating numerous finite element analyses, established the Delta8 geometry as the preferred cell, shown in Figure 2. A number of Delta8 cells were manufactured and placed on electrical test. Cell testing has shown a power density of >250 mW/cm<sup>2</sup> and voltage stability for than 3,000 hours of operation. The improved power density of the Delta8 cell represents a five-fold improvement versus the tubular cell, as shown in Figure 3.

Cost analysis, using these actual test results and coupled with advancements made in the conceptual design of the Advanced Module, show a path to a stack cost of ~\$220/kWe, which betters the cost target of \$225/kWe.

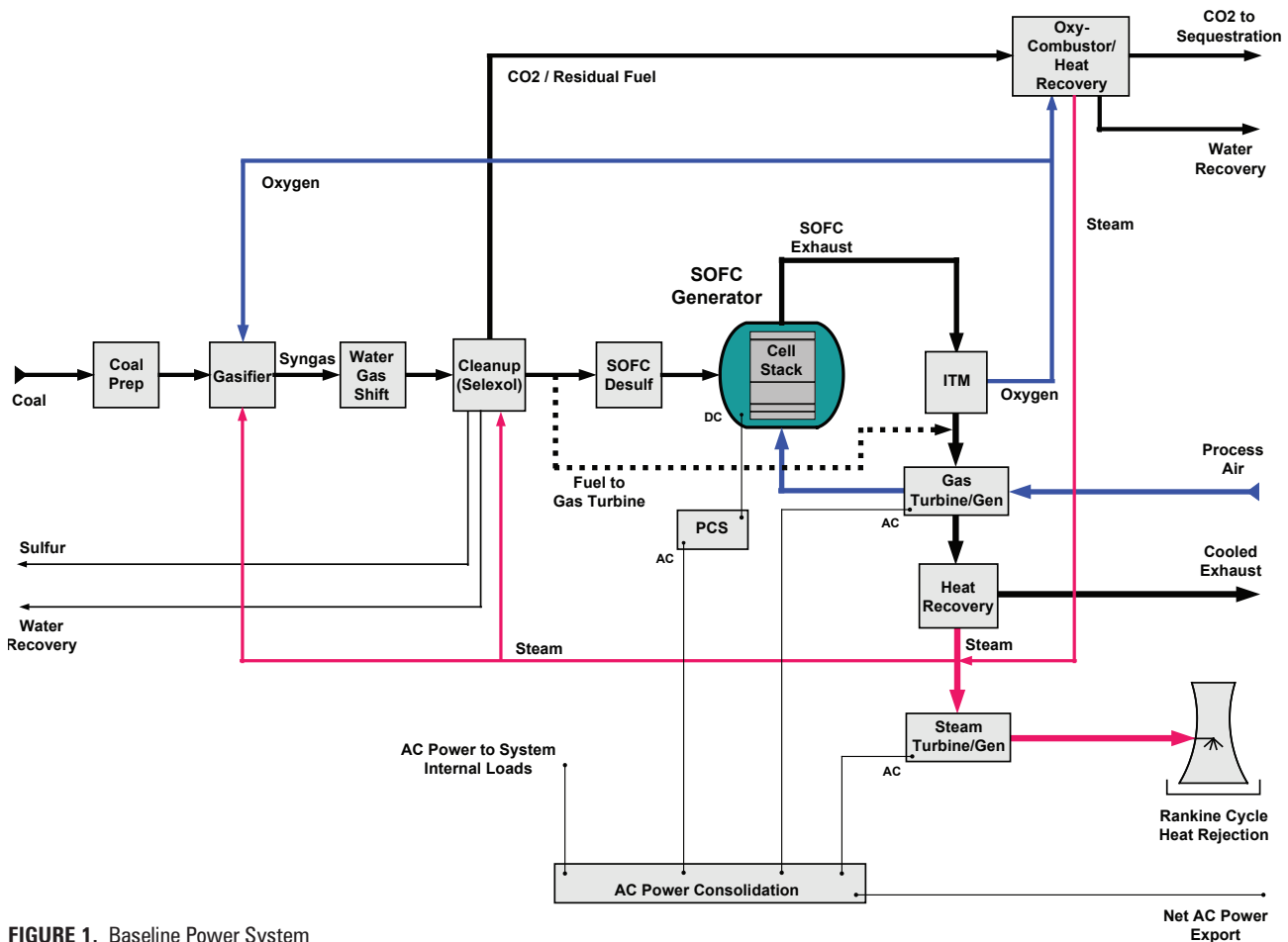


FIGURE 1. Baseline Power System

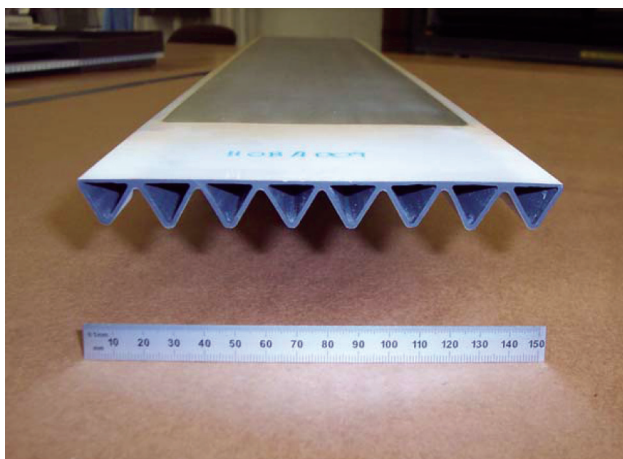


FIGURE 2. Siemens Delta8 Solid Oxide Fuel Cell

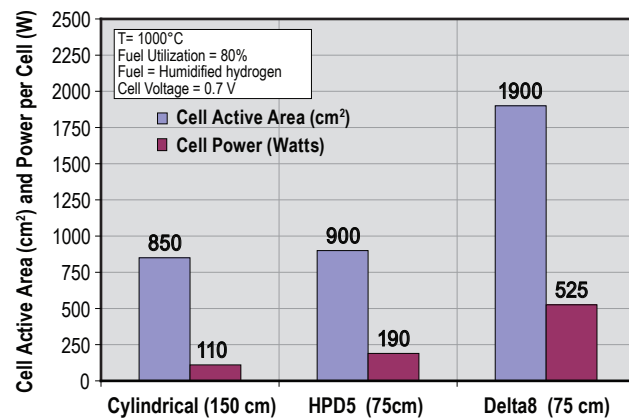


FIGURE 3. Cell Performance at 1,000°C

### Conclusions

Based on existing cell testing, systems analysis indicate the performance, CO<sub>2</sub> separation, and cost targets, respectively, for the baseline SOFC power

system can be achieved. SFC expects to exceed the performance and cost targets via the implementation of advanced cell materials and manufacturing processes, and improvements in SOFC module and balance of plant component technologies.

---

## II. SECA INDUSTRY TEAMS

### B. Cost Reduction



## II.B.1 Solid State Energy Conversion Alliance Delphi SOFC

Steven Shaffer (Primary Contact), Gary Blake, Sean Kelly, Karl Haltiner, Subhasish Mukerjee, David Schumann, Gail Geiger, Larry Chick, Ellen Sun

Delphi Automotive Systems LLC  
5725 Delphi Drive  
Troy, MI 48098  
Phone: (585) 359-6615; Fax: (585) 359-6061  
E-mail: steven.shaffer@delphi.com

DOE Project Manager: Maria Reidpath  
Phone: (304) 285-4140  
E-mail: Maria.Reidpath@netl.doe.gov

### Subcontractors:

- Battelle/Pacific Northwest National Laboratory, Richland, WA
- Electricore, Inc., Valencia, CA
- United Technologies Research Center, East Hartford, CT

Contract Number: 41246

Start Date: July 1, 2002  
Project End Date: December 31, 2011

### Objectives

- Develop a 3-5 kW solid oxide fuel cell (SOFC) power system for a range of fuels and applications (see Figure 1).
- Develop and demonstrate technology transfer efforts on a 3-5 kW stationary distributed power generation system that incorporates reforming of methane, and then natural gas.
- Develop a 3-5 kW auxiliary power unit (APU) for heavy-duty trucks and military power applications.

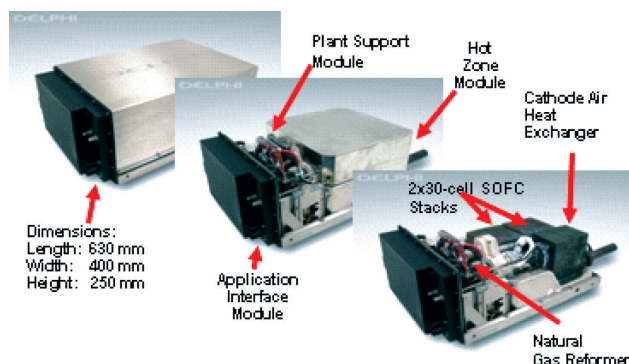


FIGURE 1. Generation 3 SOFC System

- Develop system modeling and cell evaluation for high efficiency coal-based SOFC gas turbine hybrid system.

### Accomplishments

- Systems
  - Successfully integrated a full-scale hot-reformate desulfurizer, diesel endothermic reformer, and SOFC stacks.
  - Demonstrated 50 thermal cycles on a natural gas-powered SOFC system.
  - Completed integration and test of a diesel-fueled SOFC system to support heavy-duty commercial vehicle applications.
  - Successfully tested the 12 V power electronics interface for heavy-duty commercial vehicle applications including SOFC system, 12 V DC/DC converter, lead-acid battery, and software and controls.
  - Designed and procured a heavy-duty vehicle application development chassis.
- Stack
  - Successfully fabricated and integrated multiple 30-cell Generation 3.2 stack modules into the system.
  - Improved manufacturing process for cell and stack fabrication.
  - Accelerated tests for cell and stack robustness.
  - Developed new concepts for next generation cell and stack.
- Reformer/Catalyst
  - Performed reformer subsystem and systems level testing of a diesel catalytic partial oxidation (CPOx) reformer design.
  - Designed a new air and fuel mixing approach that is expected to have benefits with respect to pre-combustion and fuel condensation/pyrolysis.
  - Investigated a platinum-based mixed-metal oxide catalyst formulation which may be very effective for natural gas hydrogenolysis.
  - Prepared a novel FeCrAlY-based thick wall honeycomb monolith that may be useful for chemical reactions requiring significant heat input.
- Balance of Plant (BOP)
  - Sourced new process air blowers and recycle pumps for the next generation system.

- Initiated internal development on a more robust igniter to survive the aggressive thermal environment.
- Continued testing of chromium volatility from various materials.
- Fabricated a three piece Inconel casting for our Integrated Component Manifold.

---



---

## Introduction

Delphi has been developing SOFC systems since 1999. After demonstrating its first generation SOFC power system in 2001, Delphi teamed with Battelle under the Solid State Energy Conversion Alliance (SECA) program to improve the basic cell and stack technology, while Delphi developed the system integration, system packaging and assembly, heat exchanger, fuel reformer, power conditioning and control electronics, along with other component technologies. Compared to its first generation system in 2001, the Delphi-led team has reduced system volume and mass by 75 percent. By January 2005, the Delphi team was able to demonstrate test cells with power density more than required to meet the SECA 2011 goals.

In addition to its compactness, another key advantage of the SOFC is its high system fuel efficiency, particularly when its high temperature co-product heat can be used in combination with its electrical output. For example, SOFCs can be teamed with gas turbines driven by the SOFC's co-product heat to potentially generate power at 55 percent to 80 percent thermal efficiency (depending on scale and fuel used). This is significantly more efficient than today's typical coal-fueled power plant thermal efficiency of 35 percent to 40 percent. By co-generating power on-site at industrial facilities, commercial businesses, or even residences, the SOFC's high-grade co-product heat will enable up to 90 percent efficiency in distributed, combined heat and electrical power generation. Similarly, heavy-duty trucks will be able to utilize SOFC auxiliary power systems for both heat and electrical power when parked, to save 85 percent of the fuel that today they consume when idling their main engine, and likewise reduce idling emissions.

While size and efficiency advantages are important for many potential applications, the SOFC's most significant advantage overall is its very broad applicability due to its inherent fuel flexibility. With relatively small changes, SOFC systems can potentially operate on a full range of conventional and alternative fuels. This includes natural gas and conventional petroleum-based fuels like low-sulfur gasoline, diesel and propane; high-sulfur military fuels like JP-8 and

jet fuel; low-CO<sub>2</sub> renewable fuels from biomass like ethanol, methanol and bio-diesel; synthetic fuels from coal and natural gas; and non-hydrocarbon fuels such as hydrogen and ammonia. This will be critical for future development to make SOFCs scalable for large coal gas power plants.

## Approach

Delphi utilized a staged approach to develop a modular SOFC system for a range of fuels and applications including:

- Develop and test major subsystems and individual components as building blocks for applications in targeted markets.
- Integrate major subsystems and individual components into a "close-coupled" architecture for integrated bench testing.
- Integrate major subsystems and individual components into a stationary power unit for the stationary market.
- Integrate major subsystems and individual components into an APU for the transportation market.
- Demonstrate large-scale hybrid stack module using simulated coal gas.

## Results

SECA Phase II is a continuation of the core hardware development activities begun in Phase I. The systems efforts in Phase II are more application-driven as Delphi moves this technology closer to pilot and production releases. The Phase II program will support and address two market opportunities. The stationary market and the transportation market have unique demands, and development tasks must address specific values that are economic drivers of the design and application.

For SECA Phase II, Delphi is aggressively pursuing performance targets which drive SOFC stack, subsystem performance, and cost reduction. Delphi is also utilizing technical progress and market research to focus effort on development of a diesel Commercial Vehicle SOFC APU. In the first half of SECA Phase II, emphasis has been placed on achieving Phase II performance metrics on natural gas. Progress has been made toward Phase II system targets: specifically, thermal cycling and power degradation rate. Current results on natural gas stationary systems are on target. Reduced efficiency and power, and increased degradation rate is anticipated when using diesel fuel. This is due in part to reduced efficiency and stack thermal management capability between internal reforming (natural gas) and CPOx/ endothermic reforming (diesel).

Stack design efforts have focused on optimizing the current design and adding features such as a cassette containing thermocouples in the center of the stack to get better temperature feedback. Development also focused on investigating different concepts for scaling up the active area footprint. Work on stack models has focused on developing algorithms that describe the current-voltage (I-V) response of an SOFC cell at a particular temperature and fuel composition. Such algorithms are essential to detailed stack models, such as the MARC-SECA code, which are used to predict the temperature, current, gas composition and, indirectly, the mechanical stress distributions within a large-scale, multi-cell stack. The algorithm is used by the model to predict the I-V response of each localized node within the mesh based on the local temperature and local anode gas composition. The cathode gas composition could also have a significant effect on the I-V response if the cathode air is allowed to become appreciably depleted in oxygen.

Delphi continues to make progress with improved cell fabrication techniques by focusing on material and process improvements. Battelle Pacific Northwest Division and Delphi continue to partner in the area of cathode powder and paste development to develop cell material sets that lead to improved electrochemical performance while being robust to potential failures such as cathode layer delamination. Delphi continues to work closely with commercial suppliers of production materials to develop a consistent supply of production grade material and optimize the material properties to provide robust performance in the solid oxide fuel cell stack and ultimately the fuel cell system. The principles of the Delphi Manufacturing System Design are being applied to develop control and quality standards for each step of the manufacturing process. By focusing efforts in these areas early in the development process, Delphi will be able to scale up the fabrication process to mass quantities while maintaining the highest quality standards.

A platinum-based mixed-metal oxide catalyst formulation was found to be very effective for natural gas hydrogenolysis. This formulation reduced ethane and propane content to almost undetectable levels and provided similar levels of performance as previously tested Rh-based catalysts, but at different operating conditions. Some supplier catalysts can match the performance of the best internally developed benchmark catalysts. The use of honeycomb substrates at higher cell counts results in better performing catalysts for partial oxidation reactions while foam substrates are not useful for partial oxidation. A novel FeCrAlY-based thick wall honeycomb monolith was prepared which may be useful for chemical reactions requiring significant heat input.

Development of BOP components continued with the main efforts focused on sourcing process air blowers and new recycle pumps for the next generation system.

A new set of requirements for a 12 VDC air pump were created. A sourcing study was completed and R&D Dynamics of Bloomfield, CT was selected as a supplier. Their proposal includes the use of air foil bearings and claims a service life of over 100,000 hours with greater than 30,000 start/stop cycles. The delivery of the first units was completed in early 2008.

## Conclusions

- SECA Phase II is focused on two markets, stationary and transportation, with additional emphasis on developing the system and stack requirements for a coal gas-based MW-scale Hybrid Power System.
- Product and process improvements were initiated for the current stack design with the initial requirements and development for the next generation stack design.
- Initiated and developed a tubular diesel endothermic reformer. In addition, developed a natural gas cracking reactor.
- A cast Inconel Integrated Component Manifold was developed and fabricated. A natural gas desulfurizer was specified, purchased, and validated in an SOFC system. Engineering began on a hot reformat desulfurizer.

## Future Directions

- Demonstrate SOFC system on varying loads using the natural gas-fueled APU.
- Demonstrate the next generation stack.
- Design release the DPS 3000 system.
- Initial test complete for subsystem of next generation SOFC system.

## FY 2008 Publications/Presentations

1. June 2007: 10<sup>th</sup> International Symposium on Solid Oxide Fuel Cells (SOFC-X), Nara, Japan, Presentation: DEVELOPMENT UPDATE ON DELPHI'S SOLID OXIDE FUEL CELL SYSTEM, Dr. Subhasish Mukerjee, Delphi Corporation.
2. June 2007: Fuel Cell 2007 Conference; Rochester, New York, Presentation: DEVELOPMENT UPDATE ON DELPHI'S SOLID OXIDE FUEL CELL SYSTEM, Sean M. Kelly, Delphi Corporation.
3. June 2007: 2007 SECA Annual Review Meeting; Nara, Japan, Presentation: DEVELOPMENT UPDATE ON DELPHI'S SOLID OXIDE FUEL CELL SYSTEM, Dr. Subhasish Mukerjee, Delphi Corporation.
4. August 2007: 2007 SECA Annual Review Meeting; San Antonio, TX: Presentation DEVELOPMENT UPDATE ON DELPHI'S SOLID OXIDE FUEL CELL SYSTEMS, Steven Shaffer, Delphi Corporation.

5. October 2007: 2007 Fuel Cell Seminar in San Antonio, TX, Presentation: Delphi SOFC Technology for Transportation and Stationary Applications: Latest Development Update, Steven Shaffer, Delphi Corporation.

### **Special Recognitions & Awards/Patents Issued**

1. US Patent Office Grant Numbers: 7255157, 7270906, 7279243, 7279246, 7294421, 7294424, 7305865

---

## III. INNOVATIVE CONCEPTS



## III.1 Solid Oxide Fuel Cell Coal-Based Power Systems

Matthew Alinger

GE Global Research  
1 Research Circle, MB277  
Niskayuna, NY 12309  
Phone: (518) 387-5124; Fax: (518) 387-5576  
E-mail: alinger@research.ge.com

DOE Project Manager: Travis Shultz

Phone: (304) 285-1370  
E-mail: Travis.Shultz@netl.doe.gov

Subcontractors:

- Pacific Northwest National Laboratory, Richland, WA
- University of South Carolina, Columbia, SC

Contract Number: 42614

Start Date: October 1, 2005

Project End Date: May 31, 2008

### Objectives

- Resolve identified barrier issues concerning the long-term economic performance of solid oxide fuel cells (SOFCs).
- Develop high performance ( $>0.75$  W/cm<sup>2</sup>), low degradation ( $<1\%$ /1,000 hours power density loss) SOFCs operating at 800°C.

### Accomplishments

- Developed a 25 cm<sup>2</sup> active area ceramic test vehicle for degradation mechanism identification and evaluation of mitigation solutions.
- Demonstrated high electrical conductivity ( $<5$  mΩ-cm<sup>2</sup>) and inherent stability ( $\sim\Delta 0$  mΩ-cm<sup>2</sup>/1,000 hours) of the cathode materials set using contact resistance measurements with inert current collectors.
- Demonstrated high electrochemical performance ( $<200$  mΩ-cm<sup>2</sup>) and inherent stability ( $<\Delta 10$  mΩ-cm<sup>2</sup>/1,000 hours) of the cathode materials set using button cell testing with inert current collectors.
- Determined that lanthanum strontium cobalt ferrite (LSCF) cathode stability is critical to mitigating degradation and demonstrated a modified architecture capable of significant improvement.
- Demonstrated  $\sim 2\%$ /1,000 hours power density degradation rate capability on a 25 cm<sup>2</sup> SOFC with the modified LSCF cathode materials set using ferritic stainless steel current collectors.

### Introduction

SOFCs represent an important opportunity to utilize fossil fuels in an efficient and environmentally friendly manner. Simple cycle fuel cells have obtained efficiencies to alternating current (AC) power as high as 45-50% with NO<sub>x</sub> production less than 0.5 ppm. Power producing systems containing fuel cells in combination with other power producing components such as gas turbines, known as combined-cycle or hybrid systems, have the potential for even higher efficiencies in converting fossil fuels to AC electricity. SOFC/gas turbine hybrid systems utilizing coal synthesis gas (from a gasifier) as a fuel will provide environmentally friendly, inexpensive and dependable central power from an abundant fuel source (coal) and will make an important contribution to improving U.S. energy security.

This project aims at developing a highly efficient, environmentally benign, and cost-effective multi-MW SOFC-based power system operating on coal. The project will be a critical step towards the overall goal of realizing large ( $>100$  MW) fuel cell power systems that will produce electrical power at greater than 50% overall efficiency from coal higher heating value to AC power, including CO<sub>2</sub> separation preparatory to sequestration. Currently, commercial success of SOFC technology lies in minimizing the overall cost and dramatically reducing performance degradation over time. The overall approach for this project is to identify critical degradation mechanisms and subsequently develop, evaluate and down-select cost-effective mitigation solutions.

### Approach

The project focuses on designing and cost estimating the integrated gasification fuel cell system and resolving technical and economic barrier issues relating to SOFCs. In doing so, manufacturing options for SOFC cells were evaluated, options for constructing stacks based upon various cell configurations identified, and key performance characteristics identified. It was determined, through a manufacturing down-select study, that the economic feasibility of SOFCs are primarily dependent upon improving long-term stability of cell performance rather than choice of manufacturing process.

Therefore, critical factors affecting SOFC performance degradation for cells in contact with metallic interconnects are studied and a fundamental understanding of associated mechanisms will be

developed. Experiments and modeling are carried out to identify key processes/steps affecting cell performance degradation under SOFC operating conditions. Interfacial microstructural and elemental changes are characterized, and their relationships to observed degradation identified. Mitigation strategies, including innovative coatings and bond layers, will be developed, evaluated and down-selected to improve degradation rates. The microstructural stabilization and minimization of the area specific resistance (ASR) contribution from  $\text{Cr}_2\text{O}_3$  scale growth and other interactions at electrode/interconnect interfaces was focused on and evaluated during electrochemical testing and advanced microstructural characterization. Novel long-term and accelerated testing techniques will be developed and conducted under standard operating conditions to demonstrate capability to meet targeted performance degradation rates ( $<0.2\%/1,000$  hours).

## Results

Cathode side degradation mechanisms comprise contributions of various ohmic (e.g., oxide scale growth and interaction/reaction layers between the metal interconnect and cathode) and non-ohmic (destruction of catalytically active sites and diffusion pathways for oxygen reduction within the cathode) mechanisms. A combination of electrochemical button cell testing and electrical contact resistance experiments are employed to simulate the configuration and conditions of operating SOFCs. A quantitative comparison of the results from the experiments, in conjunction with existing models, will furnish understanding of the degradation processes that contribute to the performance degradation of LSCF-based SOFCs.

Figure 1 shows the evolution of ASR as a function of time for gold current collectors in contact with lanthanum strontium cobalt (LSC) bond paste (red line), LSCF cathode (blue line) and a stack-up of both LSC and LSCF materials (green line). Tests were conducted at  $800^\circ\text{C}$  and operated at  $0.5 \text{ A/cm}^2$ . As shown Figure 1, there is no ohmic degradation of the LSC bond paste, the LSCF cathode, or the stack-up of LSC and LSCF when in contact with gold current collectors. The electrical resistance,  $<5 \text{ m}\Omega\text{-cm}^2$ , is very low for these materials set in this configuration. In addition, the inherent stability of the electrical paths of the LSC bond paste and LSCF cathode over time is excellent and does not pose concern when using an inert gold current collector.

In order to provide confidence and accuracy in SOFC degradation testing, a new test vehicle was designed and constructed. The testing requirements to understand and measure degradation are repeatability, high performance ( $<200 \text{ m}\Omega\text{-cm}^2$ ), control of fuel utilization (20-80%) and the use of representative active cell areas. Thus, a  $25 \text{ cm}^2$  active area ceramic

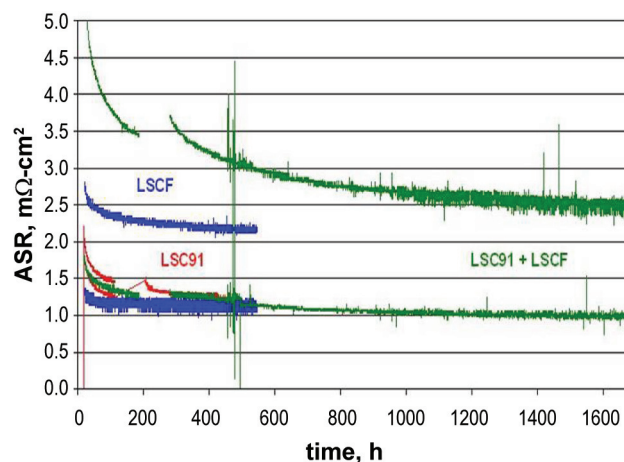


**FIGURE 1.** ASR evolution with time for LSC bond paste, LSCF cathode, and a stack-up of LSC and LSCF. Tests performed on gold interconnects at  $800^\circ\text{C}$  and  $0.5 \text{ A/cm}^2$ .

test vehicle, simulating real SOFC operating conditions with known boundary conditions was created and is shown in Figure 2. The primary goal of this test vehicle is to isolate specific degradation mechanisms, enabling a single variable approach. The current collector is interchangeable (e.g. gold, ferritic stainless steel, nickel). Initial testing was performed using five identical cell configurations with yttrium-stabilized zirconia electrolytes, LSCF cathodes and Mn,Co spinel coated GE-13L ferritic stainless steel interconnects operating at  $800^\circ\text{C}$ , 64%  $\text{H}_2$  (bal.  $\text{N}_2$ ) and 34% fuel utilization. The tests yield an open circuit voltage of  $1.059 \pm 0.003 \text{ V}$ , ASR of  $173.0 \pm 5.2 \text{ m}\Omega\text{-cm}^2$  and an initial power density at  $0.7 \text{ V}$  of  $1.12 \pm 0.013 \text{ W/cm}^2$ . These results validate the ceramic test vehicle as a useful tool for degradation mechanism identification.

Though initial performance of the ceramic test vehicle is high, 1,000-hour testing indicates that degradation rates are unacceptable. This can be seen

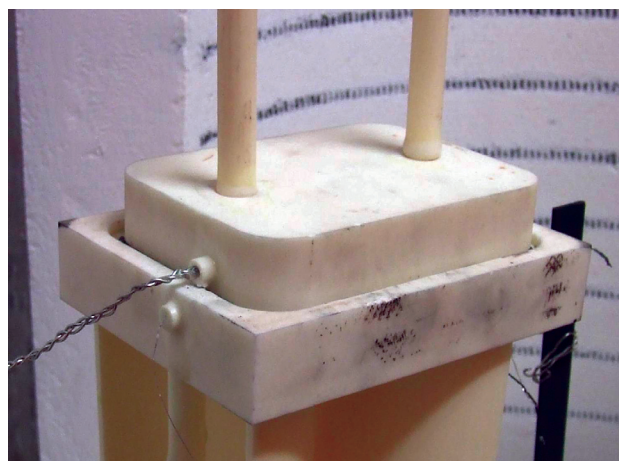


**FIGURE 2.** Ceramic Test Vehicle with a  $25 \text{ cm}^2$  Active Cell Area

in Figure 3, which plots the evolution of the power density as a function of time on the left axis and the ASR on the right. The degradation rates for this test are 18%/1,000 hours power density degradation and 110 mΩ-cm<sup>2</sup>/1,000 hours ASR increase. Detailed and thorough single variable testing using button cells and contact resistance measurement led to the conclusion that the cathode stability dominated the degradation behavior. Modifications were made to the LSCF cathode and LSC bond paste architecture to stabilize the electrochemical performance of the cathode without negatively impacting the electrical conductivity.

Figure 4 shows the effect of the stabilized cathode on the initial cell performance in addition to the degradation rate. Initial performance was high, slightly in excess of 1 W/cm<sup>2</sup>, with a time averaged power density degradation rate of ~2.2%/1,000 hours. The corresponding ASR increase is ~15 mΩ-cm<sup>2</sup>/1,000 hours. While encouraging, these test results must be shown to be repeatable and improved upon. In addition,

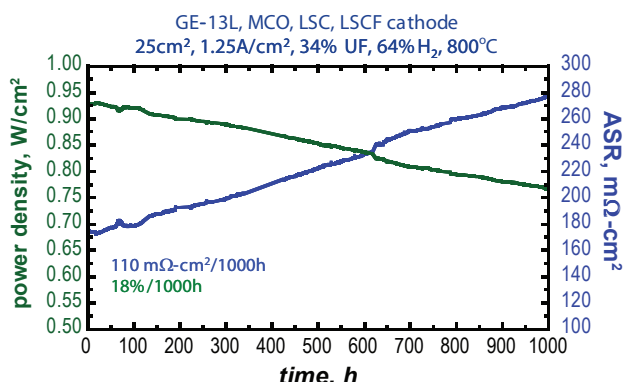


**FIGURE 3.** Ceramic test vehicle degradation data at 800°C with 64% H<sub>2</sub> (bal. N<sub>2</sub>), 34% fuel utilization driven at 1.25 A/cm<sup>2</sup>.

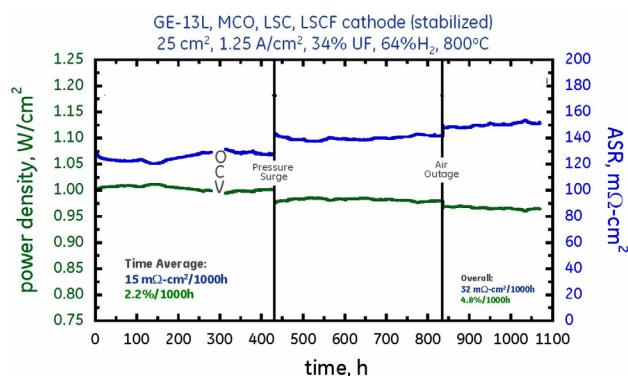


**FIGURE 4.** Ceramic test vehicle data for stabilized cathode indicating high initial performance and low degradation (at 800°C with 64% H<sub>2</sub> [bal. N<sub>2</sub>], 34% fuel utilization driven at 1.25 A/cm<sup>2</sup>).

the curve shape of the degradation behavior must be parabolic, or gradually decreasing with time, as would be anticipated from a diffusion limited growth process (i.e. chromia growth on the current collector), in order to meet targeted performances at end of life (40,000 hours).

## Conclusions and Future Directions

The inherent stability and high performance entitlement of LSCF cathode-based SOFCs has been demonstrated. The high performance of this material system plays a major role in decreasing the cost per kilowatt of SOFCs. However, a reliable solution to the degradation behavior requires more detailed knowledge of the dominant mechanisms, requiring additional investigation. This research will continue to drive toward the construction of a Pareto of cathode-side degradation mechanism impact to determine the dominant mechanism(s). Ultimately, a degradation mitigation solution for high performance SOFCs with ferritic steel interconnects, having a repeatable performance degradation of <1%/1,000 hours, will be demonstrated.

## Special Recognitions & Awards/Patents Issued

1. U.S. Patent US7211342 B2, *Fuel cell system with regenerative bed*, filed April 15, 2003, published May 1, 2007.

## FY 2008 Publications/Presentations

- Quarterly Report for 1<sup>st</sup> calendar quarter 2008, April 30, 2008.
- Solid Oxide Fuel Cell Coal-Based Power Systems*, presented at the 2008 Fuel Cell Peer Review, Pittsburgh, PA, April 21–25, 2008.
- Quarterly Report for 4<sup>th</sup> calendar quarter 2007, January 30, 2008.
- Quarterly Report for 3<sup>rd</sup> calendar quarter 2007, October 30, 2007.
- Quarterly Report for 2<sup>nd</sup> calendar quarter 2007, July 30, 2007.
- SECA SOFC Program at GE Global Research*, presented at the 8<sup>th</sup> Annual SECA Workshop and Peer Review, San Antonio, TX, August 7–9, 2007.



---

## IV. SECA CORE RESEARCH & DEVELOPMENT

### A. Cathodes



## IV.A.1 Synchrotron X-Ray Studies of SOFC Cathodes

P. H. Fuoss (Primary Contact), J. A. Eastman,  
T. T. Fister, D. D. Fong, K.-C. Chang, H. You  
Argonne National Laboratory (ANL)  
9700 S. Cass Ave.  
Argonne, IL 60439  
Phone: (630) 252-3289; Fax: (630) 252-7777  
E-mail: fuoss@anl.gov

DOE Project Manager: Briggs White  
Phone: (304) 285-5437  
E-mail: Briggs.White@netl.doe.gov

Contract Number: 49071

Start Date: June 2007  
End Date: May 2009

- Compared equilibrium, high temperature results with room temperature non-equilibrium measurements.

### Introduction

The performance of SOFCs is strongly influenced by the nanoscale structure and chemistry of electrode materials under operating conditions. However, because SOFCs are operated at elevated temperatures and at near-atmospheric pressure, the utilization of traditional surface science techniques, which typically involve vacuum conditions near room temperature, requires validation. The studies being performed in this project provide the needed understanding of *in situ*-ex situ correlations. The results also enable the development of molecular-level models for stimulating the rational design and development of high-performance cathode materials.

### Approach

We employ *in situ* X-ray scattering and spectroscopy technologies developed at ANL to both measure equilibrium structures of SOFC cathode materials at elevated temperatures and controlled oxygen partial pressures, and to examine the dynamic structural changes that occur at the cathode side of a fuel cell under conditions that simulate actual operating conditions. This work is performed in collaboration with P. Salvador's group at CMU, which grows the sample materials with pulsed laser deposition (PLD), and B. Yildiz's group at MIT which uses scanning tunneling microscopy and scanning tunneling spectroscopy to develop spatial images of electronic, topological, and electrochemical properties of cathode materials.

### Results

#### Equilibrium Structures in Active Atmospheres

We analyzed the behavior and origin of strontium surface segregation in LSM using TXRF to characterize the strontium segregation at the high temperature and pressure conditions associated with operation of present-day fuel cells.  $\text{La}_{0.7}\text{Sr}_{0.3}\text{MnO}_3$  samples on  $\text{SrTiO}_3$  (001),  $\text{DyScO}_3$  (110),  $\text{NdGaO}_3$  (110), and YSZ (001) substrates were studied as a function of temperature, partial pressure oxygen ( $p\text{O}_2$ ), and film-thickness. Comparison of samples on different substrates provides an understanding of the effects of strain and interfaces on

### Objectives

- Determine the structure of  $\text{La}_{1-x}\text{Sr}_x\text{MnO}_3$  (LSM) thin films as a function of oxygen partial pressure and temperature. Examine the role of strain state and X-ray background introduced by substrate choice and use this information to develop optimized sample geometries.
- Study the chemical and atomic structure of LSM and  $\text{La}_{1-x}\text{Sr}_x\text{CoO}_3$  (LSC) thin film cathodes on yttria-stabilized zirconia (YSZ) electrolytes in a solid oxide fuel cell (SOFC) half-cell configuration as functions of operating temperature and electrochemical potential.
- Correlate the *in situ* measurements of the first and second bullets with ex situ measurements.
- Integrate the electrochemical measurements into the controlled environment system.
- Study the operation of the cathode side of a fuel cell and correlate the structure and chemical state with those determined by ex situ measurements from the literature and supplemental measurements performed at ANL, Carnegie Mellon University (CMU) and the Massachusetts Institute of Technology (MIT).

### Accomplishments

- Completed *in situ* X-ray scattering and spectroscopy experiments on LSM and LSC thin films at the Advanced Photon Source (APS).
- Developed code for analyzing total reflection X-ray fluorescence data (TXRF).
- Analyzed collected experimental data and compiled results.

segregation behavior. For all samples, we see evidence of strontium surface segregation and observe that the segregation is approximately independent of strain state (i.e., substrate) and film-thickness but depends on  $pO_2$  and temperature.

An example of the Sr/La TXRF ratio with its corresponding theoretical prediction for a 20 nm LSM film on  $DyScO_3$  (110) at  $600^\circ C$  is shown in Figure 1. The increase in the Sr/La concentration below  $\alpha_c$  ( $\sim 0.12^\circ$ ) is clear evidence of Sr surface segregation. Furthermore, it is observed that the amount of segregation increases at lower  $pO_2$ . Based on our analysis of temperature dependent data, the enthalpy of Sr segregation to the surface region of LSM (the top  $\sim 2$  nm of our samples) is  $-3.4$  kJ/mol at 15 Torr  $pO_2$ . Behavior at temperatures below  $500^\circ C$  suggests a shift toward non-equilibrium segregation due to exponentially slower kinetics. Not displayed on Figure 1 are TXRF data we have also obtained showing the dependence of Sr segregation on  $pO_2$  at 700, 800, and  $900^\circ C$ . We also measured the 20L crystal truncation rod (CTR) and specular reflectivity at these temperatures. CTR intensities are particularly sensitive to changes in surface

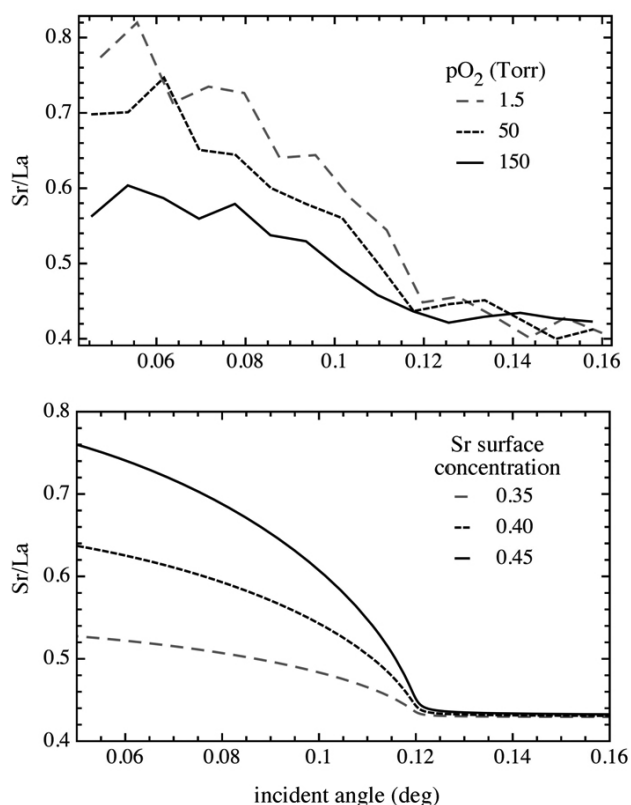


**FIGURE 1.** (a) Experimental TXRF ratios for a 20 nm epitaxial LSM film on  $DyScO_3$  (110) at  $600^\circ C$  in varying  $pO_2$ . (b) A simulation of the TXRF ratio for a 20 nm LSM film on  $DyScO_3$  where the composition of the top 2 nm of LSM is varied. The strontium surface segregation may be higher than this simulation suggests since the strontium rich layer may be less than 2 nm thick.

structure and chemistry, while reflectivity provides information on sample roughness. The 20L CTR at  $900^\circ C$ , shown in Figure 2, exhibits a distinct  $pO_2$  dependence.

### *In Situ* X-ray Studies of SOFC Cathodes

PLD-grown LSM and LSC films grown on YSZ (111) were characterized with atomic force microscopy (AFM), X-ray reflectivity and diffraction, and X-ray spectroscopy at the APS. The X-ray reflectivity and AFM results indicate that the LSC is considerably rougher and more porous than the LSM. Furthermore, out-of-plane X-ray diffraction measurements show that the LSM and LSC films grow with an (011) orientation on the YSZ (111) substrate. In-plane X-ray diffraction scans of 100 nm LSM show evidence of the six different domains that are expected with (011) in-plane epitaxy.

The Co K edge X-ray absorption near-edge structure (XANES) of LSC shows interesting variations with temperature as illustrated in Figure 3(a) and (b). At room temperature, the edge position (which is indicative of chemical state) at the surface is shifted to a lower energy compared with the bulk. Both the surface and bulk edges shift to lower energy at higher temperatures, as expected for increasing oxygen vacancy concentration in the LSC. The magnitude of the edge shift is more pronounced at higher incidence angle, suggesting that the bulk film has a lower concentration of oxygen vacancies than the surface at room temperature, but the vacancies equilibrate throughout the film at high temperature. There was no significant change in the edge position with applied electrochemical potential at either incidence angle.

The largest change in TXRF with temperature was observed in the 60 nm LSM samples as shown in Figure 4. At room temperature, we observe a 'foot' in the Sr fluorescence as a function of angle that is not present in the Mn fluorescence. The presence of

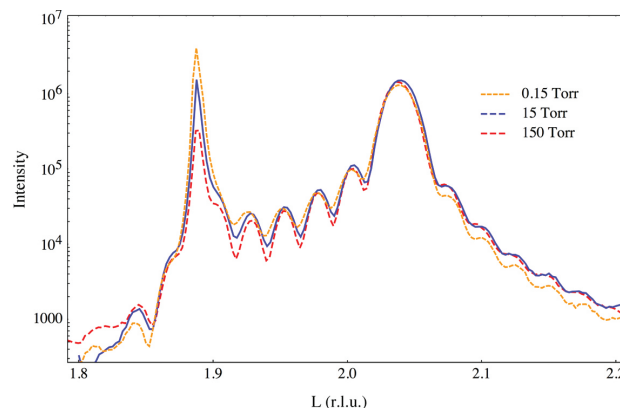


**FIGURE 2.** 20L CTR Taken from a 20 nm LSM Film on  $DyScO_3$  at  $900^\circ C$  and for  $pO_2 = 0.15 - 150$  Torr

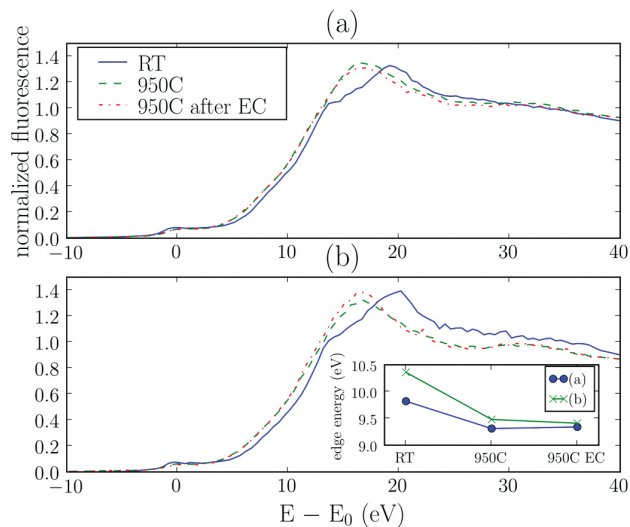


**FIGURE 3.** (a) Grazing incidence ( $Q_z \sim 0.027 \text{ \AA}^{-1}$ ) XANES and (b) high incidence angle ( $Q_z \sim 0.2 \text{ \AA}^{-1}$ ) XANES of Co measured at room temperature on 20 nm LSC on YSZ (111) both before and after applied electrochemical potential (-300 mV) at 950°C. The inset in (b) shows the change in the edge energy (defined as 0.5 point of the normalized fluorescence).

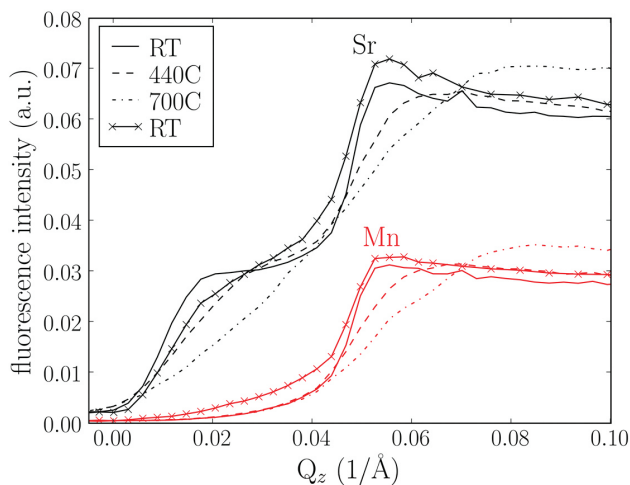


**FIGURE 4.** Strontium and Manganese TXRF Intensities Taken on 60 nm LSM on YSZ (111) at Different Temperatures

a foot feature is indicative of Sr-rich features on the surface that can be related to the rounded island-like features seen in our AFM images (not shown). The foot gradually goes away at higher temperature, suggesting that the Sr-rich regions are being incorporated into the film. The Sr migration into the film seems to depend on the holding time at high temperature and the applied potential on the sample. The foot reappears when the sample is cooled down from 700°C to room temperature, which suggests that Sr re-segregates to the surface at low temperature.

## Conclusions and Future Directions

- In controlled atmosphere experiments, Sr is observed to segregate to the surface of LSM films, the magnitude of which depends on  $pO_2$  and temperature. The enthalpy of Sr segregation is  $-3.4 \text{ kJ/mol}$  at 15 Torr  $pO_2$ .
- For electrochemical experiments, the Co K edge is observed to change with heating, suggesting that the bulk film has a lower concentration of oxygen vacancies than the surface at room temperature, but the vacancies equilibrate at high temperature. The edge does not change significantly under applied potential. Cathodic polarizations may increase the Sr segregation/desegregation rates.
- LSM and LSC cathode materials rapidly cooled from normal SOFC operating temperatures show significantly different atomic and chemical structure in the critical near surface region when compared to the same samples at elevated temperatures.

In the future, the experimental results from both systems will be integrated and compared in order to understand and differentiate the effects of oxygen partial pressure, electrochemical potential and current on perovskite oxygen electrodes. These results will be used to relate and validate ex situ measurements as a probe of structural changes in SOFC materials.

## FY 2008 Publications/Presentations

1. Quarterly Report for January-March 2008.
2. Quarterly Report for October-December 2007.
3. Quarterly Report for July-September 2007.

## IV.A.2 SOFC Cathode Surface Chemistry and Optimization Studies

Paul A. Salvador (Primary Contact), Lu Yan, Shanling Wang, and K. R. Balasubramaniam  
Carnegie Mellon University  
Department of Materials Science and Engineering  
5000 Forbes Avenue  
Pittsburgh, PA 15206  
Phone: (412) 268-2702; Fax: (412) 268-3113  
E-mail: paul7@andrew.cmu.edu

Collaborators: Drs. Paul Fuoss,<sup>a</sup> Jeff Eastman,<sup>a</sup> Dillon Fong,<sup>a</sup> Tim Fister,<sup>a</sup> Peter Baldo,<sup>a</sup> Hoydoo You,<sup>a</sup> Kee-Chul Chang,<sup>a</sup> Bilge Yildez,<sup>b</sup> Ibrahim Burc Misirlioglu<sup>b</sup>

<sup>a</sup>Argonne National Laboratory (ANL)  
9700 South Cass Avenue  
Argonne, IL 60439-4837

<sup>b</sup>Massachusetts Institute of Technology (MIT)  
Department of Nuclear Science and Engineering  
77 Massachusetts Avenue, Rm. 24-210  
Cambridge, MA 02139

DOE Project Manager: Briggs White  
Phone: (304) 285-5437  
E-mail: Briggs.White@netl.doe.gov

Contract Number: 41817

Start Date: May 1, 2007  
Project End Date: April 30, 2009

### Objectives

- Develop thin film samples having specific surface structures and chemistries using thin film preparation methods.
- Develop and employ experimental tools that provide a sensitive measure of activity/stability in operational conditions.
- Determine the stability of engineered surface chemistries as a function of thermodynamic parameters (temperature [T], pressure [P], and electrochemical parameters).
- Determine the effects of engineered surface chemistries on oxygen uptake kinetics in thin film samples.
- Determine the key correlations between surface features and electrochemical performance for solid oxide fuel cell (SOFC) cathodes.

### Accomplishments

- Developed single-crystal, epitaxial, textured, and polycrystalline thin films of (La,Sr)MnO<sub>3</sub> (LSM) and

(La,Sr)CoO<sub>3</sub> (LSC) with low roughness values on both insulating and electrolytic substrate that were/ can be used in both in-house and collaborators' experimental facilities to understand the nature of the surface chemistry.

- Developed both (100)- and (110)-epitaxial films on yttria-stabilized ZrO<sub>2</sub> (YSZ) single crystals, the former using a gadolinia doped ceria (GDC)-buffered (100)-YSZ and the latter using (111)-YSZ.
- Thin film samples were characterized at the Advanced Photon Source (APS) as a function of T, P, and electrochemistry, with the primary focus on the Sr-segregation to the surface.
- Developed electrical conductivity relaxation (ECR) testing methods for thin films over the pressure range of 10<sup>-6</sup>-10<sup>-1</sup> torr, which is also capable of ECR measurements.
- Developed a high-temperature piezoelectric crystal microbalance (PCM) capable of measuring mass changes over the pressure range of 10<sup>-6</sup>-10<sup>-1</sup> torr, which is also capable of transient mass change measurements.

---

---

### Introduction

The cathode in SOFCs is responsible for the reduction of O<sub>2</sub> gas and its incorporation into the electrolyte. To accomplish this, most SOFCs use a three-phase composite for the active cathode region. The three phases are commonly: LSM and YSZ as solid phases and O<sub>2</sub> as gas in pores. When SOFCs are operated at specific current densities/voltages, the oxygen incorporation (or uptake) process can contribute significantly to the losses of the cell, thereby limiting the performance of the SOFC system. Two major options exist for improving the cathode performance by specifically targeting the oxygen incorporation process: changing the component solid materials or adding yet another material (a catalyst) to the existing frameworks. We aim to address both approaches in this work by (1) developing an experimental project that allows us to probe the nature of atomic scale surface chemistry and its role in oxygen incorporation in LSM and related cathode materials and (2) determining the optimal catalyst chemistry from both an activity and stability perspective. Realizing these goals will lead to improved cathode performance in SOFCs and an acceleration of introduction of new materials into SOFCs to allow for the U.S. Department of Energy-Solid State Energy Conversion Alliance (DOE-SECA) program to meet performance metrics.

Generally speaking, the limitations in designing highly active cathodes for oxygen incorporation arise from the general lack of direct correlations between surface/interface chemistry/structure and performance of SOFC cathode materials. In other words, very little is quantitatively known about why specific materials/surfaces behave the way they do in SOFC operating conditions. To fill this gap, one must probe the nature of atomic scale surface chemistry or interface crystallography in fuel cell operating conditions. In this work we aim to realize this by (1) developing experimental protocols that will provide a sensitive measure of activity/stability in operational conditions and by (2) determining key correlations between structure (solid-state atomic, electronic, crystallographic, and chemical) and electrochemical performance (mass and charge transfer) parameters in surface engineered samples. Several important collaborations have been developed to realize these goals. One involves Carnegie Mellon and several groups at ANL, where thin film samples developed at Carnegie Mellon are investigated using high-energy synchrotron X-ray techniques at the APS. Another collaboration involves Carnegie Mellon and MIT, where scanning-tunneling spectroscopy and electrochemical impedance spectroscopy are carried out to determine electrical characteristics of the films. Separate reports will be provided by these collaborators. In this report, we describe the work at Carnegie Mellon on sample preparation and in two measurement techniques of the oxygen uptake kinetics.

## Approach

A key part of an experimental project that can address the above stated goals is the development of samples that allow both for controlled changes in surface chemistry and for detailed experiments to be carried out upon them. Epitaxial and textured thin films are ideal samples for these experiments. To screen for structure-performance correlations, we are producing single-crystal and textured thin film samples using pulsed laser deposition (PLD) to produce thin, flat films that can be used to characterize the structure, chemistry, and physical properties of surfaces. The long range goals are to systematically deposit various surface layers on specific bulk films and to determine key correlations between surface structure and electrochemical performance. By generating a large number of well-controlled thin film samples, we will have a high-throughput screening process that probes the identified key correlation. For the current year, we have focused on understanding the *native* surface on both LSM and LSC, as well as establishing measurement techniques that allow for the determination of surface kinetic parameters.

To establish a baseline in understanding the bulk and surface structure of LSM, epitaxial thin films of

LSM samples were grown using PLD on different single crystal perovskite substrates ( $\text{SrTiO}_3$  [STO],  $\text{NdGaO}_3$ ,  $\text{DyScO}_3$  [DSO]) as well as electrolytes (YSZ and GDC-buffered YSZ). The films were characterized for their growth rate, surface roughness, and structural nature at Carnegie Mellon using X-ray techniques and atomic force microscopy (AFM). Certain representative samples were sent to ANL and were characterized at the APS using *in situ* X-ray scattering observations, while the films were exposed to various T, P, and electrochemical environments. The observations made on these epitaxial films provide a basic scientific understanding for how LSM behaves and provide important structural information that will enable a better understanding to interpret physical property observations. Similar measurements are now being carried out on LSC films. Electrochemical performance was determined at MIT, as were scanning tunneling spectroscopy experiments to determine the electronic character of the films. An ECR measurement set-up was installed at Carnegie Mellon to determine the chemical surface exchange coefficient ( $k_{\text{chem}}$ ) at both growth and operational conditions. A PCM capable of measuring at elevated temperatures was also installed at Carnegie Mellon and was used to measure mass uptake in  $\text{LaNiO}_{3-x}$  to demonstrate the utility of this direct measurement technique in determining mass changes and exchange kinetics.

## Results

In all depositions, LSM and LSC followed cube-on-cube epitaxy on all perovskite substrates, as expected from earlier work [1,2] and exhibited low surface roughness values (on the order of unit-cell roughnesses). This allowed their use in *in situ* X-ray measurements at the APS and in scanning tunneling spectroscopy measurements at MIT. At the APS, Sr-segregation was observed for all LSM(100) films on perovskite substrates, regardless of the substrate-induced strain state or thickness of the film; segregation was a function of T and P. The Sr-surface segregation was characterized for LSM films on DSO substrates and it was shown that the surface segregation increased at low  $\text{pO}_2$  and low T. This is important because it implies that the surface composition of LSM differs dramatically from the bulk but that it is also dynamic over the range of T and P relevant to the SOFC operation.

To measure surface properties under electrochemical loads, it is necessary to generate surface engineered perovskite films on fluorite electrolyte substrates. Because the film and substrates differ in structure from one another, it is difficult to generate the cube-on-cube epitaxial state (which minimizes the microstructural complexity of the films) observed for perovskite-perovskite film-substrate combinations. By using YSZ(111) substrates, we generated epitaxial LSM(110)

and LSC(111) having low surface roughnesses. Figure 1 shows the epitaxy of the films while Figure 2 shows the surface roughnesses. From Figure 1(a), one observes that the films grow (110)-oriented on YSZ(111), and, from Figure 1(b), one observes that the in-plane alignment is such that LSM[111] is parallel to YSZ[11-2]. This

epitaxial arrangement has six degenerate orientations, leading to the 12 peaks observed in Figure 2. Hence, there are variant boundaries in these films that do not exist in the cube-on-cube epitaxial films grown on perovskite substrates. Nevertheless, these films have a well-defined microstructural state and have unit-cell roughness values, as observed in Figure 2. Such films were investigated at the APS under electrochemical loads. Again, Sr-segregation was observed as a function of T and P. Initial evidence is that the reversible Sr-segregation in these films lead to Sr-rich island-like regions at the surface at low temperatures, unlike that observed on perovskite-perovskite films. Current work is focusing on unraveling whether the substrate, the variant boundaries, or the outer (110) surface is the cause of this difference.

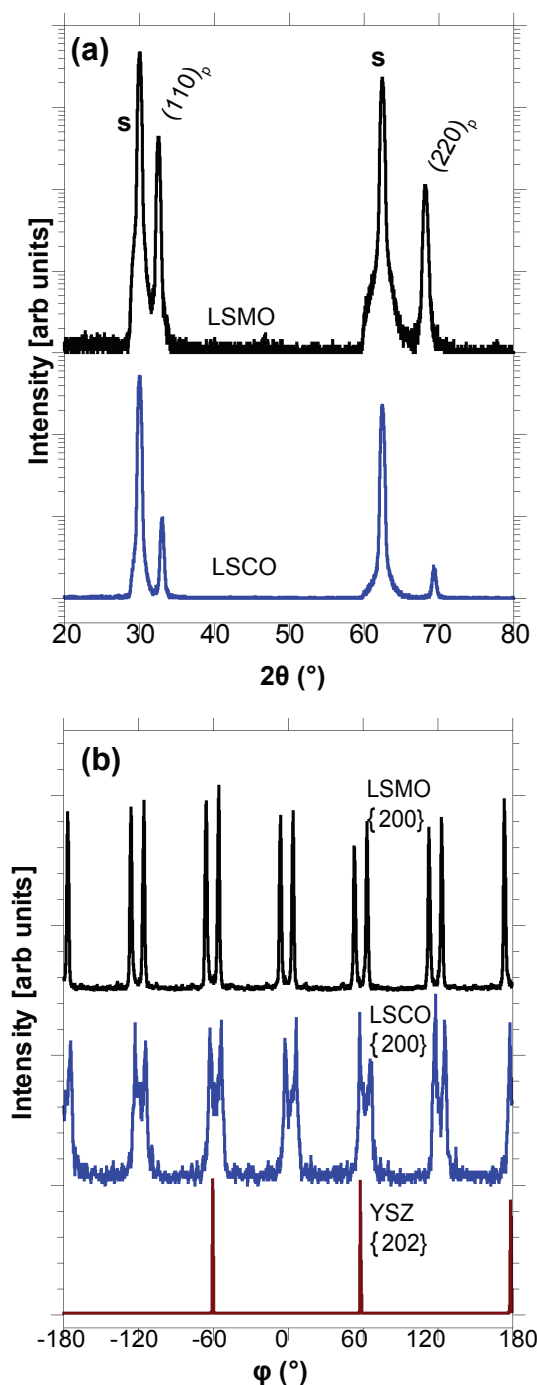


**FIGURE 1.** XRD scans of LSM and LSC films on YSZ(111). (a)  $\theta$ - $2\theta$  scans of LSM and LSC. (b)  $\phi$ -scans around the {200} reflections for LSM and LSC and the {202} of YSZ.

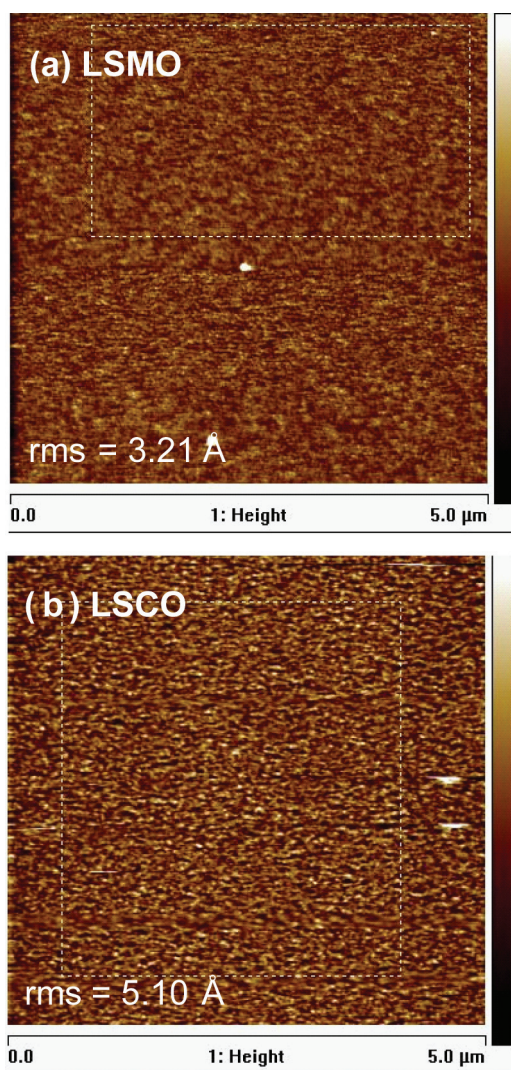


**FIGURE 2.** AFM topographs of the surfaces of LSM and LSC films on YSZ(111). The rms roughness values are given.

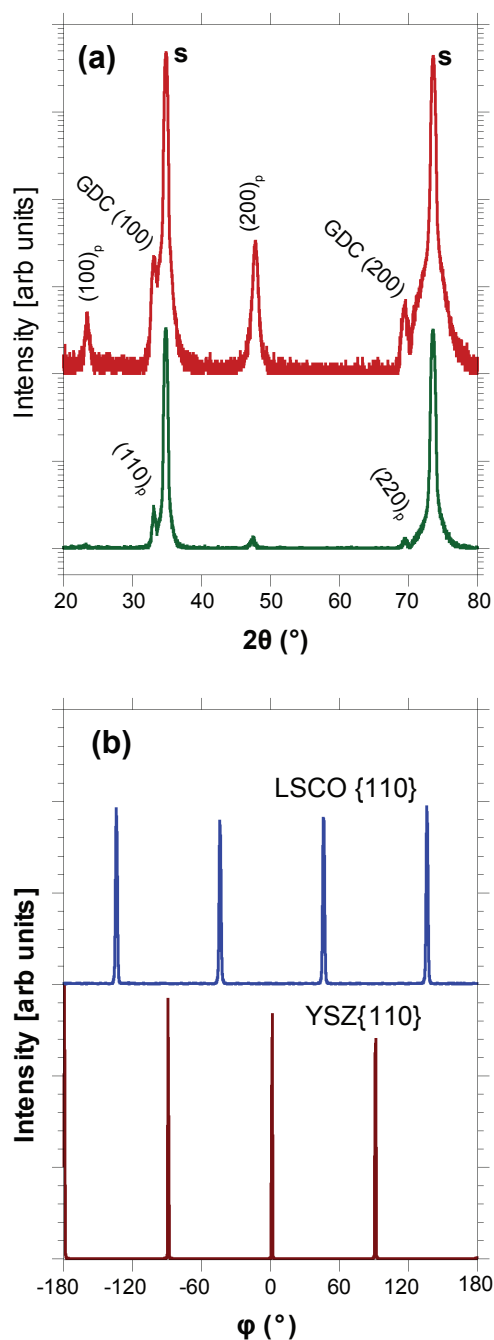


**FIGURE 3.** XRD scans of LSC films on YSZ(100). (a)  $\theta$ - $2\theta$  scans of (bottom) LSC on YSZ(100) and (top) LSC on GDC-buffered YSZ(100). (b)  $\phi$ -scans around the  $\{110\}$  reflections for LSC and the  $\{110\}$  of YSZ for the film on the GDC-buffered YSZ(110).

To directly compare the perovskite-perovskite and perovskite-fluorite film-substrate combinations it would be ideal to have similar surfaces exposed on both. We developed (110) perovskite-perovskite films on STO(110). Growing epitaxial LSM or LSC on YSZ(100) is more challenging since the films are generally polycrystalline (although the amount of specific

orientations is a function of deposition parameters). The bottom panel in Figure 3(a) shows the polycrystalline nature of LSC on YSZ(100). Similar results were observed for LSM on YSZ(100). To rectify this, and to provide chemically compatible interfaces for lanthanum strontium cobalt ferrite films to be looked at in the future, a GDC-buffer was deposited on YSZ(100), which deposits in a cube-on-cube fluorite-on-fluorite fashion. The top panel in Figure 3(a) shows the X-ray diffraction (XRD) of the LSC films deposited on the GDC-YSZ(100), which shows only an LSC(100) orientation. (Note the GDC(100) overlaps with the LSC(110), but through more detailed XRD analysis the existence of the LSC(110) orientation was ruled out.) Figure 3(b) shows the epitaxy of LSC on GDC-YSZ(100), illustrating that the LSC[011] is parallel to the GDC-YSZ[010]; therefore, there are four variants possible in this epitaxy. The root mean square (rms) roughness of the epitaxial films was on the order of unit-cell values. These films will allow for direct correlations between the perovskite-perovskite and perovskite-fluorite film-substrate combinations, allowing the effects of microstructure and surface crystallography to be deconvoluted.

Equipment for two experimental measurement techniques was installed at Carnegie Mellon to investigate the surface properties of thin films. The first is the well-known ECR technique. In our system, the pressure range is controlled using both vacuum techniques, similar to the growth chambers, and using flow rate controls, similar to those described in the literature [3]. A van der Pauw set-up was used to measure the conductivity of the films; a 100-nm thick lanthanum strontium cobalt oxide(110) film on YSZ(111) was used for this. The differences between the geometrical configurations of the voltage and current probes were  $<1\%$ , indicating the good homogeneity of the films and allowing for the use of a single configuration to determine the conductivity of the films. Figure 4 shows the normalized conductivity,

$$g(t) = \frac{s(t) - s(0)}{s(\infty) - s(0)}$$

where  $s(t)$  is the conductivity at a given time  $t$ , measured on changing the oxygen pressure from 50 mTorr to 0.01 Torr. Though this change is rather large, the overall kinetics can be fit reasonably well with a simple exponential,

$$g(t) = 1 - e^{-\left(\frac{k_{chem} t}{l}\right)}$$

where  $l$  is the thickness of the film and  $k_{chem}$  is the chemical surface exchange coefficient. The value of  $k_{chem}$  is  $3.825 \times 10^{-6}$  cm/s, which compares well to that observed for epitaxial LSC films on the perovskite  $\text{LaAlO}_3$ ,  $1.333 \times 10^{-6}$  cm/s. Current work focuses on obtaining fine gradations in pressure changes and exploring the

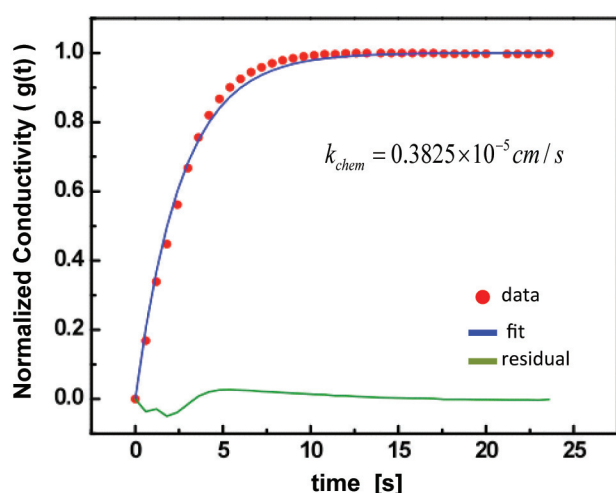


**FIGURE 4.** Normalized conductivity from an ECR measurement, the fit, and the difference (residual) for the LSC film on YSZ(111) at  $T=650^{\circ}\text{C}$ .

response of films over similar T and P as explored at the APS in which Sr-segregation was observed. Also, we are determining the effect of surface structure and microstructural complexity on the exchange kinetics.

Finally, we installed a  $\text{GaPO}_4$  piezoelectric microbalance and determined that both polycrystalline films, and epitaxial films deposited on ultrathin STO crystals could be measured using the PCM technique. Preliminary work indicated that polycrystalline lanthanum nickel oxide (LNO) films deposited on the PCM crystal could be measured for their overall oxygen content variation and for their chemical surface exchange coefficient at  $350^{\circ}\text{C}$ . Current work focuses on optimizing this approach for direct oxygen content variation measurements on various types of films and at higher temperatures.

## Conclusions and Future Directions

We have demonstrated that surface engineered films of cathode materials can be produced and characterized in detail for the structural and chemical properties. Surface segregation has been observed (on both epitaxial perovskite-perovskite and perovskite-fluorite film-substrate combinations) that is a strong function of the thermodynamic variables. Future work involves isolating the effects of surface orientation and electrochemical loading on surface segregation

and electrocatalytic properties. Both ECR and PCM equipment have been installed and used to measure surface properties of thin films. We will continue to produce a series of surface engineered films and will investigate (1) their structural properties, (2) their stabilities, (3) their oxygen uptake kinetics using specially designed crystal microbalances and electronic conductivity rigs, and (4) how electrochemical parameters affect segregation/activity. By fabricating a matrix of related materials and carrying out these measurements, we will be able to provide a large amount of data to determine the key parameters that correlate surface structure to surface activity, with the aim of providing information to the DOE-SECA program to improve cathode activity by design.

## FY 2008 Publications/Presentations

1. "In-situ synchrotron x-ray studies of domain structure and segregation behavior of epitaxially strained LSMO thin films," J.A. Eastman, P.H. Fuoss, D.D. Fong, P.M. Baldo, P.A. Salvador, K.R. Balasubramanian, J.C. Meador, *Presented at 14<sup>th</sup> International Workshop on Oxide Electronics*, Jeju, Korea, October 2007.
2. "In Situ X-Ray Studies of Domain Structure in Epitaxially Strained  $\text{La}_{1-x}\text{Sr}_x\text{MnO}_3$  Thin Films," *Presented at MRS Fall 2007*, Boston, 2007.
3. "Synthesis and in-situ X-ray studies/physical property measurements of  $\text{La}_{0.7}\text{Sr}_{0.3}\text{MnO}_3$  thin films deposited by Pulsed Laser Deposition," K.R. Balasubramanian, J. Meador, O. Maksimov, S. Wang, J. Eastman, P. Fuoss, D. Fong, P. Baldo, L. Wilson, and P. A. Salvador, *Presented at 32<sup>nd</sup> International Conference & Exposition on Advanced Ceramics and Composites*, Daytona Beach, Florida, USA, January 2008.
4. "In situ X-ray Studies of  $\text{La}_{0.7}\text{Sr}_{0.3}\text{MnO}_3$  Thin Films at Elevated Temperature and Oxygen Partial Pressure," T.T. Fister, J.A. Eastman, D.D. Fong, P.M. Baldo, M. Highland, P.A. Salvador, K.R. Balasubramanian, J.C. Meador, P.H. Fuoss, *Presented at MRS Spring 2008*, San Francisco, 2008.

## References

1. P. A. Salvador *et al.*, *Appl. Phys. Lett.* **75**, 2638 (1999).
2. B. Mercey *et al.*, *J. Mater. Chem.* **9**, 233 (1999).
3. X. Chen *et al.*, *Solid State Ionics*, **146**, 405 (2002).

## IV.A.3 TEM Investigations of Cr-Contamination in SOFC Cathodes

Paul A. Salvador (Primary Contact),  
Rumyana Petrova, and Shanling Wang  
Carnegie Mellon University  
5000 Forbes Avenue  
Pittsburgh, PA 15206  
Phone: (412) 268-2702; Fax: (412) 268-3113  
E-mail: paul7@andrew.cmu.edu

Collaborators: Drs. Michael Krumpelt  
(Primary Contact), Terry A. Cruse, and  
Brian Ingram

Argonne National Laboratory (ANL)  
9700 South Cass Avenue  
Argonne, IL 60439-4837  
Phone: (630) 252-8520; Fax: (630) 252-4176  
E-mail: krumpelt@cmt.anl.gov

DOE Project Manager: Briggs White  
Phone: (304) 285-5437  
E-mail: Briggs.White@netl.doe.gov

Contract Number: 41817

Start Date: May 1, 2007  
Project End Date: April 30, 2009

### Objectives

- Use focused ion beam (FIB) methods to prepare transmission electron microscopy (TEM) specimens from specific regions of solid oxide fuel cells (SOFCs) exposed to different operating conditions (different current [I], voltage [V], temperature [T]).
- Carry out TEM investigations on SOFCs provided by ANL collaborators to determine the local microstructure/chemistry associated with Cr contamination.
- Better understand the mechanism of Cr contamination in the active (mixed) cathode region of SOFCs.
- Compare observed microstructural features to proposed degradation mechanisms.
- Compare microstructural features and degradations at different operating conditions, including those investigated in prior reports.

### Accomplishments

- Used a FIB technique to produce reliably TEM specimens from the mixed lanthanum strontium manganate/yttria-stabilized zirconia (LSM/YSZ) (or active) cathode region of SOFCs, under the flow

channel and under the contact (landing) in ribbed interconnects.

- Determined the local microstructures and Cr-containing phases in various regions of different fuel cells, each run for 500 hours but each run under different operating conditions (temperature and current density).
- Further demonstrated that the highest contamination points were directly under the interconnect contact and near the electrolyte in all conditions.
- Established the signature of degradation as the existence of nanoparticles ( $d < 100$  nm) on solid surfaces (YSZ and/or LSM); the local number density, size, and chemical composition of such nanoparticles are factors of location, temperature, and current density.
- Clarified the mechanism of Cr contamination for SOFCs run at 700°C and 800°C.

---

### Introduction

Ferritic stainless steel alloys have been considered as interconnect materials in SOFCs whose operating temperature is in the 600-800°C range, since steels are relatively inexpensive and are stable in these conditions. However, in hydrated oxidizing atmospheres at these temperatures, Cr is volatile and forms several vapor species, such as  $\text{CrO}_2(\text{OH})_2$ . It is well known that, without the use of effective protective coatings on the steel, the gaseous Cr species can react with cathode components (in LSM/YSZ cathodes) and can cause rapid degradation of the SOFC performance [1-7]. While coatings may effectively reduce the vapor pressure of Cr species, it is still important to understand the mechanism by which Cr contamination occurs in the SOFC cathode and to establish operating conditions in which the degradation levels are acceptable for a given vapor pressure. There are considerable disagreements on the mechanism(s) by which Cr species react with the cathode components [1-5].

This work aims to determine the precise mechanism of Cr contamination. To do so, we have continued [6] to carry out TEM investigations of SOFCs operated (at ANL) under different conditions to better understand the nanoscale microstructural/chemical properties at different stages of Cr contamination. This project is part of a larger effort led by the group at ANL to understand SOFC degradation as a function of operating conditions [6,7]. At ANL, cells were operated in various fuel cell conditions and were characterized electrochemically

as well as microstructurally using scanning electron microscopy, energy dispersive spectroscopy (EDS), and high-energy X-rays at the Advanced Photon Source [7]. TEM complements these spatially averaging techniques by allowing us to locate nanosized grains and interrogate their precise chemistry/structure; for low levels – or the initial stages of – contamination, TEM allows us to identify the location and nature of Cr-contamination. The results will ultimately allow us to determine how SOFC interconnects/cathodes can be optimized to meet Department of Energy goals.

**Approach**

Anode (Ni/YSZ) supported single cells (8YSZ electrolyte and LSM/8YSZ active [mixed] cathode) were purchased from InDEC and operated under various conditions: 700°C and 800°C at several current densities [7]. E-Brite® interconnects were used for current collection on the cathode, and provided the source of chromium. Between the interconnect and the active cathode, an LSM contact paste was applied. A schematic of a cross section of the cell is shown in Figure 1(a). Such single cell SOFCs were run for 500 hours each and the operating conditions, such as temperature and current density, were varied between cells. An example of such performance degradation is given in Figure 1(b) (for a cell run at 700°C, I = -1.15A, active area = 4.6 cm<sup>2</sup>, air with 3% H<sub>2</sub>O at 160 sccm, fuel N<sub>2</sub>:H<sub>2</sub> 1:1 with 3% H<sub>2</sub>O at 400 sccm). Unless otherwise indicated the parameters used were as given above. A list of cell operating conditions is given in Table 1.

To determine the local nature of Cr-poisoning, we developed a cross-sectional TEM specimen fabrication method using a FIB that enables us to locate and later to image precise positions in the LSM/YSZ cathode.

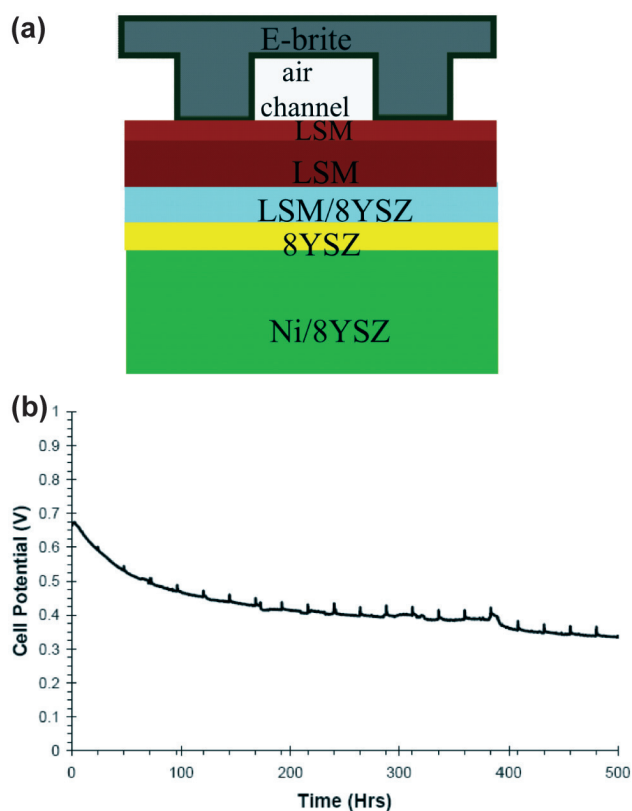


**FIGURE 1.** (a) Schematic cross-section of the cells used in this project. (b) Example of the voltage performance with time under constant current loads (see text for detail).

TEM, scanning transmission electron microscopy (STEM), EDS, chemical mapping, electron energy loss spectroscopy (EELS), and select area electron diffraction (SAED) techniques were used to analyze chemical composition and crystal structures of the Cr-containing

**TABLE 1.** The operational conditions, electrochemical performance (as the percent change in voltage over 1,000 hours), and the observed degradation are given. Here, nanoparticles indicate the observation of (Mn,Cr)<sub>3</sub>O<sub>4</sub> or Cr<sub>2</sub>O<sub>3</sub> species; the locations indicate whether Cr-solids are found at the surfaces of unperturbed LSM or YSZ or filling in the pore spaces; LSM decomposition indicates a range of particles were observed from the destruction of the LSM particles.

#	T (°C)	Inter-connect	I (A)	ΔV Per 1000h (%)	Microstructure Degradation (active cathode)	
					Location of nanoparticles	LSM decomposition
0	700	Au	1.15	0	none	none
1	800	E-brite	0.575	3	YSZ	none
2	800	E-brite	1.15	5	YSZ	none
3	800	E-brite	2.3	20	YSZ/LSM	light
4	700	E-brite	0.575	30	YSZ	none
5	700	E-brite	1.15	60	YSZ/pore-LSM	medium
6	700	E-brite	2.3	225	YSZ/pore-LSM	heavy

phases and investigate how degradation was occurred under the given operating conditions.

## Results

TEM specimens from different locations in the active (mixed) cathode of different fuel cells were studied. In this report, based on the observation made of many cells using TEM, we define degradation as the observation of changes from the original (Sample 0 in Table 1 and shown in Figure 1(a) of Ref. 6) cathode microstructure and the observation of Cr in solid phases; examples include the observation of decomposition products of LSM and of nanoparticles ( $d < 100$  nm) of  $(\text{Cr},\text{Mn})_3\text{O}_4$  and  $\text{Cr}_2\text{O}_3$ . Moreover we define the location of such degradation as: decomposed LSM (in which LSM particles are severely decomposed), LSM or YSZ surfaces (indicating the LSM or YSZ is unperturbed below its surface but that nanoparticles exist on the surface), and in the pores (indicating that the pore space is filling with Cr-containing solid phases and implying that there are nanoparticles not in direct contact with the LSM or YSZ surface). Table 1 summarizes an overall set of observations from these studies, which are described below, as well as listing the numbers of samples discussed in this report.

As discussed in last year's report [6], the amount of degradation (regardless of type) was observed to be largest at the active cathode/electrolyte interface and became less as one moved toward the pure LSM layers (in fact we continue to observe no degradation in the pure LSM layers, regardless of the operational conditions). Figure 2(a) illustrates this more clearly for sample 6 (a cell run under the highest current loads and at  $700^\circ\text{C}$ , which experienced the highest voltage degradation), where the mottled contrast near the YSZ interface is circled as a guide to observe severe degradation. A schematic of this inhomogeneous degradation is given in Figure 2(b). We also always observed a lateral inhomogeneity where the degradation was largest below the center of the landing and decreased slightly as one moved toward the location below the center of the air channel. It should be noted that the lateral variation is less pronounced than the vertical variation (the channel regions still exhibited degradation when significant degradation was observed under the landing), and could arise from variations in the electrochemical conditions or the Cr concentration under the air channel; a description of either is outside the scope of this work.

The degradation observed in the sample shown in Figure 2(a) is shown in schematic form in Figure 2(c). Nanoparticles are observed on the surface of YSZ, on the surface of the decomposed LSM particle, and filling the pores, and the LSM is severely decomposed. In Table 1 this type of degradation corresponds to nanoparticles at YSZ/pores-LSM with heavy LSM

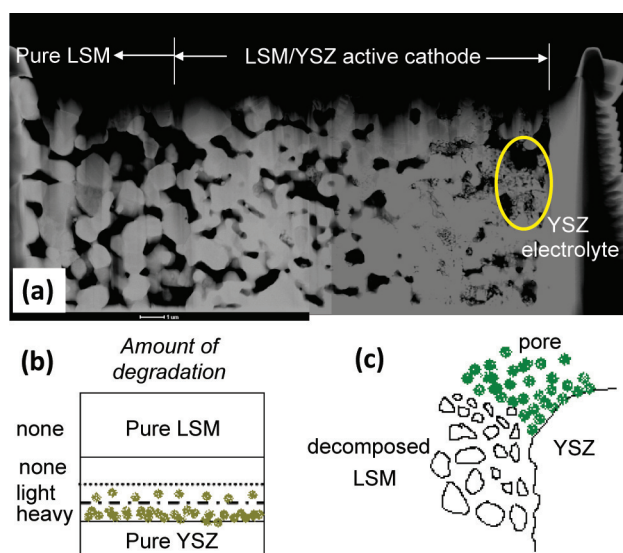


**FIGURE 2.** (a) Bright field image of a cross-section of the Sample 6. The ellipse guides the eye to the location of large-scale degradation. (b) A schematic of the amount of degradation observed in all cells investigated, where the green splotches indicate degradation. (c) The type of degradation observed in the region of highlighted in (a). Green circles indicate Cr- and Mn,Cr-containing nanoparticles on YSZ and in the pores, while white shapes indicate decomposed LSM.

decomposition. One of our goals is to understand the initial microstructural location of Cr-deposition, which cannot be determined by this sample alone.

By increasing the temperature to  $800^\circ\text{C}$ , the degradation rate is slowed and helps capture the initial stages of LSM decomposition. Figure 3(a) shows the bright field image near the YSZ-interface for Sample 4, which shows a diminished microstructural degradation from the Sample 6 [Figure 2(a)]. Figure 3(b) is a higher magnification bright field image showing the nature of the phases determined from STEM, EDS, and SAED (as discussed in Ref. 6). Note that the YSZ particles are covered with a single layer of nanoparticles, that the LSM is decomposed at its surface, and that Cr-containing particles exist at the surface of the LSM particle (not really filling the pores drastically). A schematic of this is shown in Figure 3(a). In Table 1 this type of degradation corresponds to nanoparticles at YSZ/LSM with light LSM decomposition.

Figure 4(a) shows the last kind of degradation that we observed (massive pore-filling was discussed in Ref. 6). Figure 4(a) is a bright field image of a blown-up region of Sample 2, illustrating that light degradation leads to  $\text{Cr}_2\text{O}_3$  and  $(\text{Mn},\text{Cr})_3\text{O}_4$  nanoparticles [6] being observed on YSZ surfaces with clean LSM and triple phase boundaries (TPBs). Figure 4(b) is a schematic of this type of degradation and in Table 1 corresponds to nanoparticles at YSZ surfaces and no LSM degradation (Sample 1, 2, 4). Note that these are the cells with the least amount of degradation and that nanoparticles are

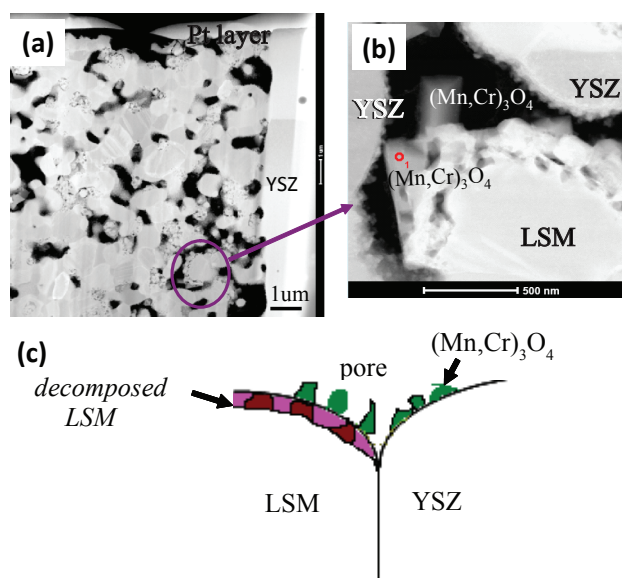


**FIGURE 3.** (a) Bright field image of a cross-section of the Sample 3. The ellipse guides the eye to the location of large-scale degradation. (b) A higher magnification image of the region highlighted in (a). (c) A schematic of the type of degradation observed in the region of highlighted in (a). Green shapes indicate Cr- and Mn,Cr-containing nanoparticles on YSZ and on the old surface of LSM, while purple shapes indicate decomposed LSM surface region.

observed on YSZ for all cells, indicating that this is likely the initial stage of microstructural degradation.

A consistent model for microstructural degradation, based on the literature and our observations, is as follows. Mn-rich islands form on the surface of YSZ and LSM [6] (which we observed both on LSM and YSZ even without Cr) near the interface of the active cathode and YSZ. It is possible that these are reduced Mn-species [2,3], especially in the more reducing portion of the cathode near the YSZ interface where degradation occurs. These Mn-rich islands react with Cr (though we cannot indicate whether it is surface species or gaseous species) and form  $(\text{Cr,Mn})_3\text{O}_4$  [6] nanoparticles on the YSZ surface (see Figure 4(b)), in a manner consistent with thermodynamic and electrochemical preferences [7], leading to higher degradation at lower temperatures/higher overpotential (or current densities). Such nanoparticles then grow (and more nucleate), leading to Cr-rich particles and even  $\text{Cr}_2\text{O}_3$  far away from the nucleation sites (several areas of YSZ were found where the center of the Cr-containing solid area was Mn-rich but the outer regions were  $\text{Cr}_2\text{O}_3$ ). These nanoparticles impact the performance of the cell by either perturbing processes that occur on the surface of YSZ or by blocking electrochemical reactions at the TPBs [1] if (as they grow) they encounter a TPB. The latter seems consistent with degradation being observed in Samples 1, 2, and 4, wherein we observed increasing amount of nanoparticles on YSZ with increasing

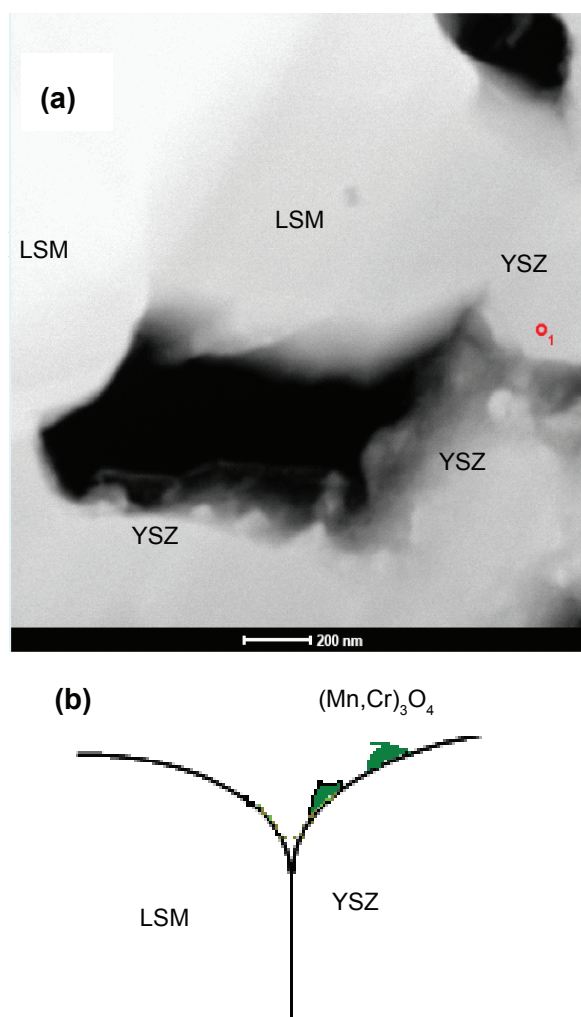


**FIGURE 4.** (a) Bright field image of a cross-section of the Sample 2. (b) A schematic of the type of degradation observed in (a). Green shapes indicate Cr- and Mn,Cr-containing nanoparticles on YSZ.

degradation, which would statistically lead to more TPBs being isolated. By comparing a large set of observations from light and heavy degradation at two temperatures, it seems that the TPB is not the location where nucleation of Cr-solids occurs, owing to the fact that nanoparticles of Cr-containing solids were rarely observed at TPBs unless a large amount of other degradation had occurred elsewhere. (On the other hand, Cr vapor could be captured at TPBs and converted to surface species that then diffuse to and react with Mn-rich islands.)

When the nanoparticles reach the LSM particles they interact with them, leading to both nanoparticle formation on LSM particles and subsequent decomposition of LSM. Both of these occur more readily under high current densities/overpotential. It should be emphasized that we cannot be sure that, under the aggressive conditions to which Samples 3, 5, and 6 were exposed, Cr-solids did not form directly on

LSM surfaces. However, when LSM decomposition was observed, there was also significant coverage of YSZ with Cr-containing solids. In other words, direct attack of Cr-species on LSM (or even Mn-rich islands on LSM) only occurs when the driving force is increased and always occurs with formation of Cr-solids on YSZ. Determining the initial stages of attack on LSM could be investigated by carrying out similar experiments on cells run for less time than 500 hours under identical conditions. Under such conditions, the LSM is then attacked and forms a variety of phases on decomposition and promotes Cr-phase formation into the pores of the cell [6]. These latter events severely degrade the performance of the cell.

### Conclusions and Future Directions

We investigated severely degraded SOFCs and, in combination with earlier work on less degraded cells, developed a model for Cr-attack on InDEC-Cells operated over a range of parameters. Although the features are consistent with earlier works, the details of degradation in real fuel cells were determined using advanced TEM methods and using many different cells. In these cells, both electrochemistry and the existence of Mn-rich islands on surfaces of LSM and YSZ play an important role in the local microstructural degradation. These results imply that by minimizing the Cr-concentration in the cathode by using coatings, by choosing electrochemical parameters that minimize the amount of severely reducing areas in the cell, by minimizing the surface concentration of (reduced) Mn-species, and by choosing a temperature that diminishes the driving force for formation of Cr-species, one can limit the degradation of SOFCs.

### FY 2008 Publications/Presentations

1. "Effects of cell operating conditions on degradation by chromium," T.A. Cruse, B.J. Ingram, M. Krumpelt, S. Wang, and P.A. Salvador, *published* in "TMS 2008 Annual Meeting Supplemental Proceedings Volume 1: Materials Processing and Properties," pp. 571-580 (2008).
2. "Examination of Chromium's Effects on a SOFC Cathode," T. Cruse, M. Krumpelt, B. Ingram, S. Wang, and P. Salvador, *presented* at the 5<sup>th</sup> International Symposium on Solid Oxide Fuel Cells (SOFC)," at 32<sup>st</sup> International Cocoa Beach Conference & Exposition on Advanced Ceramics & Composites, Daytona Beach, January 27 – February 1, 2008.

3. "Investigation of Chromium Contamination in SOFC Cathodes using Transmission Electron Microscopy," S. Wang, T. Cruse, M. Krumpelt, B. Ingram, and P. Salvador, *presented* at the 5<sup>th</sup> International Symposium on Solid Oxide Fuel Cells (SOFC)," at 32<sup>st</sup> International Cocoa Beach Conference & Exposition on Advanced Ceramics & Composites, Daytona Beach, Florida, USA January 27 – February 1, 2008.
4. "Effects of cell operating conditions on degradation by chromium," T. A. Cruse, B. J. Ingram, M. Krumpelt, S. Wang, and P. A. Salvador, *presented* at 2008 TMS Annual Meeting & Exhibition, New Orleans, Louisiana, USA, March 9–13, 2008.

### References

1. K. Hilpert *et al.*, *J. Electrochem. Soc.*, **143**, 3642 (1996).
2. S. Jiang *et al.*, *J. Electrochem. Soc.*, **147**, 4013 (2000).
3. S. Jiang *et al.*, *J. Electrochem. Soc.*, **147**, 3195 (2000).
4. S.C. Paulson and V.I. Birss, *J. Electrochem. Soc.*, **151**, A1961, (2004).
5. A. Hagen *et al.*, *J. Electrochem. Soc.*, **153**, A1165, (2006).
6. P.A. Salvador *et al.*, FY 2007 Office of Fossil Energy Fuel Cell Program Annual Report, US Department of Energy, Paper IV.A.5 (2007).
7. T.A. Cruse *et al.*, in "TMS 2008 Annual Meeting Supplemental Proceedings Volume 1: Materials Processing and Properties," p. 571 (2008).

## IV.A.4 Characterization of Atomic and Electronic Structure of Electrochemically Active SOFC Cathode Surfaces

Meilin Liu (Primary Contact), YongMan Choi,  
Matthew E. Lynch

Georgia Institute of Technology  
771 Ferst Drive  
Atlanta, GA 30332  
Phone: (404) 894-6114; Fax: (404) 894-9140  
E-mail: meilin.liu@mse.gatech.edu

DOE Project Manager: Briggs White  
Phone: (304) 285-5437  
E-mail: Briggs.White@netl.doe.gov

Contract Number: 42735

Start Date: February 13, 2006  
Project End Date: February 12, 2009

### Objectives

- Examine the interactions of oxygen species and cathode materials under solid oxide fuel cell (SOFC) operating conditions (e.g.,  $T = 873$  to  $1,273$  K at  $p_{O_2} = 0.2$  atm).
- Elucidate the mechanisms for oxygen reduction on  $La_{0.5}Sr_{0.5}MnO_{3-\delta}$  and predict rate constants for individual steps.
- Predict surface and bulk properties (e.g., diffusivities) of  $La_{0.5}Sr_{0.5}MnO_{3-\delta}$  and  $La_{0.5}Sr_{0.5}CoO_{3-\delta}$  cathode materials.

### Accomplishments

- The thermodynamic-correction formalism showed that the stability of adsorbed  $O_2$  species on  $LaMnO_3$  depends on adsorption energies, surface orientations, and surface coverage.
- Rate-constant predictions using statistical-theory techniques along with mechanistic studies verified that oxygen vacancies influence the kinetics for  $O_2$  reduction on SOFC cathode materials.
- Diffusivity calculations using transition state theory (TST) manifested that surface mobility and bulk oxygen ion conductivity of  $LaCoO_3$ -based cathode materials are much higher than those of the  $LaMnO_3$ -based ones.

### Introduction

Understanding of detailed mechanisms for oxygen reduction and ionic conduction plays a crucial role in achieving rational design of novel cathode materials for SOFCs. However, it is extremely difficult to experimentally characterize the electrode kinetics due to the complexity of the involved charge and mass transfer processes. We report our computational findings using density functional theory (DFT) and statistical-theory calculations for oxygen reduction and ionic conduction on cathode surfaces, aiming to establish a computational framework for rational design of more efficient  $ABO_3$ -type SOFC cathode materials.

### Approach

DFT calculations [1,2] along with statistical-theory approaches [3] have been used to establish a computational framework for rational design of novel  $ABO_3$ -type cathode materials with fast  $O_2$  reduction kinetics and rapid ionic conduction. The details of the computational methods are described elsewhere [1,2].

### Results

To estimate the adsorption energies of oxygen species on cathode materials under SOFC operating conditions (i.e.,  $p_{O_2} = 0.2$  atm and  $T = 873$  to  $1,273$  K), we considered the effects of temperature and pressure on gas-surface interactions by means of thermodynamic-correction formalism. We examined the thermodynamic properties for  $O_2$ - $LaMnO_3$  interactions with superoxo- and peroxy-like species ( $O_2^-$  and  $O_2^{2-}$ , respectively) at 1/6 coverage. To examine the surface-orientation effect, we applied two typical adsorbed oxygen species on  $LaMnO_3(110)$  (superoxo- and peroxy-like species with the adsorption energies of  $-1.76$  eV and  $-2.20$  eV, respectively) at 1/3 coverage. As shown in Figure 1, molecularly adsorbed oxygen species may be stable at temperatures up to  $\sim 1,050^\circ\text{C}$  at  $p_{O_2} = 0.2$  atm, depending on adsorption energies, surface orientations, and surface coverage. This information is vital to design of experiments for probing oxygen species using vibrational spectroscopy. For example, it is unlikely to observe the superoxo- and peroxy-like species on the (100) surface at high temperatures; on the (110) surface, however, they are much more stable at high temperatures.

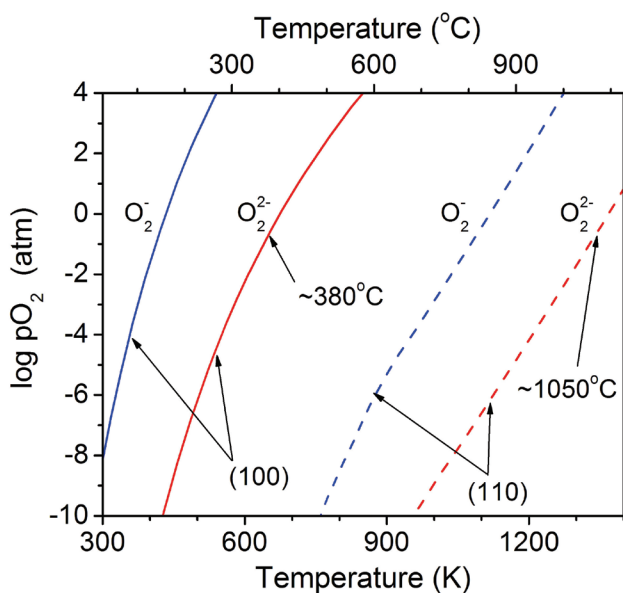


**FIGURE 1.** A Typical Phase Diagram for the Interactions Between  $O_2$  and  $LaMnO_3(100)$  and  $(110)$  Surfaces at  $1/6$  and  $1/3$  Coverage, Respectively

As depicted in Figure 2, for the interaction between  $O_2$  and the  $La_{0.5}Sr_{0.5}MnO_{3-\delta}$  surface, the first step is the formation of the superoxo-like **super-lsm1** intermediate with an exothermicity of 1.36 eV. The **diss-lsm1** species can be produced by overcoming a reaction barrier of 0.36 eV which is much lower than that on the perfect  $LaMnO_3$  ( $\sim 0.45$  eV). This means that oxygen vacancies formed by Sr doping enhance the adsorption of  $O_2$ . Then, the dissociated oxygen species is incorporated into the doubly charged oxygen vacancy ( $V_o^{**}$ ) forming **inc-a1** or **inc-b1** with the same exothermicity of 3.90 eV. The adsorbed oxygen species on **inc-a1** can further diffuse to the Mn ion on **inc-b1** by overcoming a barrier of 2.09 eV. The oxygen species incorporated into the lattice can diffuse away by the hopping mechanism. In addition to molecular adsorption, oxygen molecules can directly be incorporated into oxygen vacancies via **ts3-lsm1**, producing **inc-c1** with an exothermicity of 2.06 eV. The predicted rate constants for the  $O_2$  adsorption process on  $LaMnO_3$  (**lm**) and  $La_{0.5}Sr_{0.5}MnO_{3-\delta}$  (**lsm**) at  $T = 873$  to  $1,273$  K can be represented respectively by  $k_{ads,lm} = 1.30 \times 10^2 T^{2.56} \text{ cm}^3 \text{ s}^{-1}$  and  $k_{ads,lsm} = 3.46 \times 10^2 T^{2.52} \text{ cm}^3 \text{ s}^{-1}$ , where the rate constants are related to the rate equation,  $d[X]_{surf}/dt = k_i(\theta/A_s)[X]_g$ , which has the units of a flux: molecule  $\text{cm}^{-2}\text{s}^{-1}$ . In the rate equation,  $\theta$  represents the fraction of available surface sites,  $A_s$  is the surface area, and  $[X]_g$  is the gas phase concentration of  $O_2$  in molecules  $\text{cm}^{-3}$ . Figure 3 shows the dissociation of adsorbed oxygen species on  $La_{0.5}Sr_{0.5}MnO_{3-\delta}$  dominates over the temperature range studied, leading to the expression of  $k_{diss,lsm} = 2.15 \times 10^{12} \exp[-0.23 \text{ eV}/RT] \text{ s}^{-1}$  at  $P = 1$  atm and  $T = 873 - 1,273$  K. The predicted rate constants on the perfect  $LaMnO_3$  can

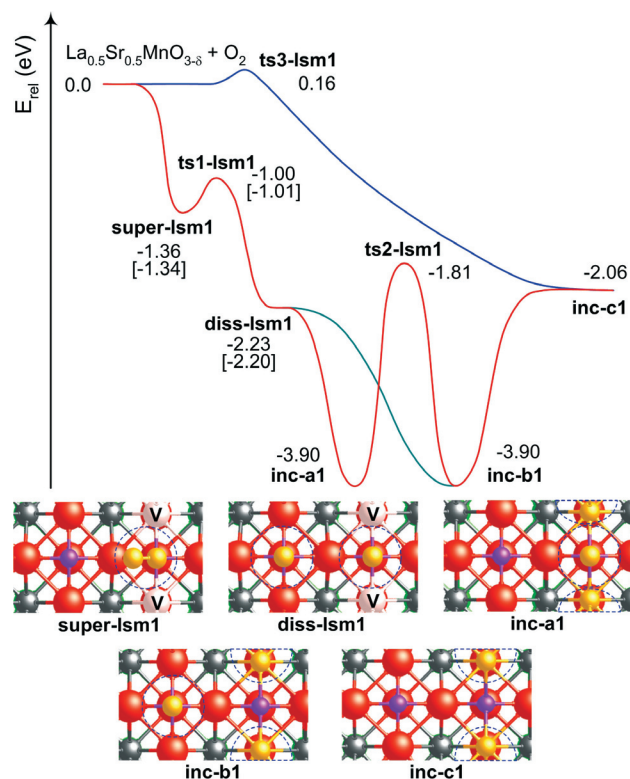


**FIGURE 2.** Potential energy profiles and top views of an intermediate state and products for  $O_2-La_{0.5}Sr_{0.5}MnO_{3-\delta}$  interactions. **V** denotes an oxygen vacancy. Dashed circles and **V** represent adsorbed oxygen species and an oxygen vacancy on the surface, respectively. Relative energies in brackets are ZPE-corrected.

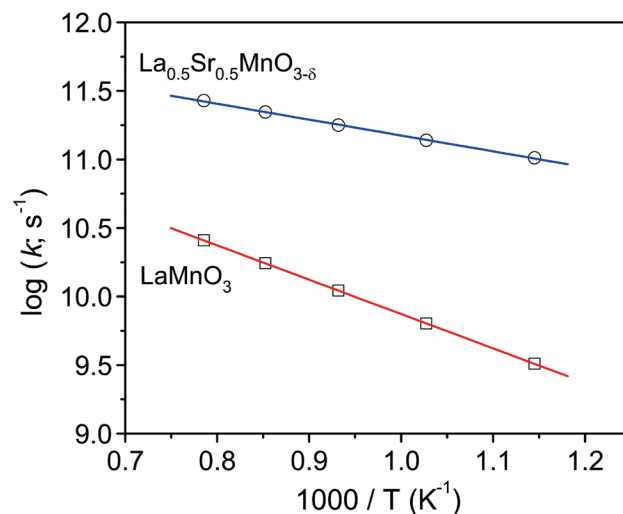


**FIGURE 3.** Comparison of predicted rate constants for the dissociation process of  $O_2$  on the perfect  $LaMnO_3$  and  $La_{0.5}Sr_{0.5}MnO_{3-\delta}$ . Solid lines are fitted using the linear-squared method.

be expressed:  $k_{\text{diss,lm}} = 2.35 \times 10^{12} \exp[-0.50 \text{ eV}/RT] \text{ s}^{-1}$ . Our rate-constant predictions along with the mechanistic studies verify that oxygen vacancies influence  $\text{O}_2$  kinetics on SOFC cathodes. The predicted rate constants may be employed for kinetic modeling on the operation of a practical SOFC system.

Understanding surface diffusion of oxygen species on the cathode in SOFCs is very crucial to rational design of efficient cathode materials since surface diffusivity is closely related to the incorporation of oxygen into the lattices of cathodes or electrolytes, including diffusion to triple-phase boundaries (TPBs). Bulk diffusivities of oxygen ions in the cathode are also a significant factor because of the direct relevance to ionic conductivity. Characterizing the two diffusion phenomena under SOFC operating conditions is very important for the development of novel cathode materials; to the best of our knowledge, little information is available in the literature due to the difficulty of experimentally distinguishing the two properties. In this study, we predicted surface and bulk diffusivities of oxygen species on and in  $\text{La}_{0.5}\text{Sr}_{0.5}\text{MnO}_{3-\delta}$  (**LSM50**) and  $\text{La}_{0.5}\text{Sr}_{0.5}\text{CoO}_{3-\delta}$  (**LSC50**). In order to estimate surface and bulk diffusivities, we applied TST. The (100) surface was applied for the characterization of the surface interactions, while the (110) surface was used for bulk property calculations. As shown in Figure 4a, an adsorbed oxygen species at the Mn ions on **LSM50** can migrate on the surface with a well-defined transition

state. In particular, the reaction barrier for **LSC50** is much lower than that for **LSM50** (1.09 eV vs. 1.93 eV). Therefore, one can expect that the hopping of adsorbed oxygen species on **LSC50** occurs more easily than on **LSM50**. As shown in Figure 4b, our TST predictions of surface diffusivities clearly support that LSC-based cathode materials have a much higher mobility than LSM-based ones. Similar to the predictions of surface diffusivities of adsorbed oxygen species, we also predicted bulk diffusivities of oxygen ions in **LSM50** and **LSC50**, showing that oxygen ion conduction through LSC-based cathode materials is much faster than that through LSM-based ones.

## Conclusions and Future Directions

In the past year, we have established a computational framework to predict diffusivities of oxygen species using first-principles-based calculations to provide more insight into rational design of efficient cathode materials. We demonstrated that surface diffusion is correlated with ionic transport. Future studies are briefly outlined as follows:

- The predicted diffusivities will be applied for continuum modeling to examine electrochemical properties of SOFCs. These values are directly applicable to our continuum models that examine transport/kinetics inside and on the surface of mixed ionic electronic conductors.

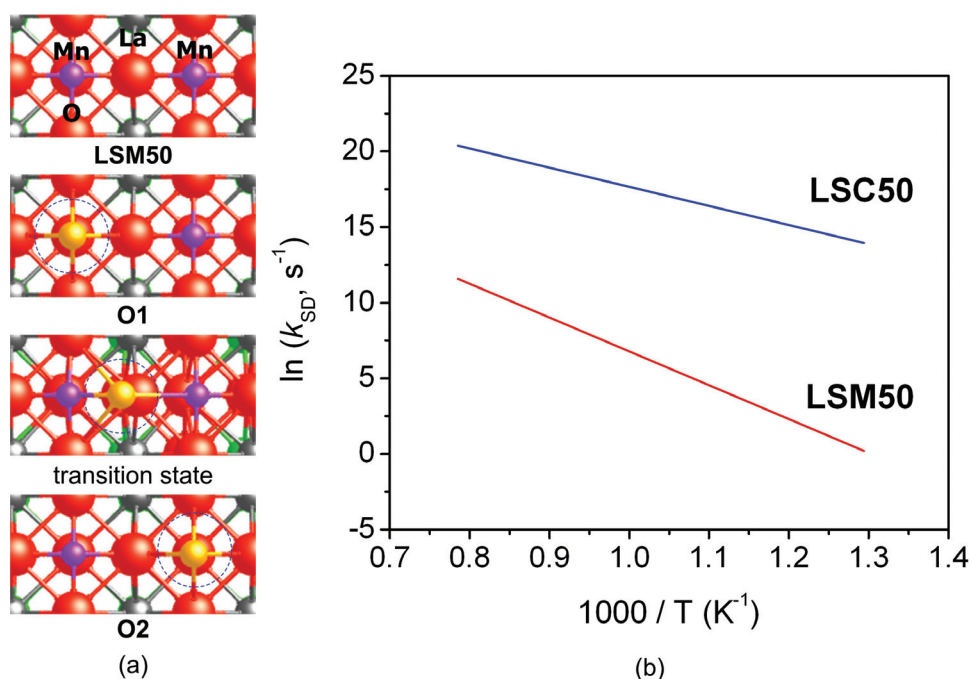


**FIGURE 4.** (a) Top views of the **LSM50(100)** surface model and stable states (**O1** and **O2**) and a transition state of adsorbed oxygen species on **LSM50**. (b) Predicted surface diffusivities ( $k_{\text{SD}}$ ) of adsorbed oxygen species on **LSM50** and **LSC50**.

- In addition to diffusivities, the techniques employed here will be used in the future to obtain estimates of other surface parameters, including reaction rate constants for adsorption, incorporation, and TPB reactions. Continued use of first-principles calculations will aid our understanding of electrochemical performance of SOFCs using multi-scale modeling.

### Special Recognitions & Awards/Patents Issued

1. Invited participant in US-Japan Frontier of Engineering – National Academy of Engineering, Nov. 4-6, 2007.
2. Invited editorial board member, "Research Letters in Materials Science," <http://www.hindawi.com/journals/rlms/editors.html>.
3. Invited editorial board member, "Advances in Materials," <http://www.hindawi.com/journals/ams/editors.html>.

### FY 2008 Publications/Presentations

#### Publications

1. Y.M. Choi, M.C. Lin, M. Liu, "Computational Study on the Catalytic Mechanism toward Oxygen Reduction on  $\text{La}_{0.5}\text{Sr}_{0.5}\text{MnO}_3(110)$  in Solid Oxide Fuel Cells," *Angewandte Chemie, International Edition*, 46, 7214-7219, 2007.
2. Y.M. Choi, D.S. Mebane, J.H. Wang, and M. Liu, "Continuum and Quantum-Chemical Modeling of Oxygen Reduction on the Cathode in a Solid Oxide Fuel Cell," *Topics in Catalysis (Invited)*, 46, 386-401, 2007.
3. D.S. Mebane, Y.J. Liu, and M. Liu, "Refinement of the Bulk Defect Model for  $\text{La}_x\text{Sr}_{1-x}\text{MnO}_{3\pm\delta}$ ," *Solid State Ionics*, 178, 1950-1957, 2008.

4. J.H. Wang, Y.M. Choi, and M. Liu, "Quantum Chemical Calculations of Surface and Interfacial Reactions in Solid Oxide Fuel Cells," In *Quantum Chemical Calculations of Surfaces and Interfaces of Materials* (Editors: V. A. Basiuk and P. Ugliengo), Chapter 14, p.p. 289-304, American Scientific Publishers, Los Angeles, 2008.
5. M.E. Lynch, D.S. Mebane, Y. Liu and M. Liu, "Triple Phase Boundary and Surface Transport in Mixed Conducting Patterned Electrodes," *Journal of the Electrochemical Society*, 155, B635-B643, 2008.
6. Y.M. Choi, M.C. Lin, and M. Liu, "A computational framework for characterization of  $\text{O}_2$  kinetics on undoped and Sr-doped  $\text{LaMnO}_3$  cathode materials for solid oxide fuel cells," *Journal of Physical Chemistry C*, submitted.

#### Presentations

1. H. Abernathy, Z. Cheng, X. Lou, and M. Liu, "Probing and mapping SOFC anode reactions using *in situ* Raman spectroscopy," 233<sup>rd</sup> ACS National Meeting, IL, 2007.

#### References

1. Y.M. Choi, D.S. Mebane, M.C. Lin, M. Liu, "Oxygen Reduction on  $\text{LaMnO}_3$ -based Cathode Materials in Solid Oxide Fuel Cells," *Chemistry of Materials*, 19, 1690-1699, 2007.
2. Y.M. Choi, M.C. Lin, M. Liu, "Computational Study on the Catalytic Mechanism toward Oxygen Reduction on  $\text{La}_{0.5}\text{Sr}_{0.5}\text{MnO}_3(110)$  in Solid Oxide Fuel Cells," *Angewandte Chemie, International Edition*, 46, 7214-7219, 2007.
3. K.J. Laidler, *Chemical Kinetics*, Harper and Row, New York, 1987.

## IV.A.5 Functionally Graded Cathodes for Solid Oxide Fuel Cells

Meilin Liu (Primary Contact), Lei Yang, Ze Liu, Jaewung Lee

Georgia Institute of Technology  
School of Materials Science and Engineering  
771 Ferst Drive  
Atlanta, GA 30332-0245  
Phone: (404) 894-6114; Fax: (404) 894-9140  
E-mail: meilin.liu@mse.gatech.edu

DOE Project Manager: Briggs White

Phone: (304) 285-5437  
E-mail: Briggs.White@netl.doe.gov

Contract Number: 41572

Start Date: May 1, 2007

Project End Date: April 30, 2008

losses arise in the cathode, more so at lower operating temperatures. One of the reasons that LSCF shows much better performance than LSM is because LSCF has much higher ionic and electronic conductivity than LSM, extending the active sites beyond the triple-phase boundaries to the entire surface of the LSCF [1]. One obvious downfall for LSCF is that it reacts adversely with yttria-stabilized zirconia (YSZ), which can be mitigated by the use of a buffer layer of doped-CeO<sub>2</sub> between LSCF and YSZ [2]. However, the catalytic activity of the stand-alone LSCF cathodes is likely to be limited by the surface catalytic properties. Further, the long-term stability of LSCF cathodes is a concern. Thus, it is hypothesized that the *performance* and *stability* of a porous LSCF cathode may be improved by the application of a catalytically active coating through infiltration [3]. The selection of the catalytic materials as well as the detailed microstructures of the porous LSCF and the catalyst layer may critically impact the performance of the proposed cathodes. The objective of this project is to validate the hypothesis and to optimize the composition and morphology of the catalyst layer and microstructure of the LSCF backbone for better performance.

### Objectives

- Determine if the *stability* and/or *catalytic properties* (or the performance) of porous La<sub>x</sub>Sr<sub>1-x</sub>Co<sub>y</sub>Fe<sub>1-y</sub>O<sub>3-δ</sub> (LSCF) cathodes can be further enhanced by infiltration of other catalytically active materials.
- Investigate the effect of surface modification of porous LSCF (by infiltration of another catalyst) on the area-specific polarization resistance.
- Evaluate stability of infiltrated cathodes.

### Accomplishments

- Designed a cell testing configuration for determining the surface catalytic properties of candidate infiltration catalysts.
- Developed a methodology for optimizing the thickness of infiltrated catalyst coatings.
- Fabricated high quality thin films of cathode materials for evaluating their intrinsic catalytic activities.
- Demonstrated that the surface activity of LSCF can be improved by infiltration of suitable catalysts.
- Demonstrated that LSCF cathodes infiltrated with a thin coating of La<sub>x</sub>Sr<sub>1-x</sub>MnO<sub>3±δ</sub> (LSM) have improved performance stability.

### Approach

Our novel cathode consists of a porous backbone of high ionic and electronic conductivity (such as LSCF) infiltrated with a thin coating of catalysts having high stability and catalytic activity toward O<sub>2</sub> reduction. The novelty of our cathodes is in the selection and the detailed microstructure of materials that create a better performing cathode. The hypothesis is that the performance of such a cathode can be enhanced by either improving the transport properties of the backbone or the catalytic activity of the catalyst, or both. The uniqueness of this approach is to integrate materials of different properties and make the best use of them. Since LSCF has excellent ionic and electronic conductivity, the performance of stand-alone LSCF cathodes is likely limited by the surface catalytic activity. Thus, infiltrating a porous LSCF backbone with a catalytically active coating material to enhance the catalysis of oxygen reduction at the gas-solid interface should further enhance the performance of the cathodes.

### Results

#### Demonstration of Surface Limitations

Shown in Figure 1 are the interfacial polarization resistances of a dense LSCF electrode deposited on a gadolinia-doped ceria electrolyte with a highly

### Introduction

The cathode is an important area of solid oxide fuel cell (SOFC) development since most of the cell power

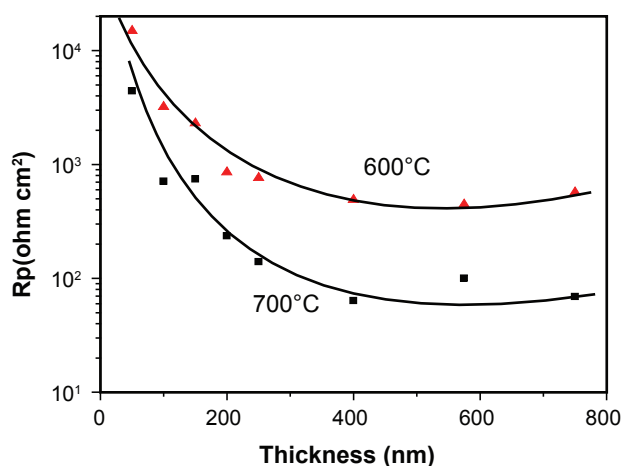


**FIGURE 1.** Polarization Resistances of Dense LSCF Electrodes of Different Thickness (Prepared by Sputtering) Measured in a Cell with a Porous Counter Electrode at 600 and 700°C

porous counter electrode. The polarization resistances decreased initially with the thickness of the LSCF layers until about 400 nm, implying that a minimum of 400 nm is needed to minimize the effect of sheet resistance. Further, the polarization resistance increased as the oxygen partial pressure was reduced, suggesting that it is the surface catalytic property (not the bulk transport property) that limits the performance of such a dense LSCF electrode. If it is limited by the ionic transport across the LSCF layer, the polarization resistance should decrease as the oxygen partial pressure is reduced since oxygen vacancy concentration and ionic conductivity are increased. Indeed, the electrode polarization resistance should decrease with the concentration of reactants (oxygen in this case).

#### Performance of Cells with SSC or LSM Infiltrated Porous LSCF Electrodes

Shown in Figure 2 are some typical scanning electron microscopy pictures of porous LSCF electrodes with or without a coating of small strontium samarium cobalt oxide (SSC) particles introduced by an infiltration process [4]. The polarization resistance ( $R_p$ ) of LSCF cathodes infiltrated with different concentrations of SSC, as determined using impedance spectroscopy, decreased with the concentration of SSC precursor solution, as shown in Figure 3. The performance of the LSCF backbone infiltrated with LSCF showed only slight improvement, suggesting that SSC infiltration has significantly improved the performance of LSCF due to its higher surface catalytic activity toward oxygen reduction.

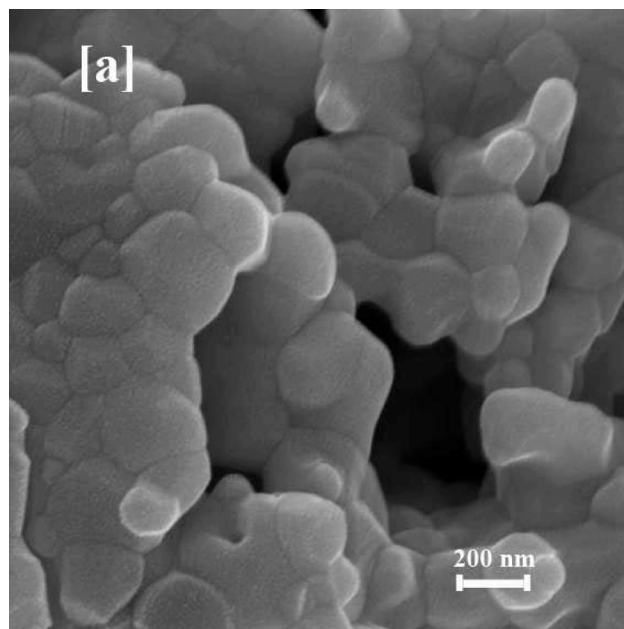


**FIGURE 2.** Cross-sectional images of porous LSCF cathodes: (a) blank LSCF and (b) LSCF infiltrated with SSC (concentration of SSC solution: 1.44 mol/L).

#### Stability

The stability and performance of test cells with LSCF cathodes infiltrated with LSM and SSC have been tested for about 100 hours. Shown in Figure 4 are the cell voltages of two test cells, with and without infiltration of LSM, as a function of time under a constant current of 833 mA/cm<sup>2</sup> at 825°C. The cell infiltrated with LSM showed higher terminal voltage and better stability compared with the blank cell without LSM infiltration.

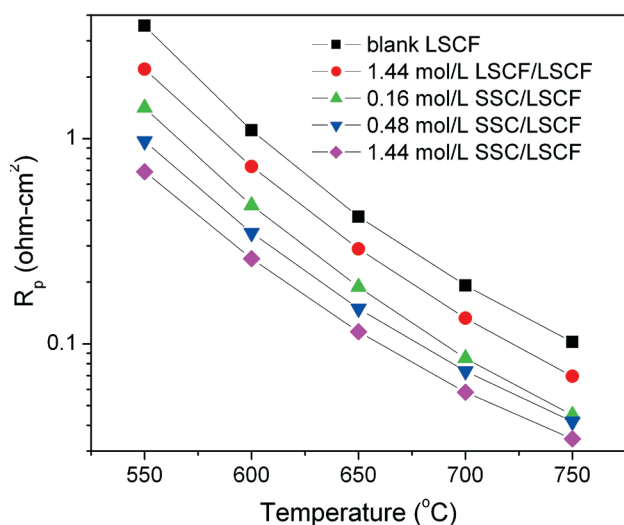


**FIGURE 3.** Electrode Polarization Resistances of Porous LSCF Electrodes Infiltrated with Different Concentrations of SSC

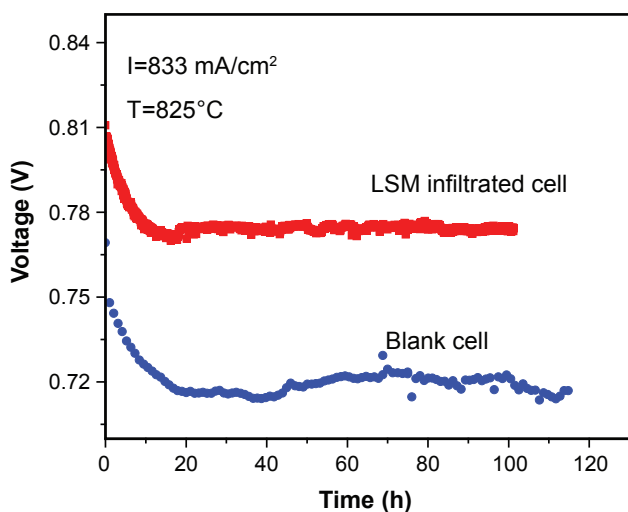


**FIGURE 4.** Terminal Voltages of Test Cells with LSCF Cathodes with and without Infiltration of 0.0312 M LSM, as Measured Under a Constant Current of 833 mA/cm<sup>2</sup> at 825°C

## Conclusions

We have successfully developed a platform for reliably evaluating the surface catalytic properties of cathode materials. It is confirmed that the surface catalytic activity limits the performances of LSCF-based cathodes. Also, the stability and performance of LSCF-based cathodes have been enhanced by infiltration of a catalytically active coating. However, several fundamental questions still remain; it is not clear why the degradation rates of LSCF cathodes are relatively high, what the degradation mechanism is, and why a LSM coating improves the stability of LSCF cathodes. While the concept feasibility of the electrode architecture is demonstrated, other catalytically more active catalysts and more conductive matrixes are yet to be identified or developed for further enhancement of the performance and stability of SOFC cathodes. Further, the long-term stability of the interfaces (e.g., LSM/LSCF) is yet to be confirmed.

## References

1. S. Shaffer, "Development update on Delphi's solid oxide fuel cell power system", technical report, Delphi Corporation, 2006.
2. S.P. Simner, M.D. Anderson, M.H. Engelhard, and J.W. Stevenson, "Degradation Mechanisms of La-Sr-Co-Fe-O SOFC Cathodes", *Electrochemical and Solid-State Letters*, 9(10) A478-A481, 2006.
3. D. Mebane, M. Liu, L. Wilson, W. Surdoval, "Novel cathode design for solid oxide fuel cells using particle infiltration technology", Provisional Patent Application, April 2007.
4. T.Z. Shoklapper, C. Lu, C.P. Jacobson, S.J. Visco, and L.C. De Jonghe, "LSM-infiltrated solid oxide fuel cell cathodes", *Electrochemical and Solid-State Letters*, 9(8): A376-A378, 2006.

## IV.A.6 Development of Metal Supported SOFC

Steven J. Visco (Primary Contact),  
Craig Jacobson, and Lutgard De Jonghe  
Lawrence Berkeley National Laboratory (LBNL)  
Materials Science Division  
Berkeley, CA 94720  
Phone: (510) 486-5821; Fax: (510) 486-4881  
E-mail: sjvisco@lbl.gov

DOE Project Manager: Briggs White  
Phone: (304) 285-1336  
E-mail: Briggs.White@netl.doe.gov

Contract Number: MSD-NETL-01

Start Date: October 1, 2007  
Project End Date: September 30, 2008

### Objectives

- Development of technologies enabling improvement of solid oxide fuel cell (SOFC) performance at equivalent (or lower cost) relative to existing SOFC components.
- Target high risk/high benefit strategies and basic science (rather than incremental engineering advances that are better suited to industrial developers).
- Characterization of performance improvement.
- Transfer of technology to industrial teams, national labs, and/or university teams.

### Accomplishments

- Demonstrated stable short-term performance of a Ni-scandia stabilized zirconia (SSZ) anode supported cell with doped ceria infiltration at 800 ppm H<sub>2</sub>S.
- Designed and fabricated standard 2-cell 5 cm x 5 cm test stacks as a platform for testing (standard stacks are now available through McAllister Technical Services and through FuelCellMaterials.com).
- Improved Cr tolerance of strontium doped lanthanum manganate-yttria stabilized zirconia (LSM-YSZ) cathodes in the presence of Cr vapor with ceria interconnected nanoparticulate coating.
- Determined trend line from stainless steel oxidation experiments indicating a time greater than 50,000 hours at 700°C before chromia scale will show any noticeable spallation for surface modified 430 alloy.

### Introduction

The main focus of the LBNL project is to support industrial Solid State Energy Conversion Alliance (SECA) teams in their effort to commercialize SOFC technology that meets the SECA performance and cost targets. In order to achieve this goal, it is necessary to improve the performance of SOFC components through the introduction of novel yet inexpensive techniques such as infiltration to improve the low temperature performance of conventional air cathodes and improve the sulfur tolerance of the fuel electrode. Such innovations may allow the industrial developers to lower the operating temperature of SOFC systems and/or tolerate larger thermal gradients while maintaining high system efficiency. Over the last decade, many SOFC developers have focused on replacing ceramic components with metallic ones (particularly interconnect plates) in an effort to further reduce SOFC stack costs and improve system reliability. If successful, this approach could lead to a cost competitive system and penetration of the clean energy market. Among the various commercial (and specialty) alloys studied, it is relatively clear that the ferritic steels (particularly the 400 series) are the best option due to the slow growth (and reasonable electronic conductivity) of the Cr<sub>2</sub>O<sub>3</sub> scale, and the close match of the thermal expansion coefficient with that of the other stack components. The introduction of stainless steel into the SOFC stack also constrains the operating temperature range to about 600-800°C.

### Approach

Accordingly, in fiscal year 2008 the LBNL core effort has been focused on the following issues:

1. Infiltration of perovskites and other appropriate catalysts into composite cathodes to form a interconnected network nanoparticulate coating;
2. Determination of baseline performance and long-term stability of infiltrated and non-infiltrated commercial electrodes;
3. Infiltration of ceria and other appropriate materials into Ni-zirconia anodes to improve sulfur and coking tolerance;
4. Design and fabrication of 2-cell stack for national labs and industrial teams as a standard platform for testing electrodes, interconnects, contact paste, and seals in a manner that allows reliable comparison across research teams.

## Results

### Performance of Ni-zirconia Anodes in the Presence of Sulfur

A Ni-SSZ anode supported cell with an SSZ electrolyte was infiltrated with ceria using the LBNL technology and tested with 800 ppm H<sub>2</sub>S/balance H<sub>2</sub>. The power density shown in Figure 1 shows an initial drop after the introduction of H<sub>2</sub>S and then relatively stable performance for the next 50 hours of testing. These preliminary tests are under sufficiently high sulfur levels so as to accommodate any commercial or military fuel, suggesting that with further optimization of the anode microstructure and infiltration composition, stable sulfur tolerant anodes can be achieved using the conventional composite Ni-zirconia material set.

### Standard 2-Cell Test Stack

The standardized stack test platform shown in Figure 2 was completed and a 2-cell stack tested. This will allow testing of electrodes, seals, contact pastes, in a uniform manner and allows comparison of results between labs, universities, and industry. The design fits in inexpensive furnaces suitable for university labs. This stack is not intended as a precursor to commercial device but as a common test platform available from a commercial supplier.

### Cr Vapor Effects on Composite Cathodes Infiltrated with Ceria

Anode supported cells with conventional LSM-YSZ cathodes are known to degrade in the presence of Cr vapor and means of preventing or decreasing the degradation are needed. LBNL has developed a low-cost metal salt infiltration technology to boost the performance of the air electrode, particularly at temperatures below 700°C, and in this fiscal year we

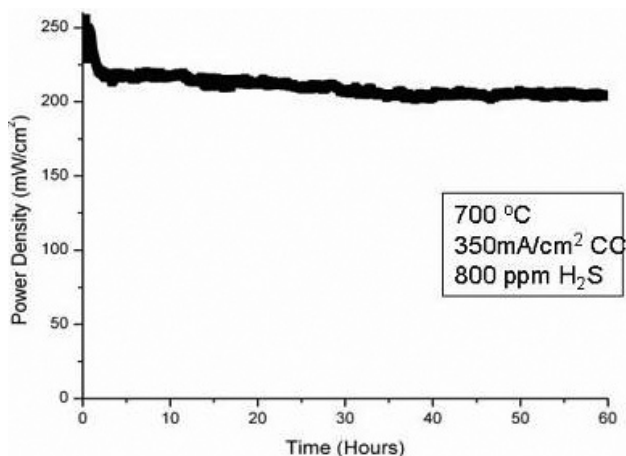


FIGURE 1. Power Density versus Time after Introducing 800 ppm H<sub>2</sub>S

determined the effect of ceria nanoparticulate coatings on tolerance to Cr vapor. Ceria infiltrated cells and non-infiltrated cells were tested at 700°C in the presence of air saturated with Cr vapor. Figure 3 shows the voltage drop of LSM-YSZ cathodes in the presence of steel with and without infiltrated ceria. The ceria infiltration greatly reduces the degradation of the cathode, however, it does not eliminate the degradation of the cell performance under the influence of chromium

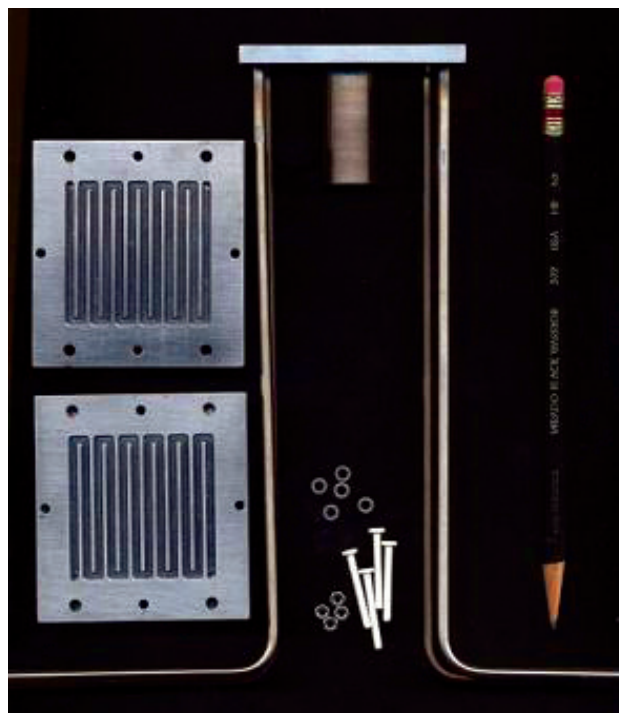


FIGURE 2. LBNL Designed 2-Cell Test Stack

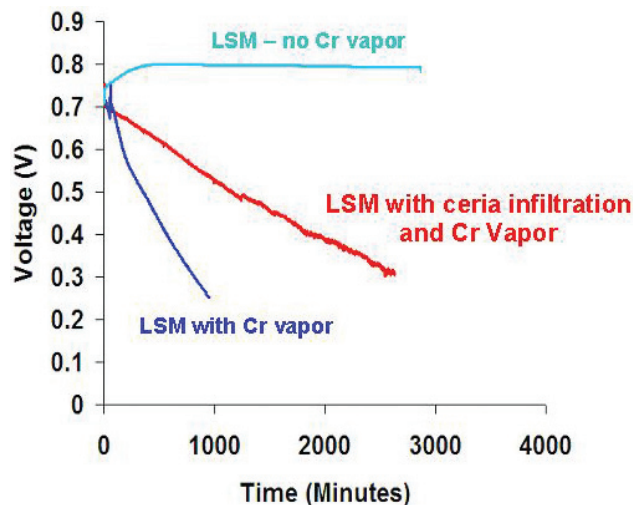
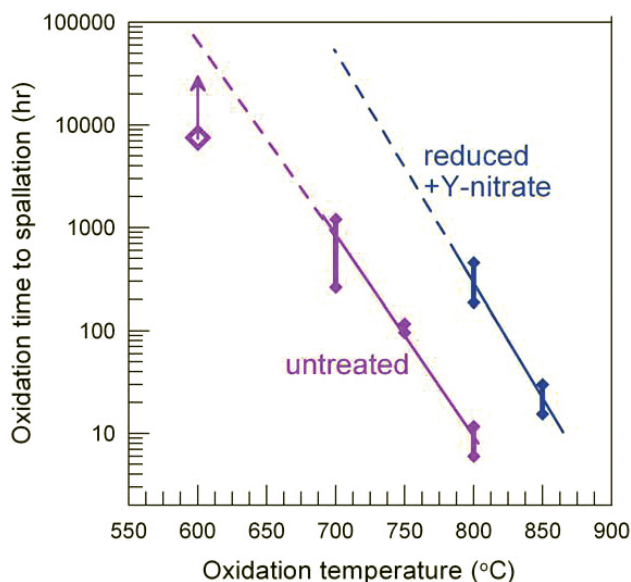


FIGURE 3. Voltage Drop of LSM Cathodes in the Presence of Steel with and without Infiltrated Ceria

contamination. Future work will investigate the mechanism of the improved performance.

### Effect of Surface Treatment on 430 Stainless Steel Scale Spallation

This work focused on determining the effect of various surface treatments on 430 stainless steel. Oxidation work was done in air between 600-850°C for various lengths of time. The time to spallation was determined by scanning electron microscopy of a series of samples oxidized for different lengths of time at a given temperature. Adhesion strength was measured using a tensile test via gluing a stub onto the surface of the oxide. Primary failure mechanism in oxide spallation was the formation of voids at the oxide/alloy interface. Voids formed preferentially along polishing marks or alloy grain boundaries, making polishing techniques none desirable. Sandblasting and firing in a reducing atmosphere prior to oxidation gave rise to noticeably improved scale adhesion. The effect of the former was to create a tortuous oxide/alloy interface and of the latter was to remove surface impurity, which resulted in the lowest interface void density and hence the highest adhesion strength. Combining the reducing treatment with a Y-nitrate surface coating further enhanced scale adhesion, shifting the failure location from the oxide/alloy interface to within the oxide. The range of oxidation time at which spallation took place after isothermal oxidation and fast cooling to room temperature, for the untreated and the reduced plus yttrium nitrate coated 430 stainless steel time is shown in Figure 4. The untreated sample oxidized at 600°C for



**FIGURE 4.** Range of Oxidation Time at Which Spallation Took Place after Isothermal Oxidation and Fast Cooling to Room Temperature, for the Untreated and the Reduced Plus Yttrium Nitrate Coated 430 Stainless Steel

the longest time did not show any spallation; the arrow points to expected longer failure time. Extrapolation from the trend line indicates a time greater than 50,000 hours at 700°C before the scale will show any noticeable spallation. These findings identify a simple surface modification technique for  $\text{Cr}_2\text{O}_3$ -forming metallic components whether independently or beneath a protective coating.

### Conclusions and Future Directions

- The LBNL approach specifically targets low-cost alternatives and/or modifications to existing SOFC technology.
- Improvement of low-temperature performance of air electrodes through infiltration could improve current distribution in the stack, reduce thermal stresses and improve stack lifetime. Long-term testing of commercially available cells is ongoing.
- Infiltration process technology should be inexpensive to implement in a commercial product and raw materials costs are low. The technology has been transferred to a number of labs and companies.
- Improved sulfur tolerance of anodes due to infiltration could substantially lower the cost of sulfur cleanup needed for coal-based SOFCs. Testing infiltrated anodes with coal gas is the next logical step.
- Development of Cr tolerant cathodes could extend the life of metal-based stacks. The mechanism of the improved performance will be determined.
- Development of a standard stack platform should facilitate comparison of stack data between teams; stack design has been transferred to U.S. companies (McAllister Technical Services and FuelCellMaterials.com).
- Extrapolation from the oxidation trend line of surface modified 430 stainless steel indicates a time greater than 50,000 hours at 700°C before the scale will show any noticeable spallation.

### Special Recognitions & Awards/Patents Issued

1. Doctor of Philosophy in Materials Science and Engineering and the Designated Emphasis in Nanoscale Science and Engineering, University of California, Berkeley, awarded to Tal Sholklapper, December 2007.
2. Low cost fuel cell project winner of UC Berkeley's Center for Entrepreneurship & Technology Clean Tech Innovation Prize, April 2008.

**FY 2008 Publications/Presentations**

1. P.E. Gannon, V.I. Gorokhovskiy, M.C. Deibert, R.J. Smith, A. Kayani, P.T. White, S. Sofie, Zhenguo Yang, D. McCready, S. Visco, C. Jacobson, H. Kurokawa, "Enabling inexpensive metallic alloys as SOFC interconnects: An investigation into hybrid coating technologies to deposit nanocomposite functional coatings on ferritic stainless steels", **International Journal of Hydrogen Energy**, Volume 32, Issue 16, pages 3672-3681, November 2007.
2. M. Tucker, G. Lau, C. Jacobson, L. De Jonghe, S. Visco, "Stability and robustness of metal-supported SOFCs", **Journal of Power Sources**, Volume 175, Issue 1, pages 447-4513, January 2008.
3. T. Sholklapper, V. Radmilovic, C. Jacobson, S. Visco, L. De Jonghe, "Nanocomposite Ag-LSM solid oxide fuel cell electrodes", **Journal of Power Sources**, Volume 175, Issue 1, pages 206-210, January 2008.
4. I. Belogolovskiy, P. Hou, C. Jacobson, S. Visco, "Chromia scale adhesion on 430 stainless steel: Effect of different surface treatments", **Journal of Power Sources**, Volume 182, Issue 1, pages 259-264, July 2008.
5. M. Tucker, G. Lau, T. Sholklapper, C. Jacobson, S. Visco, L. DeJonghe, "Metal Supported SOFCs", presentation at **Fuel Cell Seminar and Exposition**, San Antonio, TX, October 15-19, 2007.
6. Craig Jacobson, "Solid Oxide Fuel Cells", **San Francisco Electrochemical Society Short Course on Fuel Cells**, Berkeley California, November 9, 2007.
7. T. Sholklapper, C. Jacobson, S. Visco, L. De Jonghe, "Long-Term Stability of Infiltrated Commercially Available SOFC Cathodes", presentation at **32<sup>nd</sup> International Conference & Exposition on Advanced Ceramics and Composites**, Daytona Beach, FL, January 27 - February 1, 2008.
8. G. Lau, M. Tucker, C. Jacobson, S. Visco, L. De Jonghe, "Mechanism of Chromium Transport on Cathode Materials of Solid Oxide Fuel Cell", presentation at **32<sup>nd</sup> International Conference & Exposition on Advanced Ceramics and Composites**, Daytona Beach, FL, January 27 - February 1, 2008.
9. M. Tucker, G. Lau, C. Jacobson, L. De Jonghe, S. Visco, "Longevity of Metal-Supported SOFCs", presentation at **32<sup>nd</sup> International Conference & Exposition on Advanced Ceramics and Composites**, Daytona Beach, FL, January 27 - February 1, 2008.
10. T. Sholklapper, C. Jacobson, S. Visco, L. De Jonghe, "Enhanced Sulfur/Coking Tolerance of Infiltrated Ni-YSZ Anodes", presentation at **32<sup>nd</sup> International Conference & Exposition on Advanced Ceramics and Composites**, Daytona Beach, FL, January 27 - February 1, 2008.
11. S. Visco, "Development of Metal Supported SOFC", **SECA Core Peer Review**, Pittsburgh, PA, April 21-24, 2008.
12. M. Sogaard, T. Sholklapper, M. Wandel, M. Mogensen, "Infiltration of SOFC Cathodes", presentation at **8<sup>th</sup> European SOFC Forum**, Lucerne, Switzerland, June 30 - July 4, 2008.
13. M. Tucker, T. Sholklapper, C. Jacobson, L. De Jonghe, S. Visco, "Overview of Metal-Supported SOFCs", presentation at **8<sup>th</sup> European SOFC Forum**, Lucerne, Switzerland, June 30 - July 4, 2008.
14. S. Visco, C. Jacobson, T. Sholklapper, G. Lau, L. De Jonghe, "Development of Metal Supported SOFC", **9<sup>th</sup> Annual SECA Workshop**, Pittsburgh, PA, August 5-7, 2008.

## IV.A.7 Local Electronic Structure and Surface Chemistry of SOFC Cathodes

Bilge Yildiz (Primary Contact) and  
I. Burc Misirlioglu

Massachusetts Institute of Technology (MIT)  
Nuclear Science & Engineering Department  
77 Massachusetts Avenue, 24-210  
Cambridge, MA 02139  
Phone: (617) 324-4009; Fax: (617) 258-8863  
E-mail: byildiz@mit.edu

DOE Project Manager: Briggs White

Phone: (304) 285-5437  
E-mail: Briggs.White@netl.doe.gov

Contract Number: 49071

Start Date: June 2007  
Project End Date: May 2009

after electrochemical treatment, using STM and identified their current-voltage (I-V) characteristics.

- Characterized the electrochemical features of the LSM and LSC cathode films grown on YSZ single crystal substrates at three different thicknesses. Found out that surface reactions were the rate-limiting transport process in nearly all cathode films.
- Identified the Mn-enrichment and La-depletion on the surface of the 100 nm-LSM cathode films on 0.7Nb-STO using Auger electron spectroscopy (AES) with depth profiling. Such segregation behavior is contrary to the La- and Sr-segregation on LSM on YSZ, and is likely to impact the surface electronic properties and the electrochemical activity of the cathode films.
- Using the STM, found that fine segregate particles of few-nm size exist on the surfaces of the 100 nm-LSM film, and a clear re-texturing of the cathode films takes place upon high temperature electrochemical treatment.

### Objectives

- Determine the key correlations between the stable structural and electronic bonding properties at  $\text{La}_{1-x}\text{Sr}_x\text{MnO}_3$  (LSM) and  $\text{La}_{1-x}\text{Sr}_x\text{CoO}_3$  (LSC) thin film cathode surfaces, in the presence of inhomogeneities such as grain boundaries, segregate particles and crystallographic domains.
- Examine the role of strain state in the cathode film introduced by the substrate and film thickness, and use this information to design favorable cell geometries.
- Link the spatially resolved local surface electronic behavior and topological inhomogeneities measured with scanning tunneling microscopy and spectroscopy (STM, STS) at ambient conditions and at high temperature to the electrochemical behavior.
- Identify and explain the differences in the electronic transport characteristics between LSM and LSC.
- Correlate the structure and chemical state with those determined by synchrotron X-ray measurements at Argonne National Laboratory (ANL) and provide the needed understanding of *in situ*-*ex situ* correlations.
- Utilize the results on prototype cathode structures to propose favorable cathode structures with high efficiency and stability at intermediate temperatures.

### Accomplishments

- Probed the surfaces of the initial set of LSM and LSC dense cathode films grown on 0.7% Nb-SrTiO<sub>3</sub> (0.7Nb-STO) and Y<sub>2</sub>O<sub>3</sub> stabilized ZrO<sub>2</sub> (YSZ) substrates at three different thicknesses before and

### Introduction

Lowering the operation temperature of solid oxide fuel cell (SOFC) systems without sacrificing electrochemical activity is important for maximizing long-term stability and performance. The surface structure has a major influence on the electrocatalytic activity and stability of the cathodes. For this purpose, at MIT, we are investigating the correlations of the crystallographic structure and strain to the electronic structure, defect chemistry, and electronic and ionic transport characteristics of SOFC cathode surfaces. The presence and understanding of the activity at the inhomogeneities on the surfaces, namely grain boundaries and surface segregates [1,2], is especially important for our research. The effectiveness of these surface inhomogeneities is essential for the design of infiltrated cathodes, where both the solid-gas and solid-solid interfaces play an important role for cathode activity and stability. The information gathered from our characterization work will serve to demonstrate the prototype of favorable structures to promote higher activity in oxygen electrocatalysis on SOFC cathodes.

### Approach

We employ STM and STS in our research as an analytical agent to probe the localized topological and electronic properties at the nanoscale confined features and inhomogeneities on the cathode surfaces. The

STM/STS analysis has two phases of characterization: 1) at room temperature and ambient pressure at MIT, and 2) at high temperature and ultra-high vacuum (UHV) and non-UHV conditions at the Center for Nanoscale Systems (CNS) at Harvard University. We correlate the surface structure and electronic properties found by STM/STS to electrocatalytic activity using electrochemical characterization in a high-temperature furnace set-up. Our prototype structures include the epitaxial single crystal and textured polycrystalline dense thin-films in the presence of nano-scale grain boundaries. The samples consisted of three different thicknesses, 200 nm, 50 nm and 10 nm for LSM and LSC, on YSZ and 0.7Nb-STO substrates, and were provided by Carnegie Mellon University.

## Results

For the first stage of our investigation at MIT, we carried out STM/STS analysis on epitaxial (100) LSM films grown on 0.7Nb-STO and YSZ. The morphologies we retrieved from our analysis are shown in Figure 1. A retexturing of the film in the form of small rectangular islands has occurred after electrochemical treatment at 300 mA/cm<sup>2</sup> and 800°C (Figure 1a-b). The reason for the restructuring can be related to the preferential stabilization of an in-plane crystallographic epitaxy domain that LSM and LSC can form on the YSZ upon electrochemical treatment. Furthermore, using the UHV-STM at CNS, we found that fine segregate particles of few-nm size exist on the surfaces of the 200 nm LSM film (Figure 1-c).

Following the surface topography scans, we calculated the tunneling conductances at small bias near the Fermi level using the I-V measurements on different regions of the surface on each sample. The I-V behavior of the samples are not yet correlated to the specific sites or surface features in these experiments. Figure 2 presents a summary of the characteristic Fermi level tunneling conductance data from the surfaces of LSM films on 0.7Nb-STO compiled in the form of

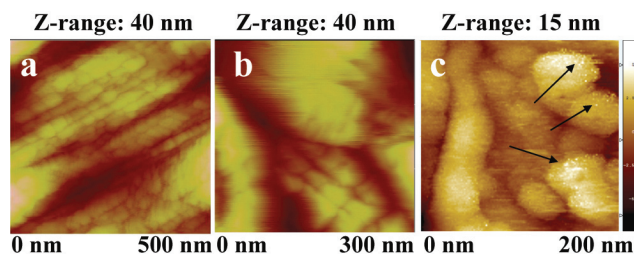


**FIGURE 1.** The surface topography scans of (a) 200 nm thick LSC and (b) 200 nm thick LSM after electrochemical treatment at 800°C, and (c) 200 nm LSM after 1/2 hour annealing at 500°C. We acquired the scan in (c) at CNS of Harvard using the Omicron VT-STM under UHV conditions. The segregated speckles on some of the grains are shown with arrows.

histograms. The Fermi level conductances of the sample surfaces exhibited a clear trend with varying thickness. The comparison of the three histograms clearly indicate that the 10 and 50 nm samples have low near-Fermi level tunneling conductances compared to the 100 nm sample, while the 100 nm sample displays a large spread in the number of sites with  $dI/dV$  greater than zero. Given these results, we expect that the 100 nm thick sample will have more available electronic states to exchange electrons with oxygen in the vicinity of the surface, and thus higher activity. Non-zero tunneling conductances on the 100 nm LSM film could also indicate a relatively high density of free carriers that depend on defect density, deviation from exact stoichiometry, and the local and overall strain states at a given temperature. Furthermore, the band-gap values

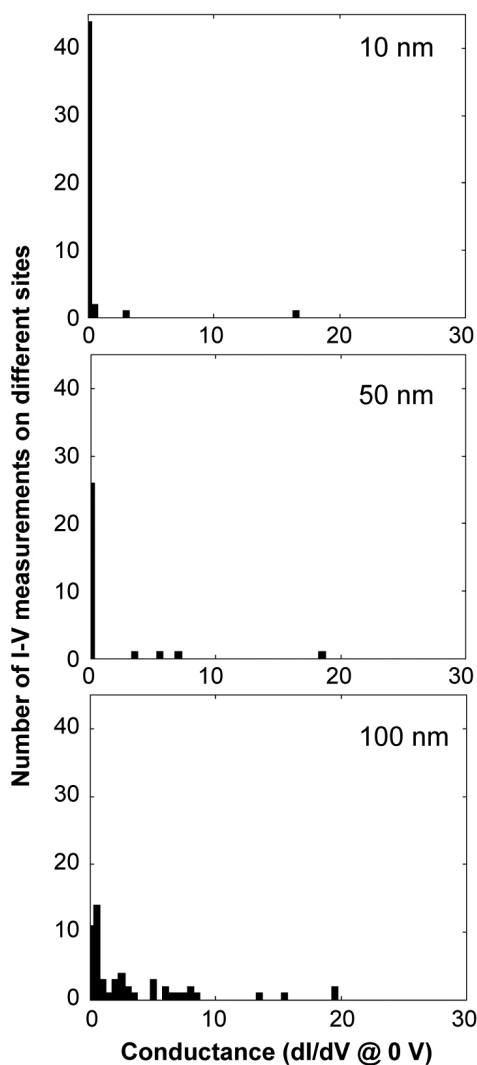


**FIGURE 2.** The Fermi level conductance histograms compiled from various measurements at ambient conditions on different sites on the 10 nm, 50 nm and 100 nm thick LSM films grown on (100) 0.7% Nb-SrTiO<sub>3</sub>.

found from the I-V measurements using STS for the 10 nm and 50 nm LSM films ranged as 1.5-2.2 V.

We performed electrochemical impedance spectroscopy (EIS) measurements to characterize the dynamic bulk electrochemical response of the LSM and LSC electrodes and to correlate the STM/STS results to electrocatalytic activity of the cathode films. There were three main observations we made in our EIS work thus far:

- We found activation energies of 1.8 eV to 2.2 eV, implying that the surface reactions [3,4] are the rate-limiting process on almost all LSM films except the 100 nm-thick LSM at the low temperature range (Figure 3a). This result is consistent with our STS

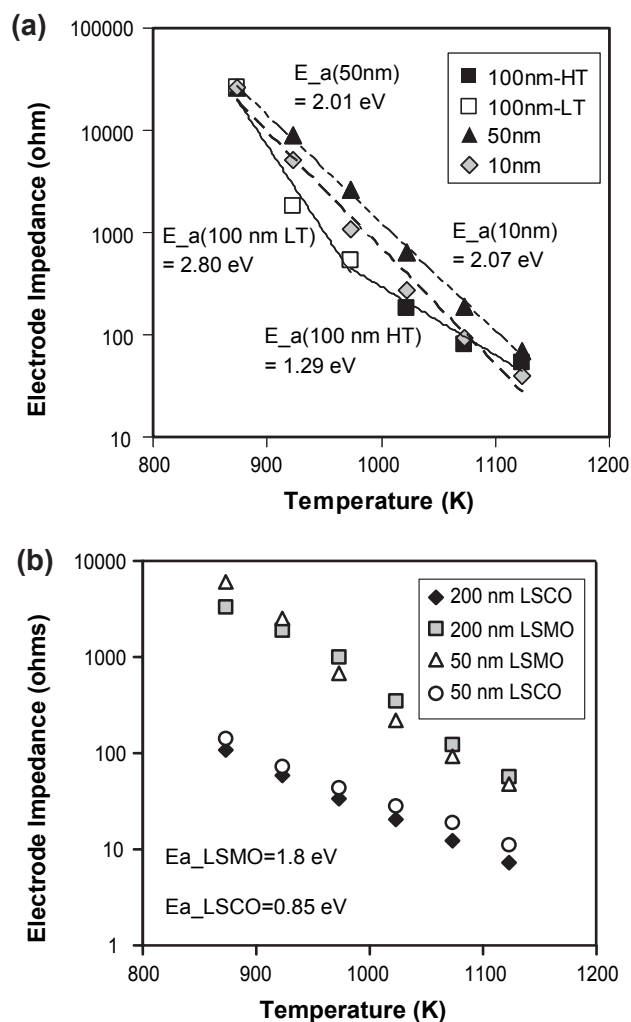


**FIGURE 3.** (a) The activation energy, in eV, for total impedance ( $Z_{tot}$ ) – low-frequency intercept on the real axis (see highlighted). The data of the 100 nm thick sample were fitted both for a low temperature (LT) range and a high temperature (HT) range as it exhibits a distinct slope change around 700°C that might be an indication of change in the type of the limiting-process. (b) Resistance vs. temperature plots of the 50 nm thick LSM and LSC, 200 nm thick LSM and LSC (resistance is given in logarithmic scale).

characterization that revealed higher tunneling conductance on the surface of the 100 nm LSM as shown in Figure 2.

- We observed orders of magnitude of difference between the total impedance of the LSM and LSC dense thin-film cathodes (Figure 3b).
- All samples, except from the 100 nm LSM at lower temperature range, had the surface reactions as the rate-limiting processes as there was no clear indication that the film thickness was impacting total impedance results.

Complementary with the structural, electronic, and electrochemical characterization is the surface chemical analysis. At MIT, we carried out our first preliminary AES on the 100 nm thick LSM on a 0.7% Nb-STO substrate. The analysis consisted of depth profiling of the La, Sr, Mn and O elements using a 3 keV incident electron beam (Figure 4). Presently, the AES results are not fully quantitative. However, it is clear that there is an enrichment of Mn (B-site). The La (A-site main cation) signal gets stronger with depth, implying a depletion of this element near the surface. In this preliminary analysis, we cannot conclude whether Sr is enriched or depleted near the surface because the 1.6 keV electrons can penetrate from the subsurface region, too. Such segregation behavior is contrary to the A-site segregation on the surface of LSM on YSZ substrate, and is likely to impact the surface electronic properties and the electrochemical activity of the cathode.

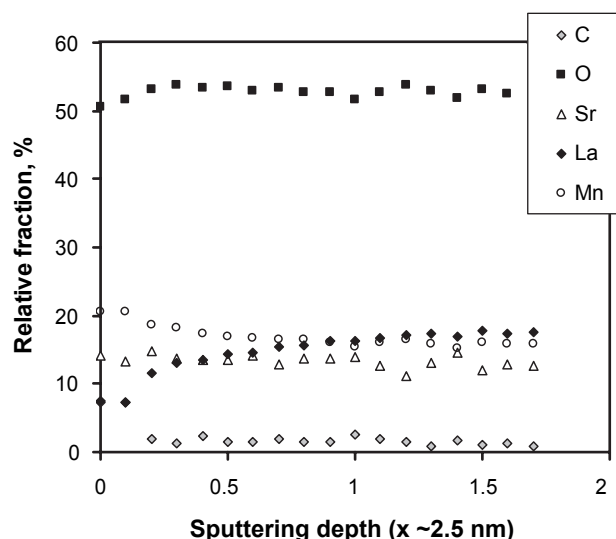


**FIGURE 4.** Near-surface depth profile of the 100 nm thick LSM composition using Auger electron spectroscopy. The analysis was terminated when the relative change in concentrations reached a constant ratio. The predicted sputtered depth corresponds to approx. 5 nm. (Source of carbon is the overall carbon-contamination of surface of the films due to prior handling of films.)

## Conclusions and Future Directions

- Electronic and topological characterizations show that thinner LSM films (10-50 nm thick) have lower near-Fermi level conductance on their surface than 100 nm samples. Consistently with this result, EIS measurements indicate that the diffusion of oxide ions dominates the electrode impedance for the 100 nm film while resistive surface processes dominate for the thinner electrodes.
  - We identified the LSC films grown on YSZ to be much more active than the LSM films on YSZ. We will compare the electronic behavior of the surfaces of the LSC and LSM electrodes using the STM/STS.
  - AES and STM results imply that surface enrichment of A-site or B-site elements in fine segregate particles is possible and can impact the surface electronic states of the cathode film. We will identify the origin and consequences of these surface segregates and whether they form during growth, annealing or electrochemical conditions will be sought.
  - We will evaluate the ex situ AES and STM data in the light of the synchrotron X-ray measurements by the ANL group at the Advanced Photon Source to provide an understanding of *in situ*-ex situ correlations.
- We will expand our STM/STS analysis from ambient conditions to high temperature (up to 1,000 K) under UHV and non-UHV (mild-UHV) conditions using the Omicron VT STM at the National Science Foundation facility of Center for Nanoscale Systems.

## FY 2008 Publications/Presentations

1. Progress Report to ANL as of January 2008.
2. Progress Report to ANL as of March 2008.
3. Quarterly Report to SECA for the second calendar quarter, April 25 2008.

## References

1. T. Becker, C. Streng, Y. Luo, V. Moshnyaga, B. Damaschke, N. Shannon and K. Samwer, Phys. Rev. Lett. 89, 237203 (2002).
2. S. Kar, J. Sarkar, B. Ghosh and A.K. Raychaudhuri, Phys. Rev. B 74, 085412 (2006).
3. E.P. Murray, T. Tsai, S.A. Barnett, Solid State Ionics 110, 235 (1998).
4. S.P. Jiang, J.G. Love, Y. Ramprakash, J. Power Sources 110, 201 (2002).

---

## IV.A.8 Intermediate Temperature Solid Oxide Fuel Cell Cathode Enhancement through Infiltration Fabrication Techniques

Matthew Seabaugh (Primary Contact),  
Scott Swartz, Michael Day, Buddy McCormick  
NexTech Materials Ltd.  
404 Enterprise Drive  
Lewis Center, OH 43035  
Phone: (614) 842-6606; Fax: (614) 842-6607  
E-mail: m.seabaugh@nextechmaterials.com

DOE Project Manager: Briggs White  
Phone: (304) 285-5437  
E-mail: Briggs.White@netl.doe.gov

Contract Number: 84881

Phase I Start Date: June 20, 2007  
Phase I End Date: March 19, 2008

values, reducing non-ohmic resistance considerably at low temperatures.

- Microstructural analyses of the resulting cathodes have further demonstrated an impressive degree of dispersion of the catalytic materials in the structures, with typical crystallite sizes of less than 100 nm. These structures show strong surface ordering.
- Fuel cell performance tests and electrical impedance spectroscopy (EIS) analysis show a strong correlation between infiltrant additions and improved cell performance and further suggest that the additives particularly affect the oxygen reduction reaction, with the critical reactions having characteristic relaxation times of ~0.5-2.0 milliseconds.

### Objectives

- Assess the contribution of three cathode enhancement strategies: gadolinium doped ceria (GDC), strontium samarium cobaltite (SSC), and Pd infiltration through the comparative testing of button cells of anode-supported and electrolyte supported designs.
- Demonstrate impact of infiltration approaches on cell performance and microstructure.
- Determine through electrical impedance analysis the mechanism of infiltrant impact on cathode performance.
- Demonstrate the infiltration approach on commercially relevant platforms.

### Accomplishments

- Infiltrants were demonstrated to provide improvement to the oxygen reduction reaction kinetics for both the lanthanum strontium manganese (LSM)/GDC and lanthanum strontium zinc ferrite (LSZF)/GDC composites cathodes, resulting in 30% enhancements in cell performance for both systems at 0.7 V and 700°C.
- Enhanced cells exhibit consistent performance improvements on large area tests, and equivalent or improved performance stability in comparison with the baseline cathode.
- Half-cell performance tests have shown that infiltration approaches translate between planar and tubular cell geometries; infiltration significantly reduces tubular cell area specific resistance (ASR)

---

### Introduction

As discussed above, great interest has recently surfaced relating to the improvement of physically and chemically stable cathodes, such as LSM, through various microstructural modifications. One method is focused on the incorporation of highly mixed-conductive nano-particles within an existing LSM architecture to improve the oxygen reduction kinetics. This principle of supported nano-catalyst is fundamental in the field of heterogeneous catalysis; only recently have fuel cell researchers borrowed these principles when designing and processing solid oxide fuel cell (SOFC) anodes and cathodes, which are essentially electro-catalysts for oxygen reduction and hydrocarbon oxidation. Research groups at Lawrence Berkeley National Laboratory [1-3], Nanyang Technical University [4,5], and the University of Pennsylvania [6-8] have demonstrated different approaches to cathode infiltration with excellent results. In this project, NexTech Materials has assessed infiltration technology for cost effectiveness and scalability for cell and materials manufacturing, while contributing to the understanding of the microstructural and mechanistic aspects of the technology.

NexTech Materials has developed cathode infiltration technologies for SOFCs and performed a comparative study of their impact on the performance of state-of-the-art composite cathodes based on LSM and LSZF. Three materials have been evaluated for infiltration, representing three technological approaches adopted from the catalyst literature: precious metal infiltration (with Pd), high oxygen exchange coefficient electrolyte additions (with GDC), and high conductivity perovskites (SSC).

GDC infiltration has been demonstrated to enhance cell performance on various cell platforms including high, intermediate and low temperature planar cells as well as cathode supported electrolyte tubes. Ultimately, infiltration of SOFC cathodes appears to be a promising route to lowering the operating temperature and/or improving performance of SOFCs. Such cross-cutting applicability across SOFC design platforms and applications presents tremendous market opportunity for this technology.

## Approach

The infiltration process developed on this project leveraged two simple processes – infiltration of precious metal and oxide precursors from aqueous solutions. NexTech performed a number of experiments to validate the effectiveness of infiltration materials and approaches for improving cathode performance.

Initial testing focused on optimizing experimental procedures and precursors to achieve consistent results and identify areas of enhancement. Pd, GDC, and SSC infiltration were found to have a positive influence on cell performance at 700°C. All the additives evaluated in Phase I produced varying degrees of cell performance enhancement, for both anode and electrolyte supported cells. The infiltration of GDC was selected for further analysis, and scale-up to 28 cm<sup>2</sup> based on cost, simplicity and impact on cell performance.

GDC infiltration was investigated for electrolyte supported cells and compared with a baseline cell by analyzing SOFC performance, EIS response, and the resultant microstructures to understand what structures develop and how they may impact cathode performance.

## Results

NexTech Materials has developed cathode infiltration technologies for SOFCs and performed a comparative study of their impact on the performance of state-of-the-art composite cathodes based on LSM, LSZF and SSC. These demonstrations have shown that 30 to 50% higher power density can be achieved for cells operating at 600-850°C, with enhancement particularly significant in the range of 600-700°C in 28 cm<sup>2</sup> cells. Testing has shown that this technology can be applied to a range of cell architectures and applications, including both planar and tubular cells. Cell performance stability of the infiltrated and baseline cells is similar.

Microstructural analysis confirmed that the infiltration processes have deposited a nanoscale catalytic distribution of the GDC and Pd additives which are stable through operation over 100 hours. An example of post-testing GDC distribution within an LSM cathode is shown in Figure 1. The fine scale, light

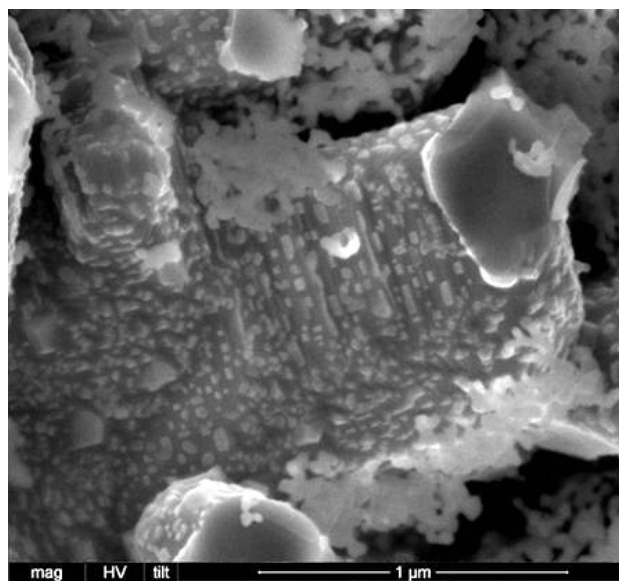


FIGURE 1. Ordering of the GDC Infiltrant Phase on the Surface of an LSM Particle

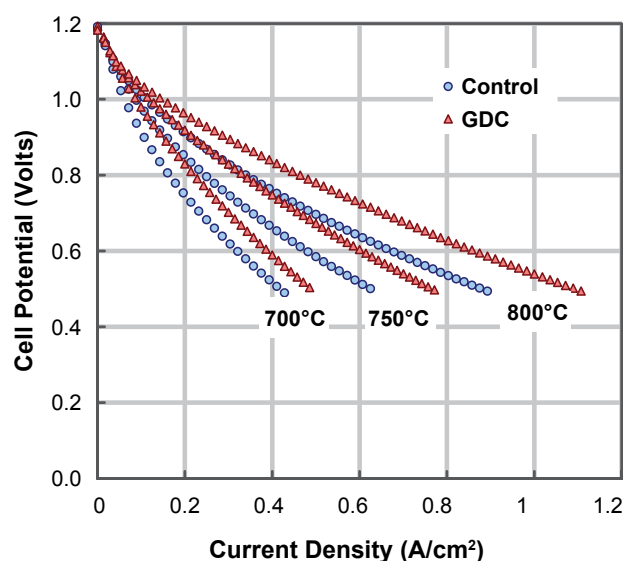
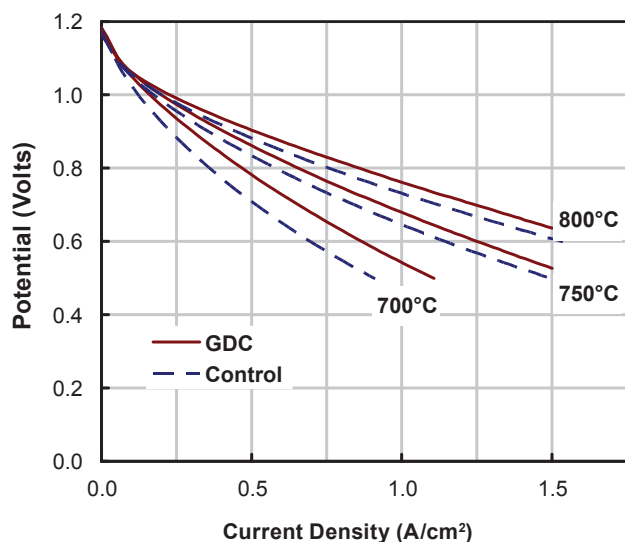


FIGURE 2. Effect of GDC Infiltration on LSM Cathode SOFC Polarization

color phase in the micrograph are GDC particles. The ordering of this addition on the LSM particle suggests preferential deposition at crystallographic ledges on the particle.

EIS analyses of the cells show that these infiltrants reduce cathode resistance in LSM-based cells by 2/3 at 650°C and by half at 700°C. The same infiltration approaches improve the power density of Zn-doped LSF cathode materials by 30% at 700°C, providing critical performance boost to cells operating in the cooler portions of an intermediate temperature stack. See Figures 2 and 3 for specific data supporting these claims.



**FIGURE 3.** Effect of GDC Infiltration on LSZF Cathode Cell Polarization

Phase I results indicate that this route will not significantly increase the cell cost, compromise long-term cell stability, or alter well-developed cell fabrication methods. Consequently, we believe further development in this arena will provide an excellent cost/benefit ratio.

### Conclusions and Future Directions

In further associated work, NexTech will confirm the applicability of infiltration approaches to SOFC manufacturing processes and evaluate the impact of the improved cell performance. Infiltration technology will be refined to improve upon the performance and stability of the down-selected GDC-infiltration approach, identify best paths for cost-effective implementation, and determine the impact of infiltration SOFC stacks performance at realistic conditions.

### FY 2008 Publications/Presentations

1. Tailored Cathodes for Solid Oxide Fuel Cells, M.M. Seabaugh, B.E. McCormick, K. Chenault, S. Ibanez, M.J. Day, and S.L. Swartz, Poster Presentation at the 5<sup>th</sup> International Symposium on Solid Oxide Fuel Cells (SOFC): Materials, Science, and Technology, American Ceramic Society, Daytona, FL, January 27 - February 1, 2008.

### References

1. Y.B. Matus, *Solid State Ionics* 176, 443-449 (2005).
2. T. Shoklapper, et al., *Electrochemical and Solid-State Letters* 9 [8], A376-A378 (2006).
3. S. Visco, et al., Presentation at the 7<sup>th</sup> Annual SECA Workshop and Peer Review Meeting, September 13<sup>th</sup>, 2006.
4. S.P. Jiang, et al., *Solid State Ionics* 176, 1351-1357 (2005).
5. S.P. Jiang, et al., *Journal of Electrochemical Society* 152 [7], A1398-A1408 (2005).
6. Y. Huang, et al., *Journal of Electrochemical Society* 153 [6], A951-A955 (2006).
7. W. Wang, et al., *Journal of Electrochemical Society* 153 [11], A2066-A2070 (2006).
8. R.J. Gorte, et al., Presentation at the 7<sup>th</sup> Annual SECA Workshop and Peer Review Meeting, September 13<sup>th</sup>, 2006.

## IV.A.9 SECA Coal-Based Systems Core Research – University of Florida

Eric D. Wachsman  
University of Florida  
Gainesville, FL 32611-6400  
Phone: (352) 846-2991; Fax: (352) 846-0326  
E-mail: ewach@mse.ufl.edu

DOE Project Manager: Briggs White  
Phone: (304) 285-5437  
E-mail: Briggs.White@netl.doe.gov

Contract Number: 44036

Start Date: January 10, 2005  
Project End Date: September 30, 2008

### Objectives

- Determine oxygen reduction mechanism for lanthanum strontium manganate (LSM) and lanthanum strontium cobalt ferrite (LSCF) solid oxide fuel cell (SOFC) cathodes.
- Identify key elements of catalytic activity for oxygen reduction.
- Identify the effects of aging on the catalytic activity of LSCF.
- Combine catalysis and electrochemical techniques to determine the mechanism for the oxygen reduction reaction at the cathode.

### Accomplishments

- Demonstrated utility of isotopic switching experiments to probe the oxygen exchange reaction on cathode powders LSM and LSCF.
- Successfully modeled, with chemical kinetics, the mechanism of oxygen exchange in LSM and LSCF using an isotopic tracer.
- Obtained activation energy and oxygen partial pressure dependence for LSM and LSCF.
- Designed and built an experimental setup for simultaneous *in situ* measurement of electrical and chemical behavior of cathodes.
- Measured degradation of LSCF surface exchange coefficient by conductivity relaxation.
- Identified Sr segregation as the source of LSCF cathode degradation.

### Introduction

Great effort has been devoted towards lowering SOFC operating temperatures while preserving acceptable levels of performance. Substantial increase in overpotential at intermediate temperatures (600-800°C) is mainly attributed to the sluggish oxygen reduction reaction at the cathode. Unfortunately, the processes that most affect performance are those that are the least understood. The actual mechanisms and rate laws governing oxygen reduction kinetics on the cathode surface remain largely indeterminate [1]. Once the rate-determining step of the cathode reaction is clearly understood, a more focused effort to tailor the catalytic properties of cathode materials is possible. Therefore, it is of great importance to understand fundamentally what features determine a material's catalytic activity and how they can be controlled to facilitate oxygen reduction. This, in combination with other design advancements, would lead to better performance at lower operating temperatures and facilitate adoption of SOFC technology.

Our work aims to explore how the reaction occurs and what elements control catalytic activity. The strategy follows the logical progression of first using catalysis characterization techniques to determine the oxygen reduction reaction (ORR) mechanism, especially the rate limiting step(s). The second step in this progression employs electrical conductivity relaxation (ECR) to separate bulk from surface properties as a function of time and temperature. Moreover, temporal behavior gives insight into the cathode degradation process. With the understanding of oxygen exchange gained from the initial two phases, the sequence is completed by the development of a novel, *in situ* characterization technique that combines electrochemical and catalytical analysis to reveal real-time SOFC electrode performance criteria and the effect of operating conditions on the ORR.

### Approach

It is well known that LSM is not as catalytically active as LSCF; however LSCF is not as stable as LSM. Therefore, it is important to figure out what elements contribute to LSCF's catalytic activity and ascertain whether they can be incorporated into LSM. An *in situ* method, using a mass spectrometer (MS) of investigating the kinetics and mechanisms of oxygen surface exchange on LSM and LSCF was developed by combining temperature programmed desorption, reaction and isothermal switching with an isotopic tracer,  $^{18}\text{O}_2$ . The

gas exchange behavior is separated into surface and bulk originated oxygen and compared to behavior predicted by chemical kinetics. A two-step mechanism is proposed consisting of dissociative adsorption of oxygen onto the surface followed by adsorbed oxygen incorporation into the material; different  $P_{O_2}$  dependences are obtained depending on which step is rate limiting.

ECR was used to generate transient data, after a  $P_{O_2}$  step, for LSCF for long-term performance analysis. Fitting this data then permitted the differentiation of bulk ( $D_{chem}$ ) from surface ( $K_{chem}$ ) transport parameters. Samples were further characterized by X-ray diffraction (XRD), scanning electron microscopy (SEM) and transmission electron microscopy (TEM), pre- and post-ECR, to identify time-dependent morphological and compositional changes.

Nevertheless, a complete understanding of the ORR mechanism as it pertains to SOFC performance, particularly the convoluted electrochemical behavior of mixed conducting and/or (electro-) catalytically active electrode materials, requires *in situ* electrochemical and catalytic characterization. Accordingly, an experimental setup is being developed to measure/apply current/potential while simultaneously recording effluent oxygen in a controlled gas environment.

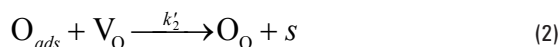
## Results

**Catalysis** – Isothermal switching experiments were conducted to determine the rate limiting step and reaction order for the ORR on LSM and LSCF. Specifically, oxygen is taken into the system and then analyzed after interacting with LSCF or LSM powders. The use of  $^{18}O_2$  allows for the extent of oxygen interaction with the surface to be determined. As  $^{18}O_2$  adsorbs onto the surface, it can exchange with the oxygen in the bulk or it can combine with a surface  $^{16}O$  to form  $^{16}O^{18}O$ . By monitoring the rise and fall of mass 32, 34, and 36 with a MS, we were able to gain insight into the ORR mechanism. The dissociative adsorption and incorporation steps are

Step (1) Dissociative Adsorption



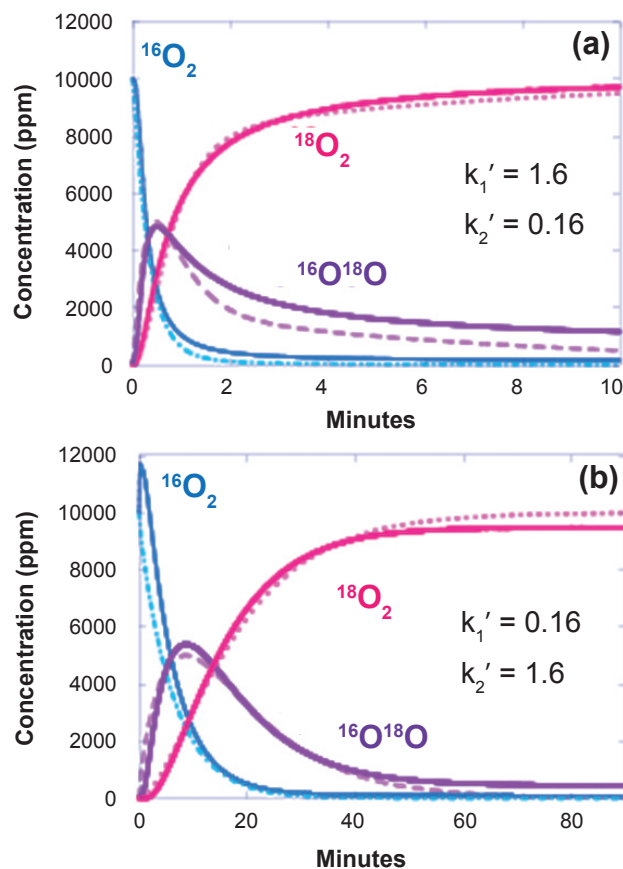
Step (2) Incorporation



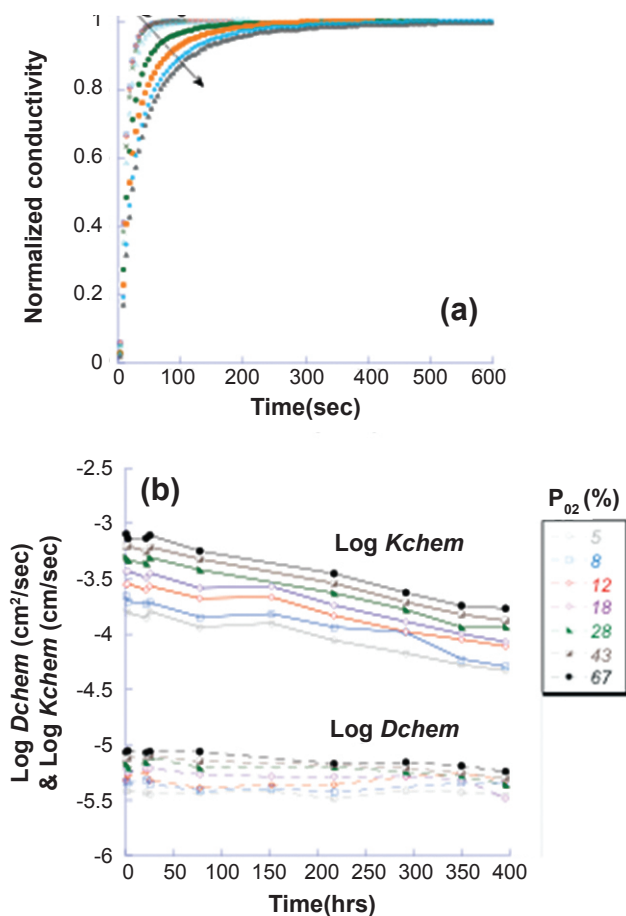
where, unfilled surface sites ( $s$ ) are assumed to be homogenous,  $V_O$  represents a vacancy at the surface and  $O_O$  represents a lattice oxygen in the surface layer. The initial reaction order with respect to  $O_2$  is predicted to be either 1 or 0.5 depending on whether dissociative adsorption (Step (1)) or oxygen incorporation (Step (2)) is the rate-limiting step.

Figure 1 shows an isothermal switching profile for LSM and LSCF where the isotopic labeling of the oxygen in the feed stream is abruptly changed. The dashed lines represent behavior predicted by the kinetic model.  $k_1'$  and  $k_2'$  are the fitting parameters and they represent the effective rate constant of the first and second step, respectively. It is seen that, at 650°C, the rate constants of LSM and LSCF differ by an order of magnitude, which indicates that LSM and LSCF have different rate limiting steps. Given a two step mechanism consisting of dissociative adsorption and incorporation, the rate limiting step for LSM was found to be incorporation at 600°C (Step (2)) and dissociative adsorption (Step (1)) at 800°C, while LSCF is limited by dissociative adsorption at either temperature. Accordingly, LSM is overall less catalytically active towards oxygen exchange than LSCF, with exchange onset occurring at 350°C in LSM and 200°C in LSCF. In addition, above 700°C, the activation energy for oxygen exchange in LSM and LSCF was found to be 0.90 eV and 0.10 eV, respectively.

**Conductivity Relaxation** – Figure 2a shows that the LSCF conductivity decreases with time while Figure 2b clarifies the roles played by chemical diffusion versus



**FIGURE 1.** Isothermal switching at 650°C in 10,000 ppm  $O_2$  for (a) LSM and (b) LSCF. The solid line represents experimental data, the dashed lines are generated from the model.



**FIGURE 2.** Aging effects on oxygen reduction kinetics. (a) Normalized electrical conductivity of LSCF after changing  $P_{O_2}$ ; (b)  $D_{chem}$  and  $K_{chem}$ , at different  $P_{O_2}$ , obtained from fitting transient data.

surface chemical exchange. Figure 2b shows that the magnitudes of the chemical diffusion coefficients in LSCF are time-independent and do not vary much with  $P_{O_2}$ . In contrast, the surface chemical exchange coefficients decrease with time and are more sensitive to  $P_{O_2}$ . This indicates that the degradation of LSCF cathodes is due to surface kinetics. Accordingly, though XRD did not reveal any obvious changes in structure between the pre- and post-ECR samples, SEM images of the sample showed a significant difference in surface morphology after ECR testing. Post-test, the sample surface was rougher and showed signs of grain growth. EDS-SEM and EDS-TEM showed that an Sr-rich and transition metals deficient (relative to bulk LSCF) phase developed in the grain boundary and a La-rich phase grew on the grain face.

Both the Sr-rich (and transition metal deficient) and the La-rich (Sr and oxygen vacancy deficient) phases likely have lower catalytic activities than LSCF6428 because transition metals and oxygen vacancies on the surface are related to the surface exchange reaction.

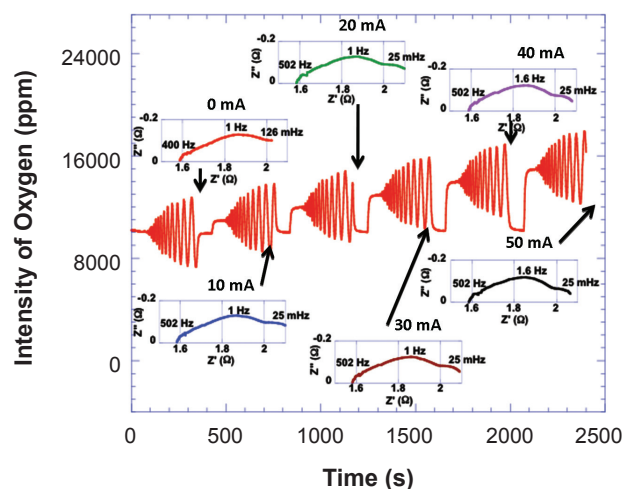


**FIGURE 3.** EIS Electrical and Chemical Behavior of LSCF on GDC at 700°C

Thus, the formation of these secondary phases appears to be the main reason for degradation of  $K_{chem}$ , and eventually, of overall SOFC cathode performance.

**Integrated Electrochemical-Catalysis System** – An integrated electrochemical-catalysis system was built and verified. Recent data from this experimental setup can be seen in Figure 3, where, for this particular experiment, electrochemical impedance spectroscopy (EIS) was used to perturb a symmetrical cell of LSCF on gadolinia-doped ceria (GDC) with a sinusoidal alternating current signal at different applied direct currents. EIS is a technique commonly used to resolve different mechanistic steps occurring in an electrochemical process, but it does not conclusively identify which steps they are. To aide in the analysis, a capillary is placed at the surface of the electrode and is connected to the inlet of the MS to monitor the gas effluent while the sample is perturbed. From Figure 3, the oxygen behavior is monitored during each EIS experiment. This demonstrates the ability of the setup to monitor, *in situ*, the electrochemical behavior of an SOFC cathode.

## Conclusions and Future Directions

In conclusion, we have:

- Demonstrated that LSCF is more catalytically active than LSM at all temperatures.
- Demonstrated that dissociative adsorption of oxygen is the rate limiting step for both LSM and LSCF at temperatures 800°C and up.
- Demonstrated that oxygen incorporation is rate limiting for LSM at 600°C.
- Determined that retardation of surface kinetics over time causes LSCF cathode degradation.

- Identified the growth of Sr-rich (and transition metal-deficient) and La-rich phases as likely reasons for reduction in LSCF surface kinetics and thereby LSCF degradation.
- Developed and demonstrated an integrated electrochemical-catalysis system for simultaneous *in situ* analysis of cathode electrochemical and catalytic performance.

For future work, we will:

- Infiltrate LSM with La, Sr, Co and Fe metal nitrate solutions to produce metal oxide nanoparticles on the surface and measure effects on catalytic activity.
- Characterize *in situ* the current-voltage characteristics of oxygen exchange reaction for SOFC (LSM and LSCF) cathodes in the integrated electrochemical-catalysis system while monitoring the gas phase composition. This not only allows us to study charge transfer but it more closely mimics the conditions in an actual working fuel cell, where applied currents/voltages and material heterojunctions are likely to affect the catalytic mechanisms.
- Elucidate the mechanistic steps for oxygen reduction in an SOFC by *in situ* tests in the integrated electrochemical-catalysis system using isotopically labeled oxygen ( $^{18}\text{O}_2$ ) in conjunction with (i) EIS, (ii) isothermal-switching experiments with applied current/potential, and (iii) potential programmed reactions.
- Determine Sr segregation mechanism—by studying effects of heat treatment, current and  $\text{P}_{\text{O}_2}$ —and investigate alternatives to Sr doping of lanthanum cobalt ferrites.
- Combine results from the different experiments to propose probable mechanisms for oxygen reduction and deduce improved cathode materials and microstructures.

### FY 2008 Publications/Presentations

1. “Investigating the Oxygen Surface Exchange Mechanisms of SOFC Cathodes Using an Isotopic Tracer,” C. Kan, F. VanAssche, E. Wachsman, *ECS Trans*, accepted.
2. “Investigating Oxygen Surface Exchange Kinetics of  $\text{La}_{0.8}\text{Sr}_{0.2}\text{MnO}_3$  and  $\text{La}_{0.6}\text{Sr}_{0.4}\text{Co}_{0.2}\text{Fe}_{0.8}\text{O}_3$  Using an Isotopic Tracer,” C.C. Kan, H.H. Kan, F.M. Van Assche IV, E.N. Armstrong, and E.D. Wachsman, *Journal of the Electrochemical Society*, submitted.
3. “Mechanical Properties of Ceria by Molecular Dynamics Simulation,” H. Xu, R. Behera, Y. Wang, F. Ebrahimi, S. Sinnott, E. Wachsman, and S. Phillpot, *Solid State Ionics*, submitted.
4. “Vacancy Ordered Structure of Cubic Bismuth Oxide from Simulation and Crystallographic Analysis,” D.S. Aidhy, J.C. Nino, S.B. Sinnott, E.D. Wachsman, and S.R. Phillpot, *Journal of the American Ceramic Society*, accepted.
5. “Characterization of Lanthanum Zirconate Formation at the A-Site Deficient Strontium-Doped Lanthanum Manganite Cathode /Yttrium Stabilized Zirconia Electrolyte Interface of Solid Oxide Fuel Cells,” A. Chen, G. Bourne, K. Siebein, R.T. DeHoff, E.D. Wachsman, and K. Jones, *Journal of the American Ceramic Society*, accepted.
6. “High Performance Composite  $\text{Bi}_2\text{Ru}_2\text{O}_7$  -  $\text{Bi}_{1.6}\text{Er}_{0.4}\text{O}_3$  Cathodes for Intermediate Temperature Solid Oxide Fuel Cells,” M. Camaratta and E.D. Wachsman, *Journal of the Electrochemical Society*, **155**, B135-142 (2008).
7. “Three-Dimensional Reconstruction of Porous LSCF Cathodes,” D. Gostovic, J. Smith, K. Jones and E. Wachsman, *Electrochemical and Solid State Letters*, **10**, B214-217 (2007).
8. “General Model for the Functional Dependence of Defect Concentration on Oxygen Potential in Mixed Conducting Oxides,” K. Duncan and E. Wachsman, *Ionics*, **13**, 127-140 (2007).
9. “Deconvolution of SOFC Cathode Polarization,” E. Wachsman, *Solid Oxide Fuel Cells X, ECS Trans*, K. Eguchi, S. Singhal, H. Yokokawa, and J. Mizusaki, Ed, **7-1**, 1051 (2007).
10. “In-situ Simultaneous Electrochemical and Catalytic Activity Measurements of SOFC Cathodes,” E. Armstrong, C. Kan, B. Blackburn, and E. Wachsman, Poster, *32<sup>nd</sup> International Conf. & Expo. Advanced Ceramics & Composites*, Daytona, FL, January 27-February 1, 2008.
11. “Oxygen Surface Exchange on Cobalt Oxide Infiltrated Solid Oxide Fuel Cell Cathodes,” C.C. Kan and E.D. Wachsman, Presentaion, *32<sup>nd</sup> International Conf. & Expo. Advanced Ceramics & Composites*, Daytona, FL, January 27-February 1, 2008.
12. “Designing for Functional Gradients in Fuel Cells and Membranes,” E.D. Wachsman, Invited Talk, *Composites at Lake Louise 2007*, October 28 – November, 2, 2007, Banff, Canada.
13. “Can Nanotechnology Play a Role in Solid Oxide Fuel Cells?” E.D. Wachsman, Invited Talk, *Materials Research Society*, April 9–13, 2007, San Francisco, CA.
14. “Evaluation of Electrochemical Processes Occuring in the Cathodic Reaction of SOFCs,” Jeremiah Smith, *Ph.D. Dissertation*, July 2007.
15. “Microstructural Engineering of Composite Cathode Systems for Intermediate and Low-Temperature Solid Oxide Fuel Cells,” Matthew Camaratta, *Ph.D. Dissertation*, November 2007.
16. “Effect of Cathode Microstructure on the Cathode Polarization in the Sintered LSM/YSZ SOFCs,” Aijie Chen, *Ph.D. Dissertation*, February 2008.

## References

1. S. B. Adler, X. Y. Chen and J. R. Wilson, *J. Catal.*, **245**, 91 (2007).

---

## IV.A.10 Electronic Structure of Cathode Materials

Walter A. Harrison  
GLAM/McCullough Bldg.  
Stanford University  
Stanford, CA 94305-4045  
Phone: (650) 723 4224  
E-mail: walt@stanford.edu

DOE Project Manager: Travis Shultz  
Phone: (304) 285-1370  
E-mail: Travis.Shultz@netl.doe.gov

Subcontractor:  
Research and Development Solutions, LLC

Contract Number: 41817

Start Date: January 7, 2008  
Project End Date: October 31, 2008

### Objectives

- Understand the electronic structure of multivalent oxides.
- Develop a simple enough description to allow treatment of other systems and properties.
- Explore the properties of  $\text{La}_{1-x}\text{Sr}_x\text{MnO}_3$  (LSM) and  $\text{La}_{1-x}\text{Sr}_x\text{Co}_y\text{Fe}_{1-y}\text{O}_3$  (LSCF) and other cathode materials using this description.

### Accomplishments

- Successful prediction of the cohesive energy of  $\text{MnO}$ ,  $\text{Mn}_2\text{O}_3$ ,  $\text{MnO}_2$ ,  $\text{FeO}$ , and  $\text{Fe}_2\text{O}_3$ .
- Extension of the theory to cohesion in the cathode materials LSM and LSCF.
- Successful use of the same formalism to predict a wide range of electrical, magnetic, and structural properties of the cathode materials.

---

---

### Introduction

We are seeking simplified methods for calculating a range of properties of transition-metal compounds. There exist highly developed computational techniques, most frequently based upon the local-density approximation, which seek the highest possible accuracy for such estimates. Our approach is essentially to make enough approximations to such methods, while retaining

the essential physics, that the estimates can be made by hand. We cannot compete with the highly developed methods for what they seek to do, except perhaps in a cleaner treatment of electron-electron interactions in these strongly correlated systems. However, we hope to provide something much better than traditional chemical arguments, which generally do not include the basic features of the electronic structure which have been made clear in the computational studies.

The simplest relevant compounds in which the transition-metal ions appear in various oxidation states, e.g.  $\text{Mn}^{2+}$ ,  $\text{Mn}^{3+}$ , and  $\text{Mn}^{4+}$ , are the oxides themselves,  $\text{MnO}$ ,  $\text{Mn}_2\text{O}_3$ ,  $\text{MnO}_2$ , and an understanding of the type we seek did not exist even for these systems. We therefore sought an understanding of these materials, seeking to estimate and test that estimate, for the cohesive energy, the energy required to separate the crystal into neutral atoms. We are not in the end primarily interested in cohesion, but it provides a good testing ground and a method for describing it will be needed in order to study vacancies and surfaces, which we will need to understand. We planned to move on to the interesting perovskite compounds which are used as cathode materials once we had successful methods for the oxides.

### Approach

The basic theoretical approach which was to be used is called *tight-binding theory*, a method which has been highly developed by Harrison for the study of semiconductors and insulators, and extensively described in his book *Elementary Electronic Structure* [1]. The theory starts from the electronic states of the constituent atoms, and estimates the modifications of the electronic states which occur when these atoms are brought together as a solid. It is in contrast to *pseudopotential theory*, of which Harrison has been a principal developer, which starts with electrons completely free to move through a solid, and estimates the modifications made by the atoms present, also documented in *Elementary Electronic Structure*, principally for metallic systems.

This is a completely natural approach for these multivalent oxides, but new and serious complications arise because a change in valence can drastically change the electronic energy levels of the atomic  $d$  states involved. These were generally taken to be unchanged from the atom in the simple compounds studied. Once we learned how to deal with such changes, the application to the properties of the various systems of interest should be tractable.

## Results

The initial study of the oxides of manganese gave a few surprises. First, the cohesive energy was dominated in all cases by the energy gained in transferring two  $s$  electrons from the Mn atoms to the oxygen atoms, just as in other divalent compounds such as MgO, CaO, CaS, etc. It was therefore very nearly the same cohesive energy *per Mn ion* for the three compounds, MnO,  $\text{Mn}_2\text{O}_3$ ,  $\text{MnO}_2$ . The small difference for the successive compounds, estimated to be 1.67 eV per Mn, arose from a *rearrangement bond*, proposed many years ago in another context by Harrison, in which occupied Mn  $d$  states and oxygen  $p$  states of about the same energy are coupled, and the electron in the antibond is transferred to some other oxygen state. This feature is much more closely related to the aspects of the electronic structure which are of interest here, than the  $s$  to  $p$  transfer which dominates the cohesion. A most important finding was that the shifts in the electronic  $d$  levels due to valence change were very much smaller than expected, partly because the extra electrostatic energy of an electron due to adding another to that atom is largely cancelled by the electrostatic energy from the removal of that electron from a neighbor atom. A second reason is that each electron is really shared by neighboring atoms, and the transfer of an electron between states, which we think of as a transfer between atoms, does not greatly modify the charge distribution.

These same features carried over to the cohesion of LSM and LSCF, but as we began to study additional properties, we found that small shifts in the energies of the levels, which were of no consequence to the cohesion, became significant. However, the extraordinary simplicity of being able to estimate properties directly, without carrying out a self-consistent computer calculation to obtain the corrections, still strongly favors using the simplest theory and that is how we are proceeding. At the same time, we can make particular self-consistent estimates on the side, and use them in relating our simple estimates to experiment. For example, we found that the two differences in cohesion in the successive compounds, MnO,  $\text{Mn}_2\text{O}_3$ ,  $\text{MnO}_2$  in the simple theory were both 1.67 eV, but a self-consistent calculation suggested that the second was smaller than the first by 0.44 eV (in comparison to an experimental difference of 0.68 eV). We do not need to abandon the simple approach for this difference, but can note it when we compare with experiment.

Once we had completed the analysis for the manganese oxides, and iron oxides, and put together an article on them [2], we began exploring the properties of LSM, in a different structure, but one based upon the same clusters of octahedral oxygen neighbors with each transition-metal ion. The treatment of cohesion, as a function of concentration  $x$  of Sr, was equally successful. We went on to an estimate of the Néel

and Curie-Weiss temperatures for  $\text{SrMnO}_3$ , which we found to be an antiferromagnetic insulator. We estimated the magnitude of a Jahn-Teller distortion in  $\text{LaMnO}_3$  which makes it also insulating. We found a magnetic state of  $\text{LaMnO}_3$  with (100) ferromagnetic planes (due to a novel double-exchange for the distorted state), antiferromagnetically stacked, as observed. We estimated the corresponding Néel temperature and its volume dependence, and the ferromagnetic Curie-Weiss temperature which applies between the Néel and Jahn-Teller temperatures. We expected that holes doped into  $\text{LaMnO}_3$  by the substitution of Sr for La would show a hopping conductivity in the context of small-polaron theory, and we obtained the conductivity as a function of temperature for that case. The results for LCSF where we had data with which to compare are shown in Figure 1. We saw that above the Jahn-Teller temperature  $\text{LaMnO}_3$  should be metallic as observed, and paramagnetic with a ferromagnetic Curie-Weiss constant which we estimate. These predictions were not so accurate, but were sufficiently close to provide a clear understanding of all of these properties in terms of a simple theory and parameters known at the outset.

We then went on to the corresponding analysis of  $\text{La}_{1-x}\text{Sr}_x\text{Co}_{0.2}\text{Fe}_{0.8}\text{O}_3$ , making comparison with extensive experiments by Tai, Nasrallah, Anderson, Sparlin, and Schlin [3] and compare with their interpretation. We agree with them that doping with Sr raises the  $\text{Fe}^{3+}$  to  $\text{Fe}^{4+}$  (rather than  $\text{Co}^{3+}$  to  $\text{Co}^{4+}$ ). We find that the spacing  $d(x)$  variation arises largely from the presence of these  $\text{Fe}^{4+}$  ions, as do the orthorhombic and rhombohedral distortions. In contrast to the interpretation by Tai, et al., we find that oxygen vacancies do *not* provide doping electrons, as they would in  $\text{SrTiO}_3$ , and that disproportionation of the  $\text{Co}^{3+}$  is *not* needed to explain

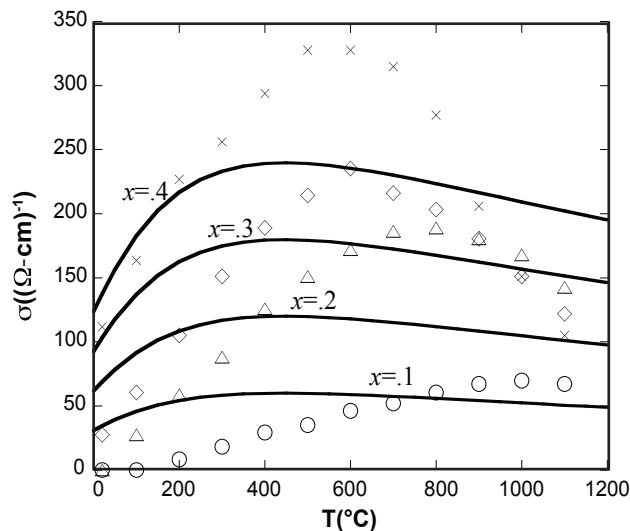
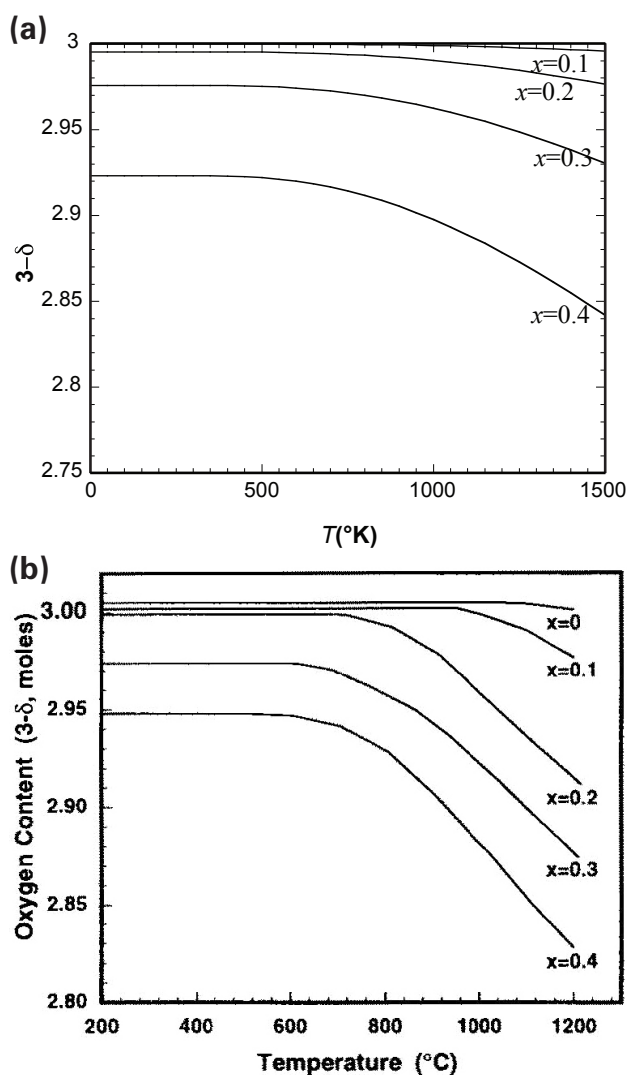


FIGURE 1. Calculated Small-Polaron Conductivity of LSCF (Lines), Compared with the Data (Points) from Reference 3

the conductivity data. We find further that such disproportionation is not favored energetically. We did agree with their interpretation that the conduction comes from small polarons, as illustrated in Figure 1. The nature of vacancies in LSCF was particularly interesting. Our estimate of the energy to form an undistorted oxygen vacancy gave a value near 2 eV. The data from Reference 3 would suggest values depending upon Sr doping concentration  $x$  and considerably smaller. Their finding of vacancy concentration (actually the number of O ions  $3-\delta$  per formula unit) as a function of temperature could be fit rather well by a model of a negative formation energy for oxygen sites with all four A neighbors (Sr or La) as Sr, 0.25 eV for only three Sr, and 0.50 eV for two Sr. The result of such a model is shown in Figure 2, and is very similar to the



**FIGURE 2.** Oxygen content, or oxygen deficiency ( $\delta$ ), as a function of temperature and Sr atom fraction ( $x$ ). Part (a) shows theoretical values if the vacancy formation energy were 0.5 eV for oxygen sites with two Sr neighbors, 0.25 eV for three Sr neighbors, and negative for four Sr neighbors. Part (b) shows the experimental (Reference 2) values.

corresponding experimental curves, also shown. We could understand such low-energy vacancies if the two Fe (or Co) ions neighboring the vacancy moved together to provide bonding minority-spin states to accommodate the two electrons from the vacancy formation, which would then insure that no doping was provided by the vacancy. At present it does not appear that we can reliably calculate the energy for such large distortions, but we proceed under the assumption that they can occur.

## Conclusions and Future Directions

The study of cohesion in the manganese and iron oxides has clarified the simplifications which can be made, and where corrections may be necessary. The study of the properties of LSM and LSCF have demonstrated the essential correctness of these simplifications and opened the door to application to a wider variety of properties, including some even more relevant to the fuel cell project. However, the study of the properties of LSM and LSCF are in a preliminary state, and the central question as to the nature of oxygen vacancies remains uncertain. We anticipate next putting these areas on firmer ground and then moving into less firm territory related to cathode surfaces.

## FY 2008 Publications/Presentations

1. Walter A. Harrison, *Tight-Binding Theory of the Oxides of Manganese and Iron*, arXiv:0803.0994, Phys. Rev. B, in press, April 2008.
2. Walter A. Harrison, *Electronic structure of Mn and Fe oxides*, paper presented at the March, 2008, meeting of the American Physical Society in New Orleans.

## References

1. Walter A. Harrison, *Elementary Electronic Structure*, World Scientific (Singapore, 1999), revised edition (2004).
2. Walter A. Harrison, *Tight-Binding Theory of the Oxides of Manganese and Iron*, arXiv:0803.0994, Phys. Rev. B, in press, April 2008.
3. L.-W. Tai, M. M. Nasrallah, H. U. Anderson, D. M. Sparlin, and S. R. Schlin, *Solid State Ionics*, **76**, 273 (1995).



---

## **IV. SECA CORE RESEARCH & DEVELOPMENT**

### **B. Anodes and Coal Contaminants**



---

## IV.B.1 Novel Sulfur-Tolerant Anodes for Solid Oxide Fuel Cells

Meilin Liu (Primary Contact), Zhe Cheng,  
Songho Choi, Jeng-Han Wang  
Georgia Institute of Technology  
School of Materials Science and Engineering  
771 Ferst Drive NW  
Atlanta, GA 30332-0245  
Phone: (404) 894-6114; Fax: (404) 894-9140  
E-mail: meilin.liu@mse.gatech.edu

DOE Project Manager: Briggs White  
Phone: (304) 285-5437  
E-mail: Briggs.White@netl.doe.gov

Contract Number: 42219

Start Date: September 27, 2004  
Project End Date: June 30, 2008

(it may involve internal reforming). Unfortunately, most hydrocarbon fuels contain sulfur, which would dramatically degrade SOFC performance at parts-per-million (ppm) levels. Low concentration of sulfur (ppm or below) is difficult to remove efficiently and cost-effectively. Therefore, knowing the exact poisoning process for state-of-the-art anode-supported SOFCs with Ni-YSZ cermet anodes, understanding the detailed anode poisoning mechanism, and developing new sulfur-tolerant anodes are essential to the promotion of SOFCs that run on hydrocarbon fuels.

In the fiscal year of 2008, the current project focused on (i) characterizing both the immediate and the slow sulfur poisoning process for state-of-the-art SOFC button cells with an anode-supported structure under various operating conditions, and (ii) understanding the mechanism of the enhanced sulfur tolerance displayed by the niobium oxide modified Ni-YSZ cermet anode.

### Objectives

- Characterize the sulfur-poisoning effect on anode-supported solid oxide fuel cells (SOFCs) under practical operation conditions.
- Investigate the sulfur-anode interaction mechanism in H<sub>2</sub>S contaminated fuels at elevated temperatures.
- Establish an effective operational window that allows SOFCs to reach lifetime targets in commercially viable power generation environments.
- Modify Ni-yttria stabilized zirconia (YSZ) anode surface to achieve enhanced sulfur tolerance.

### Accomplishments

- Characterized sulfur poisoning behavior of state-of-the-art anode-supported SOFC button cells under various operating conditions, including the concentration of H<sub>2</sub>S and cell current density.
- Revealed the mechanism for the enhanced sulfur tolerance of Ni-YSZ anode modified by a thin coating of niobium oxide.

---

### Introduction

SOFCs have a great potential to be one of the cleanest and most efficient systems that convert chemical energy to electrical energy. One of the unique advantages of SOFCs over other types of fuel cells is the potential for direct utilization of hydrocarbon fuels

### Approach

Multi-cell testing had been carried out to evaluate both the short-term and the long-term sulfur poisoning behavior for state-of-the-art anode-supported SOFC button cells. Current-voltage (I-V) curves as well as impedance spectra were collected at different stages of the sulfur poisoning experiment to deduce what might have happened to the cells exposed to fuels containing different concentrations of H<sub>2</sub>S. Meanwhile, Raman spectra of niobium oxide before and after heat treatments in fuels with and without ppm-level H<sub>2</sub>S were also collected. Further, quantum chemical calculations were used to predict the thermodynamic stability, electronic structure, and vibrational frequencies for niobium oxides and sulfides, which helped to explain the origin of the enhanced sulfur tolerance for Ni-YSZ cermet anodes modified using a thin coating of niobium oxide.

### Results

The results of the multi-cell testing indicated that the sulfur poisoning behavior for anode-supported cells are similar to that observed for electrolyte-supported cells. Figure 1 shows the results of a multi-cell sulfur poisoning test for ~2,000 hours using anode-supported cells with a lanthanum strontium manganese oxide (LSM)-based cathode at 750°C under constant current conditions. Similarly, Figure 2 shows the results of another multi-cell sulfur poisoning test (for ~1,400 hours) at 750°C under constant current conditions using anode-supported cells with a lanthanum strontium cobalt iron oxide (LSCF) cathode. From both experiments, the following

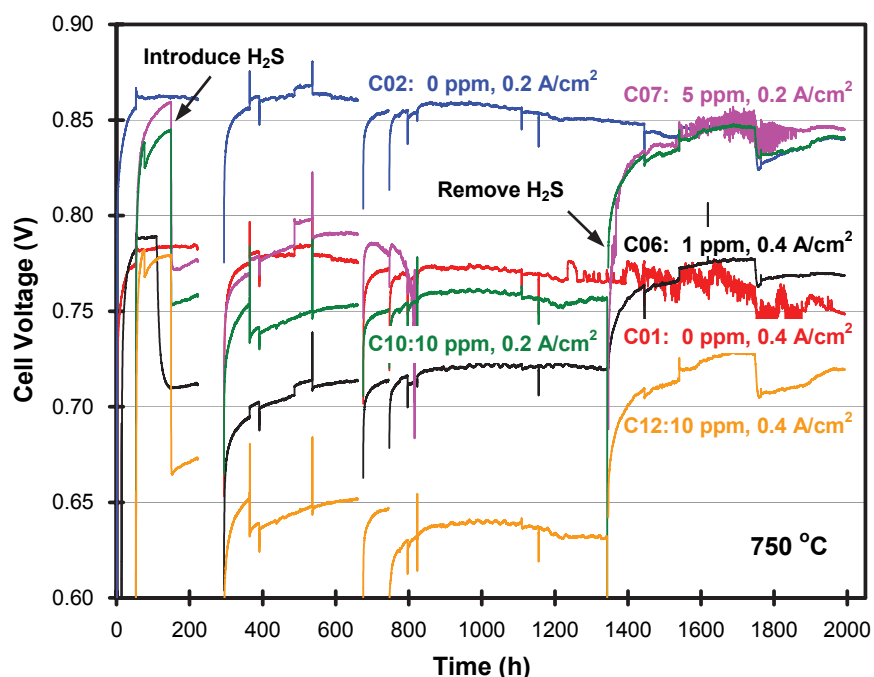


**FIGURE 1.** Plots of cell voltage versus time for a long-term multi-cell sulfur poisoning experiment using anode-supported cells with an LSM-based cathode at 750°C under constant current conditions. The  $p\text{H}_2\text{S}/p\text{H}_2$  ratios were 0, 1, 5, and 10 ppm, and the current densities were 0.2 and 0.4 A/cm<sup>2</sup>.

observations could be made. First, the relative cell power output drop (due to sulfur poisoning) increased with H<sub>2</sub>S concentration (in terms of  $p\text{H}_2\text{S}/p\text{H}_2$  ratio). Second, the relative cell power output drop increased with current density for the same H<sub>2</sub>S concentration under the constant current conditions tested. However, the change in anode resistance due to sulfur poisoning decreased with cell current density. Third, the degree of sulfur poisoning seemed to reach saturation when the  $p\text{H}_2\text{S}/p\text{H}_2$  ratio was low (i.e., 1 ppm). However, there appeared to be a second-stage, continued slower degradation when the  $p\text{H}_2\text{S}/p\text{H}_2$  ratio was 10 ppm and more. This is especially significant for cells with LSCF cathodes (see Figure 2): the cell power output continued to degrade in an almost linear fashion for about 1,000 hours after the initial dramatic drop in performance upon exposure to H<sub>2</sub>S (as seen for cells C10 and C12 in Figure 2).

Figure 3 shows some typical impedance spectra of several anode-supported cells with LSCF cathodes in the long-term multi-cell sulfur poisoning experiment at different stages. Like electrolyte-supported cells, the quick cell performance drop upon exposure to H<sub>2</sub>S is due to the large increase in the cell (anode) interfacial resistance. It is interesting to note that the so-called 2<sup>nd</sup>-stage slower degradation, as observed in Figure 2 for cells exposed to 11.8 ppm H<sub>2</sub>S, was also due to the continued increase in anode interfacial resistance instead of the change in cell ohmic resistance.

The origin of the observed 2<sup>nd</sup>-stage sulfur poisoning is not clear at the moment. Such 2<sup>nd</sup>-stage slower degradation has been observed in several independent studies using different types of cells [1-3]. Since the cell bulk resistance did not change in the 2<sup>nd</sup>-stage poisoning process and thermodynamic considerations have ruled out the formation of bulk nickel sulfide under the poisoning condition (e.g., 750°C,  $p\text{H}_2\text{S}/p\text{H}_2 = 10$  ppm) as the reason for poisoning, the most likely explanation for such behavior (i.e., 2<sup>nd</sup>-stage slower poisoning) is that it is due to the continued adsorption of sulfur onto the nickel surface towards equilibrium coverage. This is because when the nickel surface is clean, the sticking coefficient for sulfur adsorption was close to one and remains relatively constant until the surface coverage is close ~0.5-0.6 (i.e., ~50-60% of the area on the surface was covered by sulfur). Beyond that, the sticking coefficient for sulfur adsorption on nickel will decrease by several orders of magnitude [4]. This is expected to significantly lower the rate for the continued adsorption of sulfur onto the nickel surface as the area coverage goes up from ~0.5-0.6 to the ~0.8-0.9 range or even higher. As a result, the observed rate of cell performance degradation decreased dramatically and the poisoning process would last much longer beyond the quick poisoning stage.

Finally, Figures 4(a) to (c) show the Raman spectrum for niobium oxide (Nb<sub>2</sub>O<sub>5</sub>) after heat treatment in fuels with and without H<sub>2</sub>S. Upon heat treatment in

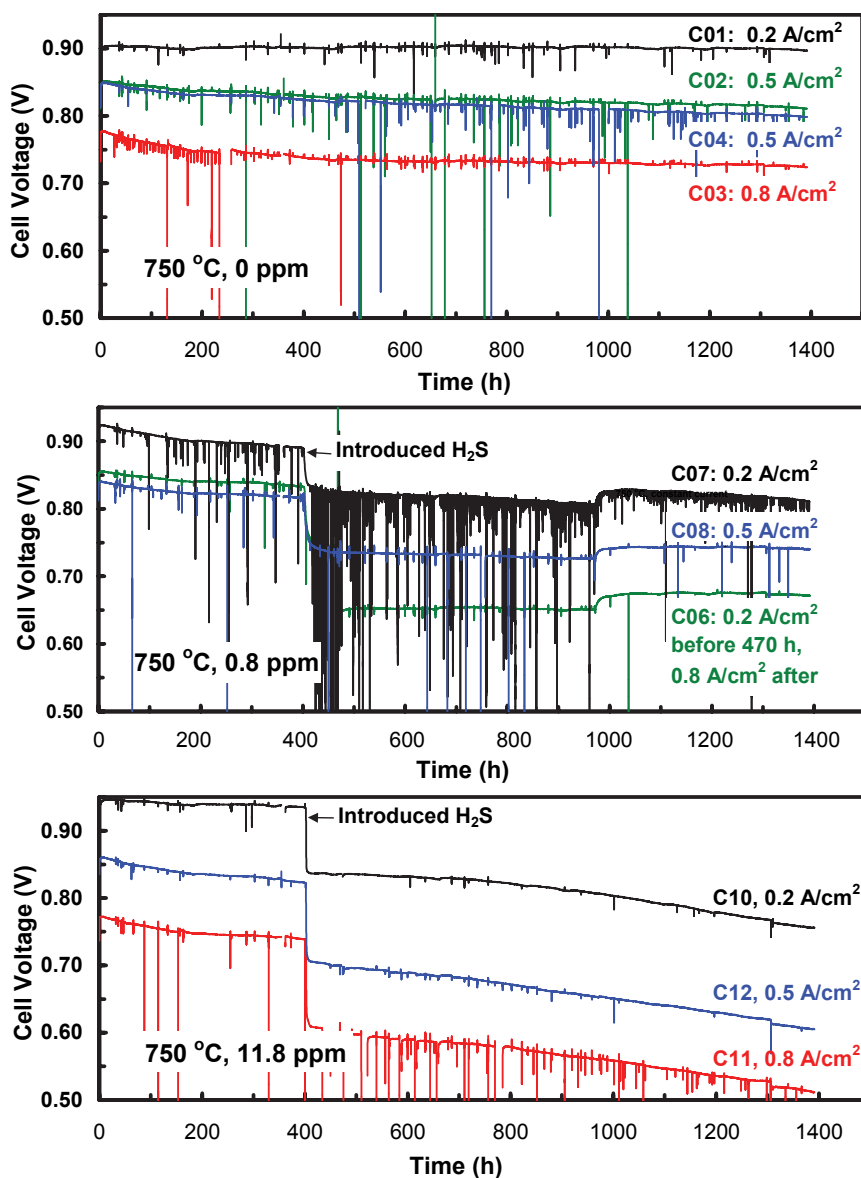


**FIGURE 2.** Plots of cell voltage versus time for a long-term multi-cell sulfur poisoning experiment using anode-supported cells with an LSCF-based cathode at 750°C under constant current conditions. The  $p_{\text{H}_2\text{S}}/p_{\text{H}_2}$  ratios were 0, 0.8, and 11.8 ppm, and the current densities were 0.2, 0.5, and 0.8  $\text{A}/\text{cm}^2$ .

$\text{H}_2$ ,  $\text{Nb}_2\text{O}_5$  was reduced to  $\text{NbO}_2$  as shown in Figure 4(a). In comparison, if  $\text{Nb}_2\text{O}_5$  was exposed to fuels containing 100 ppm  $\text{H}_2\text{S}$  at similar temperatures, the Raman peaks that corresponds to  $\text{NbS}_2$  were identified on the surface of  $\text{NbO}_2$ , as shown in Figure 4(b). Figure 4(d) shows the results of the density of state (DOS) calculation for niobium oxide ( $\text{NbO}_2$ ) and niobium sulfide ( $\text{NbS}_2$ ). The results indicate that there are no obvious band gaps around the Fermi level for both  $\text{NbO}_2$  and  $\text{NbS}_2$ , which means that  $\text{NbS}_2$  formed is still conductive just like  $\text{NbO}_2$ . In addition,  $\text{NbO}_2$  and  $\text{NbS}_2$  have similar DOS distribution indicates that both probably have similar catalytic abilities. Based on the information,

it is concluded that the enhanced sulfur tolerance for niobium oxide coated Ni-YSZ is due to the transition of the surface from niobium oxide to niobium sulfide, i.e., from  $\text{NbO}_2$  to  $\text{NbS}_2$ , which do not lead to negative impact on the electronic and catalytic properties of the anode surface.

## Conclusions and Future Directions

The initial sulfur poisoning behavior of state-of-the-art anode-supported SOFC button cells are similar to that of the electrolyte-supported cells. The observed relative cell power output drop increased with  $\text{H}_2\text{S}$

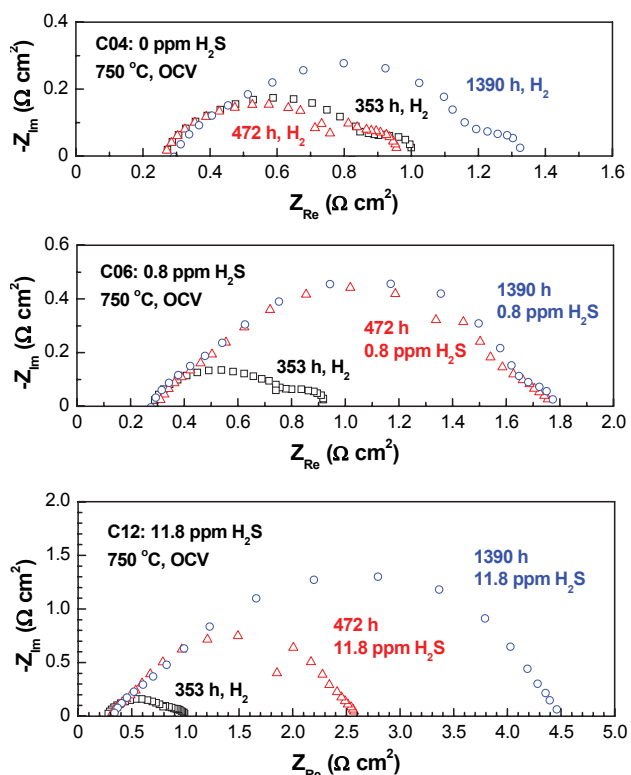


**FIGURE 3.** Full cell impedance spectra at 750°C under open circuit condition for cells C04, C06, and C12 at different stages in the long-term sulfur poisoning experiment shown in Figure 2. Note that 353 hours was before the introduction of H<sub>2</sub>S, 472 hours was after the quick poisoning stage finished, and 1,390 hours was after the cells were subject to H<sub>2</sub>S for ~1,000 hours.

concentration and with cell current density under the constant current conditions. However, the long-term sulfur poisoning behavior of those cells indicate that there might be a second-stage slower degradation due to sulfur poisoning, which would last for a thousand hours or even longer. Finally, analysis of niobium oxide indicated that the enhanced sulfur tolerance for niobium oxide coated Ni-YSZ anode is due to transformation of the niobium oxide to corresponding niobium sulfides in sulfur-containing fuels.

Future work is briefly outlined as follows:

- Characterize the long-term sulfur-poisoning effect for anode-supported SOFC button cells with LSCF cathodes under various current densities in fuels with different concentrations of H<sub>2</sub>S using a state-of-the-art sealant.

### FY 2008 Publications/Presentations

1. Z Cheng, M Liu, "Characterization of sulfur poisoning of Ni-YSZ anodes for solid oxide fuel cells using in situ Raman microspectroscopy." *Solid State Ionics* 178 (2007) 925-35.

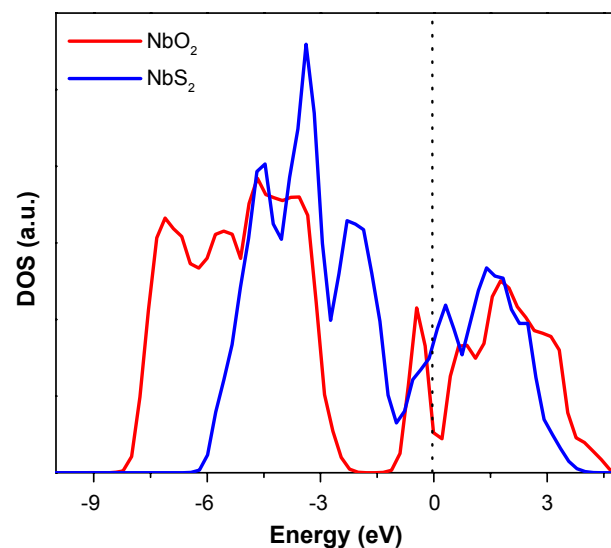
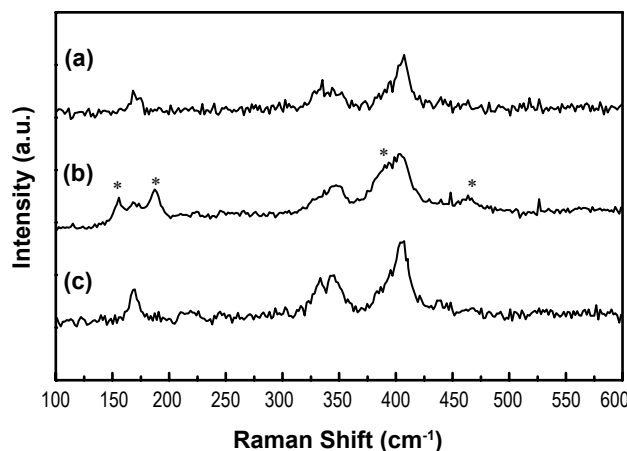


**FIGURE 4.** (a) Raman spectrum of NbO<sub>2</sub> powder after reduction in H<sub>2</sub> at 800°C for 24 hours. (b) Raman spectrum of NbO<sub>2</sub> powder after being exposed to 100 ppm H<sub>2</sub>S balanced with H<sub>2</sub> at 700°C for 15 hours; the asterisk represents the newly emerged peaks that correspond to NbS<sub>2</sub>. (c) Raman spectrum of Nb<sub>2</sub>O<sub>5</sub> powder after regeneration in H<sub>2</sub>. (d) DOS analysis for NbO<sub>2</sub> and NbS<sub>2</sub>.

2. Z Cheng, S Zha, M Liu, "Influence of cell voltage and current on sulfur poisoning behavior of solid oxide fuel cells." *Journal of Power Sources* 172 (2007) 688-93.
3. Z Cheng, H Abernathy, M Liu, "Raman Spectroscopy of Nickel Sulfide Ni<sub>3</sub>S<sub>2</sub>." *Journal of Physical Chemistry C* 111 (2007) 17997-8000.
4. S Choi, J Wang, Z Cheng, M Liu, "Surface modification of Ni-YSZ using niobium oxide for sulfur-tolerant anodes in solid oxide fuel cells." *Journal of The Electrochemical Society* 155 (2008) B449-B54.
5. J-H Wang, Z Cheng, J-L Bredas, M Liu, "Electronic and vibrational properties of nickel sulfides from first principles." *Journal of Chemical Physics* 127 (2007) 214705/1-05/8.

6. J-H Wang, M Liu, "Computational study of sulfur-nickel interactions: A new S-Ni phase diagram." *Electrochemistry Communications* 9 (2007) 2212-17.

7. J-H Wang, M Liu, "Surface regeneration of sulfur-poisoned Ni surfaces under SOFC operation conditions predicted by first-principles-based thermodynamic calculations." *Journal of Power Sources* 176 (2008) 23-30.

## References

1. S Zha, Z Cheng, M Liu, "Sulfur poisoning and regeneration of Ni-based anodes in solid oxide fuel cells." *Journal of the Electrochemical Society* 154 (2007) B201-B06.
2. JP Trembly, AI Marquez, TR Ohrn, DJ Bayless, "Effects of coal syngas and H<sub>2</sub>S on the performance of solid oxide fuel cells: Single-cell tests." *Journal of Power Sources* 158 (2006) 263-73.
3. ER Ray, "Contaminant Effects in Solid Oxide Fuel Cells," in W.J. Hubner (Ed.), *Proceedings of the Third Annual Fuel Cells Contractors Review Meeting*. U.S. Department of Energy, Washington, DC, 1992, p. 108-16.
4. CH Bartholomew, PK Agrawal, JR Katzer, "Sulfur Poisoning of Metals." *Advances in Catalysis* 31 (1982) 153.

## IV.B.2 Coal-Based Fuel Cells

Randall Gemmen

National Energy Technology Laboratory (NETL)  
3610 Collins Ferry Road  
Morgantown, WV 26507  
Phone: (304) 285-4536; Fax: (304) 285-0903  
E-mail: Randall.Gemmen@netl.doe.gov

DOE Project Manager: George Richards  
Phone: (304) 285-4458  
E-mail: George.Richards@netl.doe.gov

Contract Number: 07-220621

Start Date: October 1, 2007  
Project End Date: September 30, 2008

### Objectives

- Identify cleanup levels for trace contaminant species contained in coal syngas via solid oxide fuel cell (SOFC) performance tests on direct coal syngas and single trace coal species.
- Measure the performance of liquid tin anodes.

### Accomplishments

- A portable multi-cell test rig was constructed with the capability of testing 12 cells simultaneously at selected gasification sites. This rig was delivered to the Wilsonville, AL, Power Systems Development Facility (PSDF), and awaits testing later in FY 2008.
- Single species testing of H<sub>2</sub>Se and benzene were performed on SOFC button cells. Results showed the effect of H<sub>2</sub>Se on cell performance to behave similar to that of well characterized H<sub>2</sub>S.
- Initial testing of a liquid tin anode (LT-SOFC) showed as much as 40 mW/cm<sup>2</sup> power densities and activation energy for the overall cell resistance activation energy of 185 kJ/gm-mol. Theoretical and experimental comparisons show a mixed potential between oxidation of tin and dissolution of oxygen in tin.

### Introduction

To achieve the DOE goal of developing 60% efficient coal-based fuel cell systems will require test and evaluation of existing SOFC technology on coal syngas, and examination of novel SOFC materials and concepts. The work performed here accomplishes

the first objective by studying the impact of trace contaminant species on SOFC performance. Here, SOFC test specimens are evaluated for their voltage degradation that follows from the injection of a specific trace material. The second objective is accomplished by investigating the performance of novel liquid tin anodes. These tin anodes are formed over electrolyte supported cells and tested at high temperature to determine their voltage and power density performances. The first objective will allow us to determine levels of trace materials found in coal that are acceptable to SOFC performance and thereby set cleanup targets for gasification technology. The second objective will allow us to determine if novel tin anodes can be used in 'direct coal' conversion fuel cells and thereby allow us to simplify the SOFC plant through integration of both coal fuel processing (cleanup) and electrochemical conversion.

### Approach

The direct coal syngas tests are performed using a newly developed multi-cell test capability as shown in Figure 1. This test rig allows for 12 individual cells to be tested simultaneously thereby allowing for redundant cell testing and improved accuracy statistical analysis of the post-run data. Such capability is needed in order to maximize "data through-put" when performing tests on *real world* large-scale gasification technology. As



**FIGURE 1.** Multi-Cell Test Rig for Direct Coal Syngas Testing at the Power Systems Development Facility at Wilsonville, AL

a further measure to maximize return on investment, on-line analytical test capability is added to this work. Specifically, a gas chromatograph – inductively coupled plasma – mass spectrometer (GC/ICP/MS) unit has been configured to measure incoming gas streams for various contaminant elements and species. The data obtained from this part of the work will allow us to determine possible interaction between species and their coordinated/combined impact on SOFC performance. Results from these direct coal syngas tests are anticipated later in FY 2008. Current plans call for testing at the PSDF facility on Mississippi lignite coal ca. July, 2008.

Individual coal contaminant tests are performed using laboratory test facilities designed to deliver known amounts of contaminant to the anode of an SOFC button cell. By determining how specific contaminants attack SOFC anode materials (yttrium-stabilized zirconia [YSZ] and Ni), improved assessments for cleanup targets can be achieved.

Finally, liquid tin anode tests were performed by containing tin within a YSZ ‘cup’, where the bottom of the ‘cup’ was formed using a YSZ wafer. The cathode was made from lanthanum strontium manganite. Current was taken off the anode using a graphite electrode. For the present tests, hydrogen (50%) and nitrogen (50%) were delivered to the 6 mm thick tin anode, and air (with 3% water) was delivered to the cathode. The cell was operated over a temperature range of 600 to 950°C. Both voltage and power density data was obtained as well as data on the overall cell resistance.

## Results

Figure 2 depicts the cell voltage output as a function of operating time for a cell cyclically exposed to hydrogen, synthesis gas, and trace material. For these tests the humidified synthesis gas is mixed with the trace specie gas (in hydrogen) to the desired concentration and fed to the cell. The cell furnace is controlled at 800°C. Total fuel flow rates to the SOFC are maintained at roughly 300 mL/min for the duration of the test. The gas composition used is 29.1% H<sub>2</sub>, 28.6% CO, 12% CO<sub>2</sub>, 3.2% N<sub>2</sub>, and 27.1% H<sub>2</sub>O. The current loading on the cell was 0.25 A/cm<sup>2</sup>. The cells tested were obtained from a common lot produced by MSRI (Salt Lake City, UT). As shown in Figure 2, the cell is initially fed with pure hydrogen during the initial test period, followed by pure syngas. H<sub>2</sub>Se is then delivered to the cell at 5 ppm, which causes readily apparent degradation in performance. The cell is re-exposed to hydrogen for approximately 4 days, during which time the fresh cell output is never re-established. Finally, the cell is re-exposed to clean syngas and again shows relatively degraded output. The key result from these H<sub>2</sub>Se tests

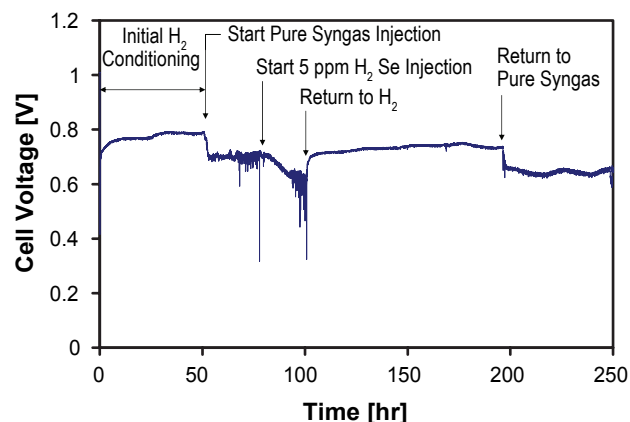


FIGURE 2. Effect of 5 ppm H<sub>2</sub>Se on Cell Voltage Performance

is the finding that selenium behaves very similarly to sulfur in regards to its effect on cell performance. This conclusion would be consistent with theoretical analyses that show no secondary phase formation between anode materials and selenium.

The effect of benzene SOFC cell performance was also evaluated following similar protocols. Results for 15 ppm benzene levels, see Figure 3, show minor influence on cell voltage over a period of 220 hours. The test at these conditions for this cell continues, and post-test analysis of the cell will be completed later to determine existence of other impacts (e.g., carbon deposition) which may be present but not noticeably impacting early voltage performance of the cell.

Results for LTSOFC testing are shown in Figure 4. The tests results shown were taken at 900°C under 50% hydrogen and 50% nitrogen on the anode. From trends understood from data taken at lower temperatures (showing an overall cell resistance activation energy of 185 kJ/gm-mol), it is expected that further improved performance is possible at higher temperatures. As

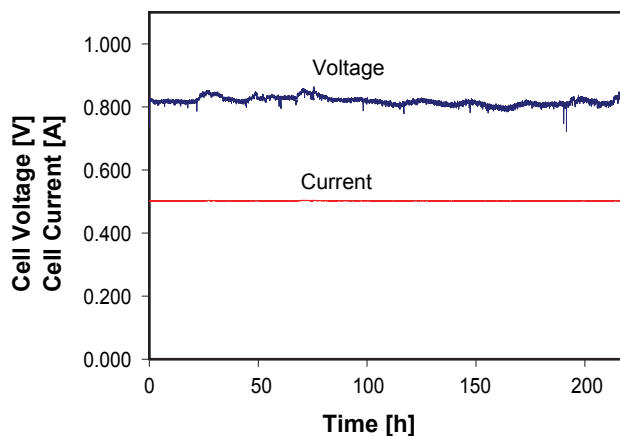
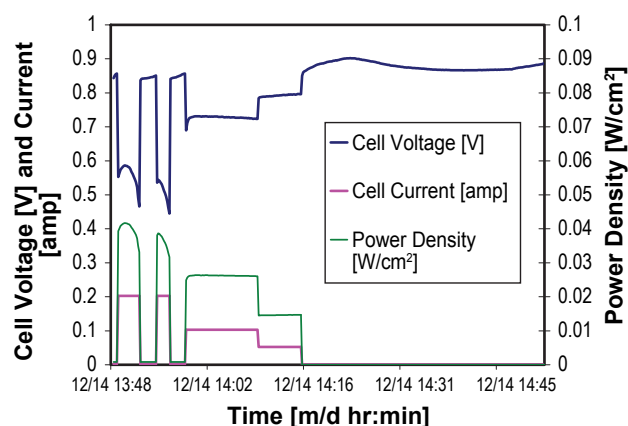


FIGURE 3. Effect of 15 ppm Benzene on Cell Performance



**FIGURE 4.** Voltage and Current Test Data of a 6 mm Thick Tin Anode on a YSZ Electrolyte Supported Cell

shown in the data, a peak power density of about  $40 \text{ mW/cm}^2$  was achieved at these conditions. Theoretical work to assess the ideal cell voltage suggests that the use of the reaction,  $\text{Sn} + \text{O}_2 \rightarrow \text{SnO}_2$  to assess the ideal potential will underestimate the actual open circuit (ideal) potential. According to the data, open circuit voltage (OCV) is about 0.9 volts. At these conditions, however, the given reaction would only predict a cell voltage a little above 0.8 volts. Instead, given the expected drive to achieve equilibrium between oxygen in the anode gas and oxygen within the tin, the reaction  $\text{H}_2 + \frac{1}{2} \text{O}_2 \rightarrow \text{H}_2\text{O}$  could be used which gives a cell potential of 1.05 volts at these conditions. These results suggest a ‘mixed potential’ exists, perhaps due to non-equilibrium remaining between gas phase and tin phase oxygen.

## Conclusions and Future Directions

Progress is being made toward understanding the effects of trace coal contaminants on SOFC performance. Clearly  $\text{H}_2\text{Se}$  will require cleanup, but perhaps given its similarity to sulfur (both in elemental electron states and in observed effect on cell performance), what measures are taken to remove sulfur to prevent degraded cell performance will also satisfactorily remove  $\text{H}_2\text{Se}$ . More work is needed to identify exact levels of contaminant removal for cleanup performance, and synergistic effects between contaminants should also be studied. Other groups, SRI and Pacific Northwest National Laboratory, and continued work by NETL on direct coal syngas testing, will set these limits in the near future.

Initial work to investigate liquid tin anode SOFC technology shows peak power density performances of near  $40 \text{ mW/cm}^2$ . To achieve higher performances, higher cell temperatures will likely be needed. Finally, it was observed that to predict OCV performance of the cell, a ‘mixed potential’ between hydrogen and tin reaction with oxygen must be assessed. While not fully understood, it appears some non-equilibrium between gas phase oxygen and oxygen dissolved in the tin can be expected at these conditions.

## FY 2008 Publications/Presentations

1. K. Gerdes and R.S. Gemmen, “Porous anode model for coal syngas fuelled SOFC: One-dimensional mass and energy transport normal to cell plane,” to be presented at the 2008 ASME 6<sup>th</sup> International Fuel Cell Science, Engineering and Technology Conference, June 16–19, 2008, Denver, CO.
2. K. Gerdes, J. Trembly, R.S. Gemmen, “Effect of  $\text{H}_2\text{Se}$  Exposure on Performance of Anode Supported SOFC,” to be presented at the 2008 International Pittsburgh Coal Conference, September 29 – October 2, 2008, Pittsburgh, PA.
3. R.S. Gemmen, M.C. Williams, K. Gerdes, “Degradation Measurement and Analysis for Cells and Stacks,” submitted to J. Power Sources.
4. R.S. Gemmen, “Fuel Cell Degradation—On Effects of Coal Trace Elements & On Degradation Measurement & Assessment,” to be presented at the 2008 ASME 6<sup>th</sup> International Fuel Cell Science, Engineering and Technology Conference, June 16–19, 2008, Denver, CO.

## IV.B.3 Combined Theoretical and Experimental Investigation and Design of H<sub>2</sub>S Tolerant Anode for Solid Oxide Fuel Cells

Gerardine G. Botte (Primary Contact),  
Damilola Daramola, Madhivanan Muthuvel  
Ohio University  
183 Stocker Center  
Athens, OH 45701  
Phone: (740) 593-9670; Fax: (740) 593-0873  
E-mail: botte@ohio.edu

DOE Project Manager: Briggs White  
Phone: (304) 285-5437  
E-mail: Briggs.White@netl.doe.gov

Contract Number: 42527

Start Date: July 21, 2005  
Project End Date: July 30, 2008

performance. However, coal syngas also contains H<sub>2</sub>S at high concentrations (0.5-5%) depending on where the coal is mined [1]. A commonly used anode material for SOFCs is Ni- yttria-stabilized zirconia (YSZ). When H<sub>2</sub>S-containing gas comes in contact with a Ni-based anode, deterioration of the anode is inevitable. Most of the experimental research in the area of SOFCs has been focused on development of new anode materials for sustaining H<sub>2</sub>S attack. In this project, we concentrate on understanding the mechanism of anode (Ni-YSZ) deterioration by H<sub>2</sub>S gas present in the coal syngas, using molecular modeling. We also want to establish validity for the predicted theoretical models by experimental analysis. Hence, objectives for this project are to determine the mechanism for H<sub>2</sub>S interaction with the Ni-YSZ anode and recommend either preventive measures for the Ni-YSZ anode or a new sulfur tolerant anode material.

### Objectives

- Determine the mechanism for solid oxide fuel cell (SOFC) anode deterioration by H<sub>2</sub>S gas found in coal syngas.
- Employ molecular modeling to study the interaction of the anode with chemical species.
- Confirm the theoretical model with experiments and surface analysis.

### Accomplishments

- The initial structure for the anode was modified beginning with the structure for zirconium oxide. This would facilitate matching experimental with theoretical Raman spectroscopy.
- The experimental setup was further improved to mitigate delaminating of current collector from the electrode and electrolyte.

### Approach

The initial anode material tested in previous quantum chemistry calculations had used monoclinic zirconium oxide as the starting material. However X-ray diffraction (XRD) analysis showed that this material had a cubic structure due to stabilization by yttrium. The error in this structure was further confirmed by a comparison between calculated Raman spectroscopy and experimental Raman spectroscopy. The structure was then rebuilt using a program called CRYSTAL [2] which is able to reproduce periodic structures better than Gaussian can.

In the experimental analysis, the sealing and mesh attachment was configured to perform better and for longer periods of time at higher temperature. The sealing was improved using a low temperature adhesive on the gold O-ring, while the mesh attachment was improved by using platinum paste between the electrodes and the current collector. Finally, the cathode was switched to lanthanum strontium manganite (LSM)-YSZ.

### Introduction

An SOFC is a high temperature fuel cell which operates at temperatures between 850 and 1,000°C. The SOFC is a viable option for a high temperature hydrogen fuel source. One of the high temperature hydrogen sources is coal syngas. Burning coal produces a gas known as coal syngas, which contains hydrogen along with other chemical species such as CO and CO<sub>2</sub>. Since an SOFC operates at high temperature, the presence of CO and CO<sub>2</sub> in coal syngas will not affect its

### Results

A comparison between the Raman spectra for the calculated (YZr5O12) and the experimental (Dong et al. [3]) structure for YSZ can be seen in Figure 1. This result, combined with XRD analysis shows that the SOFC electrolyte has a cubic structure indicating revision in the theoretical analysis was necessary. In addition to this, literature suggested a better quantum chemistry software than Gaussian 03 was suitable for

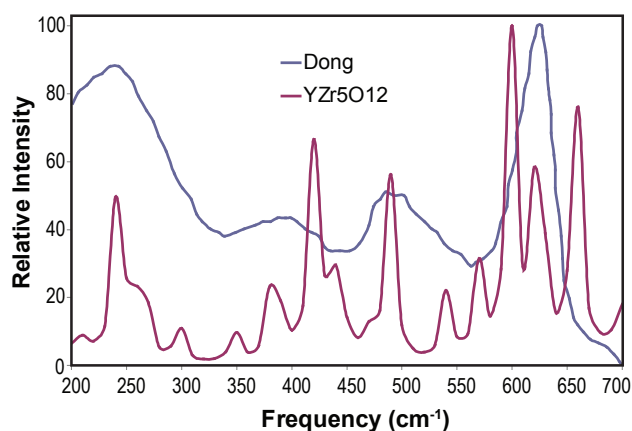


FIGURE 1. Raman Spectra of YSZ: Gaussian O3 (Red) and Experimental (Blue)

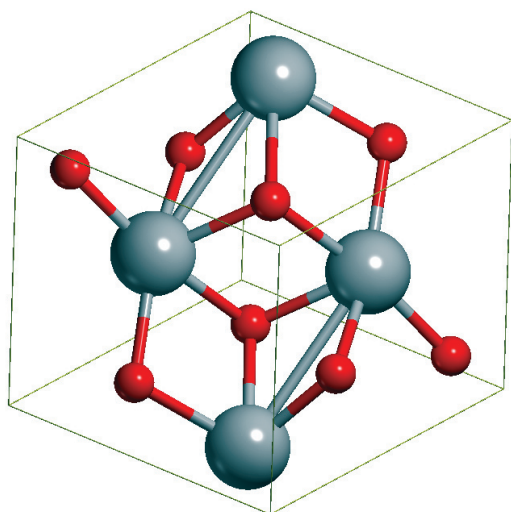


FIGURE 2. Calculated Structure of Monoclinic Zirconia

structural analysis of periodic structures i.e. crystal structures [4].

Using CRYSTAL (version 06), a preliminary analysis was performed on monoclinic zirconia based on the B3LYP level of theory. The lattice parameters (unit cell dimensions, angle, and atom coordinates) were calculated and compared to experimental values to ensure that the calculated structure (Figure 2) was valid. The average percent error was 0.75% with (3.0% being the largest error) between lattice parameters ensured that the method of calculation performed was accurate (Table 1).

After validation of the calculated structure, the frequency analysis was performed with the mean average difference calculated equaling 21 cm<sup>-1</sup> (Table 2). This was based on 13 agreed frequency modes for monoclinic zirconia. Although this difference is large,

TABLE 1. Calculated and Experimental Lattice Parameters for Monoclinic ZrO<sub>2</sub>

	Howard [5]	Calculated	% Error
a	5.151	5.2308	1.55%
b	5.212	5.2882	1.46%
c	5.317	5.3952	1.47%
β	99.23	99.35	0.12%
Zr			
x	0.2754	0.2750	-0.13%
y	0.0395	0.0407	2.96%
z	0.2083	0.2099	0.76%
O <sub>1</sub>			
x	0.07	0.0698	-0.27%
y	0.3317	0.3334	0.53%
z	0.3447	0.3462	0.43%
O <sub>2</sub>			
x	0.4496	0.4525	0.65%
y	0.7569	0.7580	0.14%
z	0.4792	0.4795	0.06%

TABLE 2. Calculated and Experimental Raman Frequency Modes for Monoclinic ZrO<sub>2</sub>

Calculated	Feinberg [6]	Difference
	92	
83	102	
190	148	
186	179	-7
200	190	-10
230	222	-8
335		
345	305	-40
358	334	-24
364	348	-16
392		
393	381	-12
512	476	-36
513	500	-13
573	534	-39
576	556	-20
641	615	-26
654	637	-17
778		

several parameters could still be adjusted including the difference between successive iteration values. However, these changes often affect the speed of the calculations performed. The effects of parameter changes are being evaluated at this present time.

For experimental analysis, the cathode to be used was switched from platinum to LSM-YSZ. This was due to problems encountered with platinum delaminating from the electrolyte. LSM-YSZ is also a more conventional cathode, less expensive and can be used as a reference electrode [7]. There had also been some problems with mesh attachment. The Ni and Ag current collectors will still be used on the anode and cathode, respectively; however, these will be attached to the electrodes with platinum paste. This was found to be more adhesive than the Ni paste previously used and did not detach the current collectors from the electrodes even after running at high temperatures for several hours. The use of a gold O-ring as the sealant was re-examined using a soap-bubble meter. The flow of gas into the setup was found to be the same as the outlet gas flow rate for the system at 850°C. Hence, we expect no leakage during the testing of various gas mixtures with our setup. These two steps were the current final step in the experimental setup before running the system with gases and since these have been completed, the setup is now ready to be tested with hydrogen gas.

### Conclusions and Future Directions

- Based on prior analysis, it is required that the models used be validated at every step using XRD and Raman spectroscopy to ensure that the structure calculated is valid.
- The agreement between lattice parameters and frequency modes and symmetry can be translated to success in other structures being calculated at the same level of theory.
- The structure factor for the monoclinic zirconia will be calculated using Cerius<sup>2</sup> [8]. This will be used to predict the XRD for the theoretical model and provide another basis for comparison of theoretical to experimental analysis.
- The above analysis (Raman and XRD) will be applied to cubic YSZ and then extended to Ni-YSZ.
- Experimental setup will be tested with 25% H<sub>2</sub> as fuel for the base run.

### FY 2008 Publications/Presentations

1. Quarterly Report for 1<sup>st</sup> calendar quarter 2008, May 7<sup>th</sup>, 2008.
2. Quarterly Report for 4<sup>th</sup> calendar quarter 2007, January 27<sup>th</sup>, 2008.
3. Quarterly Report for 3<sup>rd</sup> calendar quarter 2007, October 18<sup>th</sup>, 2007.
4. *Computational and Experimental Analysis of Solid Oxide Fuel Cell Anodes in the presence of H<sub>2</sub>S*, presented at 212<sup>th</sup> Electrochemical Society Meeting, October 7 – 12, 2007, Washington, D.C.
5. Quarterly Report for 2<sup>nd</sup> calendar quarter 2007, August 20<sup>th</sup>, 2007.

### References

1. G. Y. Lai, *High Temperature Corrosion of Engineering Alloys*, ASM International, Materials Park, OH p. 117. (1990).
2. R. Dovesi, V. R. Saunders, C. Roetti, R. Orlando, C. M. Zicovich-Wilson, F. Pascale, B. Civalleri, K. Doll, N. M. Harrison, I. J. Bush, Ph. D'Arco, and M. Llunell, *CRYSTAL06 User's Manual*, University of Torino, Torino. (2006).
3. J. Dong, Z. Cheng, S. Zha, and M. Liu, *J. Power Sources*, **156**, 461 (2006).
4. J. Kohanoff, *Electronic structure calculations for solids and molecule : theory and computational methods*. New York : Cambridge University Press (2006).
5. C. J. Howard, R. J. Hill, and B. E. Reichert, *Acta Crystallogr. B* **44**, 116 (1988).
6. A. Feinberg and C. H. Perry, *J. Phys. Chem. Solids* **42**, 513 (1980).
7. C. Grigcak, R. Green, J. Giorgi *J. Power Sources* **179**, 317 (2008).
8. Accelrys, Cerius<sup>2</sup>, Accelrys, San Diego, CA (2003).

## IV.B.4 SECA Coal-Based Systems Core Research: Anode Reactions in Coal-Derived Fuels

Olga A. Marina (Primary Contact),  
Gregory W. Coffey, Christopher A. Coyle,  
Carolyn D. Nguyen, Edwin C. Thomsen,  
and Larry R. Pederson

Pacific Northwest National Laboratory  
902 Battelle Blvd., P.O. Box 999  
Richland, WA 99352  
Phone: (509) 375-2337; Fax: (509) 375-2186  
E-mail: olga.marina@pnl.gov

DOE Project Manager: Briggs White  
Phone: (304) 285-5437  
E-mail: Briggs.White@netl.doe.gov

### Subcontractors:

- Montana State University, Bozeman, MT
- University of Florida, Gainesville, FL

Contract Number: 44036

Start Date: October 1, 2006  
Project End Date: September 30, 2008

low, 1-2 ppm, concentrations, sulfur is the most rapid to attack the nickel and is responsible for a 15-30%, depending on the temperature, performance drop. Cell performance losses due to sulfur exposure were reversible and independent of the presence of other impurities. Sulfur-nickel interactions were limited to the surface and no secondary phases were formed. Following slow second stage degradation is attributed to the presence of phosphorus and arsenic.

---

### Introduction

The coupling of coal gasification with SOFCs is being considered by the U.S. Department of Energy as a highly efficient means of electricity production [1]. Gasified coal contains high concentrations of hydrogen and carbon monoxide, which can be utilized by an SOFC to produce electricity. Gasified coal also contains many other minor and trace components that could have an impact on SOFC performance. A recent modeling study by Trembly et al. [2] identified Sb, As, Cd, Hg, Pb, P, and Se as coal gas contaminants that are most likely to affect the performance of an SOFC, some of which are predicted to form secondary bulk phases with nickel in the SOFC anode. Experimental verification of modeling calculations was identified as a critical need.

The effect of phosphorus, arsenic and sulfur impurities in the simulated coal gas on the SOFC performance was investigated under typical SOFC operation conditions. Cells tested were standard nickel/yttria-stabilized zirconia (YSZ) – supported cells with a thin YSZ electrolyte and 20 at% strontium-doped lanthanum manganese cathode. Electrodes were exposed to single and multiple contaminants at concentrations appropriate to their presence in gasified coal, and the cell electrochemical performance was evaluated.

### Approach

The ultimate goal of this project is to establish maximum acceptable concentrations of coal gas contaminants and contaminant combinations that would permit SOFCs to meet long-term standards for degradation. In the current year, the principal focus was on the effect of phosphorus, arsenic and sulfur on the standard nickel/YSZ SOFC anode when present as a single contaminant or in combination in the coal gas. Phosphorus and arsenic at parts per million

### Objectives

- Determine how contaminants found in coal gas affect the performance of nickel-based solid oxide fuel cell (SOFC) anodes, with an emphasis on those contaminants expected to form secondary solid phases with nickel.
- Establish maximum concentrations of contaminants and contaminant combinations in coal gas that would allow SOFCs operating on that fuel to meet long-term degradation standards.

### Accomplishments

- Irreversible losses in SOFC performance up to 10 percent per 100 hours were observed when exposed to low, 1-10 ppm, concentrations of phosphine ( $\text{PH}_3$ ) in simulated coal gas. Lower, but still irreversible SOFC degradation was observed in the presence of similar concentrations of arsine ( $\text{AsH}_3$ ). Both phosphine and arsine interact strongly with Ni in the upper part of the anode to form stable secondary phases such as  $\text{Ni}_3\text{P}$ ,  $\text{Ni}_5\text{P}_2$  and  $\text{Ni}_5\text{As}_2$ . No interactions of phosphorus- or arsenic-containing species with either zirconia or ceria were observed.
- In the presence of multiple contaminants such as phosphorus, arsenic and sulfur present in similar

concentrations are expected from thermochemical calculations to form secondary bulk phases with nickel, whereas sulfur is not. Though extensive studies of sulfur compound interaction with SOFC anodes have been conducted previously, little information is available with regard to sulfur in combination with other coal gas contaminants.

The long-term performances of the anode-supported button cells were evaluated as functions of contaminant concentration, temperature, fuel utilization, current density and time of the exposure. In addition, screening tests were conducted where Ni/YSZ anode support coupons were exposed to coal gas contaminants in a flow-by and flow-through arrangement. Post-test analyses were conducted with analytical scanning and transmission electron microscopies (SEM and TEM), X-ray diffraction (XRD), electron back-scatter diffraction (EBSD), X-ray photoelectron spectroscopy (XPS), and time-of-flight secondary ion mass spectroscopy (ToF-SIMS) to establish the extent and form of contaminant/anode interactions. Surface analytical probes, ToF-SIMS and XPS, are sufficiently sensitive to reveal sub-monolayer adsorption, including competitive adsorption effects, whereas electron microscopy and diffraction techniques revealed the formation of bulk or surface phases.

## Results

SOFC operation on simulated coal gas was evaluated in the presence of phosphorus, arsenic and sulfur at low (0.1 to 20 ppm) concentrations. For phosphorus exposure, introduced as  $\text{PH}_3$  in concentrations of 10 ppm or less into coal gas, no immediate change in the cell area specific resistance (ASR) was observed. After 40-250 hours, depending on the  $\text{PH}_3$  concentration and temperature, the ASR began to increase rapidly, as is shown in Figure 1. During this period of rapid change, degradation rates of 0.1-0.2% per hour were observed. With continued exposure, degradation abated and a new steady-state level of performance was reached, typically at power retention level of 70% of the initial value. This degradation appeared to be irreversible: when  $\text{PH}_3$  exposure was ended and the cell was left running under otherwise identical conditions in pure coal gas, no recovery in performance occurred.

Similar to phosphorus, when arsenic was introduced into the coal gas fuel at concentrations of 10 ppm or less, the SOFC performance did not change immediately. A period of slow (~1 percent per 100 hours) ensued, as shown in Figure 2, followed by steady-state performance at a power retention level greater than 90 percent. Figure 2 also shows results for sulfur and phosphorus exposure either alone or in combination with arsenic. Upon exposure to 1 ppm of  $\text{H}_2\text{S}$ , independent of whether  $\text{PH}_3$  or  $\text{AsH}_3$  were present, the SOFC showed an immediate drop in performance. After 30 hours of

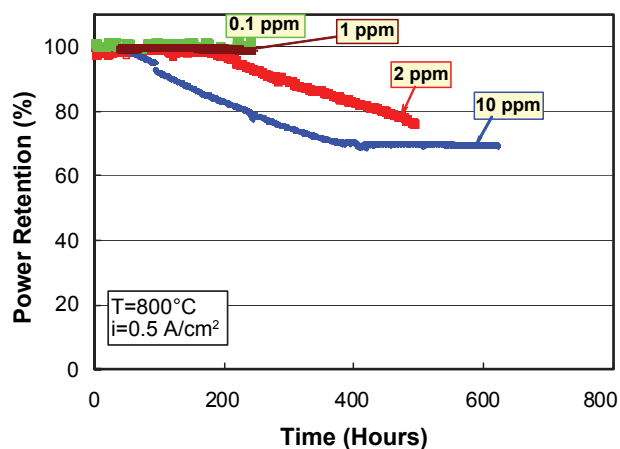


**FIGURE 1.** Effect of phosphine concentration in the coal gas on SOFC performance at 800°C and current density of 0.5 A/cm<sup>2</sup>.  $\text{H}_2/\text{CO}/\text{CO}_2/\text{H}_2\text{O} = 30/23/21/26$ .

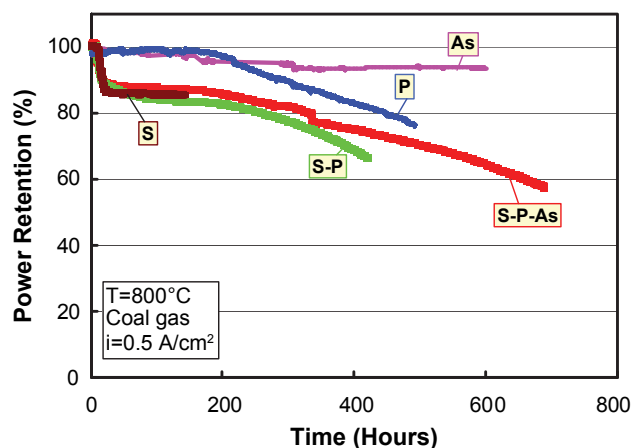


**FIGURE 2.** Effect of 1 ppm of  $\text{H}_2\text{S}$ , 1 ppm of  $\text{AsH}_3$  and 2 ppm of  $\text{PH}_3$  as well as mix of  $\text{H}_2\text{S}$  with  $\text{PH}_3$  or  $\text{PH}_3$  and  $\text{AsH}_3$  at the same concentrations on SOFC performance at 800°C.

exposure, ASR reached a new steady-state with a power retention of 85-70% of the initial value, depending on the temperature. When phosphorus or phosphorus and arsenic were also present, slow second stage degradation was observed. Thus, if sulfur is present in the gas mixture, it dominates the cell performance over the first 30 hours. Later changes in performance are attributed to the presence of phosphorus and/or arsenic, which are independent of changes due to sulfur.

Post-mortem microstructural and surface analyses were conducted on cells following extended testing in coal gas containing contaminants, which revealed secondary nickel phase formation both in the nickel current collecting grid and the Ni/YSZ anode. Depending on the time of exposure, Ni was partially or entirely converted either into nickel phosphides or nickel arsenide. SEM/EDS identified the presence of only one form of the arsenide,  $\text{Ni}_3\text{As}_2$ , while several

forms of nickel phosphides,  $\text{Ni}_3\text{P}$ ,  $\text{Ni}_5\text{P}_2$  and  $\text{Ni}_2\text{P}$ , were found depending on the  $\text{PH}_3$  concentration. In contrast, no secondary phases containing nickel and sulfur were ever observed. Although nickel arsenide and nickel phosphide phases are electrically conductive [3], electronic percolation in the outer portion of the anode support is believed to be compromised through extensive recrystallization of alteration phases. A loss of porosity can also occur. Micrographs showing extensive grain growth following phosphorus and arsenic exposure are given in Figure 3. The phases  $\text{Ni}_3\text{P}$  and  $\text{Ni}_5\text{P}_2$  are formed by eutectic reactions at 870 and 897°C, respectively [4], which are sufficiently close to test temperatures to promote high solid state diffusivities and thus substantial grain growth of alteration phases.

Tests performed with both arsenic and phosphorus added to coal gas revealed distinctive differences in the distribution of alteration phases. While  $\text{Ni}_5\text{As}_2$  was observed only in the very upper part of the anode, up to 30-40  $\mu\text{m}$  from the top,  $\text{Ni}_3\text{P}$  penetrated much deeper into the anode, up to 160  $\mu\text{m}$  following ~700 hours of operation at 800°C, as is shown in Figure 4. As such, arsenic competes effectively with phosphorus

for reaction with nickel. Both phases formed large agglomerates instead of fine nickel particles, which obviously compromised percolating Ni network as well as electronic conductivity in the upper anode layer. Further down towards the active interface, only pure nickel in the Ni/YSZ was observed, as expected. No secondary phosphorus-nickel, arsenic-nickel or sulfur-nickel phases were detected in the bulk Ni/YSZ anode away from the upper part.

Surface sensitive techniques, ToF-SIMS and XPS, were engaged to analyze whether coal gas contaminants had migrated to the active anode/electrolyte interface to form an adsorption layer. At monolayer coverage, such surface adsorption layers would not be visible by analytical electron microscopic techniques. For sulfur, surface probes showed the presence of an adsorption layer on all exposed nickel surfaces to the active interface, which is well-known to lead to reversible SOFC performance loss. Adsorbed phosphorus was similarly found on all exposed nickel surfaces by XPS point scans and ToF-SIMS line scans. Unlike sulfur, the presence of a phosphorus surface adsorption layer did not appear to have electrochemical consequences:

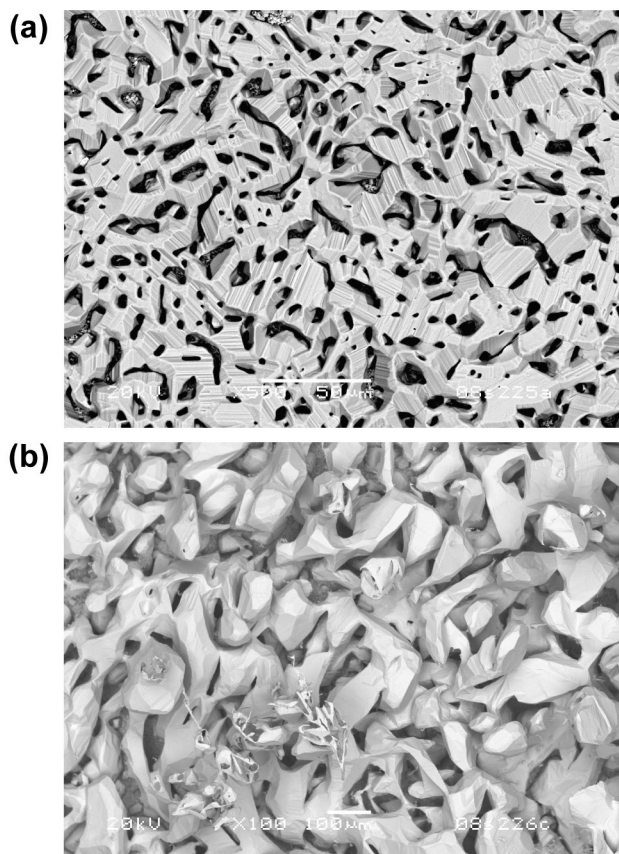


**FIGURE 3.** SEM image of the Ni/YSZ anode after 250 hour cell operation in the coal gas with 5 (a) and 20 ppm (b) of  $\text{PH}_3$  at 800°C. EDS revealed ca. 25 at% (a) and 27-30 at% (b) that corresponded to  $\text{Ni}_3\text{P}$  and  $\text{Ni}_5\text{P}_2$ , respectively.

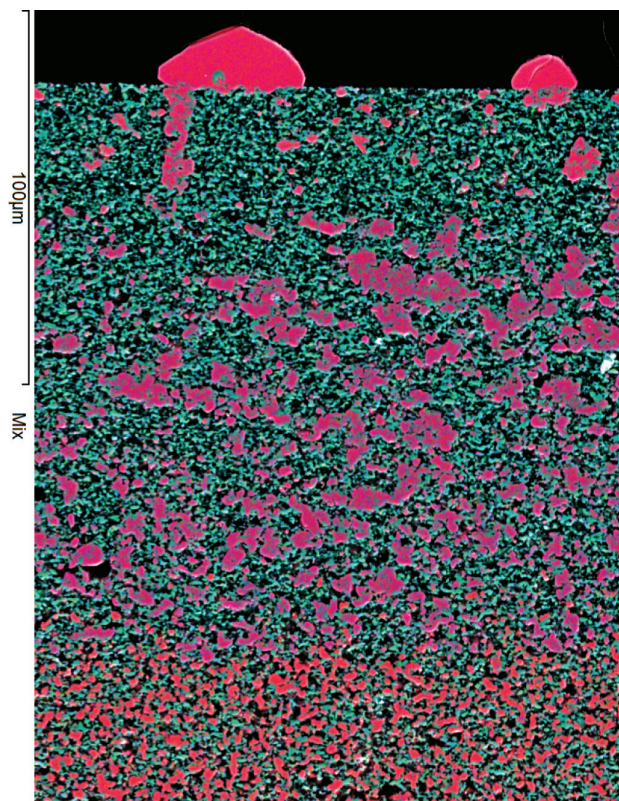


**FIGURE 4.** Cross section of the upper part of the Ni/YSZ anode after 700 hour test in the coal gas with 1 ppm of  $\text{PH}_3$ , 1 ppm of  $\text{H}_2\text{S}$  and 1 ppm of  $\text{AsH}_3$  at 800°C. In the elemental maps, zirconia is shown in teal, a mix of  $\text{Ni}_3\text{P}$  and  $\text{Ni}_5\text{As}_2$  in pink,  $\text{Ni}_3\text{P}$  is shown in purple and metal Ni is in red.

phosphorus adsorption layers formed much faster than the onset of degradation in button cell tests. For arsenic, no surface adsorption layer was detectable by surface probes at the active interface, even after hundreds of hours of exposure. Rather, arsenic was restricted to outer portions of the anode, where secondary phases with nickel were found.

### Conclusions and Future Directions

- Exposure of nickel-based SOFC anodes to phosphorus compounds in coal gas at concentrations from 0.1 to 20 ppm resulted in irreversible performance losses. Cell performance remained unchanged for periods to hundreds of hours after phosphorus exposure, followed by a period of steady power loss. Both the onset of degradation and degradation rate were related directly to the contaminant concentration. Loss of electrical percolation in the outer portion of the anode support associated with secondary phase formation is an important mode of degradation.
- Arsenic exposure of nickel anodes similarly led to irreversible performance losses, principally attributed to loss of electrical percolation in the anode support associated with secondary phase formation.
- When 1 ppm of sulfur was also present in the coal gas along with phosphorus and arsenic, it dominated cell performance during the first 30 hours of testing. Nickel-sulfur interactions were limited to the surface and no new bulk phases were detected.
- Other critical coal gas contaminants previously identified will be considered in future tests. Both anode-supported and electrolyte-supported cell configurations will be utilized, the former of which provides information on possible reduction of continuity in the anode support, and the latter of which will allow contaminants to reach the active interface more rapidly. Maximum allowable concentrations of contaminants and combinations of contaminants will be established that would permit SOFC stacks operating on coal gas to meet requirements for long-term degradation.

### FY 2008 Publications/Presentations

1. OA Marina, LR Pederson, DJ Edwards, CA Coyle, JW Templeton, MH Engelhard, and Z Zhu, "Effect of Coal Gas Contaminants on Solid Oxide Fuel Cell Operation," ECS Transactions, Volume 11: Solid-State Ionic Devices, in press.
2. OA Marina, LR Pederson, DJ Edwards, CA Coyle, JW Templeton, MH Engelhard, and Z Zhu, "Effect of Coal Gas Contaminants on Solid Oxide Fuel Cell Operation," presented at the 212<sup>th</sup> Electrochemical Society, Washington, D.C., October, 2007.
3. OA Marina, **LR Pederson, CA Coyle, JW Templeton, MH Engelhard, and DJ Edwards**, "Effect of Coal Gas Contaminants on SOFC Anode Performance and Stability," presented at 8<sup>th</sup> Annual SECA Workshop, San Antonio, TX on August 9, 2007.
4. **JW Stevenson, LA Chick, MA Khaleel, P Singh, LR Pederson, GL McVay, OA Marina, ZG Yang, GG Xia, and DL King**, "Solid Oxide Fuel Cell Technology Development at Pacific Northwest National Laboratory," Presented at 2007 Fuel Cell Seminar, San Antonio, TX on October 17, 2007.
5. OA Marina, **LR Pederson, CA Coyle, EC Thomsen, GW Coffey, DJ Edwards, and MH Engelhard**, "Effect of Coal Gas Contaminants on Solid Oxide Fuel Cell Operation," Presented at 213<sup>th</sup> meeting of the Electrochemical Society, Phoenix, AZ on May 21, 2008.

### References

1. J. P. Strakey, SECA, Coal, and FutureGen, 8<sup>th</sup> Annual SECA Workshop, 2007, [http://www.netl.doe.gov/publications/proceedings/07/SECA\\_Workshop](http://www.netl.doe.gov/publications/proceedings/07/SECA_Workshop).
2. J. P. Trembly, R. S. Gemmen, D. J. Bayless, J. Power Sources, **163**, 986 (2007).
3. G. V. Samsonov, Yu. B. Paderno, V. I. Lazorenko, P. A. Vityaz, Poroshkovaya Metallurgia, **7**, 68 (1971).
4. O. Kubaschewski, E. L. Evans, Metallurgical Thermochemistry, Pergamon (1958).

---

## IV.B.5 Effect of Coal Contaminants on Solid Oxide Fuel System Performance and Service Life

Gopala N. Krishnan (Primary Contact),  
Palitha Jayaweera, and Jianer Bao  
SRI International  
333 Ravenswood Avenue  
Menlo Park, CA 94025  
Phone: (650) 859-2627; Fax: (650) 859-2111  
E-mail: gopala.krishnan@sri.com

DOE Project Manager: Briggs White  
Phone: (304) 285-5437  
E-mail: Briggs.White@netl.doe.gov

Subcontractor:  
RTI International

Contract Number: 42627

Start Date: September 30, 2005  
Project End Date: September 29, 2008

temperature range 700 to 1,000°C and can use fuel streams containing both H<sub>2</sub> and CO. Thus, they are ideal candidates to be integrated with a gas stream from an advanced coal gasifier. However, impurities containing virtually every element in the periodic table are present in coal and many become constituents of coal-derived gas. The distribution of trace level contaminants between gaseous and solid phases depends on the individual gasification processes. The contaminants associated with the gaseous phase have deleterious effects on the performance and lifetime of coal-derived gas fed SOFCs.

The well-known impurities in the coal-derived gas stream include H<sub>2</sub>S, NH<sub>3</sub>, and HCl vapors, volatile metals such as Zn, Cd, and Hg, and metalloids such as As, P, and Sb. Some of these contaminants such as H<sub>2</sub>S are removed by several methods. This project addresses the effect of the key impurities such as H<sub>2</sub>S, methyl chloride, arsine, phosphine on the efficiency and lifetime of SOFCs.

### Objectives

- Determine the sensitivity of solid oxide fuel cell (SOFC) performance to trace level contaminants present in coal-derived gas streams.
- Assess the long-term cumulative effect of trace level contaminants.
- Assess the life expectancy of SOFC systems fed with coal-derived gas streams.

### Accomplishments

- The power densities of several Ni-cermet SOFCs were determined as a function of time when exposed to a simulated coal gas containing a combinations of select contaminants (H<sub>2</sub>S, AsH<sub>3</sub>, PH<sub>3</sub>, and CH<sub>3</sub>Cl) at ppm levels.
- Determined the stability of PH<sub>3</sub> and CH<sub>3</sub>Cl in the presence of water vapor at temperatures above 700°C using a high temperature mass spectrometer and compared the results with thermodynamic equilibrium calculations.

---

### Introduction

SOFCs have a high fuel-to-electricity conversion efficiency, environmental compatibility (low NO<sub>x</sub> production), and modularity. They operate in the

### Approach

The research project includes thermodynamic calculations, fuel cell testing, data analysis, and several characterization techniques to assess the impact of trace contaminants on SOFC performance.

In Task 1, small size (2.5 cm diameter) nickel cermet fuel cells are exposed to a simulated coal gas feed containing multiple contaminants (H<sub>2</sub>S, AsH<sub>3</sub>, PH<sub>3</sub>, and CH<sub>3</sub>Cl) for periods up to 1,000 hours at a constant temperature in the range 750 to 850°C. The tests are conducted under an electrical load to simulate the operation of a working fuel cell. The current-voltage characteristics are determined periodically. The experimental variables are the nature of the contaminant (H<sub>2</sub>S, AsH<sub>3</sub>, PH<sub>3</sub>, and CH<sub>3</sub>Cl), contaminant concentration (sub-ppm levels), temperature, and extent of gas utilization.

In Task 2, a high-temperature Knudsen cell mass spectrometer is used to identify the chemical nature of AsH<sub>3</sub>, PH<sub>3</sub>, and CH<sub>3</sub>Cl at a temperature range of 750 to 850°C and compares them with the available thermodynamic data.

In Task 3, the results from the experiments and thermodynamic calculations are used to recommend the sensitivity limits of contaminants for use with SOFCs in the temperature range of 800-1,000°C. A final assessment will be made on the degradation in the service life of SOFCs because of the presence of trace-level contaminants.

## Results

The results of the literature review and thermodynamic calculations were summarized in the 2006 annual report. Accelerated tests were conducted with small size Ni-cermet fuel cells to determine the effect of eight different contaminants on the fuel cell performance. Several potential trace level contaminants (HCl, Sb, Zn, and Hg) at relatively high levels (5 to 40 ppm) did not have a significant effect on the performance of SOFC coupons under short-term exposure conditions. Volatile species of As and P at relatively high levels (10 and 40 ppm, respectively) appear to degrade the power output of SOFCs even at short duration (<100 hours). These results were summarized in the 2007 annual report.

Long-term tests with very low level of contaminants were conducted in the fiscal year 2008. For these tests, solid oxide Ni-cermet fuel cell samples from InDec B. V., Netherlands (4.5 cm<sup>2</sup> active area) were used. They have an electrolyte layer of dense yttria-stabilized zirconia (YSZ) of 4 to 6 μm in thickness, porous anode layer of 5 to 10 μm, porous anode support layer of 520 to 600 μm, and a porous lanthanum strontium manganite-YSZ cathode layer of 30 to 40 μm thick. The cells were operated at 750 to 850°C with syngas (30% CO, 30.6% H<sub>2</sub>, 11.8% CO and 27.6% H<sub>2</sub>O) under a 1 A load. After stabilization in the simulated coal-derived gas mixture without known contaminants, the cell was exposed to a low level of H<sub>2</sub>S, PH<sub>3</sub>, and AsH<sub>3</sub> (0.5 to 1 ppmv) by adding them into the simulated gas mixture.

Figure 1 illustrates that the power density of the cell does not degrade significantly when it was exposed to 1 ppm AsH<sub>3</sub> at 750°C for 700 hours. Although these results need to be confirmed in additional tests, the results indicate that AsH<sub>3</sub> at this trace level may not

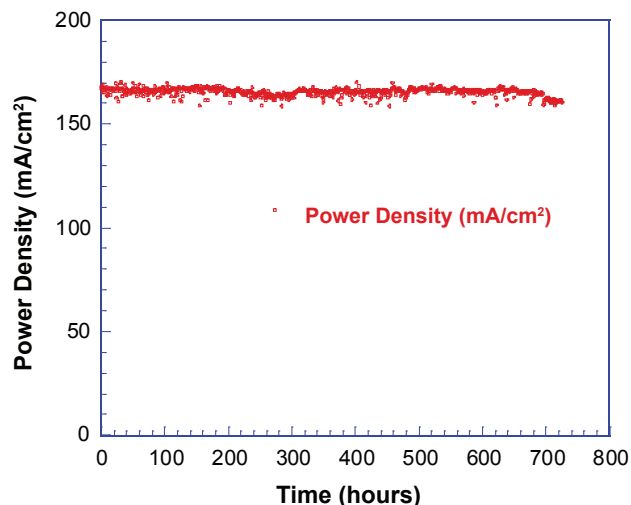
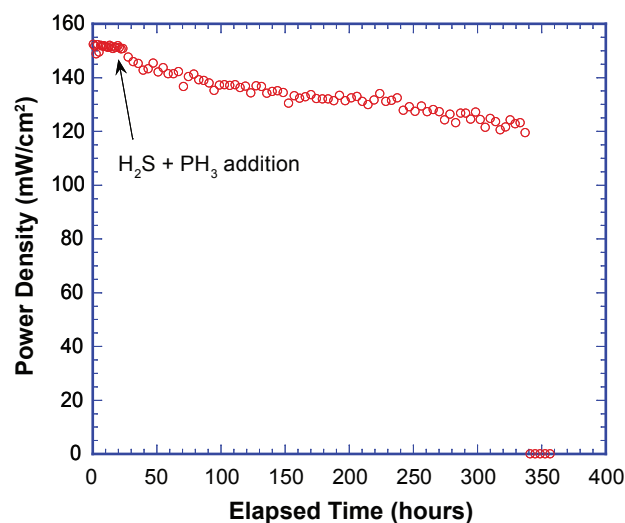


**FIGURE 1.** The Variation of the Power Density of a Cell at 750°C during Exposure to a Simulated Coal Containing 1 ppm AsH<sub>3</sub>

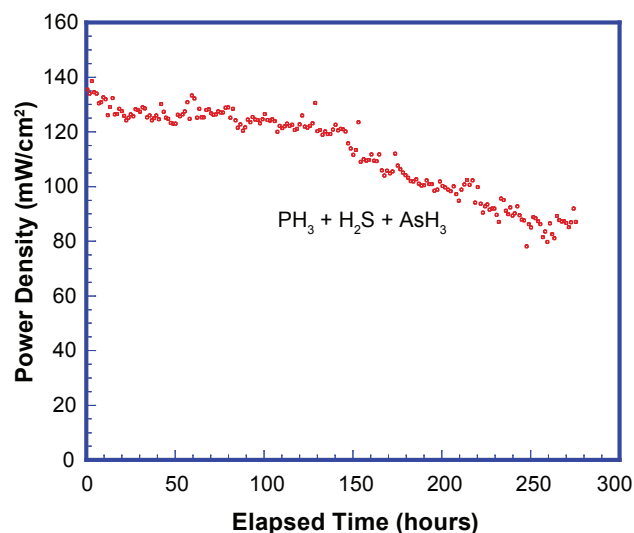
have a significant impact in the degradation of the fuel cell at this temperature.

Figure 2 shows the variation in the power density of a fuel cell when it is exposed to both H<sub>2</sub>S and PH<sub>3</sub> each at about 1 ppm. With the dual contaminants, the cell appeared to be degrading with time. This synergistic effect of contaminants is apparent when three contaminants (H<sub>2</sub>S, PH<sub>3</sub>, and AsH<sub>3</sub>) are present in the feed gas at 1 ppm or sub-ppm levels (Figure 3).

Thermodynamic equilibrium calculations indicate that species such as PH<sub>3</sub> and CH<sub>3</sub>Cl are unstable



**FIGURE 2.** The Variation of the Power Density of a Cell at 750°C during Exposure to a Simulated Coal-Derived Gas Containing PH<sub>3</sub> (1 ppm) and H<sub>2</sub>S (1.3 ppm)



**FIGURE 3.** The Variation of the Power Density of a Cell at 750°C during Exposure to a Simulated Coal-Derived Gas Containing PH<sub>3</sub> (1 ppm), AsH<sub>3</sub> (0.5 ppm) and H<sub>2</sub>S (1 ppm)

at the elevated temperatures of an operating fuel cell. However, such compounds may still be present because of kinetic limitations. A high temperature mass spectrometer was used to determine the chemical stability of these contaminants at temperatures above 700°C. These experiments showed that  $\text{PH}_3$  was stable at 725°C in the absence of water vapor in the gas, but a limited level of oxidation of  $\text{PH}_3(\text{g})$  to  $\text{HPO}_2(\text{g})$  or  $\text{HPO}_3(\text{g})$  occurs in the presence of water vapor. Similarly,  $\text{CH}_3\text{Cl}$  was converted to  $\text{HCl}$  in the presence of water vapor at 750°C, but not to the extent calculated under equilibrium calculations. This kinetically limited stability of  $\text{PH}_3$  and other contaminants indicate that they may be more prone to affect the metal components than the ceramic components of the fuel cell.

### Conclusions and Future Directions

- $\text{AsH}_3$  at sub-ppm levels did not degrade the performance of an SOFC coupon even after 700 hours of exposure.
- Synergistic effects of the contaminants appear to be more severe than individual contaminants alone. The combination of  $\text{PH}_3$ ,  $\text{AsH}_3$ , and  $\text{H}_2\text{S}$  at ppm levels appear to degrade the cell.
- $\text{PH}_3$  and  $\text{CH}_3\text{Cl}$  in the absence of water vapor appear to be more stable than the thermodynamic equilibrium calculations indicate. The above species in the presence of water vapor appear to oxidize at elevated temperatures, but they are still present at higher levels than indicated by equilibrium calculations.

Future directions will include:

- Identification of the chemical nature of the arsenic species at the operating temperature of SOFCs and compare them with thermodynamic equilibrium calculations.
- Additional long-term tests with multiple contaminants ( $\text{H}_2\text{S}$ ,  $\text{AsH}_3$ ,  $\text{PH}_3$  and  $\text{CH}_3\text{Cl}$ ) to confirm the synergistic effects.
- Use of the results from the experiments to recommend the sensitivity limits for SOFC operation.

### FY 2008 Publications/Presentations

1. Effect of Coal Contaminants on Solid Oxide Fuel System Performance and Service Life, Phase I report covering the period October 1, 2005 through September 30, 2007 under cooperative agreement No.: DE-FC26-05NT42627.
2. Effect of Coal Contaminants on Solid Oxide Fuel System Performance and Service Life, Quarterly Technical Progress Report 8 covering the period July 1, 2007 through September 30, 2007.
3. Effect of Coal Contaminants on Solid Oxide Fuel System Performance and Service Life, Quarterly Technical Progress Report 9 covering the period October 1, 2007 through December 30, 2007.
4. Effect of Coal Contaminants on Solid Oxide Fuel System Performance and Service Life, Paper presented at the 8<sup>th</sup> Annual SECA Review Meeting, San Antonio, August 7–9, 2007.

---

## IV.B.6 Direct Utilization of Coal Syngas in High Temperature Fuel Cells

Prof. Ismail Celik  
West Virginia University (WVU)  
Mechanical and Aerospace Engineering Department  
P.O. Box 6106  
Morgantown, WV 26506  
Phone: (304) 293-3111 x 2325; Fax: (304) 293-6689  
E-mail: ismail.celik@mail.wvu.edu

DOE Project Manager: Briggs White  
Phone: (304) 285-5437  
E-mail: Briggs.White@netl.doe.gov

Contract Number: 46299

Start Date: August 1, 2006  
Project End Date: July 31, 2009

### Objectives

- Characterize the effects of major trace contaminants in coal syngas on solid oxide fuel cell (SOFC) performance.
- Identify the fundamental mechanisms through which these impurities affect performance.
- Develop novel materials to minimize impact of contaminants.
- Propose remedies for adverse effects of contaminants on fuel cell performance.

### Accomplishments

- Built or extended research infrastructure: five labs and the Computational Fluid Dynamics Laboratory.
- Developed in-house capability for SOFC fabrication.
- Developed computational and experimental techniques for analysis of SOFCs.
- Performed experiments and simulations with H<sub>2</sub>S and PH<sub>3</sub> containing coal syngas.
- Disseminated results via presentations and publications.
- Organized a mini symposium on coal-based fuel cell technology.
- Trained Post Doctoral fellows, graduate and undergraduate students.

---

---

### Introduction

This project is supported under the Department of Energy Experimental Program to Stimulate Competitive

Research (EPSCoR), a program designed to enhance the capabilities of EPSCoR states in energy research and economic development through the support of advanced research at academic institutions. Our goal is to establish an internationally recognized, sustainable fuel cell research center for coal-based clean power generation which serves as a technology resource for the emerging fuel cell industry in West Virginia. Our strengths are in applying nano-technology to develop and fabricate materials for advanced coal-based fuel cells; establishing a state-of-the-art material characterization and fuel cell testing laboratory; and modeling fuel cells from atomistic to continuum scales using high performance computing. We have formed a multidisciplinary team of research professionals who have worked together for several years and have strong credentials in their respective areas of expertise. Under the present project, we will develop a laboratory infrastructure, solidify interactive working relationships, and attain national recognition for the work conducted by the center in the area of coal-based clean power generation via fuel cells. Our project will be conducted in collaboration with the National Energy Technology Laboratory.

### Approach

The research cluster is based on a multi-scale, multi-disciplinary approach conducted by nine faculty members in four departments at WVU. The work is organized under four integrated projects: (1) anode material development and experimental characterization of fuel cell anodes, (2) sub-micro-scale modeling, (3) multi-scale continuum modeling, and (4) laboratory testing of individual fuel cells and fuel cell systems. The knowledge gained from experiments (Projects 1 and 4) and multi-scale computational models (Projects 2 and 3) will be combined to understand basic mechanisms of cell performance degradation and to formulate preventive remedies.

### Results

#### Anode Materials Development and Characterization

This task seeks to characterize the behavior of SOFC anodes exposed to simulated coal syngas using a combination of *in situ* and ex-situ experimental methods including EIS (electrochemical impedance spectroscopy) and ASR (area specific resistance) measurements under operating conditions, to fabricate fuel cells with custom anodes; and to systematically explore several anode compositions and double-layered structure.

An optical setup, based on phase-shift Sagnac Interferometry method, is applied to obtain out-of-plane deformation of a button cell exposed to coal syngas with and without impurities whereby EIS, ASR and infrared measurements can be performed simultaneously. Measured interferometric fringe patterns at room temperature are in good agreement with the finite element analysis (FEA) results, with an error of less than 5%. Similar results are obtained for high temperature measurement at 800°C. The results from these simulations will be used to validate the models developed under Project 3.

Electrochemical and microstructural analyses are performed on the half cell made of Ni-yttria-stabilized zirconia (YSZ) cermet operated in the simulated coal-derived syngas containing 30.6% H<sub>2</sub>, 30% CO, 11.8% CO<sub>2</sub>, 27.6% H<sub>2</sub>O and 20 ppm PH<sub>3</sub>. Both the charge transfer resistance and the diffusion resistance increase with time (see Figure 1a) which suggests that the

incorporation of phosphorus impurity into the electrode not only impedes the charge transfer but also blocks the channels of gas diffusion. Figure 1b shows a linear tail at low frequencies, implying that the impedance is dominated by the diffusion control of the reactant gases.

X-ray diffraction and X-ray photoelectron spectroscopy (XPS) (Figure 2) measurements have demonstrated that the incorporation of P into the electrode results in the formation of the secondary phases which causes the electrode to lose the electrocatalytic activity toward oxidation of the fuel gas

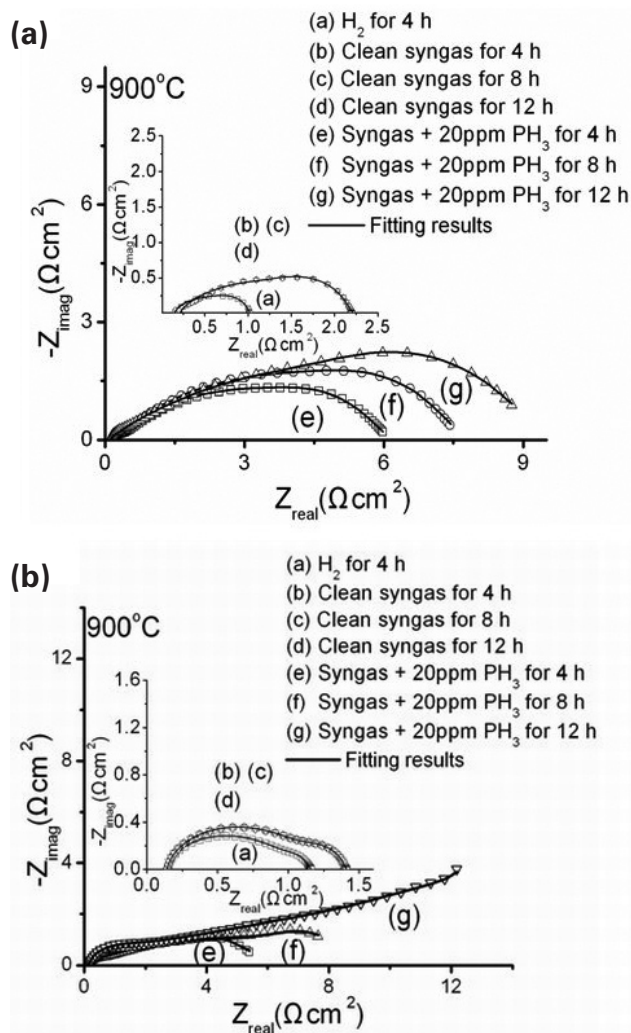


FIGURE 1. Nyquist Plot of Impedance Obtained from the Half Cell at 900°C: (a) Unloaded Cell, (b) Loaded Cell

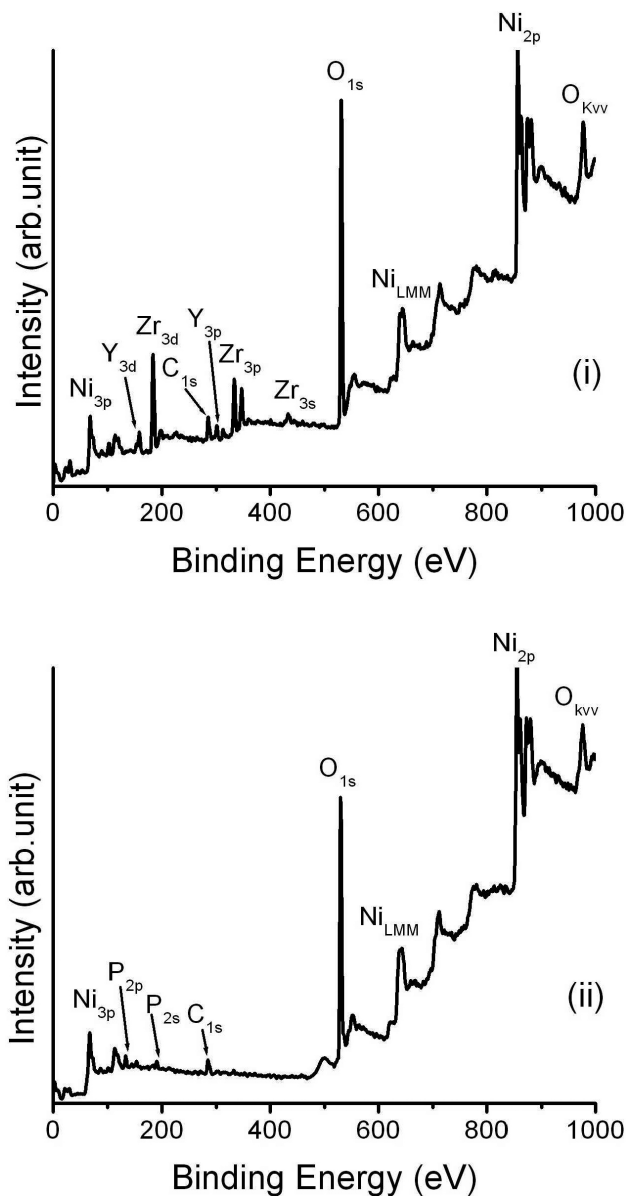


FIGURE 2. Survey Scan of the XPS Spectra Obtained from the Ni-YSZ Working Electrode under Different Conditions; (i) the Electrode after Exposure to the Clean Syngas (Clean Cell), (ii) the Electrode after Exposure to the PH<sub>3</sub>-Containing Syngas at the Open Circuit (Open Circuit Cell)

and inhibits the ability of electrode to transport oxygen ions in the electrode. Therefore, the charge transfer resistance increases with time during exposure to the  $\text{PH}_3$ -containing syngas (Zhi et al. 2008)

An advanced anode-supported planar SOFC with  $>1 \text{ W/cm}^2$  power density for direct utilization of coal syngas has been developed. These cells perform as good as if not better than the cells that are available commercially, and are being tested in Project 4. A novel sulfur-tolerant anode has been developed by impregnating doped ceria into the MSRI (Utah, U.S.) NiO-YSZ anode supported cell. The sulfur-poisoning test in simulated syngas with 20 ppm  $\text{H}_2\text{S}$  indicated the impregnated doped ceria component is able to enhance sulfur tolerance of anode supported significantly (Gong et al. 2008).

### Sub-Micro-Scale Modeling

Using an *ab initio* tight-binding method, we modeled a number of contaminant species including  $\text{H}_2\text{S}$ ,  $\text{PH}_3$  and  $\text{AsH}_3$ , and simulated their adsorption process on Ni's (1,0,0) surface. In all cases, the contaminant species are found to be chemically bonded to the Ni surface after molecular decomposition. In contrast, when the same species are placed near the Cu's (1,0,0) surface, only physical adsorption occurs.

A molecular dynamics code, ReMoDy, was developed for computing reactive gas mixtures, including catalytic reactions at active surfaces based on the Collision Theory. This is a probabilistic approach and needs input from ab-initio simulations. Simulation inside one micron pore under atmospheric conditions performed on a 2.66 GHz central processing unit, 4 GB random access memory (RAM) workstation took about one week. The program enables simulations involving up to  $10^6$  molecules per each gigabyte of RAM.

### Multi-Scale Continuum Modeling

Several sub-models were developed including multi-component mass transfer, electrochemistry with simultaneous oxidation of hydrogen and carbon monoxide, bulk reaction chemistry and surface reaction chemistry. Two gas phase mechanisms were investigated for water-gas shift and methane steam reforming: (i) a two reaction model for catalytic methane reforming and (ii) an Augmented Reduced Mechanism (ARM 9) originally developed for combustion. In addition, a detailed surface mechanism with 42 reactions and 18 species was implemented using an open source chemical kinetics code CANTERA. The calculated surface coverage of Ni agrees well with similar results in the literature.

The button cell was simulated using our in-house multi-dimensional SOFC code in parallel to the

experiments (Project 4) with simulated coal syngas. The comparison between the voltage-current (VI) curves obtained from the simulations and the experiments (Figure 3a) shows a good agreement between the two. The diffusion limitation of the cell could be predicted upon modifying the diffusion coefficients using a newly proposed correction on the effective diffusivity as a function of local current (Figure 3b) (Cayan et al. 2007, 2008).

We have identified several degradation mechanisms such as thermal stresses, thermal aging, redox cycle, and coal syngas impurities that may damage SOFC anode structural properties during long-term operation and reduce its strength and useful life. To predict long-term anode structural behavior, we are developing a

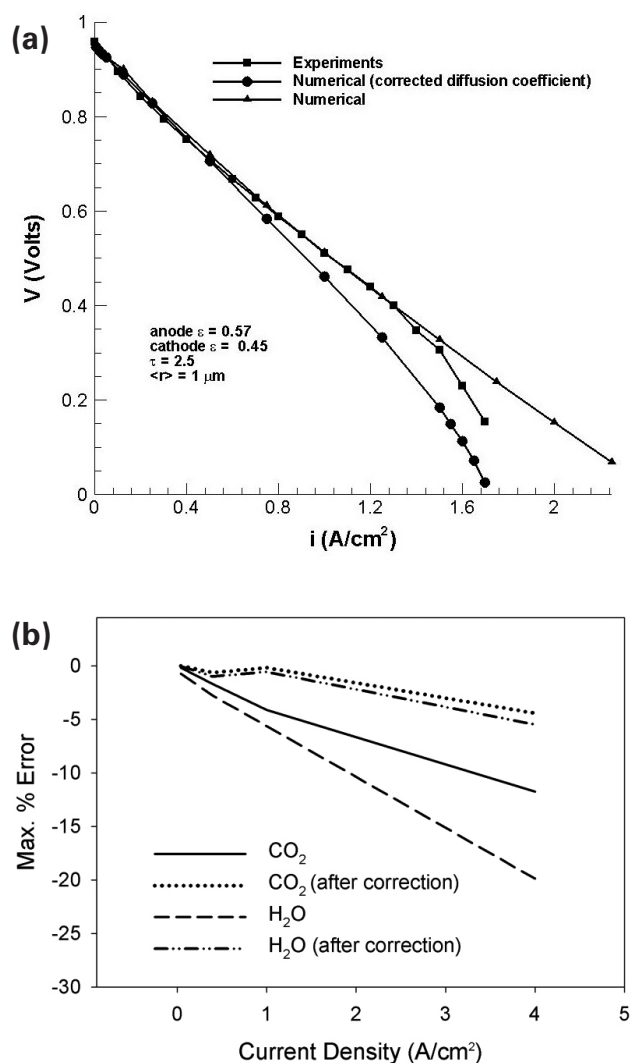


**FIGURE 3.** a) Comparison of the V-I Curve Obtained from Numerical Simulations with That Obtained from Experiments; (b) Maximum Error in Concentration over the Whole Domain in Fick's Model Predictions Plotted as a Function of Cell Current Density for Cases with and without the Proposed Correction

continuum damage model and implementing it in the FEA package ABAQUS™.

### Cell and System Laboratory Testing

The Solartron potentiostat was used to acquire open circuit voltages, polarization curves, cyclic voltammograms with and without current interrupt, and impedance spectra. Long-term tests have been conducted for the MSRI and the WVU cells manufactured under Project 1. Very stable operation is observed over 450 hours with a MSRI cell running on hydrogen fuel. The MSRI cell is also operated with a syngas mixture with and without phosphine impurities. Stable operation in the clean syngas mixture is evident for 230 hours, however, irreversible cell voltage degradation with time was observed after addition of 10 ppm PH<sub>3</sub> (Figure 4a). Impedance characterization

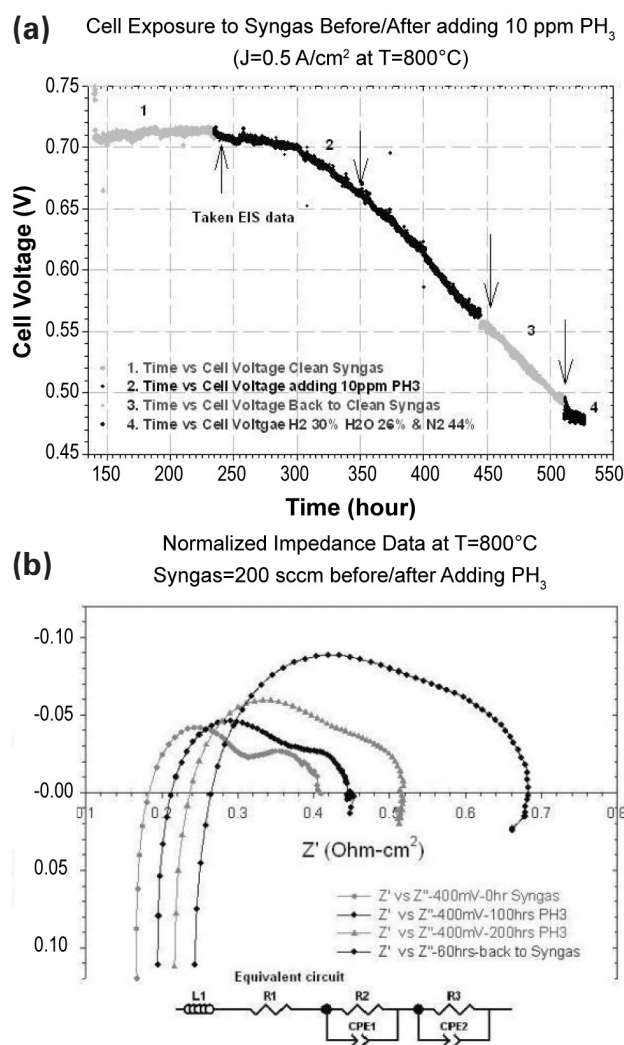


**FIGURE 4.** Results from Long-Term Tests on the MSRI Cell at T=800°C (a) Exposed to Syngas before/after Adding 10 ppm PH<sub>3</sub>, J=0.5 A/cm<sup>2</sup> (b) Normalized Impedance Data before/after Adding 10 ppm PH<sub>3</sub>

indicates that series and polarization resistances increase after addition of the phosphine (Figure 4b).

### Conclusions and Future Directions

- *Ab initio* modeling at the atomistic level indicates very different bonding and electronic states for PH<sub>3</sub>, AsH<sub>3</sub> and H<sub>2</sub>S in the presence of Ni and Cu.
- Sulfur tolerance can be enhanced using impregnated doped ceria in a NiO-YSZ anode.
- Exposing an SOFC to 5-20 ppm of PH<sub>3</sub> causes rapid irreversible performance degradation for which the mechanisms are not clearly understood.
- Multi-dimensional model results showed that the mass diffusion coefficient depends on local current density.
- A variety of observations based on *in situ* electrochemical experiments point to a lack of understanding of basic SOFC performance, a need for improving the experimental protocol, and a need for developing non-electrochemical *in situ* probes.
- In the future the infrared temperature measurement technique will be further refined in order to get a precise measurement on the small spot location of the button cell surface during SOFC testing at 800°C. The effect of P on the performance of an SOFC anode will be investigated further with different P concentrations and operating temperatures. Similar analysis will be extended to arsenic. Atomistic and molecular dynamics simulations will be continued to investigate adsorption and charge transfer mechanisms for impurities other than H<sub>2</sub>S, PH<sub>3</sub> and AsH<sub>3</sub> and noble metals and recommendations will be made with regards to potential materials to reduce degradation rates. Equilibrium and kinetic calculations will also be performed using CANTERA to estimate the most significant forms (or species) of impurities found under stable conditions. Long-term tests of commercial SOFCs and SOFCs manufactured in-house with exposure to selected impurities (phosphine, arsine) will continue. More sensitive post-mortem surface analyses and non-electrochemical *in situ* probes for SOFCs will be developed.

### FY 2008 Publications/Presentations

1. M. Zhi, X. Chen, H. Finklea, I. Celik, N.Q. Wu, Electrochemical and microstructural analysis of Ni-yttria stabilized zirconia electrode operated in phosphorus-containing syngas, J. Power Sources, DOI information: 10.1016/j.jpowsour.2008.05.055, published online (<http://dx.doi.org/10.1016/j.jpowsour.2008.05.055>).
2. M. Gong, X. Liu, J. Tremblay, C. Johnson, Sulfur-Tolerant Anode Materials for Solid Oxide Fuel Cell Application, Journal of Power Sources (2007), 168: 289-298.

3. Cayan F.N., Zhi M., Pakalapati S.R., Celik I., Wu N., Gemmen R., Effects of Coal Syngas Impurities on Anodes of Solid Oxide Fuel Cells: A Review, Accepted by Journal of Power Sources, 2008 (POWER-D-08-00834).
4. Cayan F.N., Pakalapati S.R., Elizalde-Blancas F., Celik I., On Modeling Multi-Component Diffusion Inside the Porous Anode of Solid Oxide Fuel Cells Using Fick's Model, FuelCell2008 6<sup>th</sup> International Fuel Cell Science, Engineering and Technology Conference, Denver, CO, June 16–18, 2008.
5. Cayan F.N., Zhi M., Pakalapati S.R., Celik I., Wu N., Gemmen R., Effects of Coal Syngas Contaminants on SOFC Anodes: A Review, Submitted to 2008 Pittsburgh Coal Conference, September 28 – October 2, 2008.
6. Elizalde-Blancas F., Pakalapati S. R., Escobar-Vargas J., Celik I. B., Numerical Evaluation and Comparison of Different Reduced Mechanisms for Predicting the Performance of a SOFC Operating on Coal Syngas, ASME Fluids Engineering Division Summer Conference, Jacksonville, Florida, August 10–14, 2008.
7. Zhi M., Wu N. Q., Degradation of Ni-YSZ anode in phosphorous-containing coal syngas, Army Research Office Workshop on soldier-portable power sources, College Park, MD, February 20–21, 2008 (poster).
8. Demircan O., Finklea H. O., Zondlo J., Xu C., The effect of PH<sub>3</sub> impurity in coal syngas on SOFC Performance, International Pittsburgh Coal Conference, September 28 – October 2, 2008 .

### References\*

1. Cayan F.N., Pakalapati S.R., Celik I., Modeling of Diffusion Inside the Porous Electrodes, Proceedings of the Second European Fuel Cell Technology and Applications Conference EFC2007, Rome, December 11–14, 2007.

\* See FY 2008 publications for other references



---

## IV. SECA CORE RESEARCH & DEVELOPMENT

### C. Interconnects



## IV.C.1 Evaluation of a Functional Interconnect System for SOFCs

James M. Rakowski  
ATI Allegheny Ludlum  
Technical and Commercial Center  
1300 Pacific Avenue  
Natrona Heights, PA 15065  
Phone: (724) 226-6483  
E-mail: jrakowski@alleghenyludlum.com

DOE Project Manager: Ayyakkannu Manivannan  
Phone: (304) 285-2078  
E-mail: Ayyakkannu.Manivannan@netl.doe.gov

Contract Number: 42513

Start Date: January 1, 2006  
Project End Date: December 31, 2008

### Objectives

- Evaluate commercially available ferritic stainless steels with and without coatings.
- Optimize alloy compositions and surface treatments to maximize performance in solid oxide fuel cell (SOFC) environments.
- Demonstrate significant improvement in critical SOFC-related properties for interconnect systems incorporating new or modified alloy compositions and surface modifications.

### Accomplishments

- Heats of novel and modified stainless steels have been melted and rolled to thin strip.
- Long-term oxidation testing is ongoing in simulated anode and cathode environments at 750-850°C and has produced promising results which can be related to more complex testing.
- Area specific resistance (ASR) testing of coated and uncoated alloy coupons is progressing with the initial results showing improvement in ASR evolution with minor modifications to alloy compositions.
- Post-process treatments to reduce the impact of silicon on ASR evolution with time in service were found to be effective at all conditions investigated, with the benefit increasing at higher temperatures. Reduction in ASR for a basic stainless steel ranged from nominally 50-75%.
- Material has been offered and is being produced to specifications for Industrial Team members for stack production and evaluation.

### Introduction

This project is focused on evaluating the performance of affordable materials integrated into systems for use as SOFC interconnects. Interconnects can be a source of degradation of fuel cell stack performance by the formation and growth of electrically resistive surface oxide layers. It is critical to control which types of oxides form and to minimize layer growth for an extended period of time.

The reference point for this project is a monolithic ferritic stainless steel; examples include ATI 441HP™ stainless steel (UNS S44100) and E-BRITE® alloy (UNS S44627). These were chosen for their combination of low cost, general availability, and performance characteristics. Functionality can be added to these basic interconnect materials at the cost of increased complexity. Modifications are aimed at tailoring the relevant properties of a surface to its local environment in the fuel cell and include special processing, surface treatments, and applied coatings.

### Approach

Two methods for increasing metallic interconnect performance are being explored. The first is to incorporate minor but impactful modifications to alloy compositions in what are essentially commercially available materials. A set of six alloy compositions was reduced to practice, based on current state-of-the-art information and the results from Phase I of this project.

The second approach is to alter the surface of the stainless steel by post-fabrication processing to yield long-lasting benefits by removing/sequestering elements (e.g. silicon and/or aluminum) which form resistive interfacial phases. This may be possible by annealing in specific atmospheres followed by chemical cleaning in some cases. Alternatively, an external oxidation-resistant and electrically conductive coating can be applied to remove the stainless steel surface from direct contact with the SOFC environment.

### Results

A set of six experimental compositions were melted to explore relatively minor modifications to commercially available alloys, notably E-BRITE® alloy and Type 441 stainless steel, which are iron-chromium ferritic stainless steels alloyed with a small amount of niobium. The significant difference between the two primary groups of alloys is the chromium content. The

E-BRITE<sup>®</sup> type alloys contain a high level of chromium (23-26 wt%) while the T441-type alloys have lower chromium content (nominally 17 wt%). Table 1 contains a review of the material used for testing in the current study. It is mixed between commercially available alloys and experimentally melted and processed material (designated EXP followed by a heat number).

**TABLE 1.** Overview of Test Material (weight percent)

Alloy	Cr	Nb	Si	Others
T441	17.5	0.3	0.5	0.3 Mn, 0.3 Ti
E-BRITE <sup>®</sup> alloy	26	0.2	0.3	1 Mo
EXP. 580-2	17	0.3	0.05	0.1 Ce+La
EXP. 580-5	26	0.2	0.3	1 Mo, 0.3 Mn
EXP. 580-6	17	0.3	0.15	0.3 Mn
EXP. 580-7	17	0.3	0.05	0.3 Mn
EXP. 580-8	23	0.3	0.15	0.3 Mn, 1 Mo
EXP. 580-9	24	0.3	0.05	0.3 Mn, 1 Mo

Evaluation of this set of test materials took the form of relatively simple gravimetric oxidation testing (weight change measurements) and more complex ASR testing. Oxidation testing was chosen as a measure of the rate of scale growth at temperature, permitting the use of multiple specimens and long exposure times in a relatively simple test facility. The exposures were carried out in retort furnaces using either air containing 10 vol% water vapor (to simulate the cathode/dual atmosphere environment) and in a simulated anode gas (SAG) containing 4 vol% hydrogen and 3 vol% water vapor in an argon carrier gas. The oxygen partial pressure in the SAG is estimated to be  $2.5 \times 10^{-19}$  kPa at equilibrium.

The exposure to the simulated cathode environment produced results which were consistent with the compositions of the test material. Lower-chromium alloys based on the commercial Type 441 composition generally exhibited higher weight gains than alloys based on E-BRITE<sup>®</sup> alloy-type compositions at both test temperatures (750°C and 850°C). Also, the lower-chromium alloys exhibited an irregular tendency towards accelerated oxidation, which appears to be exacerbated by the reduction of silicon to very low levels (e.g. alloys 580-2 and 580-7). Commercial E-BRITE<sup>®</sup> alloy was resistant to oxidation but was susceptible to evaporative weight loss. This was relieved in the modified variants by the addition of a small amount (nominally 0.3 wt%) of manganese, which causes the formation of an evaporation-resistant manganese chromite spinel oxide layer. Representative data from the 850°C exposure is shown in Figure 1 – the results are similar to those at 750°C in terms of overall trends. Exposure to SAG at 800°C resulted in moderate oxidation after 1,200 hours. The 17%Cr alloys (580-2, 580-6, and 580-7) tended to gain more weight than the 23-26%Cr alloys (580-8 and

580-9). Accelerated oxidation does not appear to be a significant threat in SAG. Representative data from this exposure is shown in Figure 2.

ASR testing is being carried out on both bare and coated alloy substrates. Initial test results are for commercial Type 441 stainless steel, alloy 580-2 (essentially Type 441 with very low Si content and a REE addition), alloy 580-6 (essentially Type 441 with moderately reduced Si content), alloy 580-8 (an E-BRITE<sup>®</sup>-type alloy with 24 wt% Cr, a Mn addition, and moderately reduced silicon content) and alloy 580-9 (an E-BRITE<sup>®</sup>-type alloy with 24 wt% Cr, a Mn addition, and very low silicon content). All of these alloys were tested without coatings to provide baseline data for scheduled future testing under an oxidation-resistant, electrically conductive coating. As such, the ASR values are relatively high. A plot of ASR evolution as a function of time is presented in Figure 3 for representative test stacks (multiple stacks were tested

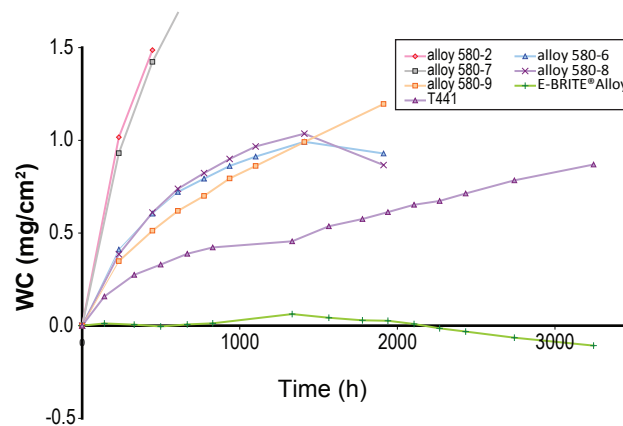


**FIGURE 1.** Oxidation Weight Change Data as a Function of Time for Samples Exposed to Air Containing 10% Water Vapor at 850°C

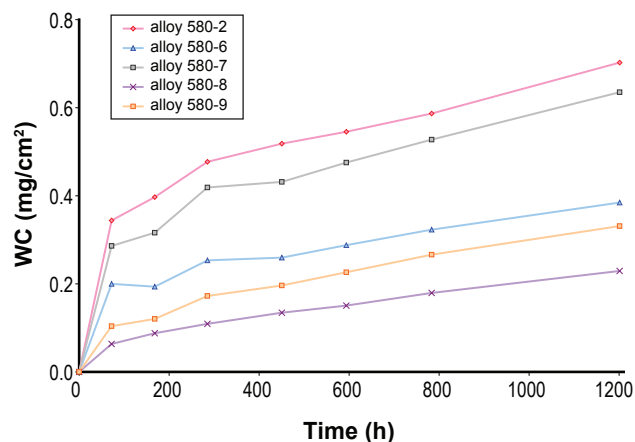


**FIGURE 2.** Oxidation Weight Change Data as a Function of Time for Samples Exposed to SAG at 800°C

but only one per alloy was plotted for clarity, with the exception of alloy 580-2, for reasons to be stated later). Further processing of the data was carried out to arrive at a plot of extrapolated expected ASR value for any given point on the ASR curve (Figure 4). As expected, the values for 40,000-hour ASR are large at first but settle down to a relatively consistent value as parabolic growth of the resistive oxide layers slows. Barring a significant change in the underlying mechanism of scale growth, this is expected to be the contribution to ASR due to the interconnect after 40,000 hours of exposure in this simulation.

- The Type 441 baseline stack exhibited a high rate of ASR increase and a high expected 40,000-hour contribution to ASR.
- Alloy 580-2, showed variable behavior – one stack showed improved performance relative to the baseline, while a duplicate stack exhibited a discontinuity early on in the test and in the end

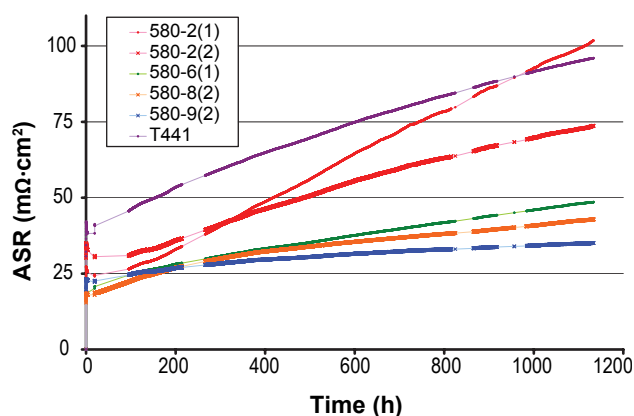


**FIGURE 3.** ASR as a Function of Time for Experimental and Commercial Alloys

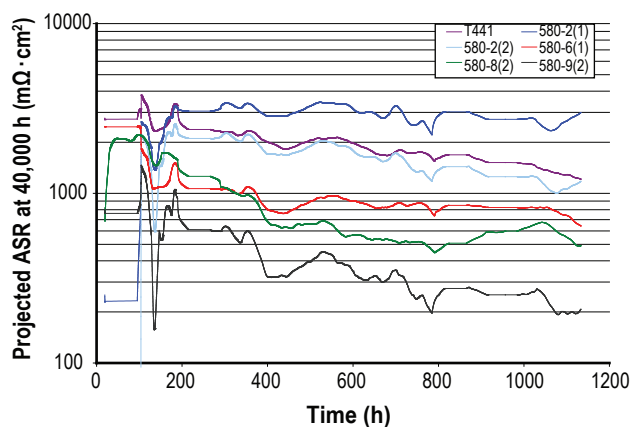


**FIGURE 4.** Predicted 40,000-hour ASR Value Extrapolated from Short-Term Test Data

exhibited a higher ASR value than the control Type 441 stack and the highest rate of increase in the test. This is consistent with the variability observed for low chromium, very low silicon alloys in the basic oxidation testing.

- Alloy 580-6 exhibited a moderate but significant improvement in performance over standard Type 441, and alloys 580-8 and 580-9 exhibited the best performance in this test. In particular, alloy 580-9 exhibited a six-fold decrease in the expected 40,000-hour ASR value.

A thermochemical process has been developed which has been shown to remove silicon from the solid-state in ferritic stainless steels. The initial results of ASR testing are encouraging based on work done by colleagues at the Pacific Northwest National Laboratory (PNNL). A desiliconized sample of Type 441 stainless steel exhibited an ASR value 33% lower than a standard Type 441 sample when tested under identical conditions (500 hours at 800°C, using a manganese cobaltite coating).

## Conclusions and Future Directions

- Alloys based on Type 441 stainless steel have shown encouraging test results. However, evaluation at the upper end of the SOFC operating temperature range has shown somewhat unpredictable behavior in terms of oxidation resistance and ASR evolution. Further work is planned to characterize causes and solutions.
- Alloy compositions based on E-BRITE® alloy have shown a substantial decrease in the rate of oxidation and in the rate of ASR increase when compared to lower chromium materials.
- Coatings have been shown to improve electrical performance significantly. Testing is beginning for commercial and novel alloy samples with applied coatings (manganese cobaltite, as provided by PNNL).
- Post-production removal may provide a way to reduce the impact of residual silicon. The silicon removal process relies on solid-state diffusion. An effect of substrate thickness is therefore expected. To quantify this effect, a master panel of Type 441 stainless steel is being rolled to several different gauges for treatment and evaluation.
- Combinations of alloying modifications, surface treatments, and coatings will be tested to determine which system is optimum for SOFC applications.
- An effort is planned to supply Type 441 stainless steel to Industrial Teams in significant quantities for stack prototyping and manufacturing.

### **Special Recognitions & Awards/Patents Issued**

1. Patents have been filed on higher-Cr content alloy compositions (application numbers 20060286433, 20060286432, and 20060285993) and on the silicon removal process (application number not yet published).

### **FY 2008 Publications/Presentations**

1. Quarterly status report for Project 42513, July 2007.
2. "Interconnect Alloys Metallurgy and Manufacturing," 8<sup>th</sup> Annual SECA Workshop, San Antonio, TX, August 8, 2007.
3. Quarterly status report for Project 42513, October 2007.
4. Quarterly status report for Project 42513, January 2008.
5. "Metallic Alloys for Solid Oxide Fuel Cell Interconnects," TMS Annual Meeting, New Orleans, LA, March 11, 2008.
6. "Evaluation of a Functional Interconnect System for SOFC's," SECA Peer Review, Pittsburgh, PA, April 22, 2008.
7. Quarterly status report for Project 42513, April 2008.

---

## IV.C.2 Oxidation Resistant, Cr Retaining, Electrically Conductive Coatings on Metallic Alloys for SOFC Interconnects

Dr. Vladimir Gorokhovskiy  
Arcomac Surface Engineering, LLC  
151 Evergreen Drive, Suite D  
Bozeman, MT 59715  
Phone: (406) 522-7620; Fax: (406) 522-7617  
E-mail: vgorokhovskiy@arcomac.com

DOE Project Manager: Ayyakkannu Manivannan  
Phone: (304) 285-2078  
E-mail: Ayyakkannu.Manivannan@netl.doe.gov

Contract Number: 42225

Phase I Start Date: September 15, 2004  
Project End Date: March 31, 2008

achieved up to 6  $\mu\text{m/hr}$  on substrates installed on a rotatable turntable 0.5 m in diameter.

- Order of magnitude reduction of surface defect density along with double of deposition rates.
- Achieved low, stable area specific resistance (ASR) ( $<50 \text{ m}\Omega\cdot\text{cm}^2$ ) for  $>1,500$  hours in  $800^\circ\text{C}$  air with porous lanthanum strontium manganite (LSM) contact.
- Significantly reduced Cr volatility. A 430 FSS with  $\sim 2 \mu\text{m}$  LAFAD nanocomposite  $\text{TiCrAlY}$  oxide coating exhibited negligible Cr volatility compared with uncoated counterparts, in spite of the coating containing  $\sim 12 \text{ at}\%$  Cr.
- Demonstrated protective, stable amorphous coatings for sealing areas with high ASR values and negligible chemical or physical changes after  $>1,500$  hours in  $800^\circ\text{C}$  air.

### Objectives

- Enable the use of inexpensive ferritic stainless steels (FSSs) as planar solid oxide fuel cell (SOFC) interconnects (ICs) via advanced physical vapor deposition (PVD) protective coatings.
- Develop and demonstrate novel, cost-effective coating deposition processes to establish dense and uniform protective and functional coatings on FSS SOFC-IC substrates.
- Evaluate protective coatings during SOFC-IC relevant exposures.
- Optimize coating deposition process parameters to maximize SOFC-IC performance and ultimately reduce cost.

### Accomplishments

- Developed and tested novel, hybrid surface engineering technologies combining large area filtered arc deposition (LAFAD), electron beam physical vapor deposition (EBPVD), unbalanced magnetron (UBM) and thermal evaporation to deposit dense, protective coatings in an economical manner.
- Engineered LAFAD coatings to combine favorable electronic conductivity and transport barrier characteristics. Diffusion-barrier amorphous Al and Cr oxide coatings were embedded with electronically conductive Co and/or Mn-containing spinel oxide crystallites.
- The maximum deposition rate of the oxiceramic coatings based on the  $\text{TiCoMnCrAlYO}$  system by one LAFAD dual arc vapor plasma source process

---

### Introduction

To achieve Solid State Energy Conversion Alliance (SECA) cost and performance goals, attention has been directed toward inexpensive FSSs as SOFC-ICs. Currently, the SOFC-IC in planar SOFC systems accounts for a dominant portion of the overall stack cost. Inexpensive FSSs meet many SOFC-IC functional requirements; however, during operation, FSSs form blanketing thermally-grown chromium oxide (TGO) scales, which dramatically degrade SOFC stack performance and limit device lifetime. To date, deleterious issues with Cr volatility, electrical resistance and thermal-chemical incompatibilities with adjoining components have restricted the use of standard FSSs as SOFC-ICs. Since 2004, Arcomac Surface Engineering, LLC (ASE) has been engaged in the development of protective and functional coatings on FSSs as SOFC-ICs. ASE has developed advanced coating deposition technologies, which show promise for resolving both SOFC-IC performance requirements in an economically-feasible manner.

### Approach

ASE has developed hybrid, filtered arc plasma deposition technologies to establish protective, functional coatings on commercially available FSSs. Coating design is aimed at inhibiting ionic transport and Cr volatility, while retaining low and stable ASR at  $\sim 800^\circ\text{C}$  in air during long-term exposures. Desired coating

compositions and architectures are determined through thermodynamic and transport modeling in addition to prior art. Appropriate deposition materials are acquired and deposition processes are designed and performed using ASE patented equipment and technologies. Coated samples are exposed to conditions simulating SOFC-IC operation, and complimentary surface analyses are conducted to evaluate performance. Results are employed to assist in developing new coating deposition process formulations. Promising coating systems from preliminary testing are then subjected to more prototypical SOFC interconnect conditions for further assessments. Concurrently, economic evaluations of coating process and SOFC-IC fabrication are ongoing.

## Results

The patented filtered arc plasma source ion deposition (FAPSID) system developed by ASE utilizes two dual filtered cathodic arc LAFAD sources in conjunction with two UBM sputtering sources, two EBPVD evaporators and a thermal resistance evaporation source in one, universal vacuum chamber layout (as illustrated in Figure 1) [1, 2]. This system has demonstrated the capability to deposit nanocomposite, nanolayered coatings with a wide variety of compositions and architectures. The FAPSID process features high deposition rate concurrent with high intensity with ion bombardment resulting in reduction of coating defects, eliminating porosity and increase of coating density up to theoretical limit. Depending on LAFAD plasma source settings, it is possible to deposit either nanolaminated architectures or uniform nanocomposite coatings.

The most promising ASE coatings yet identified are LAFAD nanostructured coatings from the MCrAlYO system (where M = Co, Ti, and/or Mn). These coatings are designed to function as effective barriers, blocking both inward and outward ionic diffusion, while providing adequate electronic conductivity through the coating thickness. The transition metal dopants are selected to increase high temperature electronic conductivity by forming nanocomposite thermistor-like oxicermet. An extensive matrix of LAFAD coatings have been successfully deposited with excellent adhesion to various FSS substrates under consideration for SOFC-ICs. Other hybrid coating deposition methods, employing filtered arc assisted thermal resistance evaporation and filtered arc assisted electron beam evaporation are also being explored. During the reported period of time, ASE's efforts were focused on optimization of LAFAD source to increase productivity while at the same time further reduce the density of defects in the coatings. The optimized LAFAD source is now capable of deposition nanocomposite MCrAlYO oxiceramic coatings with deposition rates exceeding 6  $\mu\text{m/hr}$  on substrates installed on a rotatable

0.5 m diameter turntable of the FAPSID coating system (see Figure 1). At the same time the density of

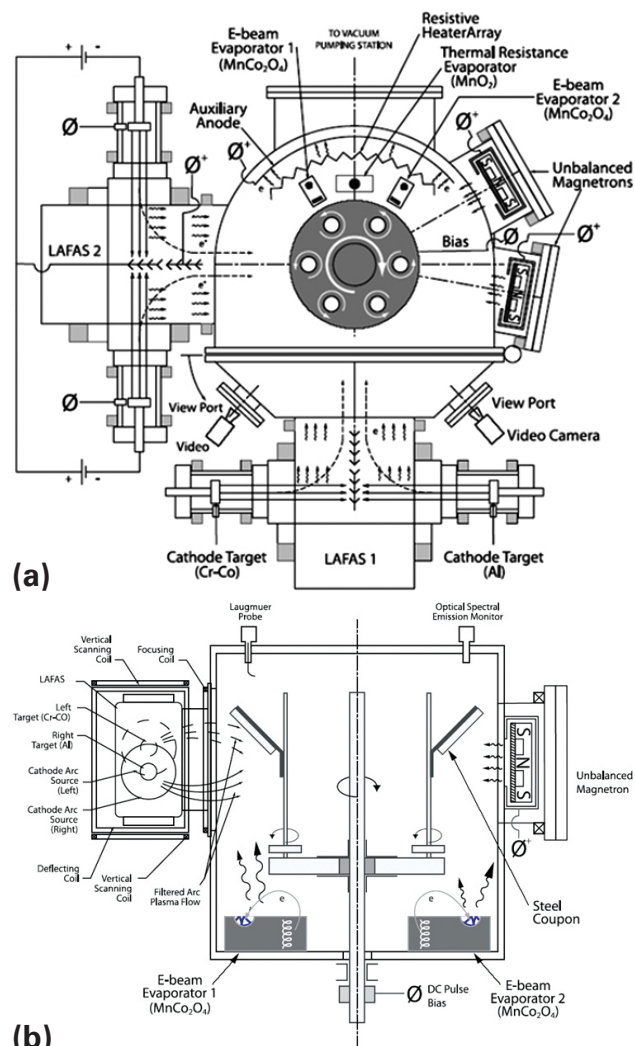


**FIGURE 1.** Schematic Illustration of the FAPSID Surface Engineering System, Showing (a) Top View; and (b) Side View

**TABLE 1.** Characteristic parameters of three unique MCrAlYO oxiceramic coatings on T430 steel processed using one LAFAD source for two hours.

Coating composition	Deposition rate, $\mu\text{m/hr}$	Hardness [GPa]	Elastic Modulus [GPa]	RMS Coeff.** [RMS/thickness]
Ti(6)Cr(10)Al(20)Y(<1)O(bal.)	6	26.1+/-2.8	262+/-16.7	0.007
TiCoCrAlYO*	4	26.8+/-2.6	258+/-19.5	TBD
TiCoMnCrAlYO*	4	21.1+/-1.2	243+/-12.0	TBD

\* Coating composition yet to be determined

\*\* Roughness was measured by Dektak 8 precision profilometer on coatings deposited on polished 440A SS

defects dropped at least an order of magnitude. The characteristic parameters of three different oxiceramic coatings deposited on SS plates simulating the SOFC metallic ICs are shown in Table 1. The testing of ASR during long term 800°C exposure in air in contact with LSM has been initiated at Montana State University.

SOFC-IC-relevant behavior of coated and uncoated samples, i.e. high temperature oxidation, ASR, and Cr volatility have been investigated in collaboration with researchers at Montana State University, Pacific Northwest National Laboratory, Lawrence Berkeley National Laboratory and Versa Power Systems. Summary ASR data (with porous LSM contact in 800°C air) from FSS with four different LAFAD coatings is shown in Figure 2. The ASR of the uncoated FSS continues to increase due to the growth of the chromia-based TGO scale. The ASR of the coated specimens generally decreases and stabilizes. The decrease is

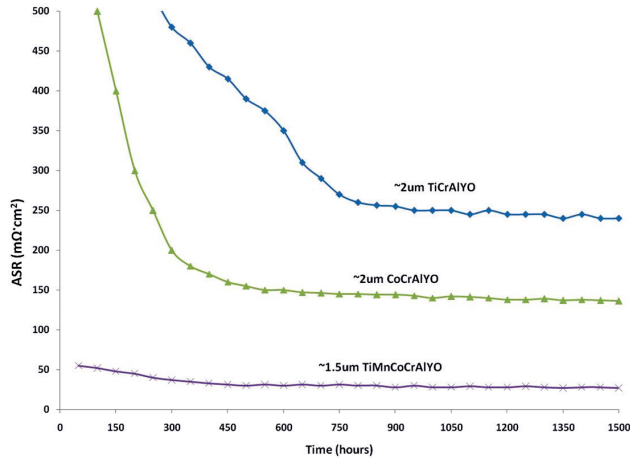


FIGURE 2. Summary ASR Data for Three Different LAFAD MCrAlYO Coatings on FSS 430

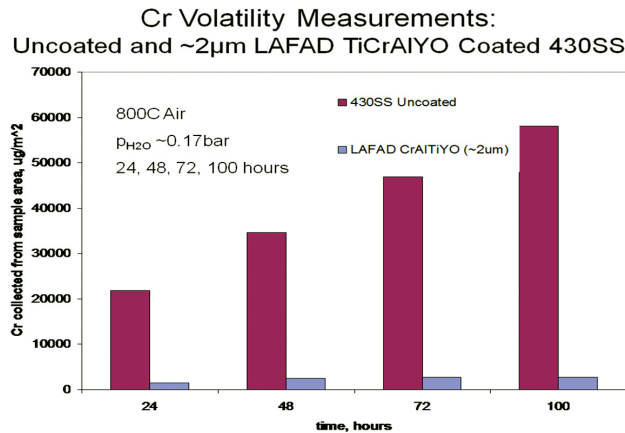


FIGURE 3. Cumulative, Time-Dependant Cr Volatility Data for Uncoated and TiCrAlYO Coated FSS

attributed to the restructuring of the as-deposited amorphous coating into a polycrystalline film. The stability is attributed to the transport-barrier properties of the coatings, whose thicknesses and chemical composition do not change appreciably during the 1,500-hour ASR test. LAFAD coatings with Co and/or Mn exhibit significantly lower initial ASR than those without. The TiCrAlYO and CrAlYO coatings are permeable to the high oxygen affinity Mn from the FSS, and evolve percolating networks of conductive Mn-containing oxides, thus lowering the ASR over time.

Figure 3 presents a summary of Cr volatility results from uncoated and LAFAD TiCrAlYO coated FSS. The graph displays the cumulative amount of Cr collected during the test. The uncoated FSS continues to volatilize Cr throughout the test, while the coated specimen demonstrates negligible Cr volatility after the first 24 hours. This coating contains ~12 at% Cr; however, the Cr is apparently sequestered in a solid solution with complex Al-containing oxides, which agrees well with thermochemical modeling. Thermochemical modeling, using the advanced “TERRA” thermodynamic equilibrium calculation code with solid solution considerations, is being used to estimate phase composition of multielemental oxiceramic coatings and their interactions with SOFC-IC operating environments. The results of thermodynamic modeling of Cr volatilization from the TiCrAlYO coating in a SOFC simulated environment as a function of Al<sub>2</sub>O<sub>3</sub> content are shown in Figure 4. It can be seen that the chromia/alumina ideal solid solution can be

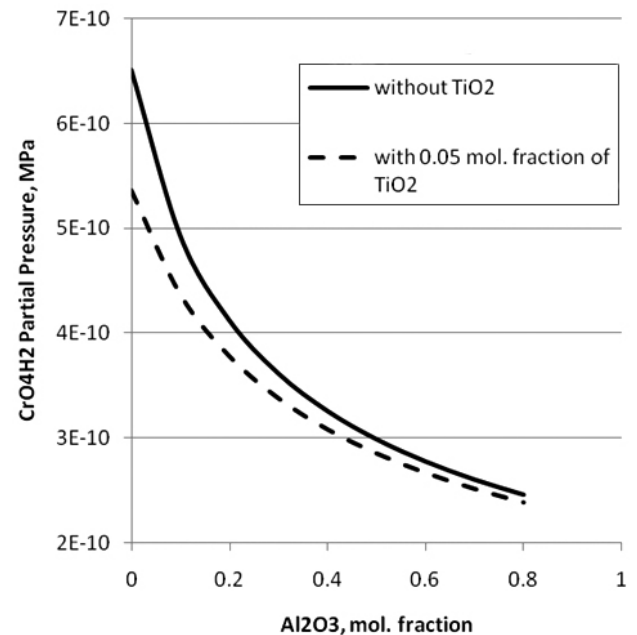


FIGURE 4. Thermodynamic Modeling Results for Cr Volatility from TiCrAlYO Oxi-Ceramic Coatings vs. Al<sub>2</sub>O<sub>3</sub> mol. Fraction at T=800°C, p=1 atm

credited for substantial reduction of the volatilization rate, but cannot explain near complete inhibiting of chromia volatilization from TiCrAlYO coatings. Kinetic mechanisms, such as formation of ultrathin Al<sub>2</sub>O<sub>3</sub> scale, have to be considered for better explanation of this phenomenon.

### Conclusions and Future Directions

ASE has developed advanced coating deposition processes, which may enable the use of inexpensive metallic alloys as IC components in planar SOFC systems. Nanostructured oxicermet coatings, deposited by hybrid filtered arc assisted techniques are being investigated to meet SECA SOFC-IC performance and cost requirements. A large-scale FAPSID surface engineering process, offering favorable economics through high yield and advanced hybrid design, is under investigation for deposition of protective coatings on SOFC-ICs. Based upon success with similar PVD processes, cost estimates for this process at full-scale production reach ~\$0.10 per SOFC-IC. Future work will focus on cross comparison with other coatings on identical FSS samples and testing in short SOFC stacks. Coating composition and architecture will be continually optimized to further improve thermal-chemical and mechanical stability, transport barrier properties and low ASR during long-term operation.

### FY 2008 Publications/Presentations

1. H. Chen, J.A. Lucas, W. Priyantha, M. Kocczyk, R.J. Smith, K. Lund, C. Key, M. Finsterbusch, P.E. Gannon, M. Deibert, V.I. Gorokhovskiy, V. Shutthanandan and P. Nachimuthu, "Thermal stability and oxidation resistance of TiCrAlYO coatings on SS430 for solid oxide fuel cell interconnect applications," Surface and Coatings Technology, accepted February 2008.

2. P.E. Gannon, M. Deibert, V.I. Gorokhovskiy, P. White, R.J. Smith, H. Chen, W. Priyantha and J. Lucas, "Advanced PVD protective coatings for SOFC interconnects," Int. Journal of Hydrogen Energy, in-press.
3. V. Gorokhovskiy et al., "High Temperature Thermal Stability of Oxi-Ceramic Coatings Deposited by Large Area Filtered Arc Deposition," Invited Presentation, International Conference on Metallurgical Coatings and Thin Films, San Diego, CA, April 30, 2008.
4. V.I. Gorokhovskiy, P.E. Gannon, M.C. Deibert, R.J. Smith, A. Kayani, M. Kocczyk, D. VanVorous, Zhenguo Yang, J.W. Stevenson, S. Visco, C. Jacobson, H. Kurokawa and S. Sofie, "Deposition and Evaluation of Protective PVD Coatings on Ferritic Stainless Steel SOFC Interconnects," Journal of The Electrochemical Society, v. 153 (10) A1886-A1893 (2006).
5. P.E. Gannon et al., "Filtered arc and hybrid PVD materials for SOFC applications," Invited Presentation, International Conference on Metallurgical Coatings and Thin Films, San Diego, CA, April 30, 2008.
6. P.E. Gannon et al., "SOFC Interconnect Research and Development at Montana State University and Arcomac," Invited Keynote Presentation, European Science Foundation Exploratory Workshop on Next Generation SOFC Materials, Genoa, Italy, October 23, 2007.

### References

1. V. Gorokhovskiy, US Patent No.6,663,7552.
2. <http://www.arcomac.com>

---

## IV.C.3 Materials Development for the Solid Oxide Fuel Cell Environment

Paul E. King (Primary Contact), David Alman, Christopher Cowen, M. Ziomek-Moroz and Paul D. Jablonski

National Energy Technology Laboratory  
Process Development Division  
1450 Queen Ave. SW  
Albany, OR 97321  
Phone: (541) 967-5948; Fax: (541) 967-5991  
E-mail: Paul.King@netl.doe.gov

### Subcontractors:

- Carnegie Mellon University, Pittsburgh, PA
- West Virginia University, Morgantown, WV

Contract Number: 08-220692

Start Date: October 1, 2007

Project End Date: September 30, 2008

### Objectives

- Fabricate and evaluate a series of low Si/Al 441-like alloys for solid oxide fuel cell (SOFC) interconnect evaluation including surface infusion.
- Produce samples of 441-series stainless steels, with and without a rare earth surface treatment for evaluation of interconnect environmental stability.
- Perform thermodynamic and kinetic modeling of interdiffusion between cladding and interconnect materials to determine potential impact on microstructural evolution.
- Evaluate novel spinel coatings for thermodynamic stability and mechanical/physical characteristics when formed on candidate interconnect substrates.

### Accomplishments

- A much better understanding of the rare earth effect has been obtained. This effect can reduce the oxidation on the metallic interconnect by a factor of 3x or more.
- Low Si/Al alloys have been produced and evaluated.
- Thermodynamic modeling of the potential oxide scales has been made.
- With proper alloy control (within commercial specifications) there is no longer a need to use extreme methods to reduce the Si to very low levels.

---

### Introduction

Fuel cells are energy conversion devices that generate electricity and heat by electrochemically combining a gaseous fuel and an oxidizing gas via an ion-conducting electrolyte [1-2]. The chief characteristic of fuel cells is their ability to convert chemical energy to electrical energy without the need for combustion, thereby giving much higher conversion efficiencies than conventional methods, such as steam turbines [2-3]. Cost remains the final obstacle that must be overcome for fuel cells to realize their full commercial potential [4-6]. Advances in solid-state material manufacturing show promise for making SOFCs applicable in any power application. Cost reduction can be achieved in component fabrication, materials used, and cell and stack designs [7-12]. This project will explore an integrated materials approach as a means of developing low cost, engineered metallic interconnects for SOFC systems fueled with syngas.

### Approach

The thermodynamic modeling software, ThermoCalc, was used to evaluate the phase stability and relative driving forces for oxide formation. Several representative alloy chemistries were formulated and small experimental heats were melted and fabricated into strip. The reactive element cerium was infused into the surface by our patent pending method. Coupons were exposed to a number of SOFC relevant fuel and air conditions for various times. Samples were subsequently characterized with scanning electron microscopy (SEM), wavelength Dispersive X-Rays (WDX), energy dispersive X-ray spectrometry (EDX) and X-ray.

### Results

The experimental Fe 6-22Cr 1Ti 0.5Mn alloys all formed multi-layered oxide scales under the test conditions (800°C in air + 3% H<sub>2</sub>O). The 6 and 9 weight percent Cr alloys both oxidized rapidly, even with the Ce surface treatment. All of the untreated experimental alloys showed a high concentration of iron in the outer scale region which is not considered to be protective. It was observed that the Ce treatment, which incorporates Ce into the alloy surface, suppressed the formation of Fe-containing oxides in the 12-22 weight percent Cr alloys. This suppression led to the formation of more protective oxide scales. Cerium treating these experimental alloys, which contained essentially no Al or Si, but did contain 1 weight percent

Ti, promoted an overgrowth of titanium oxide. This overgrowth layer does not appear to be stoichiometric  $\text{TiO}_2$  and may prove to be an effective barrier to both scale growth and Cr vaporization. These are critical features of a successful metallic interconnect in SOFC applications. *In situ* measurements are currently underway to evaluate the resistivity of the scale and thus evaluate the applicability of these alloys and the treatment in combination.

In the case of these experimental alloys we find that the minor element titanium is promoted to the surface to oxidize at the exclusion of the other elements. Titanium oxides have a significantly higher (more negative)  $\Delta G$  of formation in comparison to the other oxidizing species that might form in this alloy series (Table 1). Thus, it is not surprising that the outer layer is essentially pure titanium oxide at the exclusion of other elements (though it remains unclear why this is not also the case in the alloys without the surface treatment). This formation of a titanium oxide layer may have several positive effects for application as an interconnect material in SOFC applications. First, the oxide scale is thin, which presumably would lead to a reduced electrical resistance. Second, since the outer layer contains no Cr, the migration of Cr to the cathode which poisons its effectiveness [16-22] would be expected to be greatly reduced if not eliminated [22-25]. Finally, the Ti-rich outer oxide that forms is expected to be electrically conductive under SOFC operating conditions [26-29].

We endeavored to explore the 430/441 series of steels to understand its application as an interconnect material. Several researchers have recognized that the formation of Laves phase can be advantageous in improving oxidation resistance [13-15]. What Laves phases do is provide a sink for the silicon remaining in the material after the foundry processes. In collaboration with researchers at Pacific Northwest National Laboratory (PNNL), we have found that the application temperature, as well as material chemistry and thermal history, will likely be important to optimize the Laves phase effect. For example, in nominal chemistry 441 stainless steels, Laves phases are stable to a temperature slightly above  $800^\circ\text{C}$ , as shown in Figure 1. As such, a 441 interconnect with nominal chemistry might be prone to the formation of a silicon-rich oxide sub-scale in regions of the interconnect that get excessively hot (e.g.,  $900^\circ\text{C}$ ). However, this upper use temperature can be greatly extended by judicious selection of chemistry—still within the 441 alloy specification. For example, by raising the Nb content (a potent Laves stabilizer) from 0.05 to 0.09 weight percent the Laves formation temperature is extended to above  $900^\circ\text{C}$  (Figure 2). Furthermore, the amount of Laves phases at a given temperature is also increased (below its stability temperature). In contrast, alloy 430 does not form Laves and has been shown to form resistive silicon rich sub-scales under SOFC conditions.

**TABLE 1.** Driving force for the formation of the various oxides is given in the table below. These driving forces were calculated using ThermoCalc using the SSOL4 and SSUB3 databases with the temperature set at  $800^\circ\text{C}$  and the alloy chemistry of Fe22Cr1Ti0.5Mn without cladding.

Oxide	Driving force for formation at $800^\circ\text{C}$ (kJ/mol)
$\text{CrO}_2$	241
$\text{CrO}_3$	204
$\text{Cr}_2\text{O}_3$	271
$\text{Cr}_5\text{O}_{12}$	231
$\text{Cr}_8\text{O}_{21}$	221
$\text{Cr}_2\text{FeO}_4$	252
$\text{FeO}$	187
$\text{Fe}_2\text{O}_3$	211
$\text{Fe}_3\text{O}_4$	208
$\text{FeTiO}_3$	284
$\text{Fe}_2\text{TiO}_4$	256
$\text{MnO}$	217
$\text{MnO}_2$	208
$\text{Mn}_2\text{O}_3$	221
$\text{Mn}_3\text{O}_4$	224
$\text{Mn}_2\text{TiO}_4$	276
$\text{MnTiO}_3$	298
$\text{TiO}_2$	343
$\text{Ti}_2\text{O}_3$	321
$\text{Ti}_3\text{O}_5$	329
$\text{Ti}_4\text{O}_7$	335

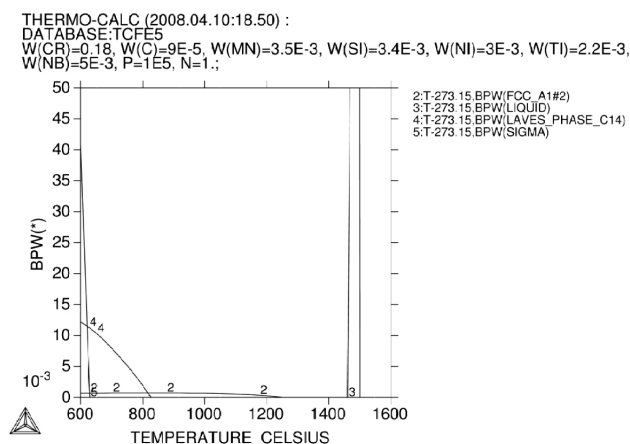


**FIGURE 1.** Weight Fraction Phase versus Temperature for Conventional 441ss

Subtleties such as these can be very important. For example, we CeOx-treat at  $900^\circ\text{C}$ . Depending upon the sample chemistry and cooling rate, Laves phases may or

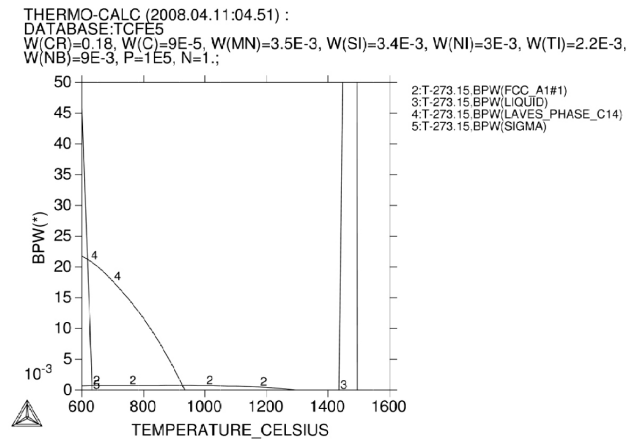


**FIGURE 2.** Weight Fraction Phase versus Temperature for 441ss Containing the Allowable Specification Maximum of Nb

may not be present in a given sample prior to exposure. It is our recommendation that a precipitation heat treatment be given to 441 interconnects prior to service to ensure that Laves phases are part of microstructure (tying up the silicon and making it unavailable for subsequent oxidation).

How does this work? When silicon is incorporated into Laves phases, its free energy is reduced relative to silicon being in solution in the matrix. Furthermore, when silicon is “evacuated” from the matrix, it is unaware of the oxygen potential at the matrix/oxide interface (where silicon oxidizes in Laves-free alloys such as 430). Thus, the reason Laves forming alloys act as though they contain no silicon is that their matrices in fact contain essentially no silicon.

We have supplied several samples of cerium-treated 441 to PNNL for additional evaluation as well as to be Co-Mn spinel coated and tested. These tests will be very helpful in describing an engineered solution for a metallic interconnect with optimum oxidation behavior.

Pulse plating of Mn-Co alloy onto low silicon 430 alloy substrates was carried out at various on-time and off-times. The coating morphology can be divided into two categories: (1) flake and porous like structures; and (2) compact, low porosity, crystalline structures. The flake-like structure shows higher Mn content than that of crystalline coatings. While the higher level of Mn is desirable, low porosity in the coating is paramount.

The surface morphology of as-deposited crystalline coatings is demonstrated in the SEM image in Figure 3(a). Some cracking across the fine particles is apparent on the surface. EDX semi-quantitative results of these as-deposited coatings indicate that Mn content is 16 at%. Also, weak Cr and Fe peaks are detected, which suggests the coating is not thick enough to prevent penetration of the electron beam to the underlying substrate. Following two hours of oxidation at 800°C, all the cracks in the

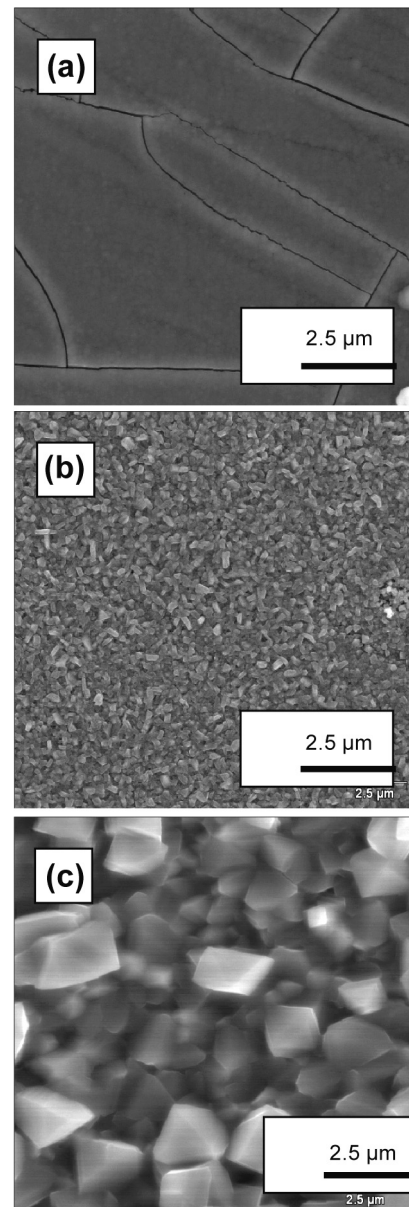


**FIGURE 3.** SEM Surface Morphology of Mn/Co Coating (a) As-Deposited Coating (Mn wt% 16.5%); (b) after Oxidation at 800°C for 2 Hours; (c) after 1,200 Hours ASR Test at 800°C

coating have healed, and only tiny spinel grains are observed, as shown in Figure 3(b).

The oxidized coating was exposed to 800°C for 1,200 hours while area specific resistance (ASR) was measured. The ASR profile is shown in Figure 4. During the initial 165 hours, the ASR value is not stable, probably due to contact problems between the platinum paste and the sample. However, the ASR then stabilizes, increasing only slightly with time. Based on this experimental data, and assuming it follows a parabolic law, the ASR value at 40,000 hours is predicted to be

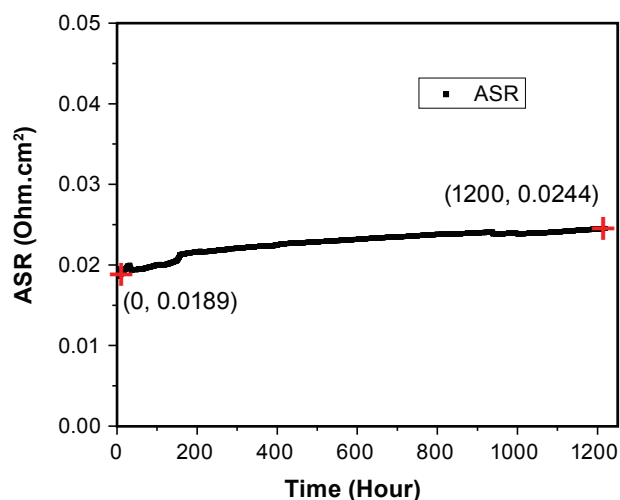


**FIGURE 4.** Contact ASR of AISI430 Substrate with Mn/Co Spinel Coating

0.0460Ω·cm<sup>2</sup>. This value is significantly lower than the target value of 0.1Ω·cm<sup>2</sup>.

Figure 3(c) shows the surface morphology of the coating after 1,200 hours of ASR measurement. The cubic grain structure typical of spinels is becoming more apparent as the oxide particles grow. A cross section of the coating shows it to be dense and compact, with good adhesion to the substrate. There is some internal oxidation observed at/near the interface, which could be from the residual silicon content in the substrate. The total scale thickness is around 3 μm. An EDX line scan profile demonstrates clearly that the coatings are composed of an ~1.5 μm Cr<sub>2</sub>O<sub>3</sub> interlayer, with an ~1.5 μm (Mn,Co)<sub>3</sub>O<sub>4</sub> coating. The manganese and cobalt levels in the top coat are essentially the same, suggesting that a significant amount of manganese has migrated from the substrate (the as-deposited surface had ~16% Mn). Chromium content remained low near the surface, indicating that little or no chromium diffuses into the coating surface. Similarly, no iron was observed to diffuse into the interlayer or coating. These results are comparable to (Mn,Co)<sub>3</sub>O<sub>4</sub> coatings achieved by thermal growth as reported by PNNL.

## Conclusions and Future Directions

The CeOx surface treatment greatly reduces the oxidation rate of interconnect materials. The selection of 441 stainless steel, with proper chemistry and thermal history, should adequately sequester silicon and thus prevent the formation of resistive sub-scale layers. It is our opinion that an engineered solution for SOFC interconnects exists (441+CeOx+Co-Mn Spinel) such that further research is not needed at this time. Once the seals and ceramic portions of the SOFC are further developed, the interconnect may need to be revisited

as these may interact with the engineered solutions recommended.

## Special Recognitions & Awards/Patents Issued

1. Paul Jablonski; Christopher Cowen; and David Alman, "Evaluation of a Ferritic Stainless Steels for SOFC Interconnect Application," TMS 2008, 137<sup>th</sup> Annual Meeting and Exhibition, New Orleans, LA, March 9–13, 2008. Invited Talk.
2. The CeOx surface treatment process patent application has been submitted (S-105,333).

## FY 2008 Publications/Presentations

### Publications

1. Paul D. Jablonski, David E. Alman, "Oxidation resistance of novel ferritic stainless steels alloyed with titanium for SOFC interconnect applications," *Journal of Power Sources* 180 (2008) 433–439.
2. M. Ziomek-Moroz, T. Adler, D. Alman, P. Jablonski, J. Clark, L. Penner, "Materials Performance of Modified 430 Stainless Steel in Simulated SOFC Stack Environments for Integrated Gasification Fuel Cell System Applications," *Electrochemical Transactions*, accepted for publication.
3. M. Ziomek-Moroz, T. Adler, P. King, "Materials Performance of Ferritic Steel in Combustion Gases for Heat Exchanger Applications in Solid Oxide Fuel Cell Systems," *Corrosion* 2008, Paper No. 08460, Houston, TX, NACE International.

### Presentations

1. M. Ziomek-Moroz, T. Adler, D. Alman, P. Jablonski, J. Clark, L. Penner, "Materials Performance of Modified 430 Stainless Steel in Simulated SOFC Stack Environments for Integrated Gasification Fuel Cell System Applications," *Fuel Cell Seminar*, San Antonio, TX, October 15–19, 2007.
2. M. Ziomek-Moroz, T. Adler, P. King, "Materials Performance of Ferritic Steel in Combustion Gases for Heat Exchanger Applications in Solid Oxide Fuel Cell Systems," *Corrosion* 2008, New Orleans, LA, March 16–20, 2008.
3. P. D. Jablonski, and D. E. Alman, "The Performance of Ce Surface Treated Ferritic Stainless Steels for Solid Oxide Fuel Cell Interconnects," 2007 Materials Science and Technology Conference, Detroit, MI, September 16–20, 2007.
4. P. D. Jablonski, and D. E. Alman, "The Influence of Si Content on the Oxidation Behavior of Type 430 Stainless Steel," 2007 Materials Science and Technology Conference, Detroit, MI, September 16–20, 2007.
5. Paul Jablonski; Christopher Cowen; and David Alman, "Evaluation of a Ferritic Stainless Steels for SOFC Interconnect Application," TMS 2008, 137 Annual Meeting and Exhibition, New Orleans, LA, March 9–13, 2008. Invited Talk.

## References

1. Fuel Cell Handbook, 7<sup>th</sup> ed., EG&G Technical Services, under contract number DE-AM26-99FT40575 with US Dept of Energy, Office of Fossil Energy, National Energy Technology Laboratory, Ch 1, (2004).
2. N.Q. Minh, Ceramic Fuel Cells, *J. Am. Ceram. Soc.* **76** (3) (1993) 563-588.
3. Mark C. Williams, Joseph P. Strakey, Wayne A. Surdoval, *J of Power Sources* **143** (2005) 101-196.
4. Mark C. Williams, Joseph P. Strakey, Wayne A. Surdoval, Lane C. Wilson, *Solid State Ionics*, **177** (2006) 2039-2044.
5. Mark C. Williams, Joseph P. Strakey, Wayne A. Surdoval, *J of Power Sources* **159** (2006) 1241-1247.
6. S. de Souza, S.J. Visco, L.C. De Jonghe, *Solid State Ionics* **98** (1997) 57.
7. H. Ishihara, H. Matsuda, Y. Takita, *J. Am. Chem. Soc.* **116** (1994) 3801.
8. M. Feng, J.B. Goodenough, *Eur. J. Solid State Inorg. Chem.* **T31** (1994) 663.
9. P. Huang, A. Petric, *J. Electrochem. Soc.* **143** (5) (1996) 1644.
10. K.Q. Huang, R. Tichy, J.B. Goodenough, *J. Am. Ceram. Soc.* **81** (1998) 2565.
11. W.Z. Zhu, S.C. Deevi, *Mat. Res. Bull.*, **38** (2003) 957-972.
12. T. Horita, Y.P. Xiong, K. Yamaji, N. Sakai, H. Yokokawa, *J. Power Sources* **118** (2003) 35.
13. J. Froitzheim, G.H. Meier, L. Niewolak, P.J. Ennis, H. Hattendorf, L. Singheiser, W.J. Quadackers, in press *J. Power Sources*, doi:10.1016/j.jpowsour.2007.12.028
14. Z. Yang, G. Xia, C. Wang, Z. Nie, J. Templeton, J. Stevenson, P. Singh, Submitted to *J. Power Sources* (2008).
15. T. Horita, H. Kishimoto, K. Yamaji, Y. Xiong, N. Sakai, M. E. Brito, H. Yakokawa, *J. Power Sources*, **176** (2008) 54-61.
16. S.P. Simner, M.D. Anderson, G.-G. Xia, Z. Yang, L.R. Pederson, J.W. Stevenson, *J. Electrochem. Soc.* **152** (4) (2005) A740.
17. M.C. Tucker, H. Kurokawa, C.P. Jacobson, L.C. De Jonghe, S.J. Visco, *J. Power Sources* **160** (2006) 130.
18. M. Kumpelt, T. Kaun, T.A. Cruse, M. Hash, SECA Annual Workshop, May 11-13, 2004, available at <http://www.seca.doe.gov>.
19. S.P.S. Badwal, R. Deller, K. Foger, Y. Ramprakash, J.P. Zhang, *Solid State Ionics* **99** (1997) 297.
20. Y. Matsuzaki, I. Yasuda, *Solid State Ionics* **132** (2000) 271.
21. S.P. Jiang, J.P. Zhand, X.G. Zheng, *J. Eur. Ceram. Soc.* **22** (2002) 361.
22. Z. Yang, G. Xia, P. Singh, J.W. Stevenson, *J. Power Sources* **155** (2006) 246.
23. X. Chen, P. Y. Hou, C. P. Jacobson, S. J. Visco, L. C. De Jonghe, *Solid State Ionics* **176** (2005) 425-433.
24. Z. Yang, G. Xia, G. Maupin and J. Stevenson, *Surface and Coatings Technology*, **201**(2006) 4476-4483.
25. Z. Yang, G. Xia, X. Li and J. Stevenson, *International Journal of Hydrogen Energy*, **32** (2007) 3648-3654.
26. S. Geng, J. Zhu, *J. Power Sources*, **160** (2006) 1009-1016.
27. S. J. Geng, J. H. Zhu, Z. G. Lu, *Scripta Mat.* **55** (2006) 239-242.
28. H. Nagai, K. Ohbayahi, *J. Am. Ceram. Soc.*, **72**, 1989, 400.
29. G. Meier, 2004 SECA Annual workshop and core technology program peer review workshop, May 11-13, 2004. Boston, MA, <http://www.seca.doe.gov>.

## IV.C.4 Cathode-Interconnect Contact and Cathode Chemical Compatibility Studies

Z.G. Yang (Primary Contact),  
X.D. Zhou (Primary Contact), G.G. Xia,  
X. Li, Z. Nie, J.D. Templeton, J.W. Templeton,  
G.D. Maupin, J.W. Stevenson, and P. Singh  
Pacific Northwest National Laboratory (PNNL)  
P.O. Box 999, MS K2-44  
Richland, WA 99352  
Phone: (509) 375-3756 (Yang), (509) 372-4468 (Zhou);  
Fax: (509) 375-2186  
E-mail: zgary.yang@pnl.gov, xiaodong.zhou@pnl.gov

DOE Project Manager: Ayyakkannu Manivannan  
Phone: (304) 285-2078  
E-mail: Ayyakkannu.Manivannan@netl.doe.gov

Contract Number: 40552

Start Date: October 1, 2007

Project End Date: September 30, 2008

the stack. The identification and implementation of suitable cathode-interconnect contact layers can be especially challenging, particularly in intermediate temperature (650-850°C) stacks, as their fabrication temperatures provide a limited amount of thermal energy for sintering and bonding of the contact material to the cathode and interconnect surfaces. Requirements for satisfactory cathode contact materials include high electrical conductivity to minimize the resistance of the contact layer and the contact interfaces, chemical compatibility with the interconnect and the perovskite cathodes, appropriate thermal expansion behavior, high thermochemical and structural stability in the SOFC operating environment, appropriate sintering activity, and low cost. During fiscal year (FY) 2008, PNNL investigated several alternative cathode contact material approaches with a primary goal of improving the sintering activity of conductive oxides in the 800-950°C temperature range. Successful development of improved, inexpensive contact materials for cathode-interconnect interfaces will assist Solid State Energy Conversion Alliance (SECA) industry developers in meeting the SECA program's cost and performance targets.

Another potential cathode-related challenge facing stack developers is degradation of cathode performance over time due to interaction between the cathode material and gas species volatilized from other stack components, such as alloy interconnects (e.g., Cr) and/or glass seals (e.g., B, Na, K). The potentially deleterious effects of volatile Cr species on cathode performance have been the subject of numerous studies, while effects of volatile seal constituents have received very limited attention to date. During FY 2008, PNNL has developed and implemented specialized cell test fixtures and procedures to shed new light on the possible impact of seal constituent evaporation on the performance and stability of intermediate temperature SOFC cathodes. Information gained in this study will assist SECA industrial developers in identifying and optimizing seal materials and designs consistent with the SECA cost and performance targets.

### Objectives

- Develop cost-effective contact materials for interconnect/cathode interfaces that exhibit long-term chemical, electrical, and structural stability.
- Investigate the effects of potential volatile seal constituents (such as B, Na, K) on solid oxide fuel cell (SOFC) cathode performance.

### Accomplishments

- Developed reaction-sintering assisted contact materials for cathode-interconnect interfaces.
- Studied effects of volatilized B species on SOFC cathode electrochemical performance.

---

### Introduction

In SOFC stacks, cells are electrically connected in series via interconnects that also separate the fuel at the anode-side of one cell from the air at the cathode-side of the adjacent cell. One interconnection-related challenge facing SOFC developers is power loss within the stack due to high contact resistances between interconnects and cell electrodes. To reduce electrode/interconnect interfacial resistances, electrical contact materials are generally applied between the interconnects and electrodes during construction of

### Approach

PNNL's contact material development focused on improving sintering activity in the intermediate temperature range through approaches involving reaction-sintering and/or materials systems with high intrinsic sintering activity. Some conductive oxides, including perovskites commonly used as cathode materials, demonstrate adequate electrical conductivity

and chemical compatibility, but these oxides typically exhibit low sintering activity in the intermediate temperature range. On the other hand, conductive oxides with lower sintering or melting temperatures tend to be highly reactive or unstable. Candidate contact materials were synthesized and characterized, and then evaluated for microstructural development, chemical stability, and electrical resistance through testing of simulated cathode/contact material/interconnect structures at  $0.5 \text{ A/cm}^2$  followed by post-test analysis (scanning electron microscopy [SEM], energy dispersive spectroscopy, X-ray diffraction analysis, etc).

PNNL also investigated boron volatility from a B-containing glass and the effects of the volatilized B on cell performance. The effect of volatile boron species on electrochemical performance of Sr-doped lanthanum manganite/yttria-stabilized zirconia (LSM/YSZ) cathodes was studied using commercial ASC3 cells purchased from H. C. Starck (Germany). The cells were tested at 700, 750, 800 and 850°C and 0.7 V with air as the oxidant and humidified  $\text{H}_2$  (~3%  $\text{H}_2\text{O}$ ) as the fuel. The boron source, consisting of sintered B-containing glass in a Pt boat, was introduced into the cathode air stream only after reasonably stable B-free performance was verified at a specific operating temperature. After the cell tests were completed, the cells were analyzed by secondary ion mass spectroscopy (SIMS) analysis. B volatility measurements were also performed to provide quantitative evaporation rates of B volatile species from the glass.

## Results

### Cathode-Interconnect Contact Materials

As reported previously, PNNL has developed a reaction-sintering based process for fabrication of manganese-cobalt spinel (MC) coatings on SOFC interconnects. In that process, a slurry containing the spinel powder is applied to the interconnect, and then heat treated in a reducing atmosphere to decompose the spinel into a mixture of MnO and Co powder. During subsequent oxidative heat treatment, the MnO and Co react to re-form the spinel phase, and in the process, create a coating which is denser than that obtained by simple oxidative heat treatment of the spinel powder. A similar approach, in which pre-reduced precursor powders are applied as contact layers, appears to be a promising means of achieving higher contact material density and bond strength than are typically obtained using the unreduced powders. Contact materials prepared in this manner have demonstrated low, stable area specific resistance (ASR) over time, as shown in Figure 1 for two different spinel compositions. A cross-sectional SEM image of one of the tested contact layers after heat treatment in air at 950°C for 1 hour (to simulate stack fabrication) and 800°C for

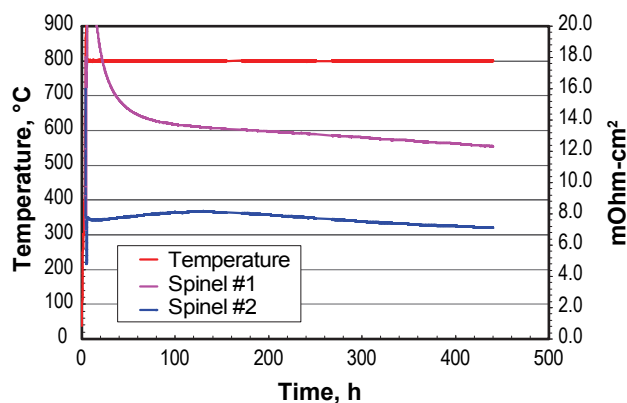


FIGURE 1. ASR Tests on Spinel Contact Materials Prepared from *In Situ* Oxidation of Pre-Reduced Precursor Powders

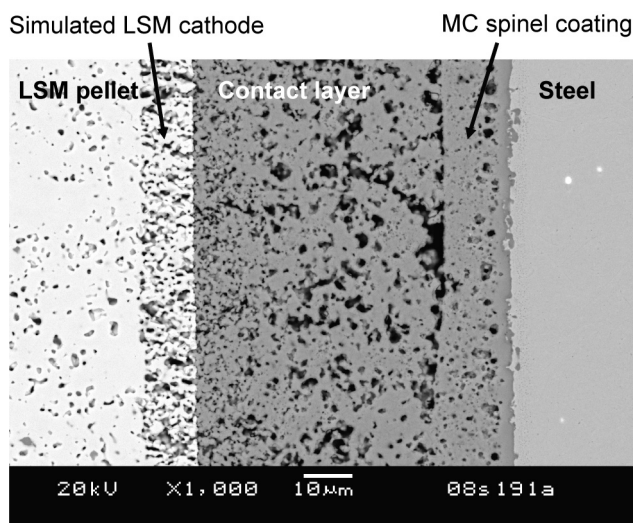


FIGURE 2. SEM micrograph of ASR test specimen with spinel contact material prepared *in situ* from pre-reduced precursor powders. Tested at 800°C for 500 hours after initial heat treatment at 950°C for 1 hour.

500 hours is shown in Figure 2. The contact layer exhibited reasonably high density and appeared to be well adherent to the LSM cathode material (on left) and spinel-coated interconnect steel (on right).

### Effects of B Volatility on Cathode Performance

Boron is known to exhibit high volatility at temperatures of interest to SOFC developers due to its propensity to form gaseous reaction products in the presence of either air or fuel. To assess the effects of volatilized B on cathode performance, PNNL's standard button cell test fixtures were modified to allow for the introduction of B glass-containing Pt boats into the cathode air stream in mid-test after the B-free baseline cell performance had been established. The B source selected for the present study was a glass (provided by Prof. Richard Brow at Missouri University of Science

and Technology) consisting of 20 wt% Sr, 20 wt% Ba, 20 wt% B, and 40 wt% Si. The goal of the present study was to study the performance of cathodes under somewhat exaggerated B dosing conditions, assuming that this would provide “worst case scenario” information regarding the sensitivity of the cathodes to the presence of volatile B species. Based on a generic stack geometry, it was assumed that the exposed surface area of the sealing glass is likely to be ~5% of the area of the cathode. The active cathode area of the button cells was 2 cm<sup>2</sup>, corresponding to exposed glass area of ~0.1 cm<sup>2</sup>. The dosage in the tests was intended to be 10 times that in stack operation conditions, so the B-dosing glass specimens were prepared with an exposed surface area of ~1 cm<sup>2</sup>.

As shown in Figure 3, introduction of the B source (at  $t = 150$  hours) resulted in an immediate reduction of cell performance. It should be noted that the open circuit voltage was monitored periodically during all cell tests, and found to be stable during the test period. Thus, it is safe to conclude that the observed changes in cell performance were not caused by changes in the Nernstian driving force due to seal leaks, electrolyte cracks, etc. Also, control experiments were conducted by using empty Pt boats instead of the glass containing boats. Changes to the electrochemical performance of these control cells were much smaller than the changes in the B-dosed cells, suggesting that the short-term performance reductions shown in Figure 3 were primarily a result of the presence of B species in the cathode air stream. In some cases, the B-dosed cells showed a recovery of power density over time. One possible explanation for this phenomenon is a reduction in the B dosing level over time, resulting in a decreasing concentration of B in the cathode. This is consistent with results of a set of cell tests in which the B sources

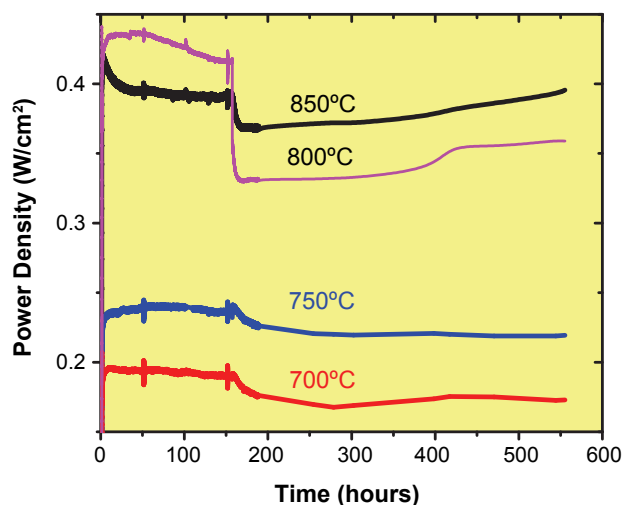


**FIGURE 3.** Electrochemical performance of anode-supported cells with LSM/YSZ cathodes tested at the indicated temperatures. The B source was introduced into the cathode air stream at 150 hours.

were inserted into the test fixtures but later removed from the fixtures; some recovery of cell performance was observed when the B sources were removed. As shown in Figure 4, SIMS analysis verified that removal of the B source during testing resulted in a lower residual B content in the cathodes compared to cathodes for which the B source was in place until the test was terminated. Therefore, the observed increases in power density may have resulted from gradual removal of B from the cathode. This is consistent with the anticipated glass chemistry at elevated temperatures. The B-containing glass is expected to at least partially devitrify over time at elevated temperatures, which may result in a decrease in B volatility. Also, depletion of boron from the surface region of the glass could cause a reduction in the rate of B volatilization over time. The average B transport rate from the glass-containing Pt boats over 300 hours in moist air (~3% water) was determined through volatility testing to be  $3.2 \times 10^{-12}$  g/cm<sup>2</sup>-sec at 750°C, which corresponded to a B species partial pressure on the order of  $1 \times 10^{-9}$  atm. Measurement of B volatility in relatively dry air (70 ppm water) yielded a lower B transport rate:  $2.1 \times 10^{-12}$  g/cm<sup>2</sup>-sec, which is consistent with the trend expected from thermodynamic calculation of equilibrium B species vapor pressures. Testing of B volatility over various time periods will help clarify whether or not time-dependent B dosing rates were responsible for the observed cell behavior.

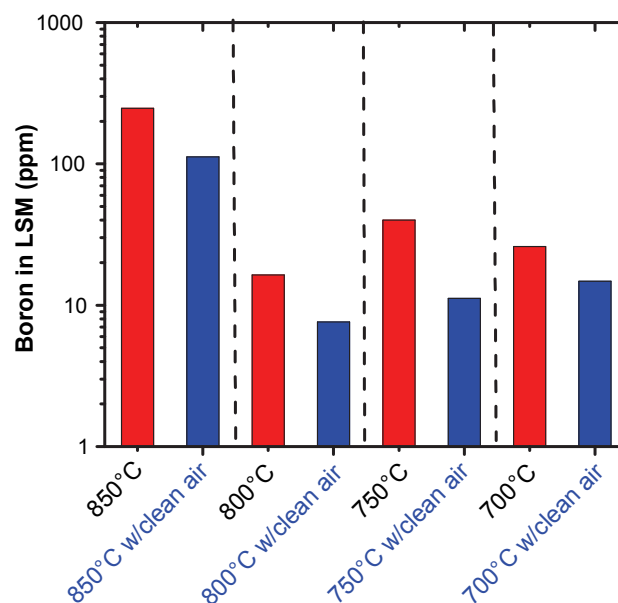


**FIGURE 4.** Boron content, as determined by SIMS cross sectional analysis, in LSM/YSZ cathode after electrochemical testing at the indicated operating temperatures. Note that the boron content in the cathodes decreased noticeably when the boron source was removed and cells were operated on clean air for 24 hours prior to termination of the test.

It should be noted that the glass used in the present study contained a relatively high B content (20 wt%). Hence, in addition to the fact that the exposure area was designed to be approximately ten times higher than expected values, it is possible that the boron source in the present study released a somewhat exaggerated concentration of volatile boron species into the ambient air stream. Therefore, in an SOFC stack, the initial performance drop due to boron poisoning of the cathode may be smaller in magnitude than the drops observed in this study. Moreover, it appears that the residual boron species in the cathode may be removed over time as the boron dosing level decreases (Figure 4).

### Conclusions and Future Directions

Encouraging results, in terms of sintered density and electrical resistance, are being achieved through novel contact material approaches such as reaction-assisted sintering. Future directions will include continued optimization of contact material compositions

for stack fabrication temperatures in the 800-1,000°C range. Developed materials will be evaluated via long-term and thermal cyclic testing of simulated cathode/contact material/interconnect structures, followed by validation via stack fixture testing. Possible issues related to mobility and/or volatility of contact material constituents, and their possible impact on cathode performance, will also be evaluated through electrochemical testing of cells with candidate contact materials.

Electrochemical testing of anode-supported cells with LSM/YSZ cathodes indicated relatively modest, possibly reversible dependence of cathode electrochemical performance on the presence/absence of B in the cathode air stream. Future directions will include further quantification of time-dependent volatility rates and testing of cells with Sr-doped lanthanum cobalt ferrite cathodes. Other potential contaminants from glass seals, such as Na and K, will also be studied in terms of their volatilization rate and effect, if any, on cathode performance.

## IV.C.5 SOFC Interconnect Materials Development at PNNL

Zhenguang "Gary" Yang (Primary Contact),  
Guanguang Xia, Joshua Templeton,  
Chong-Min Wang, Zimin Nie, Jeff Stevenson,  
and Prabhakar Singh

Pacific Northwest National Laboratory (PNNL)  
P.O. Box 999, MS K2-44  
Richland, WA 99352  
Phone: (509) 375-3756; Fax: (509) 375-2186  
E-mail: zgary.yang@pnl.gov

DOE Project Manager: Ayyakkannu Manivannan  
Phone: (304) 285-2078  
E-mail: Ayyakkannu.Manivannan@netl.doe.gov

Contract Number: 40552

Start Date: October 1, 2007  
Project End Date: September 30, 2008

### Objectives

- Develop cost-effective, optimized materials for intermediate temperature solid oxide fuel cell (SOFC) interconnect applications.
- Identify, understand, and mitigate degradation processes in interconnects and at interconnect interfaces.

### Accomplishments

- Developed Ce-modified protective spinel coating for alloy-based SOFC interconnects.
- Evaluated oxidation behavior and electrical performance of T441 ferritic stainless steel, with and without protective spinel coatings.

### Introduction

Oxidation resistant ferritic stainless steels are considered to be promising candidate materials for interconnect applications in SOFC stacks operating in the intermediate temperature range of 650-850°C. One issue associated with the use of conventional steels in this application, however, is the high electrical resistance and physical degradation that can result from the growth of the oxide scale on the alloy surface during high temperature exposure. For steels containing sufficient residual silicon, such as AISI 430, electrical resistance can be further increased by the formation of a continuous insulating silica layer at the scale/alloy

interface. Low Si ferritic alloys have been developed for interconnect applications (e.g., Crofer22APU), but the required additional processing to remove the Si and other residual elements substantially increases the material cost.

Alternatively, modification of the alloy chemistry can potentially be used to avoid silica layer formation without the need for additional expensive processing steps, such as vacuum refining. For example, Dulieu et al. [1] reported that alloy 1.4509 (German Material Number, analogous to AISI 441), which is similar in many respects to 1.4016 (AISI 430), did not form a silica sub-layer at the scale/alloy interface, in spite of the presence of over 0.5% residual Si in both alloys. The primary difference in the composition of the two alloys is the presence of small amounts of Nb and Ti in 1.4509, suggesting that these additives played a key role in preventing Si migration to the scale/alloy interface.

Based on this encouraging result, PNNL, in collaboration with Allegheny Technologies, Inc. and the National Energy Technology Laboratory, has investigated the metallurgical characteristics, oxidation behavior, and electrical performance of AISI 441. In addition, benefits of protective coatings have been examined by applying spinel-based coatings to AISI 441, and comparing the behavior of the coated steel to that of uncoated steel.

### Approach

The ferritic stainless steel studied during fiscal year 2008 was T441, a commercial grade steel manufactured by Allegheny Technologies Inc. (Mn,Co)<sub>3</sub>O<sub>4</sub> (MC) and Ce-modified MC (Ce-MC) spinel powders were prepared via glycine-nitrate combustion synthesis, applied to selected alloy coupons using a slurry-based approach, and sintered to form protective coatings. Bare and coated steel coupons were evaluated via isothermal oxidation tests in ambient air. The electrical resistance of bare and coated T441 was measured using a four-probe direct current technique, using (La<sub>0.8</sub>Sr<sub>0.2</sub>)<sub>0.98</sub>MnO<sub>3</sub> as the contact paste. Scanning electron microscopy/energy dispersive spectroscopy (SEM/EDS) and transmission electron microscopy (TEM)/EDS analyses were performed on selected samples.

### Results

SEM analysis of the as-received T441 revealed grains ranging in size from ~20 to 60 microns, with second phases randomly distributed within the grains. SEM/EDS point analysis indicated that the second phases were rich in Nb and Ti. This was further confirmed by TEM analysis, which indicated that the

intra-grain precipitates were a Laves phase, which is consistent with the  $\text{Fe}_2\text{Nb}$  Laves phase reported in the manufacturer's technical data "blue sheet" for T441 [2]. After oxidation in air at  $800^\circ\text{C}$  for 300 hours, second phase formation was observed at the grain boundaries, as shown in Figure 1. TEM analysis indicated that the grain boundary phase was a Laves phase rich in both Nb and Si, in contrast to the initial intra-grain precipitates, which contained little, if any, Si. Figure 2 shows the oxidation behavior, in terms of weight gain as a function of time, of T441 at  $800^\circ\text{C}$  in flowing air. The weight gain due to the surface oxide scale growth approximately followed the classic Wagner parabolic relationship with time. The oxidation rate was comparable to that previously measured for Crofer22APU. No spallation was observed in the early stages of oxidation, but after 900 hours, localized scale spallation was observed. Occasional delamination observed at the scale/alloy

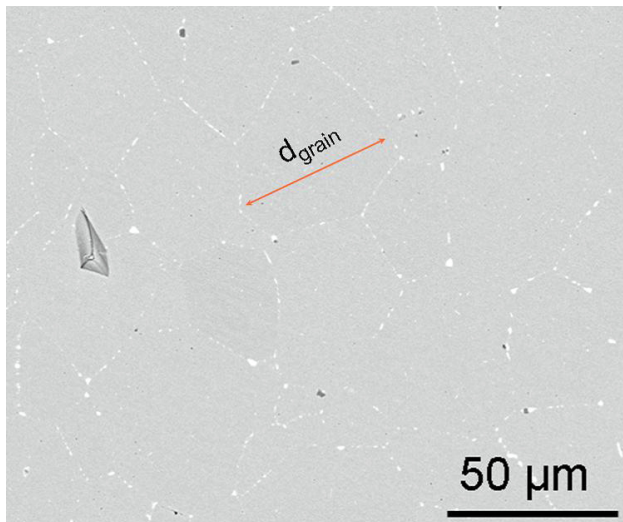


**FIGURE 1.** SEM Image of Polished T441 after Oxidation in Air for 300 Hours at  $800^\circ\text{C}$

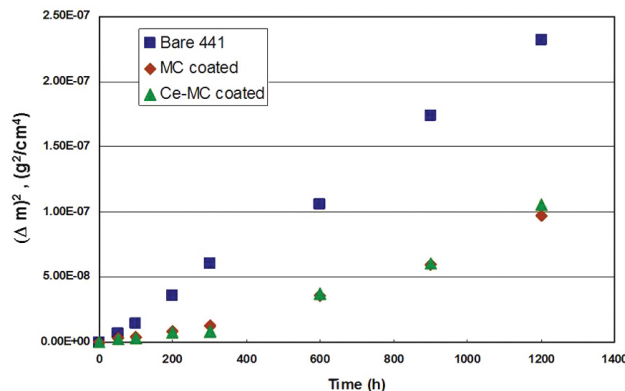


**FIGURE 2.** Weight Gain, Expressed as  $(\Delta m)^2$ , of Bare T441, MC Spinel-Coated T441, and Ce-MC Spinel-Coated T441 as a Function of Time during Oxidation in Air at  $800^\circ\text{C}$

interface during cross-sectional analysis provided qualitative evidence that the bonding of the scale to the steel substrate was weaker than that previously observed for Crofer22APU, possibly due to the absence of rare earth elements in the T441 substrate.

As mentioned above, chromia-forming ferritic stainless steels such as T441 are promising candidate materials for interconnects in SOFC stacks. During long-term operation, however, materials-related challenges may arise, including surface instability (including oxidation, spallation, and reactions with neighboring components), increasing electrical resistance due to continuous oxide scale growth, and chromia-scale evaporation, which may lead to cathode poisoning. One promising approach to overcome these issues is surface-modification of the metallic interconnects with conductive oxide coatings. For example, MC spinel coatings on stainless steel interconnects have been demonstrated to be effective in limiting inward oxygen and outward chromium diffusion [3,4]. As a result, spinel coatings are expected to improve stack performance by enhancing oxidation resistance and avoiding Cr poisoning. To fully utilize these advantages of the coatings, however, adequate adherence at the interfaces between the coating, the scale grown beneath the coating, and the metal substrate is also required. One well-established way to improve scale adherence to stainless steel substrates is to add small amounts of rare earth (RE) element(s) into the alloy. An alternative approach is to modify the alloy surface by deposition or coating with RE, usually in the form of oxides. For example, Alman et al. [5,6] reported improved oxidation resistance after surface treatment of ferritic stainless steels with Ce, via a pack cementation-based process. Preliminary testing at PNNL indicated that the surface treatment led to reduced ASR, at least in the hundreds of hours time frame. However, to obtain satisfactory long-term oxidation resistance, and to minimize Cr volatility, a protective coating (either on a bare or Ce surface-modified alloy) may be required. Recently, PNNL has worked to obtain the benefits of a spinel coating and a Ce surface treatment in a single fabrication step by the application of spinel coatings modified with Ce. Specifically, MC spinel was modified by addition of Ce (the nominal composition was  $\text{Ce}_{0.050}\text{Mn}_{1.475}\text{Co}_{1.475}\text{O}_4$ ) and then applied as a coating onto T441, which, as noted above, contains no RE additions. The properties of T441 with the Ce-modified spinel coating (Ce-MC) were investigated and compared to the properties of both uncoated T441 and T441 coated with the "standard" MC. Figure 2 shows the oxidation behavior, in terms of weight gain as a function of time, of MC and Ce-MC coated T441 at  $800^\circ\text{C}$  in air. It is clear that, during the 1200 hours of testing, the oxidation rate of the T441 was substantially reduced by the presence of the spinel coatings. SEM/EDS analysis of similarly oxidized samples found no evidence of Cr

penetration into either the MC or Ce-MC coatings. Also, there was no silica layer formation at the scale/metal interface, in spite of the relatively high residual Si content (0.47%) in the steel. This is attributed to the observed incorporation of Si into the grain boundary Laves phase, thereby reducing Si activity in the steel substrate and inhibiting the formation of an insulating interfacial silica layer.

While the MC and Ce-MC spinel coatings produced similar benefits in terms of oxidation resistance at 800°C, the structure and properties of the interface between the metal substrate and the oxide scale grown beneath the coatings appeared to differ. SEM cross-section analyses on ASR samples with the MC coating revealed cracks or gaps along the scale/metal interface which are qualitative indicators of relatively poor bonding at the scale/metal interface. In contrast, the scale grown beneath the Ce-MC coating remained adherent to the metal substrate, with no noticeable cracks or detachment

along the interface. The benefit of the Ce addition to the coating was even more evident in ASR samples tested at 850°C. The  $Mn_{1.5}Co_{1.5}O_4$  spinel (MC) coating, and the scale grown beneath it, exhibited buckling on the T441 surface (see Figure 3(a)), and detachment occurred along the scale/metal interface, as shown in the inset. In contrast, the Ce-MC coating and the scale grown beneath it were well adherent to the metal substrate, and no cracking was observed along the scale/metal interface (see Figure 3(b)).

In addition to satisfactory structural and surface stability, candidate interconnect alloys must also provide low electrical resistance in order to minimize power loss. Figure 4 shows the area specific resistance (ASR) of bare and coated T441 as a function of time, measured in air at 800°C. While the ASR of bare T441 increased to  $\sim 60 \text{ m}\Omega\cdot\text{cm}^2$  after  $\sim 5,000$  hours, the samples coated with MC or Ce-MC exhibited stable ASR of  $\sim 10\text{-}13 \text{ m}\Omega\cdot\text{cm}^2$ . It should be noted that the tests were interrupted twice by unscheduled power outages at around 650 and 2,800 hours. The unscheduled thermal events caused a discontinuous increase in the ASR of bare 441, possibly indicating damage to the interfacial contact or detachment of the scale from the metal substrate. In contrast, the ASRs of the coated samples returned to their previous level, suggesting that the coatings improved the stability of the contact material/coating/steel interface.

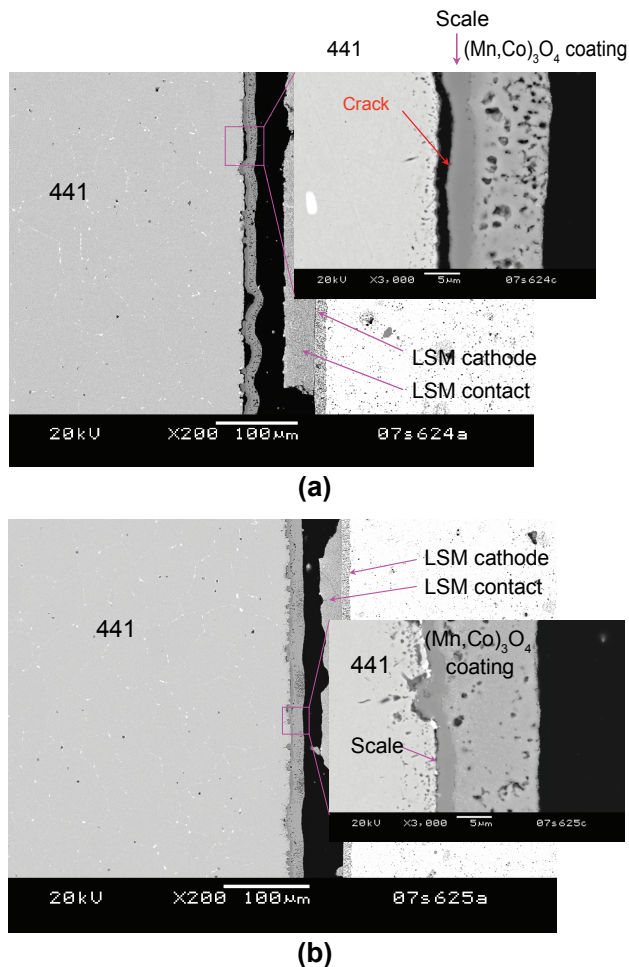


**FIGURE 3.** SEM Cross-Section Images of (a) MC Spinel-Coated T441 and (b) Ce-MC Spinel-Coated T441 after 700 Hours of Electrical Resistance Testing in Air at 850°C

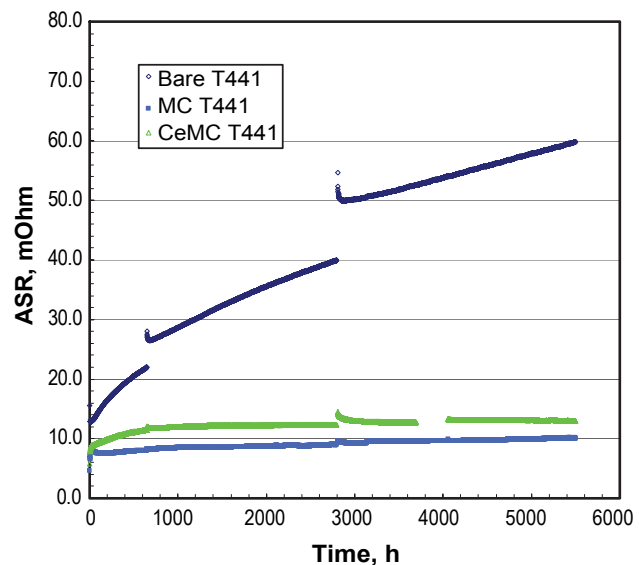


**FIGURE 4.** ASR of Bare T441, MC Spinel-Coated T441, and Ce-MC Spinel-Coated T441 as a Function of Time during Oxidation in Air at 800°C

## Conclusions and Future Directions

Investigations into the metallurgy, oxidation behavior, and electrical performance indicate that the alloy metallurgy and chemistry of T441 ferritic stainless steel remains promising for SOFC interconnect applications, although the substantial increase in ASR due to oxide scale growth over time suggest the need for a conductive protection layer, which can also minimize Cr evaporation. In particular, MC-based coatings drastically improved the electrical performance of the ferritic stainless steel T441, yielding stable ASR values at 800°C for over 5,000 hours. Ce-MC coatings retained the advantages of the unmodified spinel coatings, and also appeared to alter the scale growth behavior beneath the coating, leading to a more adherent scale. Future directions include examining effects of other rare earth additives on spinel coating performance and dual atmosphere testing of coated interconnect alloys to simulate actual SOFC interconnect operating conditions.

## FY 2008 Publications/Presentations

### Publications

1. Z.G. Yang, G.G. Xia, X.H. Li, and J.W. Stevenson, "(Mn,Co)<sub>3</sub>O<sub>4</sub> spinel coatings on ferritic stainless steels for SOFC interconnect applications," *Int. J. of Hydrogen Energy*, **32**, 3648 (2007).
2. Z.G. Yang, G.G. Xia, J.W. Stevenson, and P. Singh, "Corrosion Behavior of Interconnect Candidate Alloys under Air/Simulated Reformate Dual Exposure Conditions," in *Advances in Solid Oxide Fuel Cells III*, Ceramic Engineering and Science Proc., Wiley, **28**[4], 279 (2007).

### Presentations

1. "Surface Modification of Metallic Interconnects in SOFCs for Improved Surface and Electrical Stability," Z.G. Yang, G.G. Xia, J.W. Templeton, Z. Nie, X.S. Li, J.W. Stevenson, and P. Singh, 137<sup>th</sup> Annual TMS Meeting, New Orleans, LA, March 9–13, 2008.
2. "Investigation and Development of Cost-Effective Ferritic Stainless Steels for SOFC Interconnect Applications," Z.G. Yang, G.G. Xia, Z. Nie, J.W. Templeton, J.W. Stevenson, and P. Singh, 137<sup>th</sup> Annual TMS Meeting, New Orleans, LA, March 9–13, 2008.
3. "Advanced Interconnect Development at PNNL," Z.G. Yang, G.G. Xia, J.D. Templeton, X.S. Li, Z. Nie, C.M. Wang, G.D. Maupin, J. Coleman, J.W. Stevenson, and P. Singh, 32<sup>nd</sup> Int. Conference on Advanced Ceramics & Composites (American Ceramic Society), Daytona Beach, FL, January 27 – February 1, 2008.
4. "Advanced SOFC Interconnect Development at PNNL," Z.G. Yang\*, G.G. Xia, J. Bonnett, Z. Nie, J. Templeton, J.W. Stevenson, and P. Singh, Fuel Cell Seminar, San Antonio, TX, October 17, 2007.

## References

1. D. Dulieu, J. Cotton, H. Greiner, K. Honegger, A. Scholten, and T. Seguelong, in *Proc. 3rd Eur. SOFC Forum, European Solid Oxide Fuel Cell Forum*, Switzerland, p. 447 (1998).
2. "Stainless Steel AL 441HPTM Alloy," Technical Data Blue Sheet, Allegheny Technologies, Inc. (2005).
3. Y. Larring and T. Norby, *J. Electrochem. Soc.*, **147**, 3251 (2000).
4. Z.G. Yang, G.G. Xia, S.P. Simner, and J.W. Stevenson, *J. Electrochem. Soc.*, **152**, A1896 (2005).
5. D. Alman, C. Johnson, W. Collins, and P. Jablonski, *J. Power Sources*, **168**, 351 (2007).
6. D.E. Alman, and P.D. Jablonski, *Inter. J. Hydrogen Energy*, **32**, 3743 (2007).

---

## IV.C.6 Development of Low-Cr Fe-Ni-Based Alloys for Intermediate Temperature SOFC Interconnect Application

Jiahong Zhu (Primary Contact), Zhonghe Bi, Xiaochuan Lu

Department of Mechanical Engineering  
Tennessee Technological University  
115 W. 10<sup>th</sup> St., Box 5014, Cookeville, TN 38505  
Phone: (931) 372-3186; Fax: (931) 372-6340  
E-mail: jzhu@tntech.edu

DOE Project Manager: Ayyakkannu Manivannan  
Phone: (304) 285-2078  
E-mail: Ayyakkannu.Manivannan@netl.doe.gov

### Subcontractors:

- Oak Ridge National Laboratory, Oak Ridge, TN
- Harlan U. Anderson, Consultant, Rolla, MI

Contract Number: 42223

Start Date: October 1, 2004

Project End Date: December 31, 2007

- Electroplating of the Fe-Ni-Co alloys as a precursor to synthesize a protective spinel layer on commercial ferritic steels has been initiated to facilitate the utilization of the Cr-free spinel as a surface seal to block Cr evaporation.

---

### Introduction

With the reduction of the SOFC operating temperatures to 700-800°C, Cr<sub>2</sub>O<sub>3</sub>-forming ferritic alloys are widely used as interconnect materials in the SOFC stacks being developed by the Solid State Energy Conversion Alliance (SECA) Industrial Teams. These ferritic alloys, including Crofer 22 APU, SS 430, SS 441, Ebrite, etc., possess an overall combination of properties desirable as SOFC interconnect materials such as low cost, excellent manufacturability, adequate match in coefficient of thermal expansion (CTE) with other cell components, high electronic conductivity and thermal conductivity. Two of the major concerns (or problems) with these ferritic interconnect alloys are (1) their long-term oxidation resistance and oxide scale electrical conductivity, and (2) Cr evaporation and associated “poisoning” of the cathode under the operating environments of SOFC [1]. This SECA project has focused on the development of new low-Cr Fe-Ni-based interconnect alloys with low CTE and scale area specific resistance (ASR), suitable oxidation resistance, and reduced Cr evaporation, thus resolving the current issues for SOFC interconnect materials.

### Approach

Using alloy-design principles, a series of new low-Cr Fe-Ni-based alloys have been developed. Upon thermal exposure, these low-Cr Fe-Ni-based alloys with 6 wt% Cr maximum develops a double-layer oxide scale consisting of a Cr-free, electrically-conductive (Fe,Ni,Co)<sub>3</sub>O<sub>4</sub> spinel outer layer that acts as a surface seal for blocking Cr evaporation from the alloy surface atop a protective, electrically-conductive Cr<sub>2</sub>O<sub>3</sub> inner layer.

The double-layer oxide structure formed on the low-Cr Fe-Ni-based alloys was further studied using STEM attached with an energy-dispersive spectroscope. The tensile properties of the new alloy were determined as a function of test temperature using an *Instron* test machine, which were compared to Crofer 22 APU. In addition, the performance stability of a SOFC was studied with the new alloy as interconnect in the bare and preoxidized conditions. To reduce the overall cost

### Objectives

- Develop a series of new Fe-Ni-based alloys with low Cr for intermediate temperature solid oxide fuel cell (SOFC) interconnect application.
- Achieve low Cr volatility, adequate mechanical properties, good compatibility with the cathode, improved in-cell performance for these alloys without surface coatings.
- Explore the feasibility of electroplating of Fe-Ni-Co alloys as a precursor for synthesizing the (Fe,Ni,Co)<sub>3</sub>O<sub>4</sub> spinel to protect commercial ferritic steels.

### Accomplishments

- The compositional range of the new low-Cr Fe-Ni-based alloy system has been optimized and the double-layer oxide scale structure thermally grown on the new alloy was further confirmed using scanning transmission electron microscopy (STEM).
- In-cell testing using an anode supported cell indicates that the formation of the Cr-free spinel layer via thermal oxidation was effective in blocking the Cr migration and thus improving the cell performance stability.
- Tensile properties of the new alloy have been determined from room temperature to 900°C, with its ductility similar to Crofer 22 APU and its yield strength and tensile strength much higher than Crofer 22 APU.

of the interconnect material, electroplating of the Fe-Ni-Co alloy on commercial ferritic steels has been initiated, which is converted to a Cr-blocking surface spinel layer atop an inner  $\text{Cr}_2\text{O}_3$  layer upon thermal exposure.

## Results

STEM observation of the oxide scale thermally grown on the low-Cr Fe-Ni-Co alloy after exposure to air at  $800^\circ\text{C}$  for 3 weeks indicates the existence of a fine-grained  $\text{Cr}_2\text{O}_3$  layer next to the spinel outer layer, as shown in Figure 1(a), consistent with our earlier electron probe micro-analysis results. There were, however, a number of oxides formed at the region between the internal oxidation zone and the alloy substrate, including  $\text{Cr}_2\text{O}_3$ , Nb-Ni-Co-Si-O,  $\text{CrNbO}_4$ , etc., as shown in Figure 1(b). Furthermore,

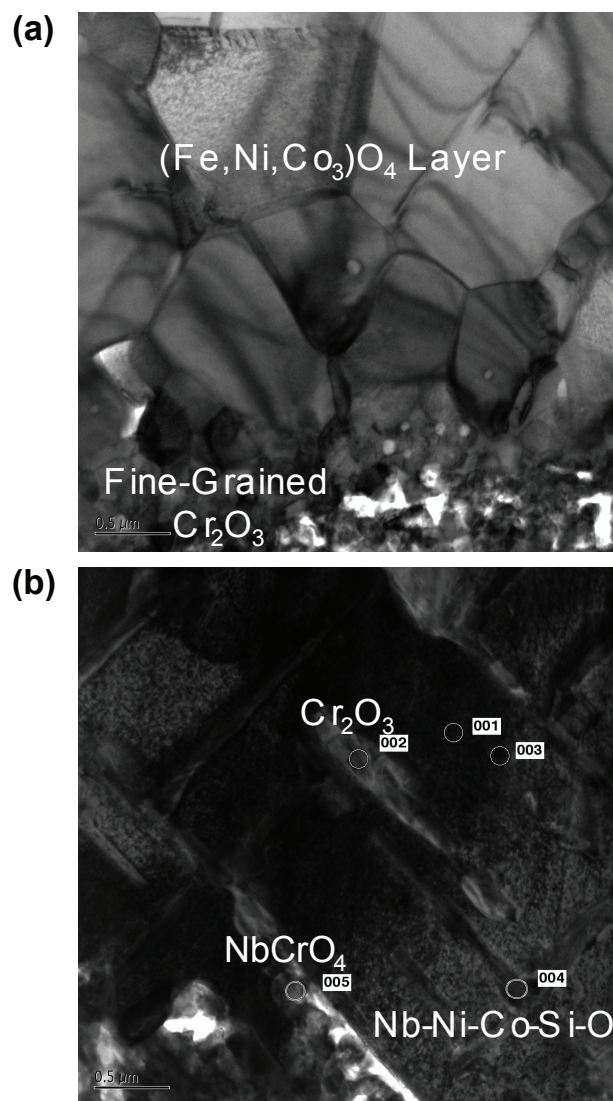


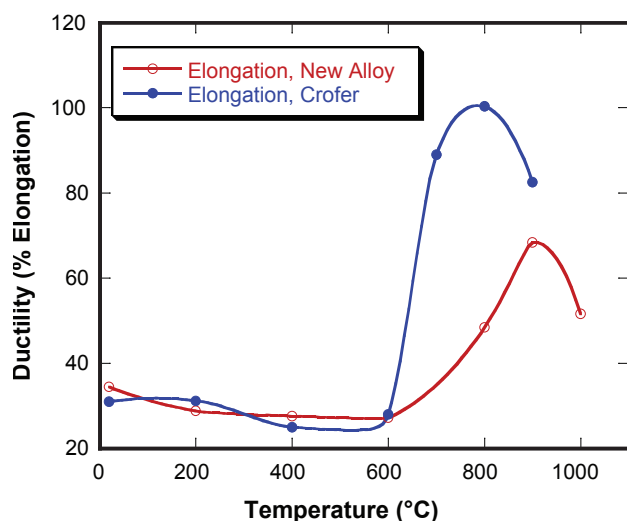
**FIGURE 1.** STEM micrographs of the oxide scale formed on the new alloy after thermal oxidation for 3 weeks at  $800^\circ\text{C}$  in air: (a) next to the spinel layer; (b) near the alloy surface.

no continuous insulating layer of  $\text{SiO}_2$  was detected across the oxide scale. This is in agreement with the low scale ASR for this alloy. It seems that Si was combined with some other metallic elements (especially Nb) to form some multi-component oxides. The electrical properties of the Si-containing oxides are currently not available.

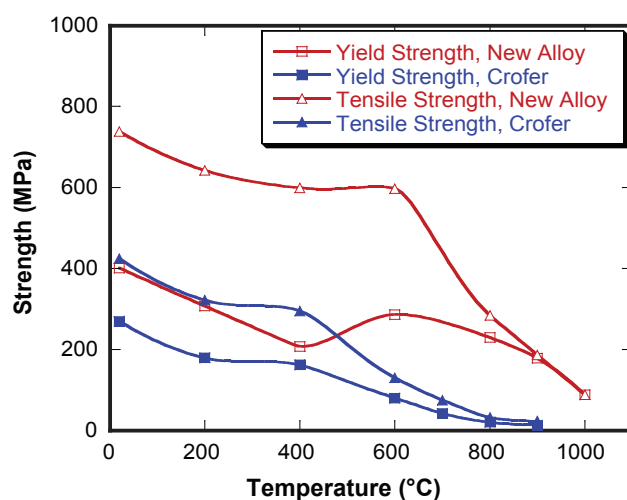
As long as the Si-containing oxides are not interconnected to form a layer, the scale ASR will not be an issue. STEM study of an alloy sample thermally oxidized for 40 weeks at  $800^\circ\text{C}$  in air also did not detect any  $\text{SiO}_2$  layer formation. Also, based on STEM observation, the oxide scale features did not change significantly upon the 40-week exposure, even though additional longer-term oxidation testing might be needed to further confirm this conclusion.

Tensile properties of the new alloy were plotted in Figure 2 as a function of test temperature. The data for Crofer was included for comparison [2]. As shown in Figure 2(a), the new alloy exhibited a ductility similar to Crofer from room temperature to  $600^\circ\text{C}$ ; however, Crofer possessed a slightly higher ductility as the temperature increased to over  $600^\circ\text{C}$ . The overall good ductility of this new alloy is in agreement with the relative ease in fabricating this alloy into sheet via hot-rolling and cold-rolling, which might also lead to the possibility of additional forming operations such as stamping to process corrugated interconnect components. The yield strength and tensile strength of the new alloy, however, were significantly higher than those of Crofer over the entire temperature range, as shown in Figure 2(b). The higher strength of this new alloy is expected to translate into better creep resistance; as a result, thinner interconnect plates might be used in SOFC stacks, thus reducing the raw material usage and lower the overall cost of the interconnect material.

Cell performance stability with the Crofer and the new alloy (both in the bare and preoxidized conditions) is shown in Figure 3. For the two bare alloys, an initial severe reduction in power density was observed, which is comparable for the two alloys. The power density continued to decrease with time, even though the degradation rate slowed down with time. The power density decrease can be attributed to the Cr poisoning effect, i.e. Cr migration from the Cr-containing interconnect alloy to the lanthanum strontium manganite (LSM) cathode, leading to a decrease in cathode electrochemical activity and thus cell performance reduction. While both the alloys exhibited a similar trend, it was noticed that the cell performance with the new alloy started to stabilize after about 120-hour operation, which is believed to be due to the *in situ* formation of the Cr-free  $(\text{Fe, Ni, Co})_3\text{O}_4$  layer on the alloy surface. The formation of this outer layer blocked the Cr evaporation from the alloy, resulting in a more stable cell performance. For one specific cell, preoxidation of the new alloy at  $800^\circ\text{C}$  in air for 120 hours was conducted to form the spinel layer on the alloy prior to cell testing.



(a)



(b)

**FIGURE 2.** Tensile properties of the new alloy and Crofer as a function of temperature: (a) ductility; and (b) yield strength and tensile strength.

The result, also shown in Figure 3, implies that with the preoxidation treatment, the initial cell performance degradation was avoided; furthermore, the power density of the cell after 150-hour testing remained as high as  $0.2 \text{ W/cm}^2$  at a fixed cell voltage of  $0.7 \text{ V}$ , which is much higher than that of the bare alloy (i.e.  $0.05 \text{ W/cm}^2$ ). The scatter in the data for the preoxidized Fe-Ni-Co alloy is presumably due to some fuel leakage/cell sealing problems apparently associated with this cell.

The best cell performance stability, however, was observed when the interconnect was Crofer 22 APU electroplated with an Fe-40%Co alloy. The electroplated alloy layer on Crofer 22 APU significantly improved the cell performance stability as compared to the bare Crofer 22 APU as well as the new alloy, as also shown in Figure 3. This clearly demonstrated the effectiveness

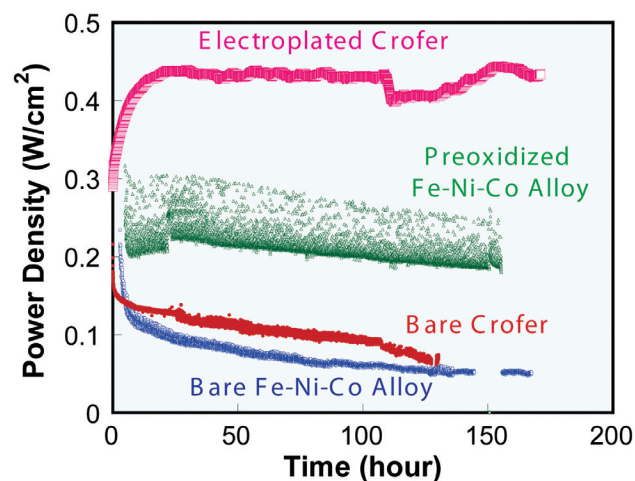


**FIGURE 3.** The cell power density vs. cell operation time for several cells with different interconnects, including bare Crofer 22 APU and Co-Fe electroplated Crofer 22 APU, bare and preoxidized Fe-Ni-Co alloy.

of the electroplated layer in blocking the Cr migration and poisoning. A surface  $\text{CoFe}_2\text{O}_4$  layer was observed on the interconnect surface after cell testing and no Cr could be detected in the surface oxide layer formed on interconnect as well as in the LSM cathode. Apparently, the Fe-Co layer was converted into a  $\text{CoFe}_2\text{O}_4$  spinel layer during the cell testing. The formation of the Cr-free spinel blocked Cr transport from the substrate alloy into the cathode.

## Conclusions and Future Directions

The design and development of new alloys which upon thermal exposure form an electrically conductive, Cr-free spinel outer layer atop a protective, electrically conductive oxide inner layer is highly desirable to mitigate the Cr poisoning problem in the SOFC stack as well as reduce the overall interconnect material cost. A new low-Cr Fe-Ni-Co alloy has been developed and optimized for SOFC interconnect application. The desired double-layer oxide structure was thermally grown on the new alloy with drastically improved oxidation resistance, low Cr volatility and scale ASR, good CTE match with other cell components, adequate mechanical property as well as good compatibility with the cathode materials. The new low-Cr alloy is a promising alternative to replace high-Cr ferritic alloys as SOFC interconnect.

While additional alloy design and production scale-up are clearly needed, this study has demonstrated that it is feasible to develop a low-Cr Fe-Ni-Co alloy with balanced properties for SOFC interconnect application. Since this alloy system contains significant amounts of Ni and Co than ferritic steels, it is suggested that this Fe-Ni-Co alloy system be combined with the ferritic steel to form a unique coating/alloy system as SOFC

interconnect material. Furthermore, it is suggested that low-cost coating processes such as electroplating should be developed for achieving such a coating/alloy system. A new interconnect material with an electroplated surface layer of the Fe-Ni-Co alloy over the ferritic steel will combine the attributes of both the new Fe-Ni-Co alloy and the low-cost ferritic steels. The surface Fe-Ni-Co layer will be converted into a Cr-free, electrically-conductive (Fe,Ni,Co)<sub>3</sub>O<sub>4</sub> spinel layer during thermal oxidation or SOFC operation. The new interconnect material system (ferritic steels electroplated with Fe-Ni-Co alloys) is expected to reduce the overall material cost and improve the durability of SOFC stacks, thus contributing to early commercialization of the SOFC technology.

### FY 2008 Publications/Presentations

1. J.H. Zhu, S.J. Geng, Z.G. Lu, and W.D. Porter, "Evaluation of Binary Fe-Ni Alloys as Intermediate-Temperature SOFC Interconnect", *Journal of the Electrochemical Society*, 154(12), B1288, 2007.
2. S.J. Geng, J.H. Zhu, M.P. Brady, H.U. Anderson, X.D. Zhou, and Z.G. Yang, "A low-Cr metallic interconnect for intermediate-temperature solid oxide fuel cells", *Journal of Power Sources*, 172, p. 775, 2007.
3. J.H. Zhu, S.J. Geng, and D.A. Ballard, "Evaluation of Several Low Thermal Expansion Fe-Co-Ni Alloys as Interconnect for Reduced-Temperature Solid Oxide Fuel Cell", *International Journal of Hydrogen Energy*, 32, p. 3682, 2007.
4. Z.G. Lu, J.H. Zhu, Y. Pan, N. Wu, and A. Ignatiev, "Improved oxidation resistance of a nanocrystalline chromite-coated ferritic stainless steel", *Journal of Power Sources*, 178, p. 282, 2008.
5. "Low-Cr Fe-Ni-Co Alloys as SOFC Interconnect", invited talk, Gordon Research Conference on High-Temperature Corrosion, New London, NH (July 29 – August 3, 2007).
6. "Low-Cr Fe-Ni-Co Alloys as Interconnect for IT SOFC", presented at SECA Core Technology Program Peer Review Meeting, San Antonio, TX (August 7–9, 2007).
7. "Electroplated Fe-Co Alloy Coatings for Protecting Ferritic Interconnect Alloys", presented at International Conference on Metallurgical Coatings and Thin Films, San Diego, CA (April 28 – May 2, 2008).

### References

1. Gindorf, C., Singheiser, L & Hilpert, K. Chromium vaporisation from Fe,Cr base alloys used as interconnect in fuel cells. *Steel Research* 72 (11-12), 528-533 (2001).
2. Hojda, R. & Paul, L., NACE Paper No. 6479, in *Corrosion* 2006 (2006).



---

## IV. SECA CORE RESEARCH & DEVELOPMENT

### D. Seals



---

## IV.D.1 Development of Seals and Seal/Interconnect Interfaces

Yeong-Shyung “Matt” Chou (Primary Contact),  
K. Scott Weil (Primary Contact), Jeff Stevenson,  
Prabhakar Singh

Pacific Northwest National Laboratory (PNNL)  
K2-44, P.O. Box 999  
Richland, WA 99354  
Phone: (509) 375-2527 (Chou); (509) 375-6796 (Weil);  
Fax: (509) 375-2186  
E-mail: yeong-shyung.chou@pnl.gov; Scott.Weil@pnl.gov

DOE Project Manager: Ayyakkannu Manivannan  
Phone: (304) 285-2078  
E-mail: Ayyakkannu.Manivannan@netl.doe.gov

Contract Number: 40552

Start Date: October 1, 2007

Project End Date: September 30, 2008

### Objectives

- To develop and validate devitrifying sealing glasses for intermediate temperature solid oxide fuel cells (SOFCs).
- To evaluate and optimize the chemical stability and mechanical integrity of interconnect alloy/sealing glass interfaces.

### Accomplishments

- Evaluated effects of surface aluminization and exposure conditions on strength of glass/alloy seals.
- Developed a powder-based aluminization process for fabrication of protective alumina layers on steel interconnects.

---

---

### Introduction

Planar SOFC stacks require adequate seals between the interconnects and cells in order to prevent mixing of the oxidant and fuel gases within the stack, and leakage of the gases from the stack. Several different approaches to sealing SOFC stacks are available, including rigid, bonded seals (e.g., devitrifying glass), compliant seals (e.g., viscous glass), and compressive seals (e.g., mica-based “gaskets”). Glass-based seals typically soften and flow slightly during stack fabrication (at a temperature above the operating temperature) but then become rigid and immobile through devitrification (to avoid excessive flow or creep) at the stack operating temperature.

While devitrifying glass seals represent a relatively easy means of sealing an SOFC stack (at least initially), they face challenges in meeting the stringent SOFC requirements, including long-term operation at elevated temperatures and thermal cycling from operating to ambient temperature. For example, the coefficient of thermal expansion (CTE) of the seals must be closely matched to the other stack components in order to avoid build-up of stresses during thermal cycling. While glass compositions can be tailored to optimize their physical properties, the selection of glasses offering appropriate thermal expansion behavior is relatively narrow. The selection of sealing glass compositions is further limited by the need for the glass to have appropriate wetting behavior and viscosity at the sealing temperature. In addition, since most SOFC sealing glasses devitrify at stack operating temperatures, the seals experience significant microstructural and crystalline phase changes over time. Thus, control of the devitrification kinetics and phases is required to assure that the long-term CTE of the seal remains compatible with other stack components. Chemical compatibility with the stack components and the gaseous constituents of the highly oxidizing and reducing environments is also of primary concern. For example, alkaline earth-containing aluminosilicate glass sealants tend to form interfacial reaction products such as barium or strontium chromate when bonded to candidate stainless steel interconnects. During long-term exposure at the stack operating temperature, growth of these high CTE (~22 ppm/°C) phases can significantly degrade interfacial strength, leading to seal failure.

Most SOFC sealing glasses are designed to seal at temperatures fairly close to stack operating conditions. Challenges associated with these glasses can include appreciable amounts of reactive (high boria content) residual glass, and changes in CTE over time as devitrification proceeds. In response to these issues, PNNL has developed devitrifying “refractory” glass seals, which are sealed at relatively high temperatures (>900°C). Refractory sealing glasses potentially offer improved stability in terms of thermal expansion, chemical compatibility, interfacial strength, and minimal interfacial reactivity during long-term operations. In addition, the higher stack fabrication temperature may result in increased strength and electrical conductivity of contact materials at the cathode/interconnect contact zones. In previous work, optimized “refractory” sealing glass compositions were developed which exhibit stable CTEs in the desired range of 11.5-12.5 ppm/°C and sealing temperatures in the 950-1,000°C range. Weight loss measurements indicated that the total material loss through vaporization should be minimal during stack lifetime. Electrical resistance tests of sealed interconnect

alloy coupons demonstrated very high electrical resistance (under direct current loading in SOFC operating conditions) which remained stable for over 1,000 hours. However, as noted above, microstructure analysis did reveal a tendency to form undesirable alkaline earth chromate (in this case, strontium chromate) at glass/interconnect alloy interfaces. Mechanical testing of the seal/joint strengths of sealed glass-alloy coupons confirmed the degradation in tensile strength during high-temperature exposure to air due to the formation of interfacial strontium chromate.

Based on these results, PNNL is investigating alloy surface modifications intended to stabilize the seal/interconnect interface by preventing the formation of the chromate phase. One of the mitigation approaches involves the formation of an aluminum oxide layer on the alloy surface, which may offer a means of preventing Cr in the Fe-Cr steel from contacting, and subsequently reacting with, alkaline earth constituents (e.g., Ba or Sr) in the glass seal material.

## Approach

In the first quarter of fiscal year (FY) 2008, environmental aging effects on seal strength were evaluated using one of PNNL's refractory sealing glasses (YSO77) and aluminized ferritic stainless steel (Crofer22APU). This work was an extension of studies in FY 2007 which found that sealing to uncoated ferritic stainless steels resulted in the formation of alkaline earth chromates (e.g., strontium chromate or barium chromate) at the glass/metal interface wherever oxygen was available. The presence of these chromates resulted in substantial degradation of the seal strength. To examine a potential means of preventing chromate formation, Crofer22APU coupons were aluminized in-house using a commercially available Al-containing aerosol spray process. The metal coupons were sprayed on both sides and heat-treated in air (900°C/2 hours) to promote the formation of an alumina layer. Residual alumina powder on the surface was subsequently removed by ultrasonic cleaning. The refractory sealing glass was applied to the coupons by screen printing, and pairs of coupons were then combined to form metal/glass/metal "sandwiches." These samples were heated to 965°C/2 hours in air for sealing and then heat-treated in air for 4 hours at 800°C to promote devitrification and microstructure development. The sealed structures were then glued to Al test fixtures with fast-setting epoxy for room temperature seal strength testing in the uniaxial tensile mode. Alternatively, some of the sealed samples were then aged either in air or in a wet reducing environment (5% H<sub>2</sub>/95% He with ~20% H<sub>2</sub>O added) prior to epoxy bonding. The samples were aged at 850°C, which may represent an upper temperature limit for planar SOFC stack operation. PNNL is also developing a new aluminization process which consists

of spraying a low viscosity Al powder/polymer solution slurry onto the surfaces of the alloy, drying the coated component in air at 80°C to drive off the solvent, and heating in air at 900°C for 1-4 hours.

## Results

The room temperature tensile seal strength of the as-sealed and aged aluminized samples are shown in Figure 1(a), together with previously obtained results for non-aluminized steel (Figure 1(b)). It is evident that the seals to aluminized steel showed no strength degradation after aging, unlike the seals to non-aluminized steel, whose strength decreased significantly during aging in air due to the formation of a strontium chromate layer at the glass/alloy interface. In fact, the strength of the aluminized samples actually increased during aging from  $5.8 \pm 1.5$  MPa (as-sealed) to  $8.2 \pm 1.5$  MPa (air aged) and  $8.4 \pm 1.2$  MPa (reducing atmosphere aged). The cause for the strength improvement is not clear at this time. Possible causes include changes in critical flaw morphology or relaxation of localized residual stresses during aging. Post-test analysis confirmed that failure in the air-aged seals to non-aluminized steel initiated in interfacial strontium chromate layers, whereas failure in the air-aged seals to the aluminized steel and in seals aged in a reducing atmosphere occurred through the

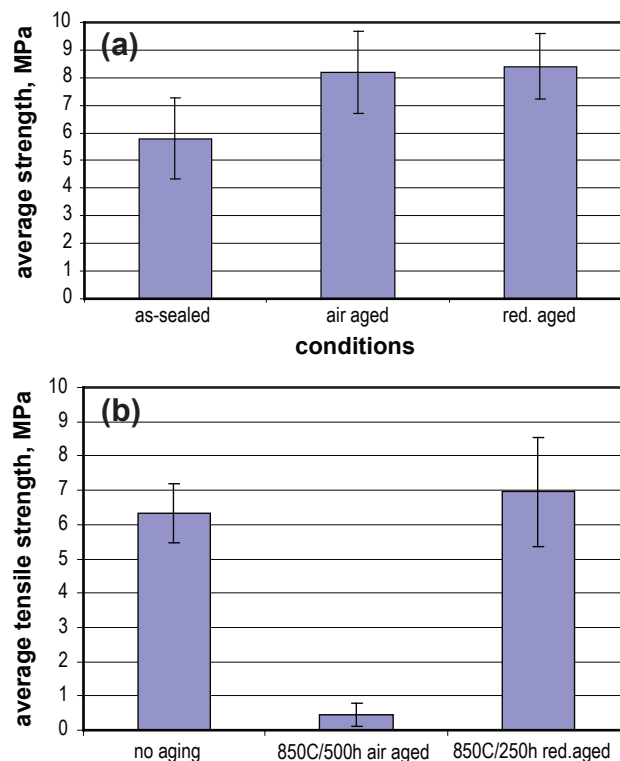


**FIGURE 1.** Effect of Environmental Aging on the Room Temperature Tensile Strength of Sealed Steel Coupons: (a) Aluminized Crofer22APU and (b) As-Received Crofer22APU

seal material itself; it should be noted that strontium chromate formation is thermodynamically unfavorable under reducing conditions. Overall, these results clearly indicate the potential benefits of an alumina coating in maintaining the mechanical integrity of glass-based seals during long-term operation at elevated temperatures in air.

Cross-sectional analysis of the aluminized steel coupons indicated that the aluminized surface layers prepared with the commercial aerosol product were irregular in structure and in some cases discontinuous. Similarly, while other commercial aluminization processes including vapor phase and pack cementation approaches exist, there are limitations to these approaches with respect to cost, dimensional changes to the components during coating (e.g. interconnect plate warpage), and/or the stability of the final coating layer. As a result, PNNL is developing a facile, low-cost aluminization technique as a potential means of improving long-term stability of glass seal/alloy interconnect interfaces. The technique (described briefly in the "Approach" section) is based on a simple powder coating method that exploits interdiffusion between an aluminum powder overlayer and the underlying stainless steel substrate, resulting in an alumina-scale forming coating. Parameters believed to affect the coating process include: powder composition (i.e. pure Al or an Al alloy), powder size, binder composition, binder concentration in the slurry, final heat treatment conditions (i.e. temperature and time), and inclusion of a secondary soluble metal compound in the binder (to further modify the composition and microstructure of the coating and/or alumina scale); some of these parameters are currently under investigation.

Shown respectively in Figures 2(a) and (b) are cross-sectional and planar micrographs of aluminized T441 stainless steel. The aluminum diffusion is apparent from the cross-sectional view, penetrating to ~100  $\mu\text{m}$  in depth for this particular set of coating conditions. It has been determined that the extent of this affected zone can be controlled predominantly by the size (i.e. average size and size distribution) of the aluminum powder particles employed in the process. Approximately 100  $\mu\text{m}$  further below the primary aluminum diffusion zone are a series of discrete aluminide precipitates that have formed. The exact composition and phase of these precipitates is currently under study. As is apparent in the planar view in Figure 2(b), some surface roughening occurs during this process.

Shown in Figures 3 and 4 are scanning electron microscopy/energy dispersive spectroscopy maps of the aluminized material, again respectively in cross-sectional and planar view. The gradient nature of the coating is obvious from the cross-sectional compositional maps in Figures 3(b)-(d). It is also apparent specifically from Figure 3(c) that the aluminization coating effectively

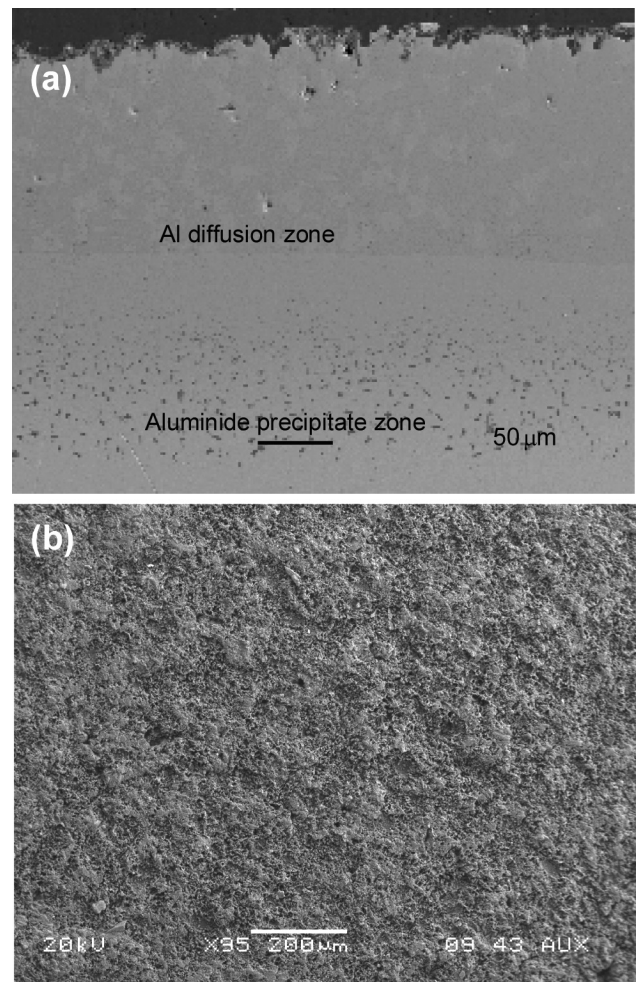


**FIGURE 2.** Aluminized T441: (a) Cross-Sectional View and (b) Planar View

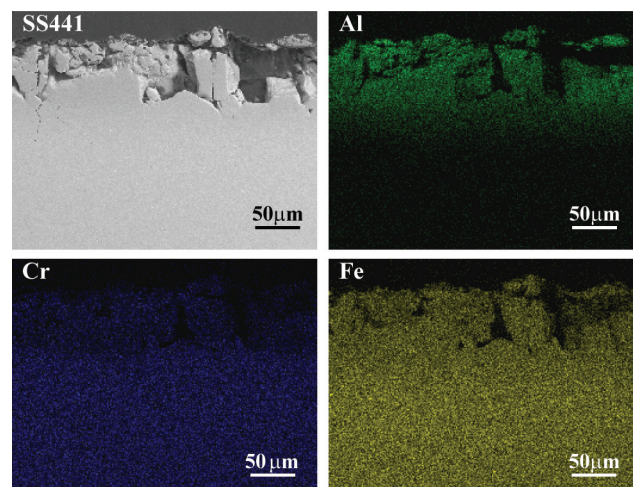


**FIGURE 3.** Cross-Sectional Views of Aluminized T441: (a) Back-Scattered Electron Image, (b) Aluminum Compositional Map, (c) Chromium Compositional Map, and (d) Iron Compositional Map

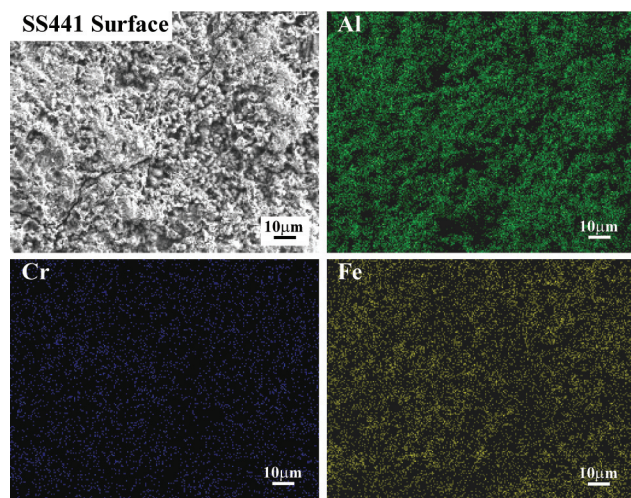


**FIGURE 4.** Planar Views of Aluminized T441: (a) Back-Scattered Electron Image, (b) Aluminum Compositional Map, (c) Chromium Compositional Map, and (d) Iron Compositional Map

blocked chromium diffusion to the top exposed surface of the coated material. Minimization of Cr volatility from steel SOFC components is another potential benefit of surface aluminization, which can thus mitigate potential issues such as runaway alloy oxidation or Cr poisoning of cathodes. Cr blocking is also apparent in the planar compositional maps shown in Figures 4(a)-(d). In particular, note that little chromium was found at the surface of the material (Figure 4(c)).

## Conclusions and Future Directions

Aluminization of steel surfaces appears to be an effective means of preventing formation of undesirable alkaline earth chromate phases which can drastically reduce the strength of glass-based seals to the steel components. As a result, PNNL is developing a cost-effective aluminization process intended to provide SOFC developers with a means of preparing stable seal/interconnect interfaces. Future directions include development of an understanding of the effects of various processing and material parameters on the thickness, microstructure, and composition of the aluminized layer. The effects of this layer in modifying thermal expansion properties of the substrate and on the strength of joints prepared with the coated materials via glass sealing, brazing, and welding will also be examined.

## FY 2008 Publications/Presentations

1. Y-S Chou, J. W. Stevenson, and P. Singh, "Effect of pre-oxidation and environmental aging on the seal strength of a novel high temperature SOFC sealing glass with metallic interconnect," *in press*.
2. "Status of Refractory Glass Seal Development at PNNL: Mechanical Property and Electrical Stability," Y.S. Chou, J.W. Stevenson, X. Li, Z.G. Yang, and P. Singh, Fuel Cell Seminar, San Antonio, TX, October 17, 2007.
3. "Adhesion Strength between Glass Sealant and Aluminized Metallic Interconnect of SOFC," S. T. Hong, J. P. Choi, Y. Hovanski, and K. S. Weil, MS&T 07, Detroit, MI, September 17, 2007.
4. "Glass-Metal Joint Strength Improvement in SOFC Stacks by Use of the Reactive Air Coating Process," J.P. Choi, S. T. Hong, and K. S. Weil, TMS Annual Meeting, New Orleans, LA, March 11, 2008.

---

## IV.D.2 Reliable Seals for Solid Oxide Fuel Cells

Ronald E. Loehman (Primary Contact),  
Erica Corral, Marlene Chavez, Scarlett Widgeon  
Sandia National Laboratories  
MS 1349  
Albuquerque, NM 87185-1349  
Phone: (505) 272-7601; Fax: (505) 272-7304  
E-mail: loehman@sandia.gov

DOE Project Manager: Ayyakkannu Manivannan  
Phone: (304) 285-2078  
E-mail: Ayyakkannu.Manivannan@netl.doe.gov

Contract Number: 68250

Start Date: October 1, 2007  
Project End Date: September 30, 2008

### Objectives

- Develop reliable, cost-effective sealing techniques for solid oxide fuel cells (SOFCs).
- Determine performance-limiting features of sealing methods.
- Optimize seal properties.
- Determine seal degradation mechanisms and predict useful seal lifetimes.

### Approach

- We are making composite seals comprising a glass matrix and powder filler whose chemical and mechanical properties can be tailored to be compatible with SOFC components.
- This composite approach allows glass and filler properties to be optimized independently.
- Thermal and mechanical strains of seals are reduced by selecting glass compositions with glass transition temperatures ( $T_g$ ) below the SOFC operating temperature.
- Viscosities, coefficients of thermal expansion (CTE), and other seal characteristics can be tailored by proper choice of the powder additive.
- With the powder filler, the volume fraction of the glass phase can be reduced to a minimum for the seal, which reduces reactivity with fuel cell materials.

### Accomplishments

- As part of a collaboration, we measured viscosities up to 1,000°C of sealing glasses made by Prof. Brow (Missouri University of Science and Technology).
- Prof. Brow, in turn, measured weight losses in forming gas (30% steam) at 750°C for two of our glasses. The glasses showed small boron losses that were higher for glasses that contained more boron. (Previously, we measured weight losses of both pure and powder filled glasses in simulated steam at 750°C for 2,000 hours and found the extrapolated 40,000-hour weight losses to be less than 5% for both linear and parabolic weight loss mechanisms.)
- X-ray photoelectron spectroscopy (XPS) measurements on borate glass compositions after 2,000 hours at 750°C show that there is no significant B gradient at the glass surface.
- Microprobe analyses of cross sections of glasses sealed to MnCo spinel-coated stainless steel (supplied by Pacific Northwest National Laboratory, PNNL) show that the coating prevents diffusion of Cr from the metal into the glass. Additionally, there is only slight ( $<3 \mu\text{m}$ ) diffusion of Mn and Co into the glass and no evidence of any new reaction product phases.
- Sealing results indicated that the MnCo coatings on the 441 stainless steel (441SS) interconnect material are weaker than either the coating-metal or the coating-glass interface. Thinner coatings are less likely to fracture, indicating there is a specific coating thickness where strength and effectiveness as a Cr barrier are optimum.
- Ag-glass composites sealed to 441SS were tested under pressure at 750°C and show good high-temperature seal strengths.

### Future Directions

- We plan to continue long-term tests of stability of seals and seal materials under realistic environmental conditions to determine potential degradation mechanisms and to demonstrate 40,000-hour performance.
- Working with PNNL staff, we will conduct functional tests of button cells sealed with these composite sealing glasses.

## Introduction

Seals for SOFC stacks face the most challenging set of performance requirements in the entire field of ceramic joining. The industry teams in the Solid State Energy Conversion Alliance program have consistently identified seal development as one of their highest priorities.

## Approach

As described in previous annual reports, we are using Department of Energy support to develop techniques for sealing SOFCs that can be tailored to the requirements of a range of different cell designs and operating conditions. The approach is based on our many years of seal development for other applications, as applied here to the special requirements for SOFC seals. It is evident that relief of thermal expansion mismatch stresses is a significant engineering requirement for any SOFC seal. Prior work has demonstrated that high-viscosity glasses can relieve thermal stresses through viscous creep. However, accommodating mismatch stresses, as well as meeting other SOFC design and operational constraints that frequently are in conflict, severely restrict the options for seal materials. Based on our prior experience in ceramic joining and on results obtained on this project, we believe ceramic-filled glasses and metal-filled glass composites provide greater design flexibility than all other options. To further validate this design concept, we previously demonstrated control of properties such as glass transition temperature and CTE by varying the compositions, amounts, and microstructures of the phases in the seal material. Use of thermochemical and composite microstructural models has allowed us to target specific seal properties for a given design. Our seals have given results in high temperature strength and 2,000-hour lifetime tests that extrapolate very favorably to 40,000 hours of operation.

## Results

Over the past year we have focused on three areas:

1. Collaboration with Professor Richard Brow of the Missouri University of Science and Technology, in which we have measured viscosities of his sealing glasses as a function of temperature, while he measured weight loss from our sealing glasses at temperature;
2. Determining the nature and extent of any reaction between our sealing glasses and the MnCo spinel-coated stainless steel interconnect material obtained from PNNL; and

3. Measurements of strengths of our seals at operating temperature.

**Glass viscosities:** We measured viscosities of R. Brow's sealing glasses as a function of temperature using the parallel plate method in our TOMMI apparatus (Thermooptical Mechanical Measuring Instrument, Fraunhofer Gesellschaft, Wurtsburg, Germany).

**Stability of boron-containing glasses in long-term tests:** Last year we conducted a number of tests of seal stability for extended times at 750-900°C. We investigated pure seal materials and seal materials in combination with different substrates, both in air and in a 30% simulated steam atmosphere made by bubbling Ar-3% $H_2$  through a 62°C water bath. Samples were heated under flowing wet hydrogen or air with periodic weighing for up to 2,000 hours. The measured weight changes as a function of time at temperature were compared to calculated upper and lower bounds for weight loss under both linear and parabolic loss mechanisms, with a conservative assumption of 5% loss at 40,000 hours. Comparison of the 2,000-hour weight losses with the predictions of the two models showed the experimental data tracked the lower parabolic limit pretty well, which strongly suggested that loss of boron or other glass constituents will not be an issue for borate glass seals in typical SOFC operating environments.

To further investigate the stability of our sealing glasses under SOFC operating conditions, we initiated a collaboration with Professor R. Brow of the Missouri University of Science and Technology in which his group measured weight loss of two of our glasses (glasses 14a and 17) at 750°C and collected the species that vaporized for subsequent compositional analysis. The weight loss data presented in Figure 1 are normalized to sample area and were collected only out to 150 hours. However, as shown in our previous experiments, the rates of weight loss in these glasses are approximately parabolic, so the largest losses occur on initial heating. According to Figure 1, the average evaporation rate for glass 14a, which has the highest boron content, was  $1.2 \times 10^{-6}$  g/cm<sup>2</sup>hr. Extrapolating that weight loss to 40,000 hours gives a total weight loss of 0.048 g/cm<sup>2</sup> of glass surface exposed to the wet steam atmosphere. The corresponding loss for glass 17 is 0.029 g/cm<sup>2</sup>. The weight loss experienced by a given seal obviously depends on how it is configured, since evaporation would occur only from the exposed edges. However, as an example, free evaporation from a 1 cm<sup>3</sup> sphere would give mass losses of about 8 and 4%, respectively, for glasses 14a and 17. These values are close to the losses predicted by extrapolation of our previous weight loss data. The collected evaporated species have not yet been analyzed by the Brow group. However, the data reported in Figure 1 are consistent with our earlier results and confirm our conclusions that seals based

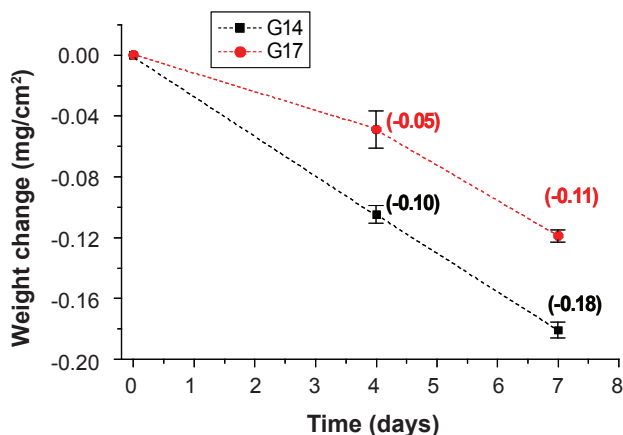


**FIGURE 1.** The Weight Change of Glass 14a and Glass 17 in Forming Gas with 30 vol% Water Vapor at 750°C

on our borate and borosilicate glasses will exhibit acceptable stability in SOFC operating environments.

Questions about preferential boron loss and possible surface concentration gradients in sealing glasses prompted us to analyze them using XPS with depth profiling. Figure 2 shows XPS spectra of the near surface of glass 14a after 2,000 hours at 750°C. As can be seen, the concentrations of all the glass constituents, including boron, do not vary with depth. Thus, boron neither concentrates nor is it preferentially lost from the glass surface at typical SOFC operating temperatures.

**Seal strengths:** As discussed in previous reports, it is difficult to measure the absolute strengths of joints in brittle materials such as ceramics. Accurate determination of the strength of a given joint geometry requires testing large numbers of specimens in a standard configuration, such as four point flexure, coupled with computational modeling. The technique can give reliable results, but it is labor intensive and it is not very efficient method for screening a lot of different process variables.

Another approach to determining seal strengths uses proof tests either of samples of the actual device or simplified versions that embody the essential features. The resulting data are not absolute materials properties, but they provide relative levels of performance. As described in last year's annual report, we designed an apparatus in which an annular seal creates a volume that can be increasingly pressurized with Ar until the seal leaks. The first-generation tests were limited to room temperature, and for them we assumed that leaks at 750°C would still be evident in specimens tested after cooling to room temperature. This year we modified the apparatus to test seals at SOFC operating temperatures. The sealed volume is placed in a furnace, heated to the test temperature, and then it is pressurized with Ar until seal leakage occurs. The apparatus permits pressure

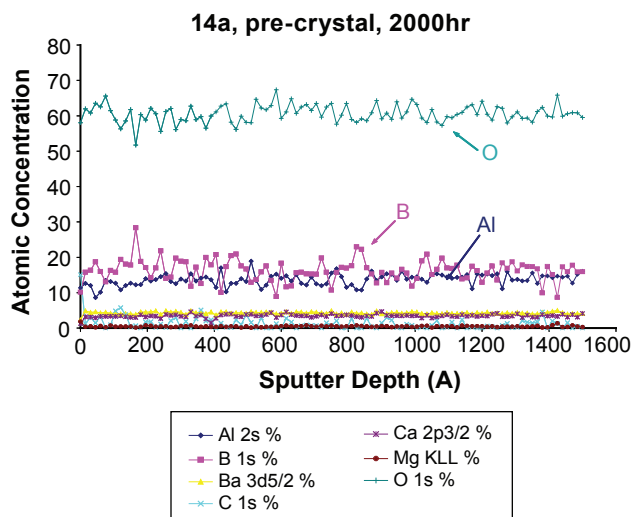


**FIGURE 2.** XPS Sputter Depth Profiles Show Borate Glass, Pre-Crystallized 14a, Have Compositional Stability at Temperature 750°C in Air for 2,000 Hours

differentials up to 2 atm., which is an extreme overtest of pressures expected on actual SOFC seals. The temperature can be cycled to simulate the effects of start-up and cool-down, and leaking seals can be resealed *in situ* and then retested without removing the fixture from the furnace. A photograph of a seal in the sample fixture is shown in Figure 3. Data from the first round of tests at 750°C are presented in Table 1.

**Compatibility of sealing glasses with spinel-coated interconnect materials:** The 400 series ferritic stainless steels are the materials of choice for SOFC interconnects because they are relatively inexpensive and have favorable mechanical and thermal properties. As with all joining, the sealing materials must not react adversely with the materials being joined. Last year we reported results of long-term tests of compatibility of uncoated 410 stainless steel with our 14a and 17 sealing glasses at 750°C, which showed the general absence of any unfavorable reactions. This year we have expanded our investigation to include the 441SS interconnect material coated with a MnCo spinel (10-20  $\mu\text{m}$  of  $\text{Mn}_{1.5}\text{Co}_{1.5}\text{O}_4$ ) that has been developed at PNNL. The spinel coating was designed, in part, to provide a barrier to Cr migration from the 441SS that might degrade seal performance. We have been evaluating the effects of those protective coatings on reactions between our two borate-based sealing glass compositions and the 441SS. We made seals between either glass 14a or glass 17 and the coated 441SS, heated them for up to 500 hours at 750°C, and then analyzed cross sections of the resulting interfaces using electron probe microanalysis to measure the elemental diffusion profiles for constituents of the glass, coating, and 441SS with a particular focus on Cr diffusion.



**FIGURE 3.** Test Apparatus Used for Measuring Burst Strength of Glass Seals at Elevated Temperature; the Bottom Insert Shows the Seal Bond Area after Rupture

**TABLE 1.** Glass Seal Strength at Temperature, 750°C

No. of Samples	Average Failure Pressure	Average Failure Strength
2	52.4 ± 2.9 kPa, 7.6 ± .85 psi	.012 N/mm <sup>2</sup> @ 1.8 psi
3*	97.2 ± 10.6 kPa 14.1 ± 1.5 psi	.020 N/mm <sup>2</sup> @ 2.9 psi
3*	Held 3 psi for 30 min at 750°C	

\* Etched 410SS

Microprobe line scans taken across the interfaces between the coated 441SS and either of the two sealing glasses show that the MnCo spinel is an effective barrier to Cr diffusion and that it does not react adversely with the sealing glasses. Figure 4 is representative of the 500-hour/750°C tests of both glass 14a and glass 17 on spinel coated 441SS. The results that are common to all the reaction experiments are:

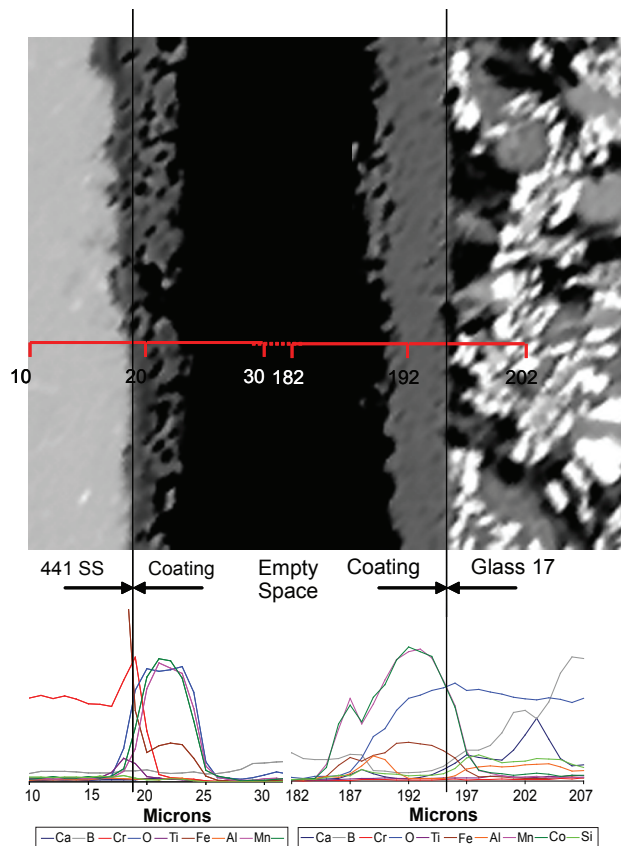


**FIGURE 4.** Line Scans of Ca, B, Cr, O, Ti, Fe, Al, Mn and Co and Scanning Electron Microscopy Image of Glass 17 on Mn<sub>1.5</sub>Co<sub>1.5</sub>O<sub>4</sub>-Coated 441SS Heat Treated to 750°C after 500 Hours

1. The coating with the nominal composition Mn<sub>1.5</sub>Co<sub>1.5</sub>O<sub>4</sub> as deposited on the 441SS, both as-received and after sealing, contains a moderate amount of Fe, probably as a substituent in the spinel structure because no separate Fe phases were seen in X-ray diffraction analysis.
2. There is no microstructural evidence in the scanning electron microscopy images for formation of any new interfacial reaction phases.
3. There is very slight diffusion of Mn, Co, and Fe from the coating into either the 14a or the 17 sealing glass, at most to a depth of 2-3 μm.
4. The glass constituents do not diffuse into the MnCoO coating to any significant extent.
5. There is a small buildup of Ti at the 441SS-coating interface, but none diffuses through the coating into the sealing glass.
6. The sealing glasses tightly bond to the spinel coating, but the thicker coatings fracture on cooling from the sealing temperature. This indicates that the coating itself is the weakest mechanical link in the 441SS-coating-sealing glass trilayer.

## Summary of Specific Accomplishments

1. We initiated viscosity measurements of some of Prof. Richard Brow's sealing glasses and provided him with some preliminary data.
2. Electron microprobe measurements of sealing glasses heated in contact with MnCo spinel-coated 441SS for up to 500 hours at 750°C showed the sealing glasses are compatible with the coatings and that there is very little interdiffusion of the glass, coating and the 441SS constituents.
3. We modified an apparatus to measure strengths of seals at 750°C. The strongest 441SS to 441SS seal using a composite glass 14a held 1 atm. overpressure at 750°C.
4. Weight loss measurements by Professor Brow's group of glasses 14a and 17 in simulated steam at 750°C for 150 hours were consistent with our earlier measurements that indicated the sealing glasses will be stable for 40,000-hour SOFC operation.

## Conclusions and Future Directions

All our results consistently show that our borate and borosilicate sealing glasses are stable in air and simulated steam for long times at 750°C. Heating experiments in air at 750°C for 2,000 hours gave weight losses of 0.2%. Weight losses measured in simulated steam in Professor Brow's group were 1.2 and 0.7  $\mu\text{g}/\text{cm}^2 \text{ hr}$  for glasses 14a and 17, respectively, which data are consistent with our earlier measurements. Analysis of glass surfaces after heating at 750°C for 2,000 hours using XPS showed there was neither depletion nor buildup of constituents in the near surface. Reaction couple experiments at 750°C showed that glasses 14a and 17 bond tightly to the MnCo spinel coated 441SS and that there were no adverse reactions between any of the members. Some couples with thicker coatings fractured through the coating, indicating the coating itself is mechanically the weakest link. Thinner coatings may be less likely to break on cooling, but if they are too thin they may not be a sufficient barrier to Cr diffusion. Thus, there is likely an engineering optimum for coating thickness.

## FY 2008 Publications/Presentations

### Publications

1. E. Corral, S.J. Widgeon, and R.E. Loehman, "Electron Microprobe Analysis of Glass-to-Metal Seals For Use in Solid-Oxide Fuel Cells," Microscopy Techniques for Ceramics and Composites, Proceedings of the Microscopy & Microanalysis Meeting 2008, Albuquerque, New Mexico, August 3-7, 2008.
2. M. Brochu and R.E. Loehman, "Hermetic Sealing of Solid Oxide Fuel Cells," in *Microjoining and Nanojoining*, Y. Zhou, ed., Woodhead Publishing, Ltd., Cambridge, England (2008) pp. 718-740.

### Presentations

1. E. Corral, and R. Loehman, "*Viscosity Properties of Glass Composites Engineered As Sealing Materials For Solid Oxide Fuel Cells*," Ceramics & Glasses Session, The Seventeenth Annual Rio Grande Symposium on Advanced Materials, The University of New Mexico, Albuquerque, NM, October 9, 2007.
2. E. Corral and R. Loehman, "*Glass Composites as Reliable Seals for Solid Oxide Fuel Cells*," Fuel Cells: Materials, Processing, Manufacturing, and Power Management Technologies: Sealing, Contact, Stack Manufacturing, and Balance of Plants of SOFC, Materials Science & Technology 2007 Conference and Exposition, Detroit, MI, September 16-20, 2007.

---

## IV.D.3 Innovative Seals for Solid Oxide Fuel Cells (SOFCs)

Professor Raj N. Singh  
University of Cincinnati  
Department of Chemical and Materials Engineering  
Cincinnati, OH 45221-0012  
Phone: (513) 556-5172; Fax: (513) 556-3773  
E-mail: Raj.Singh@uc.edu

DOE Project Manager: Ayyakkannu Manivannan  
Phone: (304) 285-2078  
E-mail: Ayyakkannu.Manivannan@netl.doe.gov

Contract Number: 42227

Start Date: July 1, 2006  
Project End Date: June 30, 2008

### Objectives

- Further develop the self-healing glasses with long-term durability through compositional modifications.
- Develop toughened glasses by fiber and filler reinforcements for enhancing toughness.
- Characterize long-term stability of the self-healing and toughened glasses through ex-situ testing.
- Measure electrical and creep behaviors of glass for use as seals in SOFCs.

### Accomplishments

- Self-healing glasses were developed for making seals for SOFCs. The seals were tested for leakage at 800°C and demonstrated self-healing ability for tests performed for 3,000 hours and 300 thermal cycles in a variety of test environments typical of an SOFC.
- Self-healing glasses have shown stability against crystallization in seal tests for 3,000 hours and in thermal annealing tests in moist fuel and air at 800°C for 1,500 hours.
- Direct current (DC) electrical resistivity of the self-healing glass between 25-800°C is measured with a value of  $0.6 \times 10^6$  Ohm-cm at 800°C.
- Creep tests were performed on a self-healing glass to determine glass flow behavior and the data were used to calculate glass viscosity useful in modeling response of the sealing glass in an SOFC stack.
- These results provide great promise towards meeting Solid State Energy Conversion Alliance (SECA) goals of seals for SOFCs.

---

### Introduction

A functioning SOFC requires seals that prevent electrode leakage and internal gas manifold leakage if internal gas manifolds are utilized. The seals must prevent the mixing of fuel and oxidant streams as well as prevent reactant to escape to the surrounding environment. The seal material must be electrically isolating and be mechanically and chemically stable in contact with interfacing cell components in humid dual reducing and oxidizing conditions. Of particular importance is the ability to seal between metallic and ceramic components with differing coefficients of thermal expansion (CTE), and do so while exposed to temperature transients over a range from room temperature up to SOFC operating temperature ( $\approx 800^\circ\text{C}$ ). This project is developing innovative sealing concepts for both short- and long-term functionality of SOFCs, addressing the aforementioned issues.

### Approach

A novel concept of *in situ* crack healing by glasses was pursued in Phase I of the project and is continued in the Phase II of our project. The fundamental idea underlying this concept is based on the fact that a glass with suitable low viscosity can heal cracks created by thermal expansion mismatch between materials that are being joined by a glass seal in an SOFC. The functionality of this innovative sealing approach based on *in situ* crack healing by a glass was demonstrated and quantified. Toughening and strengthening of the glass by fibers/particulates was pursued to minimize or eliminate bulk cracking of the seals. These concepts are pursued further in Phase II to address sealing capabilities and durability issues related to a functioning seal for an SOFC. In particular, exposure of the self-healing glasses over an extended time period is being pursued to determine long-term stability of the self-healing and reinforced glasses when exposed to environments simulating fuel and air at 800°C. In addition, compatibility of the glass in contact with 441 SS is being studied for use as interconnect material. These results are expected to provide inputs towards meeting SECA goals of 40,000 hours of seal life for an SOFC.

### Results

The object of work performed for this report is to select glasses that show self-healing behavior and long-term stability in SOFC environments. Some of the glasses used were modified by changes to their

composition to achieve long time stability in SOFC conditions. These glasses were then used for measuring electrical resistance in contact with metals at the cell operating temperature under an applied DC voltage of 1 volt. In addition, creep behavior of the self-healing glass was measured over a range of temperatures for determining the glass viscosity for use in modeling deformation of the glass when used as a sealing material of an SOFC.

The electrical resistivity of the self-healing glass under a DC-applied electric field was measured between 25-800°C between platinum electrodes in air. These measurements were done at an applied voltage of 1 volt, which is typical of a cell voltage of an SOFC. Figure 1 shows measured resistivity between 25-800°C. The data show very high resistivity values in the range of  $10^9$  ohm-cm between 25-600°C and then it decreases at higher temperatures and attains a value of  $10^6$  ohm-cm at 800°C. This value at 800°C is quite high indicating insulating characteristics for the glass. This is reasonable because the glass is ionically bonded and conduction is via movement of ions. In the presence of a DC field there is an initial high current, which subsides to a steady low value because of the ionic polarization. This leads to an insulating behavior for the glass exposed to DC field as observed from data in Figure 1.

Creep behavior of the sealing glass is important for assessing flow behavior of the self-healing sealing glass subjected to stack loads. The creep behavior of the glass samples were measured near the glass softening temperatures in a flexure mode at an applied load of 10 N. Figure 2 shows the creep data over a range of temperatures. These data were used to calculate viscosity of the glass over a range of temperatures. The results can be fitted to the following equation:

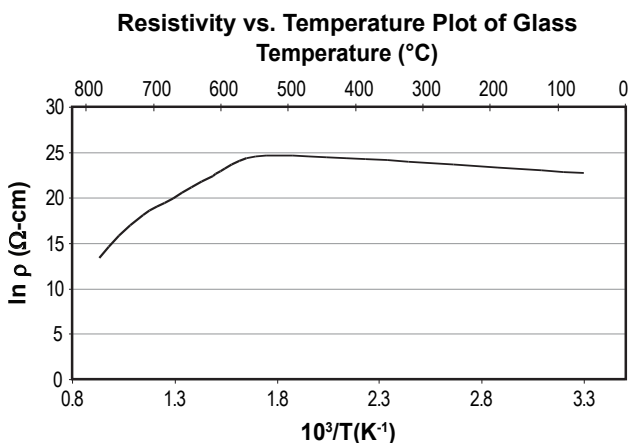


**FIGURE 1.** DC Resistivity of the Self-Healing Glass Sample Measured Between 25-800°C Indicating High Resistivity to 800°C

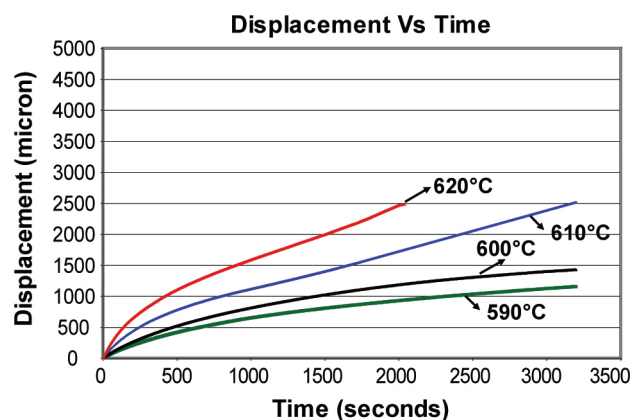


**FIGURE 2.** Creep (displacement-time) plots of a self-healing glass sample tested at high temperatures at a load of 10 N in flexure mode. The data on creep rates are useful for assessing deformation of the glass under load in seals as well as in modeling of the seal behavior in a stack.

$$y = 15.358x - 5.4587$$

where  $y = \log(\text{viscosity in Pa.s})$  and  $x = 10^3/T$  (temperature in K). The values of viscosity determined over a range of temperatures also gave an activation energy value of 125 kJ/mole. These results were provided to Pacific Northwest National Laboratory (PNNL) and used in a collaborative study on modeling of the thermomechanical response of seals in a cell stack. These results on modeling for our self-healing glass as well as those for G18-glass from PNNL were communicated.

These results on the electrical properties and creep behaviors of the self-healing glass are quite promising for developing seals to meet the SECA goals for SOFCs.

## Conclusions and Future Directions

- Seals incorporating self-healing glasses were fabricated. Effect of up to ~300 thermal cycles between 25 and 800°C and ~3,000 hours at 800°C on hermeticity of the seals was demonstrated. Self-healing behaviors of the leaking seals were also demonstrated. These results are important for achieving SECA goals of the SOFC sealing system.
- Electrical resistivity of the glass in contact with metals showed high resistivity and insulating behaviors, which are useful as sealing materials for SOFCs.
- Creep behavior of glass samples were measured for calculating viscosity of the glass. These data were then used in modeling studies to predict response of the glass as seals for an SOFC.
- Plans are to further pursue long-term stability of the self-healing glasses, reinforced glasses, stability of glasses in contact with coated 441 SS, electrical

resistivity in contact with coated 441 SS, and seals made thereof to further demonstrate long-term performance, stability, and applicability of the self-healing glass seals to SOFCs.

### **FY 2008 Publications/Presentations**

1. Program quarterly reports between July 2007 – June 2008.
2. Phase-II Annual Report (July 2007).
3. R. N. Singh, “Seals for Solid Oxide Fuel Cells (SOFC),” Invited Presentation, 32<sup>nd</sup> Int. Conf. & Expo. On Advanced Ceramics and Composites, January 27 – February 1, 2008, Florida (2008).
4. R.N. Singh, “Sealing Technology for Solid Oxide Fuel Cells (SOFC),” Int. J. Ceram. Technol. 4[2], 134-144 (2007).
5. N. Govindaraju, W.N. Liu, X. Sun, P. Singh, and R.N. Singh, “Parametric Modeling Study on the Behavior of Glass Ceramic and Self Healing Glass Seals for a Planar SOFC: Part I,” Topical Report, December (2007).

## IV.D.4 Thermochemically Stable Sealing Materials for Solid Oxide Fuel Cells

Richard K. Brow (Primary Contact),  
Signo T. Reis, Teng Zhang  
Missouri University of Science & Technology (Missouri  
S&T) (formerly the University of Missouri-Rolla)  
Department of Materials Science & Engineering  
222 McNutt Hall  
Rolla, MO 65409-0330  
Phone: (573) 341-6812; Fax: (573) 341-2071  
E-mail: brow@mst.edu

DOE Project Manager: Ayyakkannu Manivannan  
Phone: (304) 285-2078  
E-mail: Ayyakkannu.Manivannan@netl.doe.gov

Contract Number: 42221

Start Date: September 29, 2004  
Project End Date: March 31, 2008

### Objectives

- Develop 'invert' glasses with requisite properties and chemical stability for hermetic seals for solid oxide fuel cells (SOFCs).
- Develop processing techniques to fabricate hermetic seals for SOFC components, including understanding the crystallization behavior of sealing glass.
- Demonstrate hermeticity and materials compatibility, including volatility studies under SOFC operational conditions.

### Accomplishments

- Developed alkaline earth/zinc silicate glasses that form glass-ceramics with requisite thermal properties, including sealing temperatures at or below 900°C and coefficients of thermal expansion (CTE) in the range of  $10\text{-}12 \times 10^{-6}/^\circ\text{C}$ . Test seals made with candidate glasses remain hermetic to helium after up to 60 thermal cycles between 800°C and room temperature.
- Modeled borate volatilization using thermochemical calculations of volatilization reactions and determined activation energies for borate loss for two glass compositions.
- Characterized the formation of deleterious interfacial chromate phases that result when candidate glasses react with the chromium oxide scale that forms on stainless steel interconnect alloy surfaces.

### Introduction

SOFCs are multi-layered structures formed primarily from high-purity metal oxide components, including an ionic conducting electrolyte, which generate electricity from the electrochemical oxidation of a fuel source. Seals are required in an SOFC stack to prevent mixing of fuel/oxidant within stack, to prevent leaking of fuel/oxidant from stack, to electrically isolate cells in stack and also to provide mechanical bonding of components. The requirements for a sealing material include a thermal expansion match to the fuel cell components, adequate electrical resistance and thermochemical stability under the operational conditions of the stack. The seal also should be chemically compatible with other cell components, should be stable under both the high temperature oxidizing and reducing operational conditions, should be created at a temperature that is compatible with other cell components (under 900°C for some materials), and should not migrate or flow from the designated sealing region during sealing or cell operation. In addition, the sealing system should be able to withstand thermal cycling between the operational temperature and room temperature. That is, thermal stresses that develop because of mismatches in the thermal contraction characteristics of the different SOFC materials must either be reduced to well below the failure strengths of the materials or must be relieved in some fashion.

There have been many attempts to develop seals for planar SOFCs using a wide variety of glass and glass-ceramic compositions; see the reviews by Fergus [1] and Lessing [2] for many compositional examples. There are many engineering concerns with these materials, including thermal expansion mismatches, excessive sealing temperatures, and long-term interfacial reactivity with other fuel cell materials. Thus, the seal has become a critical need for meeting the long-term operational milestones of the DOE fuel cell programs [3]. The materials developed in the present project have unusual structural characteristics that contribute to a desirable set of thermal and chemical properties required for SOFC seals.

### Approach

The glasses developed at Missouri S&T have relatively low silica contents (<45 mole%) and so possess molecular-level structures that are much less connected than conventional silicate glasses. These depolymerized structures contribute to desirably low viscosities at the sealing temperatures (900°C), and

lead to the formation of crystalline phases that possess relatively high CTEs and good thermal stabilities when the seals are crystallized to form glass-ceramics.

### Results

Over eighty glass compositions have been prepared at Missouri S&T. In general, critical thermal properties, including thermal expansion coefficient, crystallization temperature, and sealing temperature, can be tailored by varying the glass composition, including the borate concentration and the type of modifying cation added. Figure 1 illustrates the latter effect. Glasses and glass-ceramics with low field strength (defined as ion charge divided by ion radius squared) modifying cations (e.g., Ba<sup>2+</sup> and Sr<sup>2+</sup>) have greater thermal expansion coefficients than materials modified by higher field strength cations (Ca<sup>2+</sup> and Zn<sup>2+</sup>). By controlling compositions, glasses with a range of desirable thermal expansion coefficients can be developed. Seals made with tapes of promising glasses between Y-stabilized zirconia (YSZ) and 430 stainless steel substrates are hermetic to helium gas after up to 60 thermal cycles between 800°C (held for 24 hours) and room temperature (Table 1). In general, when these seals failed, it was because of the failure of the YSZ, not the seal itself. (It was unclear if thermal stresses contributed to the ceramic failure, or if failure occurred because of processing defects in the ceramic.)

Borate species are the most volatile species of the common constituents of SOFC sealing glasses. As reported last year, thermo-chemical calculations indicate that BO<sub>2</sub> (g) and B<sub>3</sub>H<sub>3</sub>O<sub>6</sub> (g) have the highest vapor pressures at 800°C under conditions that simulate

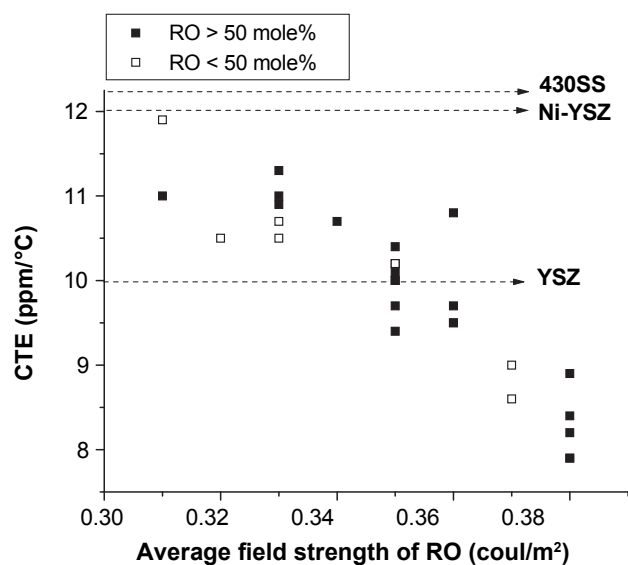


FIGURE 1. CTE Values for ‘Invert’ Silicate Glasses as a Function of the Average Field Strength of the RO-Component (R= Ca, Sr, Ba and Zn)

TABLE 1. Summary of Thermal Cycling Hermeticity Tests of Glass Seals\*

Sealing materials	Test conditions	Notes
430SS/G50 (10-12μm)/YSZ	air	Failed after 10 cycles; YSZ fracture
430SS/G50 (45-53μm)/YSZ	air	Failed after 40 cycles; YSZ fracture
430SS/G50 (10-12μm)/YSZ	forming gas	Failed after 10 cycles; YSZ fracture
430SS/G50 (45-53μm)/YSZ	forming gas	Failed after 20 cycles; YSZ fracture
430SS/G81 (45μm)/YSZ	air	60 cycles without failure
430SS/G81 (25μm)/YSZ	forming gas	Failed after 30 cycles; YSZ fracture

\*Samples were held for 24 hours at 800°C under forming gas or air, and tested for hermeticity using helium gas.

the cathode (air) and anode (fuel) sides of a fuel cell, respectively. Figure 2 shows the weight losses in air at different temperatures from a glass with 20 mole% B<sub>2</sub>O<sub>3</sub>, designated glass #59. The inset to Figure 2 shows that the weight losses are dependent on the square root of time, implying a diffusion-controlled process. The activation energy for that process, for the glass shown in Figure 2, is 371±86 kJ/mole [4]. Analyses of the gas stream that flowed over the glass surfaces are consistent with the borate-volatility model, as are surface analyses (by Auger electron spectroscopy) which show B-depleted surface layers.

The development of deleterious interfacial chromate phases was also evaluated. Figure 3 shows optical images of SOFC glass coated-430 stainless steel substrates ‘as sealed’ then after one or two weeks

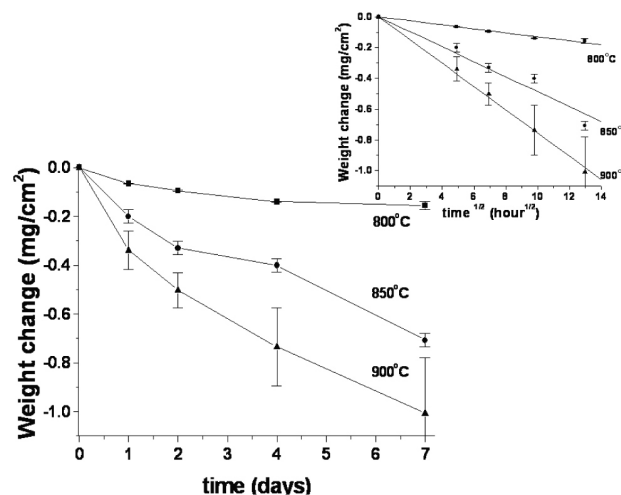
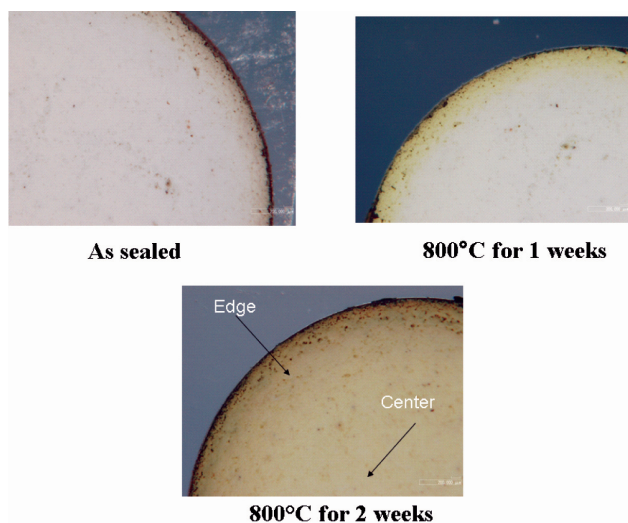
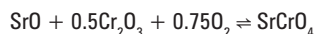


FIGURE 2. Weight Change of Glass #59 in Dry Air at Different Temperatures



**FIGURE 3.** Optical Images of Glass #36 Coatings on 430 Stainless Steel Substrates after Heating in Air at 800°C for Different Times

in air at 800°C. The yellowish reaction product is an indication of the formation of  $\text{SrCrO}_4$ , confirmed by X-ray diffraction, likely by the reaction:



These chromates have large thermal expansion coefficients and if they form at the glass-interconnect interface, can affect the mechanical integrity of the seal [5]. The kinetics of reactions like that shown here were evaluated using powder reaction couples between  $\text{Cr}_2\text{O}_3$  and various glasses. The addition of ZnO to the 'invert' glass compositions appears to impede the formation of  $\text{SrCrO}_4$  and  $\text{BaCrO}_4$ .

## Conclusions

- Hermetic seals have been fabricated and have remained hermetic after up to 60 thermal cycles from operational temperatures.
- The effect of  $\text{B}_2\text{O}_3$  on the volatility of promising 'invert' sealing glass compositions has been demonstrated.
- The reactions between SOFC glasses and chromium oxide scales on interconnect alloys have been modeled, and the effect of glass composition on reaction kinetics has been noted.

## Special Recognitions & Awards/Patents Issued

1. R.K. Brow, S. T. Reis, G. M. Benson, "Glass and glass-ceramic sealant compositions," US Patent 7,399,720, issued July 15, 2008.
2. T. Zhang, "Glass-ceramics for solid oxide fuel cell seals," PhD Thesis in Ceramic Engineering, Missouri University of Science & Technology, May 2008.

## FY 2008 Publications/Presentations

1. T. Zhang, W.G. Fahrenholtz, S.T. Reis, and R.K. Brow, "Borate volatility from SOFC sealing glasses," *J. Amer. Ceram. Soc.*, submitted February 2008; accepted March 2008.
2. T. Zhang, R.K. Brow, S.T. Reis and C.S. Ray, "Isothermal crystallization of a solid oxide fuel cell sealing glass by differential thermal analysis," *J. Amer. Ceram. Soc.*, submitted February 2008.
3. S. T. Reis, M. J. Pascual, R. K. Brow, C.S. Ray, and T. Zhang, "Crystallization Processes and Processing of SOFC Sealing Glasses," 32<sup>nd</sup> International Conference and Exposition on Advanced Ceramics & Composites, 5<sup>th</sup> International Symposium on Solid Oxide Fuel Cells: Materials, Science and Technology, Daytona Beach, FL, January 27 – February 1, 2008.

## References

1. J.W. Fergus, *J. Power Sources*, **147** 46-57 (2005).
2. P. A. Lessing, *J. Mater. Sci.*, **42**, 3465 –3476 (2007).
3. M.C. Williams, J.P. Strakey, and W.A. Surdoyal, *Int. J. Appl. Ceram. Technol.*, **2**[4] 295-300 (2005).
4. T. Zhang, W.G. Fahrenholtz, S.T. Reis, and R.K. Brow, "Borate volatility from SOFC sealing glasses," *J. Amer. Ceram. Soc.*, submitted Feb. 2008; accepted March 2008.
5. Z. Yang, K. D. Meinhardt and J. W. Stevenson, *J. Electrochem. Soc.*, **150** [8] A1095-1101 (2003).



---

## IV. SECA CORE RESEARCH & DEVELOPMENT

### E. Contact Materials



## IV.E.1 SECA Coal-Based Systems Core Research: Contact Paste Development

Larry R. Pederson (Primary Contact),  
Yeong-Shyung Chou, Gregory W. Coffey,  
Christopher A. Coyle, Benjamin P. McCarthy,  
Carolyn D. Nguyen, Edwin C. Thomsen,  
Guan-Guang Xia, and Xiao-Dong Zhou  
Pacific Northwest National Laboratory  
902 Battelle Blvd., P.O. Box 999  
Richland, WA 99352  
Phone: (509) 375-2731; Fax: (509) 375-2167  
E-mail: larry.pederson@pnl.gov

DOE Project Manager: Briggs White  
Phone: (304) 285-5437  
E-mail: Briggs.White@netl.doe.gov

### Subcontractors:

- Montana State University, Bozeman, MT
- University of Florida, Gainesville, FL

Contract Number: 44036

Start Date: October 1, 2002  
Project End Date: September 30, 2008

- A diffusion-based sintering model was developed that is consistent with observed trends in densification with regard to temperature and LSM composition.

### Introduction

Stable, low resistance electrical contacts between the electrodes and interconnect plates are needed for optimal stack performance. Contact resistance losses on the anode side are typically small, where nickel metal pastes and nickel mesh are typically utilized to provide a low-resistance metallurgical bond between the electrode and interconnect plate. It is more challenging to achieve low resistance contacts on the cathode side, where at least one ceramic-metal interface and possibly several ceramic-ceramic interfaces are present. The contact material should either be compliant or provide a good thermal expansion match to other fuel cell components, exhibit high electrical conductivity, provide good interfacial stability, and be of low cost, among other attributes. It is further preferred that the contact paste be processed at temperatures compatible with that at which glass seals are typically formed (850 to 1,050°C).

A variety of metallic and ceramic contact paste materials have been considered previously. Noble metals such as Pt, Ag, and Au provide low resistance contacts, though high cost and the tendency to electromigrate are disincentives to their use. LSM generally meets contact paste material requirements, with the exception of a higher than desired air sintering temperature (>1,200°C). Processing temperatures of LSM have been lowered through compositional modifications, though at the risk of increased interfacial instability. Unbonded LSM contact pastes may also be used, in combination with a mechanical load, but resistances tend to be variable. Sintered ceramic contacts appear to offer the most promise for low resistance and long-term stability.

### Objectives

- Develop lanthanum manganite-based contact paste compositions and forms aimed at providing a more reliable electrical connection between the cathode and interconnect plate, which can be processed at temperatures compatible with other stack components.
- Demonstrate the effectiveness of lanthanum manganite-based contact pastes and processing methods using the Solid State Energy Conversion Alliance (SECA) Core Technology Program's planar stack test fixture.

### Accomplishments

- Lanthanum strontium manganite (LSM) contact pastes were effectively sintered at low temperature by alternate exposure to air and nitrogen, without the use of any sintering aids. Accelerated shrinkage results from the creation of transient cation vacancy gradients due to alternating oxygen partial pressures.
- Bond strengths of ~3 MPa between spinel-coated interconnect plates were achieved at 900°C, which gave stable contact resistances of less than 10 milliohm-cm<sup>2</sup>.

### Approach

Alternating oxygen partial pressure exposure was explored as a means of accelerating the sintering of LSM contact pastes. This approach obviates the need for sintering aids that may otherwise impact long term stability, and would allow stack developers to take advantage of many favorable properties of LSM with regard to conductivity, thermal expansion, and compatibility with other fuel cell components. Inks composed of milled LSM powder and polyvinyl butyral binder were applied to (Co,Mn)<sub>3</sub>O<sub>4</sub>-coated ferritic steel

coupons, which were fired at 900°C in alternating air and nitrogen for ~2 hours. Fracture strengths were evaluated at room temperature in tension. Electrical properties of sandwich structures composed of coated ferritic steel bonded to a porous LSM-20 cathode were evaluated at 800°C for hundreds of hours. Dilatometry studies were additionally performed as a means of evaluating sintering kinetics in partially sintered LSM bars.

**Results**

**Accelerated Sintering Model:** Rates of intermediate-stage shrinkage of LSM compositions, where Sr=0.0, 0.05, 0.10, 0.15, and 0.20, were shown to be significantly accelerated by alternating and repeated exposure to air and to nitrogen (~10 ppm O<sub>2</sub>). This enhanced shrinkage decreased as the extent of Sr substitution for La increased, with unsubstituted lanthanum manganite yielding the highest shrinkage rates below 1,000°C, as shown in Figure 1 for 1 hour cycle times. Shrinkage curves did not follow Arrhenius behavior that is typical of LSM sintering in air. Rather, a maximum in the rate of sintering occurred at 900 to 1,000°C for compositions having the lowest levels of Sr substitution. Results are expressed as the reduced shrinkage  $Y=(V_o-V_t)/(V_o-V_f)$ , where  $V_o$ ,  $V_t$  and  $V_f$  are initial volume of the sample, the volume at time  $t$ , and final volume, respectively [1]. At temperatures >1,100°C, air/nitrogen cycling did not lead to accelerated rates of shrinkage.

A diffusion-based model was developed that is consistent with observed shrinkage rates as a function of temperature in alternating gas flows, and based on Fick’s first law. Rates of sintering  $J$  can be described as:

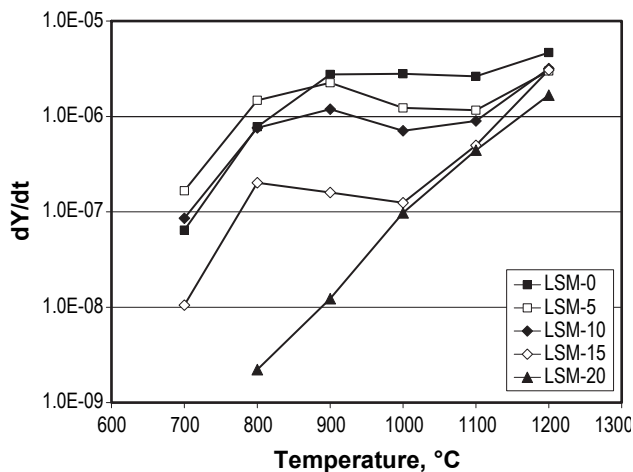


**FIGURE 1.** Shrinkage rates for LSM compositions versus temperature, resulting from repeated, alternating exposure to air (1 hour) and nitrogen (1 hour).

$$J = -D_v \frac{dC}{dr} \tag{1}$$

where  $D_v$  is the volume diffusion coefficient for cations and  $dC/dr$  is the cation vacancy gradient in a spherical particle of radius  $r$ . Lanthanum manganites are well known to contain excess oxygen, the amount of which varies with oxygen partial pressure and temperature. Because interstitial oxygen is not allowed in the perovskite lattice, this results in the formation of cation vacancies. The basic premise of the diffusion-based model is that transient cation vacancy gradients are created by the uptake and loss of more mobile oxygen as gas flows are alternated, which leads to faster rates of sintering following Equation 1.

Average cation vacancy gradients were calculated from established rates of oxygen diffusion in LSM as a function of time and temperature. The volume-weighted cation vacancy gradient in spherical particles is:

$$\frac{dC}{dr} = \frac{8(C_{i,ox} - C_{i,ox^0})}{\pi^2 a} \sum_{n=1}^{\infty} \frac{(-1)^n}{n^2} \left[ e^{-\frac{D_{ox} n^2 \pi^2 t}{a^2}} \right] \left[ n\pi \cos\left(\frac{n\pi}{2}\right) - 2 \sin\left(\frac{n\pi}{2}\right) \right] \sin\left(\frac{n\pi}{2}\right) \tag{2}$$

where  $C_{i,s}$ ,  $C_{i,ox^0}$ ,  $D_{ox}$ , and  $a$  are surface and initial bulk concentrations of oxygen, diffusion coefficient for oxygen, and particle size, respectively. The overall rate of sintering of LSM compositions is approximated as the sum of contributions: (1) that of sintering in air, and (2) additional sintering due to the creation of transient excess cation vacancy gradients from alternating air/nitrogen exposure, following:

$$\frac{dY}{dt} = \left(\frac{dY}{dt}\right)_{air} + \left(\frac{dY}{dt}\right)_{air/N_2} = (1 + A \frac{dC}{dr}) \left(\frac{dY}{dt}\right)_a \tag{3}$$

where A is a fitting constant representing a collection of geometric terms. A comparison of measured and calculated sintering rates are given for LSM-5 as a function of temperature in Figure 2. Good agreement

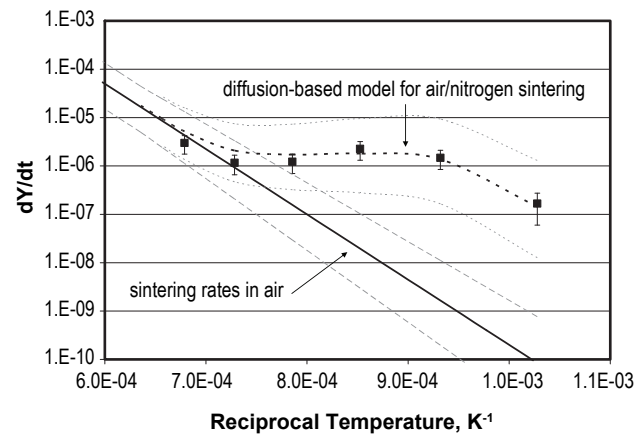


**FIGURE 2.** Comparison of intermediate-stage sintering of LSM-5 in alternating air/nitrogen to rates for air as a function of reciprocal temperature.

between experimental results and a diffusion-based model support the concept that the creation of transient cation vacancy gradients can be used to substantially accelerate sintering processes, which can be used to advantage in the processing of contact pastes for solid oxide fuel cells (SOFCs).

**Contact Paste Performance:** Lanthanum manganite contact pastes have been used to bond  $(\text{Co},\text{Mn})_3\text{O}_4$  spinel-coated ferritic steel coupons for evaluation of bond strength and to bond spinel-coated ferritic steel coupons to porous LSM-20 cathode materials for evaluation of electrical properties. A typical microstructure of the latter is shown in Figure 3, which reveals well-bonded interfaces with no obvious physical imperfections. Contact pastes were processed at  $900^\circ\text{C}$  in alternating air and nitrogen from 1 to 10 hours. Substantial interfacial bonds of at least 3 MPa were developed between ferritic steel coupons within approximately 2 hours in alternating air/nitrogen. Fracture occurred consistently within the bond paste itself, rather than at the bond paste/ferritic steel

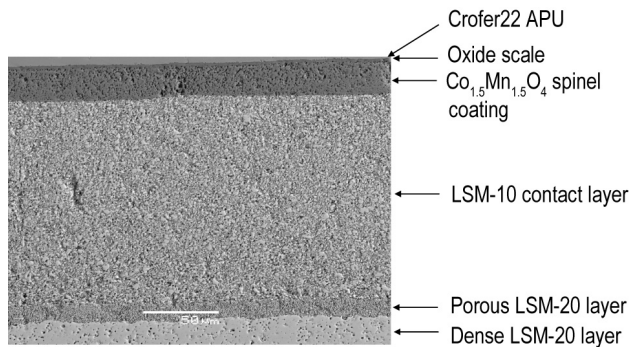


**FIGURE 3.** Polished cross-section of a  $\text{Co}_{1.5}\text{Mn}_{1.5}\text{O}_4$  spinel-coated Crofer 22 APU coupon bonded to porous LSM-20 by LSM-10 contact paste.

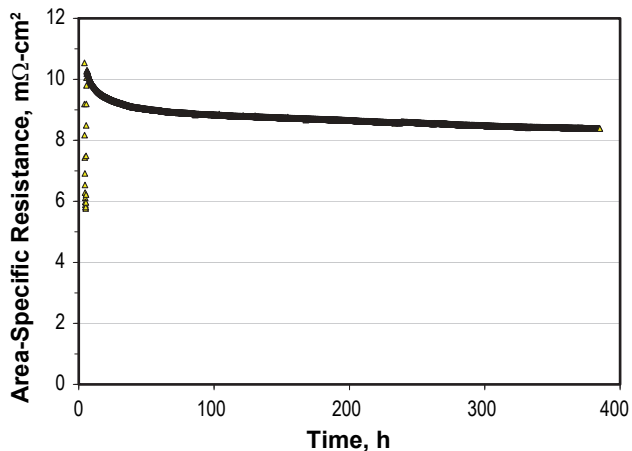


**FIGURE 4.** Electrical resistivity of spinel-coated Crofer 22 APU/LSM-10 contact paste/ $\text{Co}_{1.5}\text{Mn}_{1.5}\text{O}_4$  spinel-coated Crofer 22 APU sandwich specimen versus time, measured in air at  $800^\circ\text{C}$ .

interface. When contact pastes were processed in air for identical times, bond strengths developed between steel coupons were negligible.

Reasonably low ( $<10 \text{ m}\Omega \text{ cm}^2$ ) and stable resistivities were obtained for spinel-coated ferritic steel and LSM-20 coupons bonded with LSM contact paste, as shown for an LSM-10 contact paste in Figure 4. Resistivities were determined using test protocols established previously by Yang et al.[2], and are consistent with targets established for planar stacks.

## Conclusions and Future Directions

Alternating exposure to air and nitrogen has been shown to be an effective means of accelerating the sintering of LSM compositions. Enhancements in sintering rates decreased as the extent of Sr substitution for La increased and decreased with increased temperature, which coincides with diminished oxygen non-stoichiometry. A diffusion-based model was developed, based on the premise that transient cation vacancy gradients are created by exchange of more mobile oxygen.

This approach offers promise for the sintering of LSM-based, cathode-side contact pastes in SOFCs, where it is generally preferred that the pastes be processed at temperatures compatible with that of the glass seal ( $<1,000^\circ\text{C}$ ). Without modification of the LSM composition, sintering is negligible in air at such temperatures. An important advantage is that LSM with low Sr content can be sintered under conditions that would lead to minimal densification of LSM-20, a widely used cathode.

Demonstration of LSM contact paste processing in alternating air/nitrogen in a planar SOFC stack is planned, using a test fixture developed by the SECA Core Technology Program. The electrical performance of bonded structures will be evaluated as a function of time at constant temperature and with thermal cycles.

## Special Recognitions & Awards/Patents Issued

1. Patent Application: BP McCarthy, LR Pederson, ZD Zhou, WA Surdoval, LC Wilson. "Low-Temperature Sintering of Lanthanum Strontium Manganite-Based Contact Pastes for SOFCs," filed 2/2008.

## FY 2008 Publications/Presentations

1. BP. McCarthy, L.R. Pederson, H.U. Anderson, X.D. Zhou, P. Singh, G.W. Coffey and E.C. Thomsen, "Enhanced Shrinkage of Lanthanum Strontium Manganite ( $\text{La}_{0.90}\text{Sr}_{0.10}\text{MnO}_{3+\delta}$ ) Resulting from Thermal and Oxygen Partial Pressure Cycling," *Journal Of The American Ceramic Society*, 90 [10], 3255-3262 (2007).

2. B. P. McCarthy, L. R. Pederson, Y. S. Chou, X.-D. Zhou, W.A. Surdoval and L.C. Wilson, "Low-temperature sintering of lanthanum strontium manganite-based contact pastes for SOFC," *Journal of Power Sources*, 180, 294-300 (2008).

3. B.P. McCarthy, L.R. Pederson, BJ Koepfel, and RE Williford, "Low-Temperature Densification of Lanthanum Strontium Manganite ( $\text{La}_{1-x}\text{Sr}_x\text{MnO}_{3+\delta}$ ),  $x=0.0-0.20$ )," *Journal of the American Ceramic Society* (2008).

## References

1. Zhang XB, Liu XQ, Meng GY. *Journal of the American Ceramic Society* 2005;88:1826-1830.
2. Yang ZG, Xia GG, Singh P, Stevenson JW. *Power Sources* 2006;155:246-252.

## IV.E.2 Novel Composite Materials for SOFC Cathode-Interconnect Contact

J.H. Zhu (Primary Contact), L.T. Wilkinson,  
J.M. Shoulders, and D.A. Ballard

Department of Mechanical Engineering  
Tennessee Technological University  
115 W. 10<sup>th</sup> St., Box 5014  
Cookeville, TN 38505  
Phone: (931) 372-3186; Fax: (931) 372-6340  
E-mail: jzhu@tntech.edu

DOE Project Manager: Briggs White

Phone: (304) 285-5437  
E-mail: Briggs.White@netl.doe.gov

Contract Number: 42533

Start Date: August 1, 2005  
Project End Date: July 31, 2008

### Introduction

To reduce the electrode/interconnect interfacial resistance in SOFC stacks, electrical contact layers are often applied between the interconnect and electrodes during construction of an SOFC stack by compensating for the corrugations present on their respective surfaces. Some of the major criteria for SOFC contact materials are: (1) sufficiently high electrical conductivity over the SOFC lifetime; (2) chemical stability under high current condition and compatibility with other cell components, especially negligible effects on the formation of protective oxides on interconnect alloy; and (3) reasonable match in coefficient of thermal expansion (CTE) with other cell components. In addition, it is highly desirable for the contact materials to have some damage tolerance (possible self-healing if thermal cycle-induced cracking occurs in the contact layer) and to act as a Cr “sponge” by absorbing the Cr species migrating from the interconnect to the cathode and therefore reducing the Cr “poisoning” of the cathode. Because of the stringent criteria, finding a suitable material for the interconnect-cathode contact is very challenging.

The materials currently under consideration for cathode/interconnect contact application includes low melting-point ceramics (such as doped LaCoO<sub>3</sub>), noble metals (e.g. Ag or Pt), and their composites [1-2]. Pt, Au, and Pd are not desirable for this application because of their high raw material cost. However, Ag is an exception due to its relatively low price. Ag-ceramic composite is one of the very promising candidates for SOFC contacts due to the inherent properties of Ag, such as high chemical stability, high electrical conductivity, high ductility, and relatively low melting point. The perovskite component in the composite is expected to provide a more desirable CTE match and potentially act as a Cr absorbent and/or a barrier for Cr migration to the cathode. One major drawback of Ag as a SOFC interconnect/cathode contact material is its tendency to evaporate at SOFC operating temperatures, while for the perovskite material thermal cycle-induced cracking and damage accumulation might be an issue.

### Approach

A number of alloying additions have been selected to evaluate their effects on the Ag evaporation. The Ag-base alloys were prepared using both the arc-melting/drop-casting technique and the powder metallurgical route. These alloys were pressed into 1 mm sheets for Ag evaporation testing. Standardized evaporation conditions identified earlier were used in

### Objectives

- Elucidation of the mechanism of Ag evaporation at elevated temperatures.
- Assessment of the effect of various alloying additions on the evaporation rate of Ag.
- Evaluation of the effectiveness of the addition of the perovskite phase on the performance of Ag-based contact materials.
- Demonstration/assessment of the performance of the new contact materials in the solid oxide fuel cell (SOFC) operating conditions.

### Accomplishments

- The Ag evaporation rate of a number of Ag-base alloys with 1, 5, and 15 at% alloying additions as well as the Ag+La<sub>0.8</sub>Sr<sub>0.2</sub>MnO<sub>3</sub> (LSM) composites has been determined.
- Cross-sectional observation of the Ag-Mn and Ag-Zn alloys revealed the formation of a porous surface oxide layer, which was not adequate in blocking the Ag from evaporation.
- Similar to the Ag+(La,Sr)(Co,Fe)O<sub>3</sub> (LSCF) composite system, with the increase of Ag in the Ag-LSM composite contact layer, both the area specific resistance (ASR) and the thermal cycling-induced damage in the interconnect/contact/cathode test cells decreased.
- The abnormal growth of a thick scale of Fe oxide (about 60 μm) was observed on the Crofer 22 APU interconnect for the 100% LSM contact test cell during thermal cycling.

the evaporation test. Furthermore, the Ag evaporation rate of these alloys as a function of exposure duration was measured. Since LSM has been promoted as a potential contact material for SOFCs recently, LSM was selected for evaluation as the perovskite phase in the composite contact materials. The composite materials with different Ag-to-LSM ratios were synthesized and the effect of the LSM addition on the Ag evaporation rate was assessed.

The performance of the composite materials as an interconnect/cathode contact was further evaluated using a special testing rig which can host six cells for simultaneous testing. Six power supplies were used to supply a constant current density of 250 mA/cm<sup>2</sup> across each cell. All cells were connected via the four-point method with platinum leads. A compressive load was placed on the cells of approximately 0.16 to 0.20 kg/cm<sup>2</sup> by means of an internal rod and spring. The following contact layer compositions were tested: 0, 10, 25, 50, 75, and 100 vol% LSM with the balance being Ag. Cells were subjected to thermal cycling, which consisted of an initial 10-hour sintering at 850°C followed by cooling to 800°C and holding for another 10 hours. Next, the cells were allowed to furnace cool to 250°C before being heated to 800°C and held for ten hours. This step was repeated 50 times; the cells were then cooled down to room temperature, cross sectioned, mounted, polished, and finally evaluated with scanning electron microscopy/energy dispersive spectroscopy (SEM/EDS).

## Results

The Ag evaporation testing of a number of Ag-base alloys has been completed. While the noble metals such as Pt, Pd, and Au noticeably reduced the Ag evaporation rate, they are not suitable choices as alloying additions considering the cost of these elements. The work this year focused on the selection of low-cost alloying elements such as Ti, Fe, Co, Ni, Mn, Sn, Zn, etc. While a significant reduction in weight loss was found with the Mn and Zn additions into Ag during the initial 40-hour exposure, a constant Ag evaporation rate similar to that of pure Ag under identical conditions was observed for subsequent exposures. The initial reduction in weight loss resulted from the selective oxidation of the alloying element (which increased the alloy weight) during the initial Ag evaporation testing. Figure 1 shows the cross-sectional view near the surface of a Ag-15%Mn alloy coupon after thermal exposure for a total of 160 hours at 900°C. In addition to the formation of the discontinuous Mn-O surface layer, severe internal oxidation was observed. The dark particles, light grey regions, and the dark grey areas corresponded to Mn-O, pure Ag, and Ag-Mn, respectively, as noted on the figure. Since the Mn-O layer was highly porous and discontinuous, the formation of Mn-O had no effect on the Ag evaporation

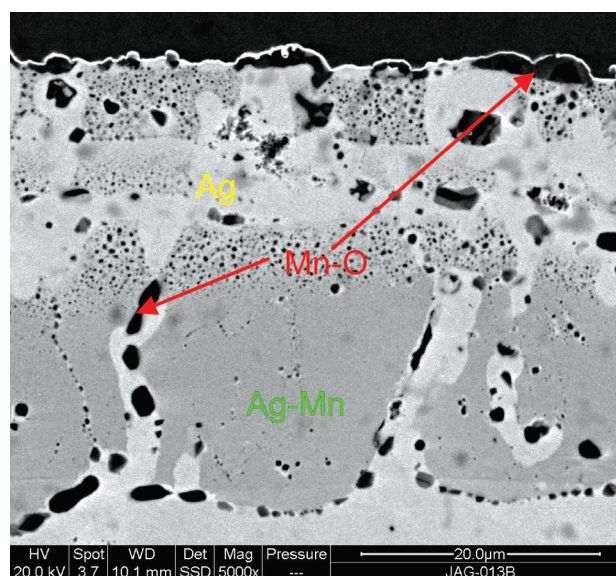


**FIGURE 1.** Cross-Sectional View near the Surface for a Ag-15%Mn Coupon after 160-hour Exposure to Air at 900°C

rate, even though its formation reduced the initial weight loss of the sample due to the pick-up of oxygen from the environment. For the Ag-5%Mn alloy coupon, it was oxidized less severely than the Ag-15%Mn alloy and oxygen penetrated mainly near the surface of the sample; however, the surface Mn-O layer was also highly porous and discontinuous, the formation of which had no effect on the Ag evaporation rate.

The Ag evaporation behavior of the Ag+LSM composites with different Ag-to-LSM ratios was also evaluated at 900°C in a moist air with a flow rate of 1.3 cm/s. The most obvious conclusion is that the addition of LSM into Ag to form a composite material did not significantly modify the Ag evaporation rate. This can be attributed to the fact that these composites were quite porous and Ag could escape from the composite materials via the interconnected voids.

Figure 2 shows the ASRs of the cells with the Ag+LSM composites as a function of the cumulative exposure time during thermal cycling. With the addition of Ag to the contact material, a significant drop in overall ASR was achieved. Even the addition of 10% Ag significantly reduced the cell ASR, as shown in Figure 1, proving the effectiveness of Ag in relaxing thermal stress and minimizing thermal cycle-induced damage. The ASR curves for the contact materials with 25 and 50% LSM overlapped and both materials exhibited a very low ASR.

It is important to relate the above information to the performance goals of contact materials in SOFC stacks. An operating lifetime of 40,000 hours is typically expected for SOFC stacks, and an ASR of less than

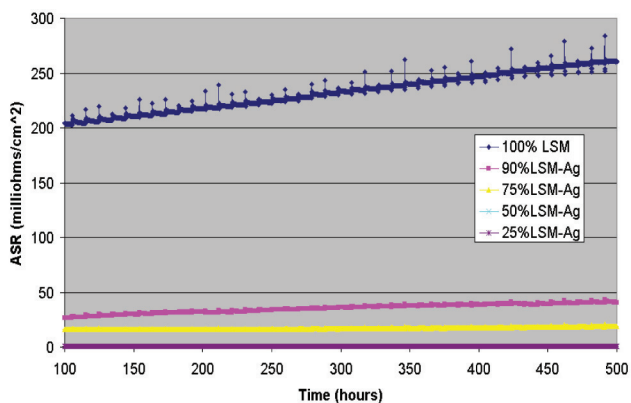


**FIGURE 2.** The Cell ASR Data vs. Cumulative Exposure Time at 800°C for the Ag+LSM Composites

100 mΩ·cm<sup>2</sup> is desired for interconnects [3]. Based on the projected values of the interconnect/contact layer ASRs after 40,000 hours using their rate of increase as determined from Figure 2, at least 25% Ag is needed to achieve the expected lifetime for the contact materials from the ASR consideration. However, these cycling test conditions are rather severe; in real SOFC stack operation (especially for stationary applications), isothermal holding will be much longer and the number of thermal cycles will be much less. ASR change during isothermal exposure with occasional thermal cycling will be monitored to assess the performance of the contact materials in such more realistic conditions.

After thermal cycling was completed, the cells with the Ag+LSM composites were removed from the test fixture, mounted, polished and examined using SEM. The most interesting observation was the presence of a thick layer of Fe oxide ( $\approx 60 \mu\text{m}$ ) on the interconnect for the 100% LSM contact material test cell. Figure 3 shows the cross section of this material. As can be seen from this figure, the pure ceramic contact material was very brittle in nature and upon removal of the cell from its fixture it separated from the interconnect. EDS analysis was performed on the oxide layer as seen in Figure 3, and the composition was verified to be close to Fe<sub>2</sub>O<sub>3</sub>.

The unique characteristic of the 100% LSM test cell is that none of the other test cells exhibited the thick oxide scale formation on the interconnect. It is proposed that the Cr<sub>2</sub>O<sub>3</sub> scale formed on the interconnect cracked repeatedly during thermal cycling due to the inability of the LSM contact material to deform and relax the thermal stress. Therefore, Fe oxides were formed on the alloy surface, which was depleted with Cr. Isothermal testing is currently under way, which will verify if the thick Fe oxide scale generated on the interconnect surface of the 100% LSM test cell is indeed related to thermal cycling.

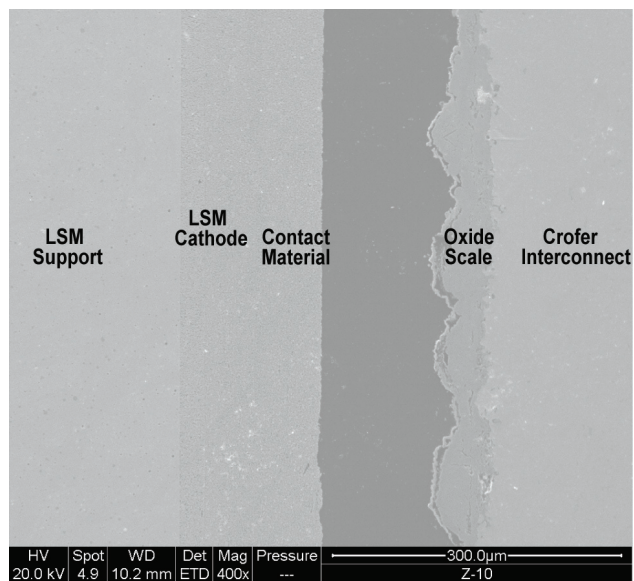


**FIGURE 3.** Cross-Sectional View of the Tested Cell with the 100% LSM Contact Material

## Conclusions and Future Directions

The following conclusions can be drawn based on this study:

- Alloying additions of Mn and Zn into Ag led to the formation of a porous surface oxide layer, which was not adequate in blocking the Ag from evaporation.
- The addition of LSM into Ag to form a composite material was not very effective in modifying the Ag evaporation rate.
- The increase of Ag in the Ag+LSM composite contact material led to the decrease in the cell ASR during thermal cycling. Even a small amount of Ag addition (e.g. 10% Ag) significantly reduced the cell ASR, indicating the effectiveness of Ag in relaxing thermal stress and minimizing thermal cycle-induced damage.

The future directions for this project are listed below:

- The evaporation behavior of Ag+perovskite composites with different microstructures will be studied.
- ASR change during isothermal exposure with occasional thermal cycling will be monitored to evaluate the performance of the composite contact materials in realistic SOFC-operating conditions.
- Cell testing with different contact materials will be conducted to further assess the effectiveness of the Ag+perovskite composite contact material in reducing Cr poisoning of the cathode.

### FY 2008 Publications/Presentations

1. "Thermal Evaporation of Pure Ag in SOFC-Relevant Environments," *Electrochemical and Solid-State Letters*, 10(10), p. B179, 2007.
2. Quarterly Report for 3<sup>rd</sup> quarter 2007, October 31, 2007.
3. Quarterly Report for 4<sup>th</sup> quarter 2008, January 30, 2008.
4. Quarterly Report for 1<sup>st</sup> quarter 2008, April 18, 2008.

### References

1. S. Koch, and P.V. Hendriksen, *Solid State Ionics*, 168, 1 (2004).
2. Z. Yang, G. Xia, P. Singh, J.W. Stevenson, *J. Power Sources*, 155, 246 (2006).
3. P. Piccardo, P. Gannon, S. Chevalier, M. Viviani, A. Barbucci, G. Caboche, R. Amendola, S. Fontana, *Surface and Coatings Technology*, 202, 122 (2007).

---

## **IV. SECA CORE RESEARCH & DEVELOPMENT**

### **F. Cross-Cutting Materials and Manufacturing**



## IV.F.1 SOFC Research and Development in Support of SECA

Michael Krumpelt (Primary Contact),  
Terry A. Cruse, Brian J. Ingram  
Argonne National Laboratory  
Argonne, IL 60439  
Phone: (630) 252-8520; Fax: (630) 252-4176  
E-mail: krumpelt@cmt.anl.gov

DOE Project Manager: Briggs White  
Phone: (304) 285-5437  
E-mail: Briggs.White@netl.doe.gov

Contract Number: 49071

Start Date: October 1, 2007  
Project End Date: September 30, 2008

### Objectives

- Explore new cathode formulations.
- Explore seals with high-temperature spring-back.

### Accomplishments

Initial results in a new task to advance the power density of cathodes are showing as much as an order of magnitude improvement.

### Introduction

In the previous two years we investigated the effect of chromium on cell potentials. When the cells were operated at 800°C and moderate current densities, the effect was within an acceptable range. At lower temperatures, lanthanum manganite cathodes were adversely impacted. Ferrite electrodes were more tolerant, but it became clear that advances in cathode performance would be beneficial. In the current fiscal year, we began to systematically explore cathodes with various combinations of manganese, iron and chromium.

We also have begun to explore a new seal concept. Most seals in industrial practice are made with an elastic o-ring that is being compressed. However, at the operating temperature of solid oxide fuel cells (SOFCs) no elastic materials are known. We conceptualized a seal configuration that would be expected to have some spring-back and have begun to develop it.

### Approach

The reduction of oxygen to oxide ions on the fuel cell cathode has many steps, each potentially rate limiting. First, the oxygen molecules need to adsorb on the surface, but it is not known where on the surface this occurs. Then, an electron needs to be transferred onto the oxygen molecule to form a peroxide ion. Then three more electrons must follow until two oxide ions are formed. These electron transfers are facilitated by the electronic properties of the material. Lastly, the oxide ions need to be transported to the electrolyte, requiring good ionic conductivity of the cathode material. We are addressing all three issues. Ionic conductivity correlates well with electrochemical performance. We screen potential new cathode materials by measuring the area specific resistance (ASR). We then measure electronic properties by X-ray photoelectron spectroscopy (XPS) and attempt to identify the surface adsorption site by Raman spectroscopy. The combination of these techniques is expected to lead to new insights into the mechanism of the oxygen reaction.

In seals, we have conceptualized a seal geometry that promises to provide some elasticity. It involves a combination of a glass and a ceramic that needs to be shaped in a specific way. We are learning to make such a seal.

### Results

The ASR of porous electrodes within the ternary system lanthanum strontium manganite (LSM)-Fe-Cr have been investigated on yttrium-stabilized zirconia (YSZ) electrolytes for compositions represented by the solid points in Figure 1. Substitution of Cr on the B-site

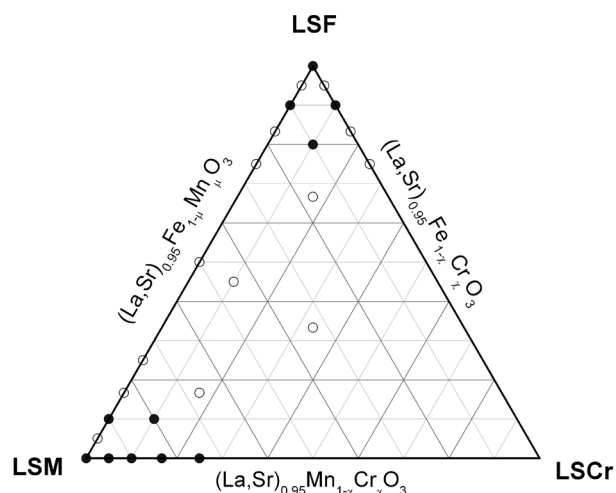
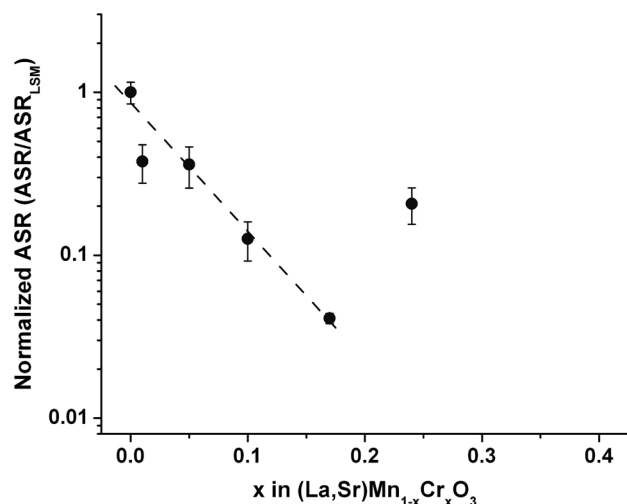


FIGURE 1. Ternary Cathode Composition Diagram



**FIGURE 2.** Normalized ASR Interpolated to 800°C of LSMCr,  $(La_{0.8}Sr_{0.2})_{0.95}Mn_{1-x}Cr_xO_{3-\delta}$  Samples as a Function of Cr Content

of LSM (LSMCr) reduces the ASR significantly as shown in Figure 2. A decrease by over an order of magnitude is observed with up to 17% Cr substitution, which corresponds to Cr statistically percolated on the B-site.

Chromium affects the electrochemical properties of LSM in two ways. First, it acts to suppress grain growth, thereby maintaining high surface area of the cathode for oxygen reduction. It also serves to alter the electronic state of LSM. The latter effect will be studied further with the use of XPS/ultraviolet photoelectron spectroscopy (UPS).

LSM substituted with Fe and Cr was investigated (see bottom left portion of Figure 1). The substitution of Fe in LSM limits the benefits of Cr addition. For instance, as shown in Figure 2 and 3, 10% Cr substitution decreases the ASR of LSM by an order of magnitude; however, in the presence of Fe the same level of Cr only decreases the ASR by a factor of 1.5. The nature of the interaction between Fe and Cr is unknown at this point. Further investigations of the physical and electrical structures are on going.

The substitution of Cr and Mn on Fe sites in lanthanum strontium ferrite (LSF) (see top portion of Figure 1) was investigated and the results are shown in Figure 4. As in the case of LSMCr, chromium substitution improves the ASR in LSF, however only by a factor of 1.5 to 2 (co-doped with Mn and without Mn, respectively). Manganese substitution, on the other hand, slightly increases the ASR of LSF. This is to be expected, since LSF is a superior cathode material than LSM. It should be noted that the two phase electrodes (50 vol% perovskite/YSZ) are screen printed on pre-sintered dense YSZ substrates. The ASR values can be improved greatly by co-sintering the composite cathodes with the electrolyte or infiltrating the perovskite into

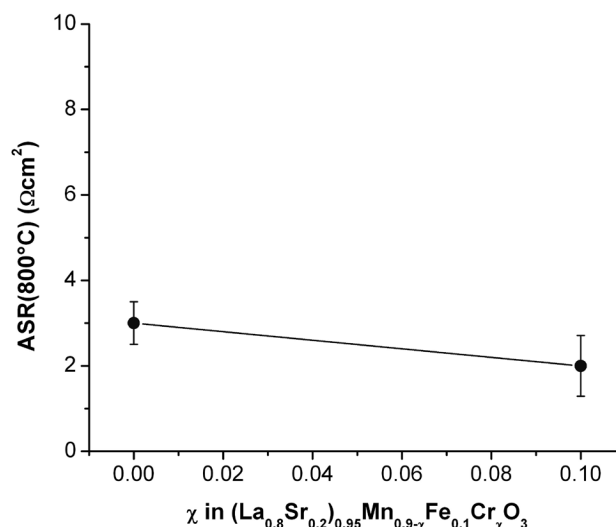


**FIGURE 3.** ASR Interpolated to 800°C of LSMFCr,  $(La_{0.8}Sr_{0.2})_{0.95}Mn_{0.9-x}Fe_{0.1x}Cr_xO_{3-\delta}$  Samples as a Function of Cr Content

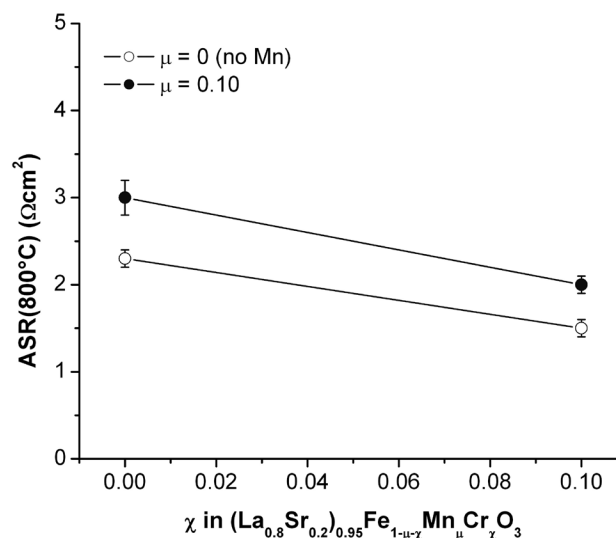


**FIGURE 4.** ASR Interpolated to 800°C of LSFMCr,  $(La_{0.8}Sr_{0.2})_{0.95}Fe_{1-\mu-\chi}Mn_{\mu}Cr_{\chi}O_{3-\delta}$  Samples as a Function of Cr Content

porous YSZ. The trends shown in Figure 4 are expected to be consistent with optimized electrode production methods.

In the area of seal development, a number of different variations of two basic geometries were produced to determine an appropriate starting configuration, with scanning electron microscopy (SEM) used as the preliminary screening technique. The SEM was used to examine cross sections of seals to help determine: processing parameters, interactions between materials and a desired starting ratio of materials. Slight modifications to the processing parameters produced specimens with desired geometries and appear to be gas

tight and chemically and mechanically stable. Presently a testing procedure is being developed to measure the mechanical properties of the seals to further determine what ratio of materials and geometries produce the best properties.

The glass presently being used is a good sealing glass for metals and ceramics with a fairly typical sealing glass composition. This glass was found to work well in the Argonne seal designs, and will be used in all the preliminary tests based on its properties and availability. The melting point of this glass is too low for ideal SOFC operating conditions, but can be considered for use in lower temperature applications. The relatively low melting point of this glass, nevertheless, has been useful in demonstrating the mechanical stability of the Argonne seal concept. At 850°C the glass readily deforms under its own weight, or that of a small piece of stainless steel, indicating that under SOFC operating conditions (a relatively high temperature and a mechanical load) the glass seal could easily fail. However, when used in the Argonne seal concept the shape of the seal was maintained at 850°C; additionally, a good bond was observed between the seal and 446 stainless steel. This observation indicates that “self-healing” glasses, which typically possess high viscosities at operating temperatures, may be utilized in the Argonne seal design, maintaining the “self-healing” characteristic while the mechanical properties are enhanced.

Some seals have also been prepared using a sealing glass developed by Dr. Brow at the Missouri University of Science and Technology. This glass, with a higher melting point than the previously discussed glass, worked well in the Argonne seal concept. There was no unexpected interaction or apparent degradation of the mechanical behavior. However, due to limited quantities of the glass further testing will be delayed until after preliminary mechanical measurements are performed and the structure and ratios are better evaluated.

## Conclusions and Future Directions

Both efforts described in this report were initiated just a few months ago. With this in mind, it appears that partially substituting other transition metals on the B-site of the lanthanum manganite or the ferrite can improve the electrochemical properties. Chromium substitution is beneficial in LSM by affecting the surface area and probably the electronic properties, which will be investigated with XPS/UPS measurements. Furthermore, correlation between the electronic surface structure and cathode performance (i.e., ASR) will be made with systematic B-site doping. The ferrite system which is a better electrode to begin with, can be further improved with chromium and other elements that cannot be discussed yet.

In our seal activity, we have been able to make the desired shapes with a combination of glass and ceramic. We will soon begin to test whether we can obtain elasticity from our configuration.

## FY 2008 Publications/Presentations

### Presentations:

1. “Examination of Chromium’s Effects on a LSM/YSZ Solid Oxide Fuel Cell Cathode”, T.A. Cruse, S.Wang, G. Chen, B.J. Ingram, P.A. Salvador, and M. Krumpelt, American Ceramic Society 32<sup>nd</sup> International Conference & Exposition on Advanced Ceramics and Composites, 2008.
2. “Investigation of Chromium Contamination in SOFC Cathodes Using Transmission Electron Microscopy”, S. Wang, P.A. Salvador, T.A. Cruse, and M. Krumpelt, American Ceramic Society 32<sup>nd</sup> International Conference & Exposition on Advanced Ceramics and Composites, 2008.
3. “Effects of Cell Operating Conditions on Degradation by Chromium”, T.A. Cruse, M. Krumpelt, B.J. Ingram, G. Chen, S. Wang, P.A. Salvador, TMS 137<sup>th</sup> Annual Meeting & Exhibition, 2008.
4. “Electrode Contamination Studies”, M. Krumpelt, T.A. Cruse, B.J. Ingram, SECA Annual Meeting, 2007.

### Publications:

1. “Potassium-assisted chromium transport in solid oxide fuel cells”, B.J. Ingram, T.A. Cruse, and M. Krumpelt, *J. Electrochem. Soc.* 154(11) B1200-B1205 (2007).
2. “Chromium reactions and transport in solid oxide fuel cells”, T. A. Cruse, B.J. Ingram, D.-J. Liu, and M. Krumpelt, *Electrochem. Soc. Trans.* 5, 335 (2007).

## IV.F.2 Reliability and Durability of Materials and Components for Solid Oxide Fuel Cells

Edgar Lara-Curzio (Primary Contact),  
Yanli Wang, Amit Shyam, Rosa Trejo,  
Beth Armstrong, Karren L. More and  
Larry Walker

Oak Ridge National Laboratory  
1 Bethel Valley Rd.

Oak Ridge, TN 37831-6062

Phone: (865) 574-1749; Fax: (865) 574-4913

E-mail: laracurzioe@ornl.gov

DOE Project Manager: Travis Shultz

Phone: (304) 285-1370

E-mail: Travis.Shultz@netl.doe.gov

Contract Number: FEAA066

Start Date: October 1, 2007

Project End Date: September 30, 2008

### Introduction

To reduce interfacial resistance, contact layers are often applied between the cathode and the metallic interconnect as part of the SOFC stack assembly process. The contact layer material must be chemically compatible in oxidizing conditions with both the interconnect material and the cathode because reactions could result in the formation of phases that could increase the contact resistance or result in thermal expansion mismatches that could lead to delamination.

One objective of this project is to identify and utilize test techniques to determine the physical and mechanical properties of cathode contact paste materials and the mechanical properties of the interfaces that exist between the cathode and the contact paste, and between the contact paste and metallic interconnects or coated metallic interconnects. The properties obtained in this study will support ongoing efforts to develop models of the thermomechanical and electrochemical behavior of SOFCs. This study will also provide insight into the mechanisms responsible for the degradation of SOFCs and in turn, strategies to overcome these limitations, particularly when SOFCs are subjected to service conditions for long periods of time, including cyclic operation.

### Approach

As part of a process to prepare test specimens for the determination of fracture properties of cathode-interconnect interfaces in SOFCs, manganese cobaltite spinel coatings were synthesized onto AL441 and Crofer 22 APU substrates using screen-printing techniques. Test specimens for the determination of interfacial mechanical properties were prepared by sandwiching a layer of lanthanum strontium manganite (LSM)-10 between two coated metallic substrates. The fracture properties of the interfaces were determined by using a 4-point test configuration. Advanced characterization techniques (e.g.- electron microprobe analysis and transmission electron microscopy) were used to characterize the microstructure of thermally grown oxides on AL441 and Crofer 22 APU, and of protective manganese cobaltite spinel coatings. X-ray diffraction techniques were used to identify the phases present in the protective coatings.

### Objectives

- To support the Solid State Energy Conversion Alliance (SECA) industrial teams in the development of reliable and durable solid oxide fuel cells (SOFCs).
- To support the SECA Core Technology Program modeling efforts by establishing material property databases.
- To establish failure criteria for SOFC materials and components.
- To determine the fracture behavior of SOFC materials, components and their interfaces.

### Accomplishments

- Used advanced techniques to characterize the scales formed on the surface of alloys AL441 and Crofer 22 APU after exposure in air at 800°C.
- Successfully screen printed  $(\text{Mn,Co})_3\text{O}_4$  spinel coatings onto strips of Crofer 22 APU and AL441 stainless steel. The composition of the coatings was consistent with specifications developed by the Pacific Northwest National Laboratory (PNNL).
- Prepared test specimens for the determination of cathode-interconnect interfacial fracture toughness and successfully obtained results for test specimens incorporating AL441 and Crofer 22 APU.

## Results

The oxide scales that form on AL441 and Crofer 22 APU when these materials are exposed to air at elevated temperatures were characterized by electron microscopy using an electron microprobe (JEOL 8200) and a transmission electron microscope (Hitachi HF-3300). The information obtained from these analyses is important to identify, in combination with interfacial fracture toughness tests, the path and the mechanisms responsible for the propagation of cracks in the region between the cathode and the metallic interconnects.

Scanning electron micrographs of the cross section of one Crofer 22 APU and two AL441 specimens that had been exposed to air at 800°C for 600 hours at PNNL are shown in Figure 1. The difference between the two AL441 specimens was the surface roughness (0.63  $\mu\text{m}$  vs. 0.08  $\mu\text{m}$ ) (Table 1). The two major components comprising the oxide scales formed on these alloys are a fine-grained layer of chromium oxide on the surface of the metal and a coarse-grained layer of (Cr,Mn) oxide on top of it. It was observed that the oxide scale that formed on the Crofer 22 APU sample

TABLE 1. Oxidized Samples

Sample I.D.	Material	Surface Roughness, Ra, $\mu\text{m}$	Nominal Thickness, mm
600-8	AL441	0.08	1.61
600-6		0.63	1.61
600I-3	Crofer 22 APU	0.1	0.53

(Figure 2) was thinner ( $\sim 2 \mu\text{m}$ ) than those formed on AL441 samples ( $\sim 4 \mu\text{m}$ ). The scale formed on Crofer 22 APU was found to be non-uniform and non-continuous, and there was evidence of spallation. A detailed analysis of the scale-metal interface revealed the presence of a non-continuous silica phase and voids, which could explain the propensity to spallation of the oxide scale. These observations are consistent with results reported elsewhere [1-2]. It was also observed that the oxide layer that formed on the surface of AL441 sample 600-8 (Figure 3) was more uniform and better bonded than the oxide layer formed on AL441 sample 600-6. These

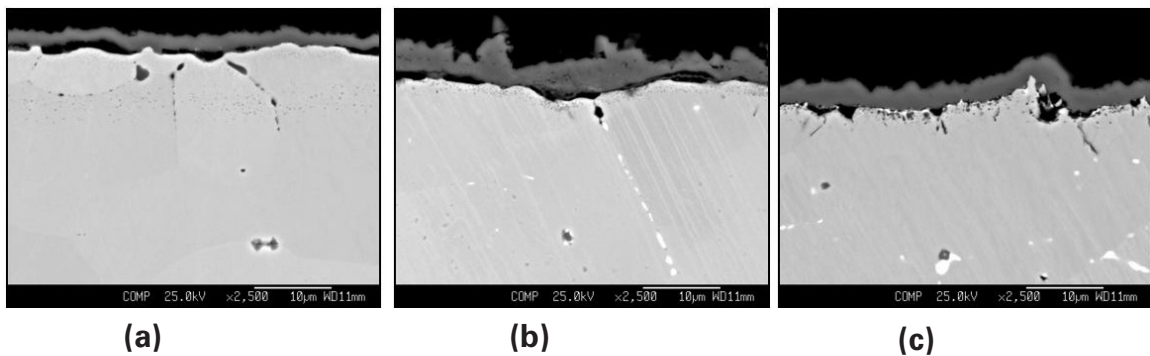


FIGURE 1. Scanning Electron Micrographs of Samples Oxidized at 800°C for 600 Hours: (a) Crofer 22 APU Sample 600I-3; (b) AL441 Sample 600-6; (c) AL441 Sample 600-8

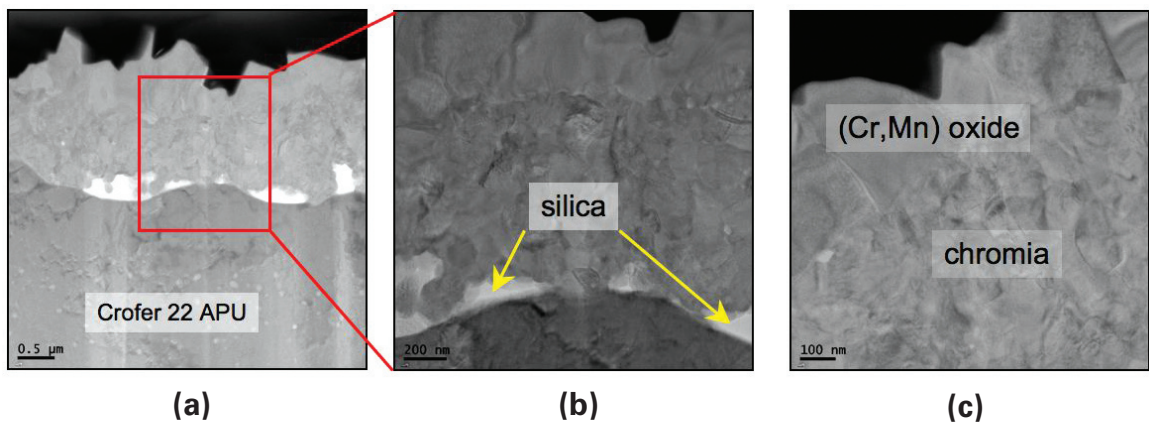
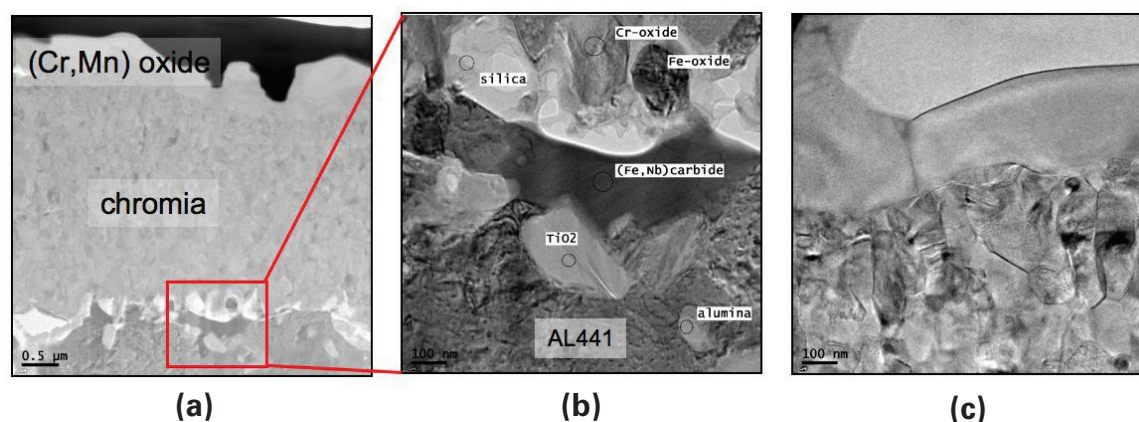


FIGURE 2. Transmission electron micrographs (bright field) of the scale formed on Crofer 22 APU sample 600I-3. (a) Structure of the scale; (b) a discontinuous silica layer was observed at the interface between the metal and the oxide scale; (c) the main components of the oxide scale are a fine-grained chromia layer and a coarse-grained (Cr,Mn) oxide layer.



**FIGURE 3.** Transmission electron micrographs (bright field) of the scale formed on AL441 sample 600-8. (a) Structure of the scale; (b) a discontinuous silica layer was observed at the interface between the metal and the oxide scale, while precipitates of alumina and Ti-Al-O were observed in the metal; (c) the main components of the oxide scale are a fine-grained chromia layer and a coarse-grained (Cr,Mn) oxide layer.

observations suggest that a finer surface finish of the alloy results in a better oxide scale microstructure.

A chemical analysis of the oxide scales revealed the presence of a non-continuous layer of titania between the AL441 substrate and the chromia layer. Also, in a 3- $\mu\text{m}$  thick region below the surface of the metal Nb-Si carbide phases were observed at the grain boundaries, along with small ( $\sim 60$  nm) precipitates of alumina, titanium-rich Ti-Al-O and acicular shaped aluminum rich Al-Ti-O.

It is known that Cr-containing oxide scales readily volatilize resulting in poisoning of the cathode and severe performance degradation of the fuel cell [3]. One approach to minimize Cr volatilization is the application of protective coatings to the metallic interconnect [4]. For this study, coatings of manganese cobaltite spinel were applied onto strips of AL441 and Crofer 22 APU according to procedures developed at PNNL [5]. Powders of  $(\text{Mn},\text{Co})_3\text{O}_4$  were synthesized via glycine nitrate combustion synthesis using  $\text{MnCO}_3$  and  $\text{Co}_3\text{O}_4$  starting powders. After screen printing and drying, the coated strips shown were reduced at  $850^\circ\text{C}$  for 4 hours using a gas mixture of 96% Ar and 4%  $\text{H}_2$  bubbled through water maintained at  $25^\circ\text{C}$ , followed by reoxidation at  $800^\circ\text{C}$  for 8 hours. An X-ray diffraction analysis of the coatings (Figure 4) revealed the presence of tetragonal  $\text{CoMn}_2\text{O}_4$  and cubic  $\text{MnCo}_2\text{O}_4$ ; after the reduction process this coating transformed into metallic cobalt and MnO; and finally into tetragonal  $\text{CoMn}_2\text{O}_4$  and cubic  $\text{MnCo}_2\text{O}_4$  at the end of the reoxidation process.

Layers of LSM-10 were deposited onto the coated strips to prepare sandwich-shaped test specimens for the determination of interfacial fracture properties. Test specimens were sintered at  $900^\circ\text{C}$  for 8 hours and the

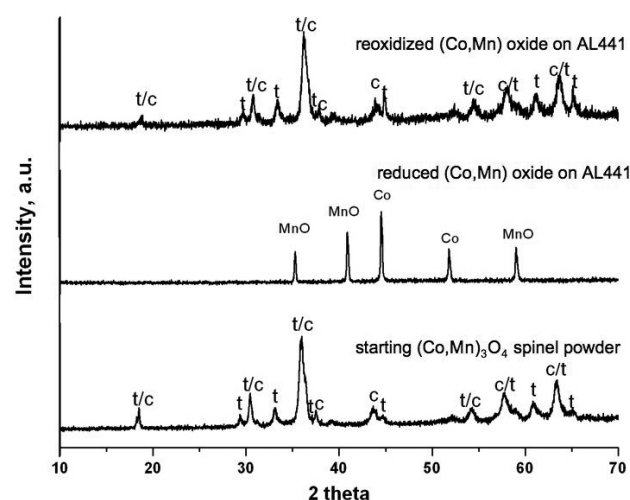


**FIGURE 4.** X-ray Diffraction Patterns for the Starting  $(\text{Mn},\text{Co})_3\text{O}_4$  Spinel Powder and the Coating Deposited onto Metallic Substrates after Reduction and Reoxidation Processes

final nominal dimensions of the test specimens were: 30 mm  $\times$  3 mm  $\times$  0.718 mm. The thickness of the spinel coating was approximately 30  $\mu\text{m}$ , while the thickness of the LSM-10 layer was approximately 40  $\mu\text{m}$ .

Alumina fixtures with 20 mm/10 mm spans were used for the mechanical evaluation of the test specimens. The results of three tests are shown in Figure 5. All the tests were performed at room temperature under a constant displacement rate of 0.5  $\mu\text{m}/\text{s}$ . The load plateau in the three curves suggests the occurrence of steady crack propagation. The value of the load plateau for steady crack propagation can be used to determine the interfacial toughness as follows:

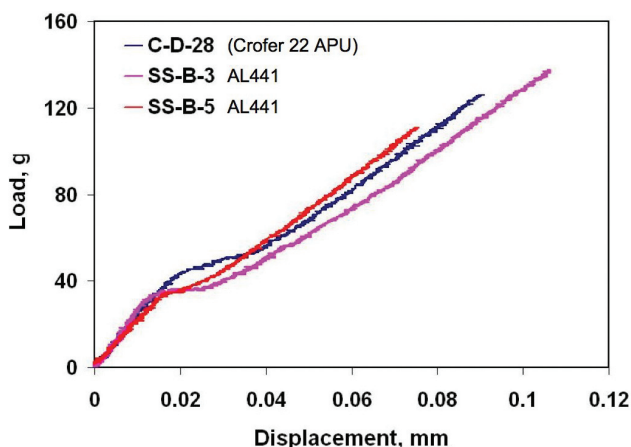


**FIGURE 5.** Load Versus Displacement Curves Obtained from the 4-Point Evaluation of Notched Sandwich Specimens

$$G = \frac{(1-\nu^2)M^2}{2E_2} \left( \frac{1}{I_2} - \frac{1}{I_c} \right)$$

$$M = Pl/2b; I_c = kh_1^3/12 + 2h_2^3/3 + h_1h_2(h_1/2 + h_2);$$

$$k = \frac{E_1(1-\nu_2^2)}{E_2(1-\nu_1^2)}; I_2 = h_2^3/12$$

where P is the load for steady crack propagation, l is the difference of the outer span and inter span, b is the sample width,  $h_1$  is the total thickness of the coatings,  $h_2$  is the thickness of the Crofer 22 APU or AL441, E is elastic modulus and  $\nu$  is the Poisson ratio. Subscript 1 refers to the coating and 2 to the metal substrate. The interfacial toughness for the samples prepared with Crofer 22 APU was  $0.42 \text{ J/m}^2$ , while the interfacial toughness for the samples prepared with AL441 was  $0.27 \text{ J/m}^2$ . Fractographic analyses suggest that crack propagation is associated with a combination of cohesive and adhesive failure, most likely associated with the high porosity (porosity higher than 45%) of the LSM-10 layer.

## Conclusions and Future Directions

Manganese cobaltite spinel coatings were successfully synthesized onto Crofer 22 APU and AL441 strips. Phase identification using X-ray diffraction revealed the presence of both tetragonal  $\text{CoMn}_2\text{O}_4$  and cubic  $\text{MnCo}_2\text{O}_4$ . Determination of the interfacial properties in sandwich test specimens of Crofer 22 APU and AL441 with the manganese cobaltite spinel coatings and layers of LSM-10 showed that the interfacial

toughness was  $0.42 \text{ J/m}^2$  for test specimens prepared with Crofer 22 APU and  $0.27 \text{ J/m}^2$  for test specimens prepared with AL441.

Failure was found to be a mixture of adhesive and cohesive failure processes. By establishing a reproducible process to prepare test specimens it has been possible to investigate the effects of important parameters (e.g., physical dimensions, processing temperature and time) on the interfacial properties of these systems. This work is in progress.

*In situ* experiments using X-ray diffraction techniques are also in progress to determine: the magnitude of growth and residual stresses associated with thermally grown oxide layers; the synthesis of protective layers; and the evolution of these stresses with time.

## FY 2008 Publications/Presentations

1. Quarterly Report for 1<sup>st</sup> quarter fiscal year 2008, January 2008.
2. Quarterly Report for 2<sup>nd</sup> quarter fiscal year 2008, April 2008.
3. Durability and reliability of SOFC Materials and Components, presented at the 8<sup>th</sup> Annual SECA Workshop and Peer Review, San Antonio, TX, August 7–9, 2007.

## References

1. S. Fontana, R. Amendola, S. Chevalier et.al. *J. Power Sources*, **17** (2007) pp. 652-662.
2. D.E. Alman and P.D. Jablonski, *Inter. J. Hydrogen Energy*, **32** (2007) pp. 3743.
3. T.S. Taniguchi, M. Kadowaki, H. Kawamura, T. Yasuo, Y. Akiyama, and Y. Miyake, *J. Power Sources*, **55**, 73 (1995) pp. 73-79.
4. S.P. Simner, M.D. Anderson, G-G Xia, Z. Yang and J.W. Stevenson, *Ceram. Eng. Sci. Proc.*, **26**, 4 (2005) pp. 83-90.
5. Z. Yang, G. Xia, S.P. Simner, and J. W. Stevenson, *Journal of the Electrochemical Society*, **152**, 9 (2005) A1896-A1901.

## IV.F.3 SECA Core Technology Program Activities - PNNL

Prabhakar Singh

Pacific Northwest National Laboratory (PNNL)  
P.O. Box 999, MS K2-44  
Richland, WA 99354  
Phone: (509) 375-5945; Fax: (509) 375-2186  
E-mail: Prabhakar.Singh@pnl.gov

DOE Project Manager: Ayyakkannu Manivannan  
Phone: (304) 285-2078  
E-mail: Ayyakkannu.Manivannan@netl.doe.gov

Contract Number: 40552

Start Date: October 1, 2007  
Project End Date: September 30, 2008

### Objective

- Direct Solid State Energy Conversion Alliance (SECA) Core Technology Program (CTP) projects.
- Identify and prioritize technology development needs that meet the cost performance and life targets of SECA.
- Develop and execute technology development plans, identify mechanistic understanding, summarize technical findings and prepare topical reports, and disseminate technical information and assist in technology transfer to SECA industrial teams.
- Develop advanced cell and stack component materials, optimize stack and systems design and configuration utilizing computational tools, and develop innovative fuel processing technologies for solid oxide fuel cell (SOFC) systems operating on coal-derived fuels.
- Participate and organize technical and topical meetings and workshops to gather and disseminate technical findings.
- Publish and present technical reports and papers in technical journals.

### Approach

- Discuss technology status and identify development needs through technical discussions with SECA CTP and industrial participants.
- Hold technical and program reviews and meetings to present the results of on-going technical work and research concepts.
- Organize topical area workshops and exchange technical information with industrial and academic experts.

- Identify and transfer key technologies to industries in a timely manner.
- Publish technical findings in quarterly, annual and topical technical reports.
- Provide leadership and organization to technical societies and outreach programs.

### Accomplishments

- A low-cost ferritic stainless steel AISI 441 has been identified and tested as the most promising cell-to-cell interconnect material. The alloy chemistry and manufacturing process utilizes the conventional metallurgical techniques amenable to large-scale manufacturing. A collaborative technology development project has been initiated with Allegheny Technologies.
- Surface coating chemistry and application techniques have been developed and long-term performance has been tested. A collaborative project with the National Energy Technology Laboratory (NETL) and AYI has been developed.
- A seal workshop was conducted to review the technology status and development needs. An analytical modeling project was established with the University of Cincinnati. A modeling workshop was also conducted and simulation tools were provided to SECA industrial teams.
- Published quarterly progress and technical topical reports. Peer reviewed journal papers were also published on topics related to cell materials, cell and stack design analysis and utilization of hydrocarbons.
- Presented invited technical lectures at technical societies, universities and industries.
- Organized ASM-MST 08, and ACerSoc Daytona Beach meetings on SOFC technology.

### Future Directions

- Continue cell and stack technology development projects in collaboration with CTP participants and industrial partners. Identify technology gaps, development needs at stack and systems level to meet the cost, life and performance targets.
- Prioritize technology development needs for SOFC operation on coal-derived fuels. Assist industries in developing and optimizing cell, stack and systems design and configurations for scale-up.
- Develop and implement cost-effective materials and fabrication processes.

- Identify long-term performance stability requirements.
- Facilitate and accelerate technology transfer to industries.
- Provide technical and topical progress reports to SECA participants.
- Organize technical society meetings to exchange technical information.
- Conduct CTP meetings and topical workshops.

---

---

## Introduction

The SECA CTP activities at PNNL coordinates, prioritizes and conducts research towards the development, testing, characterization and implementation of advanced cell and stack component materials, stack and systems design, simulation and performance optimization along with the utilization of hydrocarbons and coal-derived fuels in SOFC power systems. The PNNL project also collaborates with academic institutions, national laboratories and industries and identifies technology gaps. Research projects are focused on the development and testing of cost-effective materials and fabrication processes, electrical performance optimization and long-term stability, stack and systems design and optimization along with thermal and structural analysis, and utilization of hydrocarbons and coal-derived fuels.

Cell and stack component materials development activity at PNNL has focused on the development of lower cost bulk interconnect alloy and surface coatings for improved oxidation and corrosion resistance in an oxidizing atmosphere along with the mitigation of chromium vaporization that results in the electrochemical poisoning of the cathode electrodes [1]. Several coating approaches have been developed and evaluated [2]. Results of such studies have been provided to the SECA industry teams. Evaluation of high temperature refractory glass formulations and their testing under cell operating conditions in a newly developed stack test fixture also continued for applications in seals. Internal reforming of hydrocarbons on the cell anode was evaluated and the role of microstructural evolution on the rate of reformation was examined.

A commercial ferritic stainless steel AISI 441 alloy has been extensively tested under cathode exposure conditions. Both unmodified and coated alloy samples have been tested under isothermal and thermal cyclic conditions and corrosion processes have been identified. The alloy metallurgy utilizes conventional melt processing and ladle treatment techniques. Allegheny Technologies Inc. manufactures the alloy. Use of

selected alloy additives to the melt allow for laves phase formation and the formation of localized Si segregates that effectively results in the elimination of a continuous silica layer at the metal-oxide interface. The oxidation of laves phase results in the localized silica containing scale that does not increase the scale resistivity. Elimination of the continuous silica layer also results in improved scale adherence. The presence of Mn in the bulk alloy facilitates the formation of Cr-Mn spinel at the gas-scale interface. Although the formation of Cr-Mn spinel has the potential to lower the Cr vapor partial pressures in the oxidant, advanced coatings developed at PNNL and NETL have been found to completely block the Cr vaporization and resulting poisoning of the cathode electrode. Surface modification by ceria has shown improved oxidation resistance where as the Co-Mn spinel coating also improves the scale and interface conductivity. Several low-cost coating formulations and fabrication techniques are currently under development with emphasis on near net shape fabrication. It is postulated that a net shape coating will be desirable to coat shaped flow channels.

Our research activity related to the development of a glass seal progressed towards the identification and synthesis of a wide variety of refractory glass formulations and evaluation of their stability under nominal seal exposure conditions. Refractory glass offers the potential to utilize higher sealing temperatures for the development of the seal and interfacial contact between the cathode electrode and the interconnection material. Refractory seals also offer resistance to prolonged interactions with chromia scales formed on the underlying metallic surfaces. To prevent such interaction and the formation of respective alkali or alkaline earth chromates, surface modifications utilizing an aluminizing process has been implemented. The presence of aluminum in the metal at the exposed surface allows the formation of alumina at the expense of chromia, thus preventing the above interaction. Alumina scale also prevents “scale fluxing.”

Computational simulation and modeling activity at PNNL was predominantly focused on the structural, thermal and electrical analysis of advanced cell and stack designs. Surface and interfacial stability at cell and stack levels were investigated. Surface oxide and coating integrity with emphasis on spallation and delamination has been investigated. Refractory glass seal and compliant glass seal (in collaboration with the University of Connecticut) stability under nominal cell and stack operating conditions has been examined and results have been presented in topical reports. Work continued towards the evaluation of metal interconnection creep and deformation and the role of surface finish on the adherence of the oxide scale. Cathode electrode contact with the interconnect has also been investigated. Work on the American Society of Mechanical Engineers

(ASME) SOFC Design Basis (criteria for stability, reliability and longer life) has been initiated and will continue. Significant effort on cathode-interconnect contact aid and seal modeling will be used to assess the current state-of-the-art and guide ongoing materials development work. Modeling to assess thermal management in large SOFC stacks and high pressure electrochemistry work is included in this task. This modeling work assesses the impact of larger cells and syngas compositions on the temperature profiles and stresses on the cell, seals, and contact zones. Work will focus on cell-to-interconnect seals, interconnects and interconnect coatings, and contact aids.

Experimental and computational simulation work progressed towards the evaluation of “on anode” utilization of hydrocarbons and its role on cell temperature distribution as well as thermal management in the cell stack. As reported earlier, the above approach offers the potential to utilize the exothermic oxidative heat generation processes with endothermic reformation reactions thus providing a method for thermal management within the large stacks. Studies at bench-scale reactors have been conducted to understand the reformation kinetics and long-term structural changes. Findings have been reported in topical reports and presented at technical meetings.

The CTP coordinates and facilitates the technical information exchange among CTP participants in a timely manner. Technical and topical reports and status papers are prepared and provided to accelerate the information exchange. Quarterly reports have been prepared during the reporting period and provided to industries. Technical meetings with representatives from academia, national laboratory and industries have been held on topics of interest and importance.

## Approach

SECA CTP identifies, coordinates, prioritizes and develops advanced technologies to meet the performance, life and cost targets of the SECA program. Technology coordination is performed with universities, national laboratories and industries in order to achieve the targeted needs of the program. Technical findings are reported in topical and technical reports. Based on the identified technology gaps, topical area meetings and workshops are held with experts from industries, academia and national laboratories. Our approach consists of conducting and providing:

- Technical and topical reports and white papers
- Quarterly progress reports
- Workshops and meetings on technical areas of interest and importance
- Participation in technical society meetings
- Publications in peer reviewed journals

- Conduct meetings with SECA industrial teams to discuss technical progress.

## Results

SECA CTP activities at PNNL provide quarterly progress reports, and topical and technical reports to SECA participants. Several workshops were held during the reporting period to discuss the status of SOFC seals (San Antonio, TX), advanced interconnects and coatings (Morgantown, WV), stack test and validation (Daytona Beach, FL), and an ASME Design Basis meeting (Pittsburgh, PA and Richland, WA). Several meetings were also held with university participants namely the University of Cincinnati, University of Florida and West Virginia University. Meetings were held with SECA industrial partners to provide them with technical findings. Several invited lectures were given at technical society (ASM, ACerSoc, TMS, AVS, ECS, etc.) meetings. SOFC technology and technology status were also presented at universities (University of Connecticut, University of Pittsburgh, University of Cincinnati, Boston University, etc.) to help familiarize and train students and teaching staff. Technical society meetings were organized to bring forward experts working in the field and disseminate information to industrial participants and academia with the ongoing research activities.

## Conclusions

SECA CTP at PNNL identifies, prioritizes, and conducts research towards the development of advanced cell and stack component materials, modeling and design tools for the optimization of cell and stack designs, and fuel processing technologies for the utilization of coal-based fuels. The CTP also coordinates technology development activities at universities, national laboratories and industries. CTP facilitates the exchange and dissemination of technical findings obtained by the participants, in a timely manner to all SECA industrial team members through technical meetings and workshops, topical and technical reports as well as targeted meetings and publications.

## References

1. Yang ZG, G Xia, MS Walker, CM Wang, JW Stevenson, and **P Singh**, “High Temperature Oxidation/ Corrosion Behavior of Metals and Alloys under a Hydrogen Gradient” INTERNATIONAL JOURNAL OF HYDROGEN ENERGY 32(16):3770-3777, 2007.
2. Chen L, Jha B, Yang ZG, Stevenson JW, **Singh P**, “Clad metals by roll bonding for SOFC interconnects” JOURNAL OF MATERIALS ENGINEERING AND PERFORMANCE 15 (4): 399-403 AUG 2006.

**FY 2007-2008 Publications/Presentations**

## Publications

1. "Corrosion in Fuel Cells," **Prabhakar Singh** and Zhenguo Yang, in ASM Handbook, Volume 13C: Corrosion, ASM International, pp. 504-411, Materials Park, Ohio, 2006.
2. "Corrosion and Protection of Metallic Interconnects in Solid Oxide Fuel Cells," a book chapter by Zhenguo Yang, Jeffrey W. Stevenson, **Prabhakar Singh**, in Materials for Hydrogen Economy, edited by Russ Jones and George Thomas, Francis & Taylor (in press).
3. Chou YS, JW Stevenson, JS Hardy, and **P Singh**, "Material Degradation During Ageing and Thermal Cycling of Hybrid Mica Seal with Glass Interlayer for Solid Oxide Fuel Cells." JOURNAL OF POWER SOURCES (in press).
4. McCarthy B, LR Pederson, HU Anderson, XD Zhou, **P Singh**, GW Coffey, and EC Thomsen, "Enhanced Shrinkage of Lanthanum Strontium Manganite (La<sub>0.90</sub>Sr<sub>0.10</sub>MnO<sub>3+x</sub>) Resulting from Thermal and Oxygen Partial Pressure Cycling" JOURNAL OF AMERICAN CERAMIC SOCIETY 90(10): 3255-3262, 2007.
5. Chou YS, Stevenson JW, **Singh P**, "Novel refractory alkaline earth silicate sealing glasses for planar solid oxide fuel cells" JOURNAL OF THE ELECTROCHEMICAL SOCIETY 154 (7): B644-B651 2007.

## Presentations

1. Chou YS, Stevenson JW, Xia Gordon, Templeton Jared, Maupin Gary, Templeton Josh, **Singh P**, and Zhou Xiaodong, "SOFC materials evaluation in a standard "stack" test fixture" To be presented at MST 08, ASM International, 2008, Pittsburgh.
2. Strohm JJ, DL King, X Wang, CM Wang, **P Singh**, KP Recknagel, and Y Wang, "Effects of Activity and Deactivation of Ni-YSZ SOFC Anodes on Endotherm Profiles during Internal Reforming of Methane" American Chemical Society 234<sup>th</sup> National Meeting, 2007, Boston, MA.
3. **Singh P** "Near Zero Emissions Solid Oxide Fuel Cell (SOFC) Power Generation Systems for Operation on Hydrocarbon and Coal Derived Fuels: Technology Review." ASM (The Materials Information Society) International Los Angeles Chapter meeting, Downey, 2008, CA.
4. Chou YS, JW Stevenson, JW Templeton, GD Maupin, G Xia, XD Zhou, ZG Yang, and **P Singh**, Evaluation of SOFC sealing materials in a single cell "stack" fixture 6<sup>th</sup> International Fuel Cell Science, Engineering and Technology Conference, 2008, Denver, CO.
5. **Singh P**, "Advanced Solid Oxide Fuel Cell (SOFC) Power Generation Systems - Technology Status and Research, Development & Engineering Needs" School of Engineering, 2007, Pullman, WA.

---

## IV.F.4 Development and Implementation of Stack Fixture Tests

Yeong-Shyung “Matt” Chou (Primary Contact),  
Jeff Stevenson, Prabhakar Singh  
Pacific Northwest National Laboratory  
K2-44, P.O. Box 999  
Richland, WA 99354  
Phone: (509) 943-5233; Fax: (509) 375-2186  
E-mail: yeong-shyung.chou@pnl.gov

DOE Project Manager: Ayyakkannu Manivannan  
Phone: (304) 285-2078  
E-mail: Ayyakkanu.Manivannan@netl.doe.gov

Contract Number: 40552

Start Date: October 1, 2007  
Project End Date: September 30, 2008

### Objectives

- Develop a solid oxide fuel cell (SOFC) stack test fixture for use by Pacific Northwest National Laboratory (PNNL) and other Solid State Energy Conversion Alliance (SECA) participants.
- Implement the test fixture in evaluation/validation of the performance of new materials, processes, and design concepts developed by PNNL and other SECA Core Technology Program (CTP) participants.

### Accomplishments

- Developed cross-flow, channeled flow field, multi-seal (cell-to-frame and perimeter seals) stack test fixture on behalf of SECA CTP.
- Validated thermal cycle stability of refractory glass cell-to-frame seals in stack test fixture.

---

### Introduction

For years, PNNL and other SECA CTP participants have relied on a wide range of materials characterization techniques (X-ray diffraction [XRD], scanning electron microscopy, energy dispersive spectroscopy [EDS], transmission electron microscopy, X-ray photoelectron spectroscopy [XPS], thermal gravimetric analysis, differential scanning calorimetry, particle size analysis, electrical conductivity, single and dual atmosphere oxidation, etc.) and sub-stack multiple component tests (e.g., “button” cell testing, area specific resistance testing of interconnect/cathode/cathode structures, and leak testing of cell/seal/interconnect structures) to

evaluate the performance of newly developed materials, fabrication processes, and design concepts. Since fiscal year (FY) 2007, PNNL has been developing and implementing a new test fixture (based on an initial design provided by Lawrence Berkeley National Laboratory) intended to evaluate/validate cell and stack component performance under realistic stack conditions. It is anticipated that results from these stack fixture tests will help to bridge the gap between typical CTP tests and the full-scale cells and stacks under development by the SECA industrial teams, and thus facilitate technology transfer from the CTP to those teams.

### Approach

The test fixture, which is based on a 50 mm x 50 mm cell, includes a cell frame component as well as anode and cathode plates simulating the anode and cathode faces of an SOFC interconnect. As a result, the fixture allows for the simultaneous testing of cell-to-frame and stack perimeter seals, anode and cathode contact materials, interconnect materials (including coatings), and cell constituents (cathode, electrolyte, anode). Most components of the modified test fixture (cell frames, anode and cathode plates, contact pastes, and seals) are fabricated at PNNL. Stack fixtures are assembled and then sealed and tested in test stands consisting of a furnace, heat exchangers, gas handling system with mass flow controllers, and electrical characterization units (BioLogic VSP potentiostats). At present, the 50 mm x 50 mm cells are acquired from H.C. Starck (anode-supported cells with lanthanum strontium manganite [LSM]/yttria-stabilized zirconia [YSZ] cathodes, type ASC3). Electrochemical performance of the cells is measured under isothermal and thermal cyclic conditions. Once the tests are complete, the stacks are dis-assembled and their components are analyzed by appropriate characterization techniques such as optical and electron microscopy, EDS, XRD, XPS, etc. Results from the tests are compared to results obtained from testing of individual components and sub-stack structures to assess intrinsic stability and inter-component reactions, and their effects on performance under stack operating conditions.

### Results

The fixture design approach has been iterative in nature, i.e., results from each fixture test have been used to identify further design changes required to optimize fixture performance. The primary features of the fixture are shown schematically in Figure 1. Activities during the first half of FY 2008 focused on improving the

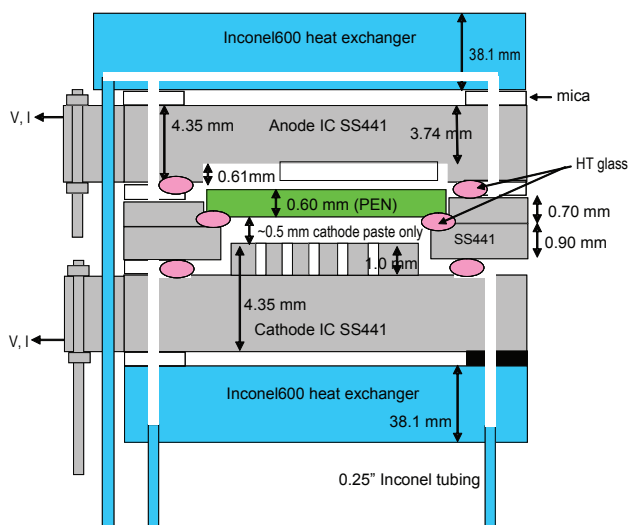


**FIGURE 1.** Schematic Illustration of Cross-Section of Stack Test Fixture

fixture design to minimize stresses on the cell, cell frame, and cell-to-frame seals, as well as the validation of the performance of refractory glass seals [1,2] under thermal cyclic conditions. The results of two recent tests (#15 and #16) are summarized in this report.

Cell Test #15 used a cross flow gas pattern with straight channel flow fields for both cathode and anode plates. The cell frame, cathode plate, and anode plate were fabricated from T441 stainless steel, provided by Allegheny Technologies, Inc. The refractory glass cell-to-frame seal was fabricated prior to test fixture assembly at 950°C/2 hours. Pastes containing LSM-20 and NiO were used as the cathode and anode contact materials, respectively. After heat treatment at 950°C for 2 hours in air (to fabricate stack perimeter seals and electrical contacts), the cell performance was measured during deep thermal cycling (room temperature to 800°C) using air and moist hydrogen as oxidant and fuel, respectively. Cell Test #15 survived only five deep thermal cycles before the open circuit voltage (OCV) at 800°C dropped from an initial value of ~1.90 V to ~1.02 V, at which point the test was terminated. Post-test analysis of Cell Test #15 indicated two types of failure. The cell-to-frame glass seal had fractured near one corner, resulting in leakage which led to alloy corrosion (arrow in Figure 2A). In addition, the cell contained several cracks (arrows in Figure 2B). The cell-to-frame seal failure may have been related to the lack of a protective coating on the T441 steel frame, which allows the formation of Sr or Ba chromate at seal edges exposed to air. The failure after five cycles was likely the result of a change in thickness (shrinkage) in the perimeter seal. This can be visualized using the cross-section schematic view shown in Figure 1. In these tests, Ni-mesh with NiO paste was used for anode side current collection while LSM contact paste was used for cathode side

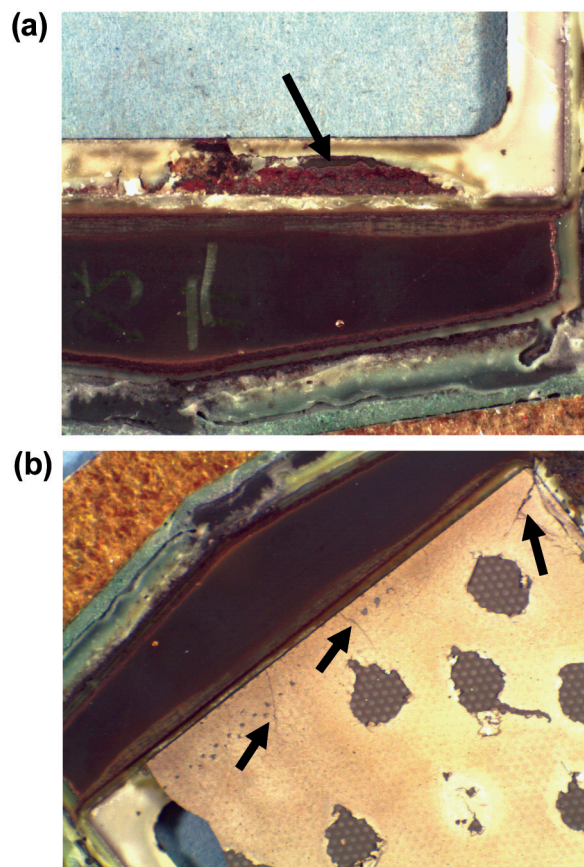


**FIGURE 2.** Optical Micrographs of Cell Test #15 after Five Deep Thermal Cycles Showing Two Types of Failure: (a) Glass Seal Failure near the Corner of Cell-to-Frame Seal (Arrow), and (b) Cell Fracture (Arrows)

current collection, without any metallic conducting mesh, which can offer some dimensional compliance. Thus, the anode side current collector was relatively compliant at elevated temperatures while the cathode side current collector remained rigid. As a result, thinning of the perimeter seals may have resulted in an "opening stress" on the cell-to-frame seals leading to the observed failure mechanisms.

Based on the post-test analyses of previous cell tests including Cell Test #15, a dimensional stabilizer was included between the cell frame and anode plate near the cell-to-frame glass seal. Cell Test #16 was then conducted to evaluate the effectiveness of the stabilizer concept. Similar to Cell Test #15, Cell Test #16 used a cross flow gas pattern with straight channel flow fields for both cathode and anode plates. The cell frame, cathode plate, and anode plate were fabricated from T441 stainless steel. The refractory glass cell-to-frame seal was fabricated prior to test fixture assembly at 950°C/2 hours. After heat treatment at 930°C for 2 hours in air (to fabricate stack perimeter seals and electrical contacts), the cell performance was measured during deep thermal cycling (room temperature to

750°C) using air and moist hydrogen as oxidant and fuel, respectively. The results of thermal cycle tests on cell #16 were promising, as a constant OCV of 1.105-1.100 V was observed at 750°C over 25 cycles, at which point the test was terminated (Figure 3). Thus, the addition of a dimensional stabilizer may have helped to balance stresses on the cell-to-frame seal (cf. Cell Test #15, which only survived five thermal cycles). During post-test analysis, no discernable fractures were evident in the refractory glass cell-to-frame seal or at the anode surface (as previously observed in Cell Test #15 [Figure 4]). However, when red dye in isopropanol was applied to the cell on the cathode side to identify possible fracture and leakage origins penetration of the red dye to the anode side of the cell indicated that fracture may have occurred within the thin YSZ electrolyte membrane during testing, although pinholes from the manufacturing process could also have been responsible for the dye penetration. Nevertheless, the results of Cell Test #16 provided an encouraging demonstration of

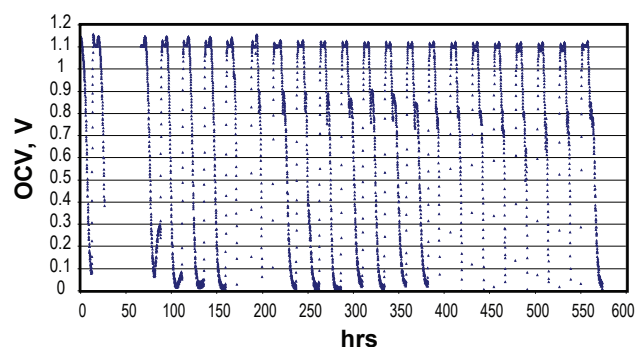


**FIGURE 3.** OCV of Cell Test #16 During Deep Thermal Cycle Testing Between Room Temperature and 750°C

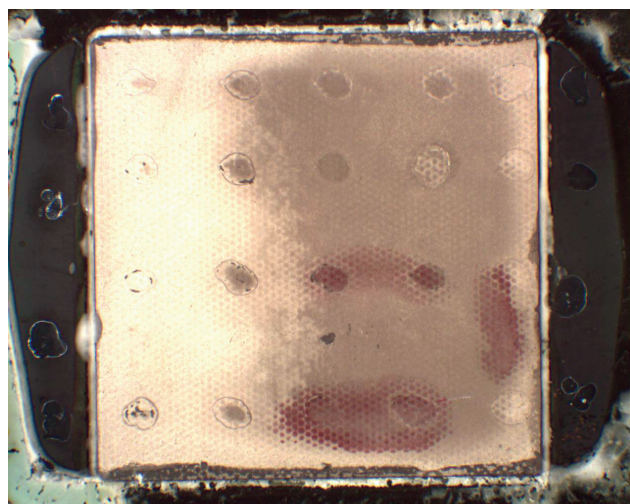


**FIGURE 4.** Post-Test Analysis of Cell Test #16 after 25 Deep Thermal Cycles

the robustness of the refractory glass cell-to-frame seals towards deep thermal cycling.

## Conclusions and Future Directions

During FY 2008, design modifications to the CTP stack test fixture led to improved performance and stability of glass seals during thermal cyclic testing. For example, a recent stack fixture test, Cell Test #16, maintained a consistent OCV of ~1.103 V at 750°C through 25 deep thermal cycles. Post-test analysis showed no degradation of the refractory glass cell-to-frame seal. Future directions will include continued fixture modification/optimization to a) minimize unbalanced stresses upon cells and cell frames, and b) allow for testing of multiple cell stacks. Near-term materials validation efforts using the stack test fixture will be focused on isothermal testing (up to 1,000 hours) of T441 steel cathode plates with Ce-modified spinel coatings [3] on exposed surfaces, and aluminized surfaces [4] in the sealing areas.

## References

1. Y-S Chou, J.W. Stevenson, and P. Singh, "Novel refractory alkaline earth silicate sealing glasses for planar solid oxide fuel cells," *J. Electrochem. Soc.*, **154**, B644 (2007).
2. Y-S Chou, J. W. Stevenson, and P. Singh, "Effect of pre-oxidation and environmental aging on the seal strength of a novel high temperature SOFC sealing glass with metallic interconnect," *in press*.
3. Z.G. Yang, G.G. Xia, J. Templeton, Z. Nie, J.W. Stevenson, and P. Singh, "Low Cost Ferritic Alloy Interconnects & Coatings Development," FY 2008 Office of Fossil Energy Fuel Cell Program Annual Report.
4. Y.S. Chou, K.S. Weil, J.W. Stevenson, and P. Singh, "Development of Seals and Seal/Interconnect Interfaces," FY 2008 Office of Fossil Energy Fuel Cell Program Annual Report.

---

## IV.F.5 Novel Low Temperature Solid State Fuel Cells

Jiang Liu, Gregory Collins, Patrick Nash, and  
Chonglin Chen (Primary Contact)

Department of Physics and Astronomy  
University of Texas at San Antonio  
One UTSA Circle  
San Antonio, TX 78249-1644  
Phone: (210) 458-6427; Fax (210) 458-4919  
E-mail: cl.chen@utsa.edu

DOE Project Manager: Patricia Rawls

Phone: (412) 386-5882  
E-mail: Patricia.Rawls@netl.doe.gov

Contract Number: 43063

Start Date: December 16, 2006  
Project End Date: December 15, 2009

### Objectives

- Develop an intermediate temperature (650-750°C) electrolyte material that is capable of ionic conduction comparable to present high temperature materials (>850°C).
- Combine electrolyte with specific cathode and anode materials that work in unison to achieve a more efficient, longer lasting solid oxide fuel cell (SOFC).
- Create and test cathode/electrolyte and anode/electrolyte half-cells as well as whole unit cells to optimize the cell function.

### Accomplishments

- New cathode material, praseodymium doped barium cobalt oxide (PBCO), deposited epitaxially onto selected substrates with characterization showing excellent mixed conductivity.
- Multilayered electrolyte material, consisting of gadolinium doped cerium oxide (GCO) and yttrium stabilized zirconia oxide (YSZ), constructed in various ratios and thicknesses and compared for functionality.
- Cathode/electrolyte half-cells produced with ionic conduction/electronic leakage tested via impedance spectroscopic methods.
- Anode material,  $Y_xBaCe_{1-x}O_3$  (YBCO), identified and preliminary investigation conducted to ascertain the optimum deposition and growth conditions.

---

### Introduction

The electrolyte in an SOFC has multiple requirements that must be met to accomplish the reactions necessary for SOFC functionality. To be successful, both ionic conduction as well as electronic insulation must be intrinsic qualities of the material. Much research has been conducted in the use of bulk materials that have a combination of these traits. However, these materials offer only mixed proportions of these properties and so a compromise must be accepted with the application of these bulk materials.

GCO offers excellent ionic conduction but is also an electronic conductor. YSZ is also ionic conductive, from approximately 500°C and above, but is also an electronic insulator. The combination of these two materials in a thin film construction offers an electrolyte that will function in a fuel cell but at a lower temperature than that of the bulk materials. This lower temperature will allow the use of less exotic interconnect materials as well as reducing thermal damage to the cell thereby extending the cell's life.

### Approach

The mixed conductive material GCO and the ionic conductive/electronic insulator YSZ will be studied in different stoichiometric combinations. The target of this research is to create a multilayered structure so that the benefits of two different materials may be combined to realize a superior electrolytic material. Construction of the structure will be accomplished through pulsed laser deposition methods. Testing and characterization of the materials will be conducted with X-ray diffraction (for crystallographic information), tunneling electron microscopy (for surface morphology) and a combination of impedance spectroscopy and a/c resistance measurements (for electrochemical analysis).

The application of this multilayered structure onto the chosen cathode material, PBCO, and the proton conductive anode material, YBCO, will be carried out to produce half-cell and whole-cell structures. The conductive properties of these structures will be analyzed with impedance spectroscopy to obtain the chemical activation energies. The application of these films onto the YBCO, which also acts as the support structure, by sputtering and other methods will also be explored.

## Results

We have fabricated highly mixed conductive PBCO thin films on various substrate materials such as SrTiO<sub>3</sub> (STO), LaAlO<sub>3</sub> (LAO), NdGaO<sub>3</sub> (NGO), and MgO. An X-ray  $\theta$ - $2\theta$  diffraction contour plot of an as-grown PBCO thin film shows that the as-grown films are predominantly *a*-oriented. The rocking curve measurement of the (200) reflection has a full width at half maximum of 0.1 degree indicating that the film on STO substrate has excellent single crystallinity and epitaxial behavior. The crystallinity and epitaxial quality of the as-grown films were further investigated by transmission electron microscopy (TEM). A dark field cross sectional TEM image shows that two types of domain structures exist on the interface, which agrees with the synchrotron studies.

The impedance measurements on the as-grown PBCO thin films suggest that the electrical conductivities of the PBCO thin films are highly dependent upon the measuring temperature and the interface strain. The lattice mismatches between the PBCO films and substrates can be simply estimated by the standard crystal lattice parameters. It is easy to find that the PBCO films are tensile on both NGO and LAO but become strain on both MgO and STO. As seen from Figure 1, the electrical conductivities of PBCO films on these substrates in air have been measured to determine the high temperature transport properties. With the increase of the temperature, the conductivity exponentially increases due to thermal activation and becomes steady around 400°C. It is interesting to note that the PBCO films tensile strain, on LAO and NGO substrates, have excellent electrical conductivity, ~102 S/cm<sup>2</sup>, over a very broad temperature

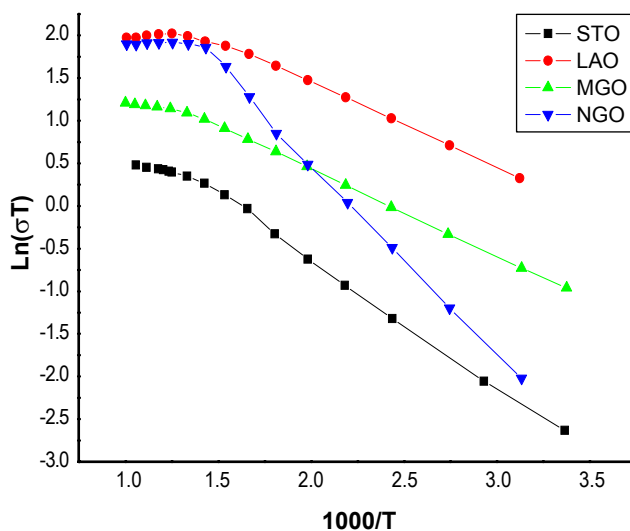
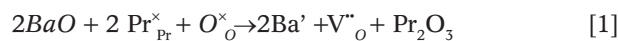


FIGURE 1. The Impedance Measurement for the PBCO Films on Various Substrates

region of 700 to 1,000 K. In contrast, the films with relaxed strain, on STO and MgO, have relative lower electrical conductivity. In the high temperature range (higher than 400°C), tensile strained films show much better conductivity. Also, compared with the traditional electrode materials such as (La,Sr)MnO<sub>3</sub> or (La,Sr)(Co,Fe)O<sub>3</sub>, PBCO thin films have much better electrical conductivity especially in the low temperature region. To understand the mechanisms of the electrical conductivity and the strain effect on the physical properties, the co-principle investigator (Prof. P. Nash) has formulated a point defect model in which mobile electrons and electron holes are assumed to be localized on specific Co-site ions. Electrons localize on Co<sup>2+</sup> = Co' = Co' Co sites and holes (small polarons) on Co<sup>4+</sup> = Co<sup>x</sup> = Co' Co. The substitution of Ba<sup>2+</sup> = Ba' = Ba' Pr for Pr<sup>3+</sup> = Pr<sup>x</sup> = Pr<sup>x</sup> Pr in the PrCoO<sub>3</sub> perovskite lattice requires charge compensation. Electroneutrality can be maintained in two ways: either by a valence change of the Co-site cation = Co<sup>3+</sup> = Co<sup>x</sup> = Co<sup>x</sup> Co (creation of holes, electronic compensation) or by the formation of oxygen vacancies V<sub>O</sub> (ionic compensation). In general, both processes occur and compete with each other, depending on composition, oxygen partial pressure and temperature. We assume that the defect chemistry of PrBaCo<sub>2</sub>O<sub>6-2δ</sub> can be described by the following three reactions:



Here the oxide lattice site anion is denoted O<sup>2-</sup> = O<sup>x</sup>O. This system of equations provides a partial mathematical expression that substitution of Ba<sup>2+</sup> for Pr<sup>3+</sup> in the PrCoO<sub>3</sub> lattice is electronically compensated by the oxidation of Co<sup>x</sup> = Co<sup>3+</sup> cations to Co<sup>4+</sup> and the formation of oxygen vacancies V<sub>O</sub>. This system of equations is completed by overall electroneutrality conditions, which can be represented by

$$[Ba'_{Pr}] + [Co'_{Co}] = [Co^x_{Co}] + 2[V_O''] \quad [4]$$

$$[Co^x_{Co}] + [Co'_{Co}] + [Co^x_{Co}] = 1 \quad [5]$$

$$[O_O^x] + \delta = 3 \quad [6]$$

We expect that when the temperature increases or the pO<sub>2</sub> (O<sub>2</sub> pressure) decreases, the equilibrium of Eq. [3] shifts to the right. As a result, oxygen vacancies V<sub>O</sub> are formed, at the expense of two holes for each V<sub>O</sub>. Therefore a loss of lattice oxygen takes occurs when the temperature increases.

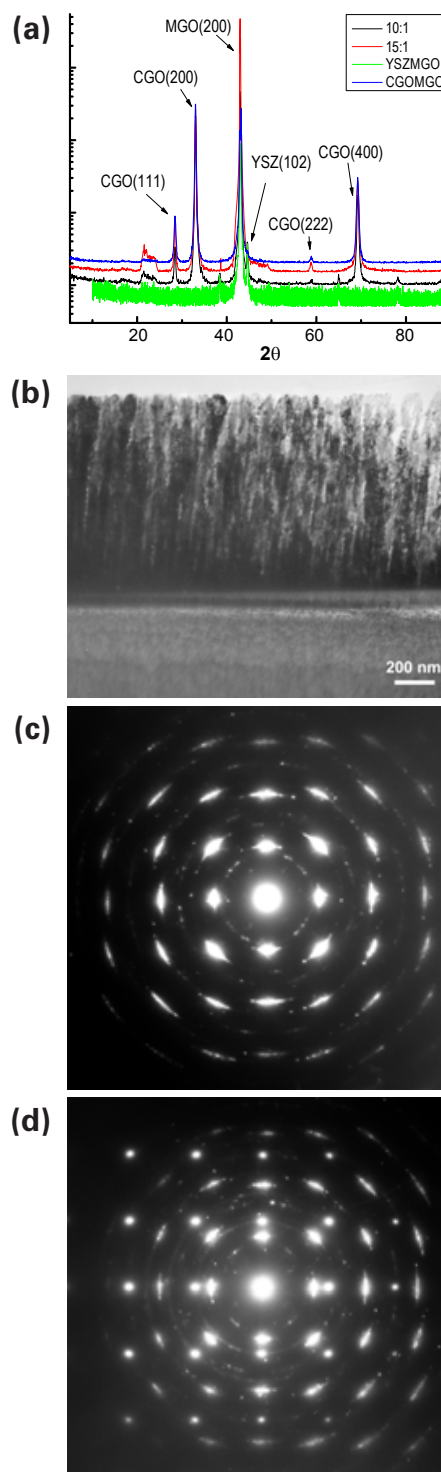
Recently, we have fabricated and systematically studied the multilayered GCO/YSZ structures for new electrolytic materials with various stoichiometric combinations on (001) MgO substrates. We have synthesized the various thickness ratio combinations (10:1, 15:1) of GCO and YSZ and different numbers of stacks (four layers, eight layers, etc.) while keeping the same total film thickness.

Figure 2(a) is the X-ray diffraction pattern showing that the as-grown multilayered GCO/YSZ systems have good crystallinity. As seen from Figure 2(b), the as-grown multilayered YSZ/GCO thin films have good crystalline quality with a columnar structure which is the typical structure for thin films grown with a large lattice misfit. The selected area electron diffractions were taken from the film, Figure 2(c), and the film/substrate interface, Figure 2(d), indicating that the as-grown multilayers are good single crystalline with c-axis oriented. The selected area electron diffraction covering the interface area reveals a surprisingly good epitaxial quality and the interface relationship can be determined to be (001)film// (001)MgO and [100]film// [100]MgO, which gives a huge lattice misfit of as large as 22%. The epitaxial nature will be investigated by using the high resolution electron microscopy soon for more detailed information since the current TEM images cannot provide detailed atomic structures in the multilayered film structures and the information about the multilayered interfaces.

The impedance measurements on the multilayered samples with the GCO/YSZ = 10:1 and different numbers of stacks have been accomplished in both pure oxygen and air within the temperature range of 600°C to 900°C, together with the single layered YSZ and GCO for comparison (Figure 3). The temperature dependence of the conductivities of the as-grown YSZ/GCO multilayer structures in air is very similar to that in pure O<sub>2</sub> for various numbers of stack (four layers, eight layers, 16 layers) but with the same total thickness. The multilayered structures were also fabricated on the (La,Sr)CoO<sub>3</sub> bottom electrodes for testing the current leakage in the multilayered structures and the experimental setup has been completed. The results for the electron leakage in the multilayered structures should be completed by the next report period.

## Conclusions and Future Directions

We continue to focus on the fabrication and characterizations of mixed conductive PBCO and multilayered ionic conductive GCO and YSZ structures on various substrate materials, and to understand the interface behavior and ionic transport dynamics of oxygen, the systematical investigation of the multilayered GCO and YSZ structures on various substrates. To better understand the interface effect on the physical



**FIGURE 2.** Microstructure characterizations indicate that the as-grown multilayered GCO/YSZ thin films have good crystallinity and highly oriented. (a) X-ray diffraction patterns showing the microstructures of the as-grown multilayered GCO/YSZ structures, (b) cross sectional TEM image showing the microstructures of the films, (c) selected area electron diffraction patterns from the multilayered film area showing film has good single crystal quality, and (d) selected area electron diffraction patterns from the interface area showing that the film and substrate have a good interface relationship.

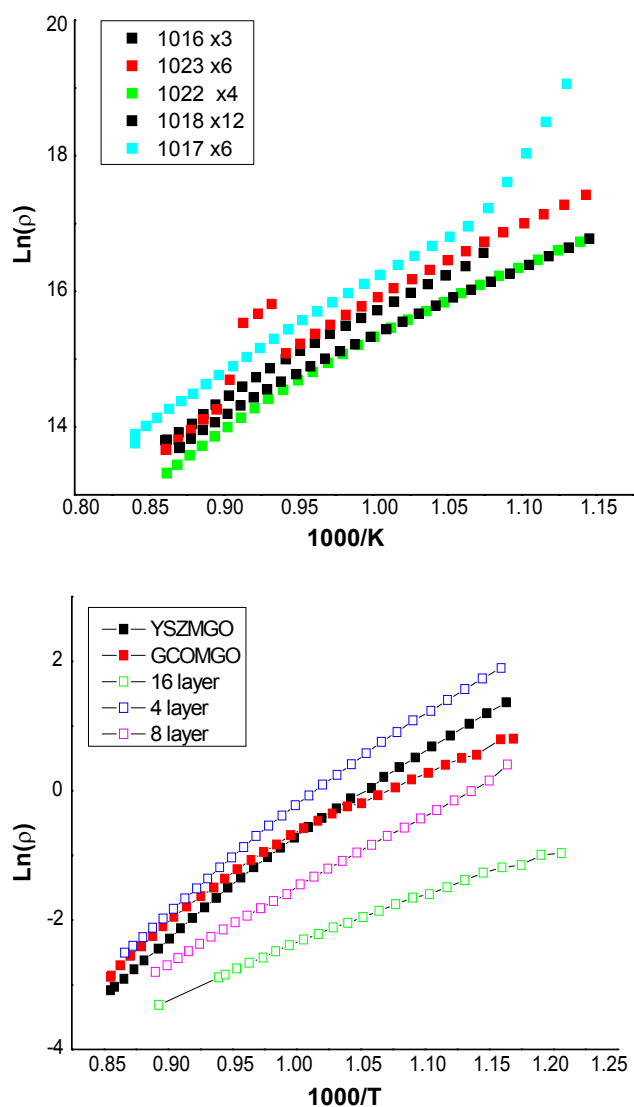


**FIGURE 3.** The impedance measurement for the multilayered GCO/YSZ structures with various combinations on (001) MgO substrates: (bottom) in pure oxygen and (top) in air.

properties, a high resolution TEM characterization will be performed in the next few weeks. Models for understanding the thickness and interface effects on the ionic transport properties of these multilayered structures are under development. The purpose of the YSZ layer in the multilayered structures is to block the electronic conduction, to enhance the quality of the electrolyte materials and to lower the operation

temperature from 800°C to 600°C. On the other hand, optimization of the half-cell structures from PBCO/YSZ and PBCO/GCO will be the next topic of focus to determine the best interface structures for the cathode/electrolyte interface. We also plan to start the fabrication and characterization of the advanced proton conductive YBCO for anode use. We will systematically study the physical properties and ionic transport behavior of each material (YBCO, PBCO, and multilayered GCO/YSZ structures). We will fabricate various crystal structures and different crystal grain sizes, and will comprehensively analyze the physical properties and interface phenomena of each material and the effects from interface, size, and strain.

The authors would like to thank the National Energy Technology Laboratory and Dr. Patricia Rawls for the support on this research.

### Special Recognitions & Awards/Patents Issued

1. C. L. Chen, J. Liu, G. Collins, “2008.024.UTSA: Multilayered YSZ/GCO structure for intermediate temperature fuel cell applications,” patent disclosure.

### FY 2008 Publications/Presentations

1. Z. Yuan, J. Liu, C. L. Chen, C.H. Wang, X.G. Luo, X.H. Chen, G.T. Kim, D.X. Huang, S.S. Wang, A.J. Jacobson, and W. Donner, “Epitaxial Behavior and Transport Properties of  $\text{PrBaCo}_2\text{O}_5$  Thin Films on (001)  $\text{SrTiO}_3$ ,” *Appl. Phys. Lett.*, **90** (2007) 212111.
2. J. Liu, G. Collins, C.L. Chen, J.C. Jiang, E.I. Meletis, “Ionic Transport Properties in Multilayered GCO/YSZ structures”, submitted to Solid State Ionics.
3. C.L. Chen (invited talk), “Remarkable new class of ionic conductive oxide thin films for intermediate temperature fuel cells”, the 2008 International Materials Research Conference, Chongqing, P.R. China, June 9–12, 2008.
4. C.L. Chen (invited talk), “Remarkable new class of ionic conductive oxide thin films for intermediate temperature fuel cells”, the Summer School Workshop on Advanced Materials, Shenyang, P.R. China, July 7–9, 2008.
5. C.L. Chen (invited talk), “Remarkable new class of ionic conductive oxide thin films for intermediate temperature fuel cells”, the 08 Materials Sciences and Technology, Pittsburgh, Pennsylvania, October 5–9, 2008.

---

## IV. SECA CORE RESEARCH & DEVELOPMENT

### G. Fuel Processing



---

## IV.G.1 Waterless 5 kWe Diesel Reformer

Craig Thompson

Aspen Products Group, Inc.  
186 Cedar Hill St.  
Marlborough, MA 01752  
Phone: (508) 480-5058 Ext. 166; Fax: (508) 480-0328  
E-mail: cthompson@aspensystems.com

DOE Project Manager: Ayyakkannu Manivannan  
Phone: (304) 285-2078  
E-mail: Ayyakkannu.Manivannan@netl.doe.gov

Contract Number: 84662

Start Date: May 20, 2007  
Project End Date: March 19, 2008

### Objectives

- Conduct a systems analysis to determine optimal reformer operating point and system mass and energy flows for a diesel fuel processor with integrated non-condensing, high-temperature water recovery.
- Identify a fuel reformer catalyst that is active and stable under conditions ranging from dry startup (catalytic partial oxidation – CPOx) to stable operation with recycled water (autothermal reforming – ATR).
- Demonstrate stable long-term operation on 50 ppm sulfur diesel, including turndown operation.

### Accomplishments

- A fuel processor design was developed that produces thermodynamically stable reformat (no danger of carbon deposition from carbon monoxide disproportionation) without the need for an external water supply.
- A fuel processor system model was developed that incorporates the fuel reformer, solid oxide fuel cell (SOFC), and high-temperature water recovery. The model was used to choose operating conditions resulting in greater than 80% efficiency (lower heating value [LHV] basis) for startup, normal, and turndown operation.
- Five catalyst formulations were screened for activity and stability at the design operating points. The chosen catalyst had the demonstrated ability to maintain high fuel reforming activity through repeated cycles of high temperature CPOx operation.

- Long-term durability of the catalyst was demonstrated over a 250-hour period that included simulated dry (no water recycle) startups followed by extended ATR operating periods.
- A turndown ratio of 4:1 was demonstrated over a 50-hour run.

---

### Introduction

SOFC-based power generation systems are attractive candidates to replace conventional diesel-fueled generators and auxiliary power units (APUs) because of their promise of greater fuel efficiency, efficient operation at part load, and low environmental signature. However, an efficient method of converting fuel into a SOFC-usable gas containing hydrogen, carbon monoxide, and methane is necessary in order to enable the use of SOFCs as APUs operating on diesel.

A fuel processor suitable for use with a fuel cell as an APU for early markets such as class 8 trucks, recreational vehicles, marine crafts, and military generators must meet the additional requirements of being light, compact, and simple, and it must operate independently of water. By reclaiming water available in the fuel cell exhaust through a high-temperature water recovery component, steam can be made available to the fuel reformer without the need for an external water source or bulky and complex water recovery equipment. Using such a method in conjunction with a reforming catalyst that can operate stably at both dry CPOx and ATR conditions, the benefits from the reactant steam content to system durability and product reformat stability can be achieved in a compact and simple package.

### Approach

A water-independent fuel processor was designed that starts up dry, in CPOx mode, and then automatically transitions to ATR or “wet CPOx” mode as water becomes available from the fuel cell exhaust. Water recovery is accomplished using a passive high-temperature water permselective membrane that does not require condensation and the associated added weight and volume of cooling hardware. The complete fuel processor design consists of a fuel reformer, fuel injector/mixer, passive water recovery component, and advanced balance of plant. A process schematic is shown in Figure 1.

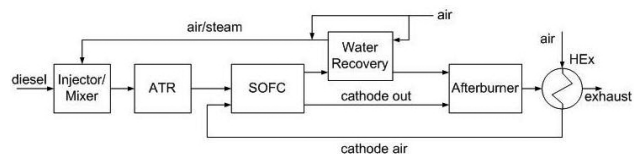


FIGURE 1. Waterless Reformer and SOFC Schematic

A system model was developed, and it was used to define representative operating points for startup, normal operation, and turndown. These operating points were used to choose test conditions for both catalyst screening and the extended run demonstrations. A catalyst was chosen from screening tests based on activity at steady state conditions and ability to maintain activity through dry startup conditions. This catalyst was then used for a long-term durability demonstration followed by a turndown ratio demonstration.

### Results

The system model developed during the project was used to predict fuel processor performance and to choose optimal operating conditions for normal, turndown, and startup conditions. A summary of the three operating points is shown in Table 1. Taking into account assumptions for parasitic power requirements and SOFC efficiency, the normal and turndown conditions correspond to 5 kWe and 1 kWe, respectively.

TABLE 1. Operating Conditions Analysis

	Normal	Turndown	Startup
Reformate LHV (kW)	15	3.8	8.5
Maximum Thermal Efficiency (%)	86	82	82
Water Recovery (%)	60	59	0
ATR Temperature (°C)	800	800	1025
Reformate H <sub>2</sub> Conc. (% dry gas)	32	30	22
Reformate CO Conc. (% dry gas)	16	15	24

Catalyst screening tests were run to identify a catalyst capable of sustained operation at the design conditions. Catalyst screening was carried out using the following procedure: (1) initial screening at three throughput levels, (2) exposure to the high temperature operating conditions present during waterless (CPOx) startup, and (3) final screening to determine effect on performance of CPOx operation.

Screening results are presented in Figure 2 and Figure 3. Results are shown for Aspen Products Group’s (APG’s) state-of-the-art CPOx catalyst, ATR catalyst, and three compositions combining elements of both CPOx and ATR. Figure 2 shows a comparison

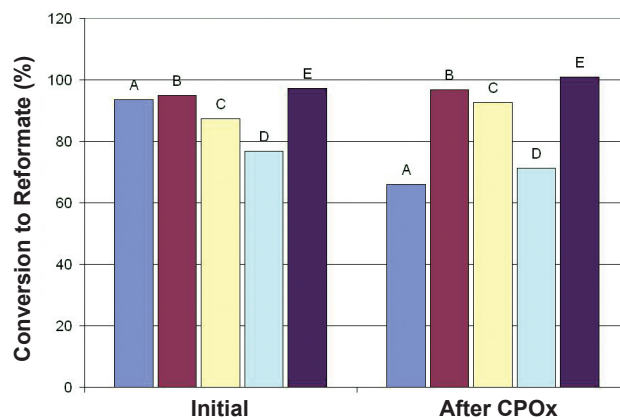


FIGURE 2. Catalyst screening comparison, conversion to H<sub>2</sub>, CO, and CH<sub>4</sub>. A - APG CPOx catalyst; B - APG ATR catalyst; C, D, E - hybrid catalyst formulations.

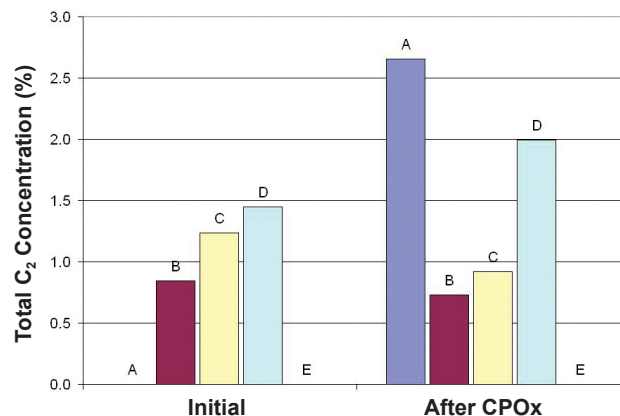


FIGURE 3. Catalyst screening comparison, sum of C<sub>2</sub>H<sub>2</sub>, C<sub>2</sub>H<sub>4</sub>, and C<sub>2</sub>H<sub>6</sub> in the product reformat. A - APG CPOx catalyst; B - APG ATR catalyst; C, D, E - hybrid catalyst formulations.

of diesel conversion for the catalysts, defined as the total carbon atoms in the product reformat (carbon monoxide, carbon dioxide, and methane) divided by the total carbon atoms in the inlet fuel (50 ppm sulfur diesel), before and after CPOx exposure. Figure 3 shows the sum of C<sub>2</sub> hydrocarbon concentrations in the product reformat. The best performing catalyst was formulation E, which had no detectable C<sub>2</sub> hydrocarbons in either the initial or final screening tests, and had complete conversion (within the limits of accuracy of the gas chromatograph analyses and the calculation method) of the diesel to reformat at the conditions tested.

Catalyst formulation E was then tested for a 250-hour extended run. The run included four simulated dry startups. Over the 250 hours of operation, thermal efficiency remained between 70% and 80%. An additional 50 hours of operation were carried out at a turndown ratio of 4:1.

## Conclusions and Future Directions

- A system analysis of the entire fuel processor/fuel cell system indicates that a system design using a multifunctional reforming catalyst and passive, high-temperature water recovery will allow operation at conditions that benefit system mechanical durability and thermal efficiency, and produce thermodynamically stable reformat.
- The design results in thermal efficiency greater than 80% at all design operating conditions.
- The catalyst formulation identified through the screening runs is capable of long-term operation with minimal performance loss from exposure to the harsh conditions of waterless startup.
- A turndown ratio of at least 4:1 is possible while maintaining thermal efficiency greater than 80%.

In the next phase of this project, research and development will take place in the areas of:

- Catalyst durability improvement
- Water recovery module development
- Diesel injector/mixer development
- Reactor and system design

## IV.G.2 SOFC Integrated Multi-Mode Diesel Reformer

Joseph J. Hartvigsen (Primary Contact),  
Piotr Czernichowski, Michele Hollist

Ceramatec, Inc.  
2425 South 900 West  
Salt Lake City, UT 84119  
Phone: (801) 978-2163; Fax: (801) 972-1925  
E-mail: jjh@ceramatec.com

DOE Project Manager: Ayyakkannu Manivannan  
Phone: (304) 285-2078  
E-mail: Ayyakkannu.Manivannan@netl.doe.gov

Contract Number: 84663

Start Date: June 20, 2007  
Project End Date: March 19, 2008

- The new reformer design successfully reformed both the current ultra-low-sulfur highway diesel fuel and military high-sulfur jet fuel.
- Reformed diesel dry with a fuel equivalent ratio  $\phi=2.7$  ( $\eta_{\text{Faradaic}}=63\%$ ).
- Reformed diesel with simulated anode tailgas recycle at  $\phi=7.2$  ( $\eta_{\text{Faradaic}}=87\%$ ).

### Objectives

- Tailor reformer design for thermal integration with a specific solid oxide fuel cell (SOFC) auxiliary power unit (APU) configuration.
- Develop process model to provide overall system mass and energy balances.
- Exercise process model to design experimental conditions and reactant flow rates.
- Create reformer solid model and fabrication drawings in computer-aided design (CAD) system.
- Source reformer components, fabricate new design, and install in test system.
- Operate reformer over the range of reactant flow rates suggested by the process model.
- Demonstrate the operational flexibility of partial oxidation diesel reforming with system efficiency values previously attainable only in thermally integrated steam reforming systems.

### Accomplishments

- A plasma-catalyzed diesel reformer was redesigned for packaging within the thermal enclosure of an SOFC APU.
- The design range of feed flow rates was mapped using process modeling software.
- The feed flow rates range from simple partial oxidation mode to endothermic reforming mode using an anode tailgas recycle configuration.
- A prototype reformer was fabricated and installed in a test system.

### Introduction

The DOE has invested in excess of \$200 million over the first few years of the Solid State Energy Conversion Alliance to bring SOFC technology to market by the year 2010. Diesel APUs for military, commercial/industrial, and consumer applications are a particularly attractive early opportunity for SOFC technology, as illustrated in Figure 1. Diesel fuel, while attractive because of its wide availability (including onboard stores of motor fuel in many envisioned applications), high energy density, safety and storability (low volatility/high flash point), poses a significant challenge to fuel cell developers because it is much more difficult to reform than lighter and cleaner fuels such as natural gas, propane, and methanol. Diesel and jet fuels have not been successfully reformed using SOFC coupled catalytic steam reforming, which is the most efficient process where feasible. Industrially, two processes, partial oxidation (POx) and high-pressure hydro-desulfurization (HDS) coupled with steam reforming, have been practiced. Currently, HDS systems are considered too large and complex to be used in the presently envisioned mobile APU applications. Some success in developing smaller systems has been achieved with partial oxidation or its variants incorporating precious metal catalysts. In the partial oxidation process (POx, catalytic POx, autothermal reforming), a sub-stoichiometric amount of air is combined with the fuel and burned, with or without a catalyst and/or steam, to reform the fuel.

One of the most attractive features of a liquid fueled SOFC generator is the potential for much higher operating efficiency than is available using an internal combustion engine driven generator. However, if the reformer utilizes a partial oxidation process, a system basis efficiency penalty as high as 40% will be incurred, reducing the overall SOFC system efficiency to below that of modern small diesel engine driven generators. Often, reformer efficiency is quoted in terms of reformate heating value or "cold gas efficiency," which may be in the 70-80% range. However, since a fuel cell is not a heat engine, a more relevant measure of efficiency would



FIGURE 1. Applications for a Diesel Fueled SOFC APU

be to compare the fuel value of reformat with that of the raw fuel, on the basis of the potential to produce current (Faradaic efficiency) in a fuel cell. Reformate produced by partial oxidation loses the potential to supply 4 electrons to the load circuit for each molecule of oxygen used in the fuel cell, relative to a hypothetical fuel cell running on the raw fuel. Consequently, the efficiency penalty of partial oxidation reformers is the direct and inescapable result of oxygen addition in the reforming process. A conceptual SOFC integrated multi-mode diesel reformer was carried forward to a detailed design, which was then fabricated and tested. This project demonstrated a means of reforming diesel fuel that minimizes the amount of oxygen needed to reform the fuel. This will enable development of diesel fueled SOFC APUs with the requisite operational flexibility and fuel efficiency.

### Approach

The reforming reaction is highly endothermic, on the order of 25-30% of the fuel heating value. When this heat is supplied by combusting a portion of the fuel, the corresponding fraction of current producing potential (Faradaic efficiency) is lost. This is true even though the remaining reformate products embody a higher heating value per unit oxygen affinity than the raw fuel, since it is the oxygen affinity or current producing capacity of the fuel and not the heating value of the fuel that produces power in a fuel cell. With an SOFC, it is not necessary to burn fuel for the purpose

of providing the heat of reformation as the SOFC stack rejects a sufficient quantity of heat to supply the heat of reformation, and does so at a temperature that is high enough to drive the reforming reaction. SOFC systems fueled by natural gas have been able to exploit this chemical recuperation effect using a thermally integrated steam reformer. However, catalytic steam reforming has not been an option for fuels with high sulfur and aromatic content such as diesel and kerosene.

The use of non-thermal plasma in place of catalyst has shown excellent results (Figure 2). The plasma creates a continuously renewed stream of active species that initiate chain reactions, wherein a large number of molecules react for each chain initiating species

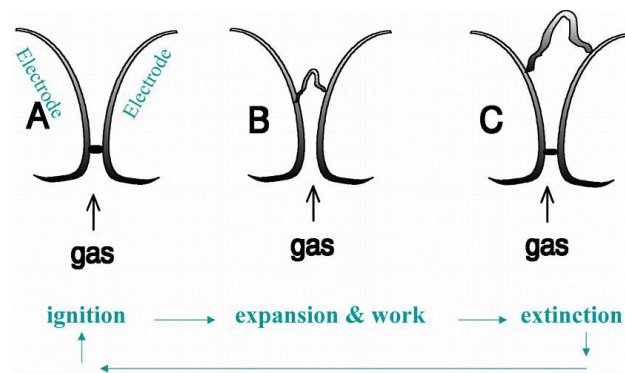


FIGURE 2. Non-Thermal Plasma Reformer Operating Principle

created in the plasma. Employing the more efficient steam reforming scheme places restrictions on the reaction vessel geometry. The larger the reactor cross-section, the lower the ratio of external surface area to reaction volume, which limits the rate at which heat can be supplied to the reformer. This is an issue that is side-stepped with partial oxidation processes, as the heat of reformation is supplied not by heat transfer, but by combustion within the vessel. The redesign of the plasma reformer created a configuration that can be physically and thermally integrated with the stacks inside the SOFC APU thermal enclosure (Figure 3). Given that the function of the reformer is to feed a fuel cell, which is used to generate electric power where none is otherwise available, a frequent objection to the use of a plasma reformer is that of electric power consumption. Our experience continues to show that the power required to produce the plasma is minimal, about 1.2% of the energy represented by the fuel reformed. The efficiency penalty associated with partial

oxidation is by far the largest loss in the fuel processor and was therefore the focus of this project. However, since steam and  $\text{CO}_2$  from anode tailgas are not available at startup and very low load conditions, and since many circumstances do not permit carrying water needed in steam reforming, the reformer must be capable of operating in simple POx mode as well as in the more efficient endothermic steam reforming mode using anode tailgas recycle.

## Results

The object of reforming is to break hydrocarbon molecules into hydrogen and carbon monoxide that can be used as fuel in the SOFC. Each carbon atom in the hydrocarbon backbone must be joined with an oxygen atom, supplied either from free oxygen in air or from bound oxygen in steam or carbon dioxide, in order to cap the severed C-C and C-H bonds of the hydrocarbon. Thus, the atom ratio of oxygen to carbon (O/C) in the feed becomes important. As a minimum, the value of O/C must be greater than 1 to make a full yield of CO possible instead of forcing the formation of solid carbon. However, only free oxygen that will support partial combustion is considered in the fuel equivalence ratio  $\phi$  that we are trying to maximize (minimize use of free oxygen) in order to increase the SOFC system efficiency. A chemical process model that computes the mass and energy balances and equilibrium thermodynamics was used to derive the reactant flow rates giving desired range of values of O/C and  $\phi$ . The  $\phi$  range of focus in this project is shown in Figure 4, where values  $\phi < 3.5$  are prior results obtained in simple partial oxidation mode, while values  $\phi > 4.5$  show results of plasma catalyzed steam reforming mode. This center range,  $3 < \phi < 5$ , covers the multi-mode transition from the purely POx operating mode to endothermic anode tailgas recycle reforming mode.

By decreasing POx air flow as stack current and anode tailgas recycle ratio are increased, the overall O/C ratio (accounting for both O and C being recycled in the form of  $\text{H}_2\text{O}$ , CO and  $\text{CO}_2$ ) can be increased while simultaneously decreasing the  $\phi$  based on raw fuel and oxygen from air. The process model assumed a stack fuel utilization of 80%. The model-calculated target operating line as  $\phi$  is increased is shown in Figure 5, with the same results as a function of anode tailgas recycle ratio shown in Figure 6.

The new configuration and detailed physical design are still proprietary until the intellectual property protection is in place. The design is an evolutionary step from the plasma catalyzed steam reformer developed under a prior Air Force Small Business Innovative Research project. Reforming runs with this earlier design were employed earlier in the project to confirm the efficiency improvement of the modeled operating modes, but the unit was too large for effective

Component	weight (kg)	#	total (kg)
1 Stack	15	4	60
2 Inlet manifold	4	4	16
3 Outlet manifold	3	2	6
4 HX	1.1	1	1.1
5 Reformer	5	4	20
6 Air blower	16	1	16
7 Fuel pump	2.7	2	5.4
8 Desulfurizer	5	4	20
9 Air filter	2	1	2
10 Insulation	40	1	40
11 Aluminum shell	11.5	1	11.5

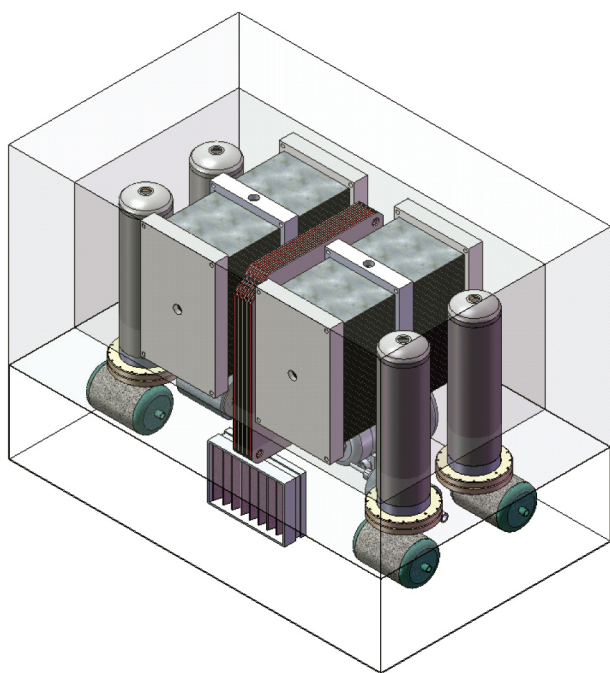


FIGURE 3. Thermally Integrated SOFC and Plasma Reformer

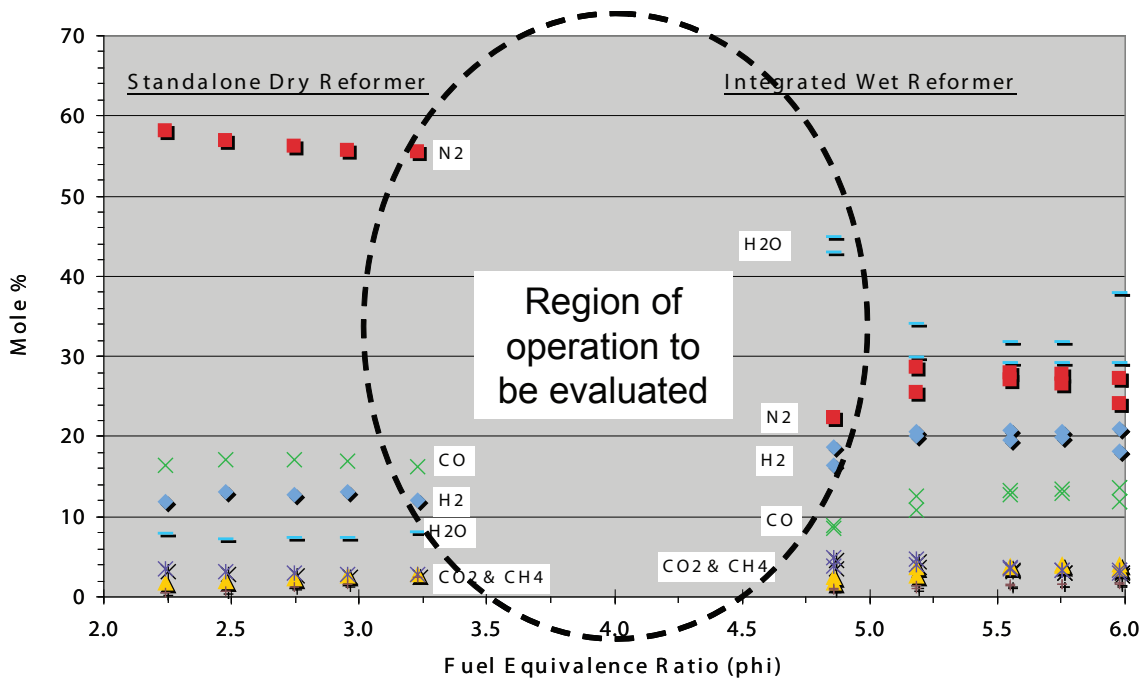


FIGURE 4. Multi-Mode Reformer Fuel Equivalence Ratio Operating Range

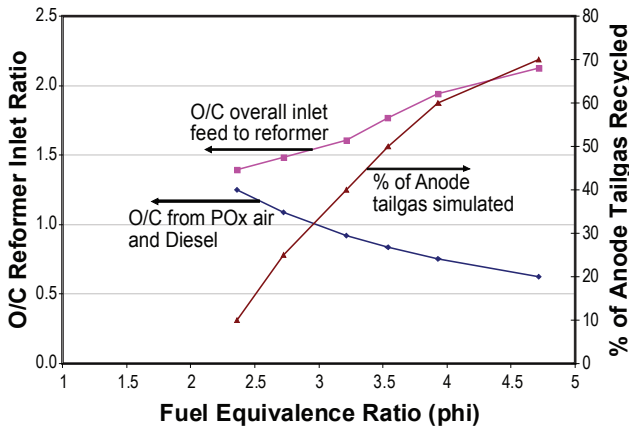


FIGURE 5. Reformer Operating Line in  $\phi$  Space

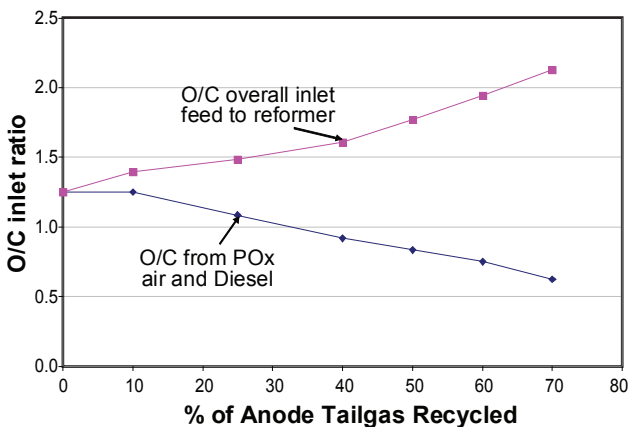


FIGURE 6. Reformer Operating Line in Anode Tailgas Recycle Ratio Space

integration within the SOFC thermal enclosure. The new configuration retains the advantages of the prior design in a form that is more compact and facilitates easier connection of the reformer to the SOFC stacks within the hot zone.

A series of runs was made with the new reformer, following the model-derived operating line. Reformate composition was analyzed using a micro-channel gas chromatograph. The results in Figure 7 show relatively constant hydrogen and carbon monoxide concentrations as  $\phi$  is increased. An earlier test comparing purely POx operation with plasma steam reforming showed a significant increase in hydrogen and CO concentration

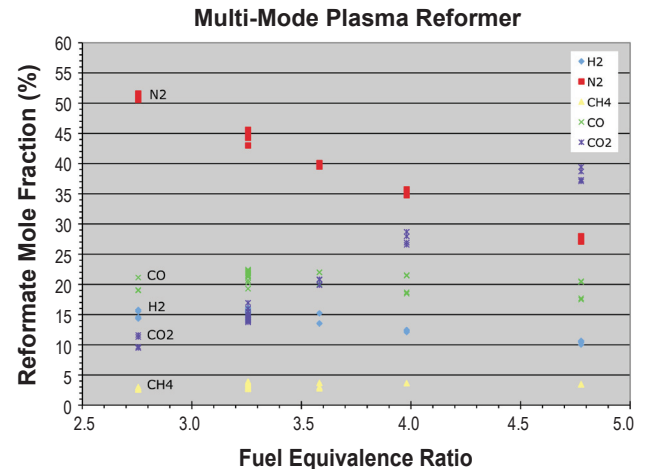


FIGURE 7. Reformate Composition Through Multi-Mode Transition

as  $\phi$  was increased (referring back to Figure 4). However, in anode tailgas recycle mode, there is a greater dilution effect from the recycle stream compared to the steam reforming mode. Notwithstanding the relatively constant  $H_2$  and CO concentrations, the SOFC system efficiency gains still accrue by increasing  $\phi$ . The reformer Faradaic efficiency expression  $\eta_F = (1-1/\phi)$ , representing the current generating potential of the fuel in the fuel cell, remains applicable for all operating modes, reformer and fuel cell types.

### Conclusions and Future Directions

This project demonstrated that the previously achieved efficiency gains of plasma catalyzed steam reforming can also be realized with a more practical combination of partial oxidation and anode tailgas recycle reforming. A redesigned implementation of the SOFC integrated plasma reformer enables more compact packaging of the reformer and SOFC within the thermal enclosure. The next step toward demonstration of a practical SOFC APU operating on diesel fuel is to build a prototype system incorporating both reformer and SOFC within a common thermal enclosure, and to operate them in combination. Such a project would require the development of a common supervisory control system. The phase I SBIR project is complete, and due to a change in small business status, Ceramatec was not eligible to pursue the phase II program. Fortunately, related work is continuing with the development of an SOFC APU reformer for the Army, targeting operation on high sulfur JP-8 fuel. Further refinements of the design are in process for the Army, addressing the plasma source, system integration and reformate sulfur cleanup.

### Special Recognitions & Awards/Patents Issued

1. Stoel-Rives Utah Innovation Awards Finalist, 2007
2. Four foundation patents pending, two issued
3. Current project patents in preparation

### FY 2008 Publications/Presentations

1. Production of Hydrogen by Cold Plasma Catalyzed Reforming of Heavy Hydrocarbons, Paper 535h, AIChE Annual Meeting, November 2007, Salt Lake City, UT.
2. SOFC Integrated Multi-Mode Diesel Reformer, 2008 Fuel Cell Seminar Abstract.

## IV.G.3 An Innovative Injection and Mixing System for Diesel Fuel Reforming

Spencer D. Pack (Primary Contact),  
John E. Short, and Nick R. Overman  
Goodrich Turbine Fuel Technologies  
2200 Delavan Drive  
West Des Moines, IA 50265-0100  
Phone: (515) 633-3460; Fax: (515) 271-7296  
E-mail: spencer.pack@goodrich.com

DOE Project Manager: Charles Alsup  
Phone: (304) 285-5432  
E-mail: Charles.Alsup@netl.doe.gov

Contract Number: 42229

Start Date: July 1, 2006  
Project End Date: December 31, 2007

### Objectives

- Develop a reliable, cost-effective diesel fuel injection mixing concept for use with auto-thermal reformers (ATR) and catalytic partial oxidation (CPOX) reformers in solid oxide fuel cell (SOFC) auxiliary power units (APUs).
- Determine operation and performance limitations of both preheat and piezoelectric injection-mixing concepts for diesel fuel reforming applications.
- Optimize both injector/mixers for diesel fuel reformers to operate with no steam/water usage and minimize air and fuel supply pressure.
- Test and analyze various anti-carbon formation coatings to improve the preheating injector life by reducing carbon formation in the injector's fuel passages.

### Accomplishments

- Completed the design and fabrication of two different preheating fuel injection concepts and an optimized piezoelectric injection concept that went through a detailed statistical design of experiment optimization study utilizing optical patterning.
- Completed Sauter mean diameter (SMD) testing of the optimized preheating injector and optimized piezoelectric injector.
- Completed a detailed computer analysis and characterization of air flow field on the preheating fuel injector with a simulated down stream porous medium (simulated reformer).
- Completed anti-carbon formation testing and down-selected to the three most promising anti-carbon

coatings using the statistical design of experiments technique.

### Introduction

Fuel reformers are a very important component of SOFC systems, enabling them to compete with conventional auxiliary power units in remote stationary and mobile power generation markets. Currently, liquid fuel processing technology is not yet viable for commercial applications in SOFC systems. One of the major technical barriers for liquid fuel processing is reactor durability. The performance of the reforming catalysts in the reactor quickly deteriorates as a result of carbon deposition, sulfur poisoning, and loss of precious metals due to sintering or evaporation at high temperatures. To mitigate these problems, research efforts are being conducted to optimize catalyst materials and to improve fuel reactor design/operation.

Problems associated with liquid fuel reactors could possibly be alleviated by improvement of feed stream preparation. Proper feed stream preparation can significantly improve reactor durability through minimizing problems due to inadequate fuel atomization, wall impingement, mixture recirculation and non-uniform mixing. These problems can easily lead to local conditions that favor carbon deposition, auto-ignition, and formation of hot spots in the reactor. Because liquid fuels are extremely difficult to reform, a proper understanding of injection and mixing systems for feed stream preparation plays an essential role in the development of reliable and durable liquid fuel reformers.

### Approach

To achieve the Solid State Energy Conversion Alliance (SECA) goals of improved feed stream preparation two promising fuel injection and mixing chamber concepts were thoroughly evaluated using both computational and laser diagnostic techniques. The key performance parameters included in the evaluation involved fuel atomization, droplet evaporation and mixing, uniformity of mixture temperature, velocity and concentration, wall impingement, flow recirculation, carbon deposits, feed stream supply pressure, power consumption, complexity and reliability of injector design/operation.

One obstacle with preheating the fuel before injection into the feed stream is carbon formation in the internal fuel passages of the fuel injector. Carbon

can restrict the fuel flow in the injector and reduce atomizer performance. Several anti-carbon coating applications were evaluated to determine their ability to reduce carbon formation within the fuel circuit of the preheating atomizer.

## Results

A carbon formation test rig was designed and fabricated to test carbon formation rates on surfaces of various sized components and test specimens. This carbon formation test rig has the ability to preheat the fuel to 200°C and heat a test specimen to 600°C inside a N<sub>2</sub>-purged oven (fuel is back pressured to prevent fuel boiling). This rig gives the flexibility to test specimens at wetted wall temperatures between 100 to 500°C. This rig was used to test six anti-carbon formation coatings via a statistical design of experiment. All six coated specimens and an uncoated baseline were tested at four different test conditions using ultra-low sulfur diesel. The specimens were tested at two fuel preheating temperature levels (150 and 175°C) inside the oven which was varied between two temperature levels (425 and 480°C). Figure 1 shows the carbon formed during a 175°C preheated fuel inside a 425°C oven with a 2.72 kg/hr diesel fuel flow rate. As seen from Figure 1 the carbon formed on the surface at a thickness less than 3.75 μm. This image was taken using a scanning electron microscope (SEM) at 2.5 K magnification. The coating tested in Figure 1 is AMCX Inertium diffusion bonded to 347 SS. Material maps of each specimen were also taken with the SEM; these material maps show the amount of carbon, silicon, chromium, iron, and nickel present in the sample area. As expected the layer of material trapped between the metal sample and the epoxy has very high carbon content.

Three coatings from the original six were further tested (AMCX Inertium, AMCX AMC26, and Restek Silcosteel AC) in a final back-to-back test with actual

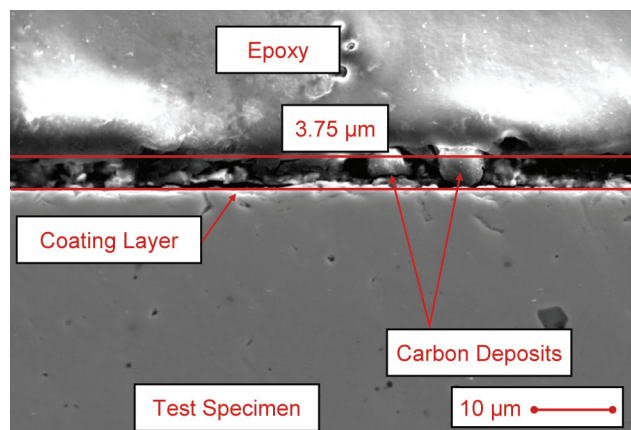


**FIGURE 1.** SEM Carbon Formation Image of Inertium Anti-Carbon Formation Coating at 2.5 K Magnification

injector component hardware. The final test was a two step test: Step 1 was 50 hours in length with the oven temperature set to 480°C, no preheating of the fuel (~21°C), and 2.72 kg/hr fuel flow rate. Step 2 was 20 hours in length with the same conditions as Step 1 but with the addition of fuel preheat to 77°C. This final test did not yield any carbon formation on any of the test specimens, so down selection to a single anti-carbon formation coating could not be determined. The leading theory for why no carbon was generated involves a fuel change prior to the testing of the final four specimens. It has been shown, from previous tests, that carbon formation rates are greatly affected by fuel changes during testing. Even though the same type of diesel was used during the testing, lot-to-lot variations in the diesel had a great impact on carbon formation rates. It is likely that any of the final three anti-carbon coatings could be selected for coating the entire fuel circuit to reduce carbon formation rate. A simple way to decide between the three coatings could be cost and coating lead time. It should be noted that these test results are preliminary. Sound conclusions could only be reached if the test results were found to be repeatable. Despite all efforts to conduct each test under identical conditions, a number of unexpected scenarios may have skewed the results.

Two preheating fuel injector concepts have been designed, fabricated, and optimized using statistical design of experiments. Build 1, for SECA Phase I utilized large flow recirculation zones to maximize fuel air mixing. However, Phase II work focused on creating a nozzle that doesn't require steam injection. Without steam, recirculation zones potentially lead to spontaneous ignition of the fuel rich mixture. Build 2 improved over Build 1 by reducing these recirculation zones. Computational fluid dynamics (CFD) was utilized to help predict flow rates, pressure drops, and flow non-uniformities associated with Build 1 and 2 design modifications. CFD was also utilized to simulate the overall flow-field structure and potential mixing capabilities, helping to provide a qualitative assessment of the injector/mixer performance under the actual reformer operating conditions. The computation domain includes the flow path from the feed stream inlets through the injector circuits, the diffuser mixing chamber and mixing chamber swirler several flow straightening screens, and ending immediately after a simulated porous medium. This porous medium was used to simulate the reformer in the ATR system. The grid system for the flow path consists of over 1.3 million computational cells, with clustering tailored to regions of expected high gradients. The solutions were obtained using FLUENT 6.2 software to solve the unsteady, Reynolds-averaged Navier-Stokes equations, with the RNG k-ε turbulence model, wall-functions, and differential viscosity models. Figure 2 shows a comparison of time-accurate velocity contours of the Build 2 preheating injector. This figure shows the CFD

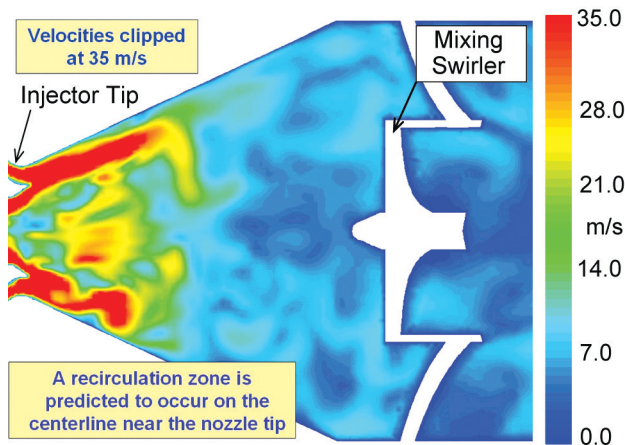


**FIGURE 2.** Time Accurate CFD Velocity Contours (m/s) of the Build 2 Preheating Injector and Large Mixing Chamber Swirler

results from the injector exit through the large mixing chamber swirler. Counter rotating air streams were utilized to produce mixing of the fuel and air. CFD predictions indicated that the preheating injector Build 2 design produces fewer recirculation zones than the Build 1 preheating injector with no separation along the mixing chamber diffuser walls.

For fuel atomization evaluation of the Build 2 preheating injector, detailed measurements were made at various operating conditions using phase/Doppler interferometry and using a SETscan OP-600 patterner produced by En’Urga Inc. The SETscan OP-600 is a high frequency statistical extinction tomography-based optical patterner. The SETscan allows detailed visual and numerical characterization of spray quality in terms of cone angle, asymmetry, streaks, voids, and patterning number. Figure 3 presents SETscan contours and radial distribution of absorption (1/mm) for the optimized preheating Build 2 injector at a simulated 5 kW load condition. This contour is taken at the diffuser exit plane (diffuser was not attached during this test). As shown the fuel/air mixture fills the 70 mm exit uniformly. The mixing chamber was able to capitalize on this optimized injector and further mix the fuel and air to allow complete vaporization of the fuel. The test point shown in Figure 3 was accomplished at ambient conditions with no preheating of the fuel. It is important to note that this injector was optimized based upon a design of experiment that varied fuel spray angle, outer swirler angle, and inner air swirl angle. The injector configuration of Figure 3 experimentally yielded the best fuel and air distribution using a 55° fuel spray angle, with a 35° outer swirler, and medium offset inner swirler.

A Phase Doppler Particle Analyzer (PDPA) system was used to measure droplet size and velocity at ambient conditions. The PDPA was used to collect droplet information via two different methods: a continuous

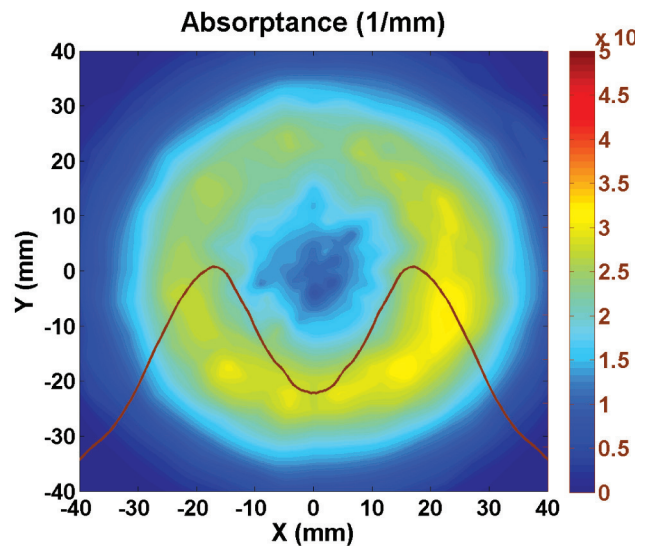


**FIGURE 3.** Fuel Absorbance Contours and Radial Distribution of the Optimized Preheating Injector 2 Inches Down Stream from Fuel Injection Point

traverse method for global spray measurement and a point-to-point method. The continuous traverse method provides mean droplet diameters that represent the entire spray and the point-to-point method offers detailed local distributions of droplet size, velocity and fuel volume flux. This information is extremely useful in determining the spray dynamic structure and to identify differences between injector concepts. Figure 4 shows point-to-point measurements taken at a location three inches below the preheating injector exit, at a simulated

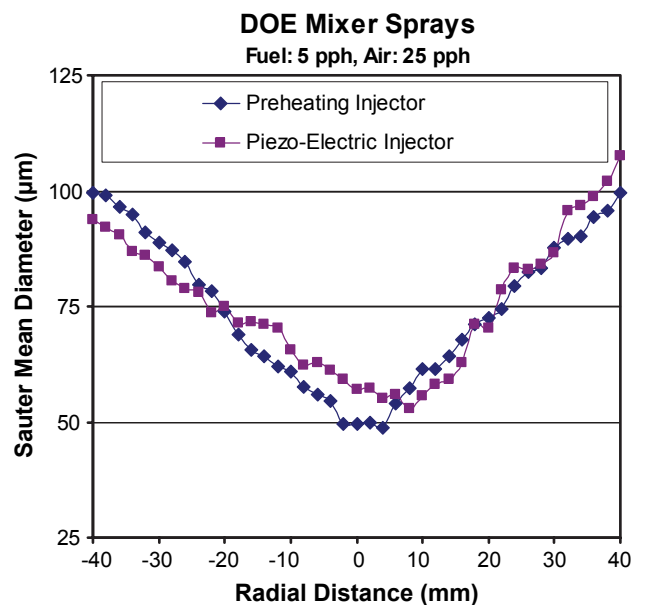


**FIGURE 4.** A Comparison of the Radial Distribution of Sauter Mean Diameter for the Build 2 Preheating Injector and Piezoelectric Injector at a Simulated 5 kW Load Condition

5 kW load condition. Fuel and air temperatures were ambient for this test. Also shown in Figure 4 are PDPA measurements of the optimized piezo-electric injector at the same flow rates.

A single piezo-electric fuel injector concept was designed, fabricated, tested, and optimized using a statistical design of experiments. Though only one concept for this injector was created, several variations of sub-components were made. As with the preheating injector design, evaluation of the piezo-electric injector was performed using both the SETscan OP-600 and the PDPA systems. This concept utilizes piezo-electric crystals to induce mechanical vibration for atomizing the fuel, rather than large pressure differentials. Employing piezo-electrics to aid in atomization allows for minimization of air and fuel supply pressures. Tests included a range of operation such that air pressures ranged between 0.10 in H<sub>2</sub>O – 3.0 in H<sub>2</sub>O, and fuel pressures less than 1 psi for flow rates up to 4.6 kg/hr. This design allows for extremely low fuel pressures, and consequently low velocities, while generating small droplets in the atomization process. When coupled with the high operating temperatures required by SOFCs, the small droplets and low velocities allowed for vaporization of the fuel within a very short distance. Therefore, this design can utilize a shorter mixing chamber and an overall more compact injector mixing unit.

## Conclusions and Future Directions

- A preheating simplex injector has been developed into a promising concept for diesel fuel processing which could be used in SOFC APUs in commercial diesel truck applications with diesel fuel flow rate applications between 5 to 20 pph.
- A piezoelectric injector has been developed into a promising concept for diesel fuel processing which could be used in SOFC APUs in commercial diesel truck applications with diesel fuel flow rate applications up to 10 pph.
- Three anti-carbon coatings applied to 347 SS have shown reduced carbon formation rates over uncoated 347 SS. These recommended coatings are AMCX Inertium, AMCX AMC26, and Restek Silcosteel AC. Further testing of these coatings should occur in attempts to obtain more repeatable data

## IV.G.4 Reformer for Conversion of Diesel Fuel into CO and Hydrogen

Michael V. Mundschau (Primary Contact),  
Christopher G. Burk, David A. Gribble, Jr.  
Eltron Research and Development Inc.  
4600 Nautilus Court South  
Boulder, CO 80301-3241  
Phone: (303) 530-0263; Fax: (303) 530-0264  
E-mail: mmundschau@eltronresearch.com

DOE Project Manager: Ayyakkannu Manivannan  
Phone: (304) 285-2078  
E-mail: Ayyakkannu.Manivannan@netl.doe.gov

Contract Number: 84394

Start Date: August 8, 2007  
Project End Date: August 7, 2008

### Objectives

- Design a reformer for converting commercial diesel fuel with a maximum of 15 parts per million by mass sulfur into a mixture of H<sub>2</sub> and CO for use in solid oxide fuel cells.
- Demonstrate the concept of self-cleaning reactor walls that prevent deposition of carbonaceous residues and plugging of reformers by effusing air through the walls.
- Develop perovskite catalysts for dry partial oxidation of diesel fuel that are sulfur tolerant, stable near 950°C, resist deactivation by sintering and contain vacancies for enhancing mobility of oxygen anions allowing rapid oxidation of hydrocarbons and inhibition of deposition of carbon.

### Accomplishments

- Tested self-cleaning reactor walls of porous yttria-stabilized zirconia (YSZ). Brought air into the reformer through porous tubular walls and demonstrated suppression of deposition of carbon onto walls in the diesel-fuel feed zones by maintaining very high local concentrations of oxygen near the inner reactor walls.
- Synthesized, characterized and tested cobalt and iron-based perovskites as “reverse” Fischer-Tropsch catalysts for converting hydrocarbons into H<sub>2</sub> + CO. Demonstrated sulfur tolerance and partial oxidation activity towards pump-grade diesel fuel containing a maximum of 15 ppmw sulfur with external reactor heating to 950°C.

### Introduction

One of the major issues in designing reformers for converting diesel fuel into a mixture of H<sub>2</sub> + CO, suitable for use in solid oxide fuel cells, is avoiding deposition of carbonaceous residues onto reformer walls and catalysts. Thermodynamic analysis predicts that the desired products will be overwhelmingly favored if the dry partial oxidation reaction, H<sub>1.8</sub>C<sub>1</sub> + 1/2 O<sub>2</sub> = 0.9 H<sub>2</sub> + CO (where H<sub>1.8</sub>C<sub>1</sub> represents the average empirical formula of the molecules in the fuel), can be brought to equilibrium above about 950°C [1]. However, thermodynamics also indicates that formation of elemental carbon will be the major product at lower temperatures [1]. A major challenge in reformer design is raising the temperature of diesel fuel from ambient to the desired reforming temperature without converting a major fraction of the fuel into elemental carbon. As diesel fuel is heated above 250-300°C, the weakest bonds in the least stable molecules break forming alkyl radicals. Under desired partial oxidation conditions, the atomic ratio of oxygen-to-carbon is limited to 1-to-1, and hydrocarbon free radicals have high probability of reacting with other hydrocarbons, rather than with oxygen, forming tars by free-radical polymerization. Free-radicals of long-chain hydrocarbons may also react intra-molecularly, forming cyclic compounds leading to nucleation of soot and graphitic carbon. Once nucleated, carbonaceous deposits are autocatalytic; they catalyze their own formation. Under both thermodynamically and kinetically favorable conditions, growth of carbonaceous deposits is exponential, rapidly plugging reactors and catalyst beds. Efficient suppression of deposition of carbon is a major goal to be addressed in any diesel-fuel reformer design.

A second major task in the development of diesel-fuel reformers employing catalytic partial oxidation is the production of catalysts that maintain high activity for dry reforming. The aromatic compounds in diesel fuel are exceptionally stable and are the most difficult hydrocarbons to oxidize. Cracking of aliphatic alkanes produces additional aromatic compounds in the reformat. To oxidize aromatics, catalysts must adsorb and dissociate molecular oxygen into highly active atomic oxygen or form other reactive species. Reforming catalysts must be stable to over 950°C if equilibrium is to be achieved while retaining the desired dry-oxidation stoichiometry of one oxygen atom per carbon atom in the fuel. Local temperatures on surfaces of catalysts may exceed 1,000°C due to the exothermic oxidation reactions, and catalysts must be able to resist thermal

deactivation due to melting, sublimation, interdiffusion with supports, sintering and loss of surface area. If deep oxidation of fuel into  $H_2O$  and  $CO_2$  occurs upstream or in the upper catalyst bed, catalysts downstream must adsorb and convert these products into  $H_2$  and  $CO$  by steam reforming:  $H_{1.8}C_1 + H_2O = 1.9 H_2 + CO$  and by dry reforming:  $H_{1.8}C_1 + CO_2 = 0.9 H_2 + 2CO$ . The catalysts must resist poisoning by sulfur and other impurities in the fuel. Reactor components must be selected to minimize production of volatile compounds which could poison partial-oxidation catalysts or fuel-cell catalysts downstream. The catalysts must also resist deactivation when cycled between highly reducing conditions during reforming and highly oxidizing conditions upon exposure to air during start-up and shut-down. Partial-oxidation catalysts must resist deactivation by deposition of carbon, a few monolayers of which can prevent adsorption of reactants. Provisions must also be made to avoid poisoning of fuel cell catalysts by sulfur and other impurities or by incompletely reacted diesel fuel.

### Approach

To suppress deposition of carbon onto reactor walls in zones where fuel is heated, air is brought into the reactor through porous walls of YSZ (see Figure 1). The

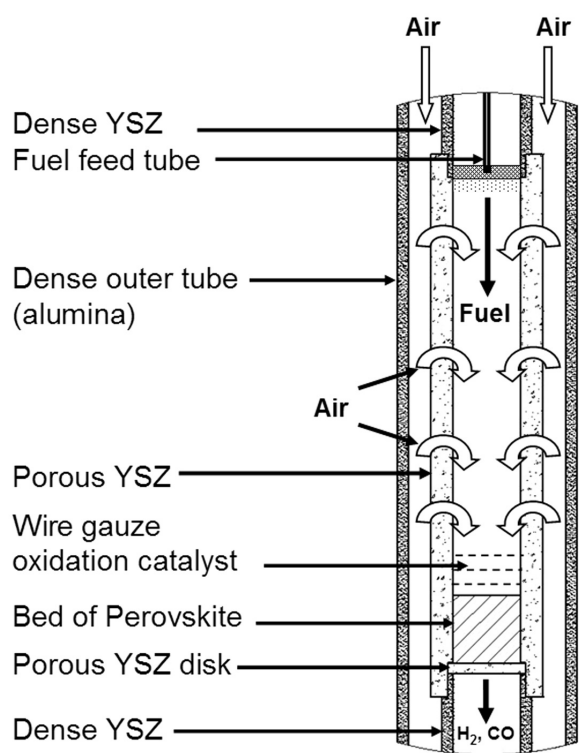


**FIGURE 1.** Schematic of a diesel fuel reformer incorporating a porous, self-cleaning wall of YSZ for the suppression of deposition of carbon in the fuel heating zones. Air is brought into the reactor through the porous walls.

concept is to maintain very high local concentrations of oxygen near the inner reactor walls such that elemental carbon is thermodynamically unstable—while retaining the overall desired atomic O-to-C ratio of 1-to-1 within the reactor. Figure 2 summarizes thermodynamic calculations predicting the equilibrium O-to-C atomic ratios required along the reactor walls as fuel is heated. The reactor walls are being designed to be self-cleaning. YSZ was chosen as the porous wall material because of its high thermal stability and low likelihood of emitting volatile species that could poison reforming catalysts and the Ni fuel-cell catalysts. In order to avoid potential phase transformations upon thermal cycling, YSZ with yttria concentrations above 9.5 mole%, are being considered in the porous walls rather than the usual Nernst Mass of 8.8 mole% (15 mass%) because the latter might undergo a cubic-to-tetragonal phase transformation.

In catalyst development, a critical criterion is resistance to poisoning by sulfur and especially formation of *bulk* sulfides that lead to irreversible deactivation. Consultation of Ellingham Diagrams [1] indicates that Pt, Rh, Co and Fe do not form thermodynamically stable bulk sulfides under desired reforming conditions with 15 ppmw sulfur in the fuel. Platinum-rhodium metal wire gauze (Pt:Rh 90:10 by mass) was selected as an ideal, albeit expensive, catalyst for commissioning reformers. The noble metals adsorb and dissociate molecular oxygen into highly active surface atomic oxygen but do not form stable

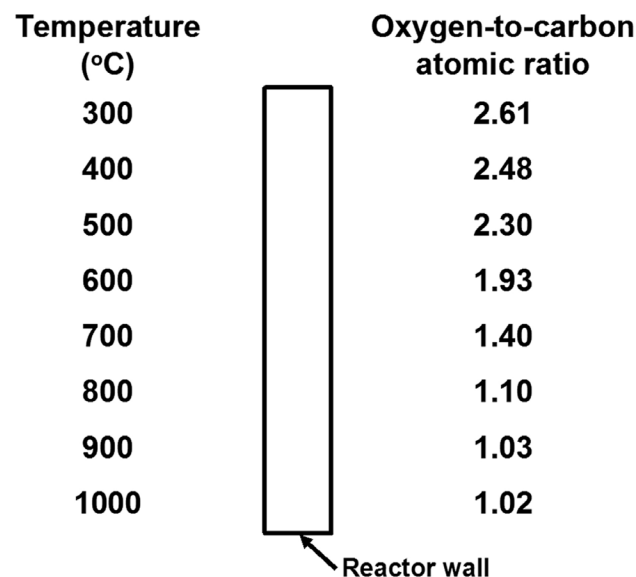


**FIGURE 2.** Summary of thermodynamic calculations for the oxygen-to-carbon atomic ratio at various temperatures needed to ensure that elemental carbon becomes thermodynamically unstable. The concept is to maintain very high local concentration of oxygen near the inner reactor walls while retaining overall the desired 1-to-1 atomic ratio in the reactor hot zone.

bulk oxides, allowing cycling between oxidizing and reducing conditions during start-up and shut-down. Platinum and rhodium have melting points of 1,772°C and 1,966°C, respectively, and their alloys are more than sufficient for resisting equilibrium temperatures. The Pt-Rh wire gauze is not deactivated by sintering, as its initial surface area is relatively low. Cobalt and iron are being pursued as low-cost reforming catalysts. Both are well-established Fischer-Tropsch catalysts, long used to synthesize hydrocarbons from H<sub>2</sub> and CO. Under appropriate thermodynamic conditions, they catalyze the reverse reactions, converting hydrocarbons into H<sub>2</sub> and CO. However, Co and Fe dispersed onto conventional supports are highly pyrophoric under oxidizing conditions and could not be cycled between oxidizing and reducing conditions. Therefore, Co and Fe are incorporated into perovskites, which are refractory oxides. They are electron-conducting and catalyze the adsorption and dissociation of molecular oxygen by the reaction:  $O_2 + 4e^- = 2O^{2-}$ . Oxygen vacancies are created in the lattices, enhancing oxygen-ion diffusion which suppresses deposition of carbon by allowing attack by mobile oxygen from beneath. Iron-based perovskites also act as reverse water-gas shift catalysts, converting CO<sub>2</sub>, if formed by deep oxidation, by the reaction:  $CO_2 + H_2 = CO + H_2O$ .

## Results

All experiments used commercial diesel fuel purchased from automotive pumps, stated to contain less than 15 ppmw sulfur. Sulfur levels were verified by two certified analytical laboratories, Intertek Caleb Brett of Chicago and Wyoming Analytical Laboratories at Golden, Colorado, which measured sulfur content of 9 ppmw and 7 ppmw, respectively, using ASTM Standard D5453, in reasonable agreement with each other and within the legal limits. A measured H-to-C atomic ratio of 1.79-to-1 (13.06 wt% H; 86.91 wt% C; balance mainly nitrogen using ASTM D5291) is taken as a representative value of the hydrogen and carbon content of low-sulfur diesel fuel. The H-to-C atomic ratio is critical for setting the reforming temperature for which elemental carbon is thermodynamically unstable. It should be appreciated that the lower H-to-C ratio in diesel fuel relative to the 4-to-1 ratio of methane, CH<sub>4</sub>, or other low-molecular weight aliphatic hydrocarbons, necessitates higher reforming temperatures to thermodynamically suppress formation of carbon. The H-to-C atomic ratio in the fuel is also critical for setting the flow of air for partial oxidation:  $H_{1.79}C_1 + 0.5 O_2 = 0.895 H_2 + CO$ . Analysis indicates that the diesel fuel contains 0.0724 moles of carbon and 0.1296 moles of hydrogen per gram and requires 0.362 mole O<sub>2</sub> = 0.811 L O<sub>2</sub> (standard temperature and pressure) (or 3.97 L air) for partial oxidation, per gram of fuel.

Layers of Pt-Rh wire gauze were used as off-the-shelf catalysts to commission the test apparatus and for comparison and evaluation of experimental perovskite-based catalysts. Seven sheets of Pt-Rh gauze separated by disks of porous YSZ (the latter used to increase turbulence and residence time) were used in the reformer hot zone. In excess oxygen, complete oxidation of diesel fuel to CO<sub>2</sub> and H<sub>2</sub>O with good mass balance was achieved [1]. As predicted, the Pt-Rh wire gauze showed no loss of activity due to the sulfur in the fuel and easily withstood temperatures above 1,000°C. The wire gauze could be cycled repeatedly between air and reducing conditions without apparent ill-effect. However, under partial-oxidation conditions it proved difficult to achieve equilibrium with limited quantities of gauze. This is attributed to its low surface area. Non-negligible quantities of CO<sub>2</sub>, H<sub>2</sub>O, CH<sub>4</sub>, and aromatic compounds escaped the reactor. Quantities of Pt-Rh wire gauze required to achieve equilibrium are likely to be cost-prohibitive in all but very specialized applications.

Catalysts with the perovskite structure (see Figure 3) were synthesized and tested [1]. Some perovskites possess catalytic oxidation activity similar to that of noble metals [1, 2], and many workers have investigated perovskites for partial oxidation of diesel fuel [1, 3, 4]. Table 1 compares lattice constants of noble metals with those of select perovskites. Lattice constants are similar and may be responsible for comparable catalytic oxidation behavior. These perovskites, especially when Ca<sup>2+</sup> and Sr<sup>2+</sup> ions are added to create oxygen vacancies, rapidly transport oxygen ions through their bulk and attack carbonaceous layers from beneath.

Figure 4 shows results of partial oxidation of diesel fuel using a bed of La<sub>0.5</sub>Sr<sub>0.5</sub>FeO<sub>3-δ</sub> in the reformer hot zone. The perovskites work very well for complete oxidation of diesel fuel in excess oxygen. Upon lowering the O-to-C atomic ratio from slightly above 3-to-1 to 1-to-1, production of CO<sub>2</sub> (and H<sub>2</sub>O) drops

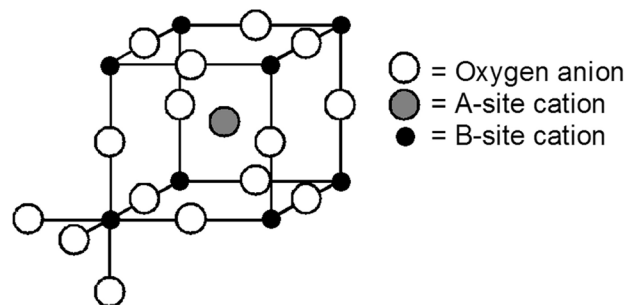


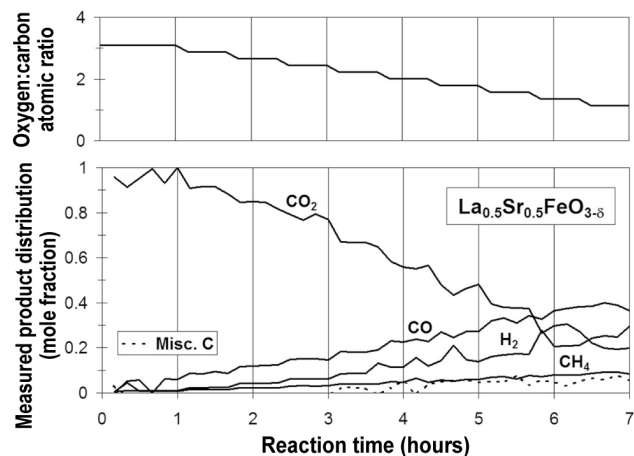
**FIGURE 3.** Ideal cubic perovskite crystal lattice. A-sites are occupied by larger-diameter cations including La<sup>3+</sup>, Sr<sup>2+</sup>, Ca<sup>2+</sup>. B-sites are occupied by smaller transition elements such as Fe<sup>3+</sup>, Fe<sup>2+</sup>, Co<sup>3+</sup>, Co<sup>2+</sup>, Mn<sup>3+</sup>, Ru<sup>3+</sup>, etc.

**TABLE 1.** Similarity of Lattice Constants of Perovskites and Noble Metals

Catalyst	Lattice Constant (Å)
Rh	3.8044(1)
Ir	3.8389(5)
Pd	3.8902(3)
Pt	3.9237(3)
LaCoO <sub>3</sub>	3.82(1)
LaCrO <sub>3</sub>	3.88
LaFeO <sub>3</sub>	3.89–3.899
LaMnO <sub>3</sub>	3.88–3.90

and concentration of H<sub>2</sub> and CO rises. Methane is also produced and a considerable fraction of diesel fuel remains unreacted, as indicated by increase in lack of mass balance. However, catalysts are by no means optimized. The porous walls of YSZ suppress sufficient deposition of carbon so that activities of various catalysts can be tested and compared. With dense walls used as controls, deposition of carbon was rapid, leading to plugging of reformers. Analysis of perovskite catalysts used in the reactor hot zone by X-ray spectroscopy showed no detectable accumulation of carbon [1], demonstrating that diffusion of oxygen from the lattice bulk eliminates build-up of carbon in catalyst beds under conditions where elemental carbon is thermodynamically unstable. Perovskites of general formula, La<sub>1-x</sub>Sr<sub>x</sub>FeO<sub>3-δ</sub> and especially La<sub>1-x</sub>Ca<sub>x</sub>FeO<sub>3-δ</sub>, are much more stable relative to their cobalt analogues [1].

Considerable work remains to produce a practical reformer. Calculations imply that heat released from partial oxidation of diesel fuel to H<sub>2</sub> + CO is just barely

**FIGURE 4.** Product distribution from dry partial oxidation of diesel fuel using a reactor with porous walls of YSZ and a bed of La<sub>0.5</sub>Sr<sub>0.5</sub>FeO<sub>3-δ</sub> in the reformer hot zone at 950°C.

enough to heat fuel and air to temperatures above 950°C without sacrificing additional fuel and greatly reducing efficiency. Reformers will need to be nearly perfectly insulating or will likely need to acquire heat from fuel cell exhaust. Sulfur even at levels of 15 ppmw in “low-sulfur” diesel fuel in the reformat is likely to poison nickel-based catalysts in solid oxide fuel cells [5], and sulfur likely will need to be reduced to much lower levels. Parasitic power consumption for fuel injection, air flow and external heating of catalysts will need to be greatly reduced if efficient systems are to be fabricated.

## Conclusions and Future Directions

- Porous, self-cleaning walls of YSZ show promise for suppressing deposition of carbon in diesel fuel heating zones but will require considerable effort to produce practical devices.
- Perovskite catalysts, especially those containing iron, show promise as sulfur-tolerant, dry partial-oxidation catalysts for diesel fuel but will require further development and may require heating from fuel cell exhaust to maintain system efficiency.

## Special Recognitions & Awards/Patents Issued

1. Michael V. Mundschau, *Catalytic Membrane Reactor and Method for Production of Synthesis Gas*, U.S. Utility Patent Application Filed September 6, 2007.

## FY 2008 Publications/Presentations

1. M.V. Mundschau, Christopher G. Burk and David A. Gribble, Jr., Diesel Fuel Reforming Using Catalytic Membrane Reactors, *Catal. Today* 136 (2008), 190-205.
2. D.S. Jack, J.H. White, J.A. Trimboli, C.G. Burk, S.L. Rolfe, D.H. Anderson and M.V. Mundschau (speaker), *Liquid Fuel Reforming Using Catalytic Membrane Reactors*, presentation, Division of Fuel Chemistry, 234<sup>th</sup> ACS National Meeting, Boston, August 19, 2007.

## References

1. M.V. Mundschau, Christopher G. Burk and David A. Gribble, Jr., Diesel Fuel Reforming Using Catalytic Membrane Reactors, *Catal. Today* 136 (2008), 190-205.
2. L.G. Tejuca, J.L.G. Fierro, and J.M.D. Tascón, Structure and Reactivity of Perovskite-Type Oxides, *Adv. Catal.* 36 (1989) 237-328.
3. D. Shekhawat, D.A. Berry, T.H. Gardner and J.J. Spivey, Catalytic Reforming of Liquid Hydrocarbon Fuels for Fuel Cell Applications, *Catalysis* 19 (2006) 184-253.

4. D.-J. Liu and M. Krumpelt, Activity and Structure of Perovskites as Diesel-Reforming Catalysts for Solid Oxide Fuel Cells, *Int. J. Ceram. Technol.* 2(4) (2005) 301-307.
5. M. Liu, J.H. Wang, S. Choi and Z. Cheng, *Novel Sulfur-Tolerant Anodes for Solid Oxide Fuel Cells*, 2007 Office of Fossil Energy Fuel Cell Program Annual Report, 73-74.

---

## IV.G.5 Low Cost, Compact Plasma Fuel Reformer for APUs

Daniel Westerheim (Primary Contact),  
Brian Hennings, Gerald Hershman

Lynntech, Inc.  
1313 Research Parkway  
College Station, TX 77845  
Phone: (979) 693-0017; Fax: (979) 694-8536  
E-mail: daniel.westerheim@lynntech.com

DOE Project Manager: Ayyakkannu Manivannan  
Phone: (304) 285-2078  
E-mail: Ayyakkannu.Manivannan@netl.doe.gov

Contract Number: 84673

Start Date: June 20, 2007  
Project End Date: March 19, 2008

---

### Introduction

One of the key components playing an integral role in the operation (and therefore commercialization) of an SOFC-based APU is the reformation system. In order to be commercially viable, an SOFC APU must be capable of operating on commonly available fuel, such as diesel or gasoline. Most SOFCs cannot do this directly and require a reformer which produces hydrogen or syngas ( $H_2/CO$  mix) from diesel.

Lynntech has developed a simplified reformer which meets the DOE requirements demanded of an SOFC APU reformer. Lynntech based their reformer on a previous design which demonstrated excellent performance at a larger scale (the original application for this reformer required higher reformate flows), but was complex, difficult to manufacture, required precision controls and had several machined components using expensive materials (quartz, Teflon™, and ceramics). The new reformer successfully re-sized the reformer for the appropriate reformate production, reduced the part count from 15 parts to less than nine parts, all standard materials and only two machined parts. The new design requires less precision to produce and to operate, while delivering comparable performance to the original, complex design.

### Approach

Lynntech began with an existing reformer design originally designed for use in exhaust after treatment systems. This reformer produced too much reformate and was too complex for the stringent low-cost requirements of an SOFC APU, although the reformer did meet virtually every performance requirement for the application (see Table 1). Lynntech analyzed the design and functionality of every component and produced a far simplified design, eliminating most of the problems associated with the original design. In the process, the new design was scaled down to produce the appropriate amount of reformate for a 1-5 kWe SOFC APU.

### Objectives

- Scale the current 8.4-25.2 kWe diesel reformer to produce 1-5 kWe of reformate.
- Improve the reformer design (simplicity, efficiency, manufacturability).
- Demonstrate the reformer's capability of meeting or exceeding DOE performance goals (i.e., turndown, sulfur tolerance, size, etc).
- Produce a preliminary design illustrating necessary areas for improvement to result in a commercially viable diesel reformer for solid oxide fuel cell (SOFC) auxiliary power units (APUs).

### Accomplishments

- Successfully scaled the system down to the required 1-5 kWe reformate production level.
- Reduced the part count from 15 precision parts with critical tolerance stack-ups to nine simple parts, only two of which are machined, without critical or tight tolerances.
- Reduced cost (no exotic materials, simple design).
- Reformer was operated and demonstrated that it met DOE SOFC APU goals in every category tested (except pressure drop: 2 psi vs. DOE goal of 1 psi).
- Simplified overall system design (lower precision air control required, lowered pressure drop from 4 psi to 2 psi).

**TABLE 1.** A Comparison of the DOE Requirements and Current Technology Status

DOE APU Requirements		Previous PFR	Lynntech Phase I PFR
Reformate Production (chemical Energy)	2 – 10 kW	16.8–50.4 kW	3 kW
Operating Temperature Range (°C)	600 – 1000	Meets	Meets
Turndown Capability	4:1	Exceeds (5:1)	Exceeds (5:1)*
Pressure Drop through Device	1 psi	4 psi	2 psi
Water Usage	Minimal	Not Required	Not Required
Carbon Suppression	Maximum	Meets	Meets
Volume	< 10 L	Exceeds (2 L)	Exceeds (~2 L)
Start-up	Rapid	< 5 sec	< 5 sec*
Power Transients	Y	< 400 ms	< 400 ms*
Part Load Operation	Y	Meets	Meets*
Sulfur Tolerance	Up to 50 ppmv	Meets	Meets*
Long-term Operation	> 5,000	Meets	Meets*
Suitable for Large Volume Mfg	80k+ units/yr	NO	Meets

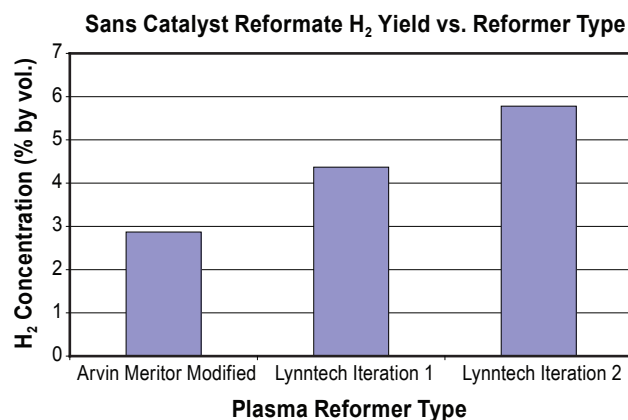
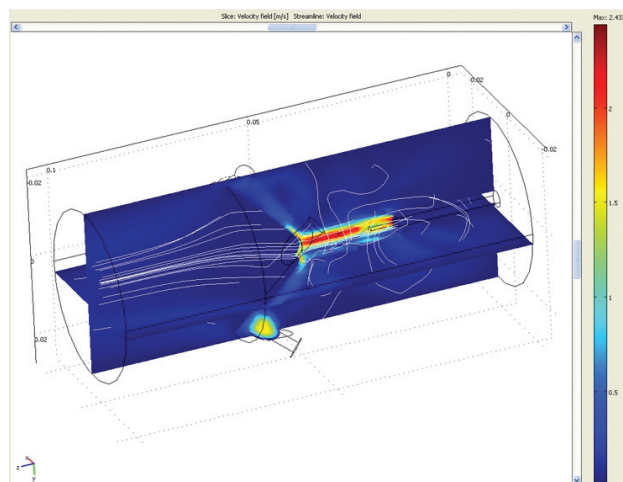
\* Note: these metrics were not measured in Phase I; however, based on previous results, they are not expected to be adversely affected by the design changes in Lynntech's Plasma Reformer. This will be verified by testing as part of the Phase II work plan.

## Results

During the course of this project, Lynntech assembled and tested a reformer of a pre-existing design, analyzed the design and operation of this reformer, used this analysis to complete the design and testing of Iteration 1 and 2 simplified reactor designs. This ultimately resulted in 30% fewer components (9 vs. 15), with no exotic or expensive components, and simplified manufacturability (only two machined components). This was accomplished without a sacrifice in performance, and actually increased performance over the baseline test performed on the previous reactor design (see Figure 1).

The Lynntech designs were modeled using Comsol and analyzed for mixing, gas flow paths and velocity (see Figure 2). Additional modeling and verification will be performed in follow-on research to further optimize the reformer design.

The primary difference between Iteration 1 and Iteration 2 was the method of fuel injection and atomization. Iteration 1 utilized a stainless steel nebulizer originally designed for use in analytical equipment. This nebulizer creates very fine droplets

**FIGURE 1.** Reformate Hydrogen Yield for Each Design Iteration, Demonstrating an Almost 200% Improvement in Phase I**FIGURE 2.** Velocity Profile in Plasma Reactor Showing Mixing Zones Behind the Plasma Region

<10  $\mu\text{m}$  mean size, but requires a high pressure gas source ( $>90$  psi). Due to this pressure requirement, a different fuel injection method was used which created slightly larger droplet sizes, but required only 30-50 psi of fuel pressure – well within range of a standard, low cost automotive fuel pump while also eliminating an air supply and control. In addition, the nebulizer created a solid cone of fuel while the fuel nozzle created a hollow cone of fuel. This was important due to the geometry of the reformer chamber and was a contributing factor in the higher performance of Iteration 2 (~5.8% H<sub>2</sub>) over Iteration 1 (~4.3% H<sub>2</sub>), both of which outperformed the baseline test (~2.9% H<sub>2</sub>).

All testing performed during the Phase I project was performed without a water-gas shift (WGS) catalyst, therefore initial H<sub>2</sub> concentration is relatively low compared to the ultimate system to be produced. Suitable commercial WGS catalysts have been identified which are sulfur tolerant and will be used in subsequent

phases of development to convert the moisture inherent in the reformat stream into hydrogen via a typical WGS reaction with the excess of CO in the reformat. For simplicity and time constraints, only hydrogen production was analyzed and optimized for in the majority of the testing procedures. Hydrogen provides a good metric of performance as to the quality of reformation, and CO levels were periodically analyzed to ensure the overall chemical energy of the reformat was within the 2-10 kW range required for a 1-5 kWe SOFC APU.

## Conclusions and Future Directions

The Phase I yielded excellent results, accomplishing all of the major milestones set forth; however, the reformer system still has areas where additional research effort is required. Although some modeling was performed in the Phase I, a more thorough analysis will be completed in the Phase II effort. This will allow for a more comprehensive model incorporating both fluidic and combustion modeling to be developed and more design iterations to be performed numerically before prototypes are built and tested.

The WGS catalyst already identified needs to be installed in the system and the performance of the overall reformer confirmed.

Additional testing is required as the time constraints of a Phase I developmental effort did not allow all of the DOE parameters to be tested. The previous reformer performed well in these tests and the new design is expected to perform similarly, but this must be confirmed by testing.

As the design is refined and eventually frozen, a long-term endurance test must be performed which would realistically simulate operation of an SOFC APU.

And finally, the reformer system must be integrated with an actual SOFC for use as an APU and the combined system rigorously tested.

## Summary of Future Efforts

- Additional modeling (fluidic and combustion) and design optimization
- Integration of WGS catalyst
- Complete performance testing to DOE requirements
- Long-term (>2,000 hours) operational testing
- Integration with SOFC
- Testing of integrated SOFC APU

---

## IV.G.6 Liquid Hydrocarbon Fuel Reforming Studies

Dushyant Shekhawat (Primary Contact),  
David A. Berry, Michael A. Lindon<sup>a</sup>,  
Earl E. Scime<sup>a</sup>

U.S. Department of Energy  
National Energy Technology Laboratory (NETL)  
3610 Collins Ferry Rd.  
Morgantown, WV 26507-0880  
Phone: (304) 285-4634; Fax: (304) 285-0903  
E-mail: Dushyant.Shekhawat@netl.doe.gov

<sup>a</sup>West Virginia University  
Department of Physics  
Morgantown, WV 26506

Contract Number: 07-220611

Start Date: October 1, 2007  
Project End Date: September 30, 2009

### Objective

- Evaluate the use of plasma energy to reform heavy hydrocarbons into hydrogen-rich synthesis gas for use by high-temperature fuel cells being developed in the Solid State Energy Conversion Alliance (SECA) program.
- Demonstrate/develop a “waterless” plasma diesel fuel reformer with 100% fuel conversion to <C<sub>3</sub> hydrocarbons with minimal carbon formation/performance decline, and parasitic power consumption of <3%.

### Accomplishments

- Modified instrumentation at NETL to use the plasma reformer.
- Demonstrated operating performance of the plasma reformer.
- Initiated plasma characterization studies.

---

### Introduction

The U.S. Department of Energy is sponsoring development of high-temperature fuel cell power systems based on solid oxide technology through its SECA program. The fuel processor is a critical and key enabling component of these systems that must be able to provide a clean, tailored hydrogen-rich synthesis gas to the fuel cell stack for long-term operation. Much of the reformer technology development thus far has

focused on catalytic systems. However, the catalytic reforming of many hydrocarbon-based fuels (coal, bio, oil-based...) is very challenging because of the catalyst deactivation by the aromatics (coke precursors) and sulfur compounds found in these fuels. Oxide-based catalysts show some promise, but are unproven at this point.

Because of this, the use of alternative non-catalytic process such as plasma reforming needs to be evaluated and considered. Catalytic processes also may be enhanced by use of such alternative approaches. Recently, Drexel Plasma Institute has developed and patented plasma technology for methane conversion into syngas [1-3] with support under a project with ChevronTexaco. A special plasma system, Gliding Arc in Tornado (GAT) reactor, was developed for this technology [1-3] and consists of non-equilibrium plasma which has demonstrated the potential advantages of combining of both thermal and non-thermal plasmas in optimized regimes. With the GAT approach, only a small portion of energy (about 2%) is supplied by plasma with the remainder being taken from the exothermic partial oxidation heat of reaction for the process itself. The GAT system may be especially promising for liquid fuel conversion, as the reverse vortex flow that stabilizes the plasma has a natural place for a second flow injection (for example, disperse fuel). According to the available information, absence of such a place in conventional vortex reactors and resulting fuel coking are major reasons for significant delay in commercialization of the technology developed elsewhere.

### Approach

NETL plans to explore the reverse vortex plasma reformer (uses a gliding arc discharge) for the reforming of hydrocarbon fuels such as diesel. This novel type of reactor design has a plasma discharge that is created and contained within a vortical counter-current flow-field. This reformer will be supplied by Drexel Plasma Institute (DPI) of Drexel University, Philadelphia, PA. This plasma reactor is designed to operate at a pressure of 15 psig and utilizes partial oxidation of gaseous or liquid hydrocarbon fuels at different oxygen-to-carbon (O/C) ratios.

Additionally, the goal of this project will be to develop a fundamental understanding of plasma-based technology as it applies to the reforming of hydrocarbon fuels for direct application to fuel cell systems. From a broader perspective, NETL is developing technology for a variety of fossil energy applications that may benefit from plasma-based processes. Some of these

applications include plasma-assisted reforming,  $\text{CO}_2$  dissociation, reduction of flue-gas  $\text{SO}_x$  to elemental sulfur, plasma-assisted combustion,  $\text{H}_2\text{S}$  conversion, etc. [4]. More specifically, this project will focus on the lower-energy plasmas (more energy efficient relative to thermal plasmas) as a means of accomplishing “plasma catalysis,” with an emphasis on trying to characterize the phenomenon and better understand the governing fundamental parameters. It is hoped that this knowledge can then be better applied to the reforming process as well as related processes/applications NETL is exploring.

The reaction vessel and lid of the plasma reformer are designed to include an external window (in the top flange) which will allow us to view the interior of the plasma reformer. Two windows into the reactor, one on the reactor lid and the other window to be located on the top flange will provide a view of the state of the discharge and location of the reaction flame. Both windows can be aligned so that it would be possible to see straight down into the reaction vessel when looking from the top of the vessel. This will provide an optical access into the plasma reformer for the plasma characterization measurements such as electron distribution and plasma density.

## Results

To assess the initial performance and ability to handle a liquid fuel compound, n-tetradecane was reformed by DPI using the plasma unit at partial oxidation conditions. Yields (actual amount of the product\*100/theoretical amount of the product expected) of various species obtained in the product stream as a function of O/C ratio are shown in Figure 1. The conversion of n-tetradecane to gaseous products was almost complete for the O/C ratio greater than 1

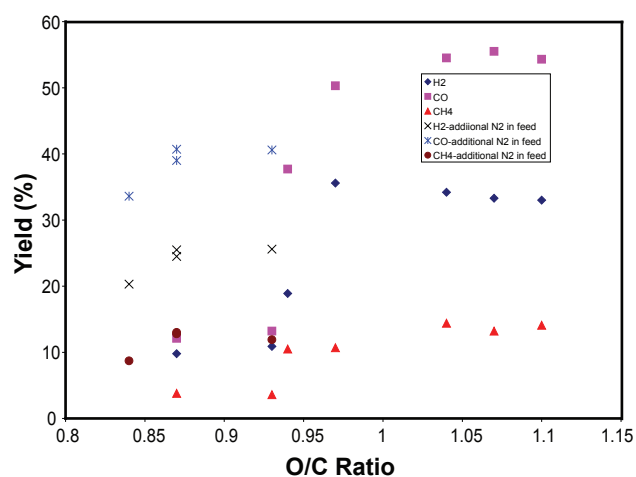


**FIGURE 1.** Yields of  $\text{H}_2$ ,  $\text{CO}$ , and  $\text{CH}_4$  from Plasma Reforming of n-Tetradecane as a Function of the O/C Ratios

and it was around 50-60% for the O/C ratio smaller than 0.97. However, a significant amount of lower hydrocarbon species ( $\text{CH}_4$ ,  $\text{C}_2\text{H}_2$ , and  $\text{C}_2\text{H}_4$ ) was also observed in the product stream. It is expected that the concentration of unsaturated hydrocarbons ( $\text{C}_2\text{H}_2$  and  $\text{C}_2\text{H}_4$ ) could be minimized once the plasma reformer is optimized for the flow, plasma power, and inlet feed temperature. Also, the reformer exhaust, a feed line coiled around the reactor outlet tube, was used to preheat the liquid fuel before it entered into the plasma reformer. The higher exhaust temperature ( $>700^\circ\text{C}$ ) observed during plasma reforming could initiate the gas phase chemistry of a liquid hydrocarbon before plasma chemistry and consequently producing unsaturated hydrocarbons. To avoid extreme preheating temperatures, the coil used to preheat the liquid feed around the reactor outlet will be replaced with a straight run of tubing which will be independently controlled at the desired preheat temperature ( $\sim 300^\circ\text{C}$ ).

The effects of the additional nitrogen fed to the reformer were also studied for the O/C ratio lesser than one. This nitrogen was added tangentially with the air to supposedly avoid any premature ignition and therefore keep the reformer in a stable region. Premature ignition outside the reaction vessel has resulted in soot formation and subsequent shorting of the arc across the ceramic dielectric ring and a reactor failure. Yields of  $\text{H}_2$ ,  $\text{CO}$ , and  $\text{CH}_4$  were significantly increased with the additional nitrogen in the feed (see Figure 1). The conversion of tetradecane to gaseous products was also significantly increased in the presence of the additional nitrogen.

Plasma characterization studies are planned to be initiated to measure the electron temperature distribution and plasma density in the plasma reaction zone during hydrocarbon reforming. Highly sophisticated probes for this purpose cannot be used due to high gas temperature as well as not enough space to insert these probes close to the plasma discharge. Therefore, optical measurements using a long focal length lens coupled with a newly acquired high resolution spectrometer is planned. Optical access into the plasma discharge can be done through two view windows located in the top and bottom flanges or through the exhaust line. With a long focal length lens coupled into a plasma spectrometer, we can perform a variety of plasma characterizing spectroscopic measurements. For example, it should be possible to determine the rotational and vibrational temperatures of nitrogen molecules in fuel-air plasmas. For most of the expected plasma conditions, the rotational states of nitrogen will be in thermodynamic equilibrium with background gas and can therefore provide a reasonable measure of the background gas temperature [5, 6]. The vibrational states are more sensitive to the non-equilibrium portion of the electron distribution and can therefore provide a measure of the non-equilibrium energy fraction of the plasma [5, 6]. Through doping

with argon gas, line ratios of argon emission lines can be used to remotely determine the plasma electron temperature and detect the presence of superthermal electron components [7]. Spectroscopic surveys of key lines can also be used to identify compounds and molecules in the plasma volume.

### Conclusions and Future Directions

Plasma technology provides an interesting and possible alternative for either full or assisted fuel reforming. A facility and reactor system has been established at NETL to allow for parametric evaluation of plasma processes with the DPI unit and/or other plasma developments efforts being undertaken to provide suitable hydrocarbon reforming for fuel cell-based systems. Parametric optimization will be conducted to obtain optimal syngas yields and hydrocarbon conversion. The parameters of interest are O/C, steam-to-carbon ratio, flow rate, preheat temperature, and power input. Plasma characterization studies are being initiated to measure the electron temperature distribution and plasma density in the plasma reaction zone during hydrocarbon reforming.

### References

1. C.S. Kalra, Y.I. Cho, A. Gutsol, A. Fridman, T.S. Rufael, V.A. Deshpande, Plasma Catalytic Conversion of Methane in Ultra Rich Flame Using Transient Gliding Arc Combustion Support, Electronic Proceedings of 2004 Technical Meeting, Central States Section, The Combustion Institute, 21–23 March 2004, University of Texas at Austin, TX.
2. C.S. Kalra, Y.I. Cho, A. Gutsol, A. Fridman, T.S. Rufael, Gliding Arc in Tornado Using a Reverse Vortex Flow, *Rev. Sci. Instrum.* 76, 025110 (2005).
3. C.S. Kalra, Y.I. Cho, A.F. Gutsol, A. Fridman, Gliding Arc Discharges as a Source of Intermediate Plasma for Methane Partial Oxidation, *IEEE Trans. Plasma Sci.* 33, No. 1, 32-41 (2005).
4. A. Czernichowski, Gliding Arc. Applications to Engineering and Environment Control, *Pure & Appl. Chem.*, Vol. 66, No. 6, 1301-1310 (1994).
5. C. Biloiu, Z Harvey, E.E. Scime, X. Sun, Determination of the Vibrational and Rotational Temperature of Helicon Generated Plasma from the Emission Spectrum of the First Positive System  $B^3\Pi_g \rightarrow A^3\Sigma_u^+$  of Nitrogen, *Rev. Sci. Instrum.* 77, 10F117 (2006).
6. C. Biloiu, X. Sun, Z. Harvey, E.E. Scime, An Alternative Method for Gas Temperature Determination in Nitrogen Plasmas: Fits of the Bands of the First Positive Systems, *J. Appl. Phys.* 101, 073303 (2007).
7. S.A. Cohen, X. Sun, N.M. Ferraro, E.E. Scime, M. Miah, S. Stange, N.S. Siefert, R.F. Boivin, On Collisionless Ion and Electron Populations in the Magnetic Nozzle Experiment (MNX), *IEEE Trans. Plasma Sci.* 34, 792-803 (2006).

## IV.G.7 Oxide-Based Reforming Catalysts: Evaluation and Development

David A. Berry (Primary Contact) and  
Dushyant Shekhawat  
U. S. Department of Energy  
National Energy Technology Laboratory (NETL)  
3610 Collins Ferry Road  
Morgantown, WV 26507-0880  
Phone: (304) 285-4430; Fax: (304) 285-0943  
E-mail: David.Berry@netl.doe.gov

### Subcontractors:

- Daniel Haynes, RDS Inc., Morgantown, WV
- Mark Smith, REM, Morgantown, WV

Contract Number: 07-220611

Start Date: October 1, 2007

End Date: September 30, 2009

### Objectives

- Evaluate performance and developmental potential of oxide-based materials as durable, low-cost catalysts to reform higher hydrocarbon fuel compounds.
- Assess the activity, selectivity, carbon deposition, and sulfur resistance of doped pyrochlore catalysts.

### Accomplishments

- Developed formulations and synthesized numerous pyrochlore catalysts.
- Evaluated the catalytic partial oxidation activity and selectivity of synthesized pyrochlore materials for reforming of n-tetradecane in the presence of 1,000 ppmw sulfur.
- Filed a patent disclosure for pyrochlore catalyst materials.

### Introduction

The Department of Energy has been sponsoring the development of high-temperature fuel cell technology for a variety of applications. This necessitates the use of current infrastructure fuels (coal, diesel, natural gas, etc.) which must be reformed into a hydrogen-rich synthesis gas before use in the fuel cell. The use of catalytic partial oxidation (CPOX) is viewed as one potentially attractive option for reforming due to its inherent simplicity that avoids the need for water addition, water management or extraneous heat exchangers and/or other costly

components. CPOX catalysts typically consist of Ni or Group-VIII noble metals incorporated onto various high surface area oxide substrates such as  $\gamma\text{-Al}_2\text{O}_3$ ,  $\text{SiO}_2$ , and more recently, mixed metal oxides. From the literature, Rh has been identified as the superior metal for CPOX due to its high selectivity to  $\text{H}_2$  and CO. This behavior is believed to be directly related to the high bond strength of Rh metal with surface oxygen, which prevents the undesirable reaction between surface oxygen and dissociated hydrogen atoms on the surface to form hydroxyl radicals and eventually water. Also, Rh has shown a high resistance to carbon formation compared to other metals.

However, carbon formation and deactivation by sulfur are still key challenges for CPOX catalysts. It has been shown that catalyst poisoning by sulfur and/or carbon is a structure sensitive reaction. Specifically, the deactivation mechanism by carbon and sulfur is influenced by the cluster size of the active metal. For example, larger metal clusters have a much stronger interaction with carbon and sulfur, than smaller, well-dispersed metal particles [1–3]. This problem becomes worse at the high reforming temperatures of CPOX, because conventional supported metals tend to sinter and agglomerate into even larger particles. Thus, the need for improved catalyst design/performance still exists.

### Approach

The development of a catalyst with spatially distributed active metal components in a structure that can tolerate the high temperatures of CPOX may provide a more durable catalyst compared to simple supported metal clusters. The formation of elemental carbon during reformation onto the surface of a catalyst has been shown to be related to both the size of the active metal cluster [4] and its coordination [5].

Dispersing the metal throughout the structure may avoid the formation of larger metal clusters at the surface that are favorable sites for sulfur poisoning and carbon deposition, and thus may make the catalyst less susceptible to deactivation. Mixed metal oxides have become increasingly popular because of the ability to substitute different metals into their structure and maintain catalytic activity [6-7]. For example, prior research at NETL has demonstrated the ability to effectively incorporate Ni into the hexaaluminate structure  $\text{ANi}_{0.4}\text{Al}_{11.6}\text{O}_{19-d}$  ( $A = \text{La, Sr, and Ba}$ ) and successfully partially oxidize n-tetradecane with reduced carbon formation [8]. Liu and Krumpelt [6] have shown that the incorporation of Ru into a perovskite type structure ( $\text{LaCr}_{0.95}\text{Ru}_{0.05}\text{O}_3$ ) is catalytically active for the

autothermal reforming of n-dodecane while exhibiting sulfur tolerance.

The general approach undertaken in this study has been to substitute catalytically active metals and dopants into the framework oxide lattice of specific pyrochlore materials to reduce the formation of large ensembles of active sites that are responsible for forming carbon and also for strongly adsorbing sulfur compounds also leading to deactivation. Select formulations of pyrochlore compounds were synthesized and evaluated for catalytic partial oxidation activity and selectivity during reforming of n-tetradecane and dibenzothiophene (1,000 ppmw of sulfur).

## Results

To assess the performance and potential of pyrochlore materials for fuel reforming, four catalyst formulations were tested for conversion of a sulfur-laden hydrocarbon fuel under partial oxidation conditions: 1) Rh/ $\gamma$ -Al<sub>2</sub>O<sub>3</sub>, 2) lanthanum zirconate (LZ), 3) lanthanum rhodium zirconate (LRZ) and 4) strontium doped lanthanum rhodium zirconate (LSRZ). Material characterizations for the catalysts are shown in Table 1.

**TABLE 1.** Catalyst Characterization

	Rh/ $\gamma$ -Al <sub>2</sub> O <sub>3</sub>	LZ	LRZ	LSRZ
Synthesis Method	Commercial Alfa Aesar	Pechini Method		
Rh Metal Loading - wt %	0.5	N/A	2.0	2.0
XRD (Phase)	N/A <sup>a</sup>	Pyrochlore	Pyrochlore	Binary phase perovskite-pyrochlore. Defect SrZrO <sub>3</sub>
Rh Dispersion by H <sub>2</sub> Pulse Chemisorption (%)	73	N/A	2	5

<sup>a</sup> did not perform X-ray diffraction (XRD) on this material.

The fuel chosen for the test was n-tetradecane (TD) with 1,000 ppm of dibenzothiophene (DBT), which was used to accentuate the effect of sulfur on catalyst degradation. Testing was conducted in a fixed bed continuous flow reactor (Autoclave Engineers, Model no. BTRS Jr.). The liquid feed was vaporized in a temperature-controlled preheating furnace set at 375°C and fed to the reactor along with the preheated air. The catalyst bed was diluted with quartz sand at a weight ratio of 5/1 quartz to catalyst to minimize temperature gradients and avoid channeling. A split-tube furnace encapsulated the reactor tube, and provided temperature control. Bed temperature was monitored by an axially centered thermocouple. All catalysts were tested under

the same conditions throughout the test and can be seen in Table 2.

**TABLE 2.** Experimental Conditions for CPOX Experiments

Reaction Conditions	
O/C ratio	1.2
GHSV (scc g <sub>cat</sub> <sup>-1</sup> h <sup>-1</sup> )	50,000
Bed Temperature (°C)	900
Catalyst Bed (mg)	480
Pressure (MPa)	0.23

A blank reactor run (CPOX of TD, no DBT) using only quartz sand in the reactor tube was performed for five hours to quantify the gas phase reactions. Comparison of the blank run relative to expected equilibrium values can be seen in Table 3. From the results, the quartz sand blank shows considerable conversion of the TD to olefins and benzene, which significantly reduces the production of hydrogen. This establishes a baseline to demonstrate the effect on product distribution and yield due to the interaction of the catalysts described later.

**TABLE 3.** Equilibrium and Blank Reactor Product Yields, and Carbon Balance for the CPOX of TD at O/C = 1.2, P = 0.23 MPa, and 900°C

	Equilibrium <sup>a</sup>	Quartz Sand (Blank) <sup>b</sup>
H <sub>2</sub> yield (%)	90	17
CO yield (%)	92	42
CO <sub>2</sub> yield (%)	8.5	17
CH <sub>4</sub> yield (%)	0.1	8
Olefin and benzene yield (%)	0.0	23
Carbon balance (%)	N/A	90
Carbon formation (g <sub>carbon</sub> /g <sub>catalyst</sub> )	0	0.4

<sup>a</sup> Calculated by a Gibb's free energy minimization using HSC Chemistry Thermodynamic software [9].

<sup>b</sup> Measured at the end of the 5-h run.

The CPOX experiments themselves involved three steps. First, the CPOX of TD only was performed for one hour to establish baseline activity and selectivity of the catalyst. Next, the feed was switched to 1,000 ppmw DBT in TD for two hours to see the effect of sulfur. Finally, the feed was switched back to TD only for two hours to examine activity recovery.

In addition, after each experiment, carbon deposition was measured by temperature programmed oxidation (TPO). The catalyst was ramped from 200-900°C by 1°C/min under 5% O<sub>2</sub>/N<sub>2</sub>, and the CO<sub>2</sub> produced was continuously monitored by a Thermo

Onix mass spectrometer (Model no. Prima 8b, a 200 a.m.u. scanning magnetic sector).

The first catalyst tested was the commercial Rh/ $\gamma$ -Al<sub>2</sub>O<sub>3</sub>, which contained a 0.05% Rh loading. Conversion of TD was effectively 100% with slightly lower than equilibrium values for hydrogen and carbon monoxide. Upon addition of the sulfur, yields of hydrogen and carbon monoxide dropped considerably with hydrogen continuing sharp decline with time (Figure 1). Upon removal of sulfur, performance improved, but nothing near initial performance.

The next test performed was on LZ (Figure 2). Although initial performance is slightly lower than Rh/ $\gamma$ -Al<sub>2</sub>O<sub>3</sub> (to be possibly expected due to absence of Rh), yields of hydrogen and carbon monoxide are similar. However, hydrogen yield is somewhat stabilized throughout the sulfur addition. In addition, catalyst recovery appears to occur to a greater degree and more rapid rate.

Upon addition of rhodium to the base LZ material, the LRZ showed near equilibrium initial performance and a much less severe drop upon sulfur addition (Figure 3). Performance did continually decline under high sulfur conditions, however, catalyst recovery approached initial catalyst performance values.

For the last test, strontium was added the LRZ to form LSRZ (Figure 4). The doping of this catalyst has the effect of increasing the ionic conductivity, which may contribute to its increased catalytic performance. Near equilibrium performance was again noted. However, the addition of sulfur resulted in a fairly modest decline in yield and performance remained relatively stable throughout this period. Removal of the sulfur saw the catalyst return very quickly to near initial values.

Measurement of carbon formation elucidated some interesting results. A TPO was conducted after each total 5-hour run (CPOX of TD only for one hour, 1,000 ppmw DBT/TD for two hours and TD only for two hours). Although catalyst activity varied among

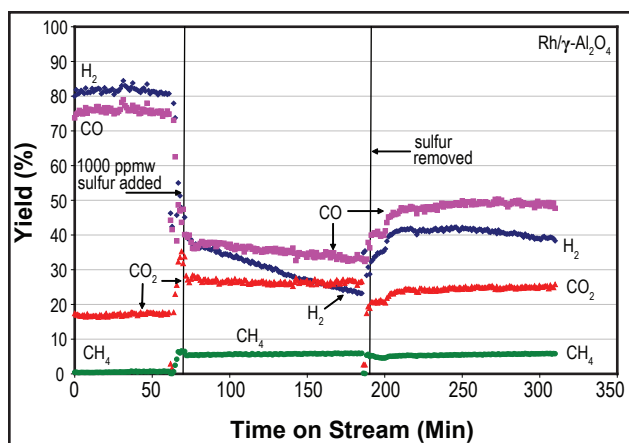


FIGURE 1. Performance of Rh/ $\gamma$ -Al<sub>2</sub>O<sub>3</sub> Catalyst

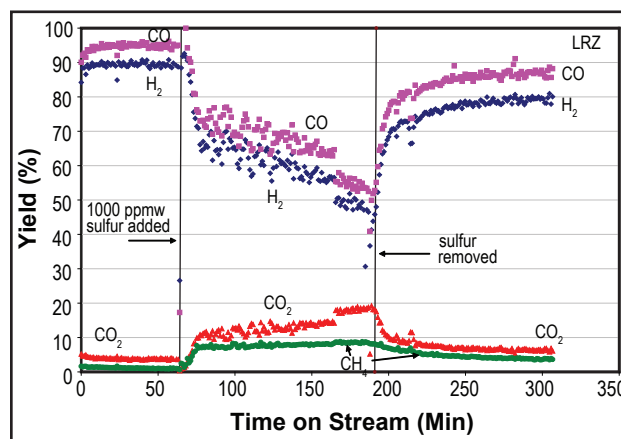


FIGURE 3. Performance of LRZ Catalyst

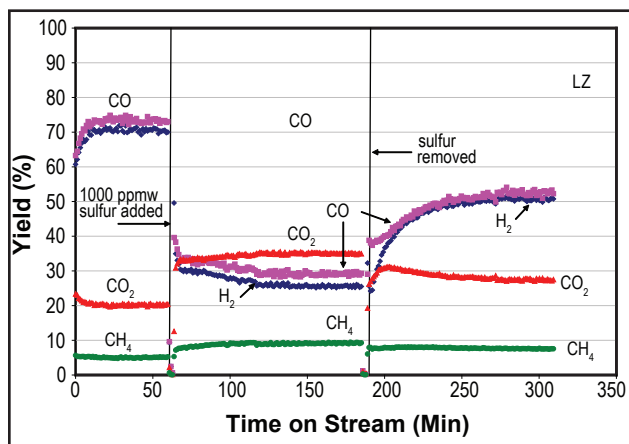


FIGURE 2. Performance of LZ Catalyst

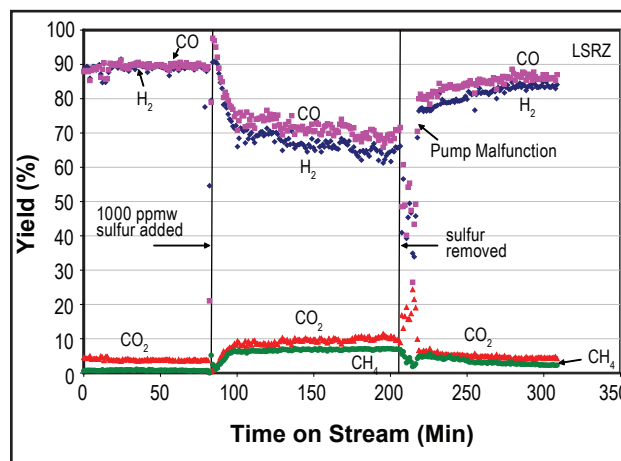


FIGURE 4. Performance of LSRZ Catalyst

the catalyst types, total carbon was similar for LZ, LRZ and Rh/ $\gamma$ -Al<sub>2</sub>O<sub>3</sub> (Table 4). However, the LSRZ showed pronounced decrease in deposited carbon.

**TABLE 4.** Amount of Carbon Formed on Pyrochlore Catalysts

	Rh/ $\gamma$ -Al <sub>2</sub> O <sub>3</sub>	LZ	LRZ	LSRZ
Carbon deposition (g <sub>carbon</sub> /g <sub>cat</sub> ) <sup>a</sup>	0.90	0.80	0.86	0.30

<sup>a</sup> As measured by TPO.

## Conclusions and Future Directions

All catalysts tested showed greater activity for hydrogen and carbon monoxide yield from TD CPOX reforming relative to the blank (sand). However, the only non-pyrochlore catalyst, Rh/ $\gamma$ -Al<sub>2</sub>O<sub>3</sub>, showed significant immediate and continuous decline upon addition of the DBT as sulfur. It is unclear over the time period of the experiment, whether activity would have reached a steady level or if hydrogen activity would have completely declined. In contrast, all of the pyrochlore catalysts exhibited either higher or more stable performance. For example, LZ showed significant initial decline, but then stabilized just slightly above the 20% hydrogen level. Upon addition of Rh to form LRZ, the next catalyst demonstrated higher initial values for both hydrogen and carbon monoxide conversion. This is to be expected if one considers Rh as the element/metal most responsible for catalytic activity. By far and away however, the LSRZ catalyst exhibited the highest product yields and most stable performance when exposed to sulfur. Perhaps the mobility of oxygen within the structure can be attributed to this tolerance. The carbon deposition data in Table 4 would seem to indicate a better ability for LSRZ to remove or retard carbon, which may also be related to better sulfur tolerance as well.

Future work will focus on exploiting the elemental substitution characteristics of the oxide pyrochlore structure in hopes of optimizing the carbon and sulfur tolerance capabilities during reformation. Once identified, long-term testing will be planned to demonstrate catalytic stability and durability.

## Special Recognitions & Awards/Patents Issued

1. D.A. Berry, D. Shekhawat, D. Haynes (LSU), J.J. Spivey, "Pyrochlore Materials for Chemical Reaction Systems", Provisional Patent Filed (2008).

## FY 2008 Publications/Presentations

1. J. J. Spivey, D. J. Haynes, D. A. Berry, D. Shekhawat, Fuel Processing of n-Tetradecane: Catalytic Partial Oxidation on Rh- and Ru-Substituted Metal Oxides, 7<sup>th</sup> International

Workshop on Catalytic Combustion, Lake Zurich, Switzerland, September 29 – October 1, 2008.

2. D. J. Haynes, D. A. Berry, D. Shekhawat, J.J. Spivey, Catalytic Partial Oxidation of n-Tetradecane Using Pyrochlores: Effect of Rh and Sr Substitution, *Catalysis Today*, 136 (2008) 206-213.
3. D. J. Haynes, D. A. Berry, D. Shekhawat, J.J. Spivey, Catalytic Partial Oxidation of TD Using Rh and Sr Substituted Pyrochlores: Effects of Sulfur, *Catalysis Today* (accepted).
4. T. H. Gardner, D. Shekhawat, D. A. Berry, M. W. Smith, M. Salazar-Villaphando, E. L. Kugler, Effect of Nickel Hexaaluminate Mirror Cation on Structure-Sensitive Reactions during n-Tetradecane Partial Oxidation, *Applied Catalysis A: General*, 323 (2007) 1-8.
5. D. J. Haynes, D. A. Berry, D. Shekhawat, T. H. Gardner, T-C. Xiao, M. H. Green, J. J. Spivey, Partial Oxidation Reforming of n-Tetradecane over Pt and Carbide Catalysts: A Comparative Study, *Industrial & Engineering Chemical Research* (accepted).
6. M. Salazar, D. A. Berry and T. H. Gardner, Partial Oxidation of Methane over Rh/Supported-Ceria Catalysts: Effect of Catalyst Reducibility and Redox Cycles, *Accepted, International Journal of Hydrogen Energy*, 2008.
7. M. Salazar, D. A. Berry and T. H. Gardner, Role of Lattice Oxygen in the Partial Oxidation of Methane over Ceria-Based Catalysts, 2007 Annual AIChE Meeting, Salt Lake City, Utah.

## References

1. B.J. Wuensch, K.W. Eberman, C. Heremans, E.M. Ku, P. Onnerud, E.M.E. Yeo, S.M. Haile, J.K. Stalick, J.D. Jorgensen, *Solid State Ionics*. 129 (2000) 111.
2. K.V.G. Kutty, C.K. Mathews, T.N. Rao, U.V. Varadaraju, *Solid State Ionics*. 80 (1995) 99.
3. P. Erri, P. Dinka, A. Varma, *Chem. Eng. Sci.* 61 (2006) 5328. Barbier, J.; Marecot, P. *J. Catal.* 102 (1986) 21.
4. Bengaard, H.S.; Norskov, J.K.; Sehested, J.; Clausen, B.S.; Nielsen, L.P.; Molenbroek, A.M.; Rostrup-Nielsen, J.R. *J. Catal.* 209 (2002) 365.
5. Xu, Z., Zhen, M., Bi, Y. and Zhen, K., *Catal. Lett.* 64 (2000) 157-161.
6. D.-J. Liu, M. Krumpelt, *Int. J. Appl. Ceram. Technol.* 2 (2005) 301.
7. J. Barbier, in: B. Delmon, G.F. Froment Eds. *Catalyst Deactivation*, Elsevier Science Publishers, Amsterdam, 1987, p. 1.
8. T.H. Gardner, D. Shekhawat, D.A. Berry, M.W. Smith, M. Salazar, E.L. Kugler, *Appl. Catal. A: Gen.* 323 (2007)
9. A. Roine, *HSC Chemistry 4.0 ed.*, Outokumpu Research Oy, Pori, Finland, 1999.

## IV.G.8 Novel Water-Neutral Diesel Fuel Processor and Sulfur Trap

Subir Roychoudhury (Primary Contact),  
Tianli Zhu, and Dennis Walsh  
Precision Combustion Inc. (PCI)  
410 Sackett Point Rd.  
North Haven, CT 06473  
Phone: (203) 287-3700 ext. 267; Fax: (203) 287-3710  
E-mail: sroychoudhury@precision-combustion.com

DOE Project Manager: Ayyakkannu Manivannan  
Phone: (304) 285-2078  
E-mail: Ayyakkannu.Manivannan@netl.doe.gov

Contract Number: 84674

Start Date: June 20, 2007  
Project End Date: March 19, 2008

- **Low pressure drop nozzle demonstrated:** Designed and tested a low pressure drop prototype nozzle with uniform mixing of fuel, air and steam. At 5 kW<sub>th</sub> (fuel throughput) stable operation was achieved.
- **ATR cost projections were expected to be consistent with long-term DOE projections.** Size of the ATR reactor was <40 cc. Weight of the ATR reactor, less housing, was <50 gms.

---

---

### Introduction

Key barriers for the Solid State Energy Conversion Alliance industrial teams are the lack of a compact and economical diesel reformer capable of operating water-neutral at very low S:C ratios and resistant to coking and sulfur poisoning. Fuel preparation for these reformers is also problematic primarily due to lack of good mixing at low pressure drop.

In Phase I, PCI identified a low pressure drop mixer, and a Microlith<sup>®</sup> diesel fuel reformer operating at low S:C ratios so as to allow overall water-neutral operation while being resistant to coking and fuel sulfur. This offers to resolve key hurdles, namely (i) reducing the pressure drop by using a low air pressure injector/mixer; (ii) system design for water neutrality by taking advantage of the very low amount of steam needed for Microlith<sup>®</sup> ATR operation; (iii) multi-thousand hour durability capability; and (iv) system simplification for cost optimization to meet commercially viable targets for the entire auxiliary power unit (APU) fuel cell system.

### Approach

The concept builds on PCI's Microlith<sup>®</sup> reforming technology which employs a mesh-based catalyst as an integrated component of a novel reformer system involving a diesel/air/steam injector, reformer, steam generator and sulfur trap. The complete 5 kW<sub>th</sub> system size was 5 liters and weighed 5 kgs. With support from the U.S. Department of Defense, PCI has developed and demonstrated such a reactor that starts up in partial oxidation mode and transitions to ATR mode, operating at low S:C ratios. It uses a limited amount of water that can be recovered from the system exhaust (via a condensing heat exchanger) and permits efficient fuel reformation without the deleterious effects of high temperatures and coke formation. Since the ATR is operated at very low S:C ratios, H<sub>2</sub>S is readily adsorbed in the downstream ZnO bed. Appropriate thermal integration of the reformer, SOFC, water recycle unit

### Objectives

- Examine feasibility of operating an integrated reformer and a solid oxide fuel cell (SOFC) system with water-neutral operation.
- Demonstrate the viability of operating the autothermal reformer (ATR) at water neutral conditions for 500 hours with Tier 2 diesel.
- Operation at low steam-to-carbon (S:C) ratio without coking and achieve complete fuel conversion (>99.9% to C1 products) with reforming efficiency of ~80% (based on ratio of lower heating value [LHV] of fuel and reformat).
- Examine and identify reduced pressure drop mixing solutions.
- System simplification for cost optimization to meet commercially viable targets.

### Accomplishments

All objectives were fully met or exceeded.

- **Water-neutral operational design achieved:** Identified and examined a design via ASPEN Engineering Modeling that would permit water-neutral operation and require only limited water recovery from the anode exhaust.
- **Demonstrated >500 hour coke-free operation** of an integrated Microlith<sup>®</sup> fuel processor (reformer reactor/sulfur trap/steam generator) operating at water-neutral design conditions on low sulfur distillate fuel (containing <15 ppm inlet sulfur). Reforming efficiency was >80%. The reformat was used to power a 1 kWe SOFC. This exceeded the proposed 500-hour Phase I objectives.

and other components in the APU system is also necessary to maximize the overall system efficiency.

PCI worked with SOFC developers to identify and develop a system approach to meet the aforementioned goals. Low pressure scenarios involving an ATR, an SOFC, an anode gas burner, and water recovery unit were explored via ASPEN process simulation software. This sought to supply the required ATR feed water via capture and recycle from process exhaust streams in order to avoid the need for water from an external source. Design approaches that enable meeting the commercially viable cost targets for the fuel cell system were identified. Development of a mixer with low pressure drop was examined. An integrated diesel fuel processor with injector/igniter/reformer was tested at a water-neutral condition to demonstrate long-term feasibility of the proposed concept.

## Results

### System Design for Water Neutrality via ASPEN Engineering Software

Water neutrality operation conditions were identified via ASPEN modeling. Two low pressure scenarios were explored involving an ATR and an SOFC. In one approach, the feasibility of achieving water neutrality was investigated by exploring water condensation and recycle from the anode exhaust; in the second configuration, recycling a vapor phase stream derived from an oxidized fraction of the anode exhaust was examined. Both approaches sought to avoid the need to supply water from an external source. The models were built based upon process configurations experimentally investigated at PCI and performance information provided by SOFC developers. The results suggested that the water condensation approach has advantages over anode exhaust gas recycle in terms of higher overall process efficiency, as well as the current availability of promising technology for water condensation. The water recovery requirement as a percentage of the total water available in the anode gas is moderate and provides sufficient water to effectively suppress coke formation in the reformer.

### Reformer Durability Under Water-Neutral and Catalytic Partial Oxidation Conditions

Long-term durability of the diesel reformer under water-neutral operation conditions is a crucial requirement for a commercially viable SOFC APU system. An ATR Microlith<sup>®</sup> reactor was operated at a low S:C ratio to permit water neutrality. Under those conditions, >500 hours stable performance was demonstrated with a 15 ppm sulfur-containing distillate fuel in a test of an integrated fuel processor

(reformer reactor/sulfur trap/steam generator) with an SOFC stack. This was done in conjunction with long-term durability efforts supported by Department of Defense programs. Almost complete fuel conversion to C1/C2 and >80% reforming efficiency (LHV) were achieved. Stable performance with no indication of coke deposition was demonstrated despite multiple shutdowns due to ancillary equipment failure. The durability testing performed so far indicates that achieving durable performance at even longer operating times (thousands of hours) may be reasonably expected in a water-neutral APU system.

### Development of a Low Air-Pressure Nozzle

An important challenge for on-board fuel reforming is the use of low pressure drop mixers for fuel, air and steam prior to entering the reactor. This reduces parasitic losses. A prototype low pressure nozzle design resulted in a very low inlet air supply pressure requirement. Nozzle tests with an ATR reactor showed a stable temperature profile with small temperature variations during ATR operation. The temperature distribution throughout the reactor was closely distributed for normal operation.

## Conclusions and Future Directions

A novel compact and efficient Microlith<sup>®</sup> diesel fuel reformer was developed for operating at low S:C ratios of <1 for overall water-neutral operation while being resistant to coking and fuel sulfur.

Water recovery approaches based on water condensation were examined and indicated the potential for a compact and cost effective water condenser. System efficiency of the APU system based on water condensation was estimated to be >30% obtained from modeling supported by experimental results.

The feasibility of the Microlith<sup>®</sup> reformer to reach long-term durability under water-neutral operating conditions was indicated by the long-term stable performance of an integrated Microlith<sup>®</sup> ATR with real world fuels. There was almost complete fuel conversion with C2 and C3 levels below 20 ppm in the reformat with >80% reforming efficiency. This provides a good likelihood for 5,000 hours of stable operation.

A prototype low pressure mixer was designed and manufactured. The performance was examined and achieved sufficient atomization/mixing for stable operation. Future development of this nozzle design will include improvement of steam injection, turn down ratio and cold start capability. Endurance testing of the nozzle is also required to examine possible formation of deposits inside the fuel injection tube.

### **Special Recognitions & Awards/Patents Issued**

1. 1 patent application filed.

### **FY 2008 Publications/Presentations**

1. Presentation scheduled for Fuel Cell Seminar 2008.

## IV.G.9 Carbon Tolerant Steam Reforming and SOFC Anode Catalysts

Eranda Nikolla, Johannes Schwank,  
Suljo Linic (Primary Contact)

University of Michigan  
2300 Hayward St.  
Ann Arbor, MI 48409  
Phone: (734) 764-7469  
E-mail: linic@umich.edu

DOE Project Manager: Ayyakkannu Manivannan  
Phone: (304) 285-1359  
E-mail: Ayyakkannu.Manivannan@netl.doe.gov

Contract Number: 42516

Start Date: July 1, 2005  
Project End Date: December 31, 2008

- The superior carbon tolerance of the alloy catalyst compared to monometallic Ni was demonstrated for different average size of metal particles and the metal loading.
- We have also implemented the Sn/Ni surface alloy as a SOFC anode catalyst.

### Objectives

- Utilize quantum Density Functional Theory (DFT) calculations and state-of-the-art experimental tools to identify underlying molecular mechanisms that govern the formation of carbon deposits on reforming catalysts.
- Use these molecular insights to formulate carbon tolerant hydrocarbon steam reforming and solid oxide fuel cell (SOFC) anode catalysts.
- Synthesize and test the potential carbon-tolerant catalysts in steam reforming of various fuels under SOFC conditions.
- Implement these catalysts as SOFC anodes.
- Determine the effect of the size of metal particles and metal loading on the performance of these catalysts.
- Utilize various spectroscopic and microscopic tools to characterize the tested catalysts.

### Accomplishments

- We have determined, using DFT, that the carbon tolerance of Ni can be improved by formulated Ni-containing surface alloys that, compared to Ni, preferentially oxidize C atoms rather than form C-C bonds and/or that have lower thermodynamics driving force associated with carbon nucleation on the low-coordinated sites on catalytic particles.
- We have found that supported Sn/Ni surface alloy catalysts are more resistant to carbon-induced deactivation than supported monometallic Ni in steam reforming of methane, propane, and isooctane at moderate steam to carbon ratios.

### Introduction

The development of efficient and environmentally friendly energy generation systems will require major advances in catalysis. Improved hydrocarbon fuel reforming catalysts and electro-catalysts need to be formulated and synthesized. These catalysts need to perform the desired reactions with utmost efficiencies, at reduced costs, and with improved durability. One of the main issues associated with the catalytic and electro-catalytic reforming of hydrocarbon fuels is that conventional catalysts, such as Ni supported on oxides, deactivate due to the formation of carbon deposits formed in the process of hydrocarbon activation.

Our objective was to utilize quantum DFT chemical calculations and various state-of-the-art experimental tools to study molecular mechanisms associated with the carbon-induced deactivation of monometallic Ni catalysts. Based on these DFT studies we have identified Sn/Ni surface alloy as potential carbon-tolerant reforming catalyst. The superior performance of supported Sn/Ni compared to Ni catalyst was demonstrated in steam reforming of methane, propane, and isooctane at moderate steam to carbon ratios [1-3]. The reactions were performed at typical SOFC operating conditions. Further tests revealed that the Sn/Ni alloy catalyst is more carbon-tolerant than monometallic Ni over a wide range of operating conditions and for different average particle size and metal loadings [4].

### Approach

We have employed quantum DFT calculations, catalyst synthesis, catalysts testing, and catalysts characterization to identify potential carbon-tolerant alloy catalysts.

DFT calculations allow us to obtain, from first principle and with high accuracy, the ground state geometries and energies of relevant reactants, products, and transition states involved in elementary chemical reactions on model catalyst surfaces [5]. These tools can be employed to guide the discovery of novel catalytic materials that might exhibit an improved performance compared to conventional catalysts.

Reactor experiments and multiple characterization techniques were applied to test novel catalytic materials identified in the DFT calculations. The novel catalysts were also tested as potential SOFC anodes.

## Results

A critical issue in catalytic hydrocarbon reforming and direct on-cell reforming in SOFCs is that currently used catalysts, such as Ni supported on oxides, facilitate the formation of extended carbon structures which deactivate the catalyst or electro-catalyst.

We have previously demonstrated that the impregnation of the supported Ni catalysts with a small amount of Sn results in the formation of a Sn/Ni surface alloy catalyst which is more resistant to carbon than the supported monometallic Ni catalysts. The surface alloy is characterized by Sn mixing with Ni in the surface layers of the Ni particles. The formation of the surface alloy was verified using various techniques. For instance, we utilized X-ray photoelectron spectroscopy (XPS) to determine that the atomic concentration of Sn in the surface layers of the reduced Sn/Ni catalysts was ~25% for the Sn/Ni particles that contained ~1 wt% of Sn with respect to Ni. Furthermore, we also performed scanning electron energy loss spectroscopy studies showing that the concentration of Sn is the highest in the surface layers of the Sn/Ni particles. The formation of the surface alloy was also supported by DFT calculations which showed that the free energy of formation of the Sn/Ni surface alloy, with Sn displacing the Ni atoms at the surface layer of Ni, is lower than the formation energy of other Sn/Ni structures, including bulk alloys and separated Sn and Ni phases. Our previous results, published in the 2006 and 2007 reports showed that for large Sn/Ni particles (~1  $\mu\text{m}$  in diameter), typical for SOFC anodes, the Sn/Ni catalyst is significantly more carbon-tolerant than monometallic Ni. In this report we focus on the role of metal loading and the size of catalytic particles.

The Sn/Ni and Ni catalysts supported on yttria-stabilized zirconia (YSZ) were prepared using two different strategies, incipient wetness and ball milling. The main difference between these synthesis strategies is that they yielded metal particles with significantly different diameters. These two approaches are generally utilized in the synthesis of steam reforming catalysts (incipient wetness) and anode electro-catalysts for SOFCs (ball milling).

The Ni/YSZ steam reforming catalyst was prepared by the standard incipient wetness technique. The appropriate amount of  $\text{Ni}(\text{NiO}_3)_3$  was dissolved in ethanol and sequentially impregnated on the YSZ support. The Ni metal loading was ~15 wt% with respect to the total amount of catalyst (Ni plus YSZ). The catalyst was calcined in air at 873 K for 2 hours

and then reduced using a gas mixture of 30%  $\text{H}_2/\text{N}_2$  at 1,073 K for 5 hours. This procedure resulted in metal particles of ~30 nm in diameter anchored on the support. The Sn/Ni/YSZ steam reforming catalyst was prepared by impregnating ~3 wt% of Sn, with respect to Ni, in the form of  $\text{SnCl}_2 \cdot 4\text{H}_2\text{O}$  on the calcined NiO/YSZ sample. The catalyst samples were then calcined again at 873 K for 2 hours and reduced under a stream of 30%  $\text{H}_2/\text{N}_2$  for 5 hours at 1,073 K.

The SOFC anode catalyst was prepared by ball milling a mixture of 50 wt% YSZ and 50 wt% of NiO in methanol for 24 hours. Once dried, the powder was pressed into 13 mm diameter pellets at 5,000 psi. The pellets were sintered at 1,673 K for 4 hours. The catalyst was further reduced at 1,173 K for 5 hours in a gas mixture of 30%  $\text{H}_2/\text{N}_2$  to insure full reducibility. This synthesis procedure yielded catalytic particles with ~0.5  $\mu\text{m}$  diameter, as measured by transmission electron microscopy (TEM). The resulting catalysts had a Ni loading of 44 wt%. The Sn/Ni/YSZ SOFC anode catalyst was prepared by impregnating  $\text{SnCl}_2 \cdot 4\text{H}_2\text{O}$  (~1 wt% with respect to Ni) on the sintered NiO/YSZ pellets via the wet incipient technique. The pellets were dried over night at 473 K and then reduced under a stream of 30%  $\text{H}_2/\text{N}_2$  for 5 hours at 1,173 K.

Figure 1 shows the conversion of isooctane in steam reforming of isooctane at a steam to carbon (S/C) ratio of 1.5 and an operating temperature of 1,073 K for four different catalysts: (1) 15 wt% Ni/YSZ steam reforming catalyst (15 wt% Ni loading with respect to the total catalyst (Ni and YSZ) and average particle diameter of 30 nm), (2) 3 wt% Sn/15 wt% Ni/YSZ steam reforming catalyst (15 wt% Ni loading with respect to the total catalyst, 3 wt% Sn with respect to Ni, and average particle diameter of 30 nm), (3) 44 wt% Ni/YSZ SOFC anode catalyst (44 wt% Ni with respect to the catalyst mass and an average particle diameter of 0.5  $\mu\text{m}$ ), and (4) 1 wt% Sn/44 wt% Ni/YSZ SOFC anode catalyst (44 wt% Ni with respect to Ni plus YSZ, 1 wt% of Sn with respect to Ni, and an average particle diameter of 0.5  $\mu\text{m}$ ). Figure 1 indicates that the conversion of isooctane for both the Sn/Ni/YSZ steam reforming and SOFC anode catalysts, irrespective of metal loading and average particle diameter was stable for as long as the catalyst was kept on stream. These longest tests lasted ~5 days. In contrast to the Sn/Ni/YSZ catalysts, the conversion of isooctane on monometallic Ni supported on YSZ deteriorated rapidly for both Ni/YSZ steam reforming and SOFC anode catalysts. The reactor tests also showed that the Ni/YSZ catalyst with smaller Ni particles was more resistant to carbon than the Ni/YSZ catalyst with larger metal particles for identical operating conditions. The carbon resistance of the smaller Ni particles is generally attributed to the high energy of carbon deposits, mainly carbon nano-tubes, which form in the process of the deactivation of the Ni particles with small diameter. This high energy of carbon deposits

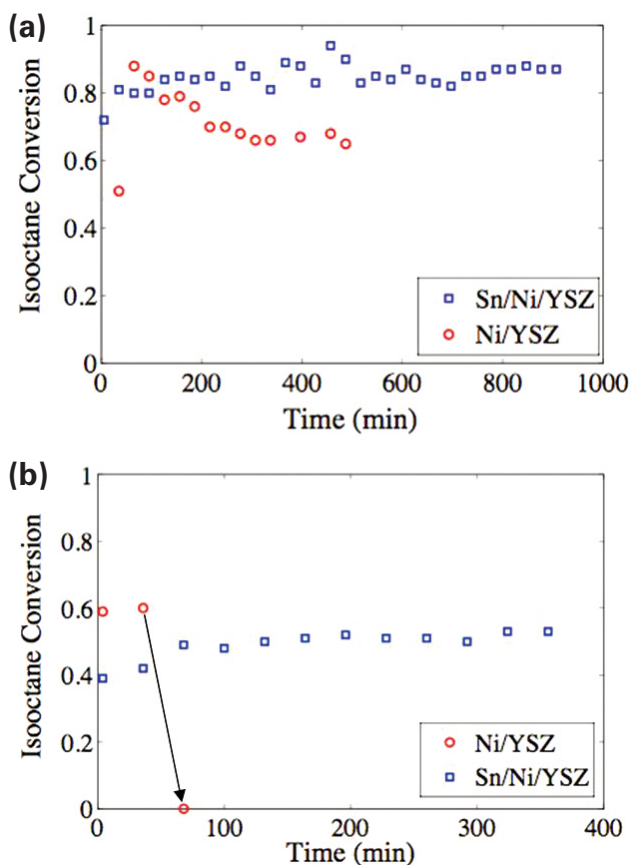


**FIGURE 1.** a) Plot of the isooctane conversion versus time under steam reforming conditions of S/C ratio of 1.5 and 1,073 K for: a) 15Ni/YSZ catalyst (15 wt% of Ni with respect to the total catalyst) and a 3Sn/15Ni/YSZ catalyst (3 wt% of Sn with respect to Ni, 15 wt% of Ni with respect to the total catalyst). Both catalysts had an average metal particle diameter ~30 nm, b) 44Ni/YSZ catalyst (44 wt% of Ni with respect to the total catalyst) and a 1Sn/44Ni/YSZ catalyst (1 wt% Sn with respect to Ni). Both catalysts had an average metal particle diameter ~0.5 μm.

results in lower driving force to form these deposits on smaller metal particles.

Characterization of the used catalysts with electron microscopy showed that the deactivation of Ni/YSZ was a consequence of the formation of carbon deposits, which led to the disintegration of Ni particles. For example, Figure 2a shows a scanning electron micrograph (SEM) of a used Ni/YSZ catalyst. It is clear that the catalytic particles were completely covered by carbon. Figure 2b shows SEM and TEM images of used Sn/Ni/YSZ. Unlike for Ni/YSZ, no carbon deposits were detected on Sn/Ni/YSZ. We have also utilized XPS to characterize the used Ni/YSZ and Sn/Ni/YSZ catalysts. These measurements showed that a substantial amount of graphitic carbon was formed on Ni/YSZ during isooctane steam reforming. On the other hand, no appreciable carbon was detected in the case of the Sn/Ni/YSZ catalyst.

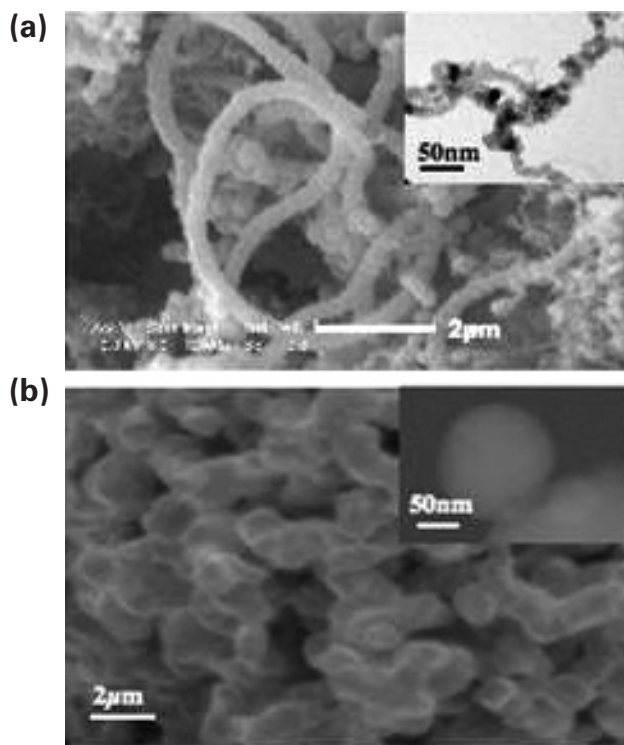


**FIGURE 2.** a) SEM and TEM (insert) images of a 44Ni/YSZ catalyst after steam reforming of isooctane. This process resulted in the formation of carbon filaments. b) SEM and TEM (insert) images for a 1Sn/44Ni/YSZ catalyst after steam reforming of isooctane. No carbon was detected on the catalyst.

### Conclusions and Future Directions

- We have demonstrated that the supported Sn/Ni surface alloy catalyst is more carbon tolerant than the supported monometallic Ni catalyst irrespective of the metal loading and average metal particle size.
- We have determined that the long-term stability of the Sn/Ni surface alloy is governed by its ability (1) to selectively oxidize carbon atoms, while preventing the formation of C-C bonds and (2) to suppress the nucleation of carbon deposits on the low coordinated catalyst sites.
- We plan to test the surface alloy catalysts as SOFC anodes for direct on-cell electrochemical oxidation of hydrocarbon fuels on SOFC anodes.

### Special Recognitions & Awards/Patents Issued

1. **Young Scientist Award of ICC 2008**, International Congress on Catalysis, Seoul, Korea, 2008.
2. **Walter J. Weber Jr. Award in Environmental and Energy Sustainability**, University of Michigan, 2007.
3. **Rackham Predoctoral Fellowship**, Horace H. Rackham School of graduate Studies, U of M, 2007-2008.

4. **Best Paper Presentations**, “Experimental/Theoretical Studies Aimed at the Development of Carbon-Tolerant Catalysts”, Michigan Catalysis Society Annual Meeting 2006, Dow Chemicals, Midland, MI, May 2006.
5. **Best Poster**, “Controlling Carbon Chemistry via alloying: Hybrid Experimental/theoretical Approach”, University of Michigan Blue and Green Engineering Competition 2006, Ann Arbor, MI, March 2006.
6. **Best Poster Award** (Eranda Nikolla, fourth year Ph.D. student), Gordon Research Conference on Catalysis, 2006, New Hampshire. (The poster was selected, along with four others, among >100 posters presented by Ph.D. students and postdoctoral fellows.)

### FY 2008 Publications/Presentations

1. Nikolla E., Schwank J., Linic S., “Hydrocarbon Steam Reforming on Ni Alloys at Solid Oxide Fuel Cell Operating Conditions”, *Catalysis Today*, in press.
2. Nikolla E., Schwank J., Linic S., “Promotion of the Long-Term Stability of Reforming Catalysts by Surface Alloying”, *Journal of Catalysis*, 250 (1), 85-93, 2007.
3. Nikolla E., Linic S., “Controlling Carbon Chemistry on Ni Surfaces by Alloying: First Principles Approaches Toward Carbon-Tolerant Alloy Catalysts and Electrocatalysts”, American Chemical Society Spring Meeting, New Orleans, LA, April 2008.
4. Nikolla E., Schwank J., Linic S., “Development of Carbon Tolerant Anodes for Solid Oxide Fuel Cells”, AIChE Annual Meeting, Salt Lake City, UT, November 2007.
5. Nikolla E., Schwank J., Linic S., “Formulation of Novel Steam Reforming Catalysts Guided by Molecular Insights”, American Chemical Society National Meeting, Boston, MA, August 2007.
6. Nikolla E., Schwank J., Linic S., “Development of Carbon Tolerant Anodes for Solid Oxide Fuel Cells”, North American Catalysis Society Meeting, Houston, TX, May 2007.
7. Linic S., Nikolla E., “Controlling Carbon Surface Chemistry on Ni by Alloying: Carbon Tolerant Hydrocarbon Reforming Alloy Catalysts”, American Chemical Society National Meeting, Chicago, IL, March 2007.

### References

1. E. Nikolla, A. Holowinski, J. Schwank, S. Linic, “Controlling Carbon Surface Chemistry by Alloying: Carbon Tolerant Reforming Catalyst”, *JACS*, 128 (35), 11354-11355, 2006.
2. E. Nikolla, J. Schwank, S. Linic, “Experimental/Theoretical Approach Aimed at the Development of a Carbon-Tolerant Alloy Catalyst”, *Fossil Fuel Cell Program Annual Review*, June 2006.
3. E. Nikolla, J. Schwank, S. Linic, “Promotion of the Long-Term Stability of Reforming Catalysts by Surface Alloying”, *Journal of Catalysis*, 250 (1), 85-93, 2007.
4. E. Nikolla, J. Schwank, S. Linic, “Hydrocarbon Steam Reforming on Ni Alloys at Solid Oxide Fuel Cell Operating Conditions”, *Catalysis Today*, in press.
5. B. Hammer, J.K. Nørskov, “Theory of adsorption and surface reactions” in (eds.) R. Lambert and G. Pacchioni, NATO ASI Series E, Kluwer Academic Publishers, Dordrecht 1997.

---

## IV. SECA CORE RESEARCH & DEVELOPMENT

### H. Power Electronics



---

## IV.H.1 Advanced Power Conditioning System (PCS) Technologies for High-Megawatt Fuel Cell Power Plants

Allen R. Hefner, Jr.  
National Institute of Standards and Technology (NIST)  
100 Bureau Dr.  
Gaithersburg, MD 20899  
Phone: (301) 975-2071; E-mail: hefner@nist.gov

DOE Project Manager: Maria Reidpath  
Phone: (304) 285-4140  
E-mail: Maria.Reidpath@netl.doe.gov

Contract Number: 43042

Start Date: October 1, 2006  
Project End Date: September 30, 2009

### Objectives

- Identify advanced technologies that may significantly reduce the cost of the power conditioning systems (PCS) required for future high-megawatt fuel cell power plants.
- Determine fuel cell power plant PCS performance requirements, including requirements for interfacing fuel cell modules and for power grid connectivity.
- Develop simulation models for advanced PCS architectures, circuit topologies, and component technologies and perform simulations required to determine overall cost and performance benefits of advanced technologies.
- Coordinate with related industry and federal government programs to enable the development of advanced high-megawatt PCS technologies necessary to meet the Solid State Energy Conversion Alliance (SECA) high-megawatt fuel cell power plant PCS goals.

### Accomplishments

- An industry/government/university consensus was reached on the process and parameters for the NIST/DOE advanced PCS technology impact analysis and on the formation of a roadmap committee and interagency task group for high-megawatt PCS technology.
- The Interagency Advanced Power Group (IAPG) Electric Systems Working Group (ESWG) reformed to serve, in part, as an umbrella organization for the High-Megawatt PCS Interagency Task Group. Two IAPG ESGW meetings were held and progress

was made in identifying common core technologies requiring development.

- The High Megawatt Power Converter Technology R&D Roadmap Workshop was held and a roadmap committee was formed.
- A National Science Foundation (NSF) workshop on Power Conditioning for Alternate Energy Systems was held and results will be used by NSF to prioritize research topics and funding opportunities in the high-megawatt PCS area.
- Initial cost estimates for low-, medium-, and high-voltage options indicate that high-voltage, high-frequency (HV-HF) SiC power semiconductor devices are a transformational technology that can enable lower cost and improved performance of future high-megawatt PCS.
- Simulation models for advanced PCS architectures, circuit topologies, and component technologies have been developed to verify the interactions between components for the technology impact evaluation.

---

### Introduction

High-megawatt PCSs are required to convert the low voltage power produced by fuel cell modules in central station scale plants to the very much higher voltage levels required for delivery to the grid. The SECA power plant PCS cost goal of \$40 - \$100/kW is generally recognized as a difficult stretch goal that cannot be met with today's technology. To address this challenge, DOE and NIST have entered into an Interagency Agreement to have NIST lead an effort to evaluate various advanced technology options for the PCS and to identify technologies requiring development to meet the cost and efficiency goals of SECA central station fuel cell power plants.

### Approach

This project aims to identify and enable development of advanced PCS architectures, circuit topologies, and component technologies that may significantly reduce the life cycle cost of the SECA central station fuel cell power plant. Various PCS approaches that focus on the use of advanced technologies for low-, medium-, and high-voltage architectures are considered. The advanced component technologies being considered include advanced power semiconductor devices made with the SiC material, advanced nano-crystalline magnetic

materials for filters and transformers, advanced capacitor technologies, advanced power electronic component cooling systems, and modular power electronic package and interconnect approaches.

Each PCS approach is being evaluated for its ability to meet the performance requirements of the fuel cell power plant including requirements for interfacing to fuel cell modules and for power grid connectivity, as well as the cost of constructing and maintaining the PCS. The cost and performance estimates are made using tabular spreadsheet calculations where detailed circuit simulations are used to verify and refine the component interaction and system performance impacts used in the spreadsheet calculations. The project thus requires the development and validation of simulation models for advanced PCS architectures, circuit topologies, and component technologies.

Evaluation of the overall impact of advanced PCS technologies requires input from, and coordination with, the broad power electronics community. To initiate this interaction and review the approach being used for the NIST/DOE Advanced PCS Technology Impact Analysis, the *High Megawatt Converter Workshop* [1] was held at NIST headquarters (in Gaithersburg, MD) on January 24, 2007. During the workshop, a consensus was reached on the parameters of the technology impact analysis. The participants of the workshop also agreed that a federal interagency task group for high-megawatt power converter technologies could play an important role in this area and that an industry roadmap process should be initiated to offer guidance for further development of more cost-effective and efficient PCSs.

In response to these recommendations, the *High Megawatt Power Converter Technology R&D Roadmap Workshop* was held at NIST headquarters on April 8, 2008 to begin to establish a roadmap process in this area. Activities of the IAPG ESWG have also been initiated to, in part, address the recommendation for coordination among federal agencies in the high-megawatt PCS area. The first meeting of the IAPG ESWG was held at the Defense Advanced Research Projects Agency (DARPA) on September 13, 2007 and a second meeting was held at NIST Headquarters on April 24 -25, 2008. The *NSF Workshop on Power Conditioning for Alternate Energy Systems* was also organized and held at NIST headquarters on May 28-29, 2008 to provide coordination with the basic research and educational needs in this area.

## Results

**High-Megawatt Converter Workshop:** The *High Megawatt Converter Workshop* held at NIST headquarters on January 24, 2007 included 42 invited participants and 21 invited presenters. Ten of the presentations described specific technologies deemed

to have the potential to reduce PCS cost and seven presentations discussed the common needs for high-megawatt PCSs across industry and government agencies. Open discussion sessions were also held to discuss the specific approach being used for the NIST/DOE Advanced PCS Technology Impact Analysis, and to discuss the merits of forming an interagency task group and an industry roadmap effort for high-megawatt PCS technologies.

### **Interagency Task Group on High-Megawatt PCS:**

The *High Megawatt Converter Workshop* participants agreed that a federal interagency task group for high-megawatt power converter technologies could play an important role in this area. It was also suggested that the IAPG would be a good organization to host such a task group. Subsequently during the IAPG Strategic Planning Meeting on April 3, 2007, the IAPG agreed that a reinitiated IAPG ESWG could serve, in part, as an umbrella organization for the High-Megawatt PCS Interagency Task Group. On September 13, 2007, a meeting of the IAPG ESWG was held at DARPA to reinitiate the group and to discuss the ongoing power conversion activities within different federal agencies. The second meeting of the IAPG ESWG was held at NIST headquarters on April 24–25, 2008 in conjunction with a meeting of the IAPG Mechanical Working Group held on April 21–23, 2008. Significant progress was made at this second meeting of the IAPG ESWG in identifying common core technologies requiring development to meet mission requirements for the participating agencies.

### **Industry Roadmap on High-Megawatt PCS:**

The *High Megawatt Converter Workshop* participants agreed that a roadmap process should be initiated to offer guidance for further development of PCSs that could meet the requirements for more cost-effective and efficient power conversion. In response to this consensus, the *High Megawatt Power Converter Technology R&D Roadmap Workshop* was held on April 8, 2008 at NIST headquarters. Forty-seven people who are active in the field participated including representatives for wind, photovoltaic, and fuel cell power generation; the power transmission/distribution industry; and high-megawatt PCS system integrators and component manufacturers. The key objective of this workshop was the formation of a Roadmap Committee, which was accomplished. The proceedings of this workshop will be available in the near future [2].

**NSF Workshop on Power Conditioning for Alternate Energy Systems:** The *NSF Workshop on Power Conditioning for Alternate Energy Systems* was held at NIST headquarters on May 28-29, 2008 to provide coordination with the basic research and educational needs in this area. The meeting brought together the interested parties from industry, government, and academia to identify power

conditioning challenges and educational needs associated with alternate/clean energy systems and the power grid. The results of the discussion will be used by NSF to prioritize research topics and funding opportunities in this area. It is envisioned that the industry roadmap, the interagency task group, and the basic research efforts will be coordinated to provide a comprehensive effort to advance technologies for high-megawatt power conditioning systems.

#### Advanced PCS Technology Impact Analysis:

During the *High Megawatt Converter Workshop*, various aspects of the NIST/DOE Advanced PCS Technology Impact Analysis effort were reviewed including: the overall approach of the study, the current and voltage boundary conditions, the grid-connectivity requirements, the fuel cell current regulation and ripple requirements, as well as, the topology and component technologies being considered by the study. An 18 kV alternating current (AC) plant collection/distribution bus was chosen for the initial study because it is similar to that being considered for integrated gasification combined cycle gas turbine plants where central station fuel cell power islands may be tested.

Various approaches were evaluated that focus on the use of advanced technologies for low-, medium-, and high-voltage architectures to convert the unregulated direct current (DC) power produced by the fuel cell modules to that required for the 18 kV AC plant distribution. Figure 1 shows an example of a low- and

high-voltage architecture for discussion, and Figures 2 and 3 show the initial cost estimates for selected architectures and component technologies. The cost estimates in Figures 2 and 3 are based upon component selection and circuit performance being validated and refined using simulations. The following cost stretch goals are also used for the future component technologies including SiC devices and advance magnetic materials to determine the cost breakpoints for the new technologies:

- 1.2 kV Schottky diodes: \$0.2/A
- 12 kV Schottky diodes: \$1/A
- 12 kV Half-bridge SiC-Metal-Oxide-Semiconductor Field Effect Transistor (MOSFET)/SiC-Schottky: \$10/A
- 15 kV SiC-PiN: \$0.4/A
- 15 kV SiC-IGBT/SiC-PiN Module: \$3.3/A
- Nano-crystalline transformer: \$2/kW
- Power Electronics DC-DC, DC-AC: 150% overhead
- 60 Hz Transformer and Switchgear: 50% overhead

**Low Voltage Inverter Approach:** The initial baseline power converter architecture for the study is a center-tapped fuel cell (approximately 700 V DC, 0.6 MW) with a DC-DC converter for fuel cell current regulation, a 480 V AC inverter, and a 60 Hz transformer to raise the output voltage to 18 kV AC for

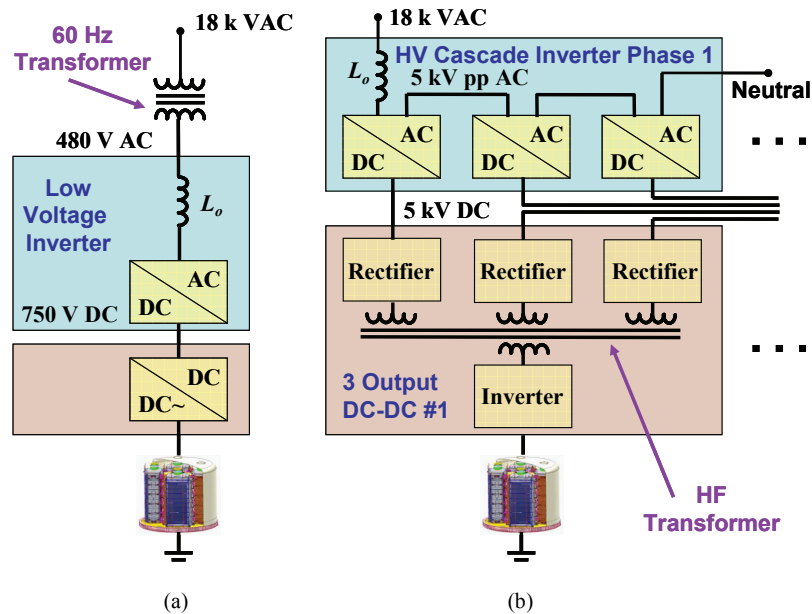
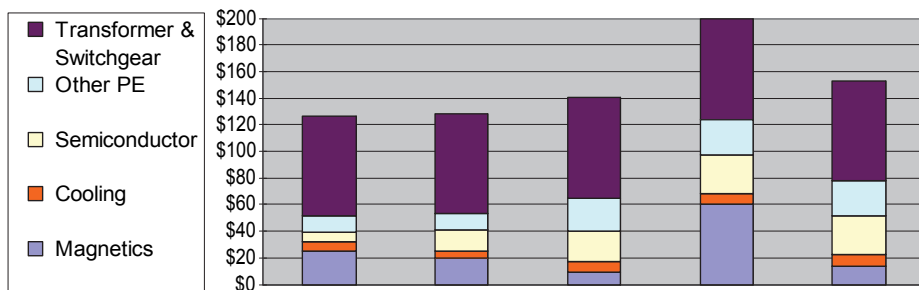


**FIGURE 1.** Example high-megawatt PCS architectures: (a) a 480 V AC inverter and a 60 Hz transformer to raise the output voltage to 18 kV AC for plant distribution and (b) an architecture that combines the output of multiple fuel cells each having a three output DC-DC converter that steps the voltage up to 5 kV, followed by a high voltage three phase cascade inverter connected directly to the 18 kV AC power plant distribution.

Estimated \$/kW: LV Inverter



<b>Inverter Voltage</b>	Low	Low	Low	Low	Low
<b>Converter Stages</b>	One	One	Two	Two	Two
<b>LV-SiC Schottky</b>		yes	yes	yes	yes
<b>HF Transformer</b>				Ferrite	Nano
<b>60 Hz Transformer</b>	yes	yes	yes	yes	yes



FIGURE 2. Initial cost estimates for selected low-voltage PCS architectures with different component technologies.

plant distribution (Figure 1a). This option was chosen as the baseline because it includes the individual functions necessary to expand to architectures having a DC common bus, and/or a medium-voltage or high-voltage inverter. The “present lowest-cost” option combines the DC-DC regulator and 480 V AC inverter functions into a single converter stage that uses the “present lowest-cost” switching power device, a 1,200 V insulated gate bipolar transistor (IGBT) module. Figure 2 shows cost estimates for several low-voltage PCS options.

**High Voltage Inverter Approach:** On the other extreme, high voltage inverter options are being considered that use DC-DC voltage step-up converters to feed high voltage inverters connected directly to the 18 kV AC power plant distribution. For example, Figure 1b shows an architecture that combines the output of multiple fuel cells each having a three output DC-DC converter that steps the voltage up to 5 kV, followed by a high voltage three-phase cascade inverter connected directly to the 18 kV AC power plant distribution bus. The three-output DC-DC converter is required because each fuel cell must power all three phases to reduce ripple current in the fuel cell.

In the case of the high-voltage inverter (e.g., architecture of Figure 1b), the voltage step-up and galvanic isolation are provided by the high-frequency transformer within the DC-DC converters as opposed to the 60 Hz transformers of the baseline low voltage inverter options (e.g., architecture of Figure 1a). The high-frequency transformer requires orders of magnitude less magnetic material and copper than the expensive

conventional 60 Hz copper-iron transformer. The cost of the advanced magnetic materials (e.g., nanocrystalline magnetic materials) for the high frequency transformers can be reduced in the near future whereas the cost of the copper required by the 60 Hz transformers is expected to increase. Figure 3 shows cost estimates for several medium- and high-voltage PCS options indicating that the high voltage inverter options have the lowest cost even with the relatively high cost SiC power semiconductor devices.

**Advanced Component Technology Development:** The high voltage inverter PCS architecture is enabled by the rapidly advancing HV-HF semiconductor devices made with the SiC material [3]. Both the *High Megawatt Power Converter Technology R&D Roadmap Workshop* and the *NSF Workshop on Power Conditioning for Alternate Energy Systems* also identified the emerging HV-HF SiC devices as a key transformational technology that will enable substantial reduction of cost and improved functionality for future grid connected PCSs. The availability and cost of these advanced components are critically important and considerable research and development will be required to meet the cost goals. It is envisioned that early investment will permit the early adoptors to utilize and advance the technology so that it will be available for future high-megawatt PCS applications.

**Modeling Advanced PCS Technologies:** Simulation models for advanced PCS architectures, circuit topologies, and component technologies are required to verify the interactions between components

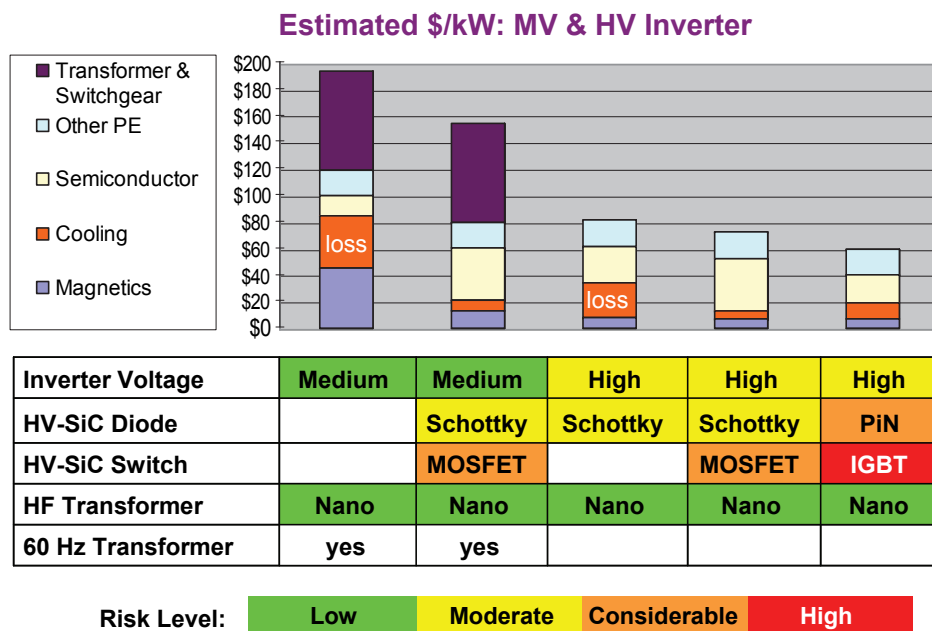


**FIGURE 3.** Initial cost estimates for selected medium and high voltage PCS architectures with different component technologies indicating that the high voltage inverter options have the lowest cost.

for the technology impact evaluation. NIST has developed and validated models for 1,200 V and 10 kV SiC MOSFETs and junction barrier Schottky diodes to be used in this work. The NIST-developed SiC power semiconductor models, in addition to the well known NIST Silicon IGBT model, are being used as part of the effort to evaluate the cost and performance advantages of the various DC-DC and DC-AC converter options. The circuit topologies/component technology options for 18 low-, medium-, and high-voltage PCS architectures have been implemented in circuit simulation schematics and are being combined with the models for the advanced component technologies to perform the comprehensive comparison of different PCS approaches.

**Conclusions and Future Directions**

It is generally recognized that the SECA cost goal of \$40-\$100/kW for the power plant PCS cannot be met with today’s technology. To address this challenge, DOE and NIST have entered into an interagency agreement to have NIST lead an effort to evaluate various advanced technology options for high-megawatt PCSs. Several workshops have been held to review the approach being used for the NIST/DOE Advanced PCS Technology Impact Analysis and to coordinate the federal, industry, and academic high-megawatt PCS research and development activities.

Various PCS architectures and advanced technologies have been identified that may lead to the cost reductions required for central station fuel cell power plants. Initial cost estimates for low-, medium-,

and high-voltage options indicate that HV-HF SiC power semiconductor devices are a transformational technology that can enable lower cost and improved performance of future PCS systems. It is envisioned that early investment in HV-HF SiC devices will permit the early adaptors to utilize and advance the technology enabling cost reduction in future high-megawatt PCS applications. Predictive simulations including advanced technologies aid in validating the interaction between components and demonstrating the overall system benefits of new high-megawatt PCS technologies.

**FY 2008 Publications**

1. Proceedings of the High Megawatt Converters Workshop, January 24, 2007, NIST Headquarters Gaithersburg, MD, [www.high-megawatt.nist.gov/workshop-1-24-07/](http://www.high-megawatt.nist.gov/workshop-1-24-07/)
2. Proceedings of the High Megawatt Power Converter Technology R&D Roadmap Workshop, April 8, 2008, NIST Headquarters, Gaithersburg, MD, [www.high-megawatt.nist.gov/workshop-4-8-08/](http://www.high-megawatt.nist.gov/workshop-4-8-08/)
3. A. R. Hefner, R. Sei-Hyung, B. A. Hull, D.W. Berning, C. E. Hood, J. M. Ortiz-Rodriguez, A. Rivera-Lopez, T. Duong, A. Akuffo, and M. Hernandez , “Recent Advances in High-Voltage, High-Frequency Silicon-Carbide Power Devices,” Proceedings of the 2006 IEEE Industry Applications Society (IAS) Annual Meeting, October 08-12, 2006, Tampa, FL, pp. 330-337.
4. J. M. Ortiz-Rodriguez, T. Duong, A. Rivera-Lopez, and A. R. Hefner, “High-Voltage, High-Frequency SiC Power MOSFETs Model Validation,” in the Proceedings of the

2007 IEEE Power Electronics Specialists Conference (PESC), June 17–21, 2007, Orlando, FL, pp. 1018-1022.

5. T. H. Duong, J. M. Ortiz-Rodriguez, R. N. Raju, and A. R. Hefner, “Electro-thermal Simulation of a 100 A, 10 kV Half-Bridge SiC MOSFET/JBS Power Module,” in the Proceedings of the 2008 IEEE Power Electronics Specialists Conference (PESC), June 15-19, 2008, Island of Rhodes, Greece, pp. 1592-1597.

6. J. M. Ortiz-Rodríguez, M. Hernández-Mora, T. Duong, S. G. Leslie, and A. R. Hefner, “Thermal Network Component Models for 10 kV SiC Power Module Packages,” in the Proceedings of the 2008 IEEE Power Electronics Specialists Conference (PESC), June 15-19, 2008, Island of Rhodes, Greece, pp. 4770-4775.

7. Allen R. Hefner, “Performance Analysis of 10 kV, 100 A SiC Half-Bridge Power Modules,” in the Proceedings of the Government Microcircuit Applications and Critical Technology Conference (GOMACTech) 2008, March 17–20, 2008, Las Vegas, NV, pp. 361-364.

8. T. H. Duong, J. M. Ortiz-Rodriguez, R. N. Raju, and A. R. Hefner, “Circuit Simulation Model for a 100 A, 10 kV Half-Bridge SiC MOSFET/JBS Power Module,” in the Proceedings of the 2008 IEEE Applied Power Electronics Conference (APEC), February 24-28, 2008, Austin, TX, pp. 913-917.

## FY 2008 Presentations

1. Allen Hefner “Power Conditioning Systems for High High-Megawatt Fuel Cell Plants,” NSF Workshop on Advanced Power Conditioning for Alternate Energy Systems, NIST, Gaithersburg, MD, May 28-29, 2008; also presented at IAPG Workshop, NIST, Gaithersburg, MD, April 21-25, 2008.

2. Allen Hefner “High-Voltage, High-Frequency Devices for Solid State Power Substation and Grid Power Converters,” 2008 High-Megawatt Converter Technology R&D Roadmap Workshop, NIST, Gaithersburg, MD, April 8, 2008.

3. Allen Hefner “SiC Devices - Status and Trends,” GE Power Electronics Symposium, Schenectady, NY, August 28, 2007.

4. Allen Hefner “Power Electronics Materials and Switching Devices,” Fuel Cells Plenary Session of the Materials Science & Technology 2007 Conference and Exhibition Energy Symposium, Detroit, MI, September 17, 2007.

5. Allen Hefner “Advanced Power Conditioning System Technologies for High-Megawatt Fuel Cell Power Plants,” Super Session Panel on Future Outlook and Application Status for Fuel Cells at the IEEE Power and Energy Society General Meeting, Pittsburgh, PA, July 22, 2008.

## IV.H.2 A Low-Cost Soft-Switched DC-DC Converter for Solid Oxide Fuel Cells

Jason Lai (Primary Contact), Sung Yeul Park,  
Hide Miwa, and Chien-Liang Chen  
Virginia Polytechnic Institute and State University  
440 Whittemore Hall  
Blacksburg, VA 24061-0111  
Phone: (540) 231-4741; Fax: (540) 231-3362  
E-mail: laijs@vt.edu

DOE Project Manager: Maria Reidpath  
Phone: (304) 285-4140  
E-mail: Maria.Reidpath@netl.doe.gov

Subcontractor:  
Southern California Edison, Los Angeles, CA

Contract Number: 41567

Start Date: October 1, 2002  
Project End Date: July 31, 2008

- Developed a wide-range active and reactive power flow controller that can precisely control the power range from zero to full power and reactive power from 0 to 100% power factor for both leading and lagging reactive power.

### Introduction

The complete SOFC power conditioning system (PCS) consists of a DC-DC converter and a DC-AC inverter to convert the low voltage unregulated DC voltage to regulated AC voltage for either standalone load or utility grid-tie applications. The primary work at Virginia Tech is to develop a highly efficient PCS for SOFCs. In the Phase I effort, a six-phase soft-switching DC-DC (V6) converter has been successfully developed and demonstrated 97% peak efficiency. With continuing improvement, the peak efficiency was improved to 98% last year by improving the transformer design and fabrication. In the Phase II effort, the focus was to develop a highly efficient soft-switching DC-AC inverter as the subsequent stage. The initial design demonstrated 98% peak inverter efficiency. However, its light-load efficiency was poor due to a fixed soft-switching delay timing control. Last year, the effort was to improve the light-load efficiency with an adjusted timing control to improve the light-load efficiency. The overall efficiency became a flat 98% from 20% load to full load. This efficiency was tested with an inductor-capacitor (LC) filter connected to the inverter output. Therefore, the inverter switching stage itself has an efficiency higher than 98%.

In addition to efficiency improvement, an advanced controller was developed to include reactive power flow control for the grid-tie application. For the Solid State Energy Conversion Alliance (SECA) 5 kW rated inverter, the range of reactive power can be controlled from 0 to  $\pm 5$  kVAr. In other words, the power factor angle can be controlled from  $-90^\circ$  to  $90^\circ$ . The power flow control can be considered as a current control with current reference generated by the active and reactive power commands, which are divided with the grid voltage to obtain two orthogonal currents and subsequently the magnitude and phase angle of the current command. The phase angle of the current command is referenced to the phase angle of the grid voltage which is obtained from the phase-locked loop (PLL). The proposed power flow control approach has been analyzed with mathematical modeling and implemented with a TMS320F2808 digital signal processor (DSP). The entire PCS has been simulated and tested to show power flow operation from  $-5$  kVAr to  $+5$  kVAr.

### Objectives

- Develop a low-cost direct current-direct current (DC-DC) converter for low- to high-voltage power conversion as the standard interface between the solid oxide fuel cell (SOFC) source and the load-side direct current-alternating current (DC-AC) inverter.
- Develop a low-cost 5 kW DC-AC inverter with a minimum energy efficiency of 99% operating with  $>400$  VDC input.
- Develop power management control strategies and demonstrate the ability to supply and consume reactive power while simultaneously supplying active power to the utility grid.
- Develop sensory and control logic to enable autonomous/semi-autonomous response to aid supporting grid voltage and frequency needs without nuisance tripping or disconnection of the fuel cell system.

### Accomplishments

- Demonstrated an adjusted timing soft-switching DC-AC inverter with improved light-load efficiency. With inclusion of filter components, the overall efficiency achieves 98% from 20% load to full load.
- Improved DC-DC converter efficiency with a homemade transformer and demonstrated V6 DC-DC converter peak efficiency at 98% with 50 V input voltage.

**Approach**

Figure 1 shows the active and reactive power control system of the inductor-capacitor-inductor (LCL) filter-based grid-tie inverter as a part of the entire fuel cell PCS. The active power command,  $P_{ref}$ , which is commanded by the fuel cell balance-of-plant, and the reactive power command,  $Q_{ref}$ , which is provided by the distributed generation control site, can be translated into the current command input,  $i_{ref}$ , by dividing the power command with the inverter output peak voltage,  $V_m$ , and subtracting the output voltage phase information,  $\theta_v$ , produced by the digital PLL. The feedback voltage and current signals including  $i_{ac}$ ,  $v_{ac}$ , and  $v_g$  are the inverter output current, filter voltage, and utility grid voltage, respectively. These signals go through the conditioning circuit to filter out the high frequency noise and to scale to low-voltage level for DSP computation. The inverter can be considered as a plant with duty cycle,  $d$ , as the input and current,  $i_{ac}$ , as the output and the plant transfer function,  $G_{id}(s)$ , can be derived as a first-order equation [1,2].

Figure 2 shows the block diagram of the complete control system with both active and reactive power flow control functions. The admittance compensator,  $G_c(s)$ , is designed to reject a disturbance, which is due to the inverter output voltage,  $v_{ac}$ , acting on the power plant transfer function,  $G_{iv}(s)$ . The current loop controller  $G_i(s)$  is designed to compensate the error between  $i_{ref}$  and the feedback sensed current,  $i_{fb}$ . The output of the current loop controller is the duty cycle control signal,  $v_d(t)$ , which is typically a sinusoidal signal. By feeding  $v_d(t)$  signal to the pulse width modulated block, the output is gating signal,  $d$ . The inverter power circuit output needs an LCL filter,  $L_{o1}-C_o-L_{o2}$ , to smooth the current and a circuit breaker to make the grid interconnection. The utility source voltage,  $v_g$ , contains a source inductance,  $L_g$ , thus the actual grid-tie voltage seen by the inverter is the voltage between  $L_{o2}$  and  $L_g$ , or

$v_{ac}$ . Both output current,  $i_{ac}$ , and interconnect voltage,  $v_{ac}$ , are fed back to the DSP through the conditioning circuit and scaling.

The key design features of the advanced power flow controller are (1) adding the admittance compensator,  $G_c(s)$ , which eliminates the power plant disturbance, (2) synchronization with a phase-locked loop, which allows precise power factor angle control, and (3) implemented with a quasi-proportional-resonant (QPR) controller, which eliminates the 60 Hz steady-state error.

Unlike most other systems where the use of a proportional-integral (PI) controller gives an infinite gain at the steady-state (or DC condition), in a DC-AC inverter, the control target is not DC but a periodical AC, which has a limited gain with the use of a PI controller. Thus, a new type of controller, the QPR controller, can be used as a bandpass filter, which only allows a 60 Hz signal to go through the controller, thus the control loop gain at 60 Hz can be very large or near infinity while the rest of the frequencies stay at the proportional controller gain. Therefore, the steady-state error at 60 Hz can be eliminated while a high stability margin can be maintained.

With the combination of the admittance compensator for disturbance rejection and the QPR controller for providing a high gain at the fundamental frequency, a scalar current control approach can be used to provide precise active and reactive power control. The main role of the controller is to generate a current reference signal with respect to the  $P_{ref}$ ,  $Q_{ref}$ , and  $v_{ac}$ . To synchronize  $i_{ac}$  with  $v_{ac}$ , a simple software PLL is adopted [1,2].

For the V6 DC-DC converter efficiency improvement, a higher voltage input was applied to the original design with the change of a different turns-ratio transformer. The efficiency with the original 25 V input inverter peaks at about 96%, but with 50 V input, the peak efficiency reached 97%. This number was further improved by using a homemade transformer, which has a wider core window area to put one more turn on the primary winding, thus the core loss is significantly reduced. The efficiency with the newly designed transformer now peaks at 98%, exceeding the original SECA goal of 97%.

For the soft-switching DC-AC inverter, the earlier version efficiency was good at the heavy load condition but poor at the light load condition. Our approach to efficiency improvement was to adjust the delay timing between the main and auxiliary switches while maintaining the originally proposed high turns-ratio

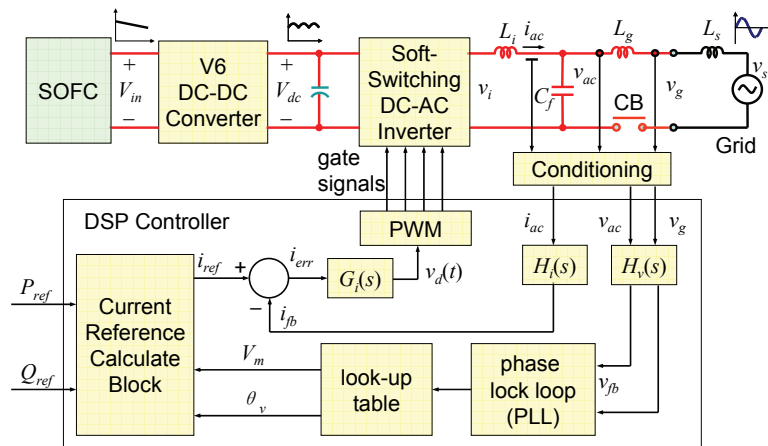


**FIGURE 1.** Block Diagram of the Complete SOFC Power Conditioning System

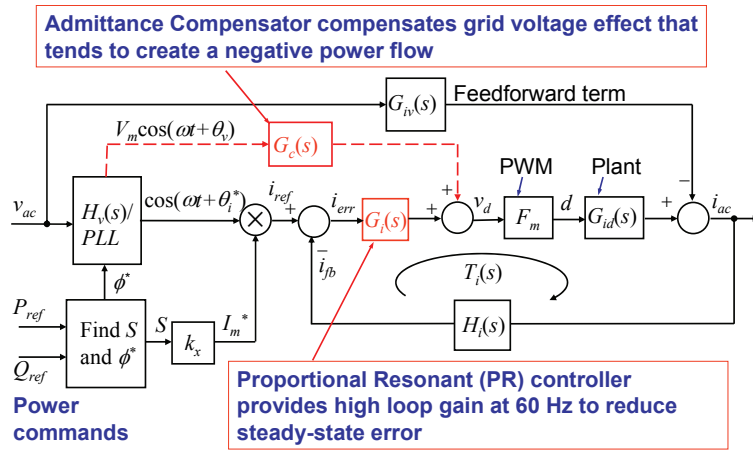


**FIGURE 2.** Advanced Control Design for Precision Active and Reactive Power Flow Control

coupled magnetics [3]. The peak efficiency of 98% remains the same, but at 20% load, the efficiency was improved from 93.8% to 97.8%.

**Results**

Figure 3 shows the full power experimental results of precision active and reactive power control. The DC bus is maintained at 400 V. The upper window indicates a pure 5 kVar leading reactive power condition, the middle window indicates a pure 5 kW active power condition, and the lower window indicates a pure 5 kVar lagging reactive power condition. With the change of power command from leading to lagging, the phase of  $i_g$  shifts from  $+90^\circ$  to  $-90^\circ$ . Notice that the  $P_{cmd}$  and  $Q_{cmd}$  voltages are all at 5 V DC. With the combination of the admittance path compensator, QPR controller, and PLL

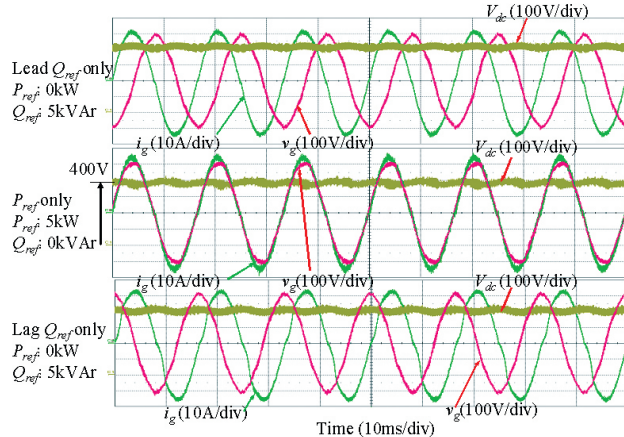
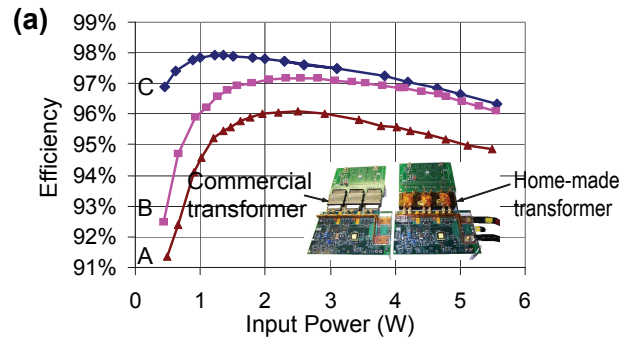


**FIGURE 3.** Precision Active and Reactive Power Flow Control Experimental Results under Grid-Tie Mode

synchronization, the output power follows the input command very well.

Figure 4(a) compares the efficiency of the V6 DC-DC converter under three different conditions. Using the custom designed commercially made transformers with 25 V as the input voltage, the peak efficiency is 96%, and the full-load efficiency is 95%. With 50 V as the input voltage, the peak efficiency is improved to 97%, and the full-load efficiency remains above 96%. By replacing the commercial transformers with the homemade transformers, the peak efficiency reaches 98%, and the full-load efficiency is higher than 96.5%. The pictures in the figure indicate that the custom made transformer is made of planar E cores, but the homemade transformer is made of conventional EE cores. The planar E cores have a limited window area to put in coppers, but the planar core-based transformer is easy to manufacture with the flat copper sheet as the high current carrying winding. The conventional EE cores have a wide open window



- A.  $V_{in} = 25$  V using custom-made commercial transformer
- B.  $V_{in} = 50$  V using custom-made commercial transformer
- C.  $V_{in} = 50$  V using in-house developed transformer

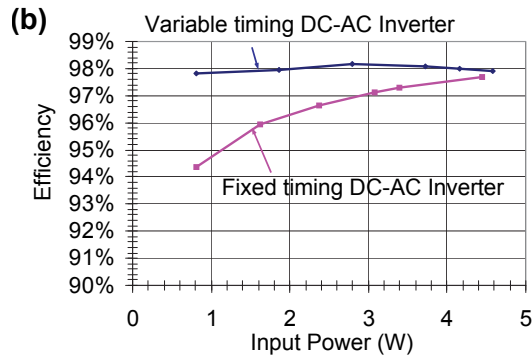


**FIGURE 4.** Measured Efficiency Results: (a) Test Results of Three V6 Converter Versions; and (b) Improved Soft-Switched DC-AC Inverter Light Load Efficiency with Adjusted Timing

area to add more turns, but it requires the use of multiple strand Litz wires for the high current carrying windings, and is more difficult to manufacture.

Figure 4(b) compares the soft-switching DC-AC efficiency with different timing control schemes. For the original design with fixed timing control, the efficiency reached 98% at the full-load condition, but its 20% load efficiency was below 95%. By properly adjusting the delay timing between the main and auxiliary switches, the 20% load efficiency is improved to 97.8%. The main reason for the efficiency improvement is the zero voltage condition appears earlier at light loads. Without adjusting the timing, the resonant voltage tends to swing back, and the voltage is no longer true zero. With the adjusted timing, the zero voltage condition can always be guaranteed. Note that the efficiency numbers for both the DC-DC converter and the DC-AC were measured without including the auxiliary fan load, which will be needed when the unit is packaged in an enclosed case. The overall peak efficiency should remain above 95% even with the inclusion of auxiliary fan load.

## Conclusions and Future Directions

A wide range active and reactive power flow control has been proposed for grid-tie power conditioning systems. The key to achieving precision power flow control is to incorporate the QPR controller in the current loop to ensure high loop gain at the fundamental frequency and the admittance compensator to ensure cancellation of the grid voltage induced negative power flow. The current loop transfer function has been systematically derived with representations of a conventional transfer function format. A 5 kVA LCL-based grid-tie inverter for the fuel cell PCS was used as the platform to show current loop controller design and admittance compensation. The QPR controller was adopted to obtain a sufficient gain at the fundamental frequency while maintaining a sufficient stability margin. Adding an admittance compensator helps cancel the negative power flow induced by the grid voltage, thus allowing precision power flow control at low power level.

The efficiency of the PCS was further improved as compared to the previous reported figures. For the DC-DC converter, the peak efficiency was improved to

98% with the use of homemade transformers running at a higher voltage condition. For the DC-AC inverter, the efficiency improvement was at the light load condition. Its 20% load efficiency was improved to above 97% with the adjusted timing control. Overall PCS efficiency was significantly improved as compared to that of the earlier version. Future work is to test the PCS with an SOFC to verify the efficiency under varying input voltage condition.

## FY 2008 Publications/Presentations

1. S.-Y. Park, C.-L. Chen, J.-S. Lai, "A Wide Range Active and Reactive Power Flow Controller for a Solid Oxide Fuel Cell Power Conditioning System," in *Proc. of IEEE APEC*, Austin, TX, February 2008, pp. 952-958.
2. C. Liu and J.S. Lai, "Low Frequency Current Ripple Reduction Technique with Active Control in a Fuel Cell Power System with Inverter Load," *IEEE Transactions on Power Electronics*, July 2007, pp.1429-1436.
3. J. Zhang, R.Y. Kim, W. Yu, J.S. Lai, "High-Power Density Design of a Soft-Switching High-Power Bidirectional DC-DC Converter," *IEEE Transactions on Power Electronics*, July 2007, pp. 1145-1153.
4. C.-L. Chen, S.-Y. Park, J.-S. Lai, and S.-R. Moon, "Admittance Compensation in Current Loop Control for a Grid-Tie LCL Fuel Cell Inverter," in *Proc. of IEEE PESC*, Orlando, FL, June 2007, pp. 520-526.

## References

1. C.-L. Chen, S.-Y. Park, J.-S. Lai, and S.-R. Moon, "Admittance Compensation in Current Loop Control for a Grid-Tie LCL Fuel Cell Inverter," in *Proc. of IEEE PESC*, Orlando, FL, June 2007, pp. 520-526.
2. S.-Y. Park, J.-S. Lai, C.-L. Chen, S.-R. Moon and T.-W. Chun, "Current Loop Control with Admittance Compensation for a Single-Phase Grid-Tie Fuel Cell Power Conditioning System," in *Proceedings of IEEE APEC*, Anaheim, CA, February 2007, pp. 1010-1016.
3. J.-S. Lai and J. Zhang, "Efficiency Design Considerations for a Wide-Range Operated High-Power Soft-Switching Inverter," *Proceedings of IEEE Industrial Electronics Conference*, Raleigh, NC, November 2005, pp. 604-609.

---

## **IV. SECA CORE RESEARCH & DEVELOPMENT**

### **I. Modeling and Simulation**



---

## IV.I.1 SOFC Design Basis Development Project

Raj Manchanda

American Society of Mechanical Engineers (ASME)  
Three Park Avenue  
New York, NY 10016-5990  
Phone: (212) 591-8500; Fax: (212) 591-7196  
E-mail: manchandar@asme.org

DOE Project Manager: Travis Shultz

Phone: (304) 285-1370  
E-mail: Travis.Shultz@netl.doe.gov

Contract Number: 05690

Start Date: September 29, 2006

End Date: July 31, 2008

### Objectives

- Develop a peer-reviewed guide which contains recommended design practices and associated modeling and analysis procedures for solid oxide fuel cells (SOFCs).
- Support Solid State Energy Conversion Alliance (SECA) strategies to accelerate commercialization of SOFCs by standardizing design requirements.
- Facilitate development of cost-effective, reliable SOFC designs.

### Accomplishments

- Identified elements integral to the SOFC peer-reviewed guide.
- Collated related research from the National Laboratories and industry.
- Drafted the SOFC Design Guide document.
- Managed peer review process with subject matter experts from the National Laboratories and industry.
- Incorporation of peer review comments and finalization of the SOFC Design Guide is in progress.

---

### Introduction

SOFCs are high-temperature devices that operate between 600-1,000°C to yield high power densities. SOFCs convert chemical energy to electrical energy through electrochemical oxidation of gaseous fuels ranging from hydrogen to hydrocarbons, including coal syngas. High efficiencies can be realized with SOFCs;

however, a substantial amount of waste heat is generated as a result of the electrochemical reactions. Long-term stable operation of cells and stacks has been found to depend upon the chemical and structural stability of the component bulk materials and interfaces, which are related to the stack thermal/mechanical design. SOFCs are ideal for distributed generation applications such as auxiliary power units, military power generation, and remote power generation.

Unlike most other types of fuel cells, SOFCs can have multiple geometries. Planar geometry is most commonly seen in fuel cell design, comprised of a flat electrolyte sandwiched between two electrodes. SOFCs can also be made in tubular geometries where the electrodes form the inside and outside of the tube. The developmental work for this guide is based primarily on evaluation of the planar geometry and planar SOFCs are assumed. However, some of the guidelines will be applicable to tubular designs, as many of the failure mechanisms affecting such designs are consistent with those seen in planar cells. It is the responsibility of the user to determine the extent to which the guide can be applied to specific designs.

Suggested analytical procedures developed by the SECA Core Technology Program to model electrochemical and thermo-mechanical performance of SOFCs, as well as how these tools and other simulation tools that can be used in designing a structurally-reliable and durable SOFC stack will be reviewed. The recommended modeling procedures attempt to quantify the variability in material properties and design parameters of all elements in the SOFC structure. These modeling procedures address the coupled electro-chemical and thermo-mechanical nature of SOFCs by quantifying the electro-chemistry activities and the associated thermal-mechanical behaviors of various SOFC components for different design configurations.

### Approach

Relevant research completed by the National Laboratories and industry was gathered to validate the design practices and associated modeling and analysis procedures for SOFCs. An ASME code writing expert has been engaged to compile the various research reports and data into standards-type format and language. The draft document has been provided for peer review by a group of SOFC subject matter experts from industry and national laboratories. A subject matter expert from industry has been engaged to provide technical support, assist with resolution of peer review comments, and provide valuable insight from industry experience.

## Results

The guidelines being developed will provide a methodology for evaluation and optimization of SOFC reliability, focusing on failure mechanisms associated with the thermo-mechanical properties and state of the SOFC. SOFCs have been considered and designed for an extremely wide range of applications, from portable power units generating a few watts of power to megawatt-scale central power plants. Each application has its own unique set of design requirements and challenges. The SOFC Design Basis Development document will address the design under steady-state operating conditions rather than long-term performance.

Preliminary agreement on the following SOFC design basis development guide elements was achieved – see Table 1.

## Conclusions and Future Directions

Many of the topics addressed herein are under on-going research and development and therefore the SOFC design basis development guide will be regularly updated so that it contains state-of-the-art knowledge and experience gained in SOFC designs.

**TABLE 1.** SOFC Design Basis Development Guide Elements

Element	Description
Symbols	
Glossary	
Acronyms	
Introduction & Background	
Scope & Assumptions	Stationary Base-loaded systems Design for initial operation SOFC stack only Manufacturing methods and tolerances
SOFC Requirements	Stack power output Stack operating voltage Fuel and oxidant flows Weight and volume Electrical load profile
Materials and Material Properties	Thermal Mechanical Electrochemical and fluid properties Existing test standards Non-conventional test methods
Cell Electrochemistry	Component function Electrolyte Anode Cathode
Analysis Procedures & Tools	Applied stresses Principal stress Delamination Load cases
Design/Failure Criteria	Structural solution Load cases Equations and calculations Mechanical failure Chemical failure Reduced power generation Bulk fracture Delamination Interconnect separation
Evaluation & Redesign	Change operating conditions Change dimensions or tolerances Change materials Reduce stresses Sensitivity study
References	
Appendices	

---

## IV.I.2 Modeling and Experiments of SOFC Stacks and Materials at PNNL

Mohammad A. Khaleel (Primary Contact),  
Xin Sun, Wenning Liu, Elizabeth Stephens,  
Kurt Recknagle, Brian Koeppel, and  
Vlad Korolev

Pacific Northwest National Laboratory (PNNL)  
902 Battelle Blvd.  
Richland, WA 99352  
Phone: (509) 375-2438; Fax: (509) 375-4392  
E-mail: moe.khaleel@pnl.gov

DOE Project Manager: Ayyakkannu Manivannan  
Phone: (304) 285-2078  
E-mail: Ayyakkannu.Manivannan@netl.doe.gov

Contract Number: 40552

Start Date: October 1, 2007  
Project End Date: September 30, 2008

stresses, and increase electrical power. The optimal performance was realized by the combined use of increased cathode air, fuel tail-gas recycling, and increased separator plate thickness.

- Developed an integrated modeling/experimental framework to predict the life of SOFC interconnect (IC) materials with and without spinel coats.
- Investigated the effect of oxide growth and metallic IC surface quality on interfacial strength of oxide scale and substrate. Reported the interfacial strength at the different interfaces in the spinel coating/oxide scale/metallic substrates tri-layer systems.
- Developed a model to evaluate the densification strains of contact materials during the sintering process and to predict the residual stress induced by the sintering process.
- Developed a homogenization model to predict glass-ceramic seal properties as a function of composition.

### Objectives

- Develop and validate multi-physics modeling tools to simulate solid oxide fuel cell (SOFC) stack performance.
- Utilize computational techniques for the mitigation of performance degradation and optimization of modular SOFC stack and system designs.
- Obtain necessary material properties to support the development and optimization of SOFC designs through modeling.
- Disseminate/transfer modeling tools to Solid State Energy Conversion Alliance (SECA) industry teams and Core Technology Program (CTP) members.

### Accomplishments

- Enhanced the PNNL-developed modeling tool SOFC-MP (Solid Oxide Fuel Cell Multi-Physics) at the request of SECA industry team members to allow N<sub>2</sub> species in the fuel composition to simulate gasifier output of coal-based fuels, to enable user-defined pressure drop calculations for the fuel and oxidant flow regions, and to enable user-defined functions for stack electrochemistry computations.
- Continued to distribute and support the SOFC-MP and Mentat-FC software packages with industry teams and CTP university researchers for modeling and development of SOFC stacks.
- Performed a numerical study of operational, and simple geometric changes for generic cross-flow stacks of 20 x 20, 30 x 30, and 40 x 40 cm cells to optimize the thermal performance, decrease

---

### Introduction

In order to efficiently develop and optimize planar SOFC stacks to meet technical performance targets, it is desirable to experiment numerically with the effects of geometry, material properties, operational parameters, and thermal-mechanical loading. The computations with representative baseline designs, validated by experimental data, have been used to develop better understanding of the stack behavior while avoiding costly and time-consuming experiments. In order to model the coupled physics associated with an SOFC stack, the simulation tool SOFC-MP was developed. This modeling tool combines the versatility of a commercial multi-physics code and a validated electrochemistry calculation routine to predict the gas flow distributions, current distribution, temperature field, and power output for stack-level simulations. The fundamental building blocks of the modeling and simulation tools are electrochemical models, heat and mass transfer simulations, computational mechanics, and experimental data.

The multi-physics modeling tools developed were then used in studying a wide range of design criteria as well as current material development and degradation challenges. A systematic methodology was developed for quantifying the interfacial strength between oxide scale and interconnect substrate and applied to predict the life of the ferritic interconnect with and without spinel coats. For SOFC materials and stack development, a homogenization model was developed to predict glass-

ceramic seal properties as a function of composition. IC scale growth was evaluated for its mechanical durability to resist growth-induced spallation. The modeling tools were also used to evaluate challenging issues anticipated for cell scale-up. The developed design methodology and stack analytical procedures are currently being documented as an American Society of Mechanical Engineers design basis for distribution within the SECA program.

## Approach

The following technical approach has been taken in the modeling task to meet program goals:

- Maintain, enhance, and provide guidance for the integrated modeling tools developed under the SECA CTP for evaluating fuel cell stack design concepts by the industry teams.
- Investigate the effects of materials degradation on cell performance and life.
- Investigate the effects of cell geometric design, material property distributions, and operating conditions on SOFC reliability.
- Perform material experiments for property data essential to constitutive and numerical model development.

## Results

### Increased Usage and Enhancement of Modeling Tools

The PNNL-developed modeling tools were greatly enhanced at the request of SECA industry team members during the past year. The modeling tools and techniques played a greater role in continued support of SOFC technology development for the SECA industry and university team members:

- The SOFC-MP and Mentat-FC modeling tools have been delivered to GE Energy, Delphi, FuelCell Energy, University of Cincinnati, and West Virginia University with accompanying technical support for usage and operation.
- The SOFC-MP solver was updated to include the use of non-reactive  $N_2$  in the thermal, flow, and species calculations. The graphical user interface (GUI) now assumes that the undefined balance of the prescribed inlet gas composition is  $N_2$ , so the existing GUI framework supports this modification.

- The flow solution, currently based on fully developed laminar flow between parallel plates, was updated to include a distributed resistance defined by a customizable user subroutine. The pressure drop is defined by  $dP/dL=RV$ , where  $P$  is the pressure,  $L$  is the length,  $R$  is the hydraulic resistance, and  $V$  is the flow velocity. This was used to simulate a simple, uniform resistance resulting in a nearly linear pressure drop across the cell and more complex fields simulating regions of different resistance (e.g. by design or from ribs, blockages). Examples showing the influence of the flow resistance on the air temperature distribution are shown in Figure 1.
- A new user-defined electrochemistry subroutine was implemented which allows the user to define the function that computes the voltage based on the input current density and the local species concentrations and temperatures.

### Modeling for Issues Related to Scale-Up

The desire to use SOFC stacks in megawatt-scale power applications using coal-based fuels provided motivation to study scale-up of cell dimensions. Larger cells are expected to have greater challenges with thermal management for mechanical reliability, electrochemical variability across the cell, and maintenance of the electrical contact path. The modeling tools were exercised to evaluate the following:

- A parametric analysis showed that increased cathode air flow, fuel tail-gas recycling, and increased separator plate thickness improved the thermal performance, decreased the stresses, and increased the electrical power of stacks. These parameters were applied to optimize the thermal management of 20 x 20 cm, 30 x 30 cm, and 40 x 40 cm cross-flow stacks.

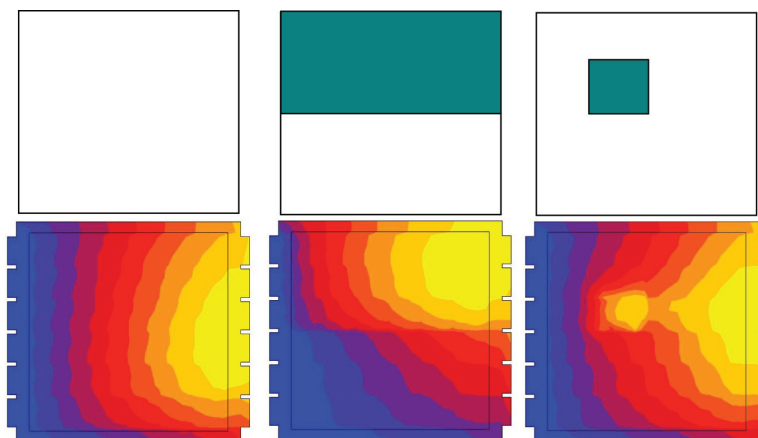


FIGURE 1. Contours of the Oxidant Temperature Field for a Cross-Flow Planar Stack

- Parametric analyses of the thermal-mechanical stresses indicated that the highest out-of-plane normal and shear stresses occurred at the edges of the contact layer. The peak normal and shear stresses were of the order of 35-80 MPa and 20 MPa, respectively. Initial parametric evaluations indicated that scale-up of cells maintained similar high stress magnitudes due to dominance by the edge effects. These stresses are very high for the contact paste layer, so the residual processing stresses will be very important for quantitative reliability calculations.

**Modeling of Material Mechanical Behavior and Experiments**

The integrated experimental/modeling method was applied to determine the interfacial strength of various interfaces. Material models were developed to describe the mechanical behavior of the contact paste and glass sealant. Experiments were conducted to provide input on the material models and to validate the modeling of the materials.

- The interfacial strength between the oxide scale and the Crofer22 substrate decreases with the growth of the oxide scale as shown in Figure 2, indicating that the growth of the oxide scale will degrade the IC reliability and therefore influence the long-term stack performance.
- IC surface roughness/finish influences the consistency of the indentation results. For those samples with  $H_o / R_a < 5.2$ , inconsistent indentation results were observed. The surface roughness of the as received SS441 is roughly three times higher than that of the Crofer22. The oxide adhesion strength of as received SS441 is lower than that of the Crofer22.
- The interfacial adhesion strength of the oxide scale/spinel-coating interface is much higher than that of the oxide scale/substrate interface.
- The interfacial strengths determined by this integrated experimental/modeling approach can be used to quantify the life of the spinel-coated metallic IC. The predicted life of the Crofer 22 APU coated with 15-micron spinel coating is around 15,500 hours as shown in Figure 3.
- A model to capture the densification behavior and developed stresses of contact materials during constrained sintering was developed. The sintering model included the effect of chemical strains due to different  $O_2$  concentrations during atmospheric cycling. For the LSM10 material at low temperatures, the cation vacancy concentration under atmospheric cycling presents a high driving force for diffusion, but the diffusion rate is very slow. At high temperatures the diffusion rate is high,

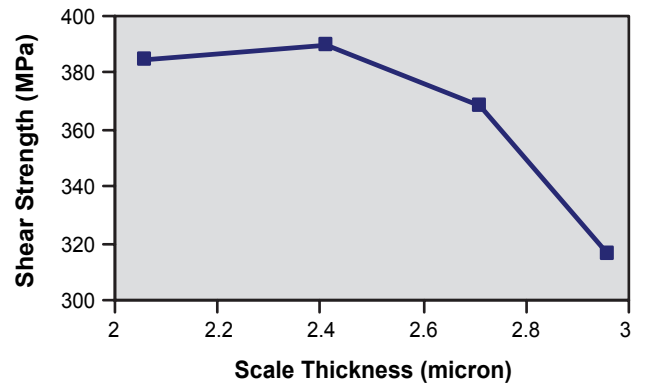


**FIGURE 2.** Predicted Interfacial Shear Strength versus Oxide Scale Thickness for Crofer 22 APU

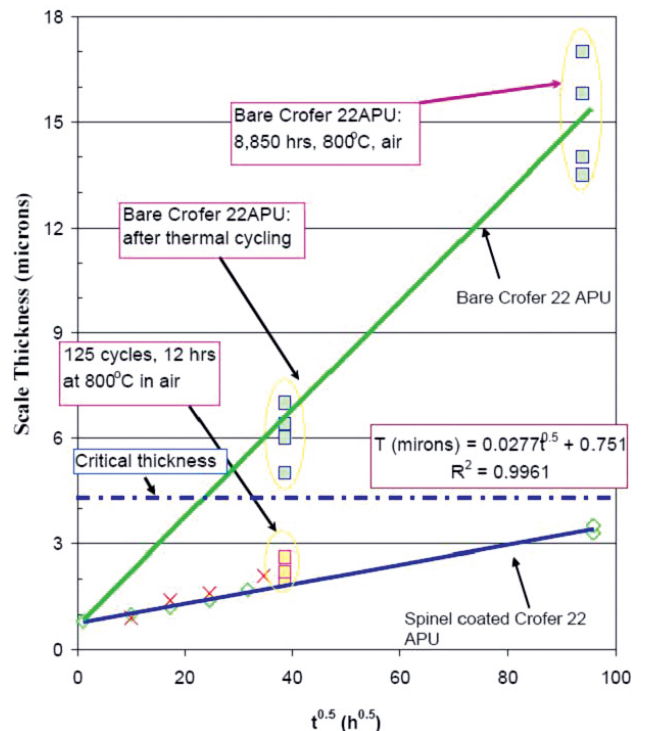
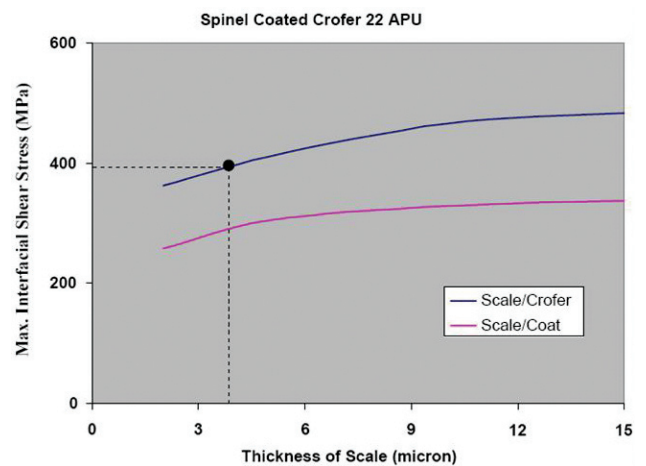


**FIGURE 3.** Life Prediction for Coated Crofer 22 APU

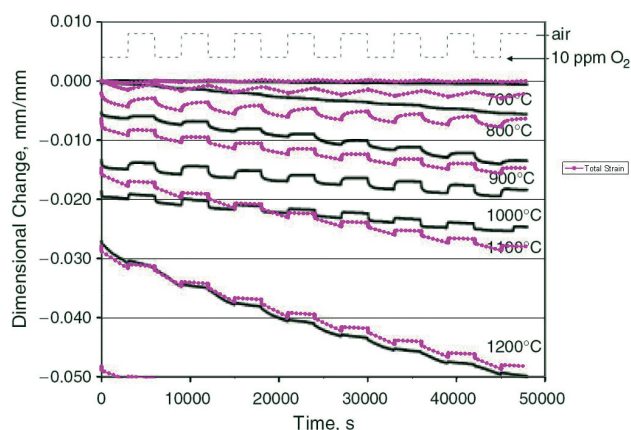


**FIGURE 4.** Experimental (McCarthy et al. 2007) and Predicted Dilatometry Results for LSM10 Specimen Strain Accumulation under  $p_{O_2}$  Cycling at Temperatures of 700-1,200°C

but the cation vacancy concentration difference between the two atmospheres is low and cycling is less influential. Figure 4 shows a comparison of the modeling and experimental results.

- Started experimental material characterization of refractory sealants and interfaces, and utilized PNNL's modeling tools to simulate stacks with self-healing glass sealants.

## Conclusions and Future Directions

During FY 2008, the modeling tools had seen continued usage among SECA teams, and additional capabilities have been developed to address durability issues. Future modeling activities will continue to focus on reliability, degradation, time-dependent response, and scale-up:

- Continue to improve the modeling tools to meet the needs of the SECA program. Continue to promote the usage of the tools by the industry and academic teams.
- Continue to add improved material models and numerical procedures to the modeling tools for simulation of time-dependent mechanical response and reliability.
- Continue modeling work on ferritic stainless steel ICs to meet the SECA target on stack life.
- Evaluate thermal management needs, influence of high pressure electrochemistry, and reliability of seal/cell structures during cell scale-up.
- Continue to support development of a robust test cell design.

- Evaluate the mechanical requirements for successful fabrication using refractory glass sealants and low-temperature sintering of cathode contact materials for reliable interconnection during operation and shutdown.
- Continue to develop seal property predictions via homogenization methods to identify reliable composite seal structures and compositions for stacks.

## FY 2008 Selected Publications/Presentations

1. X Sun, WN Liu, EV Stephens, MA Khaleel, "Determination of Interfacial Adhesion Strength between Oxide Scale and Substrate for Metallic SOFC Interconnects", *Journal of Power Sources*, v 176, n 1, 21 January 2008, p. 167-74.
2. X. Sun, A. Tartakovsky and M.A. Khaleel, Probabilistic Based Design Methodology for Solid Oxide Fuel Cell Stacks, *ASME Journal of Fuel Cell Science and Technology*, in press.
3. W. N. Liu, X. Sun, E. Stephens, and M. A. Khaleel, "Effect of IC Surface Quality on Interfacial Strength and Life Quantification of Coated Metallic IC Using an Integrated Experimental/Modeling Approach", PNNL Topical Report 17357, Pacific Northwest National Laboratory, Richland, WA 99354, January 2008.
4. W. N. Liu, X. Sun, E. Stephens, and M. A. Khaleel, "Effect of IC creep on long-term performance of one-cell stacks", presented at the 32<sup>nd</sup> Int. Con. on Advanced Ceramic and Composite, January 26 – February 1, 2008, Daytona Beach, FL.
5. W. N. Liu, X. Sun, E. Stephens, and M. A. Khaleel, "Determination of Interfacial Strength & Life Prediction by Using an Integrated Experimental/Modeling Approach", presented at the 32<sup>nd</sup> Int. Con. on Advanced Ceramic and Composite, January 26 – February 1, 2008, Daytona Beach, FL.
6. J. Milhans, H. Garmestani, S. Ahzi, X. Sun and M.A. Khaleel, "Micromechanics of the Effective Elastic and Thermal Properties of Glass-Ceramic Solid Oxide Fuel Cell Seal Materials", presented at the 32<sup>nd</sup> Int. Con. on Advanced Ceramic and Composite, January 26 – February 1, 2008, Daytona Beach, FL.
7. KP Recknagle, CL Rakowski, WN Liu, BJ Koepfel, MA Khaleel, Analysis and Optimization of Thermal and Electrical Performance of Large Scale SOFC Stacks, PNNL Topical Report 17099, Pacific Northwest National Laboratory, Richland, WA 99354, November 2007.

---

## IV.I.3 High Efficiency Coal Gasification-Based SOFC Power Plants

### Professor Scott Samuelsen

Advanced Power and Energy Program  
University of California, Irvine (UCI)  
Irvine, CA 92697-3550  
Phone: (949) 824-7302 x120; Fax: (949) 824-7423  
E-mail: gss@uci.edu

### DOE Project Manager: Travis Shultz

Phone: (304) 285-1370  
E-mail: Travis.Shultz@netl.doe.gov

### Subcontractors:

James D. Powers, Santa Monica, CA  
David M. Francuz, Rancho Santa Margarita, CA

Contract Number: 41817

Start Date: July 13, 2007

Project End Date: October 31, 2008

### Objectives

- Develop a stand-alone planar solid oxide fuel cell model based on sound first principles of operation that can be used to support system studies. The model will allow a large number of user-adjustable parameters associated with material properties and cell/stack geometry, enabling users to tailor the model to fit details of their systems or to optimize fuel cell design.
- Identify and evaluate coal gasification-based solid oxide fuel cell (SOFC) power plant concepts for large-scale central power plant applications, consistent with the Office of Fossil Energy's Fuel Cell Systems goals, targeting 60% efficiency (coal higher heating value [HHV]) while incorporating capability to isolate 90% of carbon from coal for later sequestration. Develop rough order of magnitude cost estimates for the integrated gasification fuel cell (IGFC) plants to evaluate the economic feasibility and guide design optimization.
- Produce position papers that assess benefits and synergies of fuel cells in coal-fueled central generation plants that possibly include: amenability to carbon capture/sequestration, pollutant emissions, water usage, efficiency and cost of electricity, in a format suitable for a variety of public uses.

### Accomplishments

- A planar SOFC model capable of evaluating various overpotential mechanisms (activation, ohmic and

diffusion) and physically resolving the internal current density, flow compositions and temperature profiles in fuel cell channels has been developed. The model, developed both in the MATLAB<sup>®</sup> environment and in C++, can be applied to a wide range of defined geometries (co-, counter- or cross-flow configuration, one or two dimensional), material properties and input flows. Results from the model have been validated against benchmark data. This model has been successfully linked to Aspen Plus<sup>®</sup> flow sheet simulation software as a user-defined model making it possible to analyze and optimize IGFC systems from a holistic perspective.

- IGFC plant concepts were identified that are expected to achieve very high system efficiencies (50-60%). Several different gasifiers, including Catalytic Hydrogasifier, Non-catalytic Hydrogasifier and Chemical Looping Gasifier were identified that can operate synergistically with the SOFC to maximize system performance. Functional specifications have been submitted to the gas desulfurization, CO<sub>2</sub> removal and catalyst technology vendors based on results of Aspen Plus<sup>®</sup> plant simulations.
- A survey was conducted of coal-based SOFC publications in the open literature, including papers in technical journals and feature articles in trade and popular science publications. Gaps in the available public data were identified. A strategy for publications was developed and planned papers were outlined.

---

### Introduction

Deployment of SOFC technology in coal-based power plants is essential in realizing ultra high thermal efficiencies, on the order of 60% (HHV basis), while being CO<sub>2</sub> sequestration ready. Previous conceptual analyses of SOFC-based power plants indicate that it may be possible to achieve an improved combination of efficiency, emissions, and specific power output which in turn can reduce the power generation equipment cost on a \$/kW basis. Thus, a need exists to perform a detailed systems analysis of advanced SOFC-based power plant designs in order to identify the best opportunities worthy of support by the U.S. DOE for their development. A detailed SOFC model is also required in support of such systems analyses. The University of California at Irvine's Advanced Power and Energy Program (APEP), as part of a research and development solutions team, is contracted to supply the required resources and act

as lead technical management in order to develop the necessary models, perform the systems analysis as well as report on high efficiency coal gasification-based SOFC power plants.

## Approach

**SOFC Model.** A stand-alone executable finite element SOFC model that is transferable and executable without any special software purchase requirements is under development. This model includes flexibility to accept user inputs as specified below and produce steady-state operating results based upon sound and rigorous analysis of expected future SOFC performance. The overall model requirements and specifications include cell geometry (e.g., length, width, flow channels), cell configuration (e.g., co-flow, counter-flow, cross-flow), stack geometry and size, extent of internal reforming, electrochemical loss terms (e.g., exchange current density, cell resistance), heat losses, oxidant properties (e.g., species composition), oxidant inlet thermodynamic conditions (e.g., temperature, pressure), fuel properties (e.g., species composition), fuel inlet thermodynamic conditions (e.g. temperature, pressure), fuel utilization, and operating pressure. The model consists of iterating between two interacting modules: a “Species Conservation” module that accounts for chemical (methane reformation and water gas shift reaction) and electrochemical (electrochemical oxidation of H<sub>2</sub>) reactions and calculates the chemical species profiles as well as current density distribution, and an “Energy Conservation” module that calculates the temperature distribution and heat loss terms.

**Systems Analysis.** IGFC design concepts are developed from a variety of sources, including previous work conducted by APEP, literature, discussions with the National Energy Technology Laboratory (NETL) and brainstorming sessions. When developing these concepts, special consideration is given to capturing synergies between the SOFC and the gasification systems that are not found in traditional IGCC designs. Conversely, design schemes that violate practical constraints imposed by the presence of the SOFC are disqualified. A 2020 deployment date is assumed for selection of the technologies. Design concepts that have potential for achieving the 60% efficiency, 90% CO<sub>2</sub> separation, competitive installed plant cost, acceptable reliability, low risk associated with SOFC requirements and other advanced technologies required are identified. IGFC system simulation models are then set up in Aspen Plus<sup>®</sup> with the SOFC model integrated with Aspen Plus<sup>®</sup> in order to develop overall IGFC system performance estimates. Rough order of magnitude capital, operating and maintenance cost estimates are developed in order to arrive at an indicative cost of electricity assuming the Solid State Energy Conversion Alliance (SECA) target cost for the system power block of \$400/kW (installed

cost and year 2002 dollars basis) and an SOFC stack life of 40,000 hours.

**Position Papers.** Position papers are generated that outline benefits and synergies, emanating from literature, analyses of above and prior research conducted by APEP for the DOE of fuel cells in coal-fueled central generation plants. The papers are structured to meet a variety of audiences representing stakeholders engaged in environmentally-sensitive coal utilization technologies for power generation. The primary focus of the position papers is to educate the public regarding the potential for realizing high efficiency clean coal power generation and the advantages of the SOFC in such large-scale power generation.

## Results

**SOFC Model.** The model can accept input information of inlet fuel and air thermodynamic properties (temperature and pressure) as well as chemical compositions and SOFC geometry, either from user input or from stream information in an Aspen Plus<sup>®</sup> flow sheet. Besides providing data such as fuel cell power output, heat loss, and exhaust stream properties, which are essential for systems analysis, the fuel cell model also provides the temperature, composition and current density profiles within the fuel cell that are helpful in determining if the fuel cell is being operated under realistic conditions. The planar SOFC model predictions were compared against those of the International Energy Agency’s (IEA’s) model (“IEA benchmark data”) [1] for two sets of anode feed gas compositions: “Benchmark 1” consisting of 90% H<sub>2</sub>, 10% H<sub>2</sub>O and “Benchmark 2” consisting of 26.26% H<sub>2</sub>, 17.1% CH<sub>4</sub>, 2.94% CO, 4.36% CO<sub>2</sub>, 49.34% H<sub>2</sub>O. The model predictions are in good agreement with the Benchmark 1 data but diverge somewhat from the Benchmark 2 data. This discrepancy is attributed to the difference in the methodology used in calculating the activation and diffusion polarizations between the models. The methods used for determining the activation and diffusion polarizations in the UCI model are similar to those used by Campanari [2] and Costamagna [3] while the IEA model combines the two polarizations. The activation energies appearing in these correlations are being adjusted to obtain performance projections consistent with high-performance SOFCs that have been demonstrated and are expected to be commercial in 2020. Typical temperature, current density and species flow rate distributions along the fuel cell channel as calculated by the model are presented in Figures 1 and 2.

**Systems Analysis.** Several promising IGFC plant concepts have been identified for both near atmospheric and elevated operating pressure SOFCs. Figures 3 and 4 show the overall block flow diagrams for two

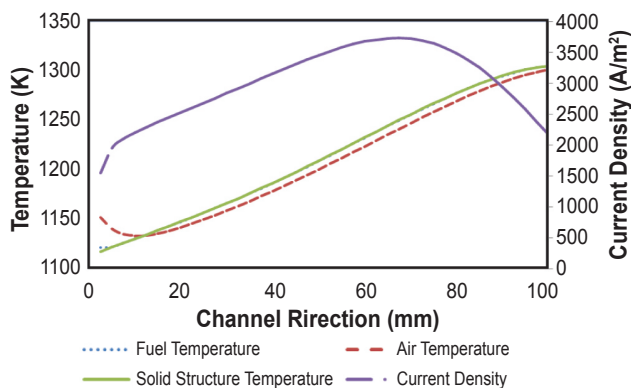


FIGURE 1. Typical Temperature/Current Density Distribution along Fuel Cell Channel - IEA Benchmark 2 Data, 1-Dimensional Co-flow

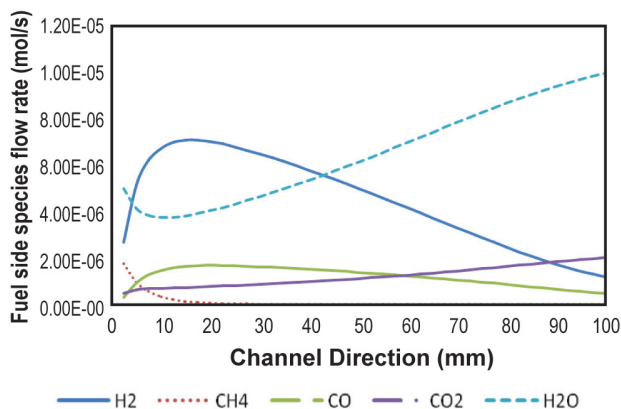


FIGURE 2. Typical Species Distribution along Fuel Cell Channel - IEA Benchmark 2 Data, 1-Dimensional Co-flow

of the concepts. The concept depicted in Figure 3 consists of a non-catalytic high pressure hydrogasifier-based plant integrated with a SOFC system operating near atmospheric pressure. The raw syngas rich in CH<sub>4</sub> after cleanup is humidified and then supplied to the reactor/expander topping cycle where additional methane is formed and the gases heated up by the exothermic methanation reaction are expanded through a turbine to recover power. The CH<sub>4</sub>-rich gas is then supplied to the SOFC system which includes a pre-reformer to chemically recuperate the sensible heat contained in the anode exhaust gas. The H<sub>2</sub> demand of hydrogasification is met partially by supply of syngas from the O<sub>2</sub> blown section of the gasifier and partially by the recycle of the anode exhaust gas after CO<sub>2</sub> separation. The fuel utilization in the SOFC is limited to about 50% in order to recycle the optimum amount of H<sub>2</sub> for the hydrogasification. A purge stream limits the concentration of N<sub>2</sub> and Ar within the recycle loop. The concept depicted in Figure 4 consists of a high pressure chemical-looping gasifier-based plant integrated with a pressurized SOFC-gas turbine (GT) hybrid. The gasification process produces a syngas stream which is

mostly H<sub>2</sub> and a separate low pressure CO<sub>2</sub> stream. The raw syngas after cleanup is humidified and then supplied to the reactor/expander topping cycle where the small fractions of CO and CO<sub>2</sub> are reacted with the H<sub>2</sub> to form CH<sub>4</sub> and the gases heated up by the methanation reaction are expanded through a turbine to recover power. The exhaust gas is then supplied to the SOFC-GT system.

**Position Papers.** Few analyses of IGFC systems have been published in the technical literature, with very inconsistent assumptions and results. Efficiencies of these systems range from 42%-63%; several of the higher-efficiency system results are not supported by rigorous analysis, but rather depend on multiplying component efficiency estimates. System designs and analyses are being developed at UCI and NETL that will demonstrate high-performance IGFC systems with SOFC performance levels and design approaches consistent with results demonstrated under the SECA program. These analyses, when published, will provide strong bases to support broad communications efforts. A large number of the benefits of IGFC have been identified with supporting data and analysis, where available. These include performance, emissions of CO<sub>2</sub>, NO<sub>x</sub> and other criteria pollutants, water demand, scalability, methane conversion capability, and capital cost advantages. A white paper and a fact sheet are being written which will outline and quantify these advantages of IGFC over competing and incumbent technologies. Further, a strategy of technical papers and feature articles has been developed that will serve to publicize and promote the advantages of IGFC systems.

### Conclusions and Future Directions

- The fuel cell model is highly configurable, which enables investigation of various parameters that may affect the performance of an SOFC. The configurable parameters of the fuel cell model include material property parameters (activation energy for exchange current density, conductivity of electrode and electrolyte materials), cell geometry parameters (length, width, number and dimensions of air and fuel channel, electrodes, electrolyte and interconnect thickness) and desired working voltage or desired working current density (the former option is more often used in system analysis).
- Promising IGFC plant concepts have been identified. Systems analysis of the various configurations will be completed to develop overall plant performances and identify the more promising concepts for developing cost estimates.
- There has been very little technical literature published on coal-based fuel cell systems that highlights the key benefits and presents realistic targets and capabilities of IGFC systems. White papers and fact sheets are being drafted to promote

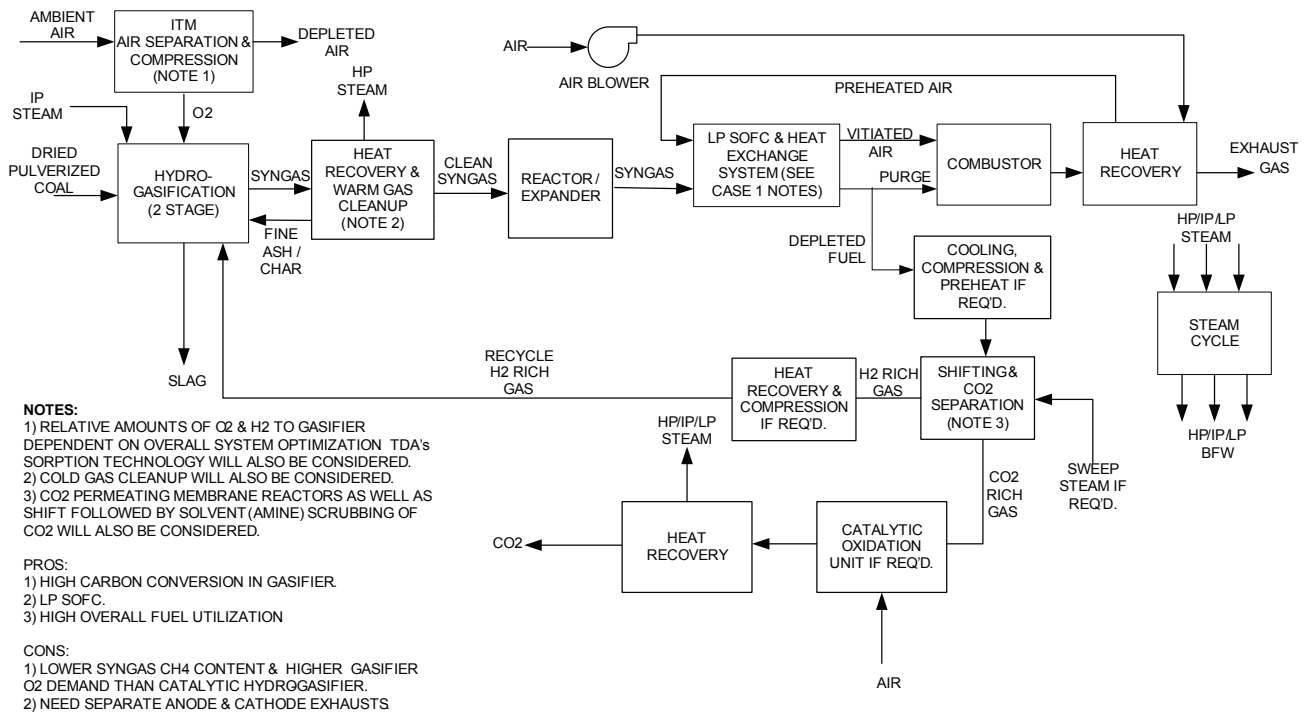


FIGURE 3. Overall Block Flow Diagram – Non-catalytic Hydrogasifier IGFC – Low Pressure SOFC

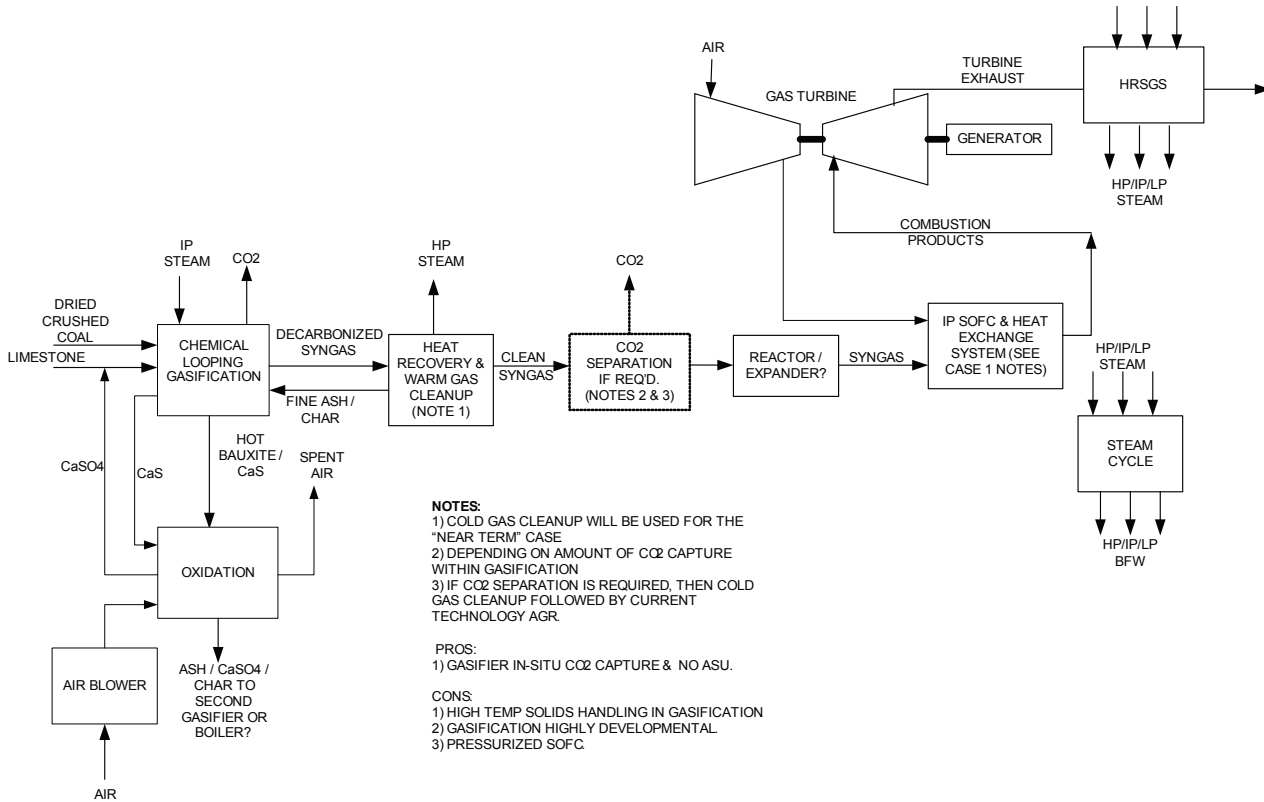


FIGURE 4. Overall Block Flow Diagram – Chemical Looping Gasifier IGFC - Pressurized SOFC

and highlight the benefits of IGFC systems. Technical paper and feature article topics have been identified and proposals will be prepared for these.

### **FY 2008 Publications/Presentations**

1. 1<sup>st</sup> Bimonthly Progress Report for August – September 2007, September 28, 2007.
2. 2<sup>nd</sup> Bimonthly Progress Report for October – November 2007, November 30, 2007.
3. 3<sup>rd</sup> Bimonthly Progress Report for December 2007 – January 2008, January 24, 2008.
4. 4<sup>th</sup> Bimonthly Progress Report for February – March 2008, March 27, 2008.

### **References**

1. E. Achenbach, "SOFC stack modeling, final report of activity A2, Annex II: modeling and evaluation of advanced solid oxide fuel cells," *International Energy Agency program on R, D&D on advanced fuel cells*, Juelich, Germany, 1996.
2. S. Campanari and P. Lora, "Comparison of finite volume SOFC models for the simulation of a planar cell geometry," *Fuel Cells*, 5(1): 34-51, 2005.
3. P. A. Costamagna, et al., "Electrochemical model of the integrated planar solid oxide fuel cell (IP-SOFC)," *Chemical Engineering Journal*, 102(1): 61-69, 2004.



---

## IV. SECA CORE RESEARCH & DEVELOPMENT

### J. Balance of Plant



---

## IV.J.1 Hybrid Ceramic/Metallic Recuperator for SOFC Generator

Mr. Anthony F. Litka (Primary Contact),  
Norm Bessette

Acumentrics Corporation  
20 Southwest Park  
Westwood, MA 02090  
Phone: (800) 332-0277; Fax: (781) 461-1261  
E-mail: tlitka@acumentrics.com

DOE Project Manager: Maria Reidpath  
Phone: (304) 285-4140  
E-mail: Maria.Reidpath@netl.doe.gov

Subcontractor:  
Blasch Precision Ceramics, Albany, NY

Contract Number: 84590

Start Date: June 28, 2006  
Project End Date: August 7, 2009

### Objectives

- Enable the use of inexpensive metallic alloys in a solid oxide fuel cell (SOFC) exhaust recuperator through the use of a ceramic heat exchange section in the high temperature region.
- Design and develop methods to mechanically integrate the ceramic and metallic sections into a recuperator assembly.
- Evaluate and characterize the performance of a hybrid ceramic/metallic recuperator under typical SOFC operating conditions.
- Demonstrate the performance and durability of the hybrid recuperator through both long-term steady-state and thermal cycle testing.

### Accomplishments

- Completed the detailed design of a cross flow ceramic/counter flow metallic hybrid recuperator for Acumentrics' SOFC fuel cell module.
- Designed and manufactured a mold to produce the cross flow ceramic monolith.
- Manufactured prototype ceramic parts.
- Completed assembly of a prototype 1-2 kW hybrid recuperator.
- Conducted preliminary testing of the hybrid recuperator.

---

### Introduction

Acumentrics Corporation continues to focus on the development of efficient, reliable, and low-cost SOFC generators. A key component of the SOFC generator is the heat exchanger, or recuperator, which preheats the incoming cathode air using available heat in the exhaust stream. Typical exhaust temperatures of an SOFC generator are in the range of 800 to 1,000°C. While the use of full metallic recuperators requires expensive high-alloy metals for oxidation resistance, these operating temperatures are well within the capabilities of lower cost ceramic and refractory materials.

In Phase I of this project, a proof-of-concept cross flow hybrid (ceramic/metallic) recuperator was designed, manufactured and tested. The hybrid design includes a ceramic monolith heat exchanger combined with additional metallic recuperator sections. This configuration takes advantage of the high temperature, low fouling capability of the ceramic section, while enabling the use of lower grade metallic alloys in the medium-to-low temperature regions. Results to date have shown that a ceramic monolith recuperator can be successfully integrated with additional metallic recuperator sections to achieve an overall heat exchange effectiveness required for use with an SOFC generator. These advances show significant promise that a recuperator capable of withstanding the severe operation conditions of an SOFC can be manufactured, while at the same time achieving significant cost reduction of the component.

### Approach

Since the start of this project, Acumentrics has made significant advances in the power density, flow distribution and sealing of its fuel cell stacks. These advances have coincided with the implementation of metallic counter flow recuperators which can achieve high effectiveness in a more compact configuration than the cross flow arrangement. The initial work in Phase II of the project has therefore focused on the design and construction of a recuperator using the ceramic monolith technology in conjunction with a counter flow metallic recuperator. Figure 1 illustrates the arrangement as configured for a 1-2 kW SOFC module. The design goal is for the ceramic section which is connected to the fuel cell stack cathode air outlet to reduce the temperature of the exhaust cathode air by approximately 100°C thereby reducing the grade of materials required for the counter flow metallic

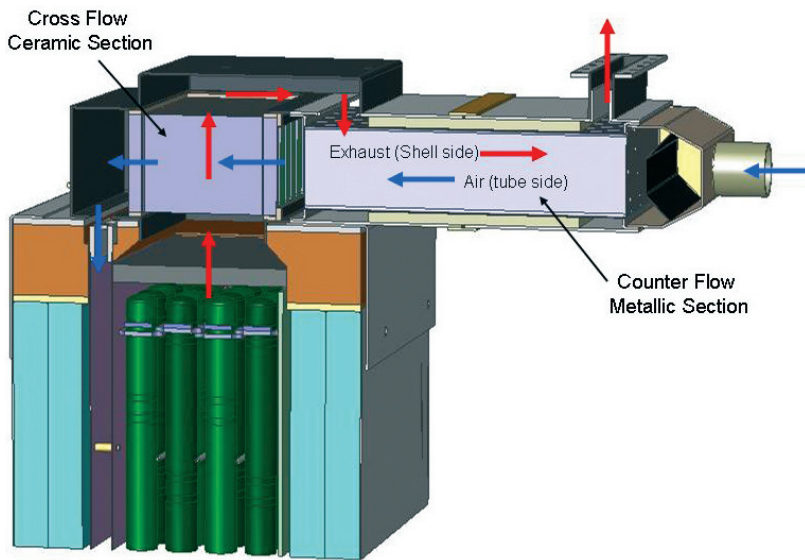


FIGURE 1. Recuperator Configuration

This core is encased in a metallic housing which directs the exhaust flow from the stack to the core exhaust passages and then directs the exhaust leaving the core to the inlet of the metallic recuperator. Expandable insulation is used to seal the core to the metallic casing preventing leakage from air to exhaust chambers. This configuration eliminates the need for complex plenums and allows for differential expansion of the heat exchange components through the use of flexible high temperature ceramic gaskets similar to that used on catalytic converters and the linear arrangement of the metallic and ceramic cores.

**Results**

Acumentrics worked closely with Blasch Precision Ceramics to design and manufacture a single pass cross flow ceramic core, made of silicon carbide, suitable for integration with a counter flow heat exchanger. A mold was manufactured to permit manufacture of ceramic cores using Blasch’s proprietary forming method capable of producing net shape ceramic parts. The ceramic monolith is shown in Figure 3. Leakage measurements were made on the cores to ensure air to exhaust side integrity. A test stand was assembled for testing the recuperator. The test configuration includes separate control and measurement of the exhaust and air streams to the recuperator. The hot exhaust entering the recuperator is produced via a combination of electric heaters and direct natural gas combustion to simulate the cathode air leaving the Acumentrics fuel cell stack. Shakedown testing of the facility has been completed and performance testing of the initial prototype is underway.

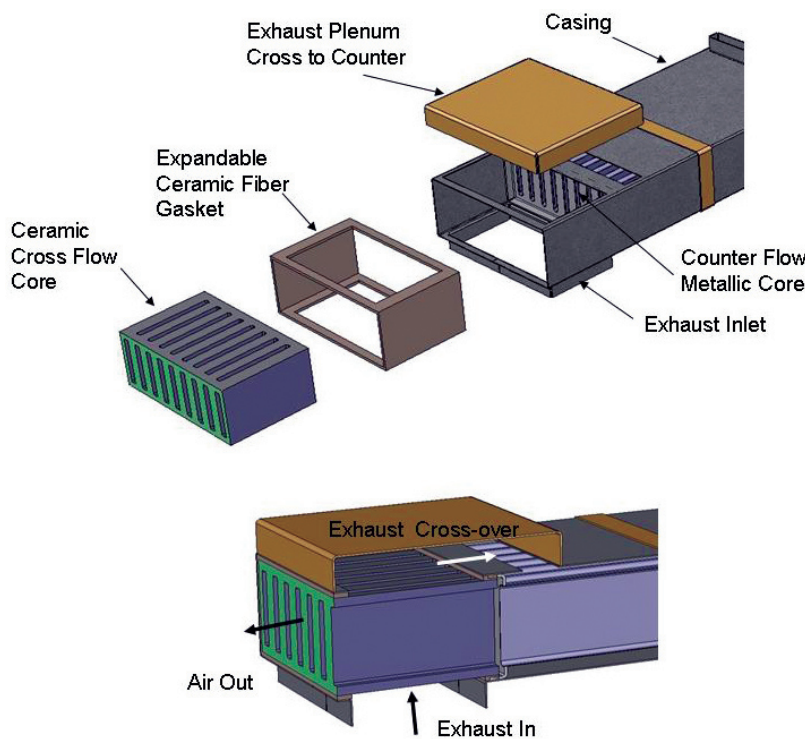


FIGURE 2. Hybrid Cross/Counter Flow Recuperator Assembly

section. Unlike in a cross flow configuration, in which different materials can be utilized in each metallic pass, in the counter flow recuperator the choice of materials is dictated by the temperature at the exhaust inlet zone.

As shown in Figure 2, a cross flow ceramic core is added to the air side outlet of the metallic recuperator.

After initial operations of the recuperator with exhaust inlet temperatures of 850°C and air preheat levels of 750°C, the recuperator was inspected to evaluate the integrity of the core. Inspection revealed that the ceramic core sealing was intact and the core was structurally sound without cracks or defects. Figure 4 shows the assembled recuperator with a close up of the ceramic core after initial shakedown testing.

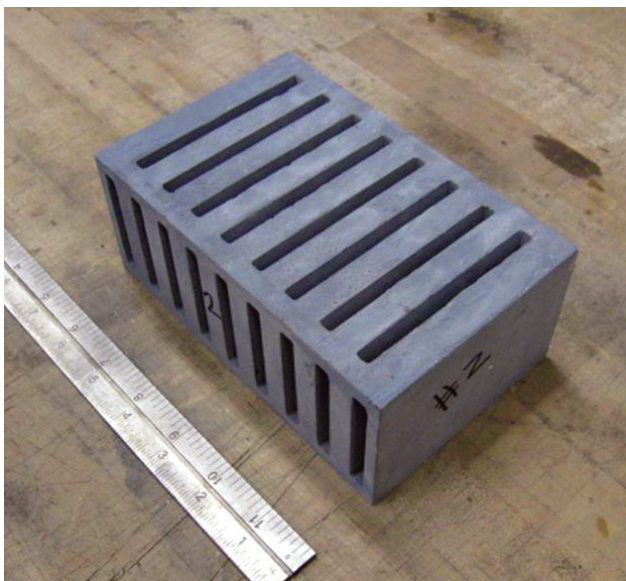


FIGURE 3. Ceramic Heat Exchanger Core



FIGURE 4. Prototype Recuperator

## Conclusions and Future Directions

Acumentrics Corporation, in conjunction with Blasch Precision Ceramics, has successfully integrated a ceramic monolith into a combination cross flow ceramic and counterflow metallic recuperator. Thermal modeling predicts that an effectiveness of  $>80\%$  with a reduction in heat transfer metal temperatures of  $100^{\circ}\text{C}$  is attainable. This will permit the use of less expensive alloys for the metallic components of the recuperator. An initial prototype of the recuperator has been manufactured and testing of the unit is underway.

The following is a summary of future technical objectives:

- Complete performance testing on the cross/counter flow hybrid recuperator.
- Evaluate ceramic component manufacturing techniques to optimize the ceramic core heat transfer rates.
- Conduct both long-term steady-state and thermal cycle testing to verify the performance and durability of the hybrid recuperator.
- Evaluate scale-up of the heat exchanger geometry to larger generator sizes.

## IV.J.2 Anode and Cathode Blower Systems for SOFC

Dr. Mark C. Johnson

Phoenix Analysis & Design Technologies (PADT)  
7755 S. Research Dr., Suite 110  
Tempe, AZ 85284  
Phone: (480) 813-4884; Fax: (480) 813-4807  
E-mail: mark.johnson@padtinc.com

DOE Project Manager: Maria Reidpath  
Phone: (304) 285-5432  
E-mail: Maria.Reidpath@netl.doe.gov

Contract Number: 84209

Start Date: August 2006  
Project End Date: August 2009

### Objectives

- Develop large multi-stage blower that can pump anode gas at 500°C (hot anode recycle blower - HARB). This unit will serve up to 500 kW power plants as part of FutureGen.
- Develop small multi-stage (SMS) blower that can pump warm anode or cathode gas at 100°C. This unit will serve up to 50 kW power plants.
- Verify bearing/seal selection and design.
- Integrate and evaluate controller/motor.
- Develop low-cost integrated assembly to provide required performance and offer low cost in high volume.

### Accomplishments

- Multi-stage blower aerodynamic technology now optimized for HARB and SMS blowers. Provisional patent has been filed.
- Developed two bearing rigs and initiated endurance testing. Goal is 40,000 hours of life. Additionally, a novel bearing system has been developed that is intended to help meet this very long life requirement.
- Complete design suitable for servicing FutureGen configurations up to 1 MW in size. Hardware now arriving for assembly.
- Complete impeller burst testing to understand durability issues with our multi-stage technology.

### Introduction

The thrust of this research and development effort is to develop technology that serves the solid oxide fuel cell (SOFC) industry and helps developers in this industry to succeed. The starting point for success rests with understanding the needs of the companies involved and this has been done through substantial discussions with these companies and the development of specifications with them. These discussions have led to two distinct designs – the HARB blower which will serve hot anode gas requirements in FutureGen demonstration units and the SMS blower, which will serve warm anode and cathode gas requirements for SOFCs and other fuel cell industries.

The challenge in this project has been to develop blowers that can make very difficult performance specifications and operate in harsh environments, while also providing low cost solutions. Therefore, the focus of this project is to develop an innovative multi-stage blower approach that is low cost and high performing. Additionally, the system must allow hot process flow while providing cool temperatures for the sensitive pump components.

### Approach

The approach used to develop this pump emphasizes design iterations with a reduction to working prototypes in rapid succession. Because of the complexities involved, side testing is used extensively. Side testing implies a test of some sub-system, or even a component, to insure suitability. Finite element analysis is used liberally whenever detailed analysis can provide insight into design tradeoffs.

Additionally, the success of this project will be dependent on close collaboration between PADT and SOFC developers. The requirements for the developers are changing continually and to glean the most out of the prototypes we build, regular feedback is needed.

### Results

Unfortunately, many of the most important results of our recent work are either PADT proprietary information or proprietary to our customers. Therefore, we can only provide high level summaries here.

One high level accomplishment is the completed design of the HARB phase II blower and the procurement of hardware. See Figure 1.

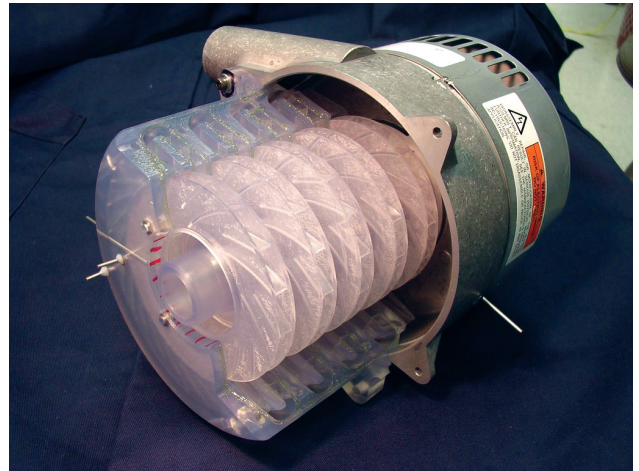
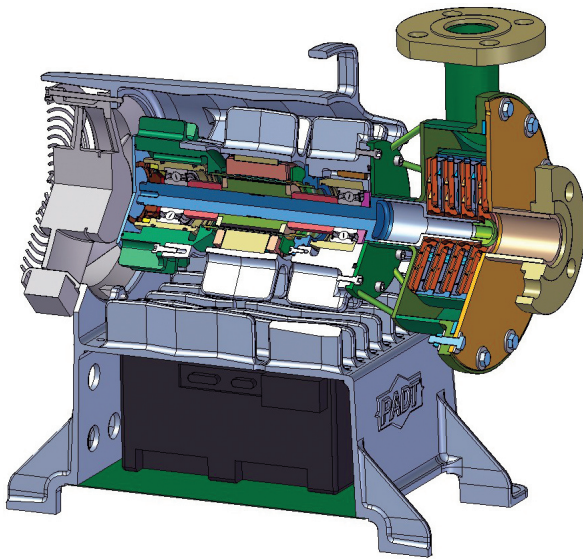


FIGURE 2. Aerodynamic Development System



FIGURE 1. PADT HARB Prototype and Early Hardware

A second major accomplishment of the last years' effort is the iterative development of highly efficient multi-stage aerodynamics. This was done using an off-the-shelf mule motor from Ametek as shown in Figure 2.

We have continued to get improved performance from our aerodynamic work on the SMS. We see this as a critical part of our multi-stage development and we have submitted a provisional patent that covers what we are trying to do. Table 1 illustrates the iterations we have completed.

TABLE 1. Description of Development Iterations for Low, Medium, and High Specific Speed Designs

	Low Specific Speed Designs	Medium Specific Speed Designs	High Specific Speed Designs
<b>Number of Iterations</b>	6	3	2
<b>Peak Efficiencies</b>	~ 68%	~ 70%	~ 75%
<b>Discussion</b>	More development is expected to increase efficiency ~ 3%.	Moderate flow and pressure is not as requested by the SOFC community. Development will stop.	Useful in very high flow cases. Again, not as requested by the SOFC community. Development will stop.

A third important result of our effort deals with blower reliability. To support this work, we have constructed two bearing rigs and mule motor, which are now running as much as possible with various bearing options. Additionally, we have conducted burst testing on impellers that are part of our aerodynamic solution. The bearing and burst rigs are shown in Figures 3 and 4.

The testing in these rigs has yielded better bearing and impeller designs. The impellers are not showing burst issues until ~44,000 RPM (about 2.5X the operating speed) and the latest bearing iterations are approaching 5,000 hours with very little sign of degradation.

### Conclusions and Future Directions

The work we have done so far has led us to the conclusion that we really need two types of blower solutions: one for FutureGen and one for small SOFC



**FIGURE 3.** Bearing Rigs for Life Evaluation and Extension

power plants. Fortunately, the technologies for the pumphead, bearing life, and thermal management will support both requirements. Additionally, we have concluded that close interaction with SOFC developers and manufacturing partners will be important for overall commercial success of our efforts.

Future work will now focus on demonstrating the durability and performance of the designs we have developed. Additionally, we will be demonstrating that the SMS-style blower can be directly retrofitted on an off the shelf motor system – thus offering a low cost solution. We anticipate a number of endurance tests will be run and some of these blowers will be tested at customer’s facilities.

**FY 2008 Publications/Presentations**

1. We presented at the 2007 SECA Workshop in San Antonio.
2. We have filed a provisional patent on our multi-stage aerodynamic technology.
3. We will be filing a full patent this year (2008).



**FIGURE 4.** Impeller Burst Rig for Impeller Life Extension

---

## IV.J.3 Foil Gas Bearing Supported High Speed Centrifugal Anode Gas Recycle Blower

Dr. Giri Agrawal (Primary Contact),  
Bill Buckley, Dennis Burr, Ali Shakil  
R&D Dynamics Corporation  
15 Barber Pond Rd.  
Bloomfield, CT 06002  
Phone: (860) 726-1204; Fax: (860) 726-1206  
E-mail: agragiri@rddynamics.com

DOE Project Manager: Maria Reidpath  
Phone: (304) 285-4140  
E-mail: Maria.Reidpath@netl.doe.gov

Contract Number: 84210

Start Date: June 27, 2005

Project End Date: August 6, 2008

- The prototype FBS-AGRB unit has been tested at elevated temperatures up to 718°C.
- A prototype unit was successfully tested by the U.S. Navy.
- Design optimization and cost reduction is in progress.

---

### Introduction

The goal of SECA is to develop commercially-viable (\$400/kW) 3 to 10 kW SOFC systems by year 2010. SOFC power generation systems are attractive alternatives to current technologies in diverse stationary, mobile, and military applications. SOFC systems are very efficient, from 40 to 60 percent in small systems and up to 85 percent in larger co-generation applications. The electrochemical conversion in a SOFC takes place at a lower temperature (650 to 850°C) than combustion-based technologies, resulting in decreased emissions – particularly nitrogen oxides, sulfur oxides, and particulate matter. These systems all offer fuel flexibility, as they are compatible with conventional fuels such as hydrogen, coal, natural gas, gasoline, or diesel. Despite these advantages, advances in balance of plant component design must be developed before the SECA program goal can be realized.

SOFC systems that incorporate some recycling of the anode exhaust gas, which is mixed with incoming fresh fuel prior to entering the pre-reformer, have a higher efficiency and offer the potential for lower overall system cost. An AGRB is an attractive solution to perform this task.

### Approach

R&D Dynamics has focused on the design and development of FBS-AGRB to achieve the goals set by SECA members. An innovative, cost-reduced, compact, high-temperature, high-speed centrifugal blower has been designed, built and tested. The FBS-AGRB rotating assembly is supported on state-of-the-art proven foil gas bearing technology. The foil gas bearing technology and the high speed permanent magnet (PM) motor design makes the FBS-AGRB very promising for meeting the technical targets and cost.

In order to reach the goal of making economically viable and efficient SOFC systems, the FBS-AGRB has been designed and built to meet the requirements of SOFC systems because of its potential for:

### Objectives

Demonstrate the feasibility of using a high-speed centrifugal foil bearing supported anode gas recycle blower (FBS-AGRB) to help members of Solid State Energy Conversion Alliance (SECA) meet their solid oxide fuel cell (SOFC) goal of higher efficiency and lower overall system cost.

### Accomplishments

- Substantial progress has been made and a prototype FBS-AGRB unit has been designed and built to meet all SECA member requirements having the following features:
  - Low cost design which incorporates design for manufacturing and assembly concepts
  - High temperature capability >850°C
  - High efficiency high-speed motor and centrifugal blower
  - Oil-free gas bearings
  - Compact
  - Scalability to larger sizes
  - No gas, sulfur, silica or heavy metal leakage
  - No purge gas required
  - No parasitic cooling required
  - Mechanical type seals were not required
  - Design explosion proof
  - No corrosion/carbon deposition
  - 40,000-hour lifetime
  - Maintenance free

- Low-cost using simple design and material.
- High-temperature capability ( $>850^{\circ}\text{C}$ ) using foil gas bearings and advanced high temperature magnets for the PM motor.
- Highest blower efficiency via high-speed centrifugal impeller, foil gas bearings, PM motor and sensorless controller.
- Contamination-free using oil-free foil gas bearings.
- High reliability requires no maintenance.
- Compactness and light weight.

## Results

The FBS-AGRB has been designed and built for an inlet temperature up to  $850^{\circ}\text{C}$ , atmospheric pressure, pressure rise of 4-10 inches of water, and a flow of 100 standard liters per minute (slpm), which is nominally composed of 46 slpm  $\text{H}_2\text{O}$ , 27 slpm  $\text{CO}_2$ , 20 slpm  $\text{H}_2$  and 7 slpm  $\text{CO}$ . Overall predicted efficiency exceeds 50% under aforementioned operating conditions. The unit has a variable speed control with a flow turndown ratio of 5 to 1. The blower unit will have a design life of  $>40,000$  hours, with a 100% duty cycle and 10,000-hour maintenance interval. The unit will be able to tolerate at least 30 thermal cycles between operating and room temperatures over its design life.

Design points for the FBS-AGRB are as follows:

Shaft speed	98,000 rpm
Pressure Ratio	1.025
Pressure Rise	25.4 cm of water (10 inches of water)
Inlet Pressure	1.01 bar (14.69 psia)
Outlet Pressure	1.08 bar (15.06 psia)
Inlet Temperature	$850^{\circ}\text{C}$ ( $1562^{\circ}\text{F}$ )
Outlet Temperature	$857.3^{\circ}\text{C}$ ( $1575.2^{\circ}\text{F}$ )
Gas Constant	$0.369 \text{ J/Kg}^{\circ}\text{C}$ ( $68.64 \text{ ft-lbf/lbm R}$ )
Specific Heat Ratio	1.274
Mass Flow	$1.54 \text{ g/s}$ ( $0.204 \text{ lbm/min}$ )
Volume Flow	100 slpm
Impeller Isentropic Power	15.6 Watt

Figures 1 and 2 show the cut-section view and the blower assembly, respectively. Figure 3 shows the shaft assembly.

Key technologies were incorporated into the blower design including state-of-the-art aerodynamics, foil gas bearings, PM motor using advanced high-temperature magnets, innovative fan design with fins mounted on shaft assembly, thermal choke to separate the hot side from the cold side and sensorless controller. Design

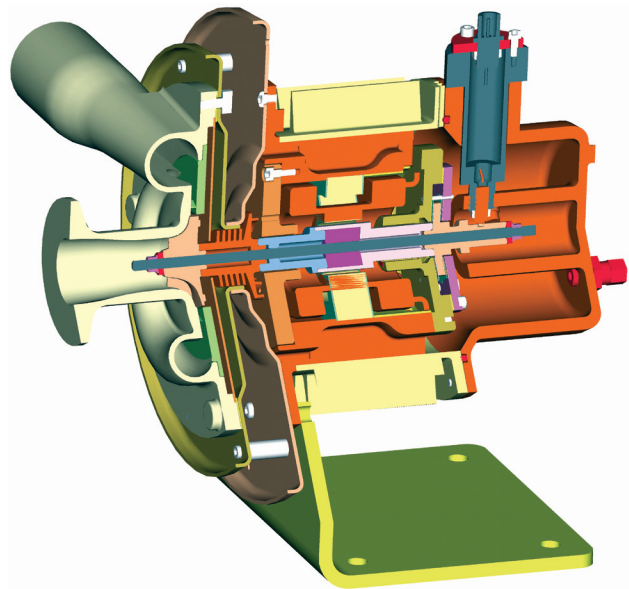


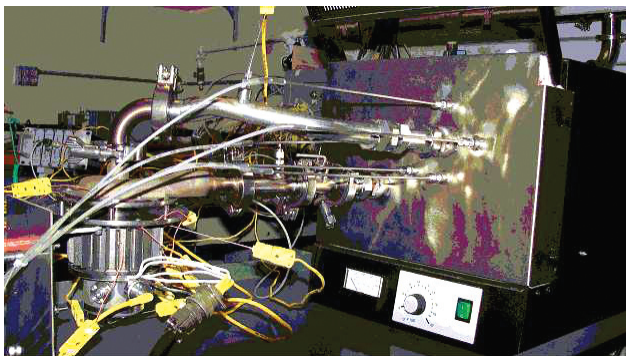
FIGURE 1. Cut-Section View of AGRB



FIGURE 2. View of the FBS-AGRB Prototype Unit



FIGURE 3. View of the Shaft Assembly



**FIGURE 4.** Elevated Temperature Test Rig with Blower Installed

analysis included performance prediction maps, preliminary design, finite element analysis including thermal, vibration and stress, computational fluid dynamics analysis, rotor dynamics analysis, cooling flow analysis, detailed design and drawings. Tests performed on AGRB components were load deflection on journal and thrust bearings and back electromotive force testing on the motor rotor and stator etc. A furnace was used to heat up the gas to elevated temperature testing of FBS-AGRB. Figure 4 shows the elevated temperature test rig with blower installed.

## Conclusions and Future Directions

- Key blower technologies were proven by extensive design analysis and testing.
- A prototype unit was designed, built and tested.
- The high-temperature blower design evolved to be a successful design to meet SECA goals.
- The blower was tested under various thermal cycles and load. It was tested successfully up to an inlet temperature of 718°C.
- A prototype unit was successfully tested by the U.S. Navy.

Work needs to be continued as follows:

- Test blower at higher temperature conditions (up to 850°C).
- Incorporate rigorous design for manufacturing and assembly techniques to further reduce cost.
- Demonstrate blower to SECA members.
- Test blower in a SECA member's fuel cell systems.

## FY 2008 Publications/Presentations

1. "Foil Bearing Supported High Speed Centrifugal Blower" Progress Report Period 04/21/07 to 03/20/08, April 20, 2008.



---

## V. ADVANCED RESEARCH



---

## V.1 Proton Conducting Solid Oxide Fuel Cell

S. (Elango) Elangovan (Primary Contact),  
J. Hartvigsen, B. Heck  
Ceramtec, Inc.  
2425 South 900 West  
Salt Lake City, UT 84119-1517  
Phone: (801) 978-2162; Fax: (801) 972-1925  
E-mail: Elango@ceramtec.com

DOE Project Manager: Ayyakkannu Manivannan  
Phone: (304) 285-2078  
E-mail: Ayyakkannu.Manivannan@netl.doe.gov

Contract Number: 84595

Start Date: August 8, 2007  
Project End Date: August 7, 2009

### Objectives

- Identification of dopant type and concentration in a perovskite host to achieve high proton conductivity and high protonic transference number under solid oxide fuel cell (SOFC) operating conditions.
- Selection of dopant type and concentration in a perovskite host to provide resistance to reactivity towards CO<sub>2</sub> and H<sub>2</sub>O.
- Evaluation of electrode materials using symmetric cells and full cells in button cell configuration.
- Test button cells using selected perovskite compositions.
- Test short stacks of nominal 100 Watts.

### Approach

- Select an appropriate B-site dopant in a perovskite matrix by evaluating protonic conductivity and transference number in SOFC relevant atmospheres.
- Investigate stability of compositions in syngas.
- Evaluate a range of perovskite compositions as potential low temperature cathodes for conductivity, thermal expansion, and reactivity with proton conducting membranes.
- Evaluate the best combination of electrolyte and electrodes using symmetric cells and full cells.
- Develop tape casting techniques to fabricate 10 x 10 cm cells.
- Test short stacks in hydrogen and natural gas reformat at 700-800°C.

### Accomplishments

- Dopant type was identified to achieve a high protonic conductivity of  $1 \times 10^{-2}$  to  $3 \times 10^{-2}$  S/cm at 800°C to 900°C.
- Selected compositions were found to be less prone to formation of BaCO<sub>3</sub> in the presence of syngas (H<sub>2</sub>O + CO<sub>2</sub>).
- High ionic transference number was demonstrated as indicated by open circuit voltage in button cells.
- A proton transference number of 0.7 was estimated at 800°C.
- Potential for high efficiency operation using a proton conductor-based SOFC relative to oxygen conductor-based SOFC was shown.
- Electrode evaluation was started using thick electrolyte discs.
- Tape cast process was developed to enable fabrication of thin electrolytes.
- A chemically compatible sintering aid was identified to achieve high sintered densities.

### Future Directions

- Optimization of electrode compositions and electrode application techniques to improve cell performance.
- Evaluation of performance in button cell and stack tests using syngas fuel.

---

### Introduction

One of the prime attractions of fuel cells is the possibility of realizing energy conversion efficiencies much higher than possible with the thermal cycle systems. The basis of this difference is that thermal cycle system efficiencies are bounded by Carnot cycle thermodynamics, whereas fuel cell efficiencies are determined by chemical equilibrium thermodynamics and non-equilibrium force-flux relationships that govern charge, mass, momentum and energy transport. Materials have been developed which function as high temperature solid electrolytes in fuel cell applications. Two of the most widely considered materials are yttria doped ZrO<sub>2</sub> (YSZ) which transports oxygen ions and gadolinium doped BaCeO<sub>3</sub> which transports protons [1].

The thermodynamic difference between proton and oxygen ion cells is manifest in reversible potential variation with reactant utilization as a function of product water location. Excess air flow, used to remove

the heat generated by cell operation, results in a lower water concentration in the cathode stream of a proton cell than in the anode stream of an  $O^{2-}$  cell.

Reversible potential variation with fuel utilization is shown for both proton and oxygen ion cells in Figure 1. The proton cell has a substantially higher reversible potential across the full range of fuel utilization. An interesting observation is that steam ratios greater than stoichiometric ( $S/C=2$ ) increase the high utilization potential of a proton cell while oxygen ion cell potentials are uniformly higher with sub-stoichiometric steam ratios. This is due to the use of carbon monoxide via the shift reaction. The oxygen ion cell generates water in the anode stream so inlet compositions can be water deficit (high potential) and still have sufficient water to drive the shift reaction as utilization increases. The proton cell, on the other hand, must have sufficient or even excess water at the inlet to drive the shift reaction at high utilizations. However, water in the anode stream does not directly enter in the calculation of proton cell potentials and thus has little effect on the potential until higher utilizations where shift produced hydrogen is important. Thus, high temperature proton conductors have a thermodynamic advantage over oxygen ion conductors.

Comparable electrolyte ionic conductivities are required to take practical advantage of the thermodynamic benefit. Applications driven by maximizing efficiency at the expense of power density would favor proton cells. Thus, the opportunity for very high efficiency operation is one of the primary motivating factors for investigating proton conducting solid oxide fuel cells (P-SOFC). However, to date the research work on P-SOFC has lagged far behind the well-known YSZ-based oxygen conducting solid oxide fuel cells (O-SOFC). The challenges that have been encountered in P-SOFC systems are discussed below.

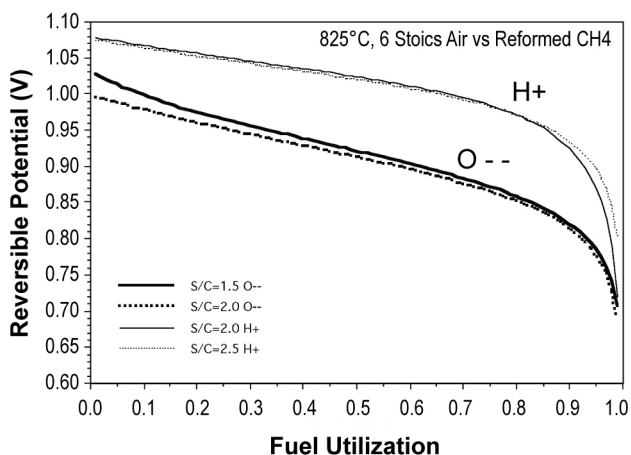


FIGURE 1. Comparison of Reversible Cell Potential

## Proton Conductivity

As mentioned earlier, the differences in electrolyte ionic conductivity may be greater than differences in driving force and must be included in any comparison of an operating cell at a fixed current density. In general the protonic conductivity of commonly known perovskite materials such as doped  $SrCeO_3$  and  $BaCeO_3$  are considerably lower than the oxygen ion conductivity of YSZ. The proton conductivity ranges from  $5 \times 10^{-3}$  to  $2 \times 10^{-2}$  S/cm at  $800^\circ\text{C}$  [2-6]. While the high end of this range is comparable to the oxygen conductivity of 8-YSZ, the perovskite materials also possess some level of oxygen ion conductivity and electronic conductivity at various temperatures. Thus, the protonic transference number varies as a function of temperature. While the doped  $BaCeO_3$  composition functions as an effective electrolyte, an increase in hydrogen conductivity is preferable to fully exploit the benefit of high efficiency with high power density.

## Stability

One of the biggest technical challenges lies in maintaining the chemical stability of the perovskite in the presence of  $CO_2$  and moisture, both are present in a typical hydrocarbon fuel. Numerous studies have confirmed the instability of the perovskite compositions.

It has been shown [7] that partial replacement of the B-site dopant with Zr completely eliminates this reaction. A similar improvement in stability in moist conditions was also reported with Zr substitution [8]. However, the stability improvement is at the expense of protonic conductivity. The proton conductivity was found to decrease monotonically with increasing Zr content [9-11].

Thus, what is required for successful development of a P-SOFC is an electrolyte material that has high proton conductivity to achieve a low area specific resistance, high protonic transference number relative to oxygen transference number to realize high efficiency, and stability in  $CO_2$  and  $H_2O$  without compromising protonic conductivity for cell operation using practical hydrocarbon fuels.

## Approach

Perovskite compositions that are known to exhibit protonic conductivity were evaluated for dopant study. The B-site dopants, typically rare earth metals, have been shown to increase the proton conductivity of perovskites such as  $BaCeO_3$ . Several dopants and dopant levels were screened to identify compositions that have high conductivity and stability. Selected compositions were evaluated in button cell tests.

## Results

A variety of B-site dopants were evaluated for their effect in total ionic conductivity and proton transference number. Protonic conductivity as high as 0.015 S/cm at 700°C and 0.02 to 0.03 S/cm at 800°C was measured. In addition, the estimated protonic transference number ranged from 0.6 to 0.7 at 800°C, while the total ionic transference number was around 0.9.

BaCeO<sub>3</sub> type perovskite materials are known to be difficult to achieve good sintered density. A small amount of a sintering aid was added to achieve a sintered density in excess of 98%. The addition of the sintering aid did not affect the ionic conduction properties of the material. Micrographs of sintered BaCeO<sub>3</sub> are shown in Figure 2. As can be seen, the addition of the sintering aid improves densification to achieve the needed density for an electrolyte.

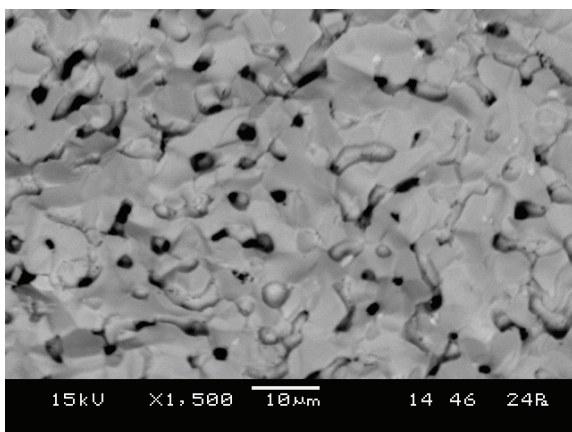
Selected compositions, baseline and modified perovskites, were also exposed to syngas at 800°C. Comparison of powder X-ray diffraction patterns showed a significant reduction in the BaCeO<sub>3</sub> for certain

modified compositions relative to the baseline material as shown in Figure 3.

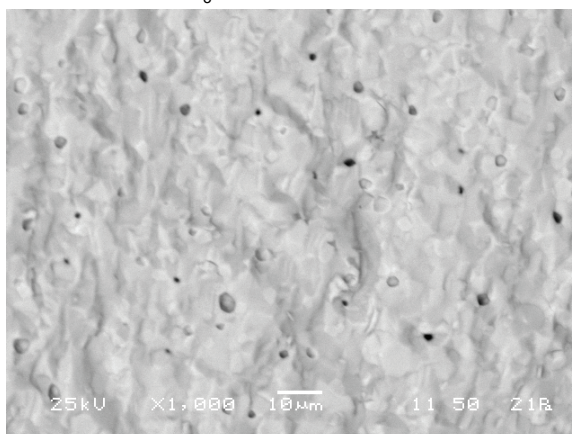
Button cell tests with 500 μm thick doped BaCeO<sub>3</sub> pellets were conducted. The cell performance was somewhat low. Post-test examination showed poor anode bonding to the electrolyte. However, comparison of proton and oxygen conducting electrolyte fuel gas potential as a function of cell current density, as measured by independent reference electrodes, showed the high efficiency potential for the proton SOFCs. This is shown in Figure 4.

Comparison of the reference voltage trace provides several interesting points:

- First, at open circuit (OCV) the proton OCV is lower than that of oxygen OCV. This again is a confirmation of pure ionic conduction of zirconia electrolyte providing near theoretical Nernst potential. The lower OCV of the proton cell is indication of the ionic transference number,  $t_{ion}$  being less than one, in this case about 0.96.



Sintered BaCeO<sub>3</sub>



Sintered BaCeO<sub>3</sub> with a sintering aid

**FIGURE 2.** Comparison of Sintered Density with and without the Addition of a Sintering Aid

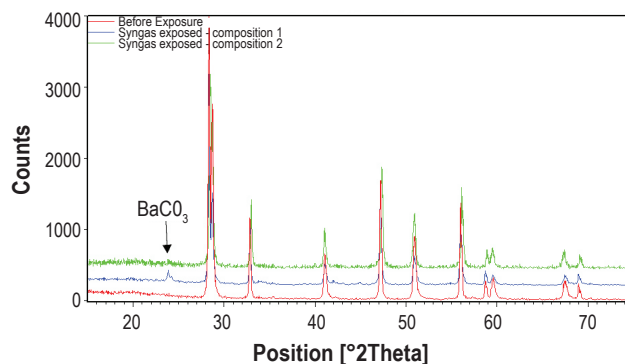


**FIGURE 3.** Powder X-ray Diffraction Patterns of 800°C Syngas Exposed Baseline and Modified Compositions

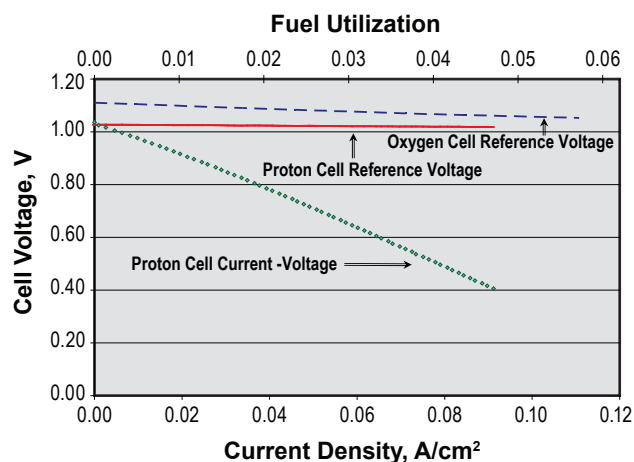


**FIGURE 4.** Comparison between Proton SOFC and Oxygen SOFC: Fuel Potential as a Function of Fuel Utilization

- As a function of utilization however, the driving potential of the oxygen cell drops more steeply than the proton cell again confirming the benefit of proton cell in maintaining higher driving force.
- Because of  $t_{\text{on}}$  being less than 1, the true benefit of the proton cell does not manifest until the cell reaches much higher utilization. The driving potential in this case will cross over at about 10 to 15% fuel utilization. It is theoretically possible to achieve very high utilization at higher operating voltage with a proton cell.
- Finally while high efficiency operation is clearly possible with the proton cell, the cell resistance must be lowered by a factor of 10 to fully realize the benefits of proton cell in terms of cost/kW as well as specific weight and volume. Improvements to electrode compositions and electrode application technique as well as the use of thin electrolyte are expected to provide the necessary performance improvement.

Additional tests with modified anode processing temperature using 500  $\mu\text{m}$  thick electrolytes showed much improved performance, as shown in Figure 5.

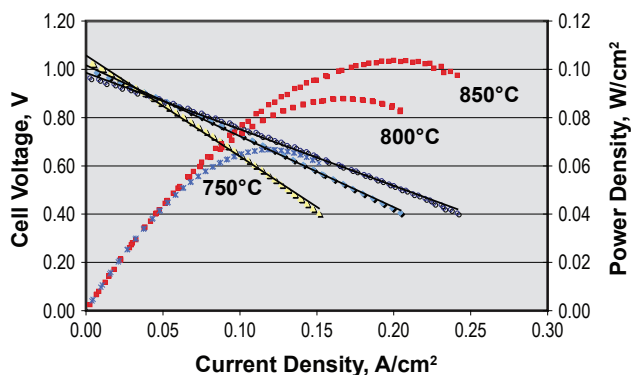


FIGURE 5. Button Cell Performance Using a 500  $\mu\text{m}$  Thick Electrolyte

## Conclusions and Future Directions

The project results re-confirm the high efficiency potential for proton conductor-based SOFCs. By proper B-site doping very high proton conductivity, comparable to that of the oxygen ion conductivity of yttria-doped zirconia, can be achieved to enable high performance cell operation. The inherent mixed ionic conductivity in the  $\text{BaCeO}_3$  type of material limits the efficiency benefit to some extent depending on the operating conditions. When the cell is operated at high utilization, significantly higher electrochemical efficiency can be realized compared to an oxygen ion conductor-based SOFC.

Electrode improvements and process development for fabrication of thin supported electrolyte cells will be the research focus for realizing the full capability of proton SOFC systems.

## References

1. Iwahara, H., Hibino, T., and Yamada, M., Proc. 3<sup>rd</sup> International Symposium on Solid Oxide Fuel Cells, p 137, Singhal and Iwahara eds., Honolulu, Hawaii, 1993.
2. H. Iwahara, T. Esaka, H. Uchida, N. Maeda, Solid State Ionics 3/4, 359 (1981).
3. H. Iwahara, H. Uchida, N. Maeda, J. Power Sources 7, 193 (1982).
4. H. Iwahara, H. Uchida, I. Yamasaki, Int. J. Hydrogen Energy 12, 73 (1987).
5. H. Iwahara, Solid State Ionics 28–30, 573 (1988).
6. N. Bonanos, K.S. Knight, B. Ellis, Solid State Ionics 79 (1995) 61.
7. T.R. Armstrong et al., “Stability of Perovskite Hydrogen Separation Membranes,” AR Materials Conference, Baltimore, MD, April 2003.
8. N. Taniguchi et al., “Endurance against moisture for protonic conductors of perovskite-type ceramics and preparation of practical conductors,” Solid State Ionics 145, 349–355 (2001).
9. K.H. Ryu and S.M. Haile “Chemical Stability and Proton Conductivity of Doped Perovskite Oxides in the  $\text{BaCeO}_3$ - $\text{BaZrO}_3$  System,” Solid State Ionics 125 (1999) 355-367.
10. K. Katahira, Y. Kohchi, T. Shimura, H. Iwahara, “Protonic Conduction in Zr-substituted  $\text{BaCeO}_3$ ,” Solid State Ionics, 138, 91-98 (2000).
11. S. Wienströer and H.-D. Wiemhöfer, “Investigation of the influence of zirconium substitution on the properties of neodymium-doped barium cerates,” Solid State Ionics 101-103, 1113-1117 (1997).

---

## V.2 Intermediate Temperature Solid Oxide Fuel Cell Development

S. (Elango) Elangovan (Primary Contact),  
Brian Heck, Mark Timper

Ceramatec, Inc.  
2425 South 900 West  
Salt Lake City, UT 84119-1517  
Phone: (801) 978-2162; Fax: (801) 972-1925;  
E-mail: Elango@ceramatec.com  
Web site: www.ceramatec.com

DOE Project Manager: Briggs White

Phone: (304) 285-5437  
E-mail: Briggs.White@netl.doe.gov

Subcontractors:

- Caltech, Pasadena, CA; Dr. Sossina Haile
- Northwestern University, Evanston, IL;  
Dr. Scott Barnett

Contract Number: 42471

Start Date: July 15, 2007  
Project End Date: June 30, 2008

### Future Directions

- Select promising cathode compositions and develop cathode application process.
- Fabricate and test short stacks.

---

### Introduction

Reducing the operating temperature of SOFCs offers several benefits: improvement in long-term stability by slowing physical and chemical changes in the cell materials, lower cost systems by the use of less expensive balance-of-plant components, compatibility with hydrocarbon reformation process allowing partial internal reformation which in turn reduces the heat exchanger duty, and finally the potential to improve thermal cycle capability. In addition, the use of stainless steel interconnects is also facilitated by the lower operating temperature. A temperature range of 600 to 700°C is ideally suited to derive the performance stability, system integration and cost benefits.

In order to derive the advantages of the lower operating temperature two factors that limit the cell performance, namely the electrolyte resistance and electrode polarization must be addressed. Lanthanum gallate compositions have shown high oxygen ion conductivity when doped with Sr and Mg. Unlike other oxygen ion conductors such as ceria and bismuth oxide that are potential candidates for lowering cell operating temperature, the Sr and Mg doped lanthanum gallate (LSGM) compositions are stable over the oxygen partial pressure range of interest. The combination of stability in fuel gas environment and the high oxygen ion conductivity makes the LSGM material a potential choice for intermediate temperature SOFCs. However, challenges in the development of electrode materials and thin cell fabrication processes need to be overcome to make use of the potential of the LSGM electrolyte.

### Approach

Tape cast process development was performed to cast LSGM tape of various thicknesses to provide sintered electrolyte thicknesses ranging from 50 to 200 microns. The process variables included: powder surface area, organic content in the tape slip, and sintering temperature. The primary objectives of the activity were to achieve sintered electrolyte density and flatness required for stacking. Single cells and symmetric cells with 2.5 cm<sup>2</sup> active area were tested for performance characteristics.

### Objectives

- Fabricate and test a thin, supported lanthanum gallate electrolyte-based solid oxide fuel cell (SOFC) stack.
- Determine operating characteristics of the stack in the intermediate temperature range.

### Approach

- Develop fabrication process for thin, supported lanthanum gallate electrolyte.
- Verify performance of thin cells in button cell configuration.
- Evaluate low temperature cathode materials using symmetric cells.
- Test the new cathode material in short stacks.

### Accomplishments

- Button cells were fabricated using the tape lamination technique.
- Preliminary cathode half-cell evaluation was conducted using new cathode compositions.
- Process for infiltration of electrode material has been developed.

While lanthanum cobaltite cathode has good intermediate temperature catalytic activity, the primary issues related to the use of cobaltite cathode are: excessive diffusion of Co into LSGM causing phase destabilization of the electrolyte, and the high coefficient of thermal expansion of cobaltite compositions. Two alternative cathode compositions were evaluated in half-cell tests. At Northwestern University, a composite of  $\text{LaSrCoFeO}_3 - \text{LaSrGaMgO}_3$  (LSCF-LSGM) was evaluated. At Caltech,  $\text{BaSrCoFeO}_3$  (BSCF) was evaluated.

**Results**

Thin electrolyte single cells were fabricated using the tape lamination technique. Both anode and cathode porous structures were evaluated as the support for the electrolyte. At least one electrode material was infiltrated into the porous structure. The performance of a cathode-supported cell is shown in Figure 1. The thin, 75 micron LSGM electrolyte cells showed an area specific resistance of  $0.5 \text{ ohm-cm}^2$  at an operating temperature of  $700^\circ\text{C}$ . The long-term performance of selected cells is shown in Figure 2. Similar performance and stability results were also obtained using cells with the anode-support configurations. A modified infiltration technique was developed in order to achieve a more uniform distribution of electrode material into the porous structure. Micrographs of cathode infiltrated structure is shown in Figure 3. Button cell tests using the new infiltration technique showed (Figure 4) an improvement in cell performance.

Cathode symmetric cells using cobalt-ferrite compositions (BSCF and LSCF+LSGM composite) were tested at the two universities. The cathode polarization losses were measured to be as low as  $0.06 \text{ ohm-cm}^2$  at  $650^\circ\text{C}$ . Some dependence of polarization on processing

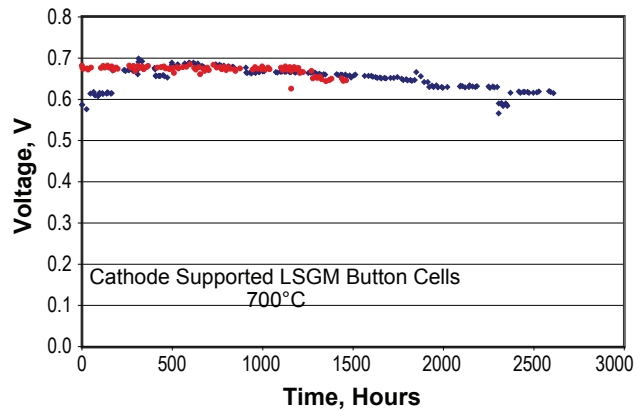


**FIGURE 2.** Long-Term Stability of Cathode Supported Cells at an Operating Temperature of  $700^\circ\text{C}$

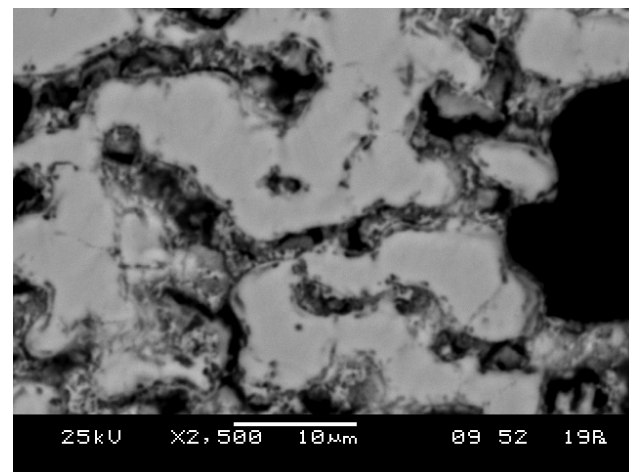


**FIGURE 3.** Micrograph of Infiltrated Cathode

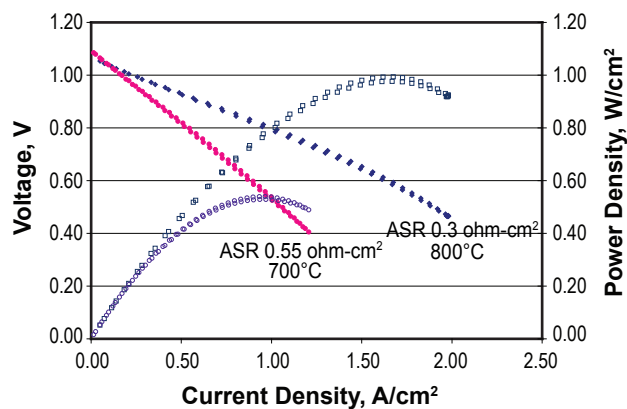


**FIGURE 1.** Performance of a cathode supported LSGM cell. Electrolyte thickness of 75 microns was used.

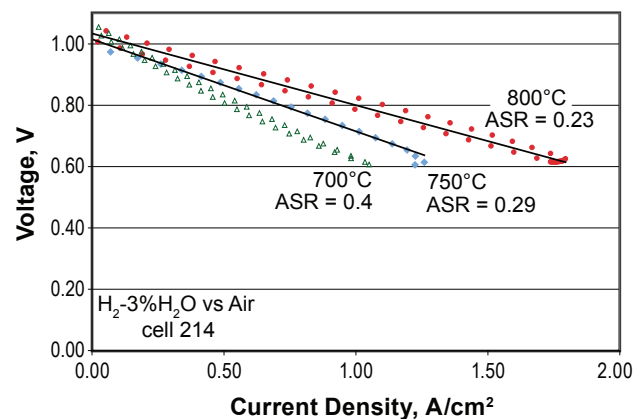


**FIGURE 4.** Button Cell Performance with Infiltrated Cathode

conditions was noted for BSCF, which requires further investigations.

Sintering process development for fabricating 10 x 10 cm electrolyte was conducted. Initial trials with thick electrolyte defined the sintering process to achieve flat, dense electrolyte. As with zirconia electrolyte-based stacks, chromium evaporation was found to contribute to stack degradation. Process development for spinel coating of stainless steel interconnects is in progress.

## Conclusions

- Thin, supported cells meet the performance target of 0.5 ohm-cm<sup>2</sup> resistance at 700°C.
- Long-term tests of single cells show stable performance.
- Alternative cathode materials show low cathode polarization at temperatures < 700°C.
- Investigations to mitigate chromium poisoning of cathode are needed.

---

## V.3 SECA Coal-Based Systems Core Research – Montana State University

Lee H. Spangler (Primary Contact),  
Richard Smith, Yves Idzerda, Hugo Schmidt,  
Hashem Nehrir, Steven Shaw, Stephen Sofie,  
Max Diebert, Hongwei Gao  
Montana State University (MSU)  
207 Montana Hall  
Bozeman, MT 59717-2460  
Phone: (406) 994-4399; Fax: (406) 994-2893  
E-mail: spangler@montana.edu

DOE Project Manager: Briggs White  
Phone: (304) 285-5437  
E-mail: Briggs.White@netl.doe.gov

Subcontractor:  
Arcomac Surface Engineering, Bozeman, MT

Contract Number: 44036

Start Date: October 1, 2002  
Project End Date: September 30, 2009

- Study SOFC component performance for niche applications (ongoing).
- Develop noble metal free, active metal brazing for SOFC sealing application.
- Initiate coal gas contaminant study.
- Develop low coefficient of thermal expansion (CTE) anodes and microstructurally engineered scaffolds for cathode infiltration.
- Evaluate SOFC efficiency considering both generated electrical power and useful exhaust heat.
- Develop a high performance load sharing control method for modularly designed direct current (DC)/alternating current inverters in large-scale SOFC power systems.
- Develop a high efficiency low cost DC/DC converter for residential fuel cell power systems.
- Investigate electrically induced degradation of SOFCs.

### Accomplishments

- Constructed and operated SOFC-IC experimental systems, including dual atmosphere corrosion test stands at 800°C in moist air and moist hydrogen.
- Anode degradation mechanisms identified due to H<sub>2</sub>S. A previously unreported degradation mechanism has been identified and reported. This is the nickel transport and depletion in cermet Ni/yttria-stabilized zirconia (YSZ) anodes.
- Developed more exact formalism for finding gas densities at the anode (or cathode) at saturation current density for which SOFC terminal voltage drops to zero.
- Demonstrated successful joining of YSZ/430SS joint with noble metal free copper-based braze in mid vacuum environment.
- Demonstrated >150 psi burst pressure and hermetic seal of braze joints.
- Developed a prototype DC/DC converter.

### Objectives

- Investigate corrosion behavior of coated and uncoated steel solid oxide fuel cell (SOFC) interconnect (IC) materials.
- Develop improved SOFC-IC coating compositions and deposition approaches.
- Develop advanced testing facilities for high-temperature exposures to controlled atmospheres.
- Continue our studies on hydrogen sulfide (H<sub>2</sub>S) degradation.
- Expand testing capabilities to address additional SOFC fuel contaminants, e.g. beyond H<sub>2</sub>S.
- Develop an *in situ* synchrotron measurement system for SOFCs.
- Measure gas flow, tortuosity, and V(i) (terminal voltage vs. current density) for SOFCs.
- Study Cr volatility for coated and uncoated steel interconnects and mechanisms related to volatility; volatility of other elements from SOFC component materials (ongoing).
- Investigate the mechanisms of Cr poisoning for SOFC cathode/electrolyte materials using ion beam analysis of oxygen diffusion and exchange at surfaces (ongoing).
- Study SOFC performance degradation associated with exposures of anode/electrolyte to synthetic coal gas using ion beam analysis (ongoing).

---

### Introduction

**Interconnects and Cr Volatility:** The requirements of low cost and high-temperature corrosion resistance for bipolar interconnect plates in SOFC stacks has directed attention to the use of steel plates with more oxidation resistant compositions. However, volatile Cr species from these steels find their way to the triple-phase boundary, leading to rapid degradation of fuel cell performance. Coatings can slow oxidation rates, and

act as diffusion barriers for the Cr-derived species from the steel, slowing the degradation process. We have also developed a relatively quick, quantitative procedure using Rutherford backscattering spectroscopy to measure the time evolution of various elemental vaporization rates.

#### **Sulfur Poisoning and Other Fuel Contaminants:**

One disadvantage of using currently available fuels is their naturally occurring, or artificially added, contaminants content such as  $H_2S$ , which is known to have detrimental effects on SOFC performance. The results presented here reveal that  $H_2S$  promotes nickel migration and can compromise the percolating nickel network in nickel/ceramic anodes, thereby destroying their electrical conductivity. We are also focusing on coal gas, and its variety of contaminants as they play an important role in future SOFC development.

**Electrode Development:** A prominent factor in SOFC failure is related to thermal cycling and hence thermal stresses within the cell/stack. While all-ceramic mixed conducting anodes yield good CTE matching, performance is still poor at best. Ni/YSZ persists as the most reliable and heavily used anode; therefore, to minimize difficulties in system integration of anode supported cell technology, the most effective near term approach is the modification of the current materials set.

#### **Engineered Pore Structures and Tortuosity:**

The use of infiltrated electrode technologies may be improved by engineering the porosity of YSZ scaffolds. In this manner the focus of this effort is to establish the infiltration of active cathode materials into an YSZ scaffold, ultimately for application into anode supported cell technology.

**Metallic Brazed Seals:** Traditional approaches to SOFC sealing have been focused on compliant and/or rigid glass or glass/ceramic seals; however, the metallic braze seal may yield a more robust, chemically bound, and true hermetic seal. While a key goal for cost effective implementation is the elimination of noble metals, additional concerns with metallic seals include: the use of inert/vacuum environments, the potential shorting of the cell due to the electrical conductivity of braze, oxidation resistance of non-noble metal base materials, metal/ceramic bonding, and substantial thermal expansion mismatch.

**Power Electronics:** Modular design is an option for design of the inverter in a large-scale fuel cell power system. Such design requires a control strategy for the inverter modules to ensure the modules share load evenly.

The model reference simulator is an electrical device that can be connected between a short stack or a single cell and full-size, full-power (3 kW) electrical loads and associated control circuitry. This device simplifies effort needed to characterize the full dynamic and nonlinear

behavior of a cell in order to predict its potential. This is especially important given that power-conditioning electronics will generally present the stack with a negative incremental resistance, which means that dynamics interactions, if any, would tend to be under damped.

The concern relative to electrically induced degradation is that a stack of slightly different cells, particularly a stack with series and parallel connections, individual cells may be exposed to unintuitive electrical terminal conditions. As an example, a cell with an abnormally high Thevenin equivalent resistance may actually be reverse-biased in the stack, a situation which would never occur if that cell were removed from the stack and connected to a resistive load.

## **Approach**

### **Interconnects and Cr Volatility**

Using filtered arc, electron beam evaporation, magnetron sputtering, electrochemical deposition, and screen printing technologies, novel SOFC-IC coatings (e.g.,  $CoMnO + Al$ ) are developed and evaluated.

Several furnace systems and corrosion testing facilities have been developed to simulate SOFC-IC operation at  $800^\circ C$ . These resources are currently employed in a variety of ongoing studies, including: dual atmosphere corrosion studies, single atmosphere corrosion studies with controlled moisture, Cr-transpiration investigations and area specific resistance measurements with SOFC cathode contact pastes (e.g., lanthanum strontium manganate [LSM], lanthanum strontium ferrite [LSF] or lanthanum strontium cobaltite ferrite [LSCF]).

We measured oxygen transport in coatings using  $^{18}O(p,\alpha)^{15}N$  nuclear reaction analysis, and exposures to  $^{18}O$  at pressures near 10 mTorr and various temperatures up to  $\sim 800^\circ C$  in an evacuated tube furnace with controlled gas environment up to several Torr pressure. The tube furnace was modified with the addition of the mass spectrometer to measure gas composition.

We are designing, constructing, and testing a new mount to hold Si wafers at the end of the tube furnace with a secondary collector to condense chromia vapors passing the first collector.

### **Sulfur Poisoning and Other Fuel Contaminants**

$H_2S$  was introduced into the fuel stream for test cells. Parts of the cells were sent to a collaborator in Taiwan to perform X-ray diffraction (XRD) as well as infrared and Raman spectroscopy. Other parts of the same cells were taken to the Advanced Light Source in Berkeley for synchrotron characterization. Design and assembly of a testing apparatus with multiple mass flow

controllers were started in order to introduce additional contaminant gases in a controlled manner. The Ni/YSZ YSZ-LSM single cell operated in lower ppm (~160 ppm)  $H_2S$  was obtained and will be evaluated by micro-Raman scattering and XRD.

### Electrode Development

MSU is developing a system with which we can perform synchrotron measurements on fuel cell materials in real fuel cells during operation. Synchrotron measurements were performed across a silicon nitride window, which is planned to be used as an interface between the ultra-high vacuum environment of the synchrotron chamber and the fuel cell chamber (in progress).

Ceramic additives (aluminum titanate and zirconium aluminum titanate) were incorporated into Ni/YSZ anode blends and tested by dilatometry and electrical conductivity, in which the lowest concentration of 5% yields substantial benefits in CTE with a small effect on conductivity.

### Engineered Pore Structures and Tortuosity

Freeze casting has been used to create open pore YSZ scaffolds for electrode infiltration. Initial infiltration runs indicate some aspects of electrode coating peeling during the  $<800^\circ\text{C}$  heat treatment process for LSCF infiltrants. The solids content, conductivity, and microstructure are currently being evaluated in a detailed study.

We developed a first-principles model for the  $V(i)$  curve for SOFCs that extends across the SOEC (solid oxide electrolyzer cell) range also. It was shown that the Butler-Volmer equation for current density,  $i$ , as a function of activation polarization,  $V_{act}$ , is based on an approximation and gives unphysical results for large applied voltage in the SOEC mode. A replacement  $i(V_{act})$  expression was developed that predicts the correct limiting current density.

### Metallic Brazed Seals

Traditional approaches to SOFC sealing have been focused on compliant and/or rigid glass or glass/ceramic seals; however, the metallic braze seal may yield a more robust, chemically bound, and true hermetic seal. While a key goal for cost effective implementation is the elimination of noble metals, additional concerns with metallic seals include: the use of inert/vacuum environments, the potential shorting of the cell due to the electrical conductivity of braze, oxidation resistance of non-noble metal base materials, metal/ceramic bonding, and substantial thermal expansion mismatch.

### Power Electronics

Theoretical analyses using thermodynamic expansions were conducted and, building upon our previously developed SOFC dynamic model, we showed that operating fuel heating values could be determined by utilizing the semi-empirical gas phase heat capacity method. This method demonstrates that more accurate, real-time efficiency measurements may be obtained from SOFC stack operational simulations based on actual thermodynamic parameters. Building on this success, an analysis was conducted of a SOFC-combined cycle system using dynamic modeling.

We are developing a high performance-fast response and high precision-load sharing control method for modularly designed inverters in large-scale SOFC power systems. We have designed the method, simulated the performance of the method, and are implementing the method in inverter modules.

We conducted a series of degradation experiments using InDEC 52 mm anode-supported cells as a standard. Our focus is to discover whether cell degradation can be detected and controlled at the electrical terminals. The experimental procedure was to mount a cell in our test fixture, reduce the anode, and collect an initial current-voltage (I-V) curve. Cells were operated at  $750^\circ\text{C}$ . These data were collected in a quasi-static manner. Then the test conditions were imposed on the cell, with periodic acquisition of an I-V curve. The experiments are stopped manually after the I-V curve shows roughly 20% degradation in terms of the extrapolated zero-voltage current-intercept. This metric was used because it integrates degradation that occurs throughout the current-voltage characteristic of the cell. Cells are then mounted in epoxy and polished so that the interfaces can be imaged under a scanning electron microscope (SEM).

## Results

### Interconnects and Cr Volatility

Numerous coatings were prepared and tested for corrosion resistance. A manuscript describing the performance of TiCrAlY oxide (Process 50) was prepared and submitted to Surface and Coatings Technology, and is under revision.

### Sulfur Poisoning and Other Fuel Contaminants

We have observed Ni transport and depletion of the anode with the presence of  $H_2S$  in the fuel stream. This depletion was shown to occur at exposed grain surfaces. We are running experiments to verify those observations.

Testing of MSU fabricated electrolyte supported cells (ESCs) (ESCs are used to minimize buffering affects

of thick anodes) indicated an irreversible degradation to H<sub>2</sub>S which was determined to be due to enhanced nickel migration. From this standpoint it appears that nickel loss, associated with a loss in electrical conducting percolation may be the mechanism by which the anode degrades permanently as opposed to reversible adsorption/desorption of sulfur. Further, it is postulated that this nickel migration is enhanced by meta-stable nickel sulfide liquid phases at operating temperature and shows considerable nickel loss at >250 ppm H<sub>2</sub>S. The characterization of sulfur degraded anodes is also being evaluated by high energy X-ray techniques to establish new methods (both post mortem and *in situ*) of evaluating sulfur degradation. Current tests are underway to establish the effects of low concentrations of H<sub>2</sub>S present after warm gas cleanup at <10 ppm to ascertain if a similar mechanism is present at these lower sulfur concentrations. In addition, facilities are being developed to allow testing of arsenic and phosphorous contaminants.

**Electrode Development**

Ceramic additives (aluminum titanate and zirconium aluminum titanate) were incorporated into Ni/YSZ anode blends and tested by dilatometry and

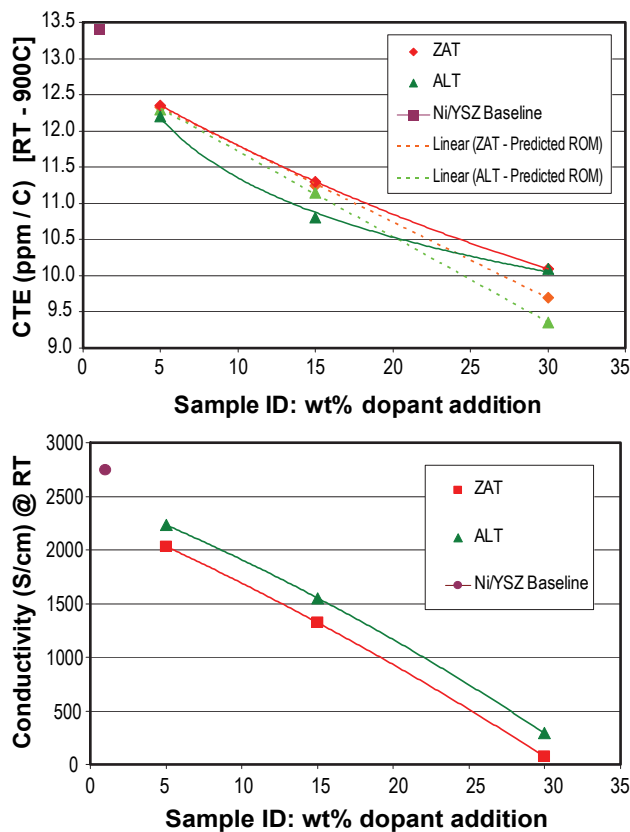


**FIGURE 1.** Thermal Expansion and Conductivity Behavior of Anode Blend Bars at Room Temperature

electrical conductivity as shown in Figure 1, in which the lowest concentration of 5% yields substantial benefits in CTE with a small effect on conductivity.

The low CTE additives also showed a dramatic improvement in flexural strength, for which the mechanism is being sought. The long-term stability of these materials as well as the effects of the dopants on electrochemical activity is currently being evaluated.

**Engineered Pore Structures and Tortuosity**

Thin functionally graded YSZ scaffolds have been successfully fabricated on YSZ electrolytes for infiltration. In addition to low viscosity nitrate solutions, the open pore structure of the freeze cast scaffolds allow higher viscosity solutions as well as colloidal solutions to increase the quality of the electrode and deposition rate for single step processing. Citrate solutions have been prepared for infiltration and comparison with nitrate solutions utilizing common LSM, LSF, and LSC-based cathode materials.

In the model used previously for finding tortuosity, the unphysical approximation made was that the fuel gas density at the anode-electrolyte interface, or oxygen at the cathode-electrolyte interface, is zero when current density, *i*, reaches the saturation current density value for which terminal voltage, *V*, drops to zero. A finite density based on results from our *V(i)* model is now employed. This improved analysis found tortuosity about 10% lower than previously found, indicating tortuosity,  $\tau$ , in the 2 to 3 range.

**Metallic Braze Seals**

Mechanical failure for commercial active metal copper brazes is driven through the YSZ without effecting the braze joint itself as shown in Figure 2.

The performance of the joint exceeded the 150 psi maximum pressure available from the testing rig and indicated a hermetic seal for over 2 hours testing at 30 psi at room temperature as shown in Figure 3. A high temperature testing chamber has been fabricated to test this material at high temperature and under thermal cycles.

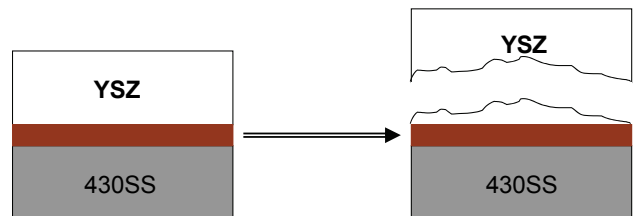


**FIGURE 2.** Schematic of Braze Joint Failure, Illustrating a Key Strength of This System Compared to Sealing Glasses

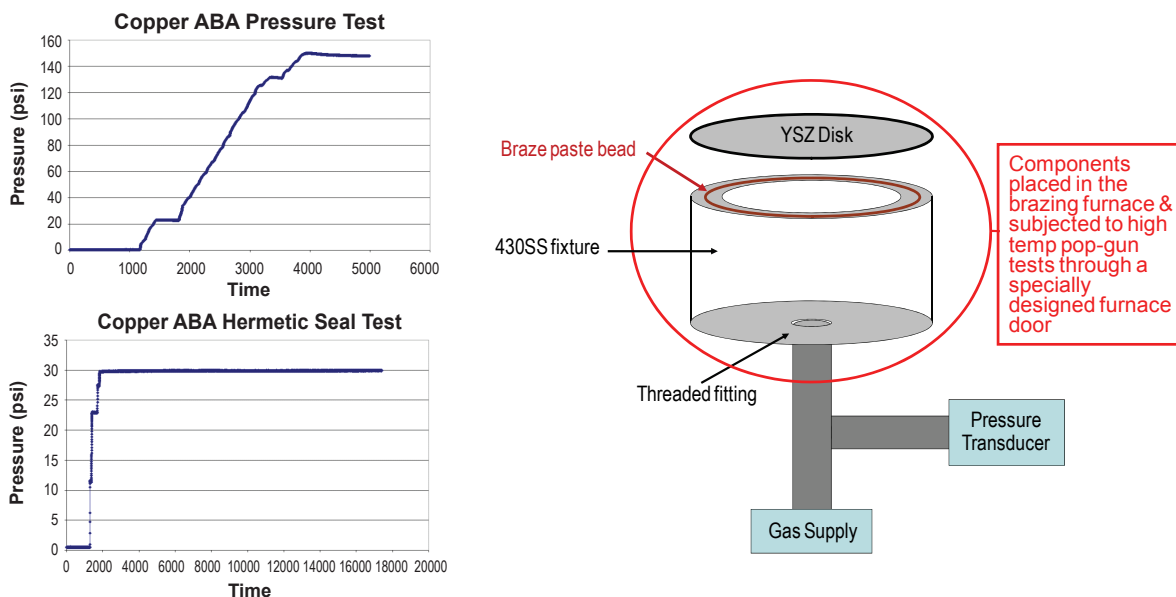


FIGURE 3. Sealing Performance of Commercial Copper Braze Compound at Room Temperature

It was established that silicon content in the copper braze diffused substantially into the YSZ raising the concern for degradation from the formation of silicon-based glassy phases. Several new custom synthesized brazes are being evaluated to mitigate silicon diffusion, which still facilitates strong bonding and oxidation resistance.

Custom braze bond strength and sealing characteristics are currently being examined. An additional concern with the copper-based braze is the relatively high CTE (19 ppm/°C) compared to SOFC components. Some evidence of residual stress-based failure has been noted and preliminary runs with aluminum titanate dopants may yield a solution. Preliminary runs with low CTE additives in the braze showed clustering of ceramic particles requiring improved means of homogenizing the braze blend prior to joining for effectiveness of this approach.

Power Electronics

We developed a method to combine the designed load sharing control method with the Space Vector Control – a popular and high performance control algorithm to control the output of an individual inverter. We also developed a computer model to simulate the performance of the combined control.

In this reporting period, we successfully achieved soft-switching, which is an advanced technique to reduce the loss in a DC/DC converter in the developed prototype.

A cell held at a reverse bias of -0.86 V for a total of 80 minutes showed significant mechanical failure at the electrolyte/anode interface, in addition to nickel

coarsening in the anode (Figure 4). The SEM image shows a chunk of nickel near the electrolyte, confirmed by energy dispersive spectroscopy.

We conducted a series of degradation experiments using InDEC 52 mm anode-supported cells as a standard. Preliminary results show a progression of degradation phenomena as the electrical conditions leading to degradation are relaxed.

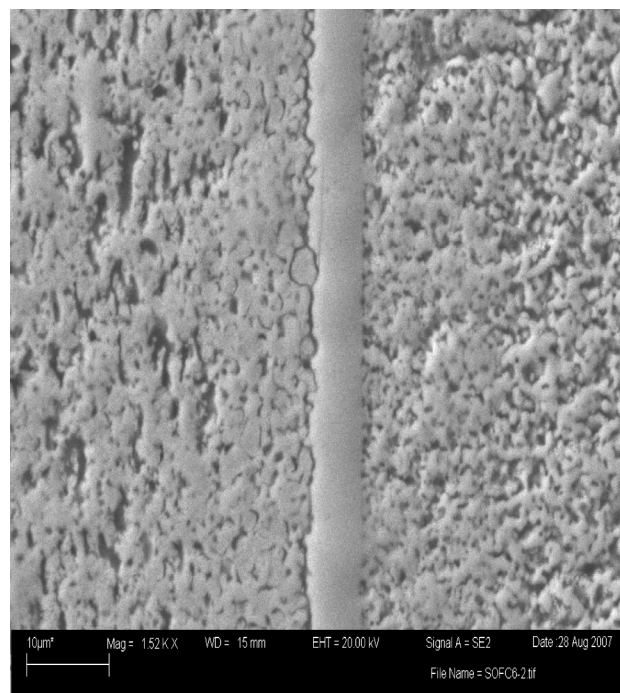


FIGURE 4. SEM of a Reverse Biased Cell Showing Interfacial Failure and Ni Coarsening

## Conclusions and Future Directions

### Interconnects and Cr Volatility

Several furnace systems and corrosion testing facilities have been developed to simulate SOFC-IC operation at 800°C. These resources are currently employed in a variety of ongoing studies, including: dual atmosphere corrosion studies, single atmosphere corrosion studies with controlled moisture, Cr-transpiration investigations (in collaboration with Richard Smith Group), and area specific resistance measurements with SOFC cathode contact pastes (e.g., LSM, LSF or LSCF). Results of these longer term tests will be available in subsequent reporting periods.

### Sulfur Poisoning and Other Fuel Contaminants

We have observed Ni transport and depletion of the anode with the presence of H<sub>2</sub>S in the fuel stream. This depletion was shown to occur at exposed grain surfaces. We are running experiments to verify those observations.

We are designing a new testing apparatus with multiple mass flow controllers to introduce multiple contaminant gases with independent control. We are currently in the design, planning, and ordering phase for this new system.

### Electrode Development

The long-term stability of the low CTE anode materials as well as the effects of the dopants on electrochemical activity will be evaluated.

### Engineered Pore Structures and Tortuosity

We will apply the improved formalism to analyses of tortuosity in various existing SOFCs and proposed SOFC designs. The existing SOFCs refer both to SOFC data in the literature, and to SOFC data to be obtained.

In collaboration with the MSU flow nuclear magnetic resonance (NMR) group, tortuosity of electrode structures will be also determined by gas flow NMR techniques. Such measurements have been reported in the literature and yield quite accurate results.

### Metallic Brazed Seals

Custom braze bond strength and sealing characteristics are currently being examined. An additional concern with the copper-based braze is the relatively high CTE (19 ppm/°C) compared to SOFC components. Some evidence of residual stress-based failure has been noted, and preliminary runs with aluminum titanate dopants may yield a solution. Preliminary runs with low CTE additives in the braze showed clustering of ceramic particles requiring

improved means of homogenizing the braze blend prior to joining for effectiveness of this approach.

### Power Electronics

We are developing a DC/DC converter of 96% efficiency and \$40/kW cost for SOFC-powered residential power systems. We have designed the topology of the DC/DC converter, simulated the performance of the DC/DC converter, developed a prototype DC/DC converter, and we are testing the prototype.

## Special Recognitions & Awards/Patents Issued

1. U.S. Patent Application filed November 10, 2006 for *Transient Recognition Control for Hybrid Fuel Cell Systems*; Inventors are Steve Shaw, Steve Leeb, and Tao Zhu; Serial No. 11/568,971.
2. Professor Richard J. Smith has been named a Fellow of the American Vacuum Society. His citation states: "For significant and sustained contributions to the understanding of the electronic and geometric structures of solid surfaces using combined ion beam channeling and electron spectroscopic techniques."
3. Professor Stephen Sofie received the MSU 2008 Mechanical & Industrial Engineering Outstanding Teacher Award. Many aspects of Dr. Sofie's teachings are founded in this research.
4. Chris Colson, graduate student, received the NSF Fellowship to work on "Intelligent Energy Management of Microgrids with Multiple Alternative Energy Power Generation Sources."
5. Professors Hashem Nehrir, Steven Shaw, and Hongwei Gao were invited to attend the NSF-sponsored workshop on "Advanced Power Conditioning for Alternate Energy Sources."

## FY 2008 Publications

1. A Physically-Based Dynamic Model for Solid Oxide Fuel Cells, C. Wang, M.H. Nehrir, *IEEE Transactions on Energy Conversion*, Vol. 22, No. 4, December 2007.
2. Advanced PVD protective coatings for SOFC interconnects, P.E. Gannon, M. Deibert, V.I. Gorokhovskiy, P. White, R.J. Smith, H. Chen, W. Priyantha and J. Lucas, *The International Journal of Hydrogen Energy*, In-press (2008).
3. Anode-Pore Tortuosity in Solid Oxide Fuel Cells Found from Gas and Current Flow Rates," Schmidt, V. Hugo, Tsai, Chih-Long, J. *Power Sources* (2008), accepted.
4. ASR evaluation of different kinds of coatings on a ferritic stainless steel as SOFC interconnects, P. Piccardo, P. Gannon, S. Chevalier, M. Viviani, A. Barbucci, G. Caboche, R. Amendola, S. Fontana, *Surface and Coatings Technology*, v 202, n 4-7, December 15, 2007, 1221-1225.

5. Determination of Anode-Pore Tortuosity from Gas and Current Flow Rates in SOFC's, Schmidt, V. Hugo, Tsai, Chih-Long, Lediaev, Laura M., *Advances in Solid Oxide Fuel Cells III: Ceramic Engineering and Science Proceedings*, Vol. 28, Is. 4, 129-140 (2007).
6. Dynamic First-Principles Molecular-Scale Model for Solid Oxide Fuel Cells, Schmidt, V. Hugo, Winter 2007, *ECS Transactions – Chicago*, Vol. 6, "Design of Electrode Structure."
7. Enabling inexpensive metallic alloys as SOFC interconnects: An investigation into hybrid coating technologies to deposit nanocomposite functional coatings on ferritic stainless steels, P.E. Gannon, V.I. Gorokhovskiy, M.C. Deibert, R.J. Smith, A. Kayani, P.T. White, S. Sofie, Zhenguo Yang, D. McCready, S. Visco, C. Jacobson, H. Kurokawa, *International Journal of Hydrogen Energy*, 32 (2007) 3672-3681.
8. In-Situ Stability Study of Proton Conducting  $\text{Ba}(\text{Zr}_{0.8-x}\text{Ce}_x\text{Y}_{0.2})\text{O}_{3-\delta}$  Ceramics in  $\text{CO}_2$  Environment," Tu, C.-S., Chien, R. R., Lee, S.-C., Huang, C.-C., Tsai, C.-L., Schmidt, V. H *Solid State Ionics* (2008), submitted.
9. Interconnect materials for next-generation solid oxide fuel cells, P.E. Gannon, P. Piccardo, S. Fontana, R. Amendola, S. Chevalier and G. Caboche, *Journal of Applied Electrochemistry*, Submitted January 2008.
10. Load Transient Mitigation for Stand-alone Fuel Cell Power Generation Systems, C. Wang, M.H. Nehrir, *IEEE Transactions on Energy Conversion*, Vol. 22, No. 4, December 2007.
11. Mechanism for SOFC Anode Degradation from Hydrogen Sulfide Exposure, Lussier, S. Sofie, J. Dvorak, Y.U. Idzerda, *International Journal of Hydrogen Energy*, in press.
12. Oxidation behavior of stainless steel 430 and 441 at 800°C in single (air-only) and dual atmosphere (air/hydrogen) exposures, J. Rufner, P.E. Gannon, P. White, M. Deibert, S. Teintze, R. Smith and H. Chen, *International Journal of Hydrogen Energy*, in-press.
13. Power Management of Stand-Alone Wind/Photovoltaic/Fuel-Cell Energy Systems, C. Wang and M.H. Nehrir, accepted for publication in the *IEEE Transactions on Energy Conversion*.
14. Short-Time Overloading Capability and Distributed Generation Applications of Solid Oxide Fuel Cells, C. Wang, M.H. Nehrir, Vol. 22, No. 4, December 2007.
15. Silver-Chromium Oxide Interactions in SOFC Environments, S. Sofie, P.E. Gannon, M.C. Deibert and V.I. Gorokhovskiy, *Journal of Power Sources*, Submitted January 2008.
16. Simulated solid oxide fuel cell interconnect performance of Crofer 22 APU with and without filtered arc Cr-Al-O-N coatings, P.E. Gannon, A. Kayani, C.V. Ramana, M.C. Deibert, R.J. Smith and V.I. Gorokhovskiy, *Electrochemical and Solid State Letters*, In-press; *Surface and Coatings Technology*, accepted (2008).
17. Stress Relaxation of LSMO and LCMO at SOFC Interfaces, A. Lussier, J. Dvorak, S. Stadler, J. Holroyd, M. Liberati, E. Arenholz, S.B. Ogale, T. Wu, T. Venkatesan, and Y.U. Idzerda, *Thin Solid Films*, 516 (6), p.880-884, January 2008.
18. Thermal stability and oxidation resistance of TiCrAlYO coatings on SS430 for solid oxide fuel cell interconnect applications, H. Chen, J. A. Lucas; W. Priyantha; M. Koczyk; R. J. Smith; K. Lund; C. Key; M. Finsterbusch; P. E. Gannon; M. Deibert; V. I. Gorokhovskiy; V. Shutthanandan; P. Nachimuthu, *Surface and Coatings Technology*, November 2007, submitted.
19. Thin Film YSZ Coatings on Functionally Graded Freeze Cast NiO/YSZ SOFC Anode Supports, P.E. Gannon, S. Sofie, M.C. Deibert, R.J. Smith and V.I. Gorokhovskiy, *Journal of Applied Electrochemistry*, submitted January 2008.

### FY 2008 Presentations

1. Applications of Ion Beam Analysis to Materials Characterization for Solid Oxide Fuel Cells, R.J. Smith, colloquium given to Physics Department, Western Michigan University, Kalamazoo, MI, September 19, 2007.
2. Development of a Novel High Performance Electrolyte Supported Solid Oxide Fuel Cell, P. Gentile and S.W. Sofie, *Materials Science and Technology 2007 Conference and Exhibition*, Detroit, MI, October 2007.
3. Extensions of a Molecular-Scale Model for Solid Oxide Fuel Cells and Electrolyzers, Schmidt, V. Hugo, Tsai, Chih-Long, The 32<sup>nd</sup> International Conference on Advanced Ceramics and Composites, Daytona Beach, FL, January 27 – February 1, 2008.
4. Flow & Diffusion Characteristics of Freeze Cast Substrates with Aligned Columnar Pores, J. McCrummen, S.W. Sofie, S. Codd, and T. Broston, 32<sup>nd</sup> International Cocoa Beach Conference & Exposition on Advanced Ceramics and Composites, Daytona Beach, FL, January 2008.
5. Growth and Characterization of Long Range Ordered Pore Structures via Freeze-Tape Casting, S.W. Sofie & J. McCrummen, *Materials Science and Technology 2007 Conference and Exhibition*, Detroit, MI, October 2007.
6. In-Situ temperature-Dependent X-Ray Diffraction Study of  $\text{Ba}(\text{Zr}_{0.8-x}\text{Ce}_x\text{Y}_{0.2})\text{O}_{3-\delta}$  Ceramics, Tu, Chi-Shun, Chien, R. R., Lee, S.-C., Tsai, Chih-Long, Keith, Alanna, Santorsola, Nick P., Hall, Sara, Schmidt, V. Hugo, The 32<sup>nd</sup> International Conference on Advanced Ceramics and Composites, Daytona Beach, FL, January 27 – February 1, 2008.
7. Investigation of bulk and grain boundary diffusion of oxygen in yttrium stabilized zirconia via nuclear reaction analysis, M. Finsterbusch, H. Chen, R.J. Smith, J.A. Schaefer, given at the 54<sup>th</sup> AVS International Symposium and Exhibition, Seattle, WA, October, 2007.

8. Metallic Braze Sealant for SOFC Application, D. Ator, S.W. Sofie, and A. Palmer, 32<sup>nd</sup> International Cocoa Beach Conference & Exposition on Advanced Ceramics and Composites, Daytona Beach, FL, January 2008.
9. Optical High Density Sintering of High Temperature Proton Conducting Ceramics, Santorsola, Nick P., Schmidt, V. Hugo, Tsai, Chih-Long, The 32<sup>nd</sup> International Conference on Advanced Ceramics and Composites, Daytona Beach, FL, January 27 – February 1, 2008.
10. Robust Copper Braze for Hermetic Sealing of Solid Oxide Fuel Cells, S.W. Sofie, D. Ator, and J. Buscher, Materials Science and Technology 2007 Conference and Exhibition, Detroit, MI, October 2007.
11. Sintering and Conductivity Study of  $\text{Ba}(\text{Zr}_{0.8-x}\text{Ce}_x\text{Y}_{0.2})\text{O}_{3-\delta}$  Ceramics, Tsai, Chih-Long, Han, Jiaping, Santorsola, Nick P., Schmidt, V. Hugo, Chien, R. R., Keith, Alanna, Hall, Sara, The 32<sup>nd</sup> International Conference on Advanced Ceramics and Composites, Daytona Beach, FL, January 27 – February 1, 2008.
12. SOFC Interconnect Research and Development at Montana State University, P.E. Gannon, Invited Keynote Presentation, European Science Foundation Exploratory Workshop on Next Generation SOFC Materials, Genoa, Italy, October 23, 2007.
13. Solid Oxide Fuel Cells: A great idea...a materials nightmare, colloquium given to Physics Department, Montana State University, Bozeman, MT, November 2007.
14. Thermal stability and oxidation resistance of protective coating on stainless steel interconnect for solid oxide fuel cells, H. Chen, J. A. Lucas, W. Priyantha, M. Kopczyk, R. J. Smith, P. E. Gannon, V. I. Gorokhovskiy, M. Deibert, V. Shutthanandan, P. Nachimuthu, 54<sup>th</sup> AVS International Symposium and Exhibition, Seattle, WA, October, 2007.

## References

1. V.H. Schmidt and C.-L. Tsai, *J. Power Sources* (2008), doi:10.1016/j.jpowsour.2008.01.073, in press.
2. V.H. Schmidt, C.-L. Tsai, and L.M. Lediaev, in: N.P. Bansal (Ed.), *Advances in Solid Oxide Fuel Cells III*, Wiley, Hoboken, NJ, 2008, pp. 129-140.
3. Y. Jiang and A.V. Virkar, *J. Electrochem. Soc.* **150**, (2003) A942-A951.
4. V.H. Schmidt and C.-L. Tsai, *J. Power Sources* (2008), doi:10.1016/j.jpowsour.2008.01.073, in press.

---

## V.4 Oxide Contaminant Removal in Liquid Tin Anode Fuel Cells by Direct Reduction with Coal

Paul E. King (Primary Contact) and  
William O'Connor

National Energy Technology Laboratory  
Process Development Division  
1450 Queen Ave. SW  
Albany, OR 97321  
Phone: (541) 967-5948; Fax: (541) 967-5958  
E-mail: Paul.King@netl.doe.gov

Contract Number: 08-220696

Start Date: October 1, 2007  
Project End Date: September 30, 2008

operating efficiencies. However, it has been shown that the liquid tin anode fuel cell (LTAFC) efficiency degrades dramatically as the tin oxide within the liquid tin bath increases. In order to maintain the efficiency of the fuel cell and to reclaim the tin oxide 'fuel', an in situ reduction process utilizing coal as the reductant has been proposed. This project proposes to investigate several issues related to the LTAFC system in an effort to develop a tin reduction unit that can be closely coupled to the fuel cell unit. Direct reduction of the tin oxide utilizing coal is the preferred method, and this project will focus on developing this technology.

### Approach

The technical approach is to evaluate the reduction efficiency of tin oxide over a range of temperatures. First, this will be accomplished by placing finely divided tin oxide and a reductant into a reaction chamber, at a predefined temperature, for a set time period in order to determine the reduction efficiency as a function of time and temperature. Chemical analysis of the product streams will yield several key pieces of information, namely a) the reduction efficiency of the tin oxide over a range of temperatures and b) the kind of contaminants that report to the liquid tin from the reductant during the reduction process. The second goal will lead naturally to questions concerning the utilization of slagging constituents for contaminant removal. The test procedure outlined will be performed utilizing a range of reductants including coke, coal, and charcoal fines in order to determine contaminant pickup as a function of reductant as well. The test procedure is as follows:

- Step 1 - Perform a complete chemical analysis of feed stocks utilized in the research and perform a differential thermal analysis of the  $\text{SnO}_2$  to determine liquidous and solidous temperatures.
- Step 2 - Perform a series of reduction tests at  $1,300^\circ\text{C}$  to determine the reduction efficiency as a function of stoichiometric fixed C addition, then use this fixed C value for the remainder of the tests (based on the stoichiometry of the equation:  $\text{SnO}_2 + 2\text{C} = \text{Sn} + 2\text{CO}$ ; stoichiometric C additions will range from ~75-125%).
- Step 3 - Perform a series of reduction tests between  $500^\circ\text{C}$ - $1,300^\circ\text{C}$  to determine reduction efficiency as a function of temperature. Analyze the products for C,  $\text{O}_2$ , Sn, SnO,  $\text{SnO}_2$  and trace contaminants by a series of analytical methods to determine reduction efficiency and the partitioning of trace contaminants to the metallic tin product.

### Objectives

The National Energy Technology Laboratory (NETL) Fuel Cell Program has identified tin (Sn) as a possible material to support concurrent electrochemistry and fossil fuel utilization. In this concept, liquid tin provides a 'fuel' for the electrochemical step. In this process, the liquid tin is converted to tin oxides as the 'fuel' is consumed. This project investigates the in situ reduction of the tin oxides through the addition of carbon to the cell. The goal is to determine whether coal can be utilized as a reductant and how to sequester contaminants introduced by the coal in the tin oxide reduction process.

### Accomplishments

A cooperative research and development agreement with CellTech, a small company working to advance liquid tin anode technology, was signed. CellTech will support NETL in order to solve the direct reduction of tin oxide with coal.

---

### Introduction

The NETL Fuel Cell Program has identified tin as a possible material to support concurrent electrochemistry and fossil fuel utilization. In this concept, liquid tin provides a 'fuel' for the electrochemical step, thereby becoming oxidized to  $\text{SnO}/\text{SnO}_2$ , and the fossil fuel (e.g., coal) is then used to reduce the oxide back to elemental Sn. It is envisioned that through this processing of the coal a greatly simplified coal-based fuel cell plant can be developed with associated cost saving and improved

Coke breeze will likely be the initial reductant investigated, with coal and charcoal substituted for the coke breeze once optimum C stoichiometry and reduction temperature have been determined in this system. The reduction tests should be conducted ideally in a controlled atmosphere furnace to limit reaction of the reduced Sn and C reductant with air. However, in the event that funding for the new furnace is not available, an existing Harrop SiC element furnace with a maximum temperature rating of 1,625°C will be used. At the end of each 2 hour test, the Harrop Furnace will be back-filled with argon during cooling in order to limit contact with air and prevent any re-oxidation reactions that may take place during the cool-down period. Chemical analysis will be performed by a combination of methods such as inductively coupled plasma, LECO<sup>®</sup>, X-ray fluorescence/X-ray diffraction or wet chemistry to determine the chemical analysis of the product streams. This information is then used to calculate a complete mass and elemental balance, thus yielding the reduction efficiency.

Task 3 of the project will investigate reduction in a multi-phase (Sn + SnO<sub>2</sub> + slag formers) system. Contaminant pick-up in the liquid Sn as a function of reductant will be determined, and potential means to remove said contaminants by a slag cleaning step will be investigated. Upon completion of Phase 2, analysis of the Sn product will identify the critical contaminants and their concentrations as a function of reductant used. A third series of reduction tests will then be conducted with the addition of slag forming oxides intended to remove specific contaminants from the liquid Sn product. Initial methods may be based on the literature, including "Extractive Metallurgy of Tin," 2<sup>nd</sup> Edition, P.A. Wright; and "A Bibliography on the Extractive Metallurgy of Tin," F. Habashi. Products will again be characterized following the procedures described for Phase 1 and 2.

In conjunction with the testing, a series of thermodynamic calculations will be performed to investigate the most likely slag formers based upon the analysis of the reductant and the chemistry of the slags produced. The object is to utilize existing techniques, where available, to encapsulate the contaminants in the slags or develop new slag formers to perform this duty. Once this is complete, a repeat of the previous reduction tests will be performed to determine the effectiveness and efficiency of the proposed slag formers. Completion of these three phases of the project will lead us naturally to the best methodology of reducing the tin oxide and slag forming.

## Conclusions and Future Directions

NETL has performed initial research into the use of liquid tin as the anode for a solid oxide fuel cell. The possible benefit of such tin technology is the ability to do both coal conversion, cleanup and separation within one process unit. Before such a fuel cell concept can be considered in system studies, a detailed assessment for the electrochemical activity and Sn – SnO diffusion within the liquid tin needs to be performed. NETL, in consultation with CellTech Power LLC, a small company working to advance liquid tin anode technology, has performed some basic electrochemical impedance and voltage interrupt studies to begin to obtain the needed performance data. Results show a peak power density of 40 mW/cm<sup>2</sup> for operation at 900°C, and an activation energy for total resistivity of 185,600 J/gm-mol for the thick (6 mm) anode tested. Higher power densities are expected with a more optimized electrolyte interface, and additional tests are being planned.

As the year progresses, and into the next fiscal year, answers to the questions of the effects and efficiencies of direct reduction of the tin oxide by coal will be answered. Following this, an effort will be put forth in order to design a fixture for operating a LTAFC system with coal as a reductant.

## References

1. Extractive Metallurgy of Tin," 2<sup>nd</sup> Edition, P.A. Wright; and "A Bibliography on the Extractive Metallurgy of Tin," F. Habashi.



steam reformer. Another 100-hour test followed, using this reformat and excess pure oxygen. The second stack was tested under similar conditions, but the oxygen outlet from the stack was closed off using a 0.3 psi check valve. The purpose of this was to approach 100% oxygen utilization, which is required for air-independent operations. The oxygen flow rate was controlled according to the stoichiometric requirement for the given current level; hence, this is called “stoichiometric oxygen control.”

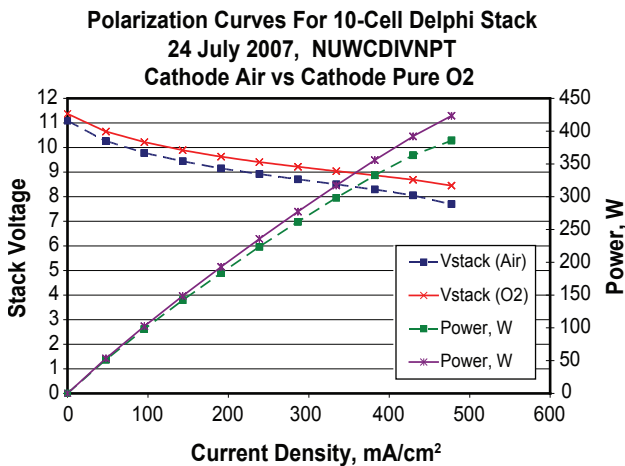
**Results**

The Delphi stack showed excellent promise for functioning well in a system that utilizes anode gas recycle and carbon dioxide removal. Under reformat and excess oxygen flows, the stack generated 550 watts at 7.9 volts. At 70 amps, the fuel utilization was 54% and the fuel efficiency was 33% on a single pass basis.

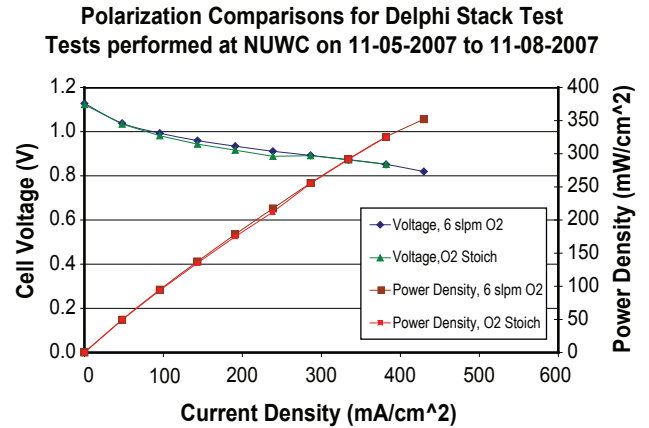
Figure 2 compares stack performance using air versus pure oxygen. While voltage enhancement is in the 2-3% range at open circuit, the boost from using pure oxygen increases as the current is ramped up. At the maximum current draw in this test, the voltage gain from using oxygen versus air was roughly 10%.

Figure 3 shows that switching from excessive oxygen flow (6 SLPM) to stoichiometric oxygen control had little effect on stack operating voltage. Figure 4 again compares excessive air flow versus stoichiometric oxygen control, but these polarization curves were taken while using diesel reformat at the anode.

Steady-state performance data over 8 hours at 50 amps is shown in Figure 5. After the stack had been run for over a combined 200 hours between testing at both Delphi’s and NUWC’s facilities, the stack showed stable



**FIGURE 2.** Use of 15 SLPM air versus 9 SLPM pure oxygen with 11 SLPM of 55% H<sub>2</sub>/45% N<sub>2</sub> at the anode. A 10% voltage gain is seen at 50 amps.



**FIGURE 3.** A 10.3 SLPM mixture of 55% H<sub>2</sub>/45% N<sub>2</sub> was bubbled through room temperature water at the anode, and the cathode feed was changed from 6 SLPM pure oxygen to a stoichiometric oxygen feed. Comparison of IV plots shows that oxygen flow rate has little effect on operating voltage.

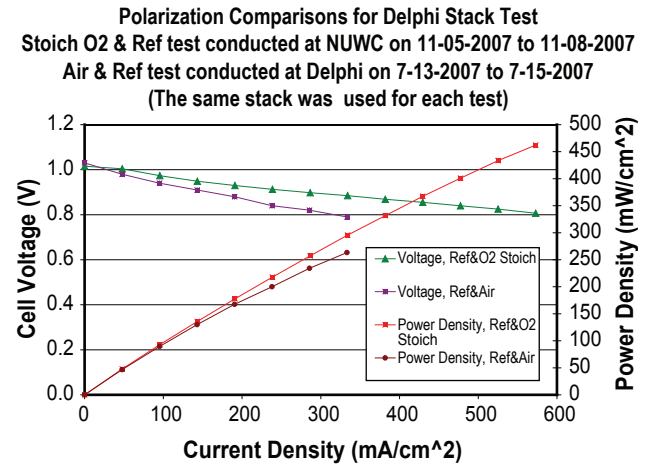


**FIGURE 4.** Polarization Plots comparing Excess Air Flow versus Stoichiometric Oxygen Flow with Reformat at the Anode

performance under the harshest conditions yet tested, i.e. diesel reformat and stoichiometric oxygen feeds.

For the 100-hour tests, the current was set at 31 amps for the steady-state analysis. Based on only the liquid fuel feed (lower heating value) into the reformer and the electricity generated by the stack, the SOFC efficiency was 76%. In a full system at steady-state, the liquid hydrocarbon feed would be the only fuel feed into the system, so there is justification for neglecting the simulated anode-recycle gas in this calculation. Parasitic power losses in a full system would likely bring the overall system efficiency down to 50-60%.

It should be noted that the fuel utilization of this stack was not pushed very high, and this may not be a strong point of this particular stack design. However,

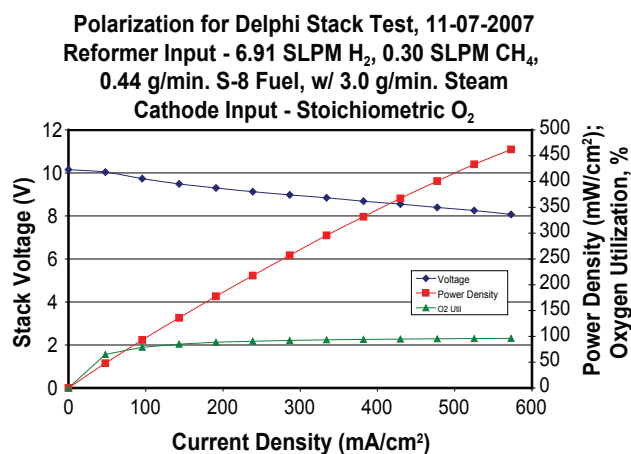


**FIGURE 5.** Polarization for a second 10-cell Delphi stack tested with furnace temperature of 725°C and the flow conditions noted above. The oxygen flow was controlled with respect to the current level by Faraday's law.

with the system concept that uses anode recycle and carbon dioxide sequestration, the single pass utilization through the stack will range from 20-35%, which is within the performance range of this stack.

There was also indication that high oxygen utilization will not adversely affect cell performance. The cathode gas feed was dead-ended by a 0.3 psi check valve in an attempt to operate at 100% oxygen utilization. The second Delphi stack was tested at 50 amps for 8 hours with a dead-ended cathode feed of pure oxygen. Oxygen utilization was near 95%, and the stack did not show any degradation. Therefore, by choosing a slightly lower operating temperature and operating current density, the concern of not using the oxidant as a stack coolant is eliminated.

## Conclusions and Future Directions

In this study, the Delphi SOFC stack showed potential for achieving much higher power density ( $>0.45 \text{ W/cm}^2$ ) while maintaining an average cell voltage of 0.8 V. Using pure oxygen at the cathode resulted in degradation rates that are acceptable for UUV applications and oxygen utilizations as high as 100% appear feasible! Therefore, the SOFC system is a promising technology that already is on the verge of meeting the requirements needed for UUV applications. Oxygen storage, system start-up, and maintenance between missions are the areas that still require development.

Targeted cell performance was set at 0.8 V for a current density of  $0.3 \text{ A/cm}^2$  at 725° C and 1 atm. The Delphi stack surpassed this goal and achieved over 0.85 V per cell at a current draw of 31 amps ( $\sim 0.3 \text{ A/cm}^2$ ). These numbers suggest that a larger current density could be targeted for the SOFC. Maintaining an average

cell voltage of 0.8 volts will ensure high stack efficiency, and increasing current density will in turn increase power density and decrease the size of stack required to meet the minimum power demands of the UUV.

If the stack can average 0.8 V/cell at  $0.6 \text{ A/cm}^2$ , as is shown in Figure 4, then it may be possible to achieve 3 kW using only a 60 cell stack (or two 30-cell modules, which are the standard stack units made by Delphi at this time).

$$(0.8 \text{ V/cell})(60 \text{ cells})(105 \text{ cm}^2)(0.6 \text{ A/cm}^2) = 3024 \text{ Watts}$$

Estimated mass and volume of two 30-cell modules are  $\sim 18 \text{ kg}$  and  $5 \text{ L}$ , respectively. If these numbers can be realized, this is much better than original estimates for the required stack size.

Minimizing the reaction of oxygen and chromium at high temperature is crucial to extending the lifetime of the stack. It is believed that a protective coating on the cathode piping/gas manifold can be used to mitigate degradation processes associated with the cathode. If a protective coating cannot prevent losses at the cathode/interconnect interface, then a diluent in the oxygen feed stream may be necessary to decrease the rate of corrosion at the cathode.

Preliminary examination of cathode pressurization and dead-ending of the cathode flow shows promise that stoichiometric oxygen control is feasible and may actually reduce cathode degradation. The low flow rate of oxygen gas could reduce the convective flow across the surfaces of the chromium-containing pipes and manifold thus minimizing the extraction of chromium in the form of an oxide. More study and longer duration testing is needed to reveal the nature of these oxidative processes at elevated pressure and low flow conditions. Tests to evaluate losses from thermal cycling are also needed to determine stack lifetime.

## FY 2008 Publications/Presentations

1. "Testing and Evaluation of Solid Oxide Fuel Cells in Extreme Conditions," extended report to DOE, delivered December 2007.
2. Visit to NETL to present work done on SOFC power systems for UUVs and review SOFC demonstrations performed at NUWC.
3. "Solid Oxide Fuel Cells for Undersea Naval Applications," 10<sup>th</sup> Electrochemical Power Sources R&D Symposium., Williamsburg, VA, August 2007, Presentation.
4. "Solid Oxide Fuel Cell Power Source for Unmanned Undersea Vehicles (UUVs)," MAST Conference, Genoa, Italy, November 2007, Paper & Presentation.
5. "SOFC Stack Performance Using Pure Oxygen and Reformate Gas Streams," 8<sup>th</sup> European Solid Oxide Fuel Cell Forum, Luzern, Switzerland, July 2008, Paper & Presentation.

## V.6 A High Temperature Electrochemical Energy Storage System Based on Sodium Beta Alumina Solid Electrolyte (BASE)

Anil V. Virkar  
University of Utah  
Department of Materials Science & Engineering  
122 S. Central Campus Drive  
Salt Lake City, UT 84112  
Phone: (801) 581-5396; Fax: (801) 581-4816  
E-mail: anil.virkar@m.cc.utah.edu

DOE Project Manager: Heather Quedenfeld  
Phone: (412) 386-5781  
E-mail: Heather.Quedenfeld@netl.doe.gov

Contract Number: 42623

Start Date: September 1, 2005  
Project End Date: March 31, 2008

### Objectives

- To synthesize planar, thin, strong BASE using a patented vapor phase process.
- To conduct kinetic studies on the conversion of  $\alpha$ -alumina + zirconia into BASE + zirconia composites by a vapor phase reaction.
- To construct electrochemical cells comprising of a sodium anode, BASE, and selected cathodes.
- To electrochemically test cells (discharge-charge) over a range of temperatures and up to the highest possible depths of discharge.
- To embed reference electrodes within BASE for electrochemical studies on electrode polarization during charge and discharge cycles.

### Accomplishments

- BASE discs were successfully fabricated by tape casting, sintering and vapor phase treatment.
- Kinetics of conversion were investigated as a function of microstructure (grain size) and temperature.
- A technique for embedding reference electrodes was explored.
- Electrochemical cells were tested and evaluated.

### Future Directions

There are no future plans under this project as the project has ended. However, work is continuing on the study of kinetics of conversion, the use of embedded

reference electrodes for electrochemical studies on solid electrolytes, and the further development of energy storage systems.

### Introduction

Electrical energy storage is gaining importance due to increased emphasis on renewable sources of energy such as wind and solar. There exists a need for an economical and efficient battery system. There also is a need for a energy storage system in the current utility industry. The demand for electricity varies depending upon the time of the day: low demand during night and high demand during day. All power plants are designed for peak power which leads to the underutilization of excess capacity during off-peak periods. One of the main reasons for the emergence of electrochemical energy storage devices such as batteries is that power plants can be designed for average demand. This will augment the capacity of power plants as the excess energy during off peak periods will be stored for use later during high peak demands. This strategy is expected to lower the capital cost.

One of the battery systems actively pursued in Europe and Japan is a high temperature battery system-based sodium beta alumina solid electrolyte. Sodium beta alumina solid electrolyte, commonly referred to as BASE, is an excellent conductor of sodium ions at 300°C. This cell has liquid sodium as the anode, BASE as electrolyte and liquid  $ZnCl_2$  as the cathode. During charging and discharging, sodium ions pass through the BASE electrolyte from the cathode to the anode and the anode to the cathode, respectively. The current applications of this solid electrolyte include the Na-S battery, the Zebra battery and the sodium heat engine. The Na-S battery has a demonstrated life of greater than 7 years in a 500 kW size. This shows that BASE has outstanding stability in rather corrosive environments – far superior than any other solid electrolyte being considered for active electrochemical devices. Work to date shows that BASE is the only known solid electrolyte with such a wide range of applicability (from as low as ~100°C to over 1,000°C), and excellent stability in strongly reducing and oxidizing environments.

### Approach

In this work, BASE bars and discs were fabricated using the method of tape casting of alumina + zirconia

and also by powder pressing followed by vapor phase conversion. The process involves first the fabrication of dense two phase materials containing insulating alpha alumina plus an oxygen ion conductor such as yttria-stabilized zirconia (YSZ). These two phase materials are then exposed to a vapor of sodium oxide. The conversion of alpha alumina into BASE occurs by coupled diffusion of sodium ions and oxygen ions. The conversion kinetics is expected to be a function of the microstructure and temperature. The main objective was to investigate the kinetics of conversion. Some work has also been initiated on the embedment of reference electrodes into BASE so that electrochemical measurements can be conducted *in situ* during cell operation. A four-cell battery with a Na/ZnCl<sub>2</sub> system at 460°C was successfully charged and discharged several times. Preliminary work conducted on aqueous systems is also reported here.

**Results**

1. A model describing the kinetics of conversion of alpha alumina + YSZ into beta"-alumina + YSZ by electrically coupled transport of sodium ions and oxygen ions was developed (Figure 1).
2. Samples of alpha alumina + YSZ and beta" alumina + YSZ over a wide range of grain sizes were fabricated (Figure 2).
3. Kinetics of conversion was investigated as a function of grain size and temperature (Figure 3). The results are in accord with the model.

4. BASE discs with embedded electrodes have been fabricated (Figure 4). These will be used to investigate electrochemical polarization in BASE in operating cells.

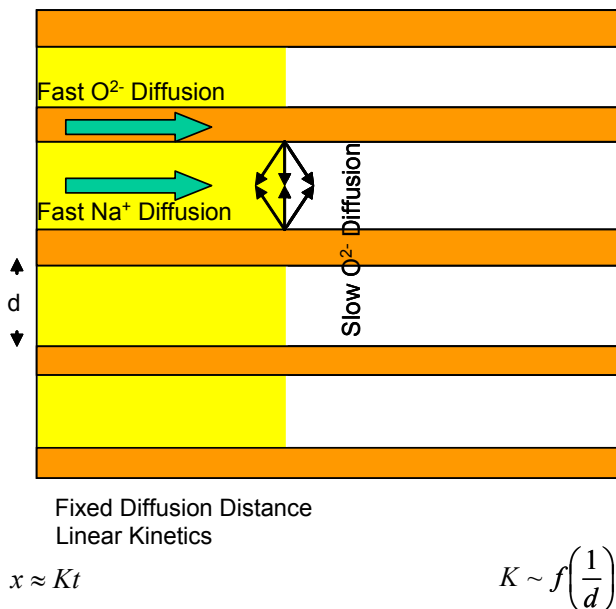


FIGURE 1. Mechanism of the Conversion Process by Coupled Diffusion

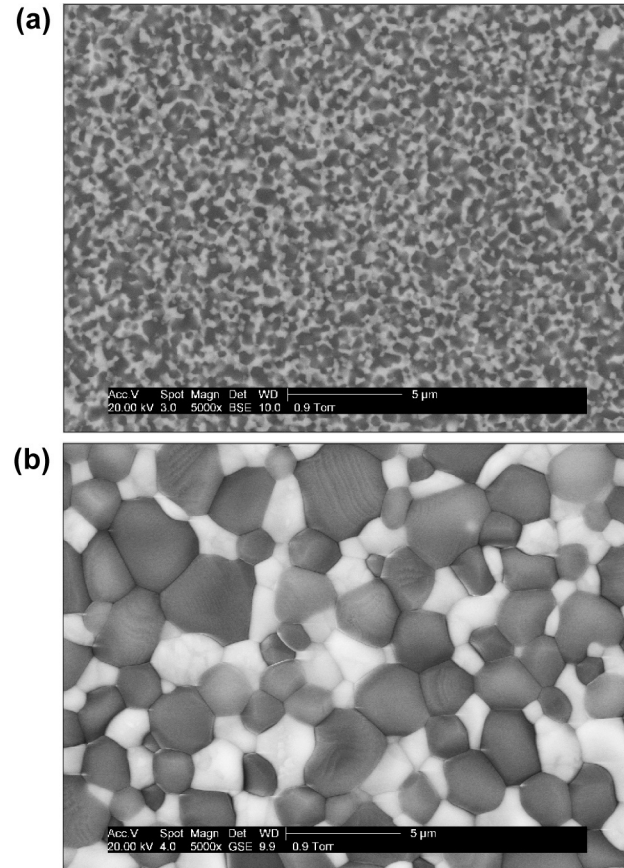


FIGURE 2. Microstructures of (a) Fine Grained and (b) Coarse Grained Alpha Alumina + Zirconia Samples

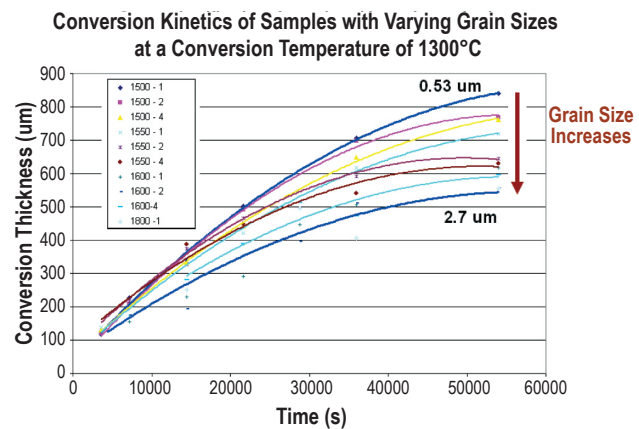
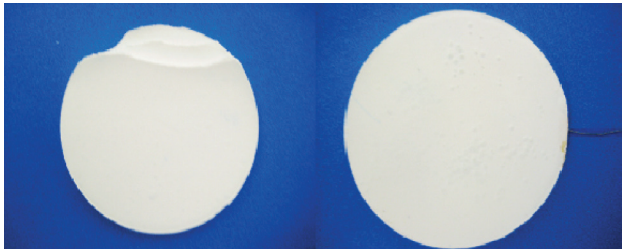
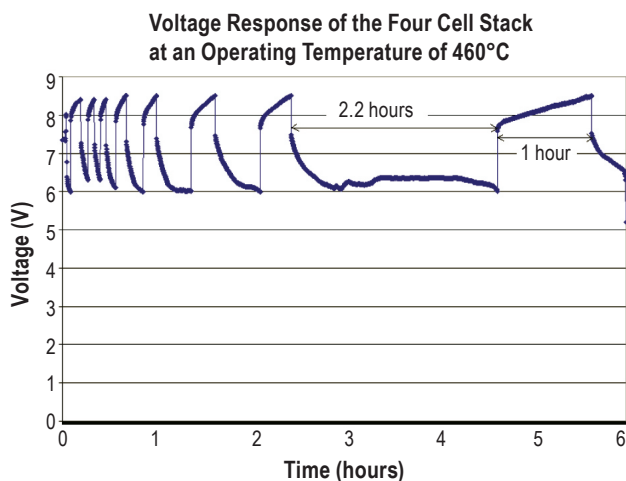


FIGURE 3. Conversion Thickness as a Function of Hold Time for the Samples with Varying Grain Sizes, Conversion Temperature – 1,300°C

5. A four cell Na/ZnCl<sub>2</sub> battery was assembled and tested at 460°C. The battery voltage was over 8 volts. The battery could be successfully charged and discharged several times (Figure 5).
6. A Cu/ZnCl<sub>2</sub> aqueous cell was constructed and successfully operated (charge-discharge) (Figures 6 and 7).



**FIGURE 4.** Delaminated BASE electrolyte with platinum electrodes embedded (left). BASE electrolyte with embedded platinum electrodes and platinum wire attached to the electrodes (right).



**FIGURE 5.** Voltage response of the planar four-cell stack at an operating temperature of 460°C – part of the charge/discharge cycles are shown. The stack was operated for four days.

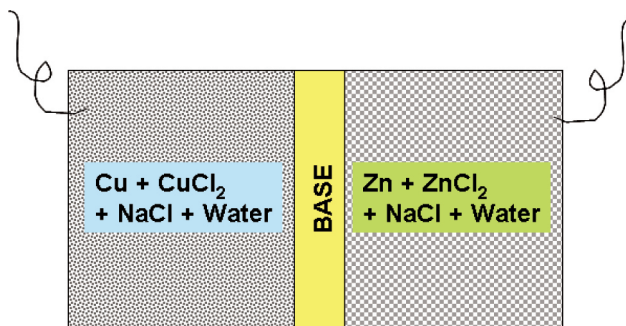


**FIGURE 6.** A Schematic of a Cu/ZnCl<sub>2</sub> Aqueous Cell

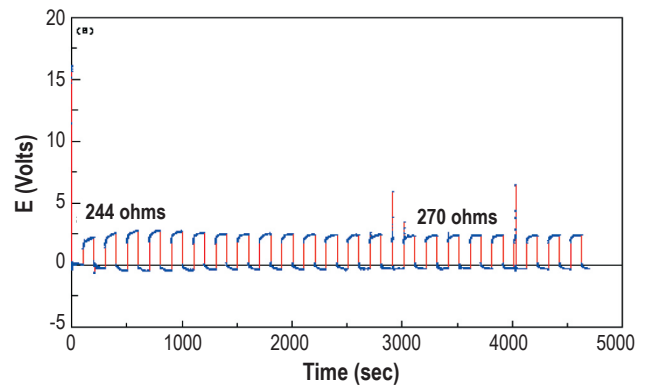


**FIGURE 7.** Charge-Discharge Cycles of Cu/ZnCl<sub>2</sub> Aqueous Cell

### Conclusions

1. The coupled transport model shows that rapid conversion of alpha alumina + YSZ into BASE + YSZ can be accomplished. This allows for the fabrication of BASE for use in numerous energy storage applications.
2. Successful operation of a Na/ZnCl<sub>2</sub> four-cell battery opens up new battery systems for energy storage. The battery is planar, compact, can be deep discharged, and can be operated over a wide temperature range.
3. The BASE made by the vapor phase process is resistant to moisture-induced degradation. As such, it can be used in aqueous electrochemical cells.



## VI. Acronyms & Abbreviations

°C	Degree(s) Celsius	ASME	American Society of Mechanical Engineers
°F	Degree(s) Fahrenheit	ASR	Area specific resistance
°K	Degree(s) Kelvin	ASTM	ASTM International, formerly American Society for Testing and Materials
Δ	Change	ASU	Air separation unit
%	Percent	ATI	Allegheny Technologies, Inc.
μm	Micrometer(s), micron(s)	atm	Atmosphere(s)
μm/s	Micron(s) per second	ATR	Autothermal reforming
Ω	Ohm(s)	Au	Gold
τ	Tortuosity	AVS	American Vacuum Society
\$	Dollars	B	Boron
A	Ampere(s), amp(s)	Ba	Barium
ABAQUS	A finite element analysis package	BaCeO <sub>3</sub>	Barium cerate
ABO <sub>3</sub>	Perovskite type materials	BASE	Beta alumina solid electrolyte
AC	Activated carbon	BFW	Boiler feed water
AC	Alternating current	BO <sub>2</sub>	Boron oxide
ACerS	Advanced Ceramics and Composites	B <sub>2</sub> O <sub>3</sub>	Boron (III) oxide
AcerSoc	American Ceramic Society	BOP	Balance of plant
A/cm <sup>2</sup>	Amp(s) per square centimeter	BPW	Biphasic waveform
ACS	American Chemical Society	BSCF	Barium strontium cobalt ferrite (BaSrCoFeO <sub>3</sub> )
AES	Auger electron spectroscopy	B.V.	Besloten vennootschap, Dutch terminology for a limited liability company (LLC)
AFM	Atomic force microscopy	C	Carbon
Ag	Silver	C	Celsius
AGR	Advanced gas-cooled reactor	Ca	Calcium
AISI	American Iron and Steel Institute	CA	California
Al	Aluminum	CAD	Computer aided design
AL	Alabama	CANTERA	An open source kinetics code
Al <sub>2</sub> O <sub>3</sub>	Alumina, aluminum oxide, sapphire	CaO	Calcium oxide
A/m <sup>2</sup>	Amp(s) per square meter	CaS	Calcium sulphide
Am.	American	CaSO <sub>4</sub>	Calcium sulfur oxide
AMCX	Advanced Materials Components Express <sup>®</sup>	C <sub>2</sub> H <sub>2</sub>	Unsaturated hydrocarbon
ANL	Argonne National Laboratory	C <sub>2</sub> H <sub>4</sub>	Unsaturated hydrocarbon
APEC	Applied Power Electronics Conference	Cd	Cadmium
Appl.	Applied	Ce	Cerium
APS	Advanced Photon Source	Ce-MC	Ce-modified manganese-cobalt spinel
APU	Auxiliary power unit	CeOx	Ceric oxides
Ar	Argon	Ceram.	Ceramics
arb.	Arbitrary	CFD	Computational fluid dynamics
ARM	Augmented reduced mechanism	Ch	Chapter
As	Arsenic	CH <sub>4</sub>	Methane
ASE	Arcomac Surface Engineering, LLC	CH <sub>3</sub> Cl	Methyl chloride
AsH <sub>3</sub>	Arsine		
ASM	ASM International, formerly American Society for Metals		

## VI. Acronyms and Abbreviations

---

chem.	Chemistry	DyScO <sub>3</sub>	Dysprosium scandium oxide
Cl	Chlorine	e-	Electron
cm	Centimeter(s)	EBPVD	Electron beam physical vapor deposition
cm <sup>2</sup>	Square centimeter(s)	E-BRITE	Fe-26Cr-1Mo alloy
CMU	Carnegie Mellon University	EBSV	Electron back-scatter diffraction
CNS	Center for Nanoscale Systems (Harvard University)	EC	Electrical conductivity
CO	Carbon monoxide	ECR	Electrical conductivity relaxation
CO	Colorado	ECS	The Electrochemical Society
Co	Cobalt	EDX	Energy dispersive X-ray
CO <sub>2</sub>	Carbon dioxide	EE	Type of transformer core with an open window area
CoMnO	Cobalt manganese oxide	EELS	Electron energy loss spectroscopy
Con.	Conference	e.g.	<i>exempli gratia</i> ; for example
Conf.	Conference	EIS	Electrochemical impedance spectroscopy
CoO <sub>3</sub>	Cobalt oxide	Electrochem.	Electrochemical
coul	Coulomb(s)	EPRI	Electric Power Research Institute
coul/m <sup>2</sup>	Coulomb(s) per square meter	EPSCOR	Experimental Program to Stimulate Competitive Research
CPOX, CPOx	Catalytic partial oxidation	ESC	Electrolyte supported cells
Cr	Chromium	ESWG	Electric Systems Working Group
CrO <sub>2</sub>	Chromium dioxide	et al.	<i>et alii</i> ; and others
CrO <sub>3</sub>	Chromium trioxide (chromic acid)	eV	Electron volts
Cr <sub>2</sub> O <sub>3</sub>	Chromic oxide	Expo.	Exposition
CT	Connecticut	FAPSID	Filtered arc plasma source ion deposition
CTE	Coefficient of thermal expansion	FBS-AGRB	Foil gas bearing supported anode gas recycle blower
CTP	Core Technology Program	FC	Fuel cell
CTR	Crystal truncation rod	FCE	FuelCell Energy, Inc.
Cu	Copper	Fe	Iron
d	Diameter	FEA	Finite element analysis
DARPA	Defense Advanced Research Projects Agency	FeCrAlY	Iron chromium aluminum yttrium
DBT	Dibenzothiophene	Fe <sub>2</sub> O <sub>3</sub>	Iron oxide
DC	Direct current	Fe <sub>3</sub> O <sub>4</sub>	Iron oxide
DC, D.C.	District of Columbia	FeO	Iron oxide
DC-AC	Direct current-alternating current	FeTiO <sub>3</sub>	Iron titanate, iron titanium oxide
DC-DC, DC/DC	Direct current to direct current	FIB	Focused ion beam
DFT	Density functional theory	FL	Florida
DOE	U.S. Department of Energy	FSS	Ferritic stainless steel
DOE-SECA	U.S. Department of Energy-Solid State Energy Conversion Alliance	ft	Foot (feet)
DOI	Digital object identifier	ft-lbf/lbm	Foot-pound(s) force per pound mass
DOS	Density of state	FY	Fiscal year
DPI	Drexel Plasma Institute	(g)	Gas
DPS	Delphi Power Systems	g	Gram(s)
DSO	Dysprosium scandium oxide (DyScO <sub>3</sub> )	Ga	Gallium
DSP	Digital signal processor	GA	Georgia
Dy	Dysprosium	GaPO <sub>4</sub>	Gallium phosphorous oxide
		GAT	Gliding arc in tornado

GC	Gas chromatograph	InDEC	InDEC B.V (Innovative Dutch Electro Ceramics), a Dutch energy technology company
GC/ICP/MS	Gas chromatograph – inductively coupled plasma – mass spectrometer		
g/cm <sup>2</sup>	Gram(s) per cubic centimeter	inorg.	Inorganic
GCO	Gadolinium doped ceric oxide	Instrum.	Instruments
Gd	Gadolinium	Int.	International
GDC	Gadolinia-doped ceria	IP	Intermediate pressure
GE	General Electric	Ir	Iridium
gms.	Grams	ISBN	International Standard Book Number
GT	Gas turbine	ITM	Ion transport membrane
GUI	Graphical user interface	I-V	Current-voltage
h	Hour(s)	J	Joule(s)
H <sub>2</sub>	Diatomic hydrogen	J/kg	Joule(s) per kilogram
HARB	High-temperature anode recirculation blower	JP-8	High sulfur military fuel
HCl	Hydrogen chloride	K	Kelvin
HDS	Hydro-desulfurization	K	Potassium
HF	High frequency	kg	Kilogram(s)
Hg	Mercury	kJ	Kilojoule(s)
HHV	Higher heating value	kJ/gm-mol	Kilojoule(s) per gram mole
HI	Hawaii	kJ/mole,	
H <sub>2</sub> O	Water	kJ/mol	Kilojoule(s) per mole
HP	High pressure	kPa	Kilopascal(s)
hr	Hour(s)	kV	Kilovolt(s)
hrs	Hours	kVA	Kilovolt-ampere(s)
HRSGS	Heat recovery steam generators	kVAr	Kilovolt-ampere(s) reactive
H <sub>2</sub> S	Hydrogen sulfide	kW	Kilowatt(s)
H <sub>2</sub> Se	Hydrogen selenium	kWe	Kilowatt(s) electric
HT	High temperature	l	Liter(s)
HV	High voltage	La	Lanthanum
HV/HF	High voltage-high frequency	LA	Louisiana
Hz	Hertz	LaCoO <sub>3</sub>	Lanthanum cobalt oxide
I	Current	LaCrO <sub>3</sub>	Lanthanum chromite
IA	Iowa	LAFAD	Large area filtered arc deposition
IAPG	Interagency Power Group	LaFeO <sub>3</sub>	Lanthanum iron oxide
IC	Interconnect	LaMnO <sub>3</sub>	Lanthanum manganite
i.e.	<i>id est</i> ; that is	LaNiO <sub>3</sub>	Lanthanum nickel oxide
IEA	International Energy Agency	LAO	Lanthanum aluminum oxide
IEEE	Institute of Electrical and Electronics Engineering	lbm	Pound(s) mass
IGBT	Insulated gate bipolar transistor	lbm/min	Pound(s) mass per minute
IGFC	Integrated gasification fuel cell	LBNL	Lawrence Berkeley National Laboratory
IL	Illinois	LC	Inductor capacitor
in	Inch(es)	LCL	Inductor-capacitor-inductor
Inc.	Incorporated	Lett.	Letter
		LHV	Lower heating value
		LLC	Limited Liability Company
		lm	Lanthanum manganite
		LNO	Lanthanum nickel oxide

## VI. Acronyms and Abbreviations

---

LP	Low pressure	MO	Missouri
LRZ	Lanthanum rhodium zirconate	mΩ	Milli-ohm(s)
LSC	Lanthanum strontium cobaltite	mOhm.cm <sup>2</sup> ,	
LSC50	La <sub>0.5</sub> Sr <sub>0.5</sub> CoO <sub>3-δ</sub>	mΩ.cm <sup>2</sup>	Milli-ohm(s) square centimeter
LSCF	Lanthanum strontium cobalt ferrite	mol	Mole(s)
LSCO	Lanthanum strontium cobaltite oxide	mol/s	Mole(s) per second
LSF	Lanthanum strontium ferrite	MOSFET	Metal-oxide-semiconductor field effect transistors
LSGM	Strontium and magnesium doped lanthanum gallate	MPa	Megapascal(s)
lsm, LSM	Lanthanum strontium manganite, strontium doped lanthanum manganite	MS	Mail stop
LSM50	La <sub>0.5</sub> Sr <sub>0.5</sub> MnO <sub>3-δ</sub>	MS	Mass spectrometer
LSMO	Lanthanum strontium manganite oxide	m/s	Meter(s) per second
LSRZ	Strontium doped lanthanum rhodium zirconate	MSRI	Materials and Systems Research, Inc.
LSZF	Lanthanum strontium zinc ferrite	MSU	Montana State University
LT	Low temperature	MT	Montana
LTAFC	Liquid tin anode fuel cell	mTorr	Millitorr(s)
Ltd.	Limited	MW	Megawatt(s)
LTSOFC	Liquid tin anode solid oxide fuel cell	mW	Milliwatt(s)
LZ	Lanthanum zirconate	mW/cm <sup>2</sup> ,	
m	Meter(s)	mW/cm <sup>2</sup>	Milliwatt(s) per square centimeter
MA	Massachusetts	MWe	Megawatt(s) electric
mA	Milliamper(s)	MWh	Megawatt-hour(s)
mA/cm <sup>2</sup>	Milliamper(s) per square centimeter	n	Number
MARC-SECA	A fuel cell stack model	N	Nitrogen
MAST	Maritime Systems and Technology	N <sub>2</sub>	Diatomic nitrogen
MATLAB	A computer programming environment	Na	Sodium
MC, MCO	Manganese-cobalt spinel (Mn,Co) <sub>3</sub> O <sub>4</sub>	Na-S	Sodium silicon
m/d	Month/day	Nb	Niobium
MD	Maryland	NbO <sub>2</sub>	Niobium oxide
mg	Milligram(s)	NbS <sub>2</sub>	Niobium sulfide
mg/cm <sup>2</sup>	Milligram(s) per square centimeter	NC	North Carolina
Mg	Magnesium	Nd	Neodymium
MgO	Magnesium oxide	NdGaO <sub>3</sub>	Neodymium gallium oxide
MI	Michigan	NETL	National Energy Technology Laboratory
min	Minute(s)	NGO	Neodymium gallium oxide
MIT	Massachusetts Institute of Technology	Ni	Nickel
mm	Millimeter(s)	NiO <sub>3</sub>	Nickel oxide
Mn	Manganese	Ni <sub>3</sub> P	Nickel phosphide
MnO	Manganese oxide	Ni <sub>5</sub> P <sub>2</sub>	Nickel phosphide
MnO <sub>2</sub>	Manganese dioxide	NiS <sub>2</sub>	Nickel sulfide
MnO <sub>3</sub>	Manganate	NIST	National Institute for Standards and Technology
Mn <sub>2</sub> O <sub>3</sub>	Dimanganese trioxide	Ni-YSZ	Nickel-yttria-stabilized zirconia
Mn <sub>3</sub> O <sub>4</sub>	Manganese oxide	nm	Nanometer(s)
MnTiO <sub>3</sub>	Manganese titanate	NMR	Nuclear magnetic resonance
Mn <sub>2</sub> TiO <sub>4</sub>	Manganese titanium oxide	No.	Number
		NOx	Oxides of nitrogen

NSF	National Science Foundation	PSDF	Power Systems Development Facility
NUWC	Naval Undersea Warfare Center	psi	Pound(s) per square inch
NV	Nevada	psia	Pound(s) per square inch absolute
NW	Northwest	P-SOFC	Proton conducting solid oxide fuel cell
NY	New York	Pt	Platinum
O	Oxygen	PVD	Physical vapor deposition
O <sub>2</sub>	Diatomic oxygen	QPR	Quasi-proportional-resonant
O/C	Oxygen to carbon ratio	R	Rankine
OCV	Open circuit voltage	RAM	Random access memory
OH	Ohio	Rd.	Road
OH	Oxyhydroxide	ReMoDy	A molecular dynamics code for computing reactive gas mixtures
Ohm.cm <sup>2</sup>	Ohm(s) square centimeter	REQ'D	Required
OR	Oregon	Rev.	Review
ORR	Oxygen reduction reaction	Rh	Rhodium
O-SOFC	Oxygen conducting solid oxide fuel cell	Rp, R <sub>p</sub>	Polarization resistance
p.	Page	RPM	Revolutions per minute
P	Phosphorous	RT	Room temperature
P	Pressure	Ru	Ruthenium
PA	Pennsylvania	s	Second(s)
PADT	Phoenix Analysis & Design Technologies	s	Surface site
Pb	Lead	S	Sulfur
PBCO	PrBaCo <sub>2</sub> O <sub>5+x</sub> , Praseodymium barium cobalt oxide	SAED	Selected area electron diffraction
PCI	Precision Combustion Inc.	SAG	Simulated anode gas
PCM	Piezoelectric crystal microbalance	Sb	Antimony
PCS	Power conditioning system	SBIR	Small Business Innovation Research
Pd	Palladium	S/C	Steam to carbon ratio
PDPA	Phase Doppler particle analyzer	Sc	Scandium
PESC	Power Electronics Specialists Conference	SC	South Carolina
PH <sub>3</sub>	Phosphine	sccm	Standard cubic centimeter(s) per minute
PhD. Ph.D.	Doctor of philosophy	Sci.	Science
Phys.	Physics	S/cm	Siemen(s) per centimeter
PI	Proportional-integral	Se	Selenium
PLD	Pulsed laser deposition	sec	Second(s)
PLL	Phase-locked loop	SECA	Solid State Energy Conversion Alliance
PNNL	Pacific Northwest National Laboratory	SEM	Scanning electron microscope
P.O.	Post office	SEM/EDS	Scanning electron microscopy/energy dispersive spectroscopy
pO <sub>2</sub>	Partial pressure of oxygen	SFC	Stationary Fuel Cells (Siemens Power Generation)
POC	Proof-of concept	Si	Silicon
POx	Partial oxidation	SiC	Silicon carbide
pp.	Pages	SIMS	Secondary ion mass spectrometry
PPH	Pound(s) per hour	SiO <sub>2</sub>	Silicon dioxide
ppm	Part(s) per million	slpm	Standard liter(s) per minute
ppmv	Part(s) per million by volume	SMD	Sauter mean diameter
ppmw	Part(s) per million by weight	SMS	Small multi-stage
Pr	Praseodymium		
Proc.	Proceedings		

## VI. Acronyms and Abbreviations

---

Sn	Tin	TPB	Triple-phase boundary
S-Ni	Sulfur-nickel	TPO	Temperature-programmed oxidation
SnO	Tin oxide	Trans.	Transactions
SnO <sub>2</sub>	Tin oxide	TST	Transition state theory
Soc.	Society	TX	Texas
SOFC	Solid oxide fuel cell	TXRF	Total reflection X-ray fluorescence
SOFC-MP	Solid oxide fuel cell multi physics	UBM	Unbalanced magnetron
SOFC-X	Symposium on Solid Oxide Fuel Cells	UC	University of California
SOx	Oxides of sulfur (e.g., SO <sub>2</sub> )	UCI	University of California, Irvine
Sr	Strontium	UF	Fuel utilization
SrCeO <sub>3</sub>	Strontium cerate	UHV	Ultra-high vacuum
SrMnO <sub>3</sub>	Strontium manganate	um	Micrometer(s)
SrTiO <sub>3</sub>	Strontium titanate	UPS	Ultraviolet photoelectron spectroscopy
SS, ss	Stainless steel	US, U.S.	United States
SSC	Strontium samarium cobalt oxide	USA	United States of America
SSZ	Scandia stabilized zirconia	UT	Utah
St.	Street	UUV	Unmanned undersea vehicles
S&T	Science and Technology	v	Volume
STEM	Scanning transmission electron microscopy	V	Volt(s)
STM	Scanning tunneling microscopy	VA	Virginia
STO	Strontium titanate (SrTiO <sub>3</sub> )	V <sub>act</sub>	Activation polarization
STS	Scanning tunneling spectroscopy	VDC	Volt(s) direct current
SW	Southwest	V(i)	Terminal voltage vs. current density
T	Temperature	V <sub>O</sub> , V <sub>O</sub> ••	Oxygen vacancy
TBD	To be determined	VPS	Versa Power Systems
TD	N-tetradecane	W	Watt(s)
Tech.	Technology	WA	Washington
Technol.	Technology	WC	Weight change
TEM	Transmission electron microscopy or tunneling electron microscopy	W/cm <sup>2</sup>	Watt(s) per square centimeter
Tg	Glass transition temperature	WDX	Wavelength dispersive x-rays
TGO	Thermally-grown chromium oxide	WGS	Water gas shift
Ti	Titanium	wt	Weight
TiCrAlY	Titanium chromium aluminum yttrium	wt%	Weight percent
TiO <sub>2</sub>	Titanium dioxide	WV	West Virginia
TiO <sub>3</sub>	Titanate	WVU	West Virginia University
Ti <sub>2</sub> O <sub>3</sub>	Titanium oxide	x	Times
Ti <sub>3</sub> O <sub>5</sub>	Titanium oxide	XANES	X-ray absorption near edge spectroscopy
Ti <sub>4</sub> O <sub>2</sub>	Titanium oxide	XPS	X-ray photoelectron spectroscopy
t <sub>ion</sub>	Ionic transference number	XRD	X-ray diffraction
TMS	The Metallurgical Society	Y	Yes
TN	Tennessee	Y	Yttrium
ToF-SIMS	Time-of-flight secondary ion mass spectroscopy	YBCO	Y <sub>x</sub> BaCe <sub>1-x</sub> O <sub>3</sub>
TOMMI	Temperature optical-mechanical measuring instrument	Y <sub>2</sub> O <sub>3</sub>	Yttrium oxide (yttria)
		YSZ	Yttria-stabilized zirconia
		Zn	Zinc
		ZnCl <sub>2</sub>	Zinc chloride

ZnO	Zinc oxide
Zr	Zirconium
ZrO <sub>2</sub>	Zirconium dioxide (zirconia)
Z_tot	Total impedance



---

## VII. Primary Contact Index

### A

Agrawal, Giri . . . . . 251  
Alinger, Matthew . . . . . 33

### B

Berry, David . . . . . 206  
Botte, Gerardine . . . . . 89  
Brow, Richard . . . . . 147  
Burke, A. Alan . . . . . 274

### C

Celik, Ismail . . . . . 99  
Chen, Chonglin . . . . . 177  
Chou, Yeong-Shyung "Matt" . . . . . 135, 174

### E

Elangovan, S. (Elango) . . . . . 257, 261

### F

Fuoss, P. H. . . . . 39

### G

Gemmen, Randall . . . . . 86  
Ghezel-Ayagh, Hossein . . . . . 17  
Gorokhovsky, Vladimir . . . . . 111

### H

Harrison, Walter . . . . . 75  
Hartvigsen, Joseph . . . . . 186  
Hefner, Allen Jr. . . . . 219

### J

Johnson, Mark . . . . . 248

### K

Khaleel, Mohammad . . . . . 233  
King, Paul . . . . . 115, 272  
Krishnan, Gopala . . . . . 96  
Krumpelt, Michael . . . . . 163

### L

Lai, Jason . . . . . 225  
Lara-Curzio, Edgar . . . . . 166  
Linic, Suljo . . . . . 213  
Litka, Anthony . . . . . 245  
Liu, Meilin . . . . . 52, 56, 81  
Loehman, Ronald . . . . . 139

### M

Manchanda, Raj . . . . . 231  
Marina, Olga . . . . . 92  
Mundschau, Michael . . . . . 195

### P

Pack, Spencer . . . . . 191  
Pederson, Larry . . . . . 153  
Pierre, Joseph . . . . . 22

### R

Rakowski, James . . . . . 107  
Roychoudhury, Subir . . . . . 210

### S

Salvador, Paul . . . . . 42, 47  
Samuelson, Scott . . . . . 237  
Seabaugh, Matthew . . . . . 67  
Shaffer, Steven . . . . . 27  
Shekhawat, Dushyant . . . . . 203  
Singh, Prabhakar . . . . . 170  
Singh, Raj . . . . . 144  
Spangler, Lee . . . . . 264

### T

Thompson, Craig . . . . . 183

### V

Virkar, Anil . . . . . 277  
Visco, Steven . . . . . 59

### W

Wachsman, Eric . . . . . 70  
Westerheim, Daniel . . . . . 200

### Y

Yang, Zhenguo "Gary" . . . . . 120, 124  
Yildiz, Bilge . . . . . 63

### Z

Zhou, X.D. . . . . 120  
Zhu, Jiahong H. . . . . 128, 157



---

## VIII. Organization Index

### A

Acumentrics Corporation . . . . . 245  
American Society of Mechanical Engineers . . . . . 231  
Arcomac Surface Engineering, LLC . . . . . 111  
Argonne National Laboratory . . . . . 39, 163  
Aspen Products Group, Inc. . . . . 183  
ATI Allegheny Ludlum . . . . . 107

### C

Carnegie Mellon University . . . . . 42, 47  
Ceramtec, Inc. . . . . 186, 257, 261

### D

Delphi Automotive Systems LLC . . . . . 27

### E

Eltron Research and Development Inc. . . . . 195

### F

FuelCell Energy, Inc. . . . . 17

### G

GE Global Research . . . . . 33  
Georgia Institute of Technology . . . . . 52, 56, 81  
Delevan d.b.a. Goodrich Turbine Fuel Technologies  
. . . . . 191

### L

Lawrence Berkeley National Laboratory. . . . . 59  
Lynntech, Inc. . . . . 200

### M

Massachusetts Institute of Technology. . . . . 63  
Missouri University of Science & Technology. . . . . 147  
Montana State University . . . . . 264

### N

National Energy Technology Laboratory  
. . . . . 86, 115, 203, 206, 272  
National Institute of Standards and Technology. . . . . 219  
Naval Undersea Warfare Center. . . . . 274  
NexTech Materials Ltd. . . . . 67

### O

Oak Ridge National Laboratory. . . . . 166  
Ohio University . . . . . 89

### P

Pacific Northwest National Laboratory  
. . . . . 92, 120, 124, 135, 153, 170, 174, 233  
Phoenix Analysis & Design Technologies . . . . . 248  
Precision Combustion Inc. . . . . 210

### R

R&D Dynamics Corporation . . . . . 251

### S

Sandia National Laboratories. . . . . 139  
Siemens Power Generation, Inc. . . . . 22  
SRI International. . . . . 96

### T

Tennessee Technological University . . . . . 128, 157

### U

University of California, Irvine . . . . . 237  
University of Cincinnati . . . . . 144  
University of Florida . . . . . 70  
University of Michigan . . . . . 213  
University of Texas at San Antonio . . . . . 177  
University of Utah . . . . . 277

### V

Virginia Polytechnic Institute and State University  
. . . . . 225

### W

Walter A. Harrison/Stanford University . . . . . 75  
West Virginia University . . . . . 99



---

## IX. Contract Number Index

05690 .....	231	42614 .....	33
07-220611 .....	203, 206	42623 .....	277
07-220621 .....	86	42627 .....	96
08-220692 .....	115	42735 .....	52
08-220696 .....	272	43042 .....	219
40552 .....	120, 124, 135, 170, 174, 233	43063 .....	177
41246 .....	27	43247 .....	274
41567 .....	225	44036 .....	70, 92, 153, 264
41572 .....	56	46299 .....	99
41817 .....	42, 47, 75, 237	49071 .....	39, 63, 163
41837 .....	17	68250 .....	139
42219 .....	81	84209 .....	248
42221 .....	147	84210 .....	251
42223 .....	128	84394 .....	195
42225 .....	111	84590 .....	245
42227 .....	144	84595 .....	257
42229 .....	191	84662 .....	183
42471 .....	261	84663 .....	186
42513 .....	107	84673 .....	200
42516 .....	213	84674 .....	210
42527 .....	89	84881 .....	67
42533 .....	157	FEAA066 .....	166
42613 .....	22	MSD-NETL-01 .....	59



## X. Index of Previous Projects

### Projects Discontinued Since the FY 2007 Annual Report

Contract Number	Performer	Project Topic
41838	Acumentrics Corporation	Development of a Low Cost 10 kW Tubular SOFC Power System
41245	GE Global Research	Solid State Energy Conversion Alliance (SECA) Solid Oxide Fuel Cell Program
42175	University of Missouri-Rolla	Resilient Sealing Materials for Solid Oxide Fuel Cells
41247	Siemens Power Generation	Small-Scale Low Cost Solid Oxide Fuel Cell Power Systems
42220	University of Utah	Electrically Conductive, Corrosion-Resistant Coatings through Defect Chemistry for Metallic Interconnects
42741	Virginia Polytechnic Institute and State University	Digital Manufacturing of Gradient Meshed SOFC Sealing Composites with Self-Healing Capabilities
84611	Mesta Electronics Inc.	DC-AC Inverter with Reactive-Power-Management Functionality
84616	R&D Dynamics Corporation	Foil-Bearing Supported High-Speed Centrifugal Cathode Air Blower
84624	TIAX LLC	Low-Cost, High-Temperature Recuperators for SOFC Fabricated from Titanium Aluminum Carbide (Ti <sub>2</sub> AlC)
83795	TDA Research, Inc.	Sorbents for Desulfurization of Natural Gas and LPG
84608	Materials and Systems Research, Inc.	A Thin Film, Anode-Supported Solid Oxide Fuel Cell Based on High Temperature Proton Conducting Membrane for Operation at 400 to 700°C
86280	Materials and Systems Research, Inc.	A High Temperature (400 to 650°C) Secondary Storage Battery Based on Liquid Sodium and Potassium Anodes
86140	FuelCell Energy, Inc.	Advanced Control Modules for Hybrid Fuel Cell/Gas Turbine Power Plants
86283	NexTech Materials, Ltd.	Component Manufacturing and Optimization of Protonic SOFCs
41244	Cummins Power Generation	10 kW Solid Oxide Fuel Cell Power System Commercialization
42184	University at Albany – SUNY	Feasibility of a SOFC Stack Integrated Optical Chemical Sensor
42624	Massachusetts Institute of Technology	Photo-Activated Low Temperature, Micro Fuel Cell Power Source
42625	Northwest University	High Temperature Fuel Cells for Co-Generation of Chemicals and Electricity
42626	United Technologies Research Center	Techno-Economic Feasibility of Highly Efficient Cost Effective Thermoelectric-SOFC Hybrid Power Generation Systems

### Projects Discontinued Since the FY 2006 Annual Report

Contract Number	Performer	Project Topic
FEAA067	Oak Ridge National Laboratory	Power Electronics for Solid Oxide Fuel Cells
FWP49100	Argonne National Laboratory	Technology Development in Support of SECA
34139	Siemens Power Generation	High Temperature Solid Oxide Fuel Cell Development
40798	FuelCell Energy, Inc.	Direct Fuel Cell/Turbine Power Plant
41562	University of Florida	Determination of Electrochemical Performance and Thermo-Mechanical-Chemical Stability of SOFCs from Defect Modeling
41566	University of Washington	Advanced Measurement and Modeling Techniques for Improved SOFC Cathodes
41569	Ceramatec, Inc.	Metal Interconnect for Solid Oxide Fuel Cell Power Systems
41571	Georgia Institute of Technology	An Integrated Approach to Modeling and Mitigating SOFC Failure
41574	<sup>1</sup> University of Illinois at Chicago <sup>2</sup> Ceramatec Inc. <sup>3</sup> Virginia Polytechnic Institute and State University <sup>4</sup> Oak Ridge National Laboratory <sup>5</sup> Pacific Northwest National Laboratory	An Investigation of Resolve the Interaction between Fuel Cell, Power Conditioning System and Application Load
41575	NexTech Materials, Ltd.	Continuous Process for Low-Cost, High-Quality YSZ Powder
41578	University of Pittsburgh	Fundamental Studies of the Durability of Materials for Interconnects in Solid Oxide Fuel Cells
41915	Southern University and A&M College	Dense Membranes for Anode Supported All-Perovskite IT-SOFCs
41959	University of Florida	Electrocatalytically Active High Surface Area Cathodes for Low Temperature SOFCs
41960	University of Houston	New Cathode Materials for Intermediate Temperature Solid Oxide Fuel Cells
42222	Chevron Energy Research and Technology Company	Development of Ni-Based Sulfur-Resistant Catalyst for Diesel Reforming
42228	Connecticut Global Fuel Cell Center University of Connecticut	Low-Cost Integrated Composite Seal for SOFC: Materials and Design Methodologies
42514	Franklin Fuel Cells, Inc.	Novel Cathodes Prepared by Impregnation Procedures
42515	Georgia Institute of Technology Center for Innovative Fuel Cell and Battery Technologies	Quantitative Characterization of Chromium Poisoning of Cathode Activity
42517	University of Michigan	Desulfurization of High-Sulfur Jet Fuels by Adsorption and Ultrasound-Assisted Sorbent Regeneration
73138	Ceramatec, Inc.	Advanced Net-Shape Insulation for Solid Oxide Fuel Cells
83528	NexTech Materials, Ltd.	Highly Textured Glass Composite Seals for Intermediate-Temperature SOFCs
84387	FuelCell Energy, Inc.	Diesel Plasma Reformer
84212	Spinworks, LLC	Low-Cost/High-Temperature Heat Exchanger for SOFCs Using Near-Net-Shape Ceramic Powder Forming Process

### Projects Discontinued Since the FY 2005 Annual Report

<b>Contract Number</b>	<b>Performer</b>	<b>Project Topic</b>
FE09	Los Alamos National Laboratory	Diesel Reforming for Solid Oxide Fuel Cell Auxiliary Power Units
40779	General Electric	SOFC Hybrid System for Distributed Power Generation
41539	Boston University	Materials System for Intermediate-Temperature SOFC
41602	University of Utah	Active Cathodes for Super-High Power Density SOFC Through Space Change Effects
41631	California Institute of Technology	Enhanced Power Stability for Proton-Conducting Solid Oxide Fuel Cells
41801	Virginia Polytechnic Institute and State University	Modeling and Design for a Direct Carbon Fuel Cell with Entrained Fuel and Oxidizer
41803	University of Akron	Carbon-based Fuel Cell
41804	Duke University	Carbon Ionic Conductors for Use in Novel Carbon-Ion Fuel Cells
83212	Ceramatec, Inc.	Lanthanum Gallate Electrolyte Based Intermediate-Temperature Solid Oxide Fuel Cell Development







**National Energy  
Technology Laboratory**

1450 Queen Avenue SW  
Albany, OR 97321-2198  
541-967-5892

2175 University Avenue South  
Suite 201  
Fairbanks, AK 99709  
907-452-2559

3610 Collins Ferry Road  
P.O. Box 880  
Morgantown, WV 26507-0880  
304-285-4764

626 Cochran Mill Road  
P.O. Box 10940  
Pittsburgh, PA 15236-0940  
412-386-4687

One West Third Street, Suite 1400  
Tulsa, OK 74103-3519  
918-699-2000

**Wayne A. Surdoval**  
Technology Manager, Fuel Cells  
412-386-6002  
wayne.surdoval@netl.doe.gov

Visit the NETL website at:  
[www.netl.doe.gov](http://www.netl.doe.gov)

Customer Service:  
**1-800-553-7681**



**U.S. Department of Energy  
Office of Fossil Energy**

Printed in the United States on recycled paper  
DOE/NETL-2009/1348, December 2008

